NASA Contractor Report 177571

Fully Automatic Guidance and Control for Rotorcraft Nap-of-the-Earth Flight Following Planned Profiles Volume II – Mathematical Model

Warren F. Clement, Peter J. Gorder, and Wayne F. Jewell

Contract Number NAS2-12640
January 1991

National Aeronautics and Space Administration

NASA Contractor Report 177571

Fully Automatic Guidance and Control for Rotorcraft Nap-of-the-Earth Flight Following Planned Profiles Volume II – Mathematical Model

Warren F. Clement, Peter J. Gorder, and Wayne F. Jewell
Systems Technology, Inc., Mountain View, California

Prepared for
Ames Research Center
Contract Number NAS2-12640
January 1991

National Aeronautics and
Space Administration

Ames Research Center
Moffett Field, California 94035-1000

FOREWORD AND ACKNOWLEDGEMENTS

The work described herein was performed under NASA Contract NAS2-12640 (SBIR Phase II) for the NASA Ames Research Center (ARC), under the technical direction of the Flight Guidance and Navigation Branch (Code FSN) as part of its automatic nap-of-the-earth flight program in cooperation with the Army Research and Technology Activity of the U.S. Army Aviation Systems Command. The NASA ARC Code FSN contract technical monitor was Harry N. Swenson. The project engineer for Systems Technology, Inc., (STI) was Warren F. Clement, and the STI technical director was Duane T. McRuer. This work was performed during the period from September 1987 through September 1990. Mrs. Sharon A. Duerksen of STI published the report. This research required the subcontracted services of McDonnell-Douglas Helicopter Company (MDHC) for whom Donald G. Caldwell served as project engineer.

The authors wish to acknowledge the assistance, in scheduling and operating the Vertical Motion Simulator at NASA ARC, of Thomas Alderete and David Astill of the NASA ARC Simulation Experiments Branch; Richard Bray of the NASA ARC Flight Dynamics and Controls Branch; and Ernest Inn, Mary Shirin Sheppard, Frederic G. Kull, Jr., and their colleagues at SYRE. A special note of thanks goes to Richard A. Coppenbarger of the NASA ARC Flight Guidance and Navigation Branch for his diligent assistance and encouragement during the NASA ARC simulation and data analysis.

ABSTRACT

Developing a single-pilot, all-weather nap-of-the-earth (NOE) capability requires fully automatic NOE (ANOE) navigation and flight control. Innovative guidance and control concepts are investigated in a four-fold research effort that: (1) organizes the on-board computer-based storage and real-time updating of NOE terrain profiles and obstacles in course-oriented coordinates indexed to the mission flight plan; (2) defines a class of automatic anticipative pursuit guidance algorithms and necessary data preview requirements to follow the vertical, lateral, and longitudinal guidance commands dictated by the updated flight profiles; (3) automates a decision-making process for unexpected obstacle avoidance; and (4) provides several rapid response maneuvers. Acquired knowledge from the sensed environment is correlated with the forehand knowledge of the recorded environment (terrain, cultural features, threats, and targets), which is then used to determine an appropriate evasive maneuver if a non-conformity of the sensed and recorded environments is observed. This four-fold research effort has been evaluated in both fixed-base and moving-base real-time piloted simulations, thereby providing a practical demonstration for evaluating pilot acceptance of the automated concepts, supervisory override, manual operation, and re-engagement of the automatic system. Volume I describes the major components of the guidance and control laws as well as the results of the piloted simulations. Volume II describes the complete mathematical model of the fully automatic guidance system for rotorcraft NOE flight following planned flight profiles.

TABLE OF CONTENTS

TABLE OF CONTENTS (CONTINUED)

TABLE OF CONTENTS (CONCLUDED)

LIST OF FIGURES

LIST OF FIGURES (CONTINUED)

LIST OF FIGURES (CONTINUED)

LIST OF FIGURES (CONTINUED)

LIST OF FIGURES (CONTINUED)

LIST OF FIGURES (CONTINUED)

LIST OF FIGURES (CONTINUED)

LIST OF FIGURES (CONTINUED)

LIST OF FIGURES (CONCLUDED)

LIST OF TABLES

LIST OF TABLES (CONCLUDED)

LIST OF ABBREVIATIONS

c.g.	Center of gravity
CPU	Computer processing unit
CRT	Cathode ray tube
deg	Degree
dm	Decameter
DMA	Defense Mapping Agency
FCS	Flight control system
FLYRT	FLY RighT Apache helicopter simulation model (MDHC)
fpm	Feet per minute
ft	Foot, feet
HUD	Head-up display
kt	Knot(s)
LHX	Light Helicopter eXperimental
MDHC	McDonnell-Douglas Helicopter Company
min	Minute
MMD	Moving map display
NOE	Nap of the earth
SCAS	Stability and control augmentation system
SCTT	Sub-critical task tester
sec	Second
VCPH	Velocity command/position hold
VMC	Visual meteorological conditions

0. INTRODUCTION

The automatic nap-of-the-earth (NOE) flight program is a cooperative National Aeronautics and Space Administration (NASA)/U.S. Army effort to develop technology that will lead to enhanced low-altitude and NOE flight path management, guidance, and control through computer aiding. Reference 1 presents a description of the necessary considerations for automatic NOE (ANOE) rotorcraft flight. Included in the description is a hierarchical apportionment of the guidance structure into three vector feedback loops (Fig. 0.1 from Ref. 1). The innermost feedback loop consists of the near-field obstacle avoidance and guidance of the rotorcraft and is the focus of this project. In contradistinction to the three loop structure in Fig. 0.1, this project presumes separation of the (preflight) mission and route planning functions from the flight guidance and obstacle avoidance activities.

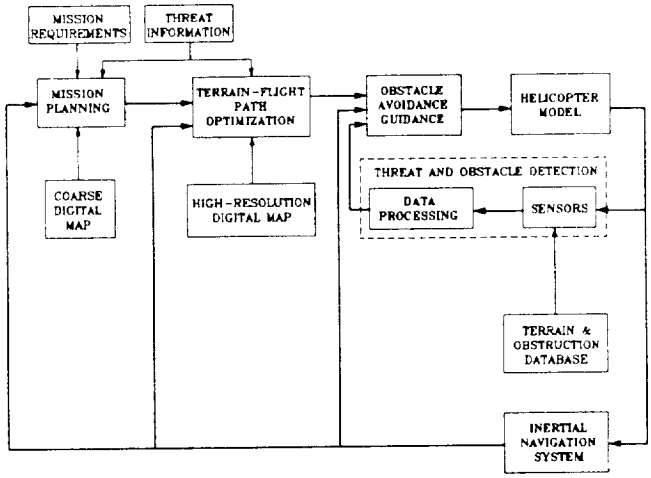

Figure 0.1. Automatic NOE Guidance Structure (from Ref. 1)

The automatic guidance and control system mathematical model is separated in this document into the individual sections depicted in Fig. 0.2: (1) the flight control system mathematical model, including pursuit feedforward guidance and programmed constrained time-optimal maneuvers, (2) the pre-planned stored flight plan, (3) the automatic guidance recapture logic, (4) the obstacle detection and avoidance maneuver selection logic, and (5) the aerodynamic model of the rotorcraft. Additionally, although not shown in Fig. 0.2, Section 6 of this report includes the head-up display (HUD) specifications; Section 7, the cockpit flight instrument specifications; Section 8, the moving map display (MMD) specifications; Section 9, the audio annunciator specification; and Section 10, the side task specifications, each of which forms a part of the NOE flight simulation for which the automatic guidance and control system mathematical model has been prepared. Appendices A through E incorporate all or parts of five working papers prepared during the course of the reported study. Appendix F provides the XFLOAT array designations, and Appendix G, the terrain approximation routine, TERRN. Finally, Appendix H is a comprehensive indexed list of symbols with special notations that indicate where symbol definitions are given algebraically and/or numerically.

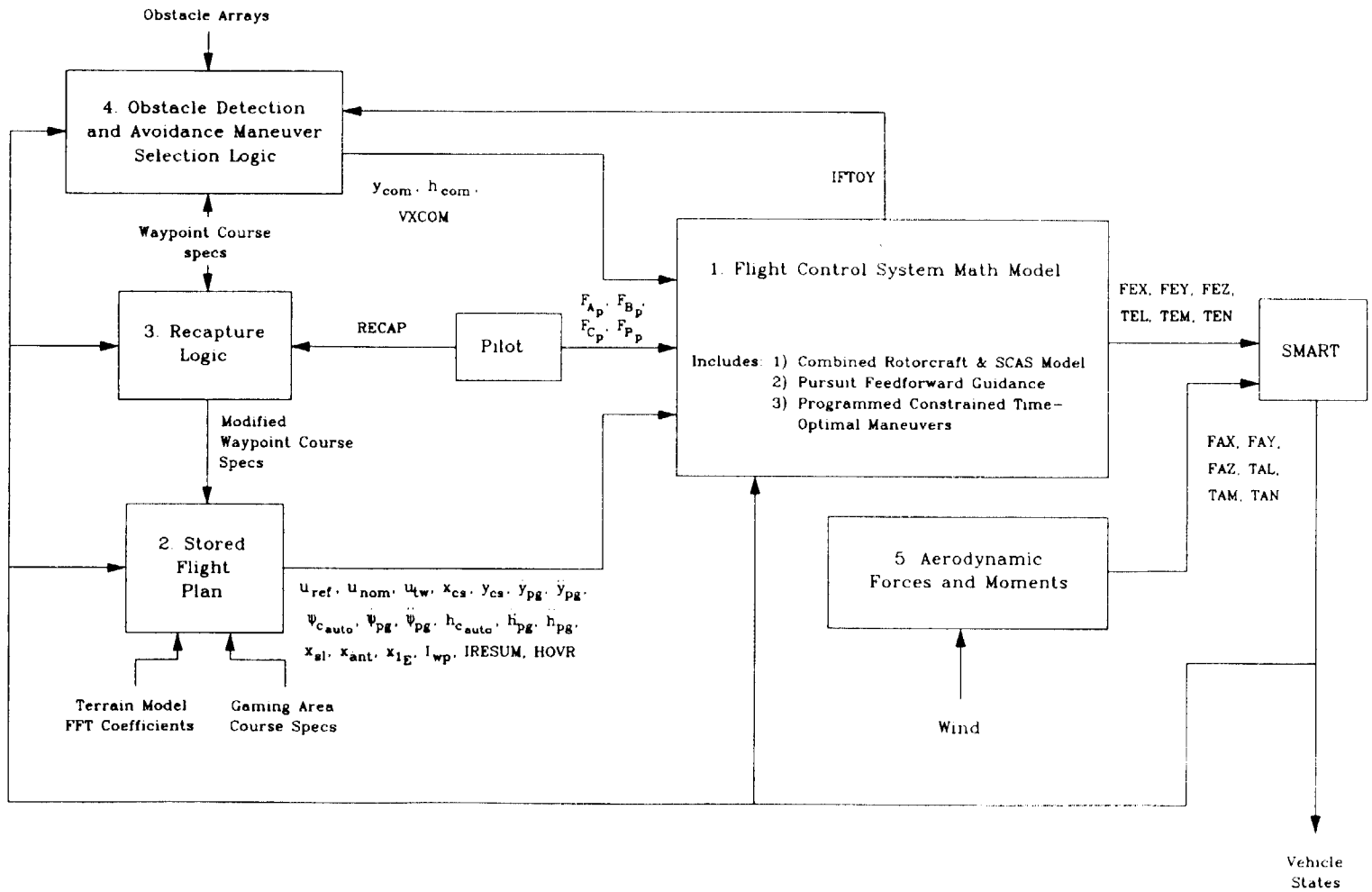

Figure 0.2. Vector Block Diagram for Multiloop Guidance and Control System Enumerating Major Mathematical Model Sections

1. FLIGHT CONTROL SYSTEM MATHEMATICAL MODEL

1.1 Combined Rotorcraft and Stability and Control Augmentation System (SCAS) Model

The helicopter dynamics were simulated using small perturbation stability and control derivatives, as shown in the block diagrams of Figs. 1.1 through 1.3. The outputs of the block diagrams are forces and moments (TEM, TEL, FEZ, and TEN), which are inputs to a kinematic model of the translational and rotational equations of rigid body motion (the displacements x, y, h, ϕ, Θ, and ψ are outputs of this model, Ref. 4). The numerical values of the derivatives, as well as the feedback variables indicated in the block diagrams, were designed to simulate a highly augmented vehicle having translational rate command, position hold capabilities. The transfer functions for vehicle response due to cockpit control under manual control (i.e., without any of the pursuit feedforward terms shown in the block diagrams) are given below. The variables indicated in the transfer functions are shown in the block diagrams of Figs. 1.1 through 1.3.

Cockpit Controller	Vehicle Response	Transfer Functions for Manual Control Under:	
		Rate Command	Position Hold
Collective	Vertical Velocity	$\frac{\dot{h}}{\dot{h}_{R_p}} = \frac{2.0}{(s+2.0)}$	$\frac{h}{h_c} = \frac{1.0}{(s+0.5)(s+2.0)}$
Pedals	Yaw Rate	$\frac{\dot{\psi}}{\dot{\psi}_{R_p}} = \frac{4.0}{(s+4.0)}$	$\frac{\psi}{\psi_c} = \frac{4.0}{(s+1.0)(s+4.0)}$
Longitudinal Cyclic	Forward Speed	$\frac{\dot{x}}{u_{R_p}} = \frac{0.8}{(s+0.8)}$	$\frac{x}{x_c} = \frac{0.16}{(s+0.2)(s+0.8)}$
Lateral Cyclic	Lateral Speed	$\frac{\dot{y}}{v_{R_p}} = \frac{0.8}{(s+0.8)}$	$\frac{y}{y_c} = \frac{0.16}{(s+0.2)(s+0.8)}$

The longitudinal and lateral cyclic, collective, and directional control systems are shown in Figs. 1.1 through 1.3, respectively. The parameters for each axis' control system are given in Tables 1.1 through 1.3. A state space derivation of the combined rotorcraft model and SCAS is presented in Appendix A.

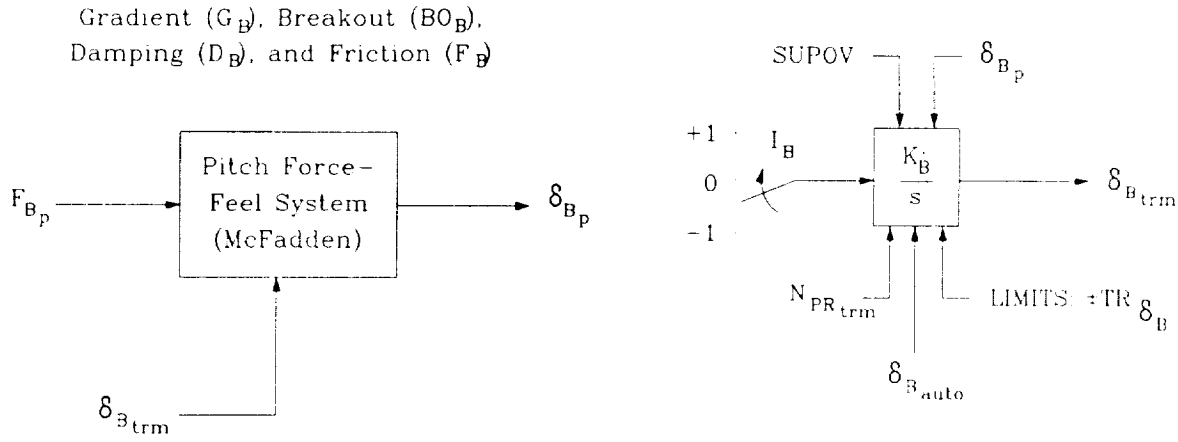

$$\delta_{B_{auto}} = TR_{\delta_B}\left(\left[\frac{u_{R_{auto}}}{2K_{\delta_B}} + \sqrt{\frac{u_{R_{auto}}^2}{4K_{\delta_B}^2} + \frac{1}{27}}\right]^{\frac{1}{3}} + \left[\frac{u_{R_{auto}}}{2K_{\delta_B}} - \sqrt{\frac{u_{R_{auto}}^2}{4K_{\delta_B}^2} + \frac{1}{27}}\right]^{\frac{1}{3}}\right)$$

Notes:

1. I_B is a two-axis trim button on the cyclic stick.

2. $N_{PR_{trm}}$ is the trim release button on the cyclic stick (button on the top of the stick).

3. $\delta_{B_{trm}}$ should be initialized to the trim longitudinal stick position. Ramp δ_{B_p} to $\delta_{B_{trm}}$ in IC.

4. In operate, if $N_{PR_{trm}} = 1$ then set $\delta_{B_{trm}}$ to δ_{B_p}, else, if $I_B = 0$ and SUPOV is false, then set $\delta_{B_{trm}}$ to $\delta_{B_{auto}}$, else set the value of $\delta_{B_{trm}}$ as shown.

5. If $N_{PR_{trm}} = 1$, $|\delta_{B_p}| \leq 0.1$ in, and $|\dot{\delta}_{B_p}| \leq 0.1$ in/sec, then disable the trim release button, set $N_{PR_{trm}}$ to 0, and set $\delta_{B_{trm}}$ to 0.0 in.

6. $G_B = (1 - N_{PR_{trm}})*2.0$ lb/in
   $BO_B = 1.25$ lb
   $D_B = 0.1$ lb/in/sec
   $F_B = 0.5$ lb

7. $K_B = 0.7$ in/sec

8. $TR_{\delta_B} = 5.5$ in
   $K_{\delta_B} = 30.0$ ft/sec

a. Pitch Force Feel System

Figure 1.1 Longitudinal and Lateral Control System

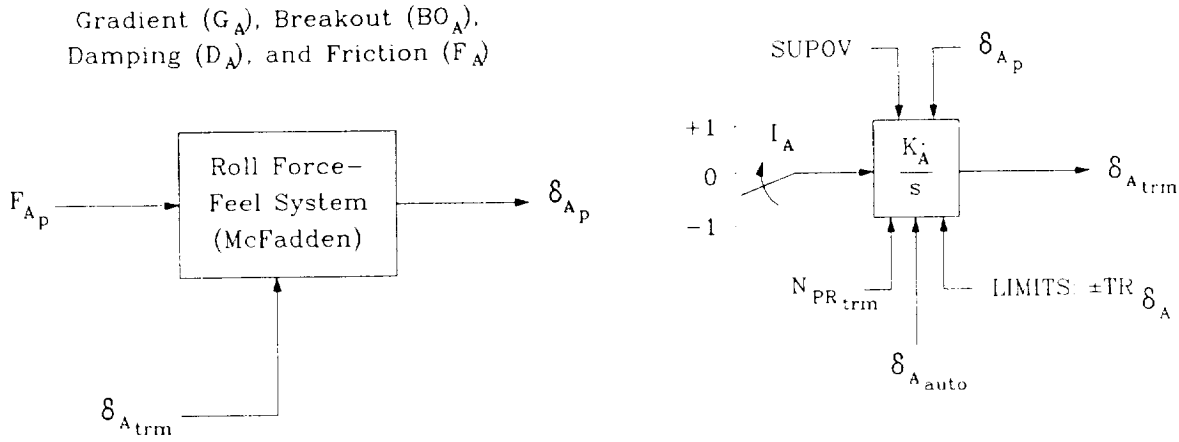

$$\delta_{A_{auto}} = TR_{\delta_A}\left(\left[\frac{V_{R_{auto}}}{2K_{\delta_A}} + \sqrt{\frac{V_{R_{auto}}^2}{4K_{\delta_A}^2} + \frac{1}{27}}\right]^{\frac{1}{3}} + \left[\frac{V_{R_{auto}}}{2K_{\delta_A}} - \sqrt{\frac{V_{R_{auto}}^2}{4K_{\delta_A}^2} + \frac{1}{27}}\right]^{\frac{1}{3}}\right)$$

Notes:

1. I_A is a two-axis trim button on the cyclic stick.

2. $N_{PR_{trm}}$ is the trim release button on the cyclic stick (button on the top of the stick).

3. $\delta_{A_{trm}}$ should be initialized to the trim lateral stick position. Ramp δ_{A_p} to $\delta_{A_{trm}}$ in IC.

4. If $N_{PR_{trm}} = 1$ then set $\delta_{A_{trm}}$ to δ_{A_p}, else if $I_A = 0$ and SUPOV is false, then set $\delta_{A_{trm}}$ to $\delta_{A_{auto}}$, else, set the value of $\delta_{A_{trm}}$ as shown.

5. If $N_{PR_{trm}} = 1$, $|\delta_{A_p}| \leq 0.1$ in, and $|\dot{\delta}_{A_p}| \leq 0.1$ in/sec, then disable the trim release button, set $N_{PR_{trm}}$ to 0, and set $\delta_{A_{trm}}$ to 0.0 in.

6. $G_A = (1 - N_{PR_{trm}}) * 1.0$ lb/in
   $BO_A = 0.75$ lb
   $D_A = 0.1$ lb/in/sec
   $F_A = 0.5$ lb

7. $K_A = 0.7$ in/sec

8. $TR_{\delta_A} = 5.5$ in
   $K_{\delta_A} = 30.0$ ft/sec

b. Roll Force Feel System

Figure 1.1 (Continued)

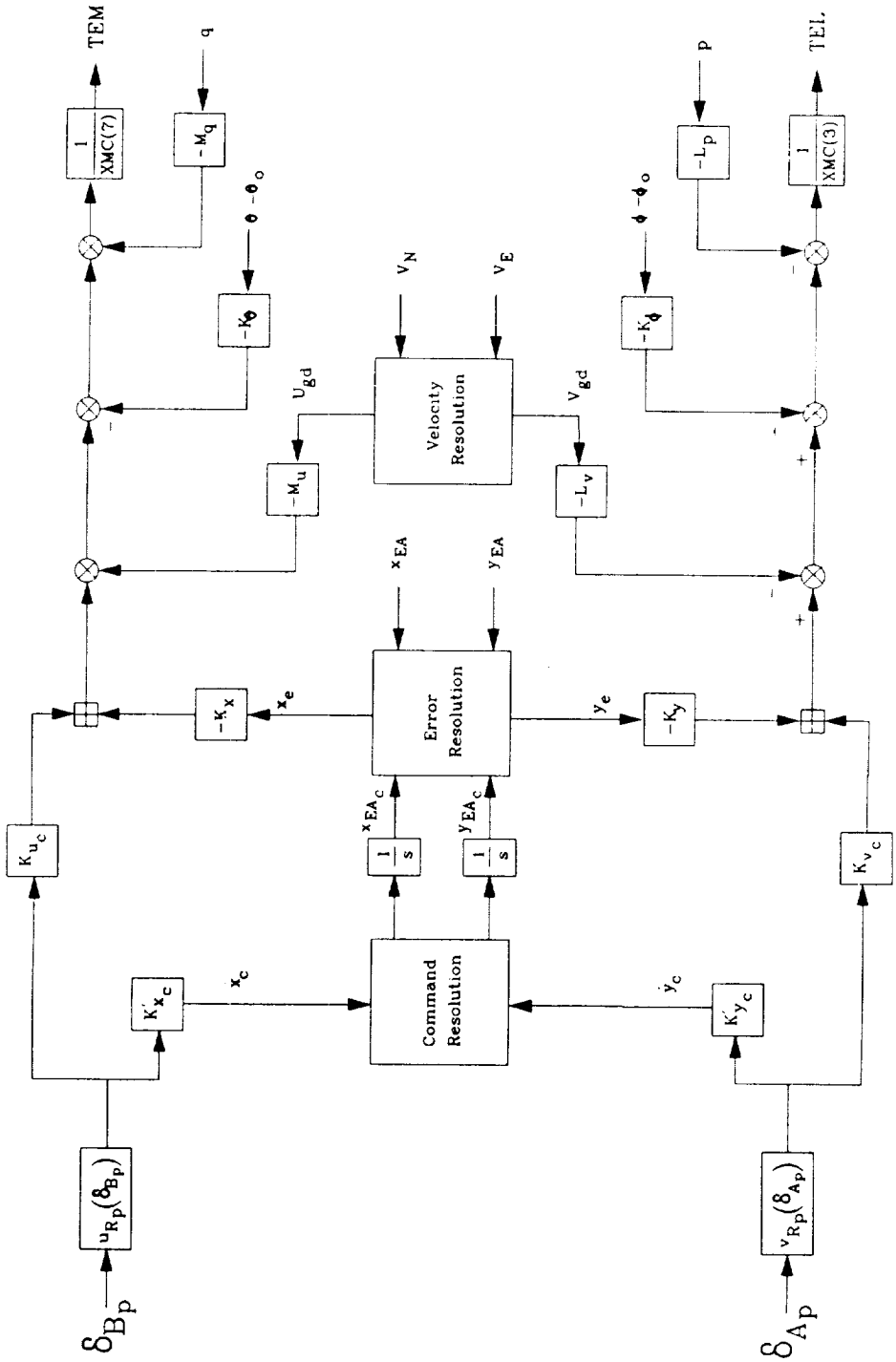

c. Longitudinal and Lateral SCAS and FCS

Figure 1.1 (Continued)

Notes for Figure 1.1c

1. The contents of the command resolution, error resolution, and velocity resolution boxes are as follows:

   Command Resolution:

$$\dot{x}_{EA_c} = \dot{x}_c \cos\psi - \dot{y}_c \sin\psi$$

$$\dot{y}_{EA_c} = \dot{x}_c \sin\psi + \dot{y}_c \cos\psi$$

   Error Resolution:

$$x_e = (x_{EA_c} - x_{EA})\cos\psi + (y_{EA_c} - y_{EA})\sin\psi$$

$$y_e = -(x_{EA_c} - x_{EA})\sin\psi + (y_{EA_c} - y_{EA})\cos\psi$$

   Velocity Resolution:

$$U_{gd} = V_N \cos\psi + V_E \sin\psi$$

$$V_{gd} = -V_N \sin\psi + V_E \cos\psi$$

2. The subscript EA denotes earth-fixed axis system.

3. V_N and V_E are the northward and eastward rotorcraft inertial velocities, respectively.

Figure 1.1 (Continued)

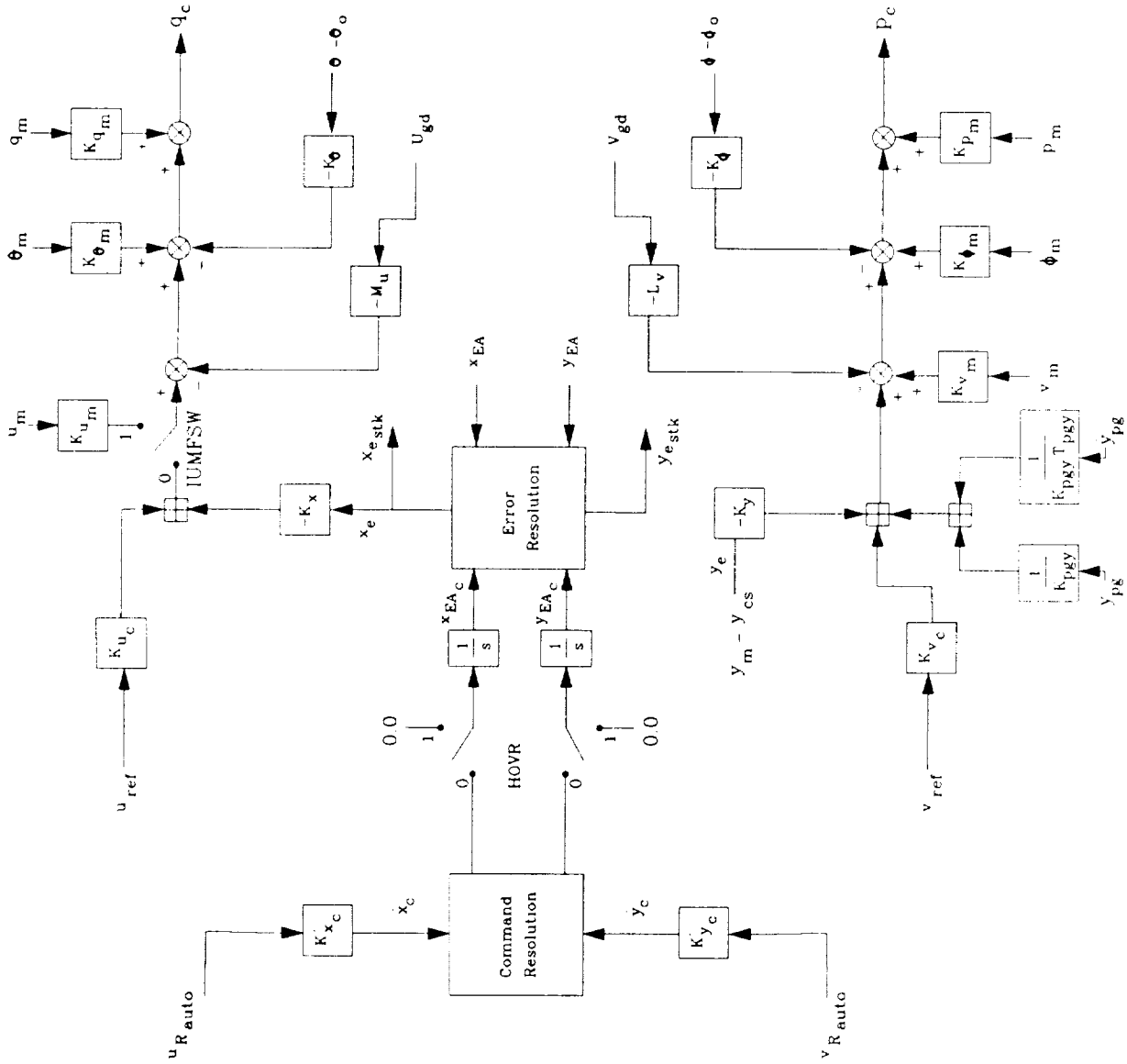

d. Longitudinal and Lateral Automatic Guidance

Figure 1.1 (Continued)

Notes for Figure 1.1d

1. The contents of the command resolution, error resolution, and velocity resolution boxes are as follows:

   Command Resolution:

$$\dot{x}_{EA_c} = \dot{x}_c \cos\psi - \dot{y}_c \sin\psi$$

$$\dot{y}_{EA_c} = \dot{x}_c \sin\psi + \dot{y}_c \cos\psi$$

   Error Resolution:

$$x_e = (x_{EA_c} - x_{EA})\cos\psi + (y_{EA_c} - y_{EA})\sin\psi$$

$$y_e = -(x_{EA_c} - x_{EA})\sin\psi + (y_{EA_c} - y_{EA})\cos\psi$$

   Velocity Resolution:

$$U_{gd} = V_N \cos\psi + V_E \sin\psi$$

$$V_{gd} = -V_N \sin\psi + V_E \cos\psi$$

2. The subscript EA denotes earth-fixed axis system.

3. V_N and V_E are the northward and eastward rotorcraft inertial velocities, respectively.

4. The state of the logical switch HOVR is determined in the waypoint sequencing portion of the stored flight plan or the condition of the supervisory override switch, SUPOV (If SUPOV = .TRUE., HOVR = .FALSE.). When TRUE, the HOVR switch holds the position command fixed in intertial space.

5. In the figure, the possible states, 1 and 0, for the logical switch HOVR correspond to .TRUE. and .FALSE., respectively.

6. IUMFSW = 0 if SUPOV = .TRUE. or IFTOX = 0, IUMFSW = 1 otherwise.

Figure 1.1 (Continued)

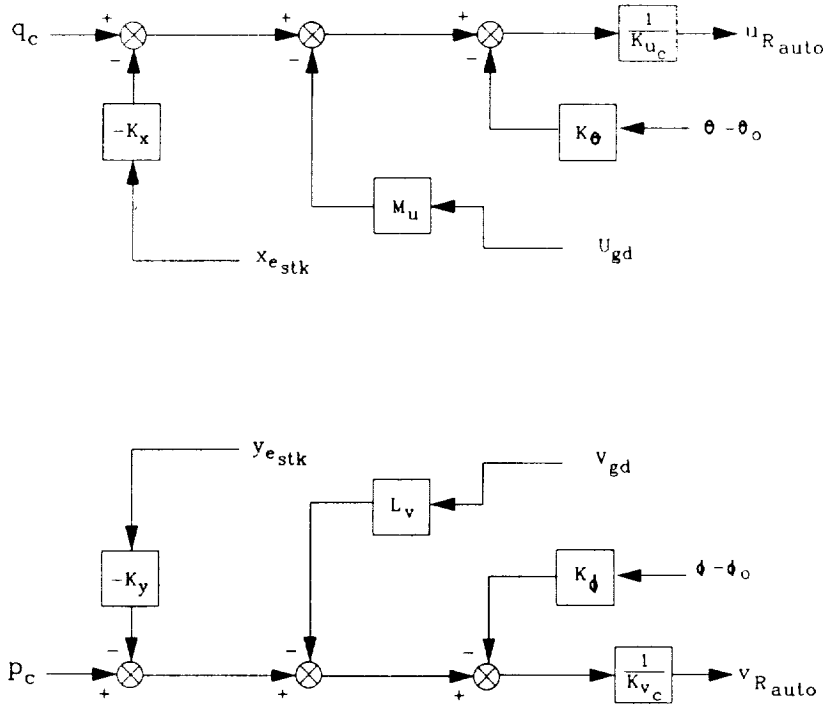

e. Automatic Guidance Velocity Commands

Figure 1.1 (Concluded)

TABLE 1.1

PARAMETER VALUES FOR LONGITUDINAL AND LATERAL CONTROL SYSTEM

$u_{R_p}(\delta_{B_p})$	Non-linear longitudinal cyclic gain: $u_{R_p}(\delta_{B_p}) = K_{\delta_B}\left(\frac{\delta_{B_p}}{TR_{\delta_B}} + \left[\frac{\delta_{B_p}}{TR_{\delta_B}}\right]^3\right)$	
K'_{x_c}	Normalized longitudinal position command gain	1.0
K_{u_c}	Longitudinal velocity command feedforward gain	-0.10 rad/ft-sec
K_x	Longitudinal position error feedback gain	0.02 rad/ft-sec^2
M_u	Augmented longitudinal velocity stability derivative	0.134 rad/ft-sec
K_θ	Pitch attitude feedback gain	-7.962 1/sec^2
M_q	Augmented pitch rate stability derivative	-4.96 1/sec
XMC(7)	Effective pitching moment of inertia	1.0 ft-lb-sec^2
$v_{R_p}(\delta_{A_p})$	Non-linear lateral cyclic gain: $v_{R_p}(\delta_{A_p}) = K_{\delta_A}\left(\frac{\delta_{A_p}}{TR_{\delta_A}} + \left[\frac{\delta_{A_p}}{TR_{\delta_A}}\right]^3\right)$	
K'_{y_c}	Normalized lateral position command gain	1.0
K_{v_c}	Lateral velocity command feedforward gain	0.1893 rad/ft-sec
K_y	Lateral position error feedback gain	-0.0374 rad/ft-sec^2
L_v	Augmented lateral velocity stability derivative	-0.215 rad/ft-sec
K_ϕ	Roll attitude feedback gain	-11.32 1/sec^2
L_p	Augmented roll rate stability derivative	-5.02 1/sec

TABLE 1.1 (CONCLUDED)

XMC(3)	Effective rolling moment of inertia	$1.0 \frac{1}{ft\text{-}lb\text{-}sec^2}$
K_{pgy}	Pursuit guidance model gain	3.3113 ft/rad
T_{pgy}	Lateral pursuit guidance model time constant	0.90334 sec
θ_0	Trim pitch attitude at hover	0.0 rad
ϕ_0	Trim roll attitude at hover	0.0 rad
K_{v_m}	Lateral model velocity feedforward gain	0.247 rad/ft-sec
K_{ϕ_m}	Lateral model roll attitude feedforward gain	10.253 $1/sec^2$
K_{p_m}	Lateral model roll rate feedforward gain	2.726 1/sec
K_{u_m}	Longitudinal model velocity feedforward gain	-0.1439 rad/ft-sec
K_{θ_m}	Longitudinal model pitch attitude feedforward gain	6.243 $1/sec^2$
K_{q_m}	Longitudinal model pitch rate feedforward gain	2.4163 1/sec

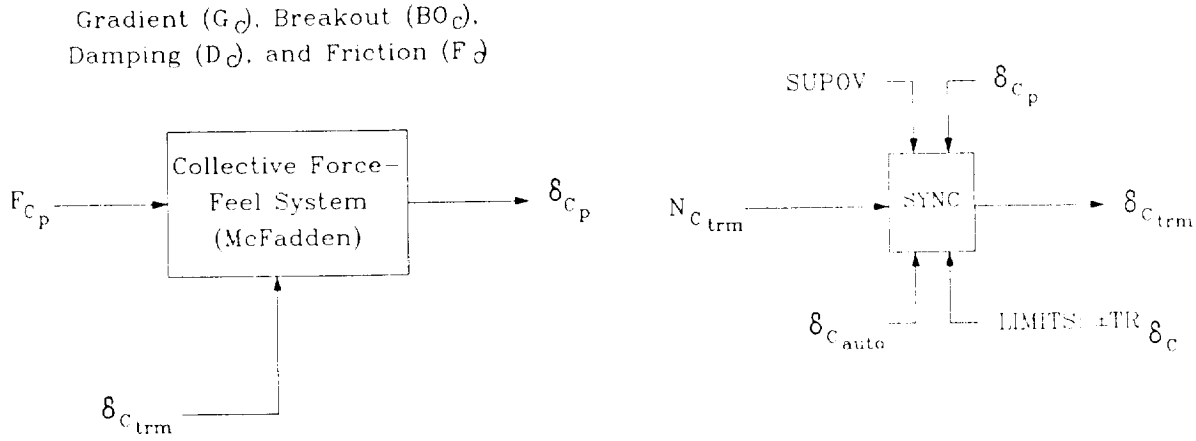

$$\delta_{C_{auto}} = TR_{\delta C}\left(\left[\frac{h_{R_{auto}}}{2K_{\delta C}} + \sqrt{\frac{h_{R_{auto}}^2}{4K_{\delta C}^2} + \frac{1}{27}}\right]^{\frac{1}{3}} + \left[\frac{h_{R_{auto}}}{2K_{\delta C}} - \sqrt{\frac{h_{R_{auto}}^2}{4K_{\delta C}^2} + \frac{1}{27}}\right]^{\frac{1}{3}}\right)$$

Notes:

1. $N_{C_{trm}}$ is the trim release button on the side-arm collective stick (button on the top of the stick).

2. $\delta_{C_{trm}}$ should be initialized to the trim side-arm collective stick position. Ramp δ_{C_p} to $\delta_{C_{trm}}$ in IC.

3. In operate, if $N_{C_{trm}} = 1$ then set $\delta_{C_{trm}}$ to δ_{C_p}, else, if SUPOV is false, then set $\delta_{C_{trm}}$ to $\delta_{C_{auto}}$, else hold the value of $\delta_{C_{trm}}$.

4. If $N_{C_{trm}} = 1$, $|\delta_{C_p}| \leq 0.1$ in, and $|\dot{\delta}_{C_p}| \leq 0.1$ in/sec, then disable the trim release button, set $N_{C_{trm}}$ to 0, and set $\delta_{C_{trm}}$ to 0.0 in.

5. $G_C = (1 - N_{C_{trm}})*2.4$ lb/in
   $BO_C = 2.0$ lb
   $D_C = 0.3$ lb/in/sec
   $F_C = 1.4$ lb

6. $TR_{\delta C} = 3.0$ in
   $K_{\delta C} = 12.5$ ft/sec

a. Collective Force Feel System

Figure 1.2 Collective Control System

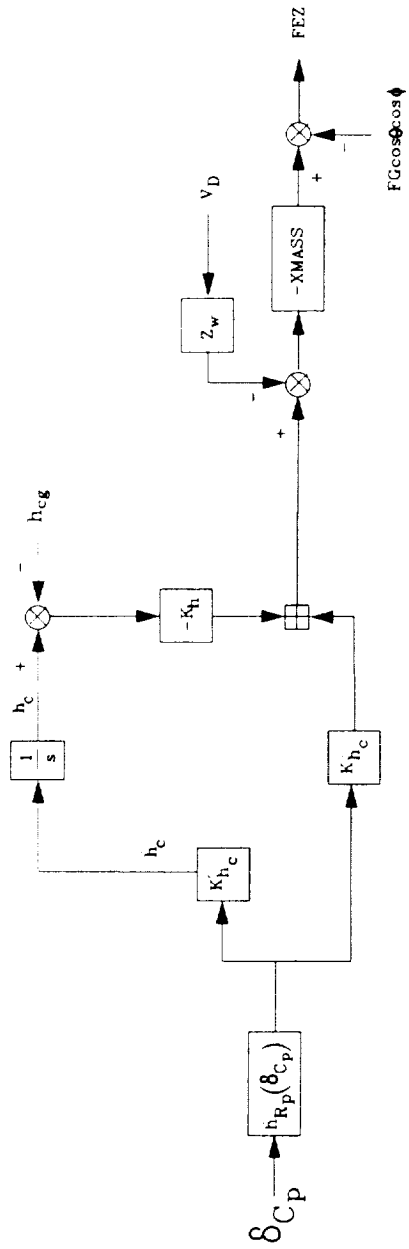

b. Vertical SCAS and FCS

Figure 1.2 (Continued)

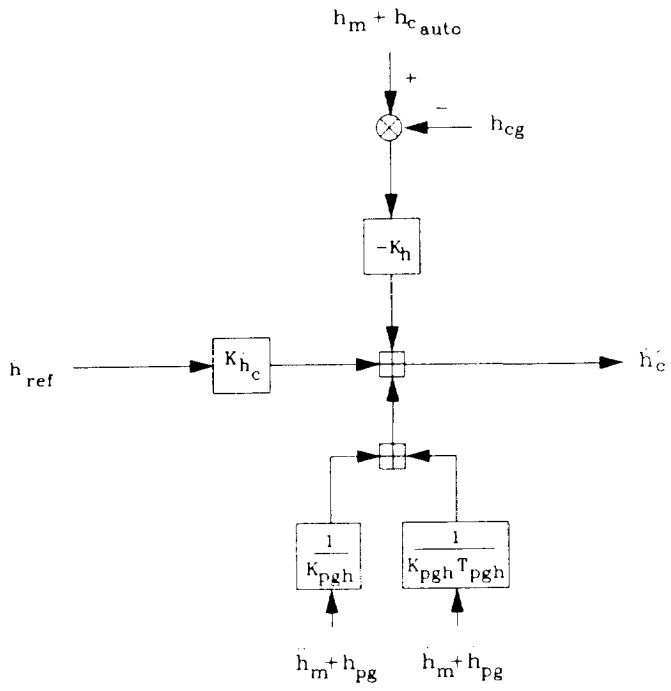

c. Vertical Automatic Guidance

Figure 1.2 (Continued)

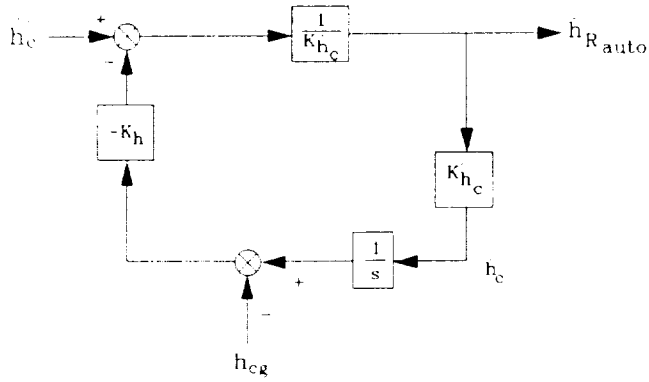

d. Automatic Guidance Vertical Velocity Command

Figure 1.2 (Concluded)

TABLE 1.2

PARAMETER VALUES FOR COLLECTIVE CONTROL SYSTEM

$h_{R_p}(\delta_{C_p})$	Non-linear collective gain: $h_{R_p}(\delta_{C_p}) = K_{\delta_C}\left(\frac{\delta_{C_p}}{TR_{\delta_C}} + \left[\frac{\delta_{C_p}}{TR_{\delta_C}}\right]^3\right)$	
K'_{h_c}	Normalized vertical position command gain	1.0
K_{h_c}	Vertical velocity command feedforward gain	2.0 1/sec
K_h	Vertical position error feedback gain	-1.0 $1/sec^2$
Z_w	Augmented vertical velocity stability derivative	-2.5 1/sec
XMASS	Effective mass	1.0 slug
K_{pgh}	Pursuit guidance model gain	1.0
T_{pgh}	Pursuit guidance model time constant	0.4 sec

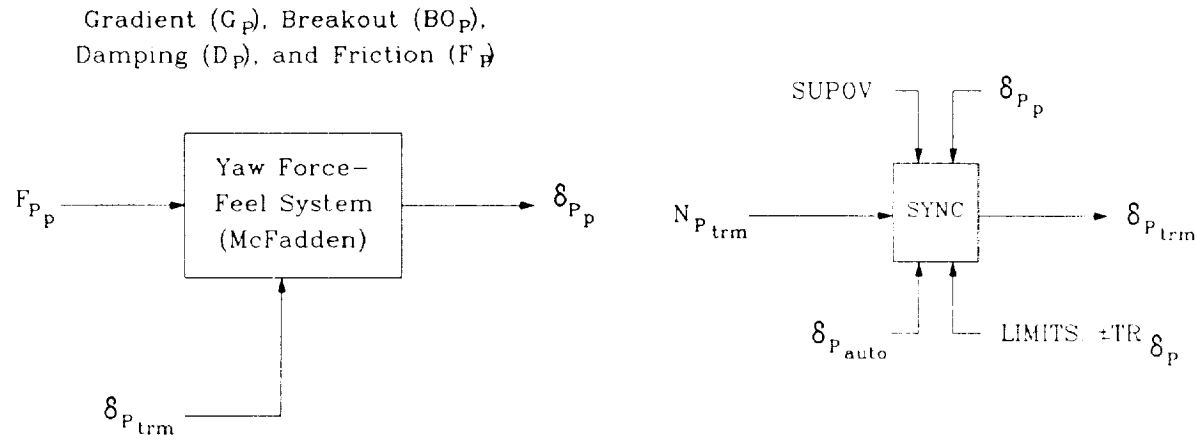

$$\delta_{P_{auto}} = TR_{\delta P}\left(\left[\frac{\dot{\psi}_{R_{auto}}}{2K_{\delta P}} + \sqrt{\frac{\dot{\psi}^2_{R_{auto}}}{4K^2_{\delta P}} + \frac{1}{27}}\right]^{\frac{1}{3}} + \left[\frac{\dot{\psi}_{R_{auto}}}{2K_{\delta P}} - \sqrt{\frac{\dot{\psi}^2_{R_{auto}}}{4K^2_{\delta P}} + \frac{1}{27}}\right]^{\frac{1}{3}}\right)$$

Notes:

1. $N_{P_{trm}}$ is the trim release button.

2. $\delta_{P_{trm}}$ should be initialized to the trim pedal position. Ramp δ_{P_p} to $\delta_{P_{trm}}$ in IC.

3. In operate, if $N_{P_{trm}} = 1$ then set $\delta_{P_{trm}}$ to δ_{P_p}, else, if SUPOV is false, then set $\delta_{P_{trm}}$ to $\delta_{P_{auto}}$, else hold the value of $\delta_{P_{trm}}$.

4. If $N_{P_{trm}} = 1$, $|\delta_{P_p}| \leq 0.1$ in, and $|\dot{\delta}_{P_p}| \leq 0.1$ in/sec, then disable the trim release button, set $N_{P_{trm}}$ to 0, and set $\delta_{P_{trm}}$ to 0.0 in.

5. $C_P = (1 - N_{P_{trm}})*6.0$ lb/in
   $BO_P = 2.75$ lb
   $D_P = 0.0$ lb/in/sec
   $F_P = 1.0$ lb

6. $TR_{\delta P} = 5.75$ in
   $K_{\delta P} = 0.35$ rad/sec

a. Yaw Force Feel System

Figure 1.3 Directional Control System

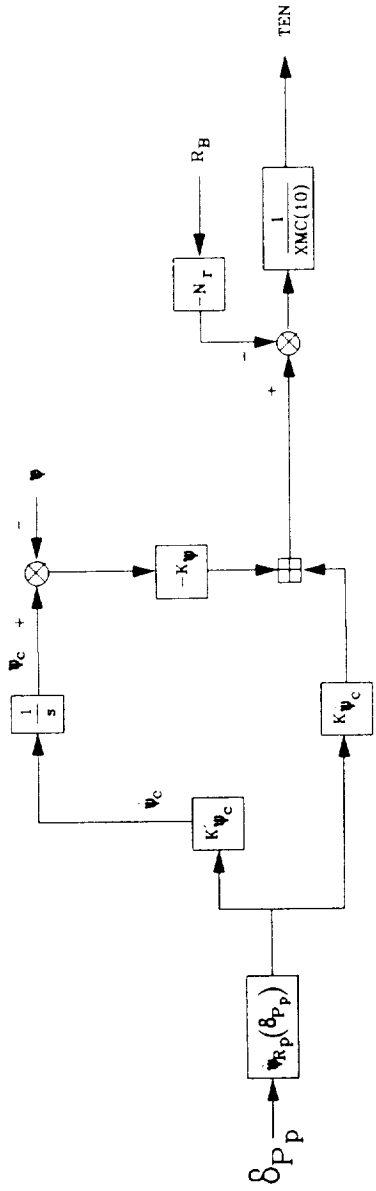

b. Directional SCAS and FCS

Figure 1.3 (Continued)

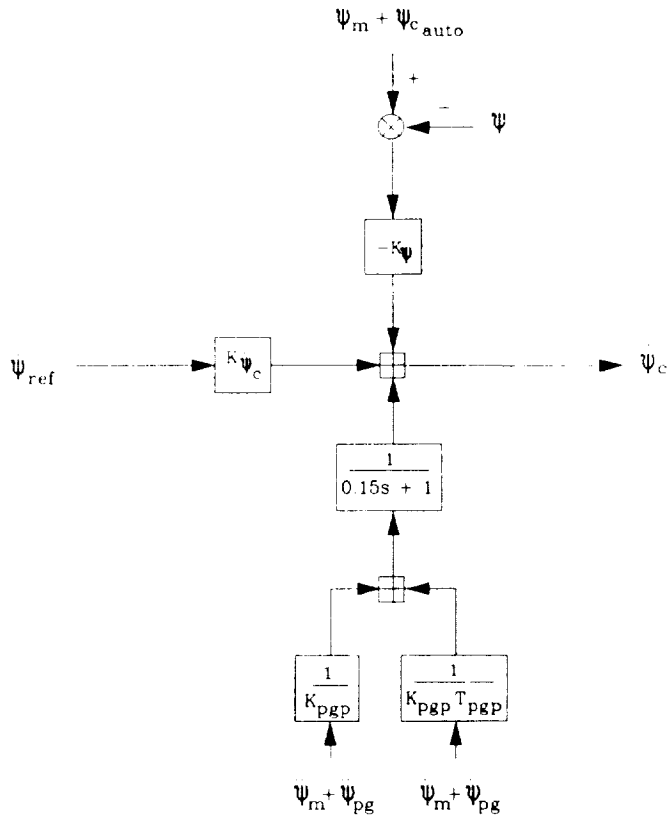

c. Directional Automatic Guidance

Figure 1.3 (Continued)

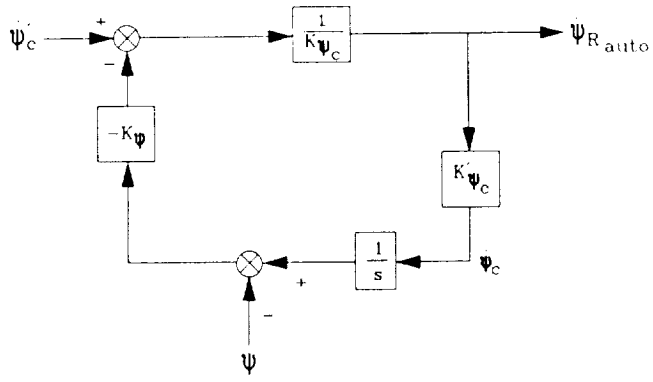

d. Automatic Guidance Yaw Rate Command

Figure 1.3 (Concluded)

TABLE 1.3

PARAMETER VALUES FOR DIRECTIONAL CONTROL SYSTEM

$\dot{\psi}_{R_p}(\delta_{P_p})$	Non-linear pedal gain: $\dot{\psi}_{R_p}(\delta_{P_p}) = K_{\delta_P}\left(\frac{\delta_{P_p}}{TR_{\delta_P}} + \left[\frac{\delta_{P_p}}{TR_{\delta_P}}\right]^3\right)$	
K'_{ψ_c}	Normalized heading command gain	1.0
K_{ψ_c}	Yaw rate command feedforward gain	4.0 1/sec
K_{ψ}	Heading error feedback gain	-4.0 1/sec^2
N_r	Augmented yaw rate stability derivative	-5.0 1/sec
XMC(10)	Effective yawing moment of inertia	1.0 ft-lb-sec^2
K_{pgp}	Pursuit guidance model gain	1.0
T_{pgp}	Pursuit guidance model time constant	0.2 sec

1.2 Pursuit Feedforward Guidance

In order to attain the desired level of precision for safety in automated NOE flight along a preplanned flight profile, it is necessary to include pursuit feedforward guidance commands in the anticipative trajectory coupler. The base rotorcraft described above FCS exhibits the following dynamics for position response to velocity command in all axes (Sec. 1.1, p. 3):

$$Y_c(s) = \frac{K_c}{s(s + 1/\tau_c)}$$

where τ_c represents the augmented surge, sway, heave, and yaw damping. To minimize the position errors, the following must then represent the pursuit feedforward guidance terms if r(s) is the general expression for the Laplace transform of the course position command array:

$$\frac{1}{K_c}(\dot{r}(s) + 1/\tau_c r(s))$$

The constants K_c and τ_c are synonymous with K_{pgy} and T_{pgy} for the lateral axis, K_{pgh} and T_{pgh} for the vertical axis, and K_{pgp} and T_{pgp} for the directional axis in the preceding section.

1.3 Programmed Constrained Time-Optimal Avoidance Maneuvers

Rapidly responding evasive maneuvers are required for automatically-piloted NOE flight operations to provide guidance in response to unforeseen obstacles. The four maneuvers chosen for automatically controlled evasive action, each involving primarily one of the four independent axes of the rotorcraft, were (a) the lateral sidestep, (b) the longitudinal acceleration/deceleration maneuver, (c) the bob-up and -down, and (d) the hover turn.

1.3.1 Constained Time-Optimal Lateral Sidestep

The constraining limits on lateral maneuvering are limits on roll attitude, roll rate, and roll angular acceleration. Ideally, therefore, the vehicle response during a constrained time-optimal lateral sidestep would resemble that depicted in Fig. 1.4. Figure 1.5 is a flow chart representation of a realization of a control scheme yielding such a vehicle response.

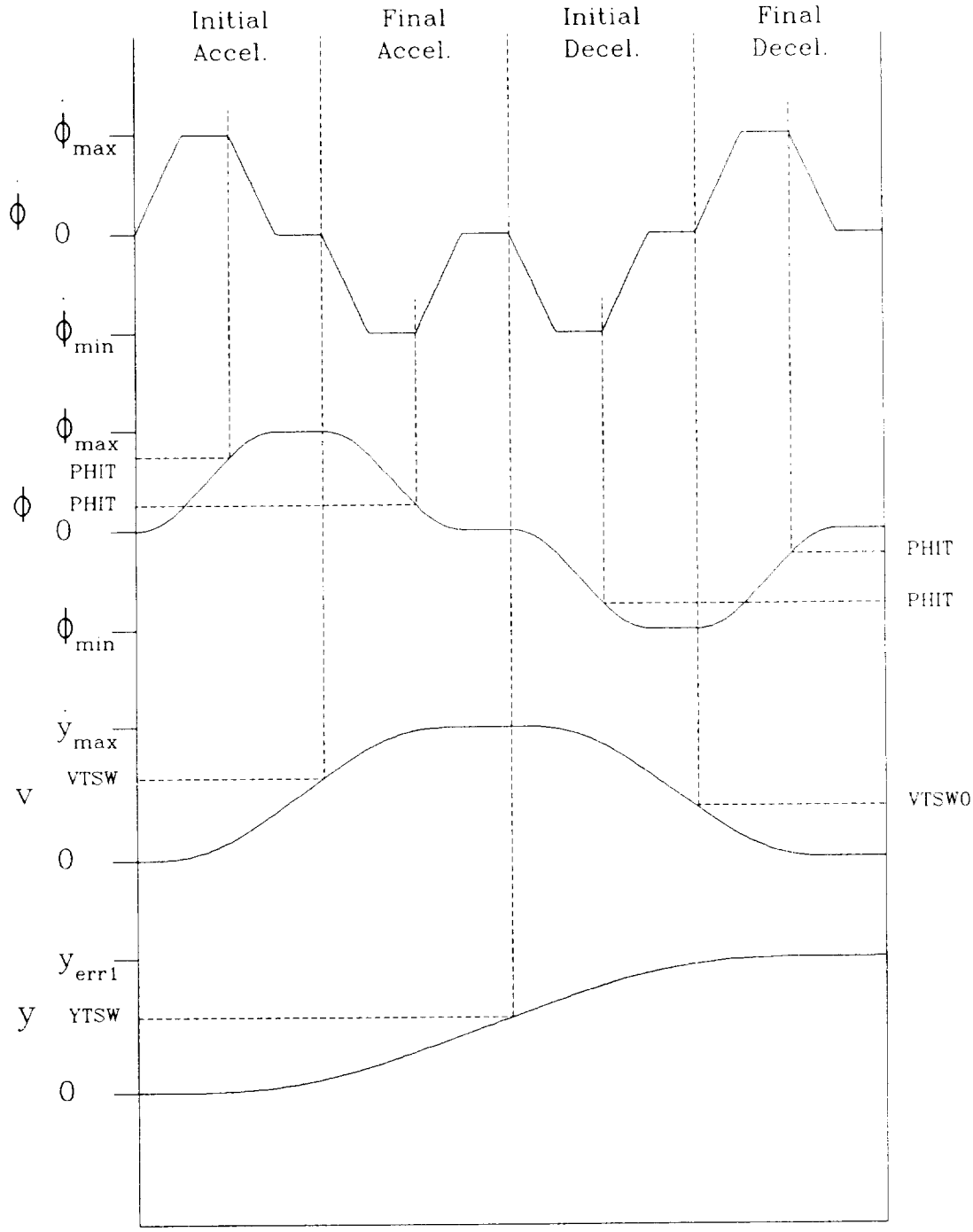

Figure 1.4 Ideal Time History of Constrained Time-Optimal Lateral Sidestep Maneuver

Inputs:	Lateral course offset	
	Vehicle roll attitude and roll rate	ϕ_m, p_m
	Lateral inertial velocity	y_m, v_m
	Lateral offset command	y_{com}
	Previous lateral offset command	y^p_{com}
	Maneuver urgency factor	MUF
Outputs:	Model commands	y_c^{TO}, ϕ_c^{TO}, p_c^{TO}
	Command flags	IPCFG, IPHCFG, IYDCFG
	Lateral time-optimal maneuver flag	IFTOY

a. Inputs and Outputs

Figure 1.5 Flow Diagram for Lateral Constrained Time-Optimal Maneuvers

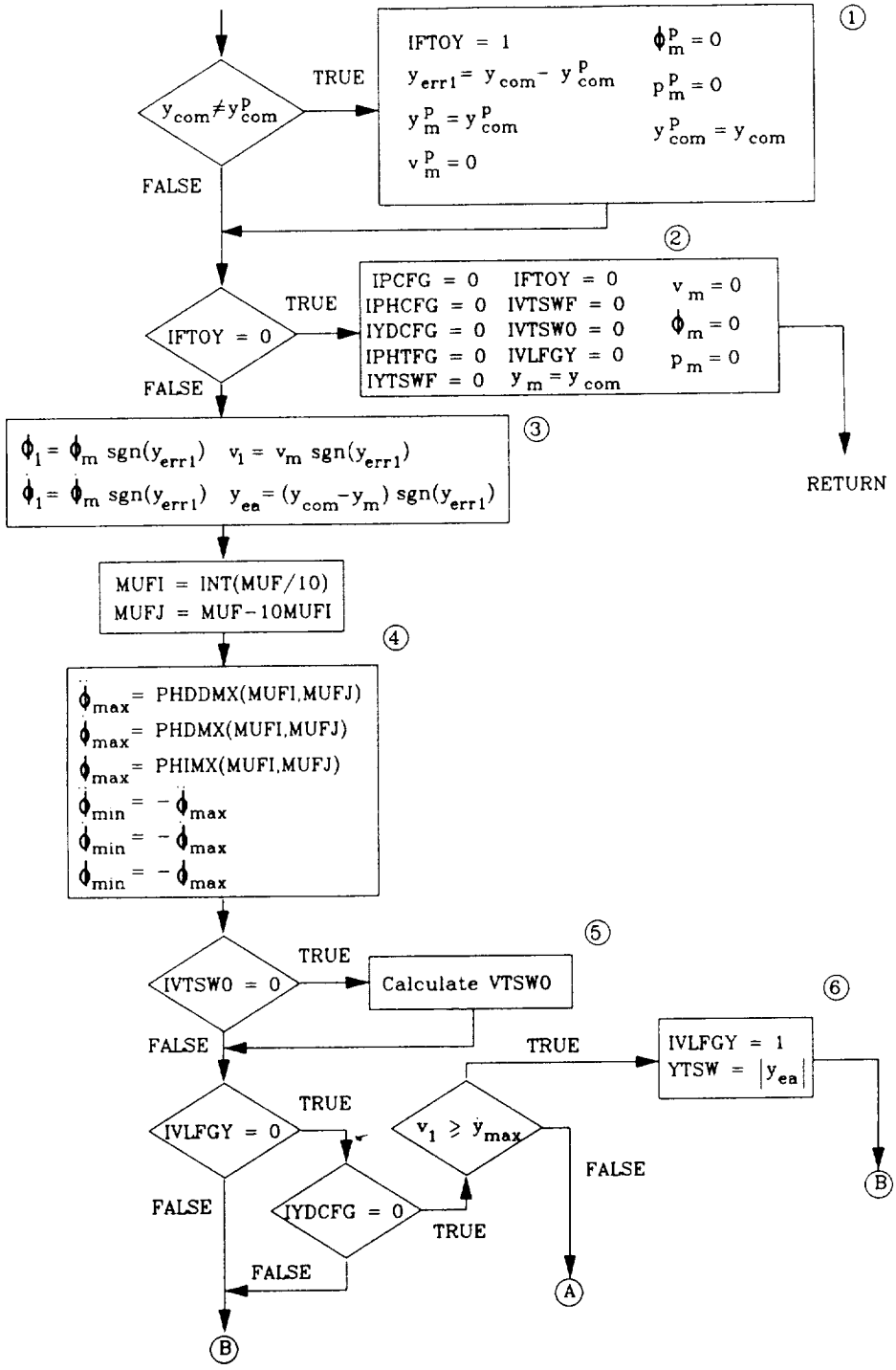

b. Calculation of Switching Criteria

Figure 1.5 (Continued)

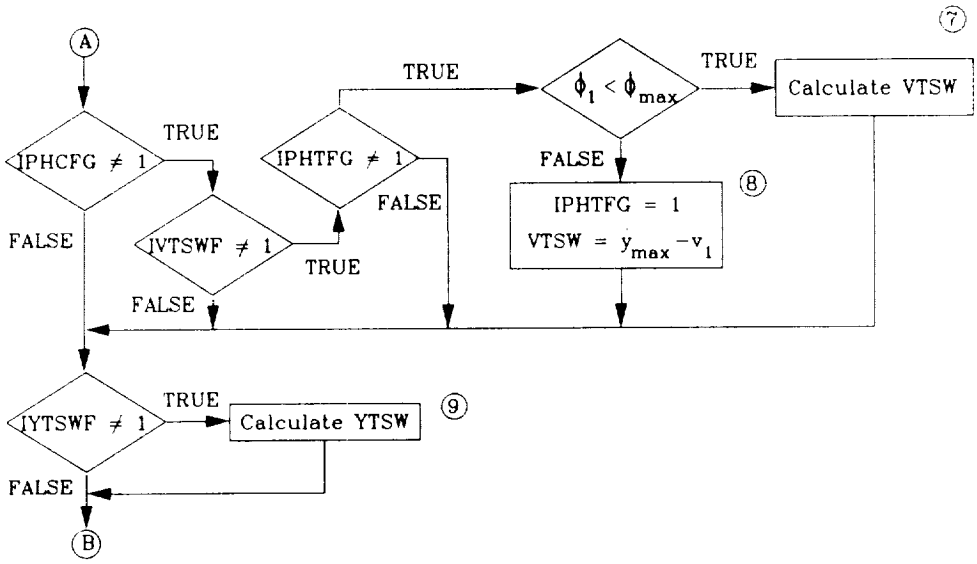

b. (Concluded)

Figure 1.5 (Continued)

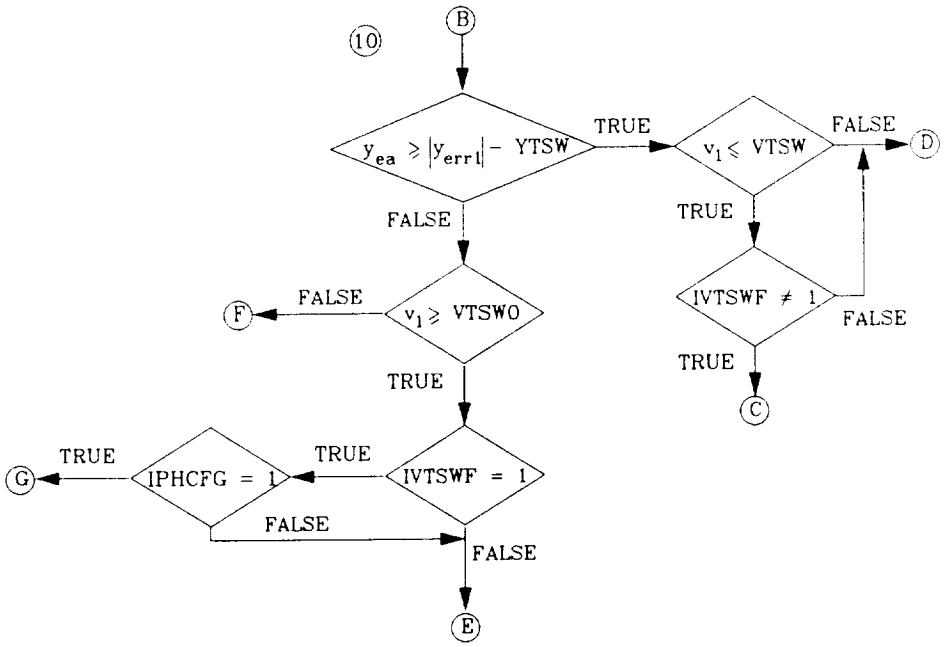

c. Selection of Appropriate Response Phase

Figure 1.5 (Continued)

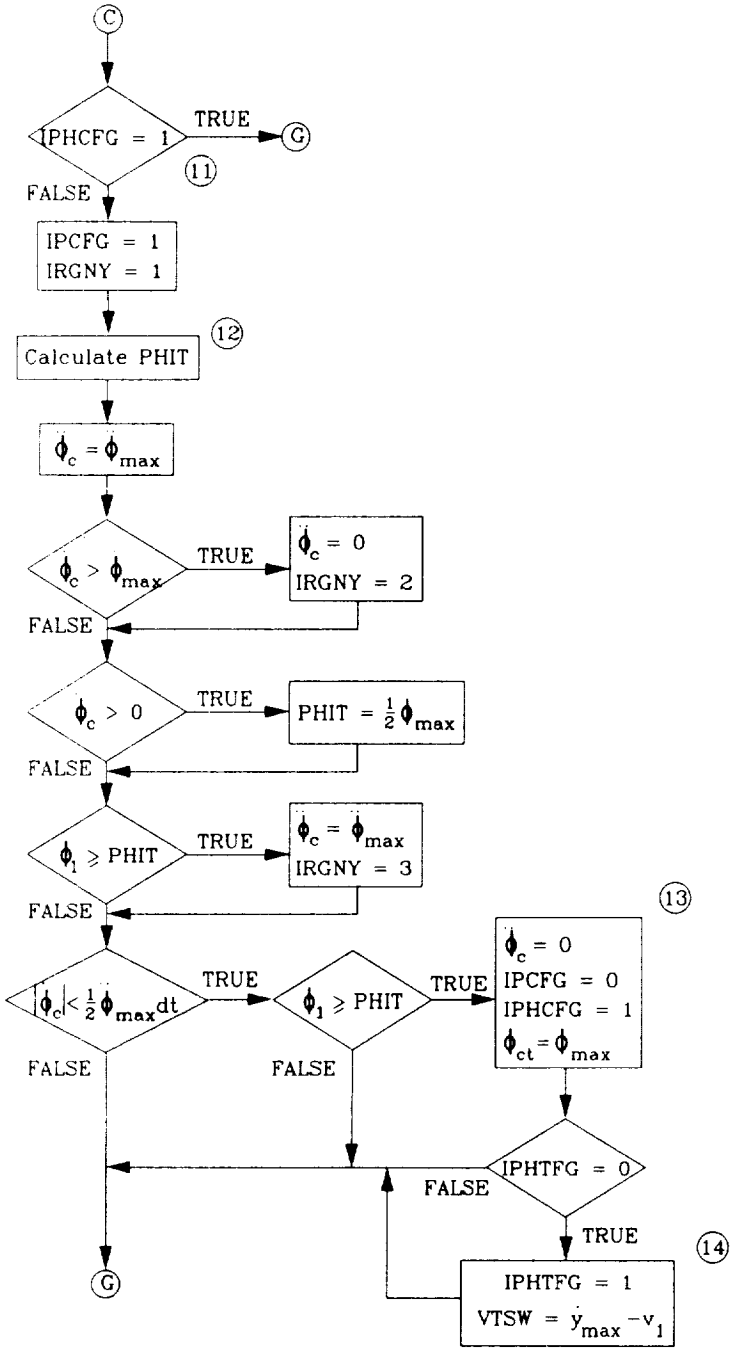

d. Initial Acceleration Phase

Figure 1.5 (Continued)

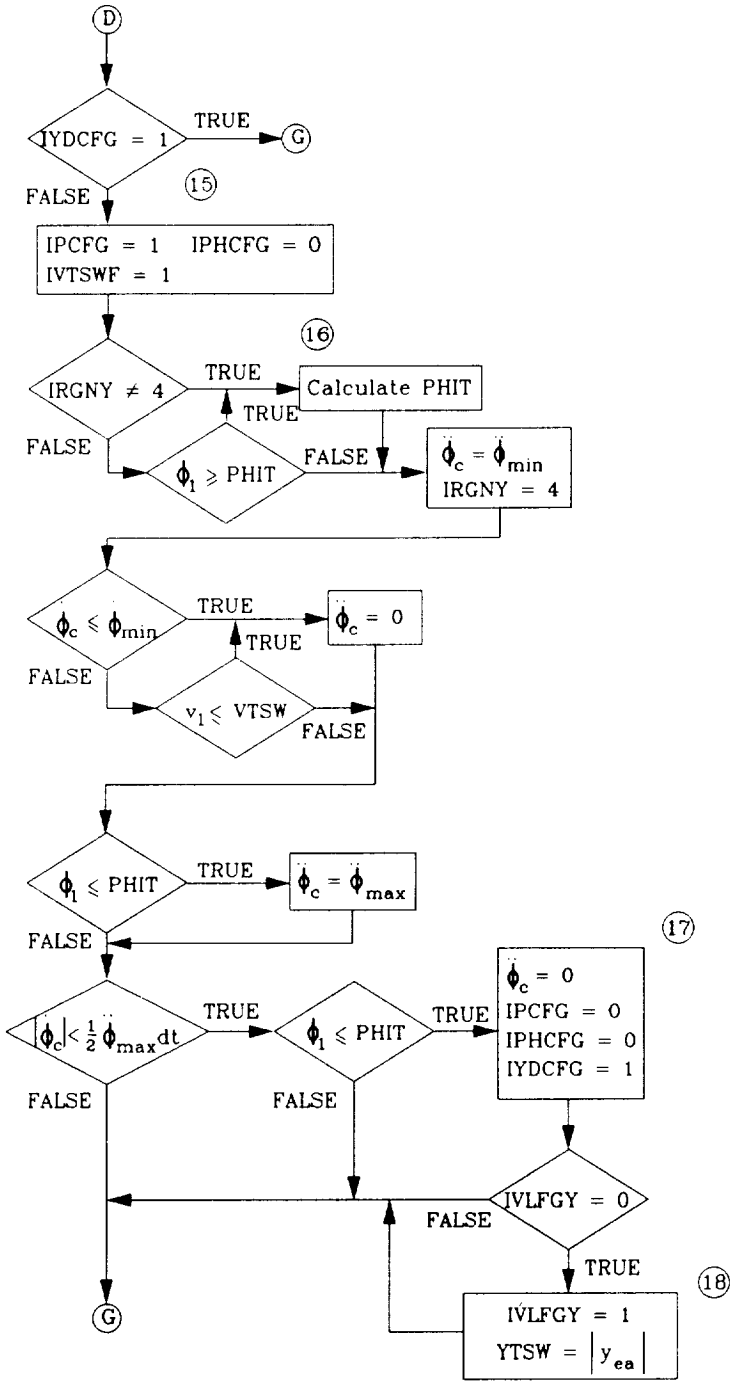

e. Final Acceleration Phase

Figure 1.5 (Continued)

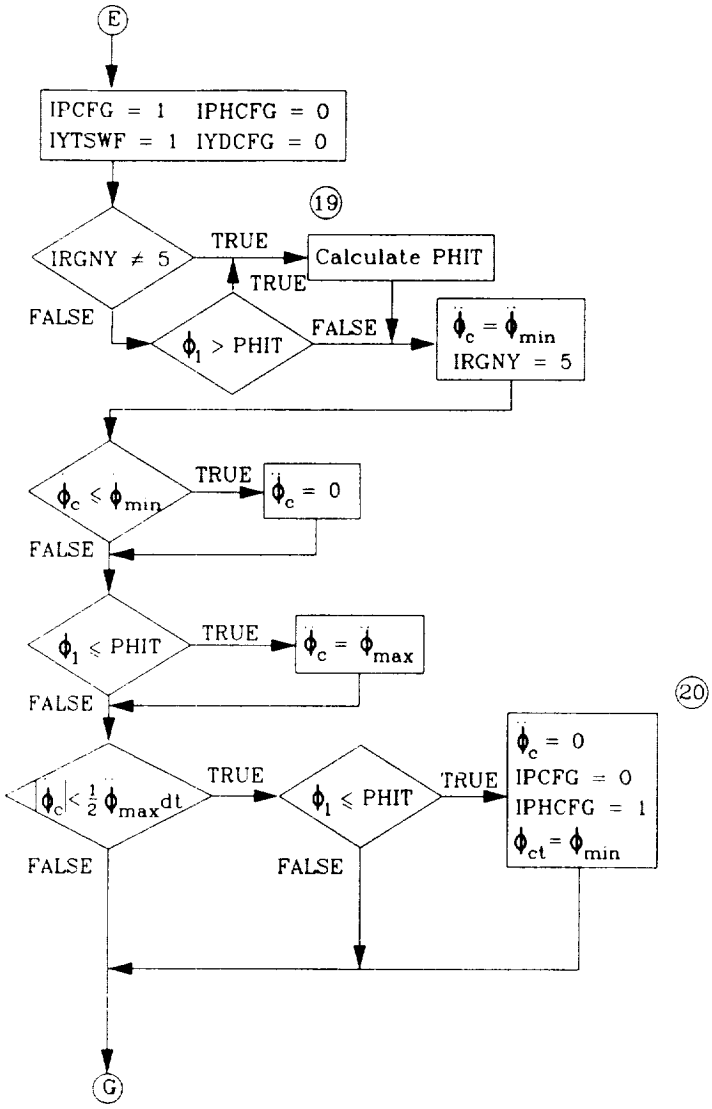

f. Initial Deceleration Phase

Figure 1.5 (Continued)

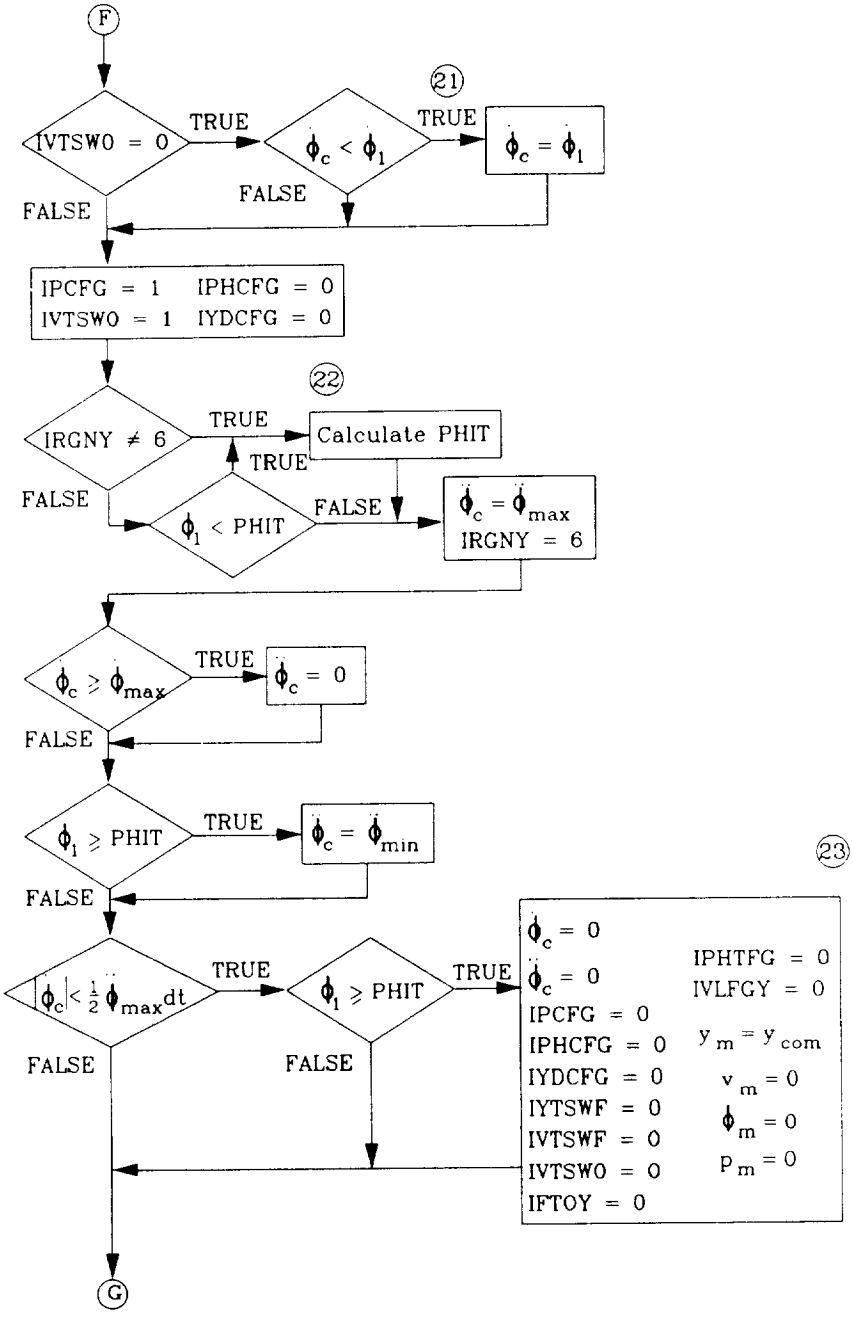

g. Final Deceleration Phase

Figure 1.5 (Continued)

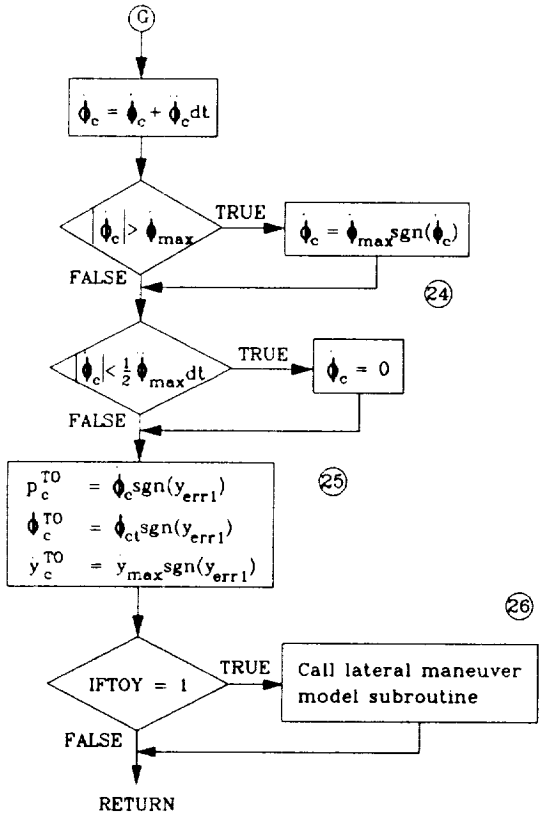

h. Calculation of Constrained Time-Optimal Commands

Figure 1.5 (Continued)

i. Notes (corresponding to circled numbers throughout figure)

1. If the current lateral offset command is not equal to the previous value, a lateral offset command has been issued. The initial error resulting from this command is calculated (y_{err_I}), and the "past" model states are initialized in preparation for the constrained time-optimal maneuver. Also at this time, the lateral time-optimal maneuver flag is set to 1.

2. If IFTOY = 0, the intermediate control flags are reinitialized to 0.

3. The model roll attitude, roll rate, lateral inertial velocity, and lateral offset are normalized with respect to the sign of the initial error. This allows the same logic to be employed for both left and right sidesteps.

4. The roll acceleration, rate, and attitude limits are determined based on the maneuver urgency factor (see Table 1.4 for values).

5. The velocity switching criterion that initiates the final deceleration phase of the maneuver, VTSW0, is calculated as follows:

$$VTSW0 = g\left[-\frac{\dot{\phi}_I^3}{3\ddot{\phi}_{max}^2} + \frac{\dot{\phi}_{max}\dot{\phi}_I^2}{4\ddot{\phi}_{max}^2} - \frac{\dot{\phi}_{max}\phi_I}{2\ddot{\phi}_{max}} + \frac{\dot{\phi}_I\phi_I}{\ddot{\phi}_{max}} - \frac{\phi_I|\phi_I|}{2\dot{\phi}_{max}} - \frac{\dot{\phi}_I^2\phi_I}{2\dot{\phi}_{max}\ddot{\phi}_{max}} + \frac{\dot{\phi}_I^4}{8\dot{\phi}_{max}\ddot{\phi}_{max}^2}\right]$$

It is only calculated until the switch IVTSW0 is set to 1.

6. If the model velocity exceeds the maximum lateral velocity but the velocity switch IVLFGY has not yet been set to 1, the position switching criterion, YTSW, is calculated as the lateral error at the time of reaching the maximum lateral velocity. This could result from an overshoot in the constrained time-optimal velocity response.

7. The velocity switching criterion that initiates the final acceleration phase of the maneuver, VTSW, is calculated as follows:

$$VTSW = \frac{1}{2}\left[\dot{y}_{max} - g\left(\frac{2\dot{\phi}_I^3}{3\ddot{\phi}_{max}^2} + \frac{2\phi_I\dot{\phi}_I}{\ddot{\phi}_{max}}\right)\right]$$

It is only calculated using this expression until the switch IVTSWF is set to 1, the switch IPHTFG is set to 1, or the attitude command flag, IPHCFG, is set to one.

Figure 1.5 (Continued)

i. Notes (Continued)

8. An alternate expression is used to calculate the velocity switching criterion, VTSW, in the event that the model reaches the maximum roll attitude before the attitude command flag, IPHCFG, is set to one and before the velocity switch IVTSWF is set to 1. This could result from an overshoot in the constrained time-optimal roll attitude response. In this case, the velocity switching criterion is calculated as the difference between the current lateral velocity and the maximum allowable lateral velocity at the time the rotorcraft achieves the maximum roll attitude.

9. The calculation of the lateral position switching criterion that initiates the initial deceleration phase varies with the progress through the acceleration phases of the response (see Appendix B). This progress is quantified using the IRGNY counter.

IRGNY = 1: There are two subregions in this first region of the response.

If $\dot{\phi}_c \leq \frac{1}{\sqrt{2}}\dot{\phi}_{max}$, then:

$$YTSW = \frac{1}{2}\left[|y_{err1}| - g\frac{5.577\dot{\phi}_1^4}{\dot{\phi}_{max}^3} \right]$$

else:

$$YTSW = \frac{1}{2}\left[|y_{err1}| - g\left(\frac{2\dot{\phi}_1^6}{3\dot{\phi}_{max}^2\dot{\phi}_{max}^3} + \frac{2\dot{\phi}_1^5}{\dot{\phi}_{max}\dot{\phi}_{max}^3} + \frac{2.0833\dot{\phi}_1^4}{\dot{\phi}_{max}^3} + \frac{\dot{\phi}_1^3\dot{\phi}_{max}}{\dot{\phi}_{max}^3} + \frac{\dot{\phi}_1^2\dot{\phi}_{max}^2}{6\dot{\phi}_{max}^3} \right) \right]$$

IRGNY = 2:

$$YTSW = \frac{1}{2}\left[|y_{err1}| - g\left(\frac{5\dot{\phi}_1^3}{3\dot{\phi}_{max}^2} + \frac{65\dot{\phi}_1^2\dot{\phi}_1}{12\dot{\phi}_{max}^2} + \frac{6\dot{\phi}_1^2}{\dot{\phi}_{max}} + \frac{3\dot{\phi}_{max}^4}{2\dot{\phi}_{max}^3} \right) \right]$$

IRGNY = 3:

$$YTSW = \frac{1}{2}\left[|y_{err1}| - g\left(\frac{2\dot{\phi}_1^3}{3\dot{\phi}_{max}^2} + \frac{\dot{\phi}_1^2}{\dot{\phi}_{max}} + \frac{\dot{\phi}_{max}^2\dot{\phi}_1}{\dot{\phi}_{max}^2} + \frac{2v_1\dot{\phi}_1}{g\dot{\phi}_{max}} + \frac{v_1\dot{\phi}_{max}}{g\dot{\phi}_{max}} \right) \right]$$

Figure 1.5 (Continued)

i. Notes (Continued)

IRGNY = 4:

$$YTSW = \frac{1}{2}\left[|y_{err1}| - g\left(\frac{2\phi_1^3}{3\dot{\phi}_{max}^2} + \frac{2v_1\phi_1}{g\dot{\phi}_{max}} \right) \right]$$

10. This section selects the appropriate phase of the response based on the position and velocity switching criteria.

11. If the roll attitude command flag, IPHCFG, is set to 1, the initial acceleration phase is complete and is awaiting the satisfaction of the velocity or position switching criteria to initiate another phase of the response.

12. The attitude switching criterion, PHIT, is calculated in this phase as follows:

$$PHIT = \phi_{max} - \frac{\dot{\phi}_{max}^2}{2\ddot{\phi}_{max}}$$

except during the initial part of the roll-up, where $\ddot{\phi}_c = \ddot{\phi}_{max}$, in which case:

$$PHIT = \frac{1}{2}\phi_{max}$$

13. At the conclusion of the roll-up to the maximum roll attitude, switch to attitude command.

14. If the attitude command stage is reached prior to IPHTFG being set to 1 (see Note 8), the velocity switching criterion is calculated as the difference between the current lateral velocity and the maximum allowable lateral velocity.

15. If the lateral inertial velocity command flag, IYDCFG, is set to 1, the final acceleration phase is complete and is awaiting the satisfaction of the position switching criterion to initiate the deceleration phase of the response.

Figure 1.5 (Continued)

i. Notes (Continued)

16. The attitude switching criterion, PHIT, is calculated in this phase as follows:

$$PHIT = \frac{\dot{\phi}_1^2}{2\ddot{\phi}_{max}}$$

It is calculated only until the criterion is satisfied.

17. At the conclusion of the roll-back to the steady-state roll attitude for constant maximum lateral velocity, switch to velocity command.

18. If the velocity command stage is reached prior to IVLFGY being set to 1 (see Note 6), the position switching criterion, YTSW, is calculated as the current lateral error.

19. The attitude switching criterion, PHIT, is calculated in this phase as follows:

$$PHIT = \phi_{min} + \frac{\dot{\phi}_1^2}{2\ddot{\phi}_{max}}$$

It is calculated only until the criterion is satisfied.

20. At the conclusion of the roll-up to the minimum roll attitude, switch to attitude command.

21. To help compensate for the lag between the commanded and actual roll rates, the roll rate command is initialized to the minimum of its former value and the actual roll rate.

22. The attitude switching criterion, PHIT, is calculated in this phase as follows:

$$PHIT = -\frac{\dot{\phi}_1^2}{2\ddot{\phi}_{max}}$$

It is calculated only until the criterion is satisfied.

Figure 1.5 (Continued)

i. Notes (Concluded)

23. At the conclusion of the roll-back to zero roll attitude, exit the time-optimal control, and reinitialize necessary flags and switches.

24. Limit the roll rate command, and provide a buffer about zero where the roll rate command is identically equal to zero.

25. Calculate the constrained time-optimal commands.

26. If a lateral evasive maneuver is in progress, call the model subroutine to update the model states for the next pass.

Figure 1.5 (Concluded)

TABLE 1.4

PARAMETER VALUES FOR THE CONSTRAINED TIME-OPTIMAL LATERAL MANEUVERING CONTROL LOGIC

y_{errt}	Lateral offset error threshold	15 ft
PHDDMX	Roll acceleration limits associated with the two digits of the maneuver urgency factor	

$$PHDDMX(MUFI,MUFJ) = \begin{bmatrix} 10 & 15 & 20 & 30 \\ 20 & 25 & 40 & 50 \\ 30 & 40 & 50 & 50 \end{bmatrix} \quad deg/sec^2$$

PHDMX Roll rate limits

$$PHDMX(MUFI,MUFJ) = \begin{bmatrix} 5 & 7.5 & 10 & 15 \\ 10 & 15 & 20 & 25 \\ 15 & 20 & 30 & 30 \end{bmatrix} \quad deg/sec$$

PHIMX Roll attitude limits

$$PHIMX(MUFI,MUFJ) = \begin{bmatrix} 10 & 10 & 10 & 15 \\ 10 & 15 & 20 & 25 \\ 15 & 20 & 30 & 30 \end{bmatrix} \quad deg$$

$\dot{y}_{max}$	Lateral velocity limit	50.667 ft/sec (30 kt)
Y_v	Sway damping stability derivative	-0.12 1/sec

1.3.2 Constained Time-Optimal Speed Change Maneuver

The constraining limits on longitudinal maneuvering are on pitch attitude, pitch rate, and pitch angular acceleration. Ideally, the vehicle response during a constrained time-optimal longitudinal speed change would resemble that depicted in Fig. 1.6. Figure 1.7 is a flow chart representation of a control scheme yielding such a vehicle response. Constrained time-optimal longitudinal speed change maneuvers will be used to perform the forward speed changes necessitated by commands from the obstacle detection and avoidance maneuver selection logic or from the waypoint sequencing logic.

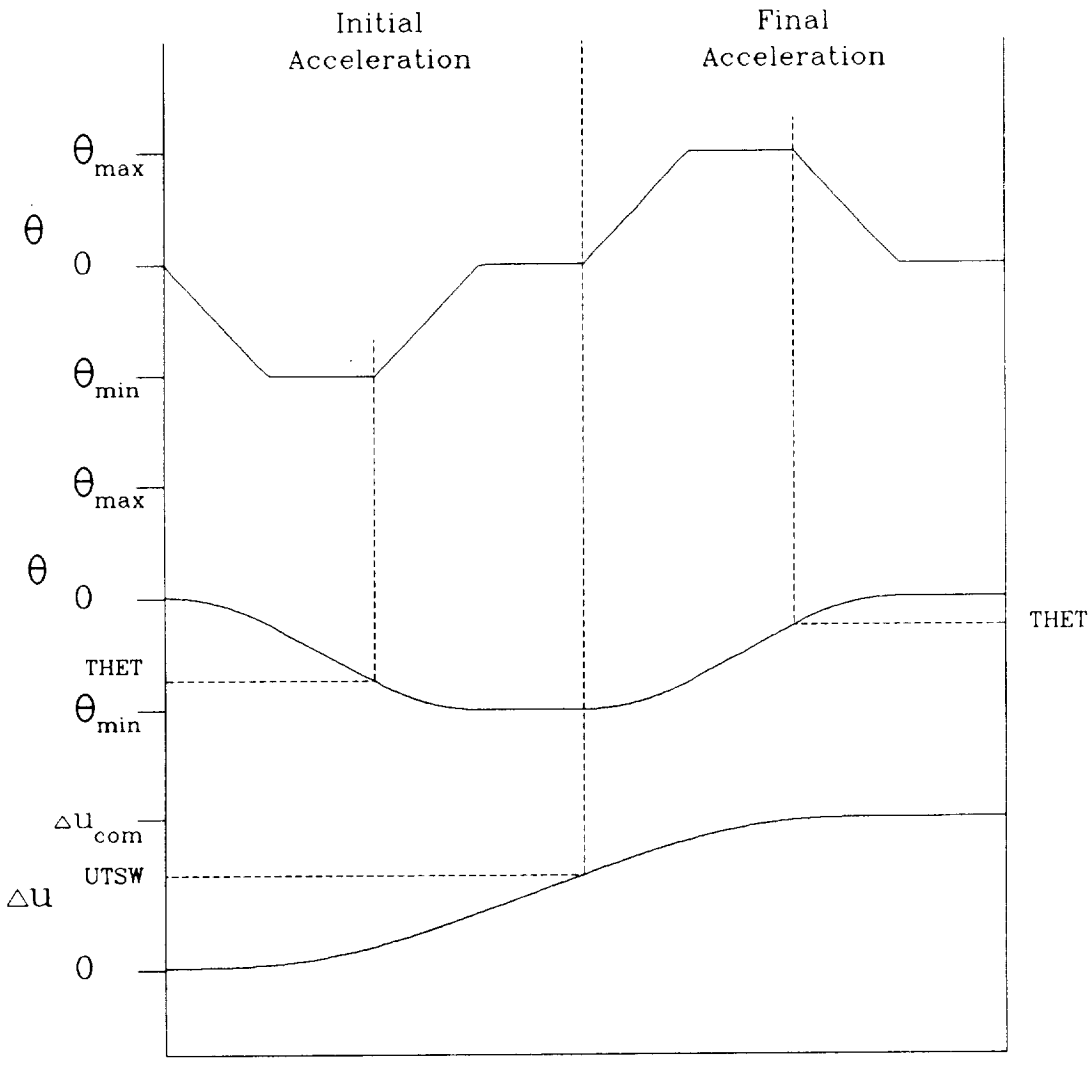

Figure 1.6 Ideal Time History of Constrained Time-Optimal Longitudinal Speed Change Maneuver

Inputs:	Longitudinal along-course velocity command	
	from waypoint sequencing	u_{tw}
	from obstacle detection logic	$V_{x\,com}$
	Previous along-course velocity command	u_{ref}^{p}
	Model pitch attitude and pitch rate	θ_m, q_m
	Longitudinal model velocity	u_m
	Along-course distance from next waypoint	x_{cs}
	Waypoint course parameters	x_{sl}, x_{lE}, and x_{ant}
	Nominal velocity resumption flag	IRESUM
Outputs:	Longitudinal inertial velocity command	u_{ref}
	Command flags	IQCFG, ITHCFG
	Model commands	q_c^{TO}, θ_c^{TO}
	Longitudinal time-optimal maneuver flag	IFTOX

a. Inputs and Outputs

Figure 1.7 Flow Diagram for Longitudinal Constrained Time-Optimal Maneuvers

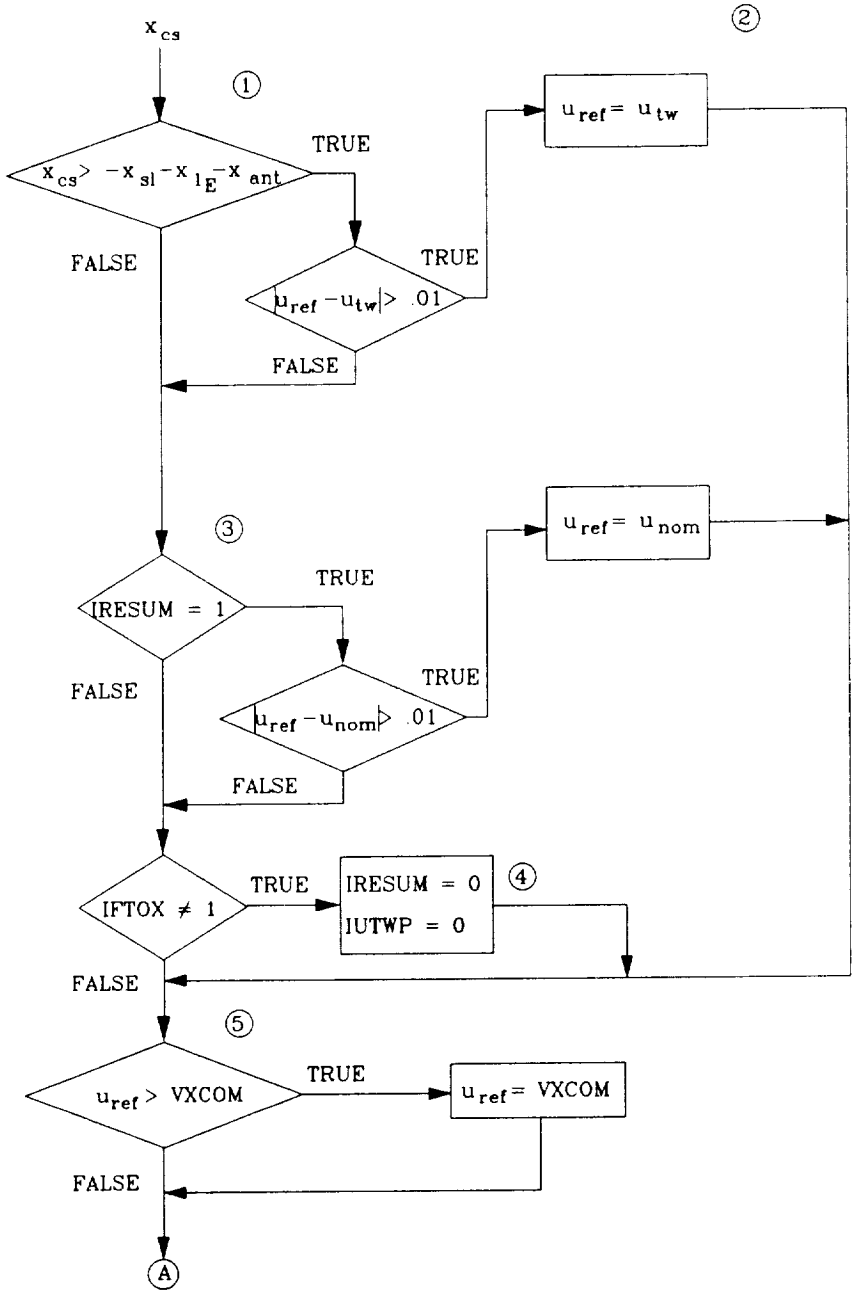

b. Initiation of a Constrained Time-Optimal Speed Change

Figure 1.7 (Continued)

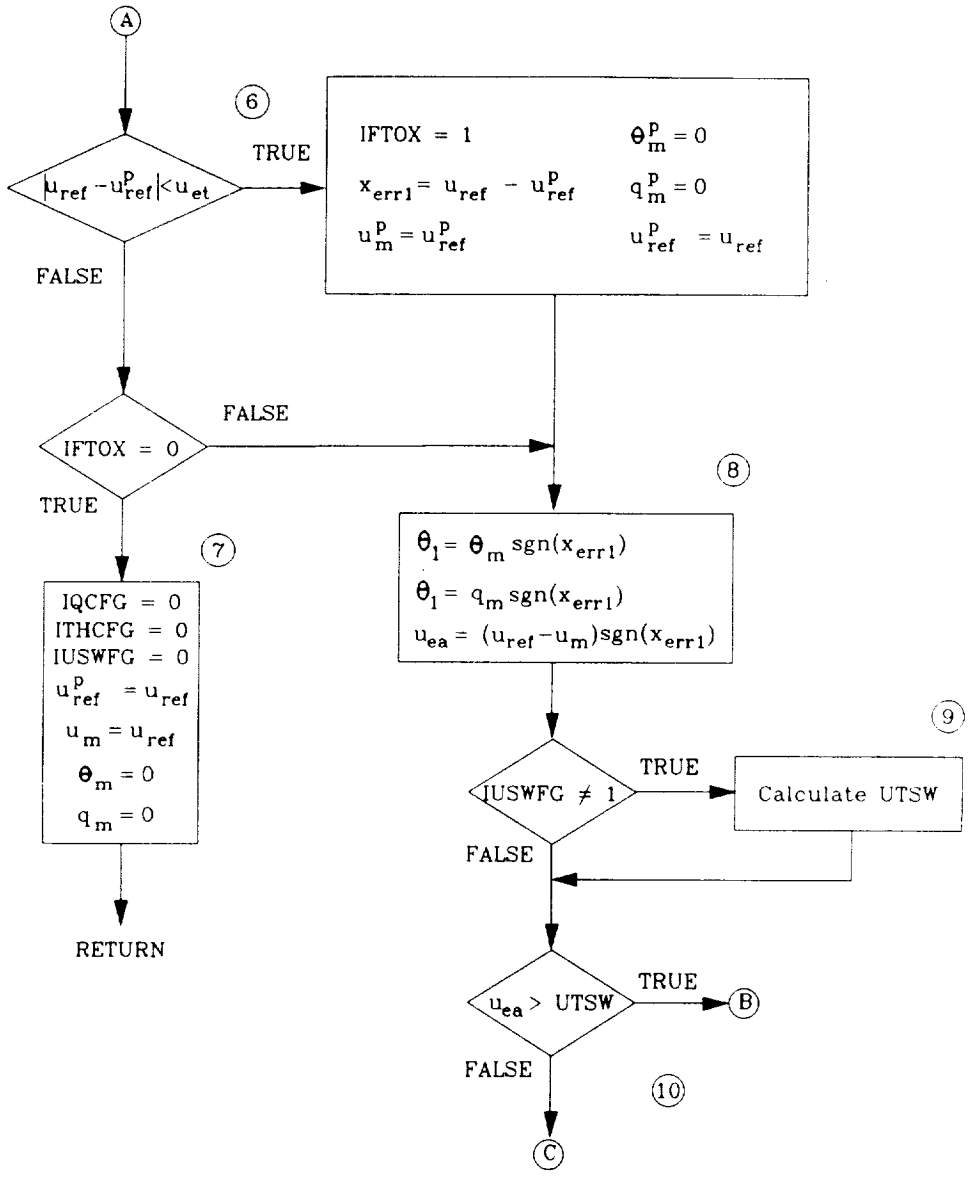

c. Calculation of a Velocity Switching Criterion and Selection of an Appropriate Response Phase

Figure 1.7 (Continued)

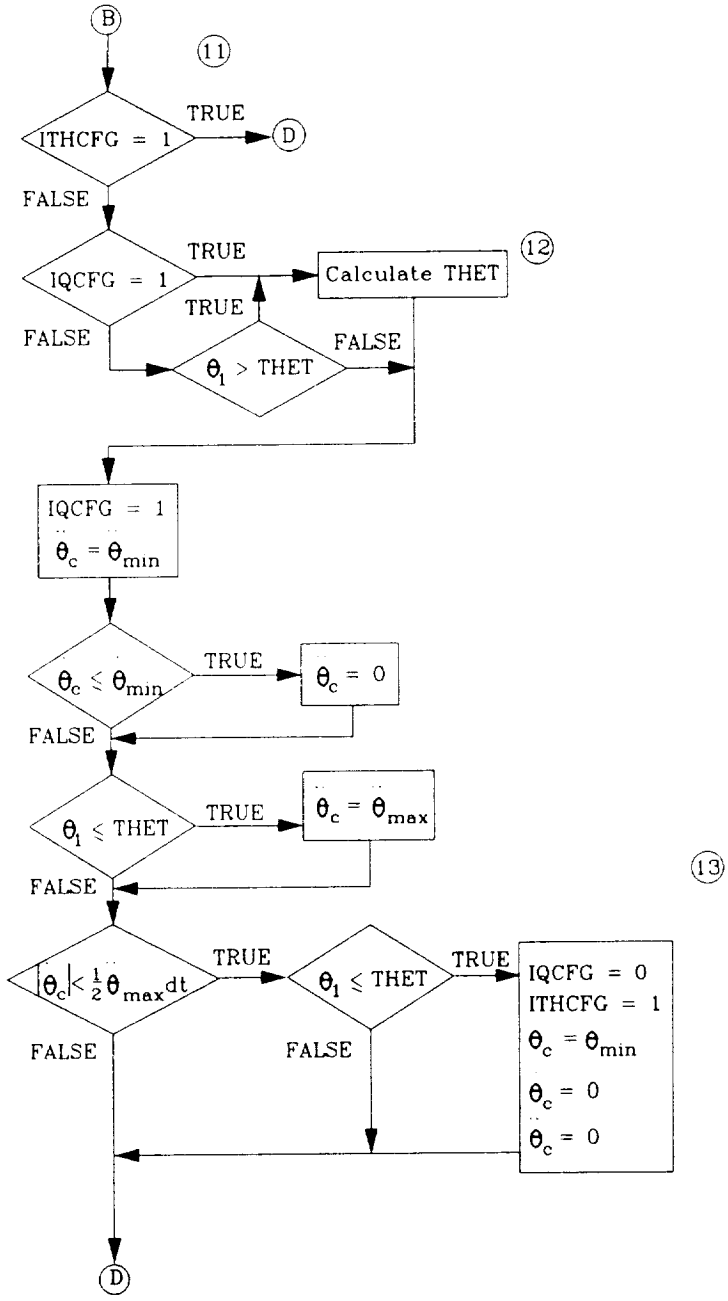

d. Initial Acceleration Phase

Figure 1.7 (Continued)

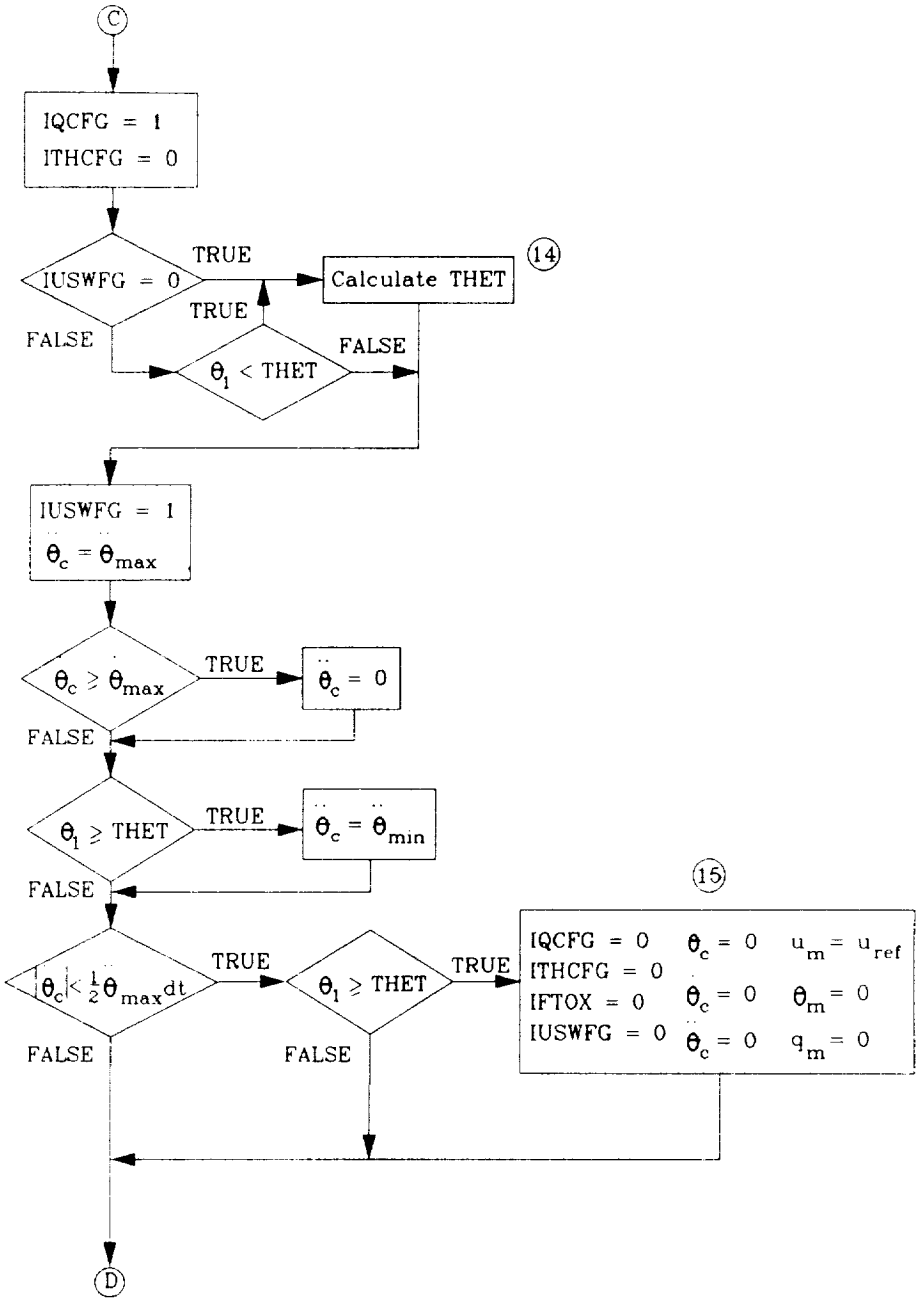

e. Final Acceleration Phase

Figure 1.7 (Continued)

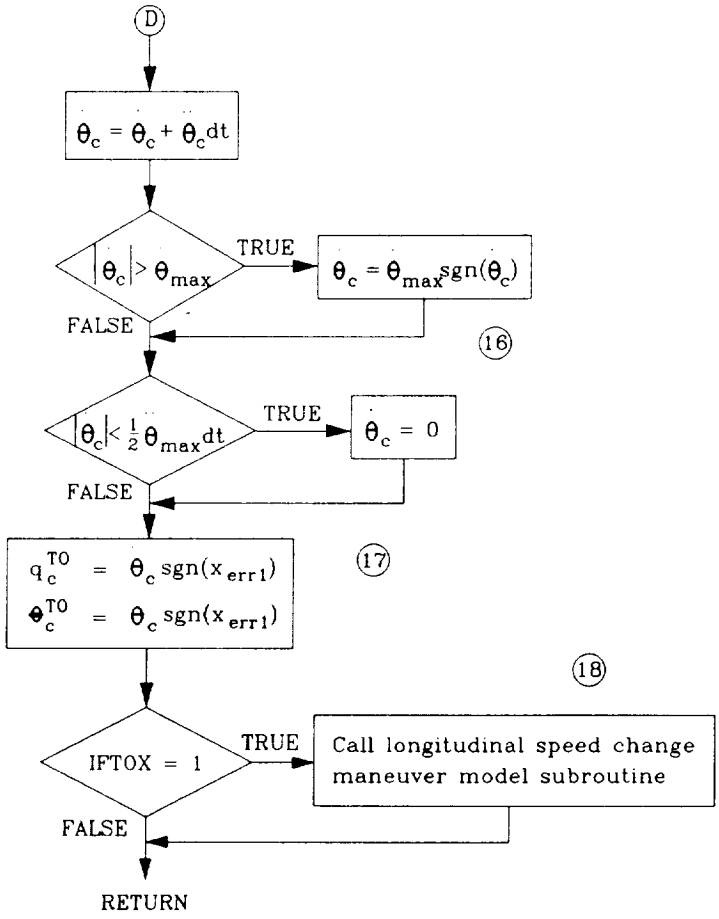

f. Calculation of Constrained Time-Optimal Commands

Figure 1.7 (Continued)

g. Notes (corresponding to circled numbers throughout figure)

1. If the distance to the "to" waypoint, $-x_{cs}$, is less than the anticipative distance to the transition speed change and the transition speed is other than the current velocity command, initiate the transition speed change.

2. Set the along-course velocity command to the necessary value, and set the obstacle avoidance velocity command, VXCOM, to the minimum of the value from the obstacle detection and avoidance maneuver selection logic and this new along-course velocity command.

3. If the post-transition IRESUM flag is equal to 1 and the current velocity command is not equal to the nominal course velocity command, initiate a speed change back to the nominal velocity.

4. Upon completion of a constrained time-optimal speed change (IFTOX set back to 0), reset IRESUM and IUTWP to 0.

5. If the obstacle avoidance velocity command from the obstacle detection and avoidance maneuver selection logic, VXCOM, is less than the current velocity command, then initiate a speed change to VXCOM.

6. If the difference between the current and past along-course velocity commands is greater than a threshold value, then a speed change command has been issued. The initial velocity error is calculated (x_{err1}), and the "past" model states are initialized in preparation for the constrained time-optimal maneuver. Also at this time, the longitudinal time-optimal maneuver flag is set to 1.

7. If IFTOX = 0, the intermediate control flags are reinitialized to 0.

8. The model pitch attitude, pitch rate, and longitudinal velocity are normalized with respect to the sign of the initial error. This allows the same logic to be employed for both acceleration and deceleration maneuvers.

Figure 1.7 (Continued)

g. Notes (continued)

9. The velocity switching criterion that initiates the final acceleration phase of the maneuver, UTSW, is calculated using the following five-step procedure.

1)
$$T_{r1} = -\frac{q_1}{\ddot{\theta}_{max}}$$

$$q_{c_{r1}} = \ddot{\theta}_{max}$$

$$q_{0_{r1}} = q_1$$

$$\theta_{0_{r1}} = \theta_1$$

$$UTSW_1 = -g\left(\frac{1}{6}T_{r1}^3 q_{c_{r1}} + \frac{1}{2}T_{r1}^2 q_{0_{r1}} + T_{r1}\theta_{0_{r1}}\right)$$

2)
$$\theta_{0_{r2}} = \frac{1}{2}T_{r1}^2 q_{c_{r1}} + T_{r1} q_{0_{r1}} + \theta_{0_{r1}}$$

$$q'_{mx} = \min\left(\dot{\theta}_{max}, \sqrt{\frac{-\theta_{0_{r2}}}{\ddot{\theta}_{max}}}\right)$$

$$T_{r2} = -\frac{q'_{mx}}{\ddot{\theta}_{max}}$$

$$q_{c_{r2}} = \ddot{\theta}_{max}$$

$$q_{0_{r2}} = 0$$

$$UTSW_2 = -g\left(\frac{1}{6}T_{r2}^3 q_{c_{r2}} + \frac{1}{2}T_{r2}^2 q_{0_{r2}} + T_{r2}\theta_{0_{r2}}\right)$$

3)
$$\theta_{0_{r3}} = \frac{1}{2}T_{r2}^2 q_{c_{r2}} + T_{r2} q_{0_{r2}} + \theta_{0_{r2}}$$

$$\theta_{0_{r4}} = -\frac{q'^2_{mx}}{2\ddot{\theta}_{max}}$$

$$T_{r3} = \frac{\theta_{0_{r4}} - \theta_{0_{r3}}}{\dot{\theta}_{max}}$$

Figure 1.7 (Continued)

g. Notes (continued)

If $T_{r3} > 0$ then

$$\dot{q}_{c_{r3}} = 0$$

$$q_{0_{r3}} = \dot{\theta}_{max}$$

$$UTSW_3 = -g\left(\frac{1}{6}T_{r3}^3\dot{q}_{c_{r3}} + \frac{1}{2}T_{r3}^2 q_{0_{r3}} + T_{r3}\theta_{0_{r3}}\right)$$

else

$$UTSW_3 = 0$$

4)
$$T_{r4} = \frac{q'_{mx}}{\dot{\theta}_{max}}$$

$$\dot{q}_{c_{r4}} = -\dot{\theta}_{max}$$

$$q_{0_{r4}} = q'_{mx}$$

$$UTSW_4 = -g\left(\frac{1}{6}T_{r4}^3\dot{q}_{c_{r4}} + \frac{1}{2}T_{r4}^2 q_{0_{r4}} + T_{r4}\theta_{0_{r4}}\right)$$

5)
$$UTSW = \sum_{i=1}^{4} UTSW_i$$

It is only calculated using this expression until the switch IUSWFG is set to 1.

10. This selects the appropriate phase of the response based on the velocity switching criterion.

11. If the pitch attitude command flag, ITHCFG, is set to 1, the initial acceleration phase is complete and is awaiting the satisfaction of the velocity switching criterion to initiate the final acceleration phase of the response.

Figure 1.7 (Continued)

g. Notes (concluded)

12. The attitude switching criterion, THSWT, is calculated in this phase by the following expression:

$$THSWT = -\theta_{max} + \frac{q_1^2}{2\ddot{\theta}_{max}}$$

It is only calculated until the attitude switching criterion is satisfied.

13. At the conclusion of the roll-up to the minimum pitch attitude, switch to attitude command.

14. The attitude switching criterion, THSWT, is calculated in this phase by the following expression:

$$THSWT = -\frac{q_1^2}{2\ddot{\theta}_{max}}$$

It is only calculated until the attitude switching criterion is satisfied.

15. At the conclusion of the pitch-back to the steady-state pitch attitude for the new velocity command, exit the time-optimal control, and reinitialize the necessary flags and switches.

16. Limit the pitch rate command and provide a buffer about zero, where pitch rate command is identically equal to zero.

17. Calculate the constrained time-optimal commands.

18. If a speed change maneuver is in progress, call the model subroutine to update the model states for the next pass.

Figure 1.7 (Concluded)

TABLE 1.5

PARAMETER VALUES FOR THE CONSTRAINED TIME-OPTIMAL LONGITUDINAL MANEUVERING CONTROL LOGIC

u_{et}	Longitudinal velocity error threshold	6.756 ft/sec (4 kt)
$\dot{\theta}_{max}$, $-\dot{\theta}_{min}$	Pitch angular acceleration limit	40 deg/sec^2
θ_{max}, $-\theta_{min}$	Pitch rate limit	20 deg/sec
θ_{max}, $-\theta_{min}$	Pitch attitude limit	20 deg

1.3.3 Constained Time-Optimal Bob-Up/Down Maneuver

The constraining limits on vertical maneuvering are vertical velocity, vertical acceleration, and vertical acceleration rate. Figure 1.8. presents the constrained time-optimal velocity command profile. This command signal is realized through the same control strategy as that for the pursuit guidance feedforward control. As with the previous constrained time-optimal maneuvers, the objective is to force the rotorcraft response to the limits of acceptable performance. Figure 1.9 is a flow chart representation of the control scheme yielding such a vehicle response.

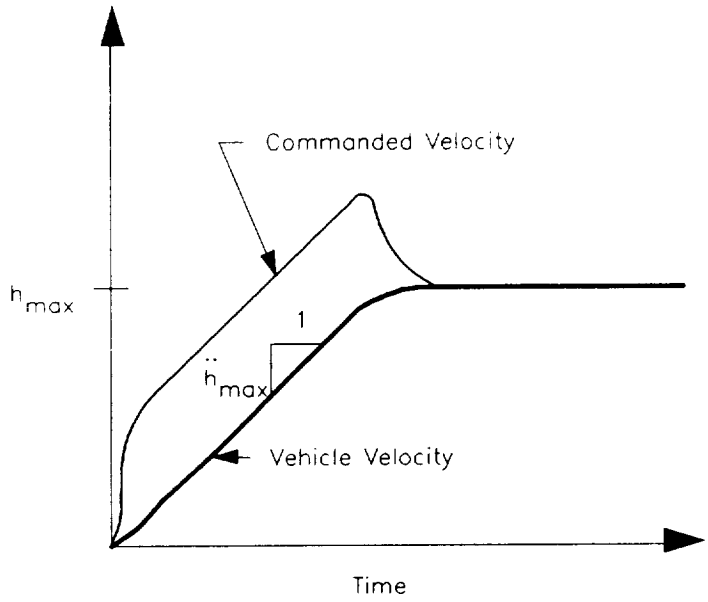

Figure 1.8 Constrained Time-Optimal Vertical Velocity Profile

Inputs:	Previous and current altitude offset commands	h^{p}_{com}, h_{com}
	Vertical model states	$\dot{h}_m$, $\ddot{h}_m$, h_m
Outputs:	Command flags	IAZCFG, IHDCFG
	Model commands	$\ddot{h}^{TO}_c$, h^{TO}_c
	Vertical time-optimal maneuver flag	IFTOH

a. Inputs and Outputs

Figure 1.9 Flow Diagram for Constrained Time-Optimal Vertical Maneuvers

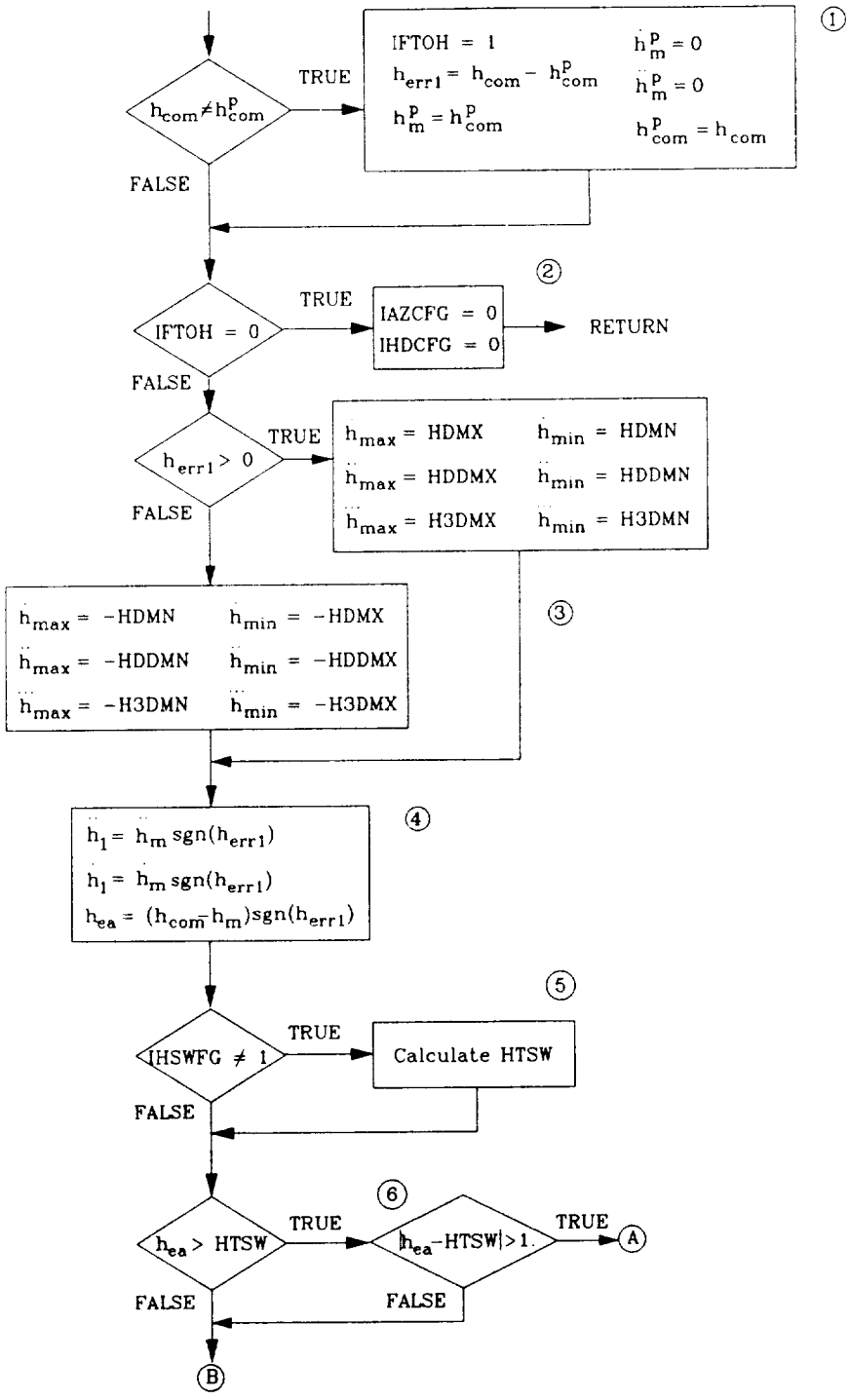

b. Calculation of Vertical Velocity Switching Criteria and Selection of Appropriate Response

Figure 1.9 (Continued)

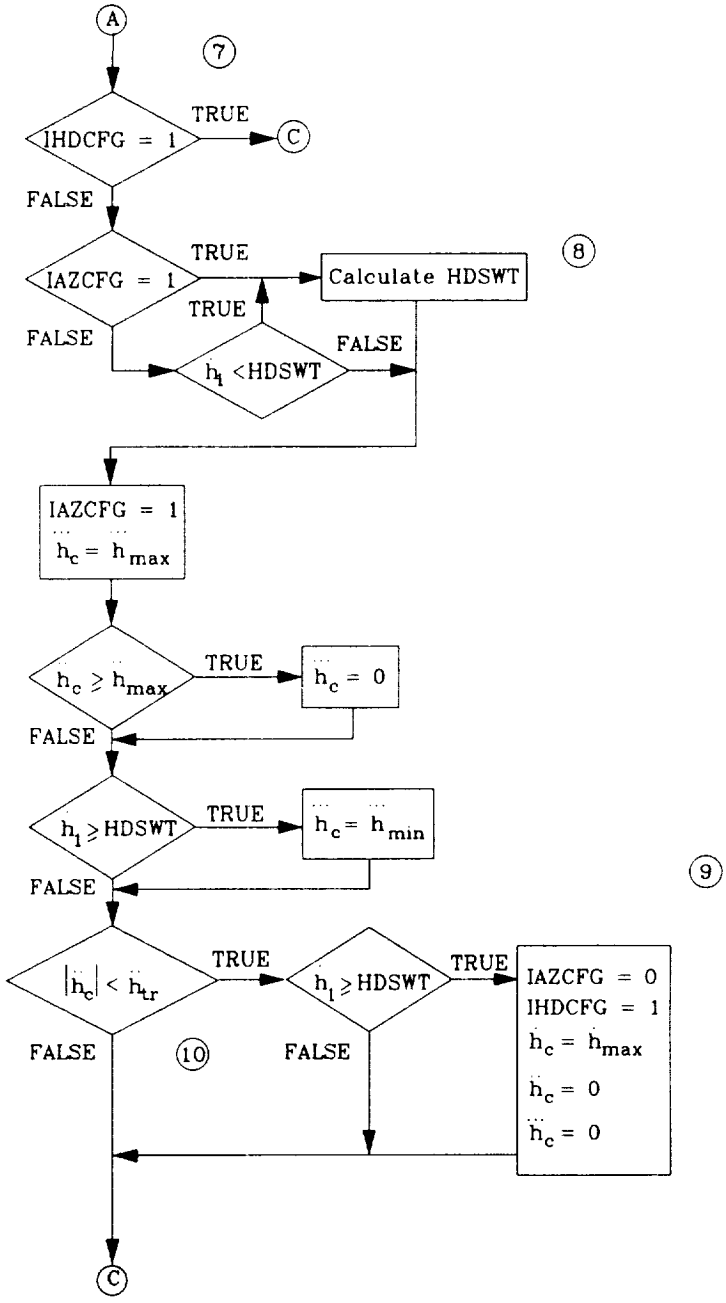

c. Initial Phase - Vertical Acceleration

Figure 1.9 (Continued)

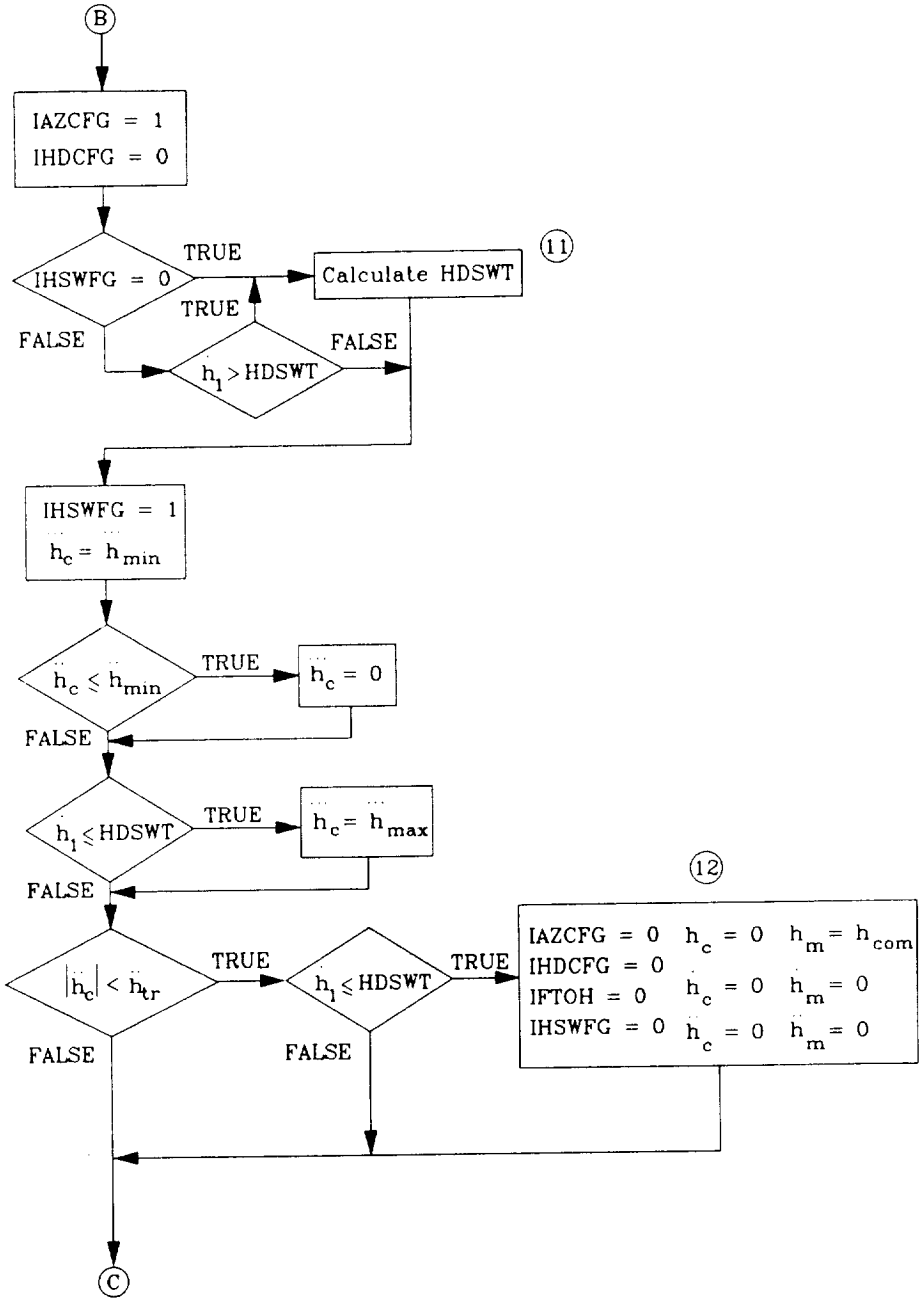

d. Final Phase - Vertical Deceleration

Figure 1.9 (Continued)

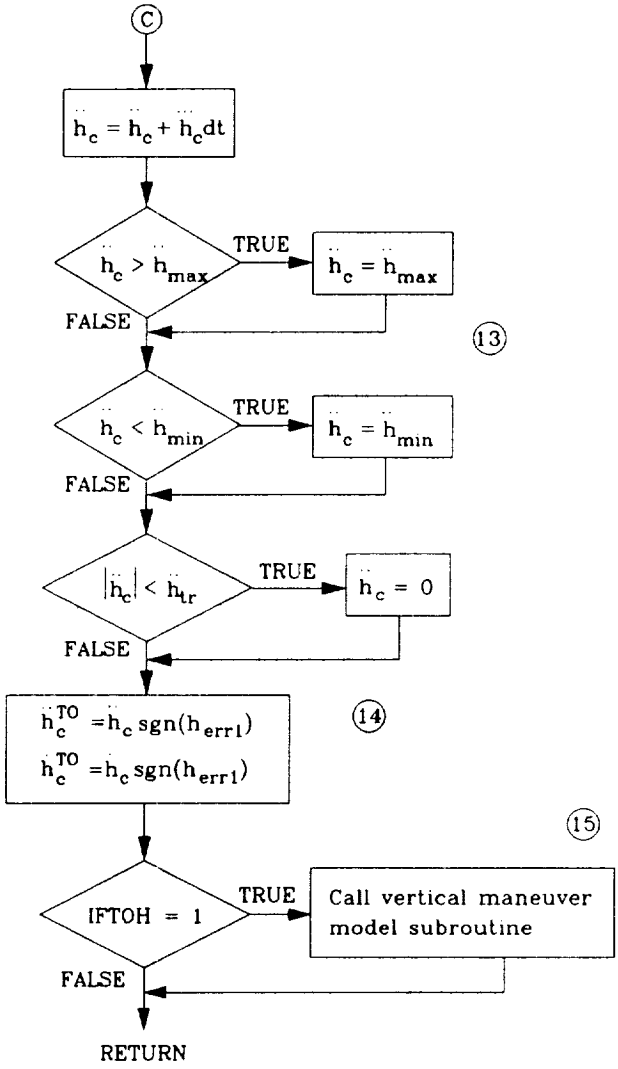

e. Calculation of Constrained Time-Optimal Vertical Velocity Command

Figure 1.9 (Continued)

f. Notes (corresponding to circled numbers throughout figure)

1. If the current altitude offset command is not equal to the past command, a vertical offset command has been issued. The initial altitude error is calculated (h_{err1}), and the "past" model states are initialized in preparation for the constrained time-optimal maneuver. Also at this time, the vertical time-optimal maneuver flag is set to 1.

2. If IFTOH = 0, the control flags are reinitialized to 0.

3. The vertical state limits are set, based on the sign of the initial altitude error. This is due to the fact that the positive and negative limits are not necessarily the same.

4. The model vertical acceleration, velocity, and position offset are normalized with respect to the sign of the initial error. This allows the same logic to be employed for both bob-up and -down maneuvers.

5. The altitude offset switching criterion that initiates the deceleration phase of the maneuver, HTSW, is calculated using the following five-step procedure.

1)
$$T_{r1} = -\frac{\dddot{h}_1}{\dddot{h}_{min}}$$

$$\dddot{h}_{cr1} = \dddot{h}_{min}$$

$$\ddot{h}_{0r1} = \ddot{h}_1$$

$$\dot{h}_{0r1} = \dot{h}_1$$

$$HTSW_1 = \frac{1}{6}T_{r1}^3\dddot{h}_{cr1} + \frac{1}{2}T_{r1}^2\ddot{h}_{0r1} + T_{r1}\dot{h}_{0r1}$$

2)
$$\dot{h}_{0r2} = \frac{1}{2}T_{r1}^2\dddot{h}_{cr1} + T_{r1}\ddot{h}_{0r1} + \dot{h}_{0r1}$$

$$\ddot{h}'_{mn} = \max\left(\ddot{h}_{min}, -\sqrt{\frac{2\dot{h}_{0r2}}{\frac{1}{\dddot{h}_{max}} - \frac{1}{\dddot{h}_{min}}}}\right)$$

Figure 1.9 (Continued)

f. Notes (Continued)

$$T_{r2} = \frac{\ddot{h}'_{mn}}{\ddot{h}_{min}}$$

$$\ddot{h}_{cr2} = \ddot{h}_{min}$$

$$\ddot{h}_{0r2} = 0$$

$$HTSW_2 = \frac{1}{6}T_{r2}^3\ddot{h}_{cr2} + \frac{1}{2}T_{r2}^2\ddot{h}_{0r2} + T_{r2}\dot{h}_{0r2}$$

3)

$$\dot{h}_{0r3} = \frac{1}{2}T_{r2}^2\ddot{h}_{cr2} + T_{r2}\dot{h}_{0r2} + \dot{h}_{0r2}$$

$$\dot{h}_{0r4} = \frac{\dot{h}'^2_{mn}}{2\ddot{h}_{max}}$$

$$T_{r3} = \frac{\dot{h}_{0r4} - \dot{h}_{0r3}}{\ddot{h}_{min}}$$

If $T_{r3} > 0$ then

$$\ddot{h}_{cr3} = 0$$

$$\ddot{h}_{0r3} = \ddot{h}_{min}$$

$$HTSW_3 = \frac{1}{6}T_{r3}^3\ddot{h}_{cr3} + \frac{1}{2}T_{r3}^2\ddot{h}_{0r3} + T_{r3}\dot{h}_{0r3}$$

else

$$HTSW_3 = 0$$

4)

$$T_{r4} = -\frac{\ddot{h}'_{mn}}{\ddot{h}_{max}}$$

$$\ddot{h}_{cr4} = \ddot{h}_{max}$$

Figure 1.9 (Continued)

f. Notes (Continued)

$$\ddot{h}_{0_{r4}} = \ddot{h}'_{mn}$$

$$HTSW_4 = \frac{1}{6}T_{r4}^3 \dddot{h}_{c_{r4}} + \frac{1}{2}T_{r4}^2 \ddot{h}_{0_{r4}} + T_{r4}\dot{h}_{0_{r4}}$$

5) $$HTSW = \sum_{i=1}^{4} HTSW_i$$

It is only calculated using this expression until the switch IHSWFG is set to 1.

6. This selects the appropriate phase of the response based on the vertical offset switching criterion.

7. If the vertical velocity command flag, IHDCFG, is set to 1, the acceleration phase is complete and is awaiting the satisfaction of the vertical offset switching criterion to initiate the deceleration phase of the response.

8. The vertical velocity switching criterion, HDSWT, is calculated in this phase by the following expression:

$$HDSWT = \dot{h}_{max} + \frac{\ddot{h}_1^2}{2\dddot{h}_{min}}$$

It is only calculated until this switching criterion is satisfied.

9. At the conclusion of the acceleration to the maximum vertical velocity, switch to the vertical velocity command.

10. The band about zero defining the vertical acceleration threshold is calculated using the downward jerk limit, as the magnitude of this limit is less than that of the upward jerk limit, thus minimizing the buffer zone.

$$\ddot{h}_{tr} = -\frac{1}{2}H3DMN\,dt$$

Figure 1.9 (Continued)

f. Notes (Concluded)

11. The vertical velocity switching criterion, HDSWT, is calculated in this phase by the following expression:

$$HDSWT = \frac{\ddot{h}_1^2}{2\dddot{h}_{max}}$$

It is only calculated until this switching criterion is satisfied.

12. At the conclusion of the deceleration to zero vertical velocity at the new altitude command, exit the time-optimal control and reinitialize the necessary flags and switches.

13. Limit the vertical acceleration command, and provide a buffer about zero where vertical acceleration command is identically equal to zero.

14. Calculate the constrained time-optimal commands.

15. If a vertical evasive maneuver is in progress, call the model subroutine to update the model states for the next pass.

Figure 1.9 (Concluded)

TABLE 1.6

PARAMETER VALUES FOR THE CONSTRAINED TIME-OPTIMAL VERTICAL MANEUVERING CONTROL LOGIC

H3DMX	Positive vertical acceleration rate limit	20 ft/sec^3
H3DMN	Negative vertical acceleration rate limit	-15 ft/sec^3
HDDMX	Positive vertical acceleration limit	16 ft/sec^2
HDDMN	Negative vertical acceleration limit	-10 ft/sec^2
HDMX	Positive vertical velocity limit	20 ft/sec
HDMN	Negative vertical velocity limit	-15 ft/sec

1.3.4 Constained Time-Optimal Pedal Turn Maneuver

The constraining limits on directional maneuvering are yaw rate and yaw acceleration. The yaw rate command signal is realized via the same control strategy as that for the pursuit feedforward control. As with the previous constrained time-optimal maneuvers, the objective is to force the rotorcraft response to the limits of acceptable performance. Figure 1.10 is a flow chart representation of the control scheme yielding such a vehicle response.

Inputs:	Directional model states	ψ_m, $\dot{\psi}_m$, $\ddot{\psi}_m$
	Previous and current heading command	ψ^P_{com}, $\psi_{c_{auto}}$
Outputs:	Model commands	ψ^{TO}_c, $\dot{\psi}^{TO}_c$
	Directional time-optimal maneuver flag	IFTOPS

a. Inputs and Outputs

Figure 1.10 Flow Diagram for Constrained Time-Optimal Directional Maneuvers

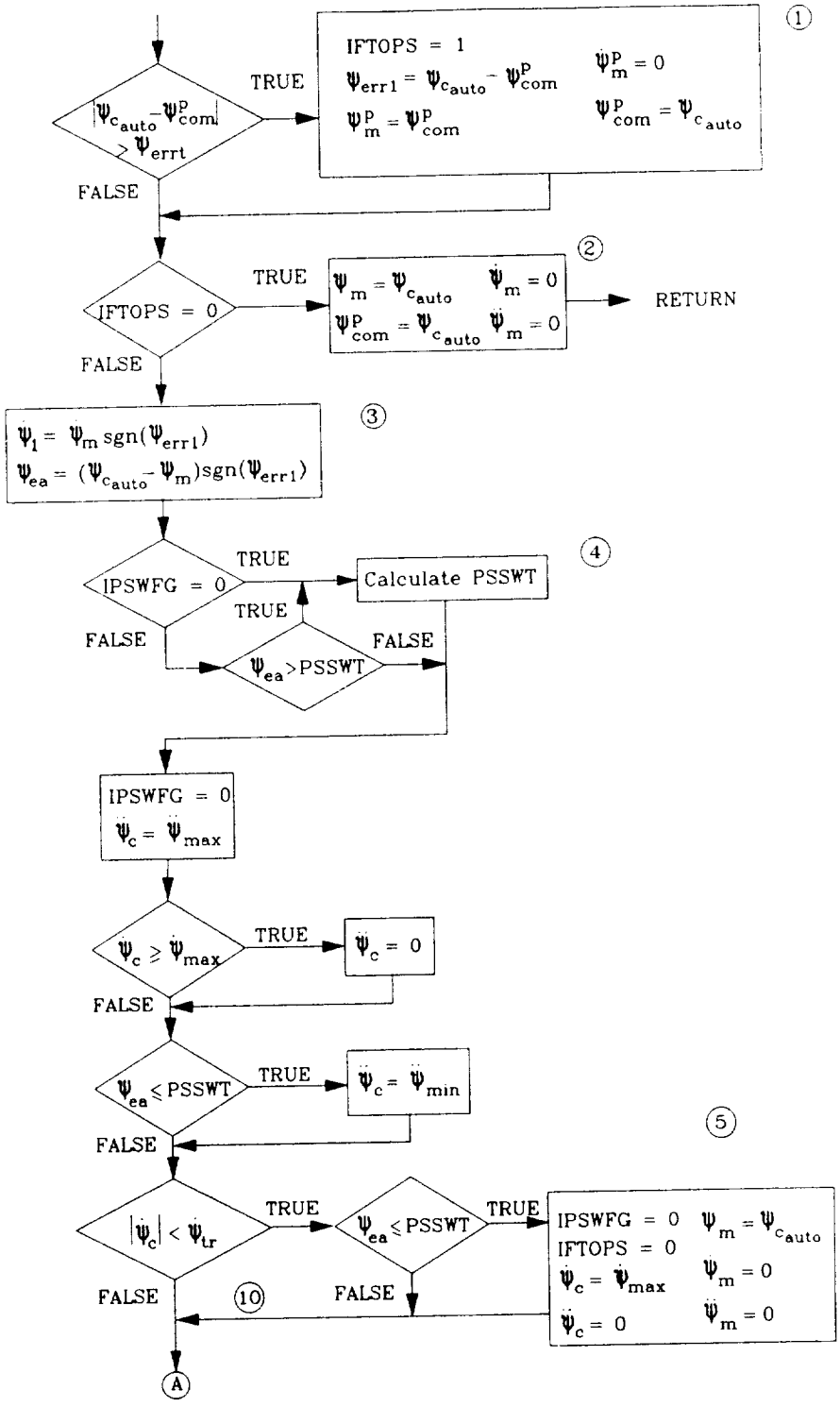

b. Constrained Time-Optimal Pedal Turn

Figure 1.10 (Continued)

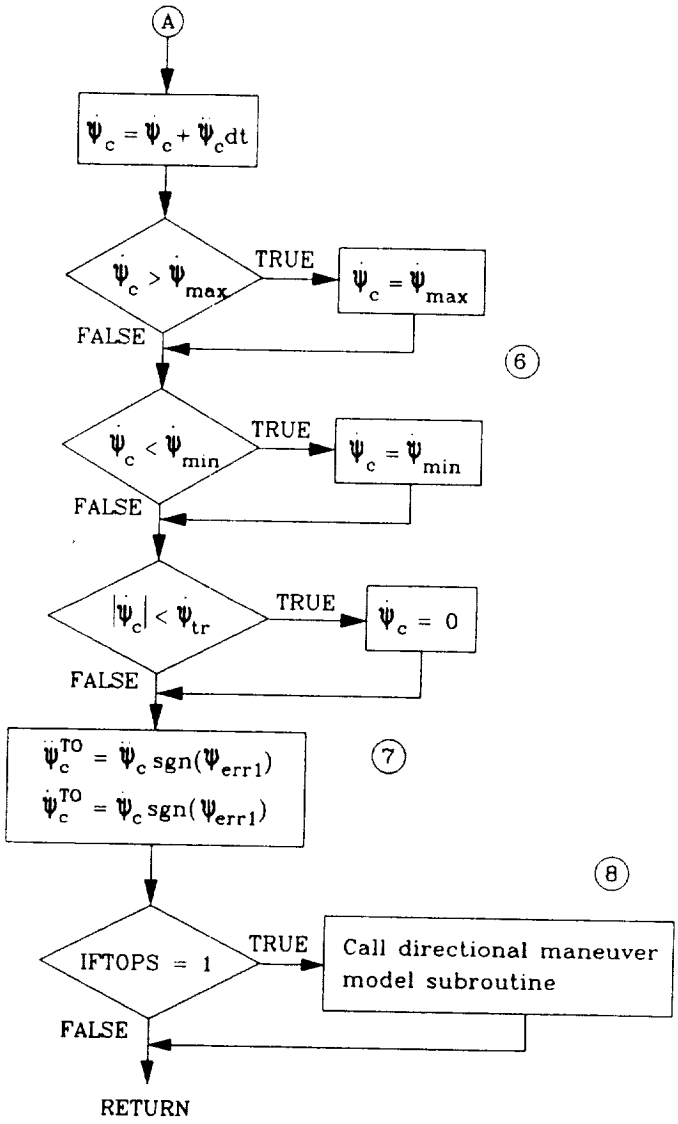

c. Calculation of Constrained Time-Optimal Yaw Rate Command

Figure 1.10 (Continued)

d. Notes (corresponding to circled numbers throughout figure)

1. If the difference between the current and past heading commands exceeds the error threshold, then a heading change command has been issued. The initial heading error is calculated (ψ_{err1}), and the "past" model states are initialized in preparation for the constrained time-optimal maneuver. Also at this time, the directional time-optimal maneuver flag is set to 1.

2. If the directional time-optimal maneuver flag is equal to zero, bypass the time-optimal control logic, and set the control flags to zero.

3. The model heading error and yaw rate are normalized with respect to the sign of the initial heading error. This allows the same logic to be utilized for both clockwise and counter-clockwise pedal turns.

4. The heading error switching criterion for the pedal turn is calculated as follows:

$$PSSWT = \frac{\dot{\psi}_1^2}{2\ddot{\psi}_{max}}$$

This switching criterion is only calculated until the criterion is satisfied.

5. At the conclusion of the deceleration to zero yaw rate at the new heading command, exit the time-optimal control, and reinitialize the necessary flags and switches.

6. Limit the yaw rate command, and provide a buffer about zero, where yaw rate command is identically equal to zero.

7. Calculate the constrained time-optimal commands.

8. If a constrained time-optimal heading change maneuver is in progress, call the model subroutine to update the model states for the next pass.

Figure 1.10 (Concluded)

TABLE 1.7

PARAMETER VALUES FOR THE CONSTRAINED TIME-OPTIMAL DIRECTIONAL MANEUVERING CONTROL LOGIC

ψ_{errt}	Heading error threshold	10 deg
$\ddot{\psi}_{max}$	Yaw angular acceleration limit	0.25 rad/sec^2
$\dot{\psi}_{max}$	Yaw rate limit	0.5 rad/sec

1.4 Evasive Maneuver Models

As introduced in the previous section, the constrained time-optimal evasive maneuvers will be accomplished using a model-following technique. Models for each of the maneuvers are defined in Figs. 1.11 through 1.14.

Inputs:	Previous lateral maneuver model states	y_m^p, v_m^p, ϕ_m^p, p_m^p
	Constrained time-optimal commands	$\dot{y}_c^{TO}$, ϕ_c^{TO}, p_c^{TO}
	Command flags	IYDCFG, IPHCFG, IPCFG
Outputs:	Lateral maneuver model states	y_m, v_m, ϕ_m, p_m

a. Inputs and Outputs

Figure 1.11 Flow Diagram for Lateral Maneuver Model

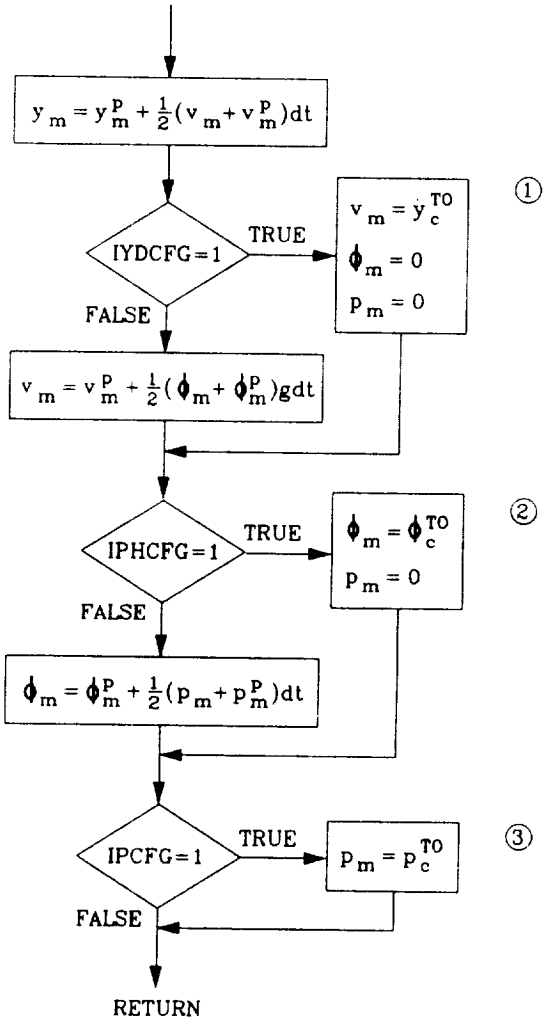

b. Integration of Model States

Figure 1.11 (Continued)

c. Notes (corresponding to circled numbers throughout figure)

1. If the time-optimal logic dictates a velocity hold, set the model velocity to the command, and set the model roll attitude and roll rate to zero. Otherwise, integrate the model roll attitude to get the model velocity.

2. If the time-optimal logic dictates a roll attitude hold, set the model roll attitude to the command, and set the model roll rate to zero. Otherwise, integrate the model roll rate to get the model roll attitude.

3. If the time-optimal logic dictates a roll rate command, set the model roll rate to the command.

Figure 1.11 (Concluded)

Inputs:	Previous longitudinal maneuver model states	u_m^p, θ_m^p, q_m^p
	Constrained time-optimal commands	θ_c^{TO}, q_c^{TO}
	Command flags	ITHCFG, IQCFG
Outputs:	Longitudinal maneuver model states	u_m, θ_m, q_m

a. Inputs and Outputs

Figure 1.12 Flow Diagram for Longitudinal Maneuver Model

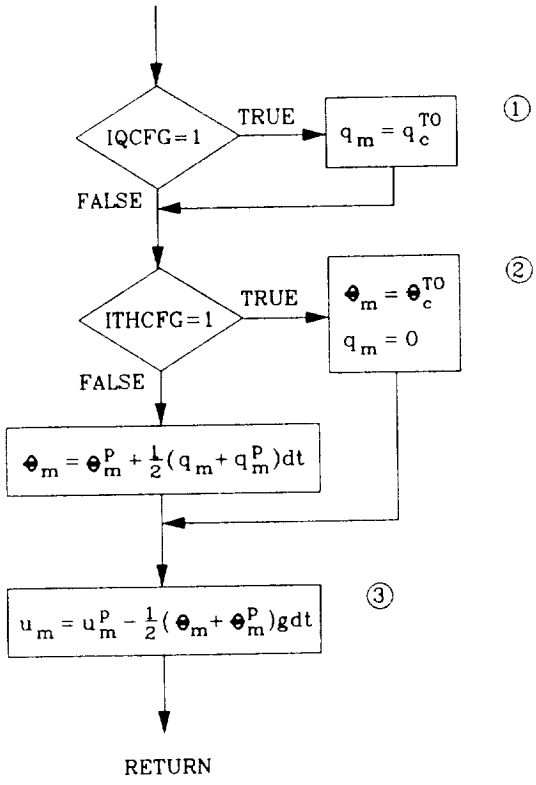

b. Integration of Model States

Figure 1.12 (Continued)

c. Notes (corresponding to circled numbers throughout figure)

1. If the time-optimal logic dictates a pitch rate command, set the model pitch rate to the command.

2. If the time-optimal logic dictates a pitch attitude hold, set the model pitch attitude to the command, and set the model pitch rate to zero. Otherwise, integrate the model pitch rate to get the model pitch attitude.

3. Integrate the model pitch attitude to get the model velocity.

Figure 1.12 (Concluded)

Inputs:	Previous vertical maneuver model states	h_m^p, $\dot{h}_m^p$, $\ddot{h}_m^p$
	Constrained time-optimal commands	$\dot{h}_c^{TO}$, $\ddot{h}_c^{TO}$
	Command flags	IHDCFG, IAZCFG
Outputs:	Vertical maneuver model states	h_m, $\dot{h}_m$, $\ddot{h}_m$

a. Inputs and Outputs

Figure 1.13 Flow Diagram for Vertical Maneuver Model

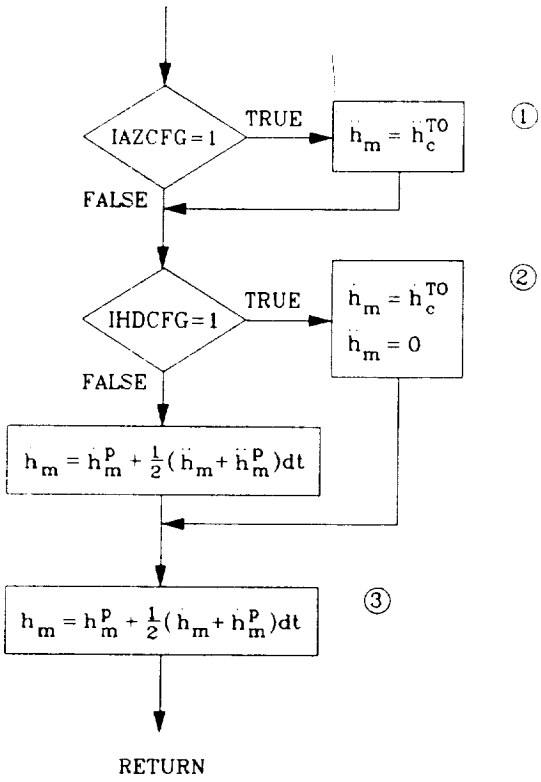

b. Integration of Model States

Figure 1.13 (Continued)

c. Notes (corresponding to circled numbers throughout figure)

1. If the time-optimal logic dictates a vertical acceleration command, set the model vertical acceleration to the command.

2. If the time-optimal logic dictates a vertical velocity hold, set the model vertical velocity to the command, and set the model vertical acceleration to zero. Otherwise, integrate the model vertical acceleration to get the model vertical velocity.

3. Integrate the model vertical velocity to get the model altitude.

Figure 1.13 (Concluded)

Inputs:	Previous directional maneuver model states	ψ_m^p, $\dot{\psi}_m^p$
	Constrained time-optimal commands	ψ_c^{TO}, $\ddot{\psi}_c^{TO}$
Outputs:	Directional maneuver model states	ψ_m, $\dot{\psi}_m$

a. Inputs and Outputs

Figure 1.14 Flow Diagram for Directional Maneuver Model

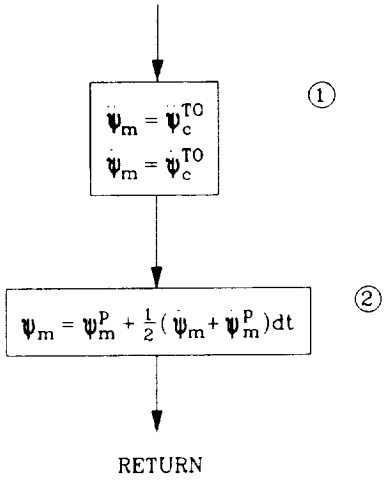

b. Integration of Model States

Figure 1.14 (Continued)

c. Notes (corresponding to circled numbers throughout figure)

1. Set the model yaw rate and yaw acceleration to the appropriate command.

2. Integrate the model yaw rate to get the model heading.

Figure 1.14 (Concluded)

2. STORED FLIGHT PLAN

The stored flight plan is characterized in the locally horizontal plane by waypoint sequencing logic, discussed below in Subtopic 2.1, and is characterized in the locally vertical dimension by the terrain surface approximating function, discussed subsequently in Subtopic 2.2, p. 100.

2.1 Waypoint Sequencing Logic

The pre-planned flight path consists of a series of waypoints, each comprised of latitudinal and longitudinal coordinates ($x_{wp}(I_{wp})$ and $y_{wp}(I_{wp})$) and a transitional velocity, $u_{tw}(I_{wp})$. To maintain lateral guidance and control throughout the course, hyperbolic arcs are used as defined transition legs between the straight legs entering and exiting waypoints that call for nonzero transition velocities, and hover turns are employed at waypoints designating hover transitions. Appendix C contains a complete description and derivation of the hyperbolic transition logic. The latter transitions are called for at waypoints where the rotorcraft is to perform aggressive unmask/mask maneuvers and are referred to as stations of aggressive maneuvering while on watch.

The waypoint sequencing logic provides the lateral, longitudinal, and directional guidance commands for the automated flight. This includes pursuit feedforward guidance commands along with lateral position and heading commands, both of which enable the automatic guidance algorithms to minimize the errors from the prescribed course. Also, at stations of aggressive maneuvering while on watch, the series of commands controlling the aggressive maneuvering are provided, with the resumption of the nominal preplanned course following these maneuvers. Figure 2.1 is a flow diagram representation of the waypoint sequencing logic. The definition of various parameters for the hyperbolic transition legs is presented in Fig. 2.2, with values of some of these parameters presented in Table 2.1. In addition, the initialization steps required, including the calculation of the remainder of the hyperbolic transition leg parameters, are presented in the flow diagram of Fig. 2.3.

Inputs:	Waypoint specifications:	
	Number of waypoints	N_{wps}
	Longitudinal coordinates of the waypoints	$x_e(I_{wp})$
	Latitudinal coordinates of the waypoints	$y_e(I_{wp})$
	Transitional velocities at the waypoints	$u_{tw}(I_{wp})$
	Aggressive maneuver specifications:	
	Observation heading	$\psi_{mum}(I_{AMC})$
	Observation radar altitude	$h_{mum}(I_{AMC})$
	Observation time	$T_{mum}(I_{AMC})$
Outputs:	Lateral course command	y_{cs}
	Along-course distance to next waypoint	x_{cs}
	Course command heading	$\psi_{c_{auto}}$
	Lateral pursuit feedforward guidance commands	$\dot{y}_{pg}$, $\ddot{y}_{pg}$
	Directional pursuit feedforward commands	$\dot{\psi}_{pg}$, $\ddot{\psi}_{pg}$
	Nominal course resumption flag	IRESUM
	Hover logical switch	HOVR
	Index of current waypoint	I_{wp}
	Waypoint course and hyperbolic transition parameters for current waypoint leg	$u_{tw}(I_{wp})$, $x_{sl}(I_{wp})$, $x_{lE}(I_{wp})$, and $x_{ant}(I_{wp})$
	Waypoint leg heading	$\lambda_{I_{wp}}$
	Waypoint leg length	$R_{I_{wp}}$

a. Inputs and Outputs

Figure 2.1 Flow Diagram for Waypoint Sequencing Logic

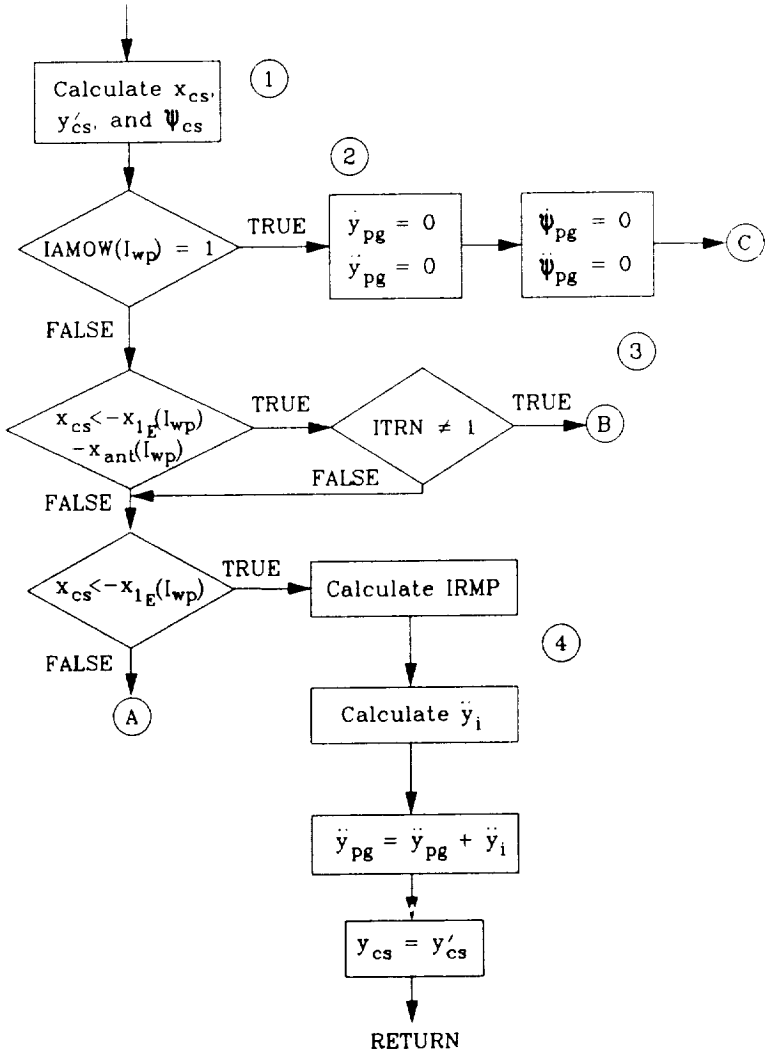

b. Initial Roll-Up for Transition

Figure 2.1 (Continued)

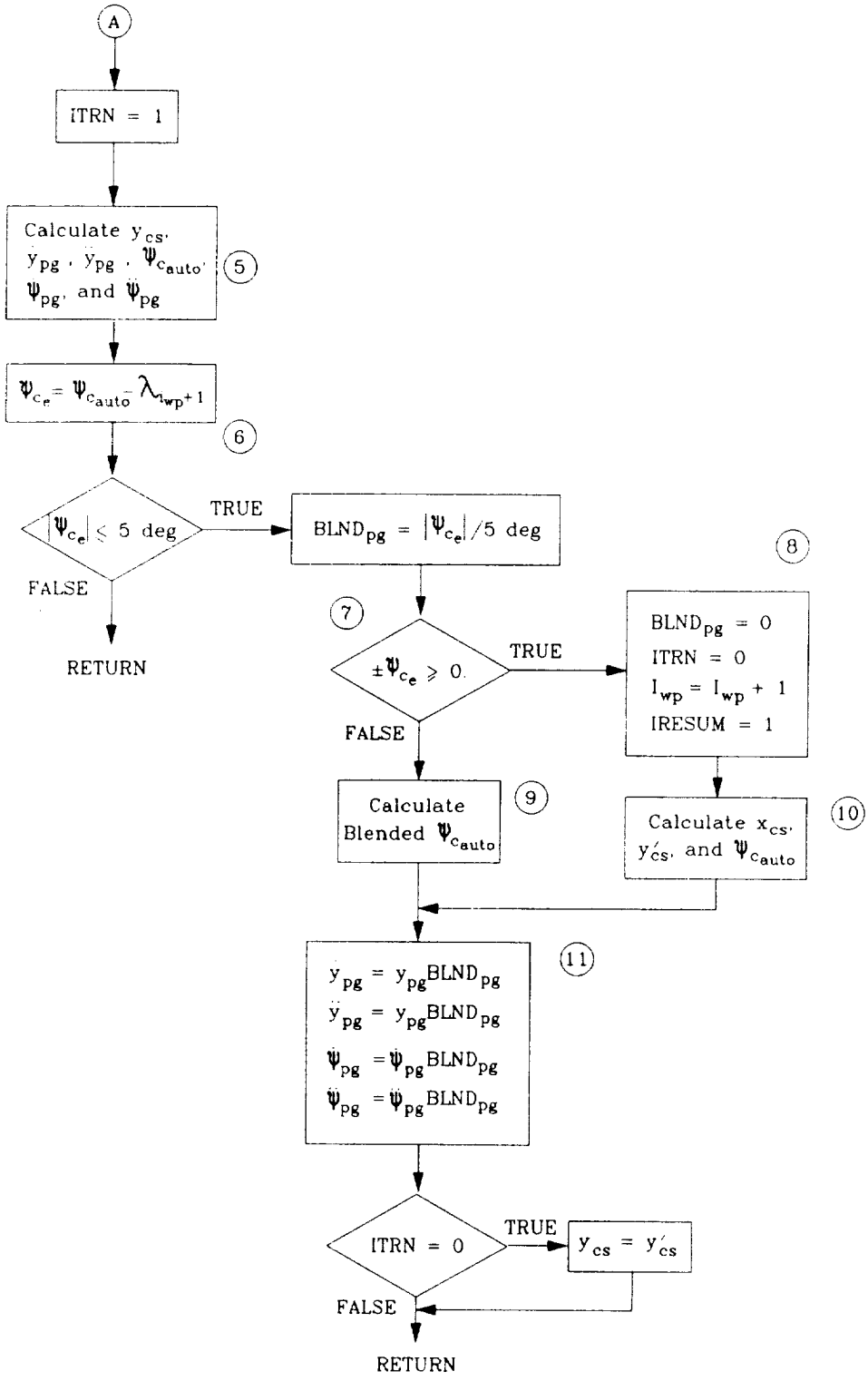

c. Hyperbolic Transition Logic

Figure 2.1 (Continued)

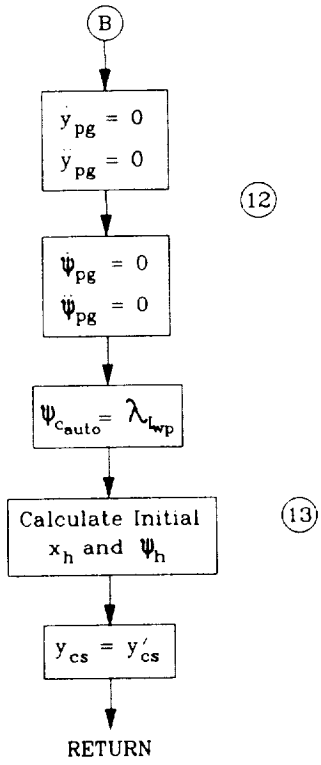

d. Preparation for Future Hyperbolic Transition

Figure 2.1 (Continued)

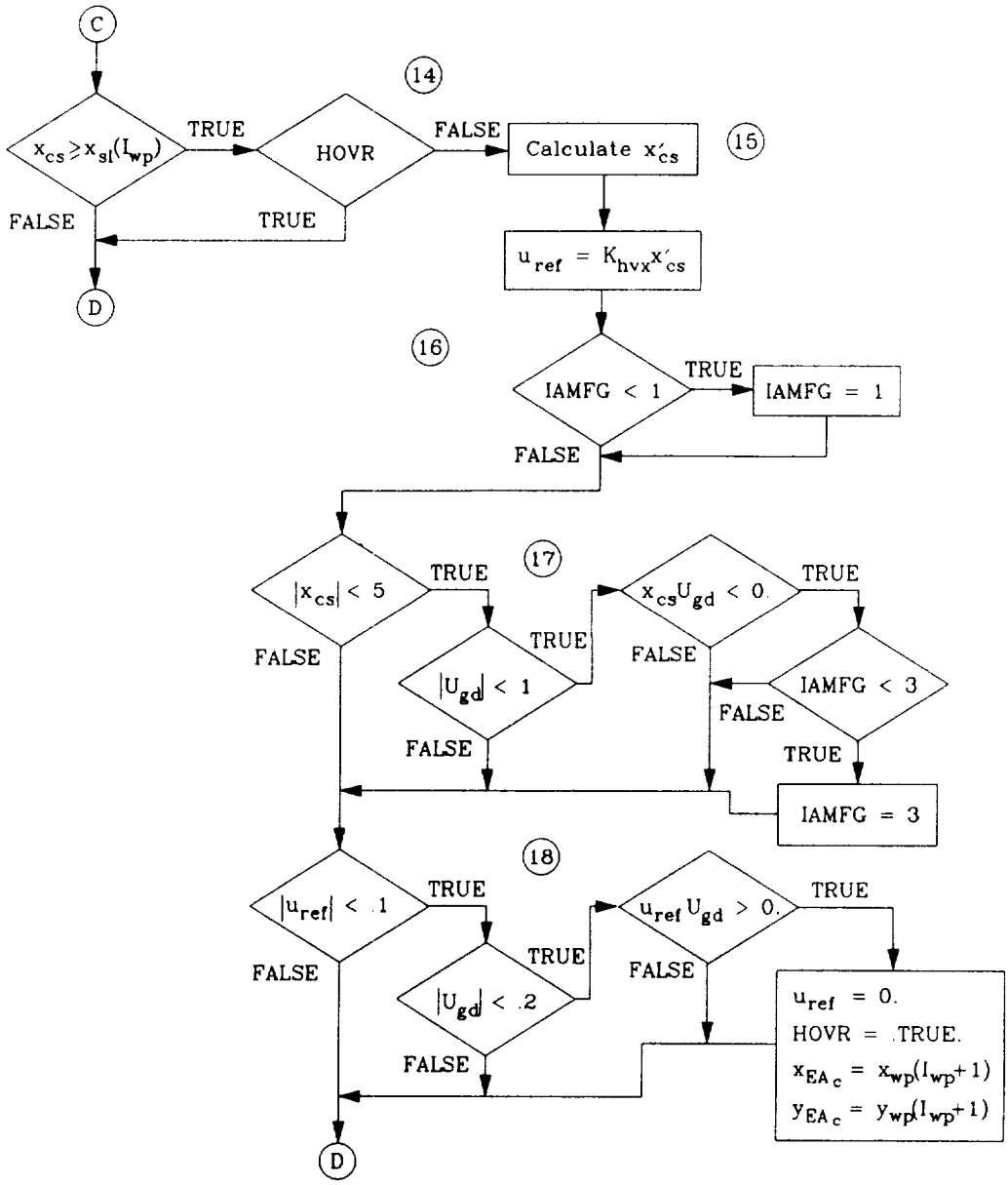

e. Deceleration to Hover at Station for Aggressive Maneuvering While on Watch

Figure 2.1 (Continued)

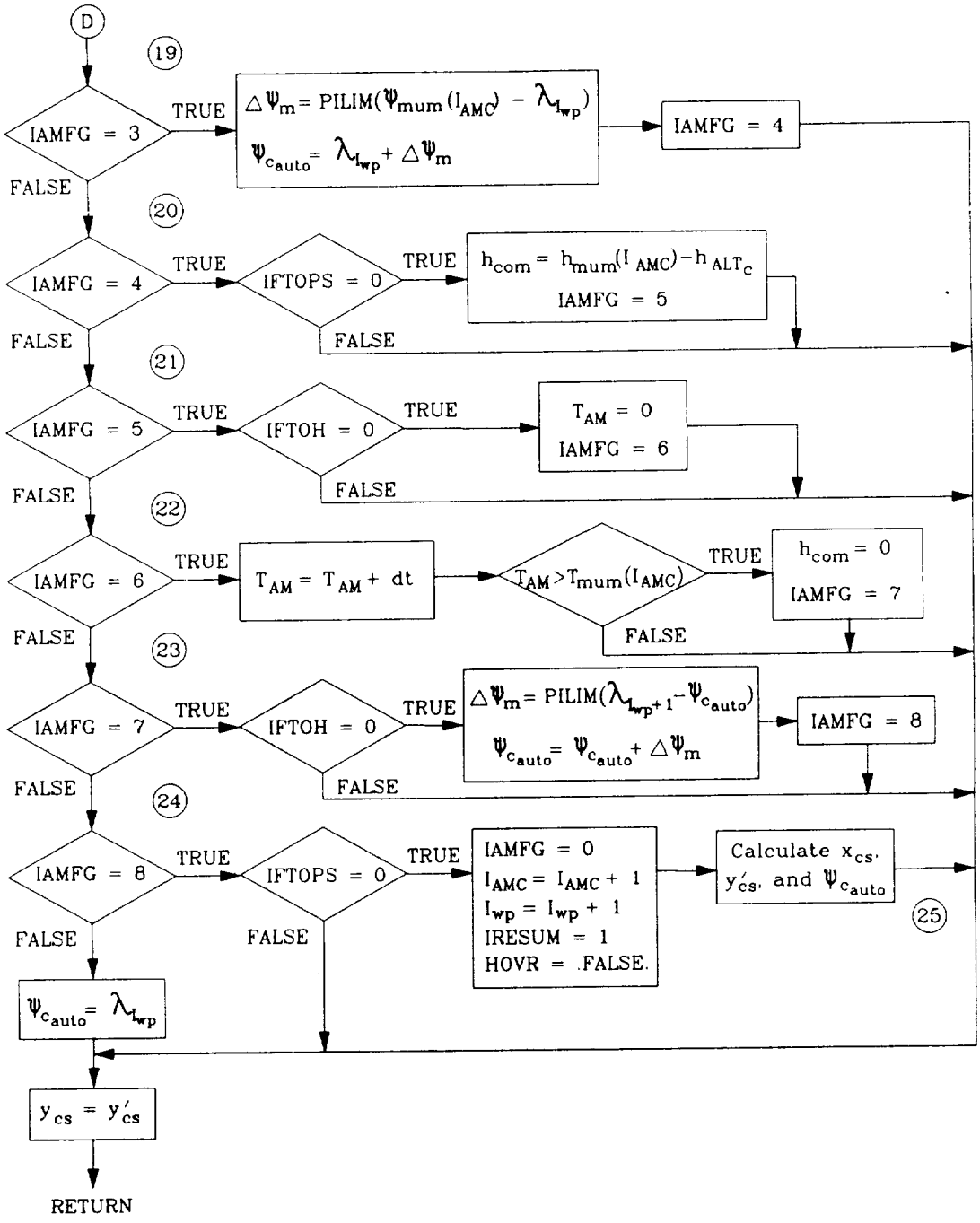

f. Performing Aggressive Maneuvering While on Watch

Figure 2.1 (Continued)

g. Notes (corresponding to circled numbers throughout figure)

1. Calculate the along-course distance to the next waypoint, the lateral offset from the current waypoint leg, and the difference between the current heading and the heading of the current waypoint leg as follows:

$$x_{cs} = (x_{EA} - x_{wp}(I_{wp}+1))\cos(\lambda_{I_{wp}}) + (y_{EA} - y_{wp}(I_{wp}+1))\sin(\lambda_{I_{wp}})$$

$$y'_{cs} = -(x_{EA} - x_{wp}(I_{wp}+1))\sin(\lambda_{I_{wp}}) + (y_{EA} - y_{wp}(I_{wp}+1))\cos(\lambda_{I_{wp}})$$

$$\psi_{cs} = \psi - \lambda_{I_{wp}}$$

2. A waypoint leg for which $IAMOW(I_{wp}) = 1$ is designated as a station for aggressive maneuvering while on watch.

3. If the distance to the next waypoint is greater than the necessary anticipative distance, bypass the transitioning logic.

4. An anticipative roll-up is required prior to entering the hyperbolic transition leg to insure that the entrance roll attitude is sufficient to keep the rotorcraft on the prescribed curved trajectory. This is accomplished by ramping up to the entrance roll attitude at the maximum rate utilizing the following equations:

$$IRMP = \frac{x_{ant}(I_{wp})}{U_{gd}\,dt}$$

$$\ddot{y}_i = \left(\frac{b^2(I_{wp})}{a^2(I_{wp})} - \tan^2(\alpha_{I_{wp}})\right)\frac{U_{gd}^2\cos^3(\alpha_{I_{wp}})}{y_{I_h}(I_{wp})IRMP}$$

5. The hyperbolic transition commands are calculated through the following set of equations:

   1. $x_h = x_h + U_{gd}\cos(\psi_h)dt$

   2. $y_h = \pm b(I_{wp})\sqrt{1 + \frac{x_h^2}{a^2(I_{wp})}}$

   3. $\psi_h = \tan^{-1}\left(\frac{b^2(I_{wp})x_h}{a^2(I_{wp})y_h}\right)$

Figure 2.1 (Continued)

g. Notes (Continued)

4. $$\frac{\partial y_h}{\partial x_h} = \frac{b^2(I_{wp})x_h}{a^2(I_{wp})y_h}$$

5. $$\frac{\partial^2 y_h}{\partial x_h^2} = \frac{\frac{b^2(I_{wp})}{a^2(I_{wp})} - \left(\frac{\partial y_h}{\partial x_h}\right)^2}{y_h}$$

6. $$\frac{\partial^3 y_h}{\partial x_h^3} = -\frac{3\left(\frac{\partial^2 y_h}{\partial x_h^2}\right)\left(\frac{\partial y_h}{\partial x_h}\right)}{y_h}$$

7. $$\dot{x}_h = U_{gd}\cos(\psi_h)$$

8. $$\dot{y}_h = U_{gd}\sin(\psi_h)$$

9. $$\ddot{x}_h = -\frac{\frac{\partial^2 y_h}{\partial x_h^2}\dot{x}_h\dot{y}_h}{1+\left(\frac{\partial y_h}{\partial x_h}\right)^2}$$

10. $$\ddot{y}_h = \frac{\frac{\partial^2 y_h}{\partial x_h^2}\dot{x}_h^2}{1+\left(\frac{\partial y_h}{\partial x_h}\right)^2}$$

11. $$\dot{\psi}_h = \frac{\frac{\partial^2 y_h}{\partial x_h^2}\dot{x}_h}{1+\left(\frac{\partial y_h}{\partial x_h}\right)^2}$$

12. $$\ddot{\psi}_h = \frac{\frac{\partial^3 y_h}{\partial x_h^3}\dot{x}_h^2 + 3\frac{\partial^2 y_h}{\partial x_h^2}\ddot{x}_h}{1+\left(\frac{\partial y_h}{\partial x_h}\right)^2}$$

13. $$\psi_{c_{auto}} = \lambda_{I_{wp}} - \alpha_{I_{wp}} + \psi_h$$

14. $$\dot{\psi}_{pg} = \dot{\psi}_h$$

15. $$\ddot{\psi}_{pg} = \ddot{\psi}_h$$

16. $$\dot{y}_{pg} = -\dot{x}_h\sin\psi_h + \dot{y}_h\cos\psi_h$$

17. $$\ddot{y}_{pg} = -\ddot{x}_h\sin\psi_h + \ddot{y}_h\cos\psi_h$$

Figure 2.1 (Continued)

g. Notes (Continued)

18. $$y'_h = y_h \mp \sqrt{b^2(I_{wp}) - a^2(I_{wp})\tan^2(\alpha_{I_{wp}})}$$

19. $$x_0 = x_h \cos(\alpha_{I_{wp}}) + y'_h \sin(\alpha_{I_{wp}})$$

20. $$y_0 = -x_h \sin(\alpha_{I_{wp}}) + y'_h \cos(\alpha_{I_{wp}})$$

21. $$y_{cs} = -(x_{cs} - x_0)\sin(\psi_h - \alpha_{I_{wp}}) + (y'_{cs} - y_0)\cos(\psi_h - \alpha_{I_{wp}})$$

These equations are to be solved in order, with the initial values of x_h and ψ_h discussed in Note 13. Note that the sign of the $\mp$ in Eqn. 18 is determined by the direction of the turn, i.e., - for rightward turns and + for leftward turns.

6. When the commanded heading is within 5 deg of the heading of the next course leg, begin blended exit from hyperbolic trajectory.

7. When the difference between the commanded heading and the heading of the next waypoint leg changes sign (from - to + for rightward turns or from + to - for leftward turns), the hyperbolic transition is complete.

8. Upon completion of a hyperbolic transition, increment the waypoint counter, I_{wp}, and set the nominal trajectory resumption flag, IRESUM, to 1.

9. Calculate the blended value of the commanded heading as follows:

$$\psi_{c_{auto}} = \lambda_{I_{wp}} + (\lambda_{I_{wp}+1} - \lambda_{I_{wp}})(1 - BLND_{pg}) + (\psi_h - \alpha_{I_{wp}})BLND_{pg}$$

10. Calculate the along-course distance to the next waypoint, the lateral offset from the new waypoint leg, and the commanded heading of the new waypoint leg as follows:

$$x_{cs} = (x_{EA} - x_{wp}(I_{wp}+1))\cos(\lambda_{I_{wp}}) + (y_{EA} - y_{wp}(I_{wp}+1))\sin(\lambda_{I_{wp}})$$

$$y'_{cs} = -(x_{EA} - x_{wp}(I_{wp}+1))\sin(\lambda_{I_{wp}}) + (y_{EA} - y_{wp}(I_{wp}+1))\cos(\lambda_{I_{wp}})$$

$$\psi_{c_{auto}} = \lambda_{I_{wp}}$$

11. Calculate the blended values of the pursuit feedforward guidance commands.

12. While following the straight legs of the waypoint course, the pursuit feedforward guidance commands are zero.

Figure 2.1 (Continued)

g. Notes (Continued)

13. In preparation for the next waypoint leg transition, the initial values for x_h and ψ_h are calculated as follows:

$$x_h = x_{I_h}(I_{wp}) - u_{tw}(I_{wp})\cos(\alpha_{I_{wp}})dt$$

$$\psi_h = \alpha_{I_{wp}}$$

14. If the along-course distance to the next waypoint is less than the prescribed deceleration distance and the logical hover switch, HOVR, is still false, decelerate the rotorcraft to hover.

15. Calculate the along-course distance to the next waypoint as follows:

$$x'_{cs} = (x_{EA} - x_{wp}(I_{wp} + 1))\cos(\psi) + (y_{EA} - y_{wp}(I_{wp} + 1))\sin(\psi)$$

The forward velocity command is proportional to this distance.

16. IAMFG is a counter to mark the progress through the aggressive maneuvering while on watch. Upon initiating the deceleration to the hover location, the counter is set to 1.

17. Upon satisfaction of the specified criteria, the counter IAMFG is set to 3, enabling the initiation of the aggressive maneuvers. These criteria are intended to signify an acceptable proximity to the desired hover location and may be modified during real-time testing of the system.

18. Upon satisfaction of stricter hover proximity criteria, the logical hover flag, HOVR, is set to TRUE, and the inertial position commands are defined as the longitudinal and latitudinal coordinates of the desired hover location.

19. Once the IAMFG counter is set to 3, a pedal turn is initiated to the desired observation heading using constrained time-optimal logic if the magnitude of the heading change warrants it. The counter is then set to 4. A π limiter function is used to limit the change in heading command to $\pm\pi$ by adding $2K\pi$.

20. Upon completion of the pedal turn, the unmasking bob-up maneuver is initiated, again using constrained time-optimal logic if the magnitude of the bob-up warrants it.

Figure 2.1 (Continued)

g. Notes (Concluded)

21. Following the bob-up, the time on station, T_{AM}, is initialized.

22. The observation height is held until the time on station, T_{AM}, exceeds the observation time, $T_{mum}(I_{AMC})$, after which the masking bob-down maneuver is initiated.

23. Following the bob-down maneuver, a pedal turn is initiated to the heading of the the next waypoint leg.

24. After this pedal turn, the waypoint course is resumed.

25. Calculate the along-course distance to next waypoint, the lateral offset from the new waypoint leg, and the commanded heading of the new waypoint leg as follows:

$$x_{cs} = (x_{EA} - x_{wp}(I_{wp}+1))\cos(\lambda_{I_{wp}}) + (y_{EA} - y_{wp}(I_{wp}+1))\sin(\lambda_{I_{wp}})$$

$$y'_{cs} = -(x_{EA} - x_{wp}(I_{wp}+1))\sin(\lambda_{I_{wp}}) + (y_{EA} - y_{wp}(I_{wp}+1))\cos(\lambda_{I_{wp}})$$

$$\psi_{c_{auto}} = \lambda_{I_{wp}}$$

Figure 2.1 (Concluded)

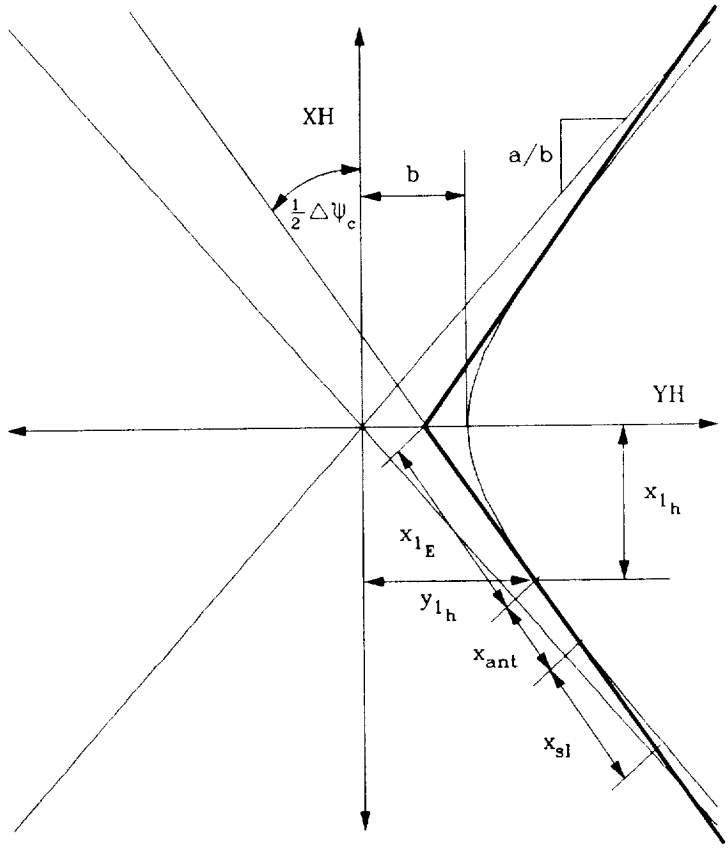

Figure 2.2 Diagram Depicting Various Hyperbolic Transition Parameters

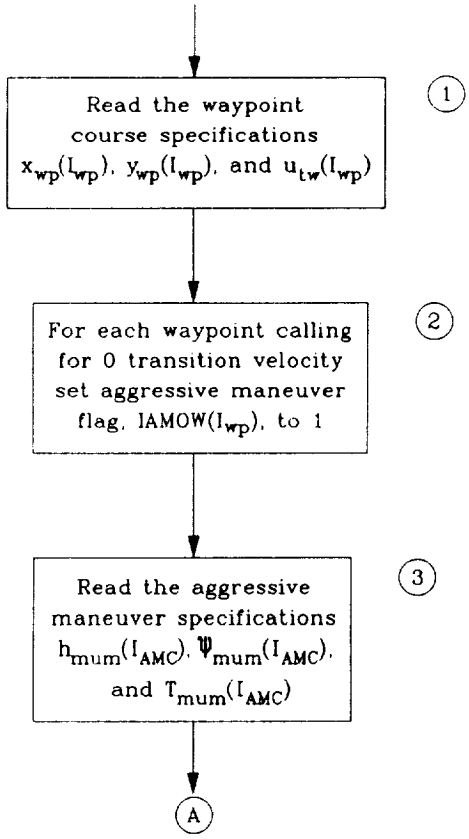

a. Reading the Waypoint Course Specifications

Figure 2.3 Flow Diagram of Calculation of Hyperbolic Transition Parameters

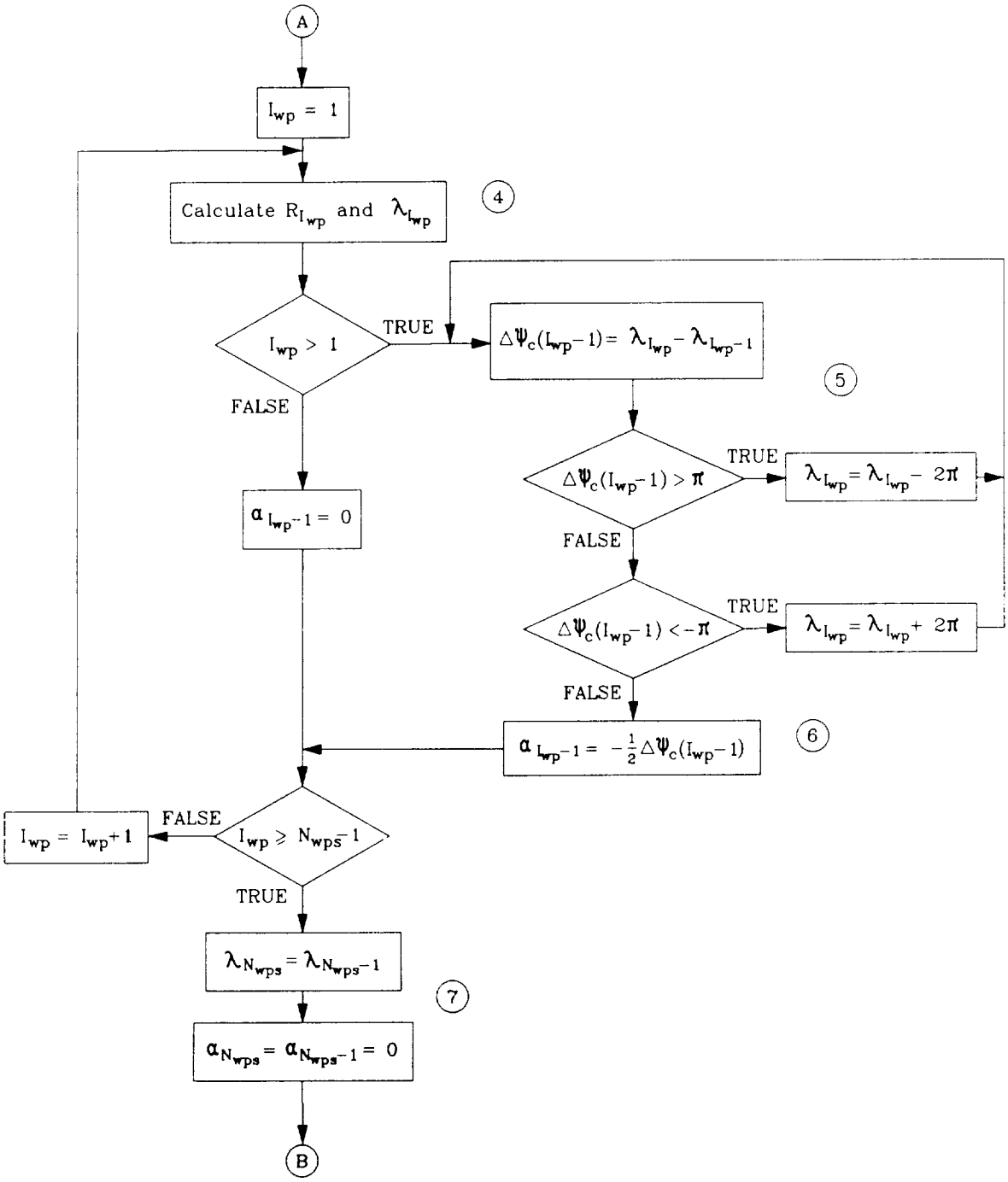

b. Calculation of Range, Heading and Heading Change Parameters

Figure 2.3 (Continued)

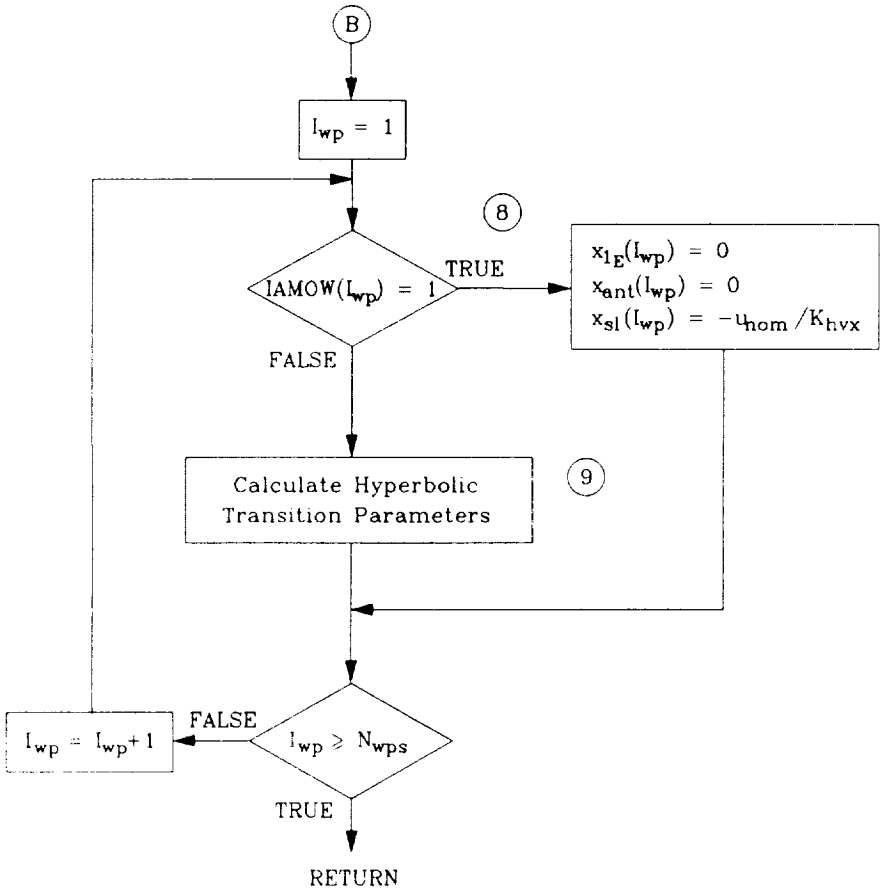

c. Calculation of Hyperbolic Transition Parameters

Figure 2.3 (Continued)

d. Notes (corresponding to circled numbers throughout the figure)

1. The waypoint course specifications are contained in the data files, WAYPTS1_NOE.DAT, WAYPTS2_NOE.DAT, WAYPTS1_AMOW.DAT, and WAYPTS2_AMOW.DAT. The format for reading these files is as follows:

   I6 - first line contains the number of waypoints, N_{wps}

   3F12.4 - next N_{wps} lines contain $x_{wp}(I_{wp})$, $y_{wp}(I_{wp})$, and $u_{tw}(I_{wp})$.

2. Also count the number of waypoints commanding zero transition velocity. This number, N_{AMC}, will define the number of sets of aggressive maneuver specifications needed for the waypoint course ($N_{AMC} = 3$ for the simulation flights requiring aggressive maneuvering while on watch along the first waypoint course, $N_{AMC} = 4$ for the simulation flights requiring aggressive maneuvering while on watch along the second waypoint course, and $N_{AMC} = 0$ for the simulation flights for NOE traveling for both courses).

3. The aggressive maneuver specifications are contained in the data files WPAMOW1.DAT and WPAMOW2.DAT. The format for reading these files is as follows:

   3F12.4 N_{AMC} lines contain $\psi_{mum}(I_{AMC})$, $h_{mum}(I_{AMC})$, and $T_{mum}(I_{AMC})$.

4. The following equations are used to calculate the range and heading of the waypoint legs:

$$R_{I_{wp}} = \sqrt{(x_{wp}(I_{wp}+1) - x_{wp}(I_{wp}))^2 + (y_{wp}(I_{wp}+1) - y_{wp}(I_{wp}))^2}$$

$$\lambda_{I_{wp}} = \tan^{-1}\left(\frac{y_{wp}(I_{wp}+1) - y_{wp}(I_{wp})}{x_{wp}(I_{wp}+1) - x_{wp}(I_{wp})}\right)$$

   Note that all of the hyperbolic transition parameter arrays, as well as the waypoint course specification arrays, should be dimensioned from 0, with the only exceptions being $R_{I_{wp}}$ and $\alpha_{I_{wp}}$ which should be dimensioned from -1. These requirements are further discussed in the waypoint course recapture logic. All of these arrays should be initialized to contain all zeros prior to the initial calculations discussed here.

5. The waypoint leg heading is modified so that the change of heading at the waypoint is limited to $\pm\pi$ rad.

Figure 2.3 (Continued)

d. Notes (Continued)

6. $\alpha_{l_{wp}}$ is equal to minus half the change in heading at the waypoint.

7. The heading at the last waypoint is equal to the heading of the last waypoint leg; therefore, the change in heading at that waypoint is zero.

8. If the waypoint in question is a station for aggressive maneuvering while on watch, the anticipative roll-up distance and the hyperbola entrance distance are set to zero, and the deceleration distance is calculated as shown.

9. The calculation of the hyperbolic transition parameters is as follows:

If the change in heading is less than 35 deg,

1a. $$a(I_{wp}) = \frac{u_{tw}^2(I_{wp})\tan\left(\left|\frac{1}{2}\Delta\psi_c(I_{wp})\right| + 5\text{deg}\right)}{g\tan\phi_{max}}$$

2a. $$b(I_{wp}) = a(I_{wp})\tan\left(\left|\frac{1}{2}\Delta\psi_c(I_{wp})\right| + 5\text{deg}\right)$$

If the change in heading is greater than 35 deg,

1b. $$a(I_{wp}) = \frac{u_{tw}^2(I_{wp})\tan(|0.643\Delta\psi_c(I_{wp})|)}{g\tan\phi_{max}}$$

2b. $$b(I_{wp}) = a(I_{wp})\tan(|0.643\Delta\psi_c(I_{wp})|)$$

3. $$y_{l_h}(I_{wp}) = \pm\frac{b^2(I_{wp})}{\sqrt{b^2(I_{wp}) - a^2(I_{wp})\tan^2(\alpha_{l_{wp}})}}$$

4. $$x_{l_h}(I_{wp}) = y_{l_h}(I_{wp})\frac{a^2(I_{wp})}{b^2(I_{wp})}\tan(\alpha_{l_{wp}})$$

5. $$x_{sl}(I_{wp}) = \frac{u_{nom}^2 - u_{tw}^2(I_{wp})}{10.7\,\text{ft/sec}^2}$$

Figure 2.3 (Continued)

d. Notes (Concluded)

6. $$x_{ant}(l_{wp}) = \pm \frac{b^2(l_{wp}) - a^2(l_{wp})\tan^2(\alpha_{l_{wp}})(u_{tw}\cos\alpha_{l_{wp}})^3}{y_{l_h}(l_{wp})a^2(l_{wp})g\dot{\phi}_{max}}$$

7. $$x_{l_E}(l_{wp}) = \frac{x_{l_h}(l_{wp})}{\cos(\alpha_{l_{wp}})}$$

Note that the sign of expressions 3 and 6 is determined by the direction of the turn at the waypoint, i.e., + if $\Delta\psi_c(l_{wp}) > 0$, and - if $\Delta\psi_c(l_{wp}) < 0$.

Figure 2.3 (Concluded)

TABLE 2.1

PARAMETER VALUES FOR HYPERBOLIC TRANSITION CALCULATIONS

u_{nom}	Nominal along-course velocity	33.778 ft/sec (20 kt)
K_{hvx}	Position error feedback gain	0.2 1/sec
h_{ALT_c}	Commanded radar altitude	20 ft
ϕ_{max}	Turn bank angle limit (different from time-optimal lateral maneuver limit)	20 deg
$\dot{\phi}_{max}$	Turn roll rate limit (different from time-optimal lateral maneuver limit)	20 deg/sec

2.2 Terrain Surface Approximating Function

This section describes the method for interpolating within the resolution of a stored data base to provide guidance for following flight profiles. This method employs compressed data storage of terrain heights using pre-flight parameter identification of the planned gaming area course. The storage and real-time updating of terrain profiles and obstacles have been organized in gaming area course coordinates that are indexed to the defined gaming area course. A complete description of this method is presented in Appendix D.

2.2.1 Gaming Area Course Transformation

The gaming area course is a 100 decameter (dm) wide corridor specified prior to the NOE mission that defines the geographic boundaries of the mission. This course is transformed from an earth coordinate system to its own (course-oriented) coordinate system for convenience in defining the approximate surface of the terrain, as will be further discussed in the next section. In its own coordinate system, the entire gaming area course is straightened into a rectangular corridor 100 dm wide. This corridor is divided into a number of rectangular sections, each defining a course leg, based on the number of course points used to define the gaming area course.

The gaming area course coordinate system has a nonlinear relationship with the earth-fixed axis system because, although the lengths of the two sides of the course leg sections are of equal length in the course-oriented coordinate system, the actual distances these two sides represent in the earth-fixed axis system are, in general, different due to turns in the gaming area course. This is demonstrated in Fig. 2.4, where a sample course leg of a defined gaming area course is isolated. The procedure presented in Fig. 2.5 is used to transform earth coordinates into gaming area course coordinates for a given course leg. Necessary initialization calculations are presented in the flow diagram of Fig. 2.6, while values af parameters are presented in Table 2.2.

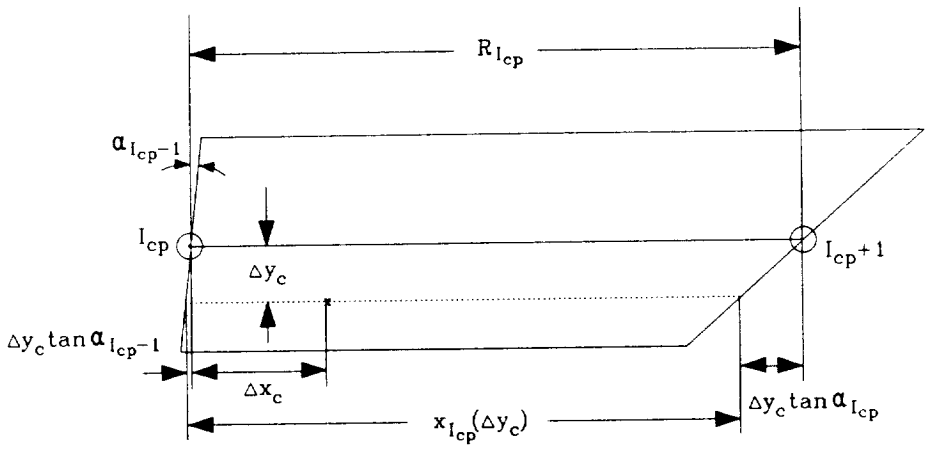

where

$$x_{I_{cp}}(\Delta y_c) = R_{I_{cp}} + \Delta y_c \tan \alpha_{I_{cp-1}} + \Delta y_c \tan \alpha_{I_{cp}}$$

Figure 2.4 Sample Course Leg of a Gaming Area Course in Earth Coordinates

Inputs:	Gaming area course specifications:	
	Number of course points	N_{cps}
	Northerly (latitude) coordinates of the course points	$x_{cp}(I_{cp})$
		$y_{cp}(I_{cp})$
	Easterly (longitude) coordinates of the course points	x_{EA} and y_{EA}
	Northerly and easterly coordinates of current rotorcraft location	V_N and V_E
	North and East inertial velocity components	$\dot{V}_N$ and $\dot{V}_E$
	North and East linear acceleration components	
Outputs:	Gaming area course coordinates	x_{gc} and y_{gc}
	Gaming area course inertial velocity components	$\dot{x}_{gc}$ and $\dot{y}_{gc}$
	Gaming area course linear acceleration components	$\ddot{x}_{gc}$ and $\ddot{y}_{gc}$

a. Inputs and Outputs

Figure 2.5 Flow Diagram for Gaming Area Course Transformation

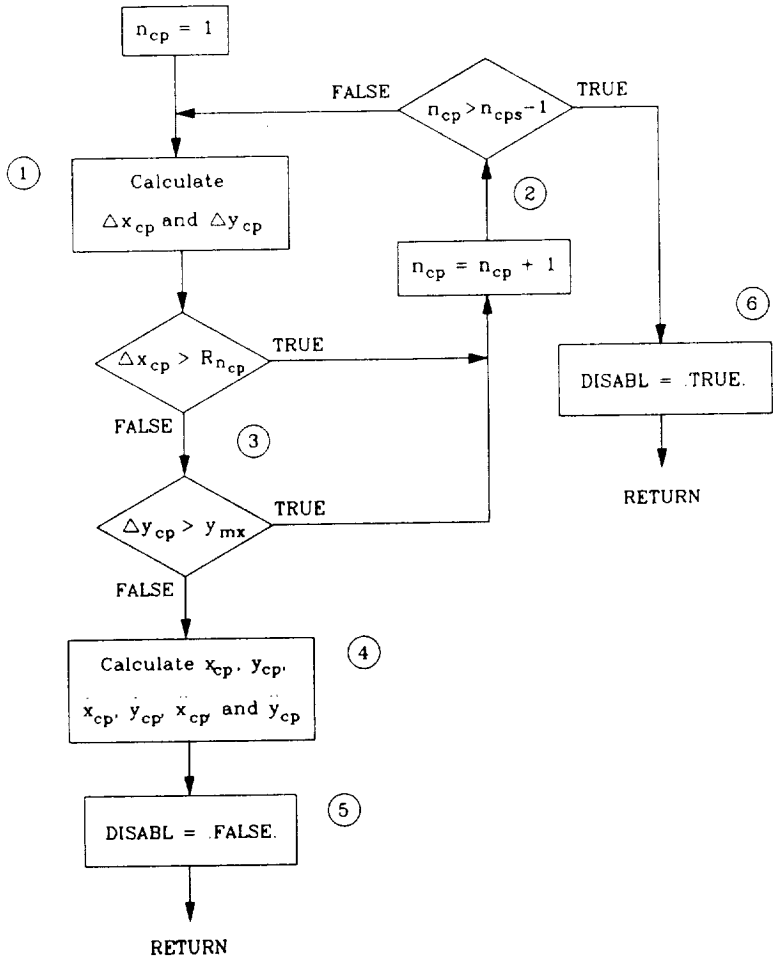

b. Gaming Area Course Transformation

Figure 2.5 (Continued)

c. Notes (corresponding to circled numbers throughout the figure)

1. The position, velocity components, and acceleration components must be converted from feet to decameters by multiplying each by FT2DM.

2. The following steps are performed to calculate the incremental distances Δx_{gc} and Δy_{gc}:

   Step 1. Calculate the distance from the course point I_{cp} and the current rotorcraft location.

   $$\Delta x_e = x_{dm} - x_{cp}(I_{cp})$$

   $$\Delta y_e = y_{dm} - y_{cp}(I_{wp})$$

   Step 2. Project the distances from Step 1 into the course leg direction.

   $$\begin{bmatrix} \Delta x_c \\ \Delta y_c \end{bmatrix} = \begin{bmatrix} \cos(\lambda_{I_{cp}}) & \sin(\lambda_{I_{cp}}) \\ -\sin(\lambda_{I_{cp}}) & \cos(\lambda_{I_{cp}}) \end{bmatrix} \begin{bmatrix} \Delta x_e \\ \Delta y_e \end{bmatrix}$$

   Step 3. Account for distortion in the along-course coordinate caused by unequal lengths of course leg sides. Because the lengths of the sides of the course leg rectangle in the gaming area course coordinates are equal to the distances between the two course points that define the course leg, any distance along a line parallel to the centerline of the course leg can be considered as a fraction of the total length in earth coordinates of that parallel line multiplied by the total length of the centerline. From Fig. 2.4, this translates into

   $$\Delta x_{gc} = R_{I_{cp}} \left(\frac{\Delta y_c \tan \alpha_{I_{cp}-1} + \Delta x_c}{\Delta y_c (\tan(\alpha_{I_{cp}-1}) + \tan(\alpha_{I_{cp}})) + R_{I_{cp}}} \right)$$

   $$\Delta y_{gc} = \Delta y_c$$

3. If the incremental distance along a gaming area course leg is greater than the length of that leg, or the lateral offset from the leg is greater than half the width of the gaming area course, then the rotorcraft location is not within the defined boundaries of the gaming area course leg in question. Increment the leg counter and try again.

Figure 2.5 (Continued)

c. Notes (Continued)

4. Once the correct gaming area course leg has been identified, calculate the transformation of the position, velocity, and acceleration into gaming area coordinates as follows:

Step 1. Add previous course leg lengths to the incremental distances calculated previously.

$$x_{gc} = \sum_{i=1}^{l_{cp}-1} R_i + \Delta x_{gc}$$

$$y_{gc} = \Delta y_{gc}$$

Step 2. Transform velocities and accelerations into along-course leg direction.

$$\begin{bmatrix} \Delta \dot{x}_{gc} \\ \Delta \dot{y}_{gc} \end{bmatrix} = \begin{bmatrix} \cos(\lambda_{l_{cp}}) & \sin(\lambda_{l_{cp}}) \\ -\sin(\lambda_{l_{cp}}) & \cos(\lambda_{l_{cp}}) \end{bmatrix} \begin{bmatrix} \Delta \dot{x}_{dm} \\ \Delta \dot{y}_{dm} \end{bmatrix}$$

$$\begin{bmatrix} \Delta \ddot{x}_{gc} \\ \Delta \ddot{y}_{gc} \end{bmatrix} = \begin{bmatrix} \cos(\lambda_{l_{cp}}) & \sin(\lambda_{l_{cp}}) \\ -\sin(\lambda_{l_{cp}}) & \cos(\lambda_{l_{cp}}) \end{bmatrix} \begin{bmatrix} \Delta \ddot{x}_{dm} \\ \Delta \ddot{y}_{dm} \end{bmatrix}$$

Step 3. Calculate gaming area course velocities and accelerations as

$$\dot{x}_{gc} = \frac{\partial x_{gc}}{\partial \Delta y_c} \Delta \dot{y}_{gc} + \frac{\partial x_{gc}}{\partial \Delta x_c} \Delta \dot{x}_{gc}$$

$$\dot{y}_{gc} = \Delta \dot{y}_{gc}$$

and

$$\ddot{x}_{gc} = \frac{\partial x_{gc}}{\partial \Delta y_c} \Delta \ddot{y}_{gc} + \frac{\partial x_{gc}}{\partial \Delta x_c} \Delta \ddot{x}_{gc} + \frac{\partial^2 x_{gc}}{\partial \Delta y_c^2} \Delta \dot{y}_{gc}^2 + \frac{\partial^2 x_{gc}}{\partial \Delta x_c^2} \Delta \dot{x}_{gc}^2 + \frac{\partial^2 x_{gc}}{\partial \Delta x_c \partial \Delta y_c} \Delta \dot{x}_{gc} \Delta \dot{y}_{gc}$$

$$\ddot{y}_{gc} = \Delta \ddot{y}_{gc}$$

Figure 2.5 (Continued)

c. Notes (Concluded)

where

$$\frac{\partial x_{gc}}{\partial \Delta y_c} = \frac{R_{l_{cp}}^2 \tan(\alpha_{l_{cp}-1}) - R_{l_{cp}} \Delta x_{gc}(\tan(\alpha_{l_{cp}-1}) + \tan(\alpha_{l_{cp}}))}{[\Delta y_{gc}(\tan(\alpha_{l_{cp}-1}) + \tan(\alpha_{l_{cp}})) + R_{l_{cp}}]^2}$$

$$\frac{\partial x_{gc}}{\partial \Delta x_c} = \frac{R_{l_{cp}}}{\Delta y_{gc}(\tan(\alpha_{l_{cp}-1}) + \tan(\alpha_{l_{cp}})) + R_{l_{cp}}}$$

$$\frac{\partial^2 x_{gc}}{\partial \Delta y_c^2} = -2\frac{\left[R_{l_{cp}}^2 \tan(\alpha_{l_{cp}-1}) - R_{l_{cp}} \Delta x_{gc}(\tan(\alpha_{l_{cp}-1}) + \tan(\alpha_{l_{cp}}))\right](\tan(\alpha_{l_{cp}-1}) + \tan(\alpha_{l_{cp}}))}{[\Delta y_{gc}(\tan(\alpha_{l_{cp}-1}) + \tan(\alpha_{l_{cp}})) + R_{l_{cp}}]^3}$$

$$\frac{\partial^2 x_{gc}}{\partial \Delta x_c^2} = 0$$

$$\frac{\partial^2 x_{gc}}{\partial \Delta x_c \partial \Delta y_c} = \frac{-R_{l_{cp}}(\tan(\alpha_{l_{cp}-1}) + \tan(\alpha_{l_{cp}}))}{[\Delta y_{gc}(\tan(\alpha_{l_{cp}-1}) + \tan(\alpha_{l_{cp}})) + R_{l_{cp}}]^2}$$

These velocities and accelerations are required in order to determine the time rate of change of terrain elevation and slope discussed in the next section.

5. The logical switch DISABL governs the ability of the automatic guidance system to resume control following a supervisory override. If false, the automatic guidance system is enabled.

6. If the location of the rotorcraft is outside the bounds of the gaming area course, disable the automatic guidance system. In this case, the pilot, upon depressing the recapture toggle switch, will maintain control of the rotorcraft. The lighted toggle will flash red in this case to alert the pilot that the automatic guidance system has been disabled.

Figure 2.5 (Concluded)

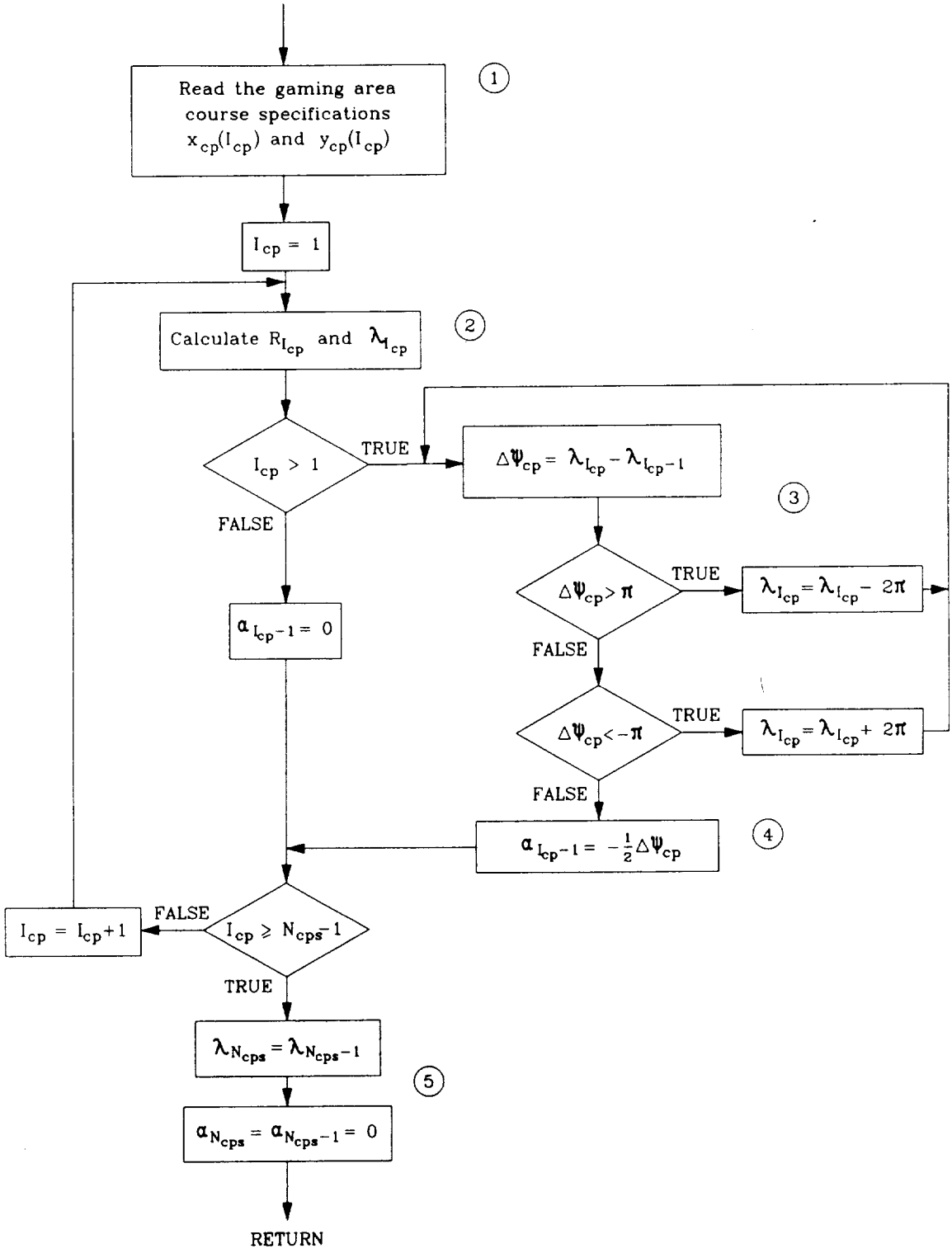

Figure 2.6 Calculation of Range, Heading, and Heading Change Parameters for the Gaming Area Course

Notes (corresponding to circled numbers throughout the figure)

1. The gaming area course specifications are contained in the data file CRSPTS_GAC.DAT. The format for reading this file is as follows:

   I6 - first line contains the number of course points, N_{cps}

   2F12.4 - next N_{cps} lines contain $x_{cp}(I_{cp})$ and $y_{cp}(I_{cp})$

2. The following equations are used to calculate the range and heading of the gaming area course legs:

$$R_{I_{cp}} = \sqrt{(x_{cp}(I_{cp}+1) - x_{cp}(I_{cp}))^2 + (y_{cp}(I_{cp}+1) - y_{cp}(I_{cp}))^2}$$

$$\lambda_{I_{cp}} = \tan^{-1}\left(\frac{y_{cp}(I_{cp}+1) - y_{cp}(I_{cp})}{x_{cp}(I_{cp}+1) - x_{cp}(I_{cp})}\right)$$

3. The gaming area course leg heading is modified so that the change of heading at the course point is limited to $\pm\pi$ rad.

4. $\alpha_{I_{cp}}$ is equal to minus half the change in heading at the course point.

5. The heading at the last course point is equal to the heading of the last gaming area course leg; therefore, the change in heading at that course point is zero.

Figure 2.6 (Concluded)

TABLE 2.2

PARAMETER VALUES FOR GAMING AREA COURSE TRANSFORMATION CALCULATIONS

y_{mx}	Half the gaming area course width	50 dm
FT2DM	Conversion from feet to decameters	0.03048 dm/ft

2.2.2 Using the Terrain Approximating Surface

In order to create a continuous representation of the terrain profile and threat exposure height, the rectangular gaming area course corridor is mapped with an approximate terrain surface and threat exposure height function to reduce the storage requirements and facilitate the interpolation within the resolution of the stored data base. This approximating surface is stored in the form of coefficient matrices in the file TERRN.DAT. The following procedure is used to retrieve the coefficient matrices from this file.

9A1,2I5	9 characters precede the integer values of NX and NY on the first line of the data file.
9A1,2I5	9 characters precede the integer values of MX and MY on the second line.
12A1,2G11.4	12 characters precede the real values of XRES and YRES on the third line.
6A1	6 characters designate the name of the first coefficient matrix on the next line.
5G13.5	The values in that coefficient matrix follow with 5 values per line.

These last two lines characterize how all of the coefficient matrices are stored in the data file. The order in which they appear in the file and the manner in which to read each are listed below.

1. $((D_{ij}, j = 1, MY), i = 1, MX)$
2. $((E_{ij}, j = 1, MY), i = 1, MX)$
3. $(F_{0_i}, i = 1, MX)$
4. $(F_{1_i}, i = 1, MX)$
5. $((G_{ij}, j = 1, MY), i = 1, MX)$
6. $((H_{ij}, j = 1, MY), i = 1, MX)$
7. $(I_{0_i}, i = 1, MX)$
8. $(I_{1_i}, i = 1, MX)$
9. $(J_j, j = 1, MY)$
10. $(K_j, j = 1, MY)$
11. L_0
12. L_1
13. $(M_j, j = 1, MY)$
14. $(N_j, j = 1, MY)$
15. P_0
16. P_1

With these coefficient matrices read from the data file prior to the simulation test flights, the following steps are taken to calculate the approximate elevation of the terrain at the given gaming area course coordinates:

Inputs:	Gaming area course coordinates	x_{gc} and y_{gc}
	Gaming area course inertial velocity components	$\dot{x}_{gc}$ and $\dot{y}_{gc}$
	Gaming area course linear acceleration components	$\ddot{x}_{gc}$ and $\ddot{y}_{gc}$
Outputs:	Automatic guidance altitude command (based on approximate terrain surface)	$h_{c_{auto}}$
	Pursuit feedforward guidance commands (derivatives of the approximate terrain surface)	$\dot{h}_{pg}$ and $\ddot{h}_{pg}$

1. The gaming area course lateral coordinate is modified such that the (0,0) coordinate corresponds to the lower left corner of the gaming area course corridor:

$$x_{ter} = x_{gc}$$

$$y_{ter} = y_{gc} + y_{mx}$$

2. The approximate terrain elevation is calculated as follows:

$$h(x_{ter}, y_{ter}) = C_0(y_{ter}) + C_1(y_{ter}) \cdot (x_{ter} + 1) + \sum_{i=1}^{MX} [A_i(y_{ter})\sin(\omega_i x_{ter}) + B_i(y_{ter})\cos(\omega_i x_{ter})]$$

where

$$A_i(y_{ter}) = F_{0_i} + F_{1_i}(y_{ter} + 1) + \sum_{j=1}^{MY} [D_{ij}\sin(\omega_j y_{ter}) + E_{ij}\cos(\omega_j y_{ter})]$$

$$B_i(y_{ter}) = I_{0_i} + I_{1_i}(y_{ter} + 1) + \sum_{j=1}^{MY} [G_{ij}\sin(\omega_j y_{ter}) + H_{ij}\cos(\omega_j y_{ter})]$$

$$C_0(y_{ter}) = L_0 + L_1(y_{ter} + 1) + \sum_{j=1}^{MY} [J_j\sin(\omega_j y_{ter}) + K_j\cos(\omega_j y_{ter})]$$

$$C_1(y_{ter}) = P_0 + P_1(y_{ter} + 1) + \sum_{j=1}^{MY} [M_j\sin(\omega_j y_{ter}) + N_j\cos(\omega_j y_{ter})]$$

$$\omega_i = \frac{2\pi i}{NX} \quad \text{and} \quad \omega_j = \frac{2\pi j}{NY}$$

3. The derivatives are calculated for use in the pursuit feedforward guidance algorithm using the following expressions.

$$\dot{h}(x_{ter}, y_{ter}) = \frac{\partial}{\partial x_{ter}}(h(x_{ter}, y_{ter}))\cdot \dot{x}_{gc} + \frac{\partial}{\partial y_{ter}}(h(x_{ter}, y_{ter}))\cdot \dot{y}_{gc}$$

$$\ddot{h}(x_{ter}, y_{ter}) = \frac{\partial}{\partial x_{ter}}(h(x_{ter}, y_{ter}))\cdot \ddot{x}_{gc} + \frac{\partial^2}{\partial x_{ter}^2}(h(x_{ter}, y_{ter}))\cdot \dot{x}_{gc}^2$$
$$+ 2\frac{\partial^2}{\partial x_{ter}\partial y_{ter}}(h(x_{ter}, y_{ter}))\cdot \dot{x}_{gc}\dot{y}_{gc} + \frac{\partial^2}{\partial y_{ter}^2}(h(x_{ter}, y_{ter}))\cdot \dot{y}_{gc}^2$$
$$+ \frac{\partial}{\partial y_{ter}}(h(x_{ter}, y_{ter}))\cdot \ddot{y}_{gc}$$

where

$$\frac{\partial}{\partial x_{ter}} h(x_{ter}, y_{ter}) = C_1(y_{ter}) + \sum_{i=1}^{MX}[A_i(y_{ter})\omega_i \cos(\omega_i x_{ter}) - B_i(y_{ter})\omega_i \sin(\omega_i x_{ter})]$$

$$\frac{\partial}{\partial y_{ter}} h(x_{ter}, y_{ter}) = \frac{d}{dy}C_0(y_{ter}) + \frac{d}{dy}C_1(y_{ter})\cdot(x_{ter}+1) + \sum_{i=1}^{MX}[\frac{d}{dy}A_i(y_{ter})\sin(\omega_i x_{ter})$$
$$+ \frac{d}{dy}B_i(y_{ter})\cos(\omega_i x_{ter})]$$

$$\frac{\partial^2}{\partial x_{ter}^2} h(x_{ter}, y_{ter}) = -\sum_{i=1}^{MX}[A_i(y_{ter})\omega_i^2 \sin(\omega_i x_{ter}) + B_i(y_{ter})\omega_i^2 \cos(\omega_i x_{ter})]$$

$$\frac{\partial^2}{\partial x_{ter}\partial y_{ter}} h(x_{ter}, y_{ter}) = \frac{d}{dy}C_1(y_{ter}) + \sum_{i=1}^{MX}[\frac{d}{dy}A_i(y_{ter})\omega_i \cos(\omega_i x_{ter})$$
$$- \frac{d}{dy}B_i(y_{ter})\omega_i \sin(\omega_i x_{ter})]$$

$$\frac{\partial^2}{\partial y_{ter}^2} h(x_{ter}, y_{ter}) = \frac{d^2}{dy_{ter}^2}C_0(y_{ter}) + \frac{d^2}{dy_{ter}^2}C_1(y_{ter})\cdot(x_{ter}+1) + \sum_{i=1}^{MX}[\frac{d^2}{dy_{ter}^2}A_i(y_{ter})\sin(\omega_i x_{ter})$$
$$+ \frac{d^2}{dy_{ter}^2}B_i(y_{ter})\cos(\omega_i x_{ter})]$$

$$\frac{d}{dy}A_i(y_{ter}) = F_{1i} + \sum_{j=1}^{MY}[D_{ij}\omega_j \cos(\omega_j y_{ter}) - E_{ij}\omega_j \sin(\omega_j y_{ter})]$$

$$\frac{d}{dy}B_i(y_{ter}) = I_{1i} + \sum_{j=1}^{MY}[G_{ij}\omega_j \cos(\omega_j y_{ter}) - H_{ij}\omega_j \sin(\omega_j y_{ter})]$$

$$\frac{d}{dy}C_0(y_{ter}) = L_1 + \sum_{j=1}^{MY}[J_j\omega_j\cos(\omega_j y_{ter}) - K_j\omega_j\sin(\omega_j y_{ter})]$$

$$\frac{d}{dy}C_1(y_{ter}) = P_1 + \sum_{j=1}^{MY}[M_j\omega_j\cos(\omega_j y_{ter}) - N_j\omega_j\sin(\omega_j y_{ter})]$$

$$\frac{d^2}{dy^2}A_i(y_{ter}) = -\sum_{j=1}^{MY}[D_{ij}\omega_j^2\sin(\omega_j y_{ter}) + E_{ij}\omega_j^2\cos(\omega_j y_{ter})]$$

$$\frac{d^2}{dy^2}B_i(y_{ter}) = -\sum_{j=1}^{MY}[C_{ij}\omega_j^2\sin(\omega_j y_{ter}) + H_{ij}\omega_j^2\cos(\omega_j y_{ter})]$$

$$\frac{d^2}{dy^2}C_0(y_{ter}) = -\sum_{j=1}^{MY}[J_j\omega_j^2\sin(\omega_j y_{ter}) + K_j\omega_j^2\cos(\omega_j y_{ter})]$$

$$\frac{d^2}{dy^2}C_1(y_{ter}) = -\sum_{j=1}^{MY}[M_j\omega_j^2\sin(\omega_j y_{ter}) + N_j\omega_j^2\cos(\omega_j y_{ter})]$$

4. Finally, the commanded altitude and pursuit feedforward guidance terms for the vertical axis are calculated using the following expressions:

$$h_{c_{auto}} = h(x_{ter}, y_{ter}) + h_{ALT_c}$$

$$h_{pg} = h(x_{ter}, y_{ter})$$

$$\dot{h}_{pg} = h(x_{ter}, y_{ter})$$

The FORTRAN code written to perform the above described calculations is included as Appendix G.

3. SUPERVISORY OVERRIDE AND AUTOMATIC GUIDANCE RECAPTURE LOGIC

3.1 Supervisory Override

The automatic guidance system for NOE flight is equipped with a "control-stick steering" feature, depicted in Figs. 1.1 through 1.3. This system allows the automatic guidance algorithm to guide the controller positions in the automatic mode. However, the control inputs to the rotorcraft actuators are in both the manual and automatic modes of operation, a result of controller deflection only. The pilot may thus modify the command from the automatic guidance algorithm in any axis by overcoming the breakout and gradient on the controller. When the perceived crisis has satisfactorily been averted, releasing tension on the controller will transfer full authority back to the automatic guidance algorithm.

In some instances, however, the pilot may desire full control of the rotorcraft without the encumbrance of the unsteady null force position of the controllers caused by the automatic guidance algorithm. In this case, a full supervisory override is required. The pilot may initiate this option by depressing the autoguidance toggle button. The null force positions for the controllers immediately revert to the nominal settings (those corresponding to zero controller inputs), and the automatic guidance algorithm is ignored. Because of the abrupt change in the null force positions for the controllers, the autoguidance toggle must be located either on the collective or the cyclic controller, thus allowing the pilot to prevent an abrupt change in controller position.

When the pilot takes over control by depressing the autoguidance toggle, the SUPOV logical switch is assigned the value .TRUE.. The supervisory override is terminated when the pilot again toggles the autoguidance button. At this point the recapture logic is initiated (SUPOV = .FALSE. & RECAP = .TRUE.).

3.2 Automatic Guidance Recapture Logic

There are two modes for the recapture of the pre-planned flight path using automatic guidance. The first is used in the initial capture of the waypoint course. The starting location of the rotorcraft may vary within the confines of the gaming area course. The initialization procedure generates two "temporary" waypoints that are necessary to bring the rotorcraft to the nearest waypoint down the course from the initial position. The second recapture algorithm is used to recapture the waypoint course following an interval of supervisory override. For this simulation, a restriction was placed on the pilot that he must not leave the tree-lined "tunnel" surrounding the waypoint course. The second recapture algorithm identifies the current waypoint course coordinate location of the rotorcraft and re-initializes the autoguidance algorithms to this initial condition. The procedures for these two recapture processes are depicted in the flow diagram of Fig. 3.1, with parameter values presented in Table 3.1.

Inputs:	Waypoint specifications:	
	Number of waypoints	N_{wps}
	Longitudinal coordinates of the waypoints	$x_e(I_{wp})$
	Latitudinal coordinates of the waypoints	$y_e(I_{wp})$
	Transitional velocities at the waypoints	$u_{tw}(I_{wp})$
	Waypoint leg headings	$\lambda_{I_{wp}}$
	Waypoint leg lengths	$R_{I_{wp}}$
	Aggressive maneuver station tags	$IAMOW(I_{AMC})$
	Nominal along-course velocity	u_{nom}
Outputs:	Modified waypoint specifications:	
	Longitudinal coordinates of the waypoints	$x_e(I_{wp})$
	Latitudinal coordinates of the waypoints	$y_e(I_{wp})$
	Transitional velocities at the waypoints	$u_{tw}(I_{wp})$
	Waypoint leg headings	$\lambda_{I_{wp}}$
	Waypoint leg lengths	$R_{I_{wp}}$
	Aggressive maneuver station tags	$IAMOW(I_{AMC})$
	Hyperbolic transition parameters	$x_{sl}(I_{wp})$, $x_{lE}(I_{wp})$, and $x_{ant}(I_{wp})$
	Current waypoint leg	I_{wp}

a. Inputs and Outputs

Figure 3.1 Flow Diagram for Automatic Guidance Recapture Logic

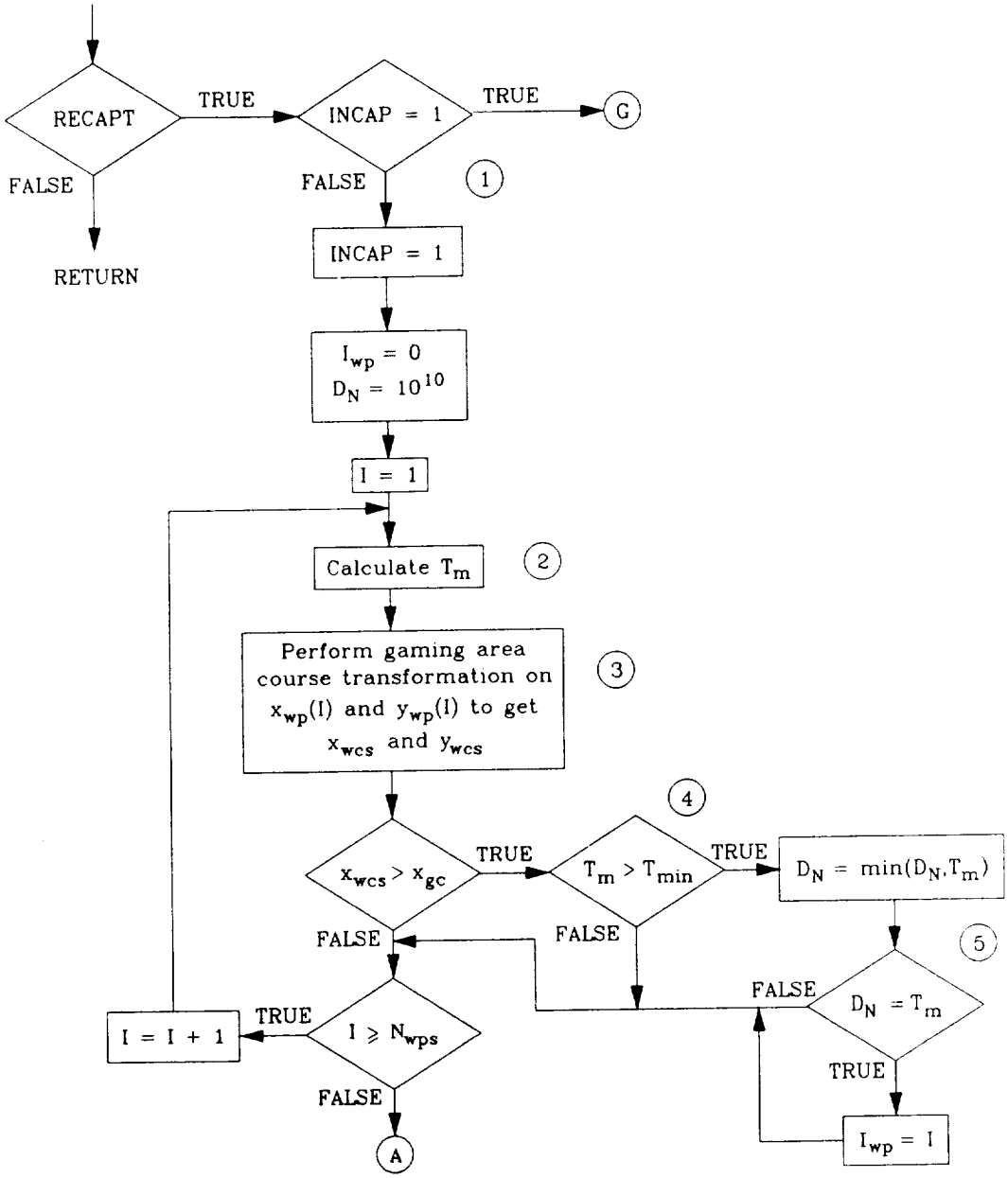

b. Identification of Nearest Waypoint

Figure 3.1 (Continued)

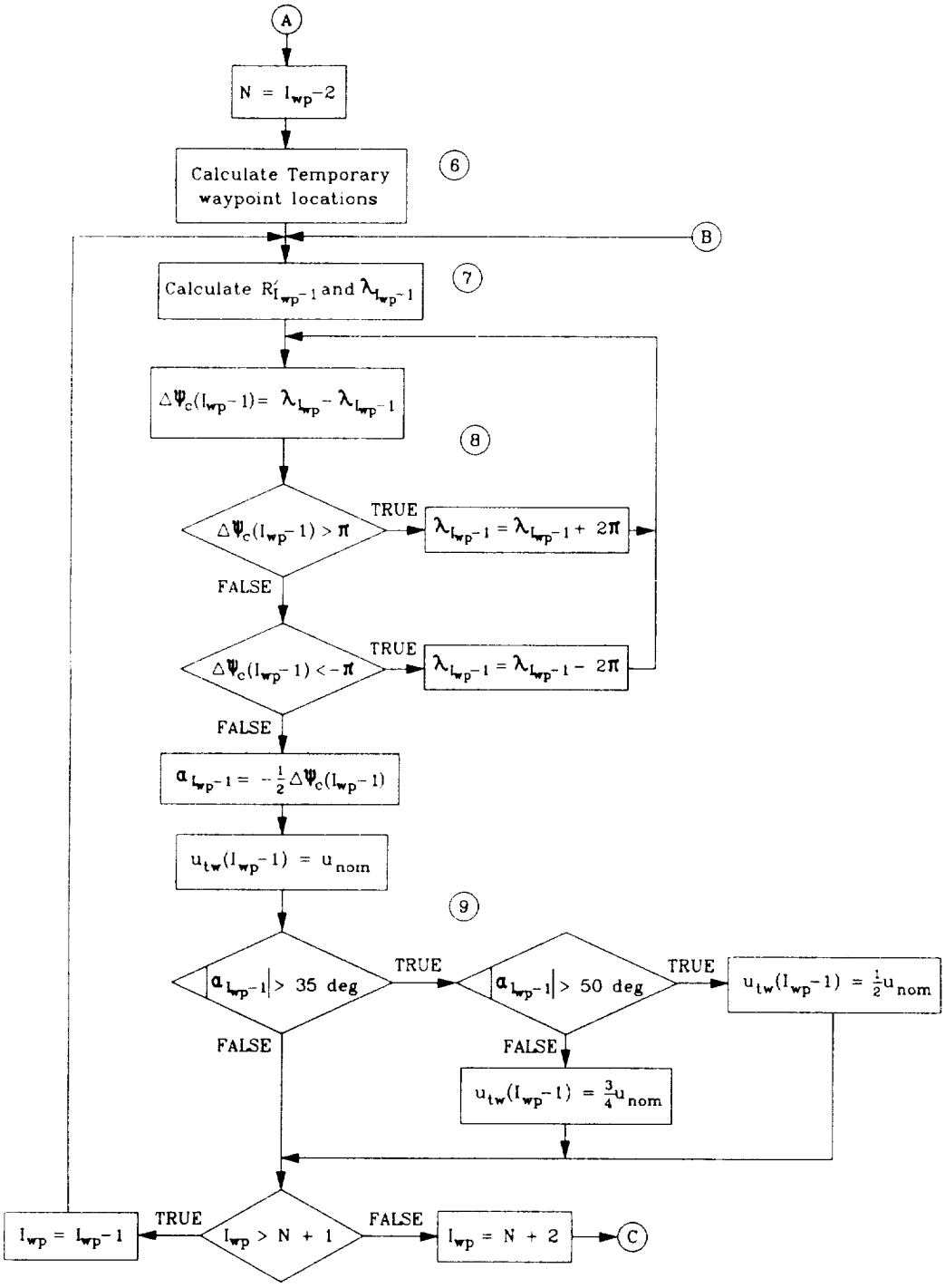

c. Calculation of Temporary Waypoint Specifications

Figure 3.1 (Continued)

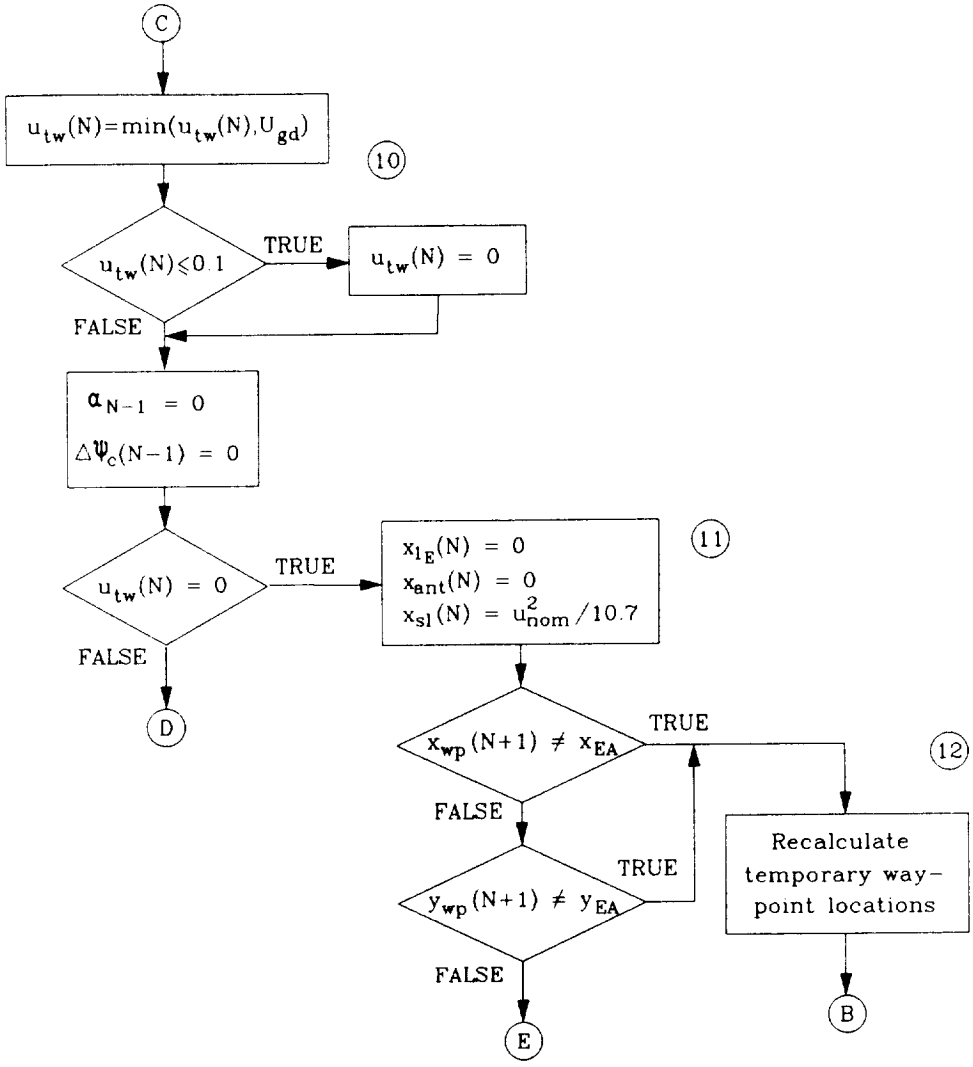

d. Calculation of First Temporary Waypoint Sequencing Parameters

Figure 3.1 (Continued)

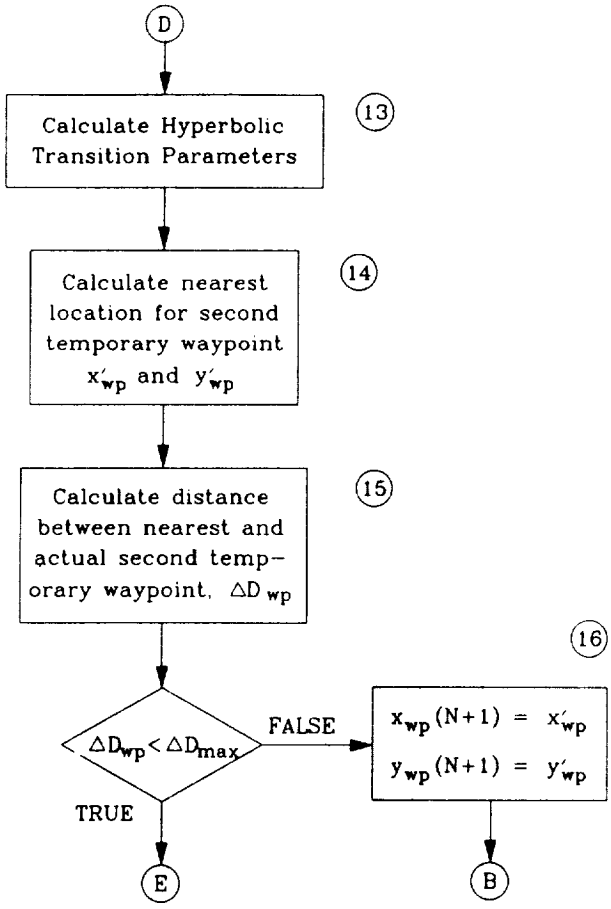

d. (Concluded)

Figure 3.1 (Continued)

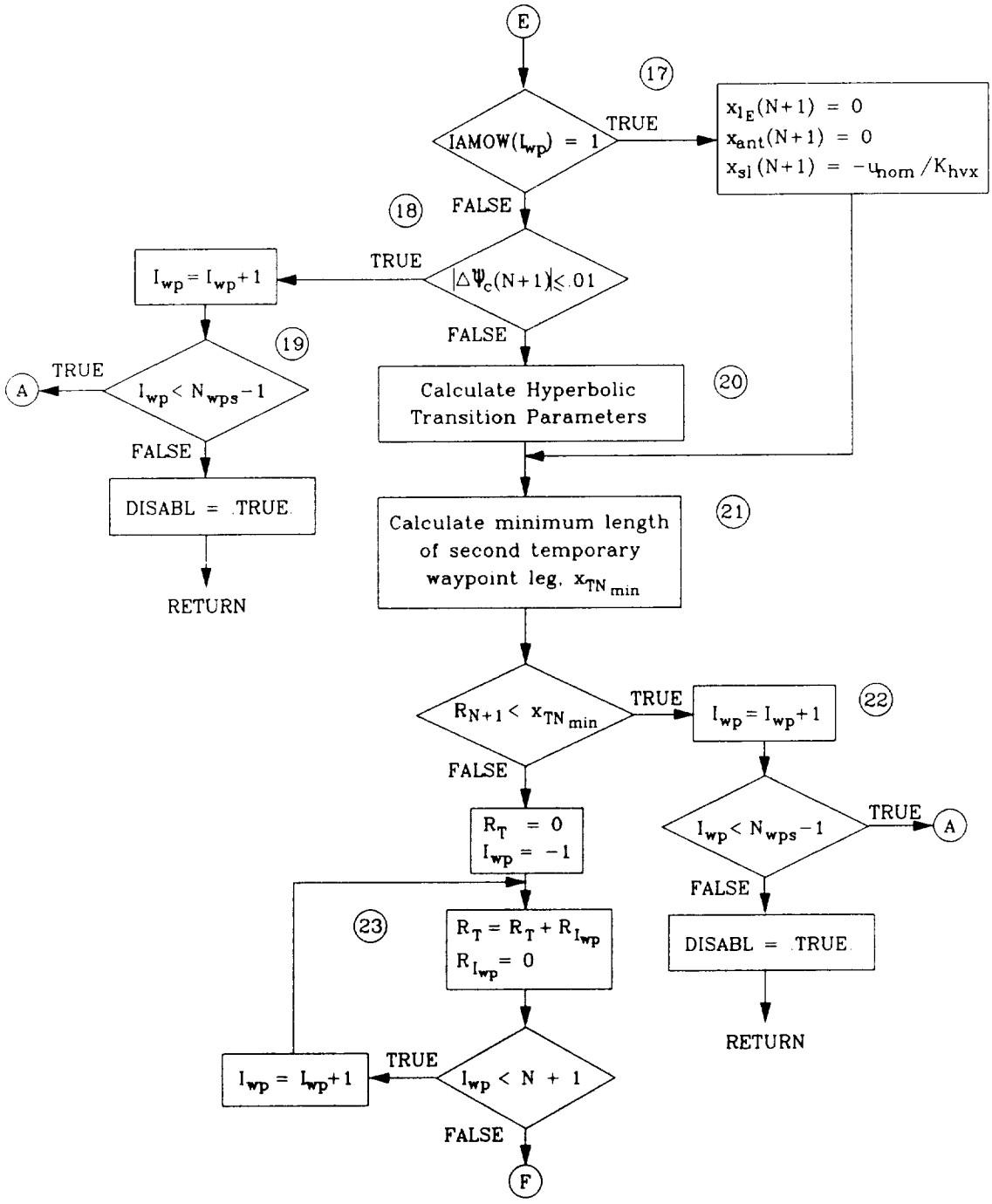

e. Calculation of Second Temporary Waypoint Sequencing Parameters

Figure 3.1 (Continued)

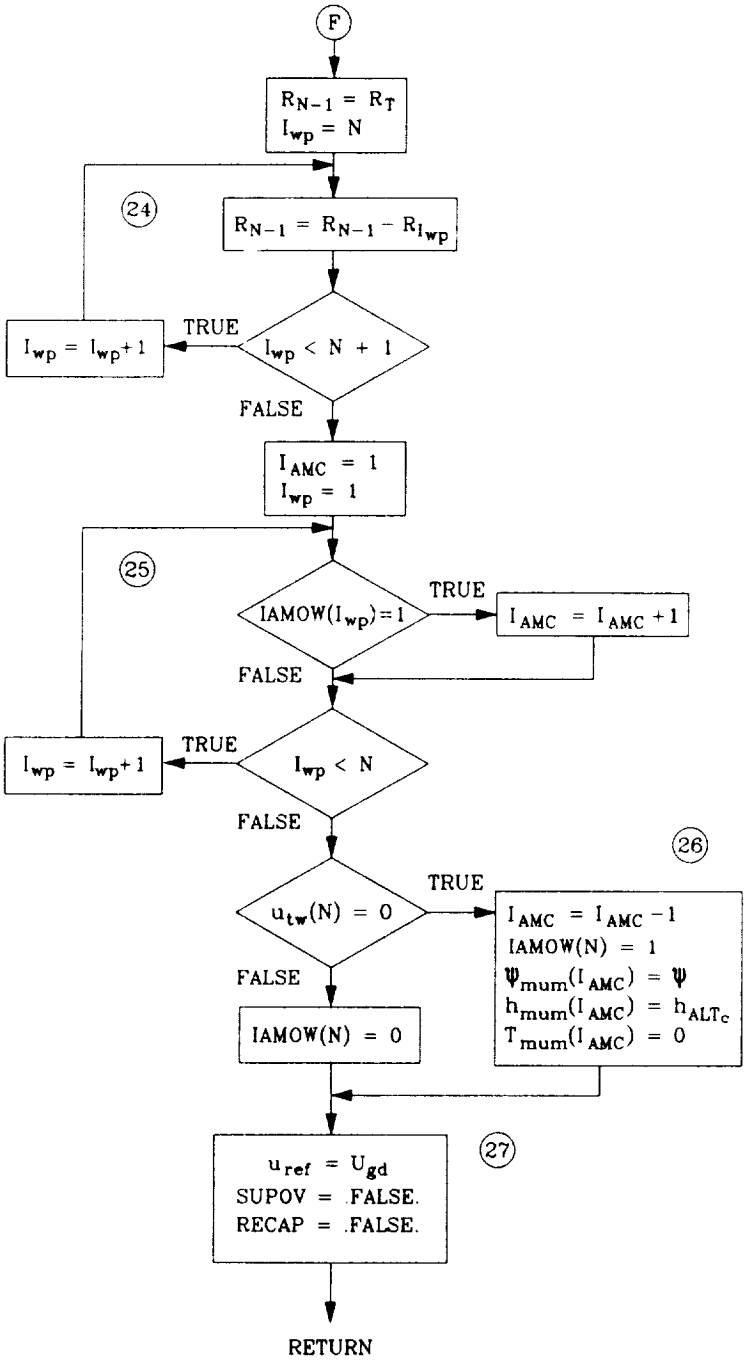

f. Preparation for Capture of Planned Waypoint Course

Figure 3.1 (Continued)

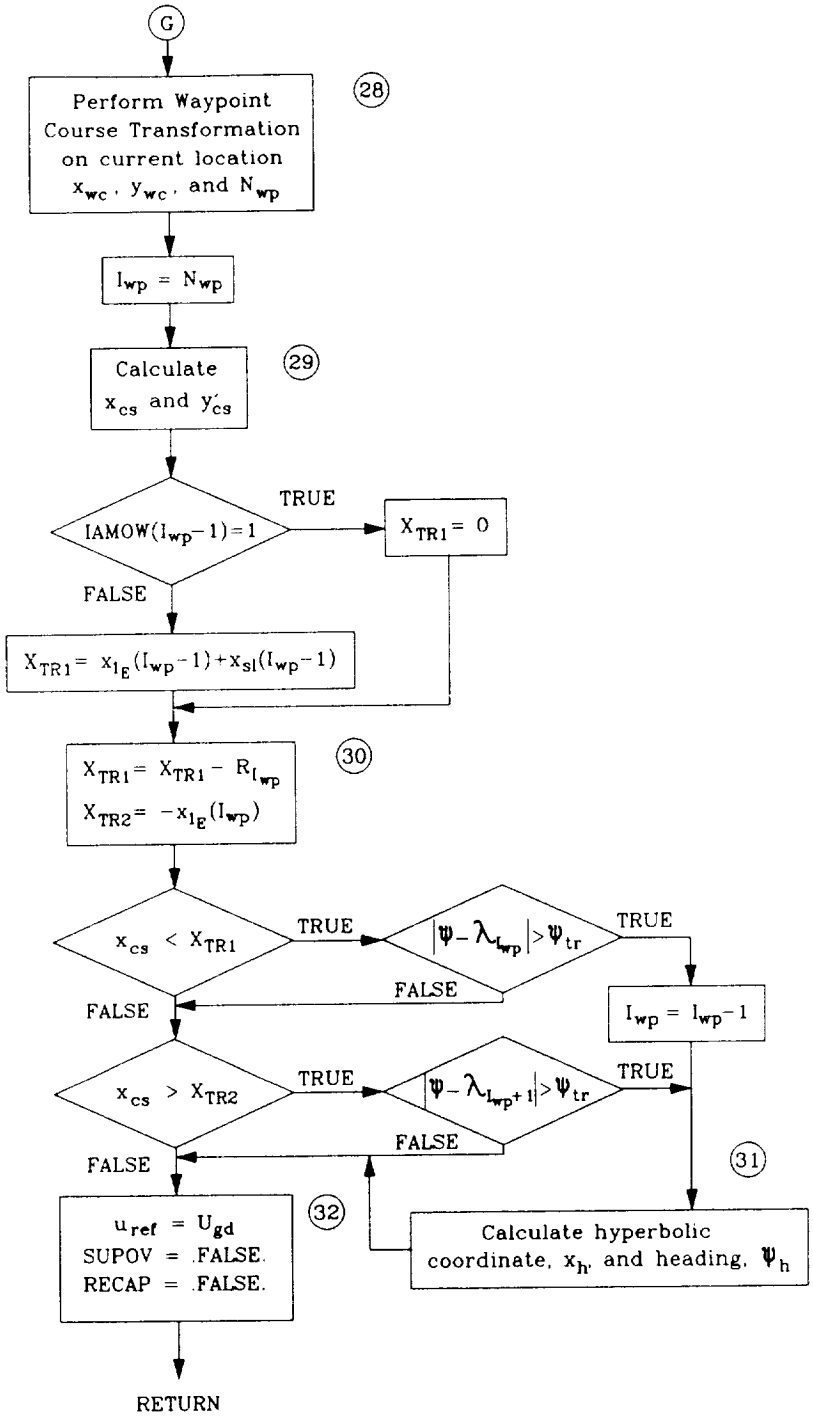

g. Re-acquisition of Preplanned Waypoint Course Following Supervisory Override

Figure 3.1 (Continued)

h. Notes (corresponding to circled numbers throughout figure)

1. INCAP is a one-way switch allowing the initial capture logic to be executed only once.

2. The distance to a particular waypoint is calculated as follows:

$$T_m = \sqrt{(x_{EA} - x_{wp}(I_{wp}))^2 + (y_{EA} - y_{wp}(I_{wp}))^2}$$

3. The gaming area course transformation described in Section 2.2.1 is used to transform the waypoint locations into gaming area course coordinates.

4. The distance along the gaming area course of the rotorcraft and the waypoint in question is compared. Only waypoints further along the gaming area course are considered for recapture. Also, the waypoint in question must be a minimum distance from the rotorcraft at the time of recapture.

5. The distance to the waypoint in question is compared to the previous minimum observed. In this way, the nearest waypoint to the rotorcraft is selected as the recapture waypoint.

6. The locations of the temporary waypoints are defined as follows:

$$x_{wp}(N) = x_{EA}$$

$$y_{wp}(N) = y_{EA}$$

$$x_{wp}(N+1) = x_{EA} + T'_{min}\cos\psi$$

$$y_{wp}(N+1) = y_{EA} + T'_{min}\sin\psi$$

7. The length of the temporary waypoint legs are stored in an array separate from that of the lengths of the planned waypoint course legs. This is necessary, because the original waypoint leg lengths are required in order to determine the proper distance along the modified waypoint course (see Note 24). This added step is unnecessary in the case of the heading of the temporary waypoint legs. These lengths and headings are calculated as follows:

$$R'_{I_{wp}-1} = \sqrt{(x_{wp}(I_{wp}) - x_{wp}(I_{wp}-1))^2 + (y_{wp}(I_{wp}) - y_{wp}(I_{wp}-1))^2}$$

Figure 3.1 (Continued)

h. Notes (Continued)

$$\lambda_{I_{wp}-1} = \tan^{-1}\left(\frac{y_{wp}(I_{wp}) - y_{wp}(I_{wp}-1)}{x_{wp}(I_{wp}) - x_{wp}(I_{wp}-1)}\right)$$

8. The temporary waypoint leg heading is modified so that the change in heading is limited to $\pm\pi$ rad. Note that the headings are calculated from the first planned waypoint leg (following the recapture waypoint) back to the first temporary waypoint leg.

9. The transition velocity is adjusted, based on the change in heading required in the hyperbolic transition. If the change in heading exceeds 70 deg, the transition velocity is 3/4 the nominal velocity; if the heading change exceeds 100 deg, the transition velocity is 1/2 the nominal velocity.

10. The transition velocity of the first temporary waypoint leg is further modified to be the lowest of the previously determined transition velocity and the current rotorcraft velocity. This prevents the automatic guidance system from speeding up initially. Also, if the rotorcraft is hovering at the time of recapture initiation, a hover transition is utilized to recapture the waypoint course.

11. For hover transitions, the anticipative distances are calculated as shown. Note that the calculation of x_{s1} differs from the previously defined expression (Section 2.1). In this case, this distance represents the approximate distance the rotorcraft will traverse in the acceleration to nominal speed following the hover transition and is used subsequently in the calculation of the minimum length for the second temporary waypoint leg.

12. The recalculation of the temporary waypoint locations in the case of a hover transition is performed as follows:

$$x_{wp}(N+1) = x_{EA}$$

$$y_{wp}(N+1) = y_{EA}$$

$$x_{wp}(N) = x_{EA} - 10\cos\psi$$

$$y_{wp}(N) = y_{EA} - 10\sin\psi$$

Figure 3.1 (Continued)

h. Notes (Continued)

Note that this definition of the temporary waypoint locations places the rotorcraft at the second temporary waypoint, even though it is still considered in the first temporary waypoint leg until it has completed the hover transition.

13. The calculation of the hyperbolic transition leg parameters is defined in Fig. 2.3, Note 9.

14. The location of the nearest possible location of the second temporary waypoint is calculated, based on the parameters of the first hyperbolic transition leg.

$$x'_{wp} = x_{wp}(N) + (x_{l_E}(N) + x_{ant}(N) + x_{sl}(N))\cos\psi$$

$$y'_{wp} = y_{wp}(N) + (x_{l_E}(N) + x_{ant}(N) + x_{sl}(N))\sin\psi$$

15. The distance between this possible second temporary waypoint and the current location is calculated as follows:

$$\Delta D_{wp} = \sqrt{(x'_{wp} - x_{wp}(N+1))^2 + (y'_{wp} - y_{wp}(N+1))^2}$$

16. If this distance is greater than a defined maximum, the location of the second temporary waypoint is re-established at the location defined as the nearest location. Note that this will altar the required heading correction at that waypoint, thus changing the first temporary waypoint hyperbolic transition leg parameters. It is necessary, therefore, to iterate until the distance between the calculated nearest possible location and the established location of the second temporary waypoint is less than the defined maximum. Since the initial capture need not take place in real time, this iteration requirement should not be a problem.

17. If the recapture waypoint was defined in the original waypoint course as a station for aggressive maneuvering while on watch, the anticipative distances are appropriately calculated.

18. If the second temporary waypoint leg is in line with the leg following the recapture waypoint, the waypoint following the recapture waypoint is considered the recapture waypoint, and the temporary waypoint specifications are recalculated.

Figure 3.1 (Continued)

h. Notes (Continued)

19. The recapture waypoint must precede the last waypoint of the course.

20. The calculation of the hyperbolic transition leg parameters is defined in Fig. 2.3, Note 9.

21. The minimum length of the second temporary waypoint leg is defined as the exit distance of the hyperbolic transition onto the leg added to the entrance distance of the hyperbolic transition onto the next waypoint leg.

22. If the second temporary waypoint leg is shorter than the required length defined above, the recapture waypoint index is incremented, and the temporary waypoint specifications are recalculated.

23. Because the distance along the waypoint course is required in the obstacle detection and avoidance maneuver selection logic, the original distance along the waypoint course to the recapture waypoint is calculated. All of the lengths of the waypoint legs that are indexed less than the recapture waypoint leg are also set to zero.

24. An imaginary waypoint leg is then considered leading up to the first temporary waypoint leg. The length of this imaginary waypoint leg is adjusted such that the sum of this length, along with the lengths of the two temporary waypoint legs, is equal to the original distance along the course up to the recapture waypoint. As will be seen in the waypoint course transformation, the waypoint course coordinates following the recapture waypoint leg will be unaffected by the waypoint course modification defined herein.

25. The aggressive maneuvering counter must also account for the exclusion of the waypoints preceding the temporary waypoints. It is incremented for each station for aggressive maneuvering that is bypassed by this waypoint course modification.

26. If a hover transition is to be used in the recapture of the waypoint course (Note 10), 1 is subtracted from the aggressive maneuvering counter, and aggressive maneuvering specifications indexed to this counter value are set to perform the hover transition.

27. The current longitudinal velocity command is defined as the current inertial longitudinal velocity.

28. For the second mode of automatic guidance recapture, the current waypoint course leg is determined using the waypoint course transformation algorithm defined in Section 4.1.

Figure 3.1 (Continued)

h. Notes (Concluded)

29. The along-course distance to the next waypoint and the lateral offset from the current waypoint leg are calculated as follows:

$$x_{cs} = (x_{EA} - x_{wp}(I_{wp}+1))\cos(\lambda_{I_{wp}}) + (y_{EA} - y_{wp}(I_{wp}+1))\sin(\lambda_{I_{wp}})$$

$$y'_{cs} = -(x_{EA} - x_{wp}(I_{wp}+1))\sin(\lambda_{I_{wp}}) + (y_{EA} - y_{wp}(I_{wp}+1))\cos(\lambda_{I_{wp}})$$

30. The entrance and exit transition distances are calculated in order to determine if the current location is in a transition region.

31. If the current location is within a hyperbolic transition region, the current hyperbolic transition coordinates are calculated as follows:

$$\psi_h = \psi - \lambda_{I_{wp}} - \alpha_{I_{wp}}$$

$$x_h = \frac{a^2(I_{wp})\tan(\psi_h)}{\sqrt{b^2(I_{wp}) - a^2(I_{wp})\tan^2(\psi_h)}}$$

32. The recapture and supervisory override logical switches are toggled to FALSE following the pass through the recapture algorithm.

Figure 3.1 (Concluded)

TABLE 3.1

PARAMETER VALUES FOR THE AUTOMATIC GUIDANCE RECAPTURE ALGORITHM

T_{min}	Minimum distance to recapture waypoint	250 ft
T'_{min}	Initial length of first temporary waypoint leg	200 ft
ΔD_{max}	Maximum change in length of first waypoint leg from previous iteration	5 ft
ψ_{tr}	Threshold heading error to be considered in hyperbolic transition leg	5 deg

4. OBSTACLE DETECTION AND AVOIDANCE MANEUVER SELECTION LOGIC

In an automatically-piloted vehicle flying in nap-of-the-earth (NOE) conditions along a prescribed course, provisions must be made for unexpected obstacle avoidance. To this end, obstacle detection and avoidance logic has been developed for the automatic guidance system defined herein. This logic invokes, as necessary, one or more rapid response avoidance maneuvers from among the several defined in Section 3.1.

4.1 Waypoint Course Coordinate Transformation

The first step of the obstacle detection and avoidance maneuver selection logic is to transform the current rotorcraft inertial position into waypoint course coordinates. This process is similar to the transformation into gaming area course coordinates described in Section 2.2.1. This transformation is required to ensure that the along-course anticipative array defined in the next section is aligned with the waypoint course. Figure 4.1 presents a flow diagram of the waypoint course transformation procedure with the parameters defined previously in Section 2 and in Table 4.1.

Inputs:	Waypoint course specifications	
	Number of waypoints	n_{wps}
	Waypoint locations	$x_{wp}(I_{wp})$ and $y_{wp}(I_{wp})$
	Waypoint leg headings	$\lambda_{I_{wp}}$
	Waypoint leg lengths	$R_{I_{wp}}$
	Longitudinal and latitudinal coordinates of current rotorcraft location	x_{EA} and y_{EA}
	Northerly and Easterly inertial velocity components	V_N and V_E
Outputs:	Waypoint course coordinates	x_{pp} and y_{pp}
	Waypoint course resolved velocity components	V_x and V_y

a. Inputs and Outputs

Figure 4.1 Flow Diagram for Waypoint Course Coordinate Transformation

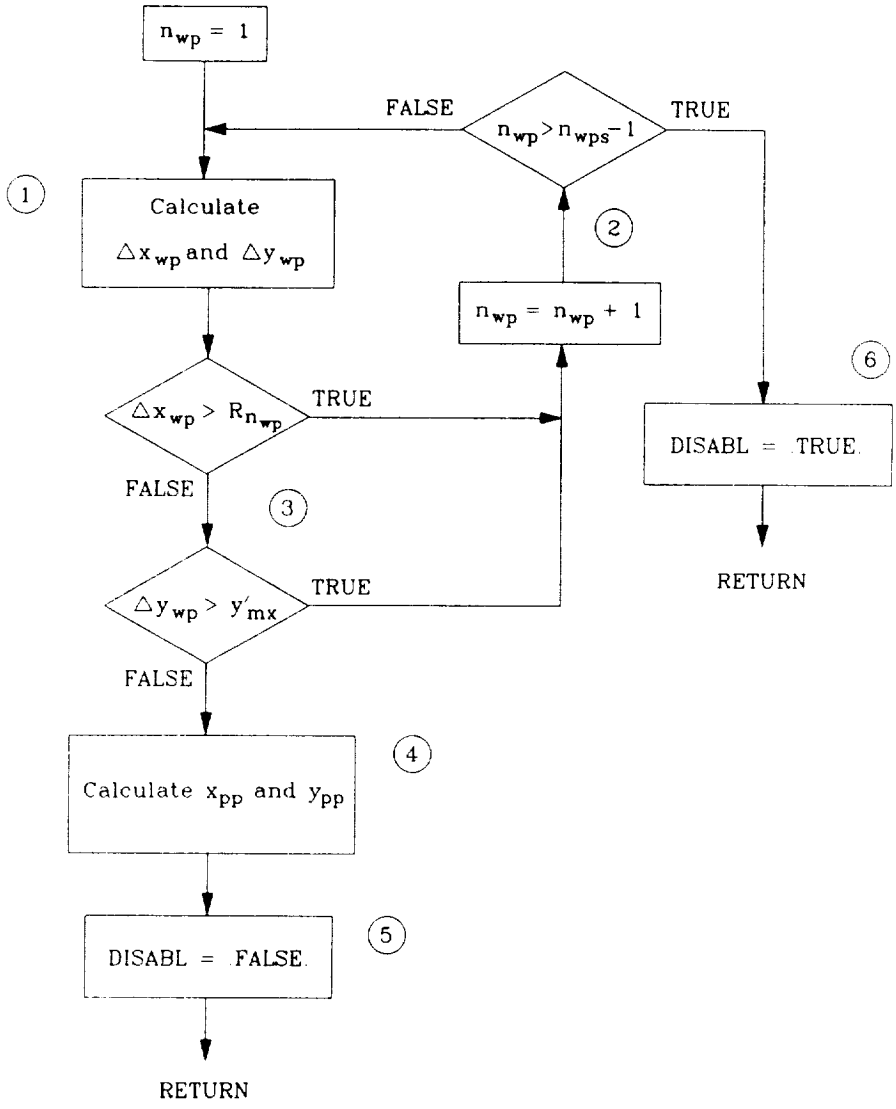

b. Waypoint Course Coordinate Transformation

Figure 4.1 (Continued)

c. Notes (corresponding to circled numbers throughout figure)

1. The incremental distance from the previous waypoint is calculated as follows:

$$\Delta x_e = x_{EA} - x_{wp}(n_{wp})$$

$$\Delta y_e = y_{EA} - y_{wp}(n_{wp})$$

$$\begin{bmatrix} \Delta x_c \\ \Delta y_c \end{bmatrix} = \begin{bmatrix} \cos\lambda_{n_{wp}} & \sin\lambda_{n_{wp}} \\ -\sin\lambda_{n_{wp}} & \cos\lambda_{n_{wp}} \end{bmatrix} \begin{bmatrix} \Delta x_e \\ \Delta y_e \end{bmatrix}$$

$$\Delta x_{wp} = R_{n_{wp}} \left(\frac{\Delta y_c \tan\alpha_{n_{wp}-1} + \Delta x_c}{\Delta y_c(\tan\alpha_{n_{wp}-1} + \tan\alpha_{n_{wp}}) + R_{n_{wp}}} \right)$$

$$\Delta y_{wp} = \Delta y_c$$

where

$$\alpha_{n_{wp}-1} = \frac{1}{2}(\lambda_{n_{wp}-1} - \lambda_{n_{wp}})$$

2. The stated criteria are used to determine if the candidate waypoint leg is indeed the current waypoint leg.

3. Each waypoint is tested as a candidate for the previous waypoint until the correct waypoint is identified or all of the waypoints are exhausted. The previous waypoint index, once identified, will correspond to the index of the current waypoint leg.

4. Once the correct waypoint leg has been identified, the transformation is completed as follows:

$$x_{pp} = \sum_{l_{wp}-1}^{n_{wp}-1} R_{l_{wp}} + \Delta x_{wp}$$

$$y_{pp} = \Delta y_{wp}$$

Figure 4.1 (Continued)

c. Notes (Concluded)

5. The automatic guidance recapture/disable switch is set to false.

6. If none of the waypoints satisfy the criteria as the index of the current waypoint leg, the automatic guidance recapture function is disabled by setting the logical flag DISABL to .TRUE..

Figure 4.1 (Concluded)

TABLE 4.1

PARAMETER VALUES FOR THE WAYPOINT COURSE COORDINATE TRANSFORMATION

y'_{mx}	Maximum deviation allowed from the waypoint course	328.08 ft (10 dm)

4.2 Obstacle Detection and Avoidance Maneuver Selection Logic

Obstacle detection and avoidance while following the flight plan depends on the correlation of acquired knowledge from the sensed environment with the forehand knowledge of the recorded environment (i.e., terrain, obstacles, threats, and targets) and the accessing of that correlated knowledge for the purpose of guidance. The correlation procedure to be demonstrated herein is performed in the along-course[1] coordinates. Similar logic could be extended to across-course coordinates. The correlation is provided in a continuous sense using an approximation of the terrain between points from the digital DMA terrain data base. Threats are represented in terms of a threat exposure height function of course coordinates. The "obstacles" are sensed by interrogating a given region for the presence of non-conformity of the observed terrain, cultural features, and threats to the terrain approximation or threat exposure height function. To simulate the sensing of these non-conformities, obstacle arrays are defined that contain the locations and dimensions of obstacles in waypoint course coordinates. These arrays are interrogated to determine the presence of obstacles in a given location. The obstacles are characterized by height increments either rising above the terrain height profile or descending below the threat exposure height profile.

A prerequisite for using the forward- and sideward-looking sensed data base to update the flight plan in real time is an independent (navigation) reference system with prescribed uncertainty that is common to the reference system of the preflight stored geodetic and cultural data base. A typical example of such a system would be an inertial system updated by a global positioning system.

Figure 4.2 illustrates a procedural flow diagram for updating and modifying the stored guidance command flight profiles in real time to provide avoidance of unexpected obstacles. Two data bases having a common navigational reference system (which provides the state vector $\underline{X}$) are identified at the top of the diagram: the stored flight profiles (vector $\underline{R}_n$) at the upper left and the sensed profiles of terrain, obstacles, and threats, together with offset bias requirements for safety, at the upper right (vector $\hat{\underline{R}}_n$).

1 For the purposes of this discussion, the terms "along-course" and "across-course" refer to the rotorcraft total velocity direction relative to the pre-planned flight profile. In the nominal case, if the rotorcraft is following the pre-planned flight profile, the across-course velocity is zero.

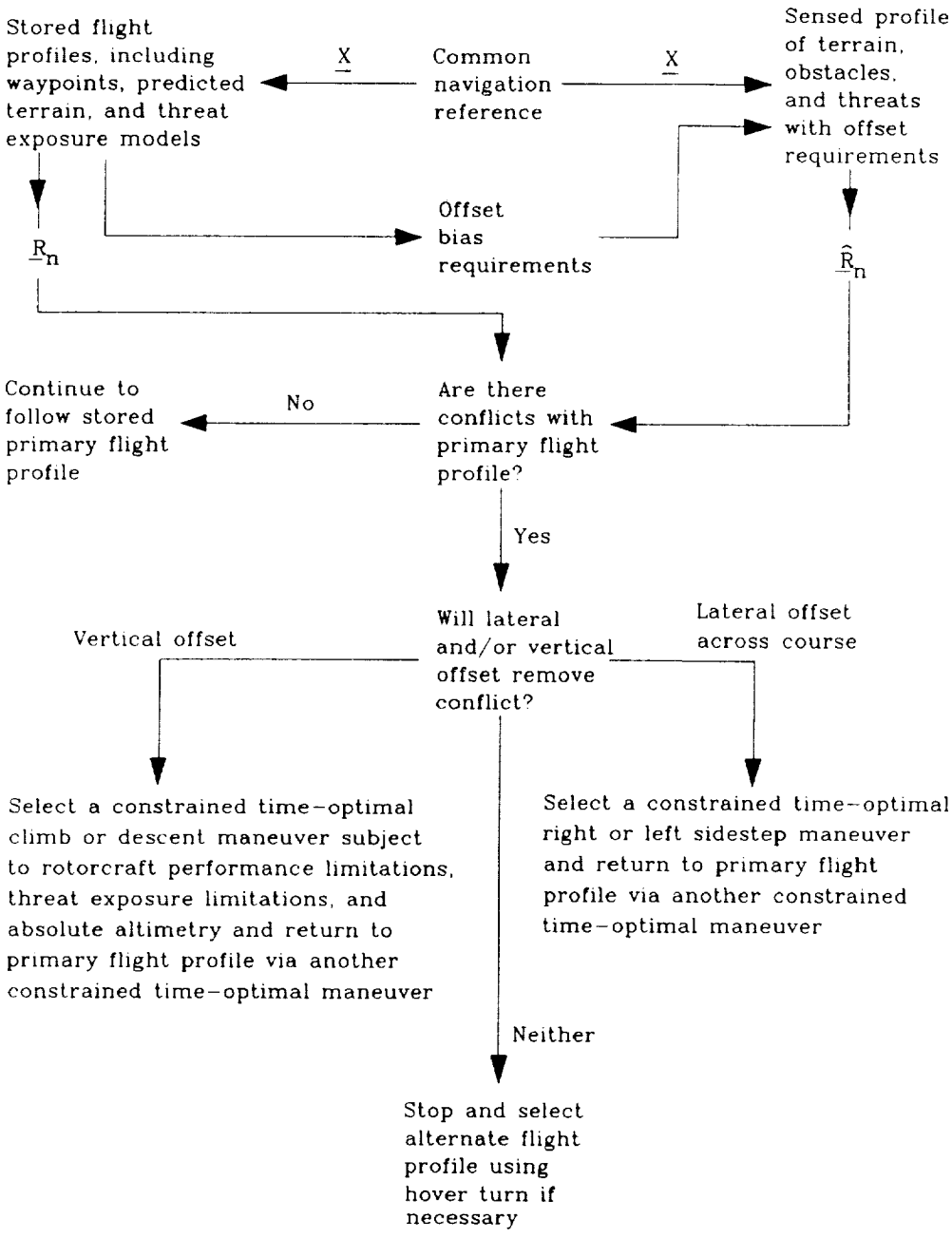

Figure 4.2 Procedural Flow Diagram for Avoidance of Unexpected Obstacles Encountered in the Along-Course Anticipative Array (Combined vertical and lateral maneuvers are possible)

In principle, it is necessary to compare $\underline{\hat{R}}_n$ with $\underline{R}_n$ in real time, resolve any conflicts with the planned flight profile by automatically selecting a combination of lateral and vertical evasive maneuvers, and return to the planned flight profile where possible. If no combination of lateral and vertical evasive maneuvers will remove a conflict between $\underline{\hat{R}}_n$ and $\underline{R}_n$, the rotorcraft is commanded to stop and let the pilot select another flight plan. Figure 4.3 presents a flow diagram of the obstacle detection and avoidance maneuver selection logic with the required parameters defined in Table 4.2. A thorough verbal description of the logic is presented in Appendix E.

Inputs:	Waypoint course coordinates	x_{pp} and y_{pp}
	Waypoint course resolved velocity components	V_x and V_y
	Defined obstacle arrays	$x_{obs}(I_{obs})$, $y_{obs}(I_{obs})$, $w_{obs}(I_{obs})$, and $h_{obs}(I_{obs})$
Outputs:	Lateral offset command	y_{com}
	Vertical offset command	h_{com}
	Forward velocity command	VXCOM

a. Inputs and Outputs

Figure 4.3 Flow Diagram for Obstacle Detection and Avoidance Maneuver Selection

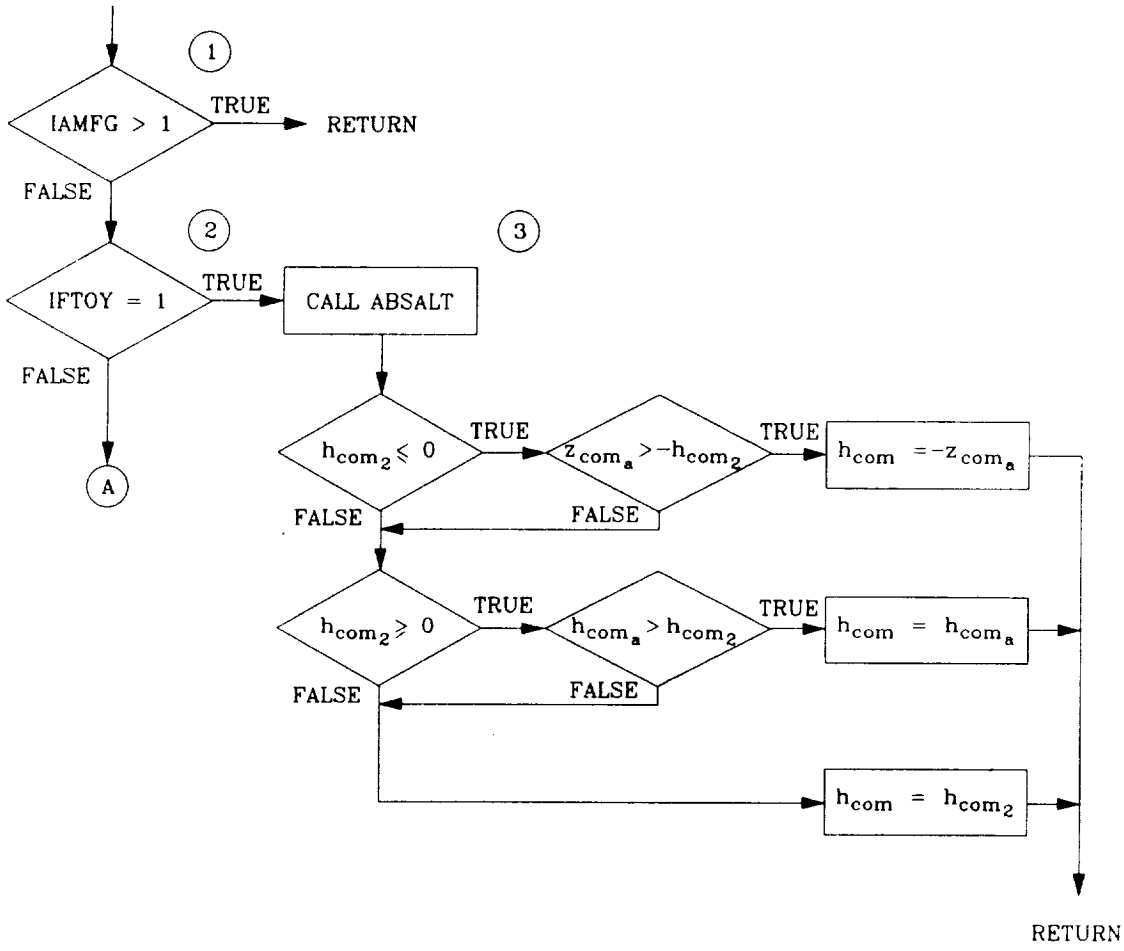

b. Bypass Avoidance Logic During Aggressive Maneuver

Figure 4.3 (Continued)

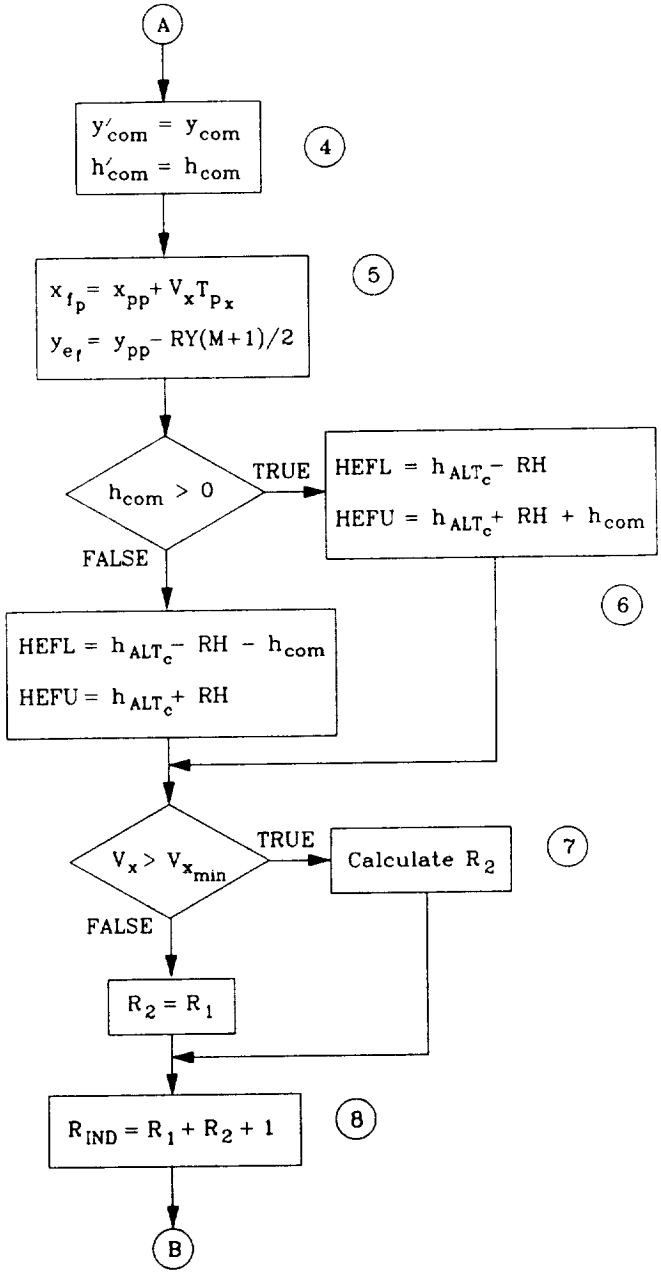

c. Define Anticipative Array

Figure 4.3 (Continued)

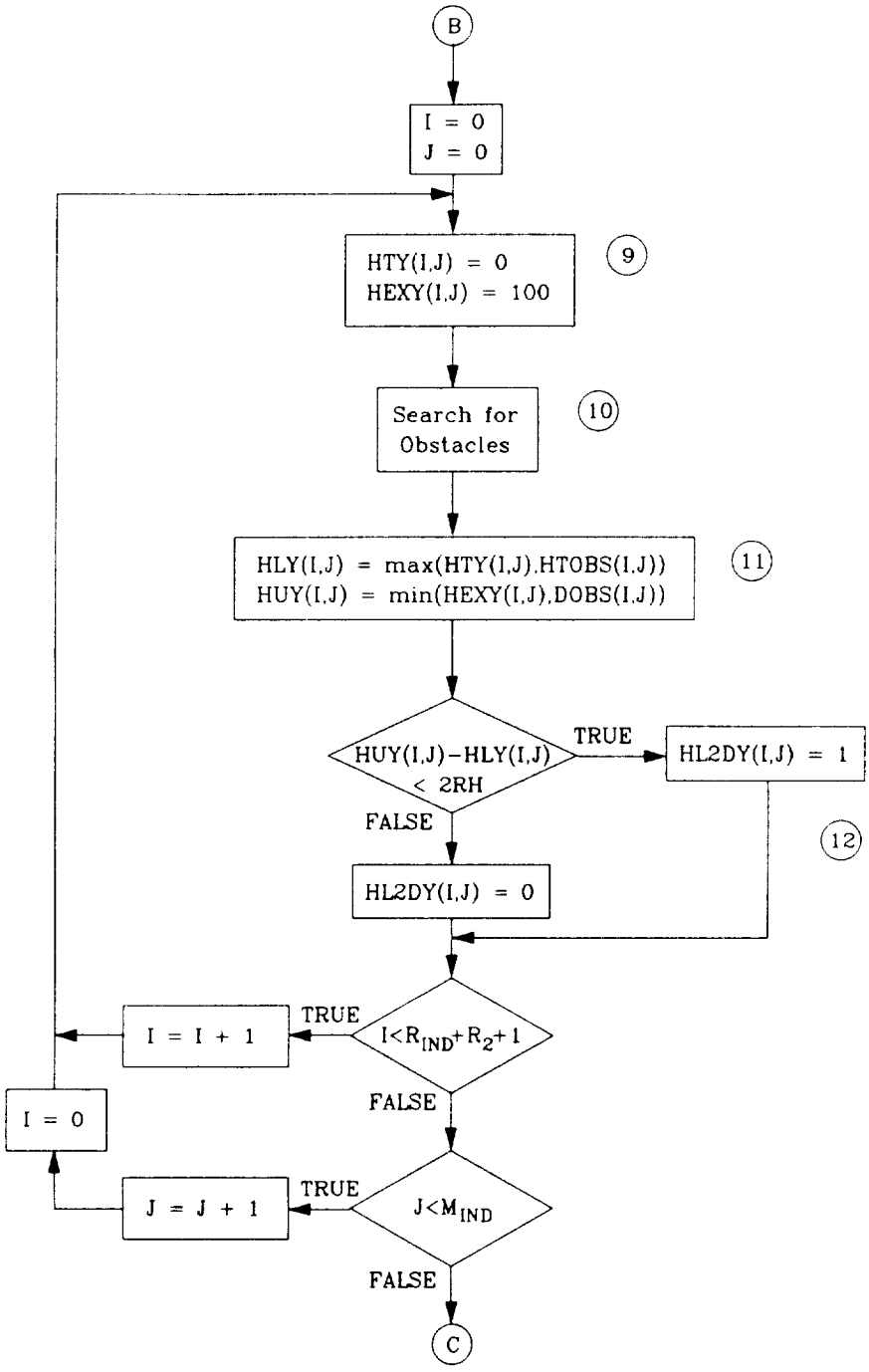

d. Search Anticipative Array for Obstacles

Figure 4.3 (Continued)

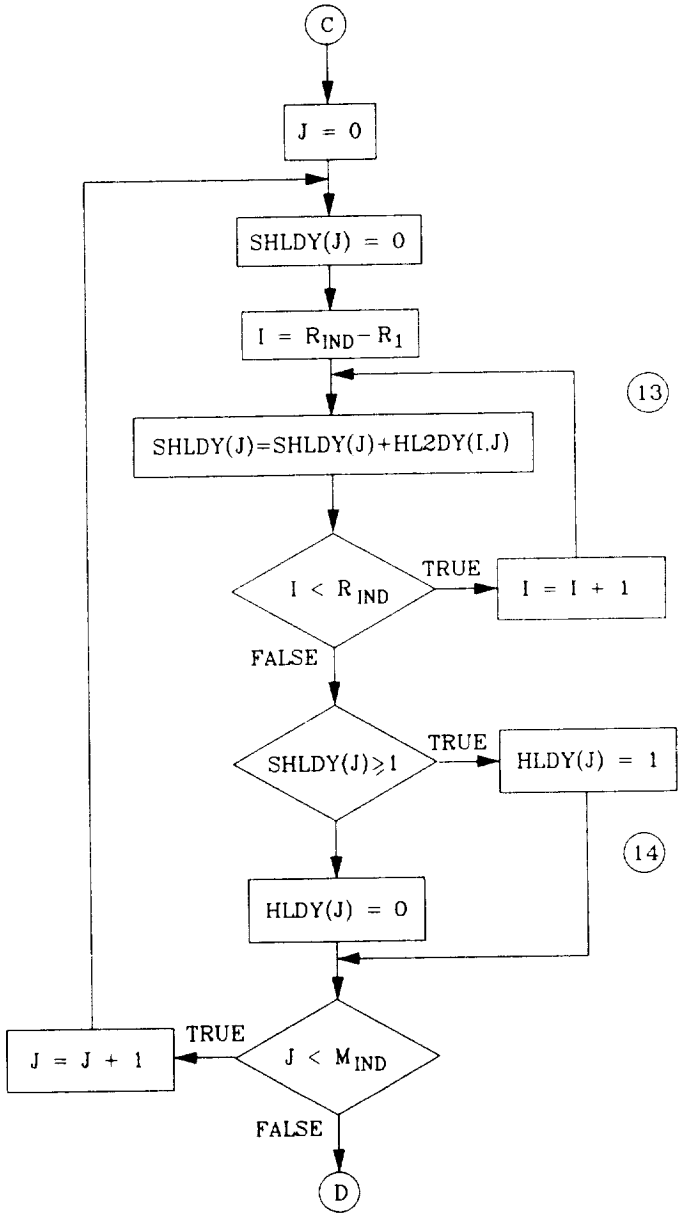

e. Identify Obstructions in the Flight Path

Figure 4.3 (Continued)

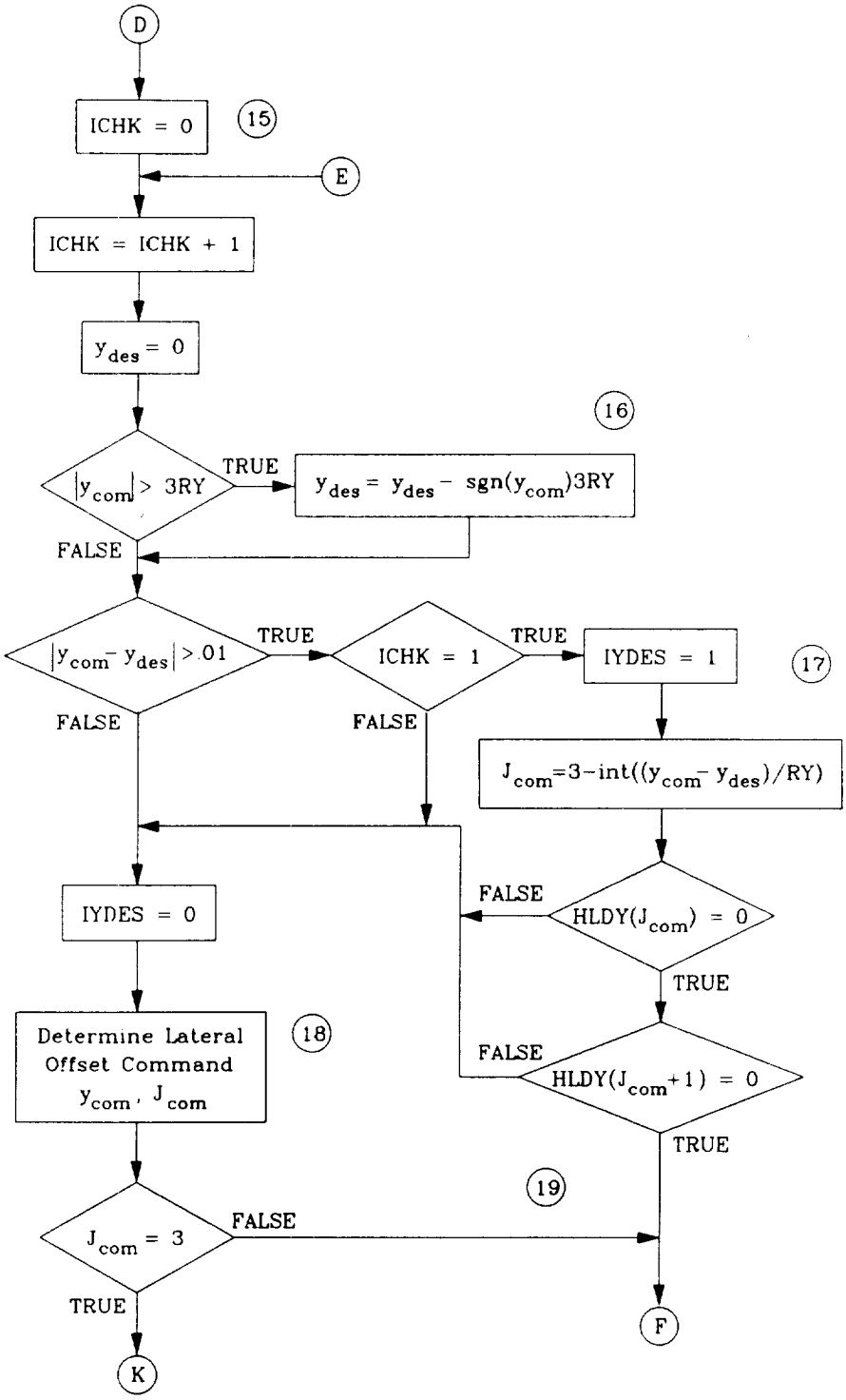

f. Determine Necessary Lateral Offset Command (Section 1)

Figure 4.3 (Continued)

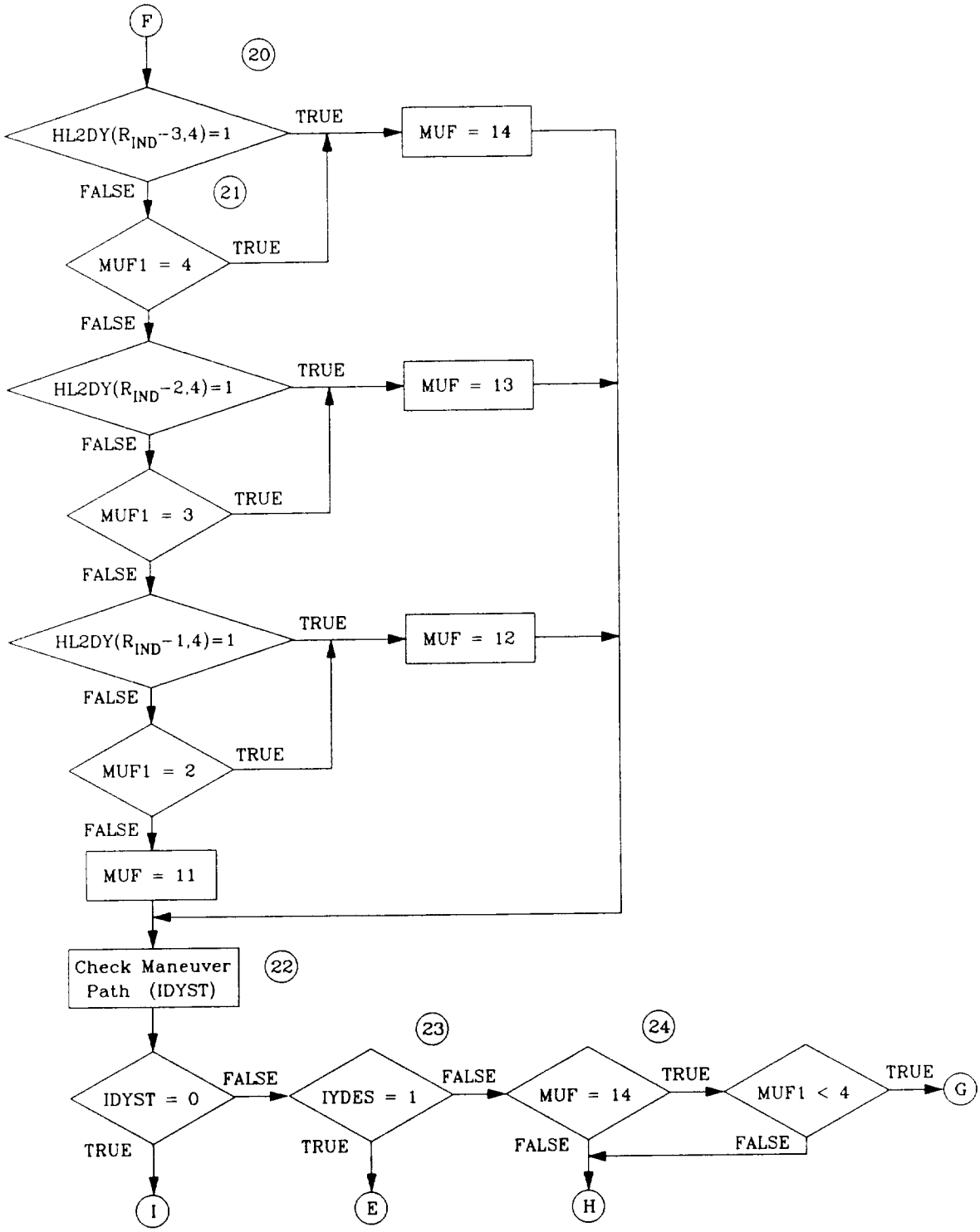

g. Check Proposed Maneuver Path (Sections 3 and 4)

Figure 4.3 (Continued)

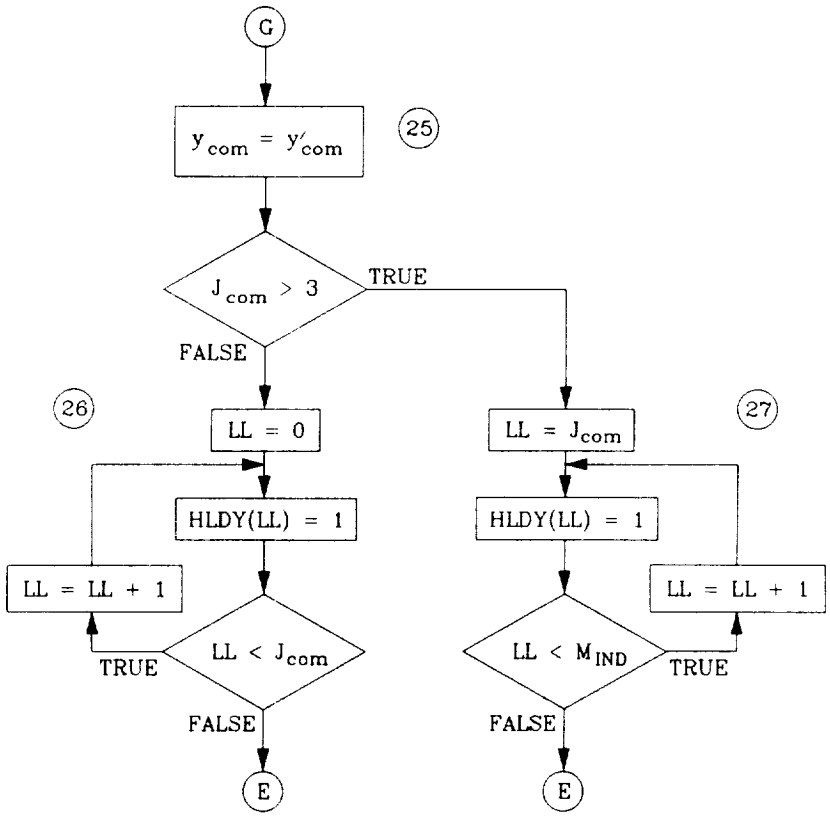

h. Choose Alternate Lateral Evasive Maneuver

Figure 4.3 (Continued)

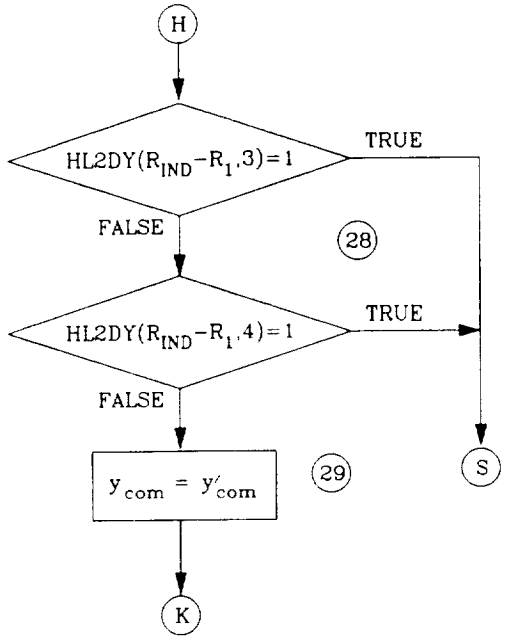

i. Continue without Evasive Action

Figure 4.3 (Continued)

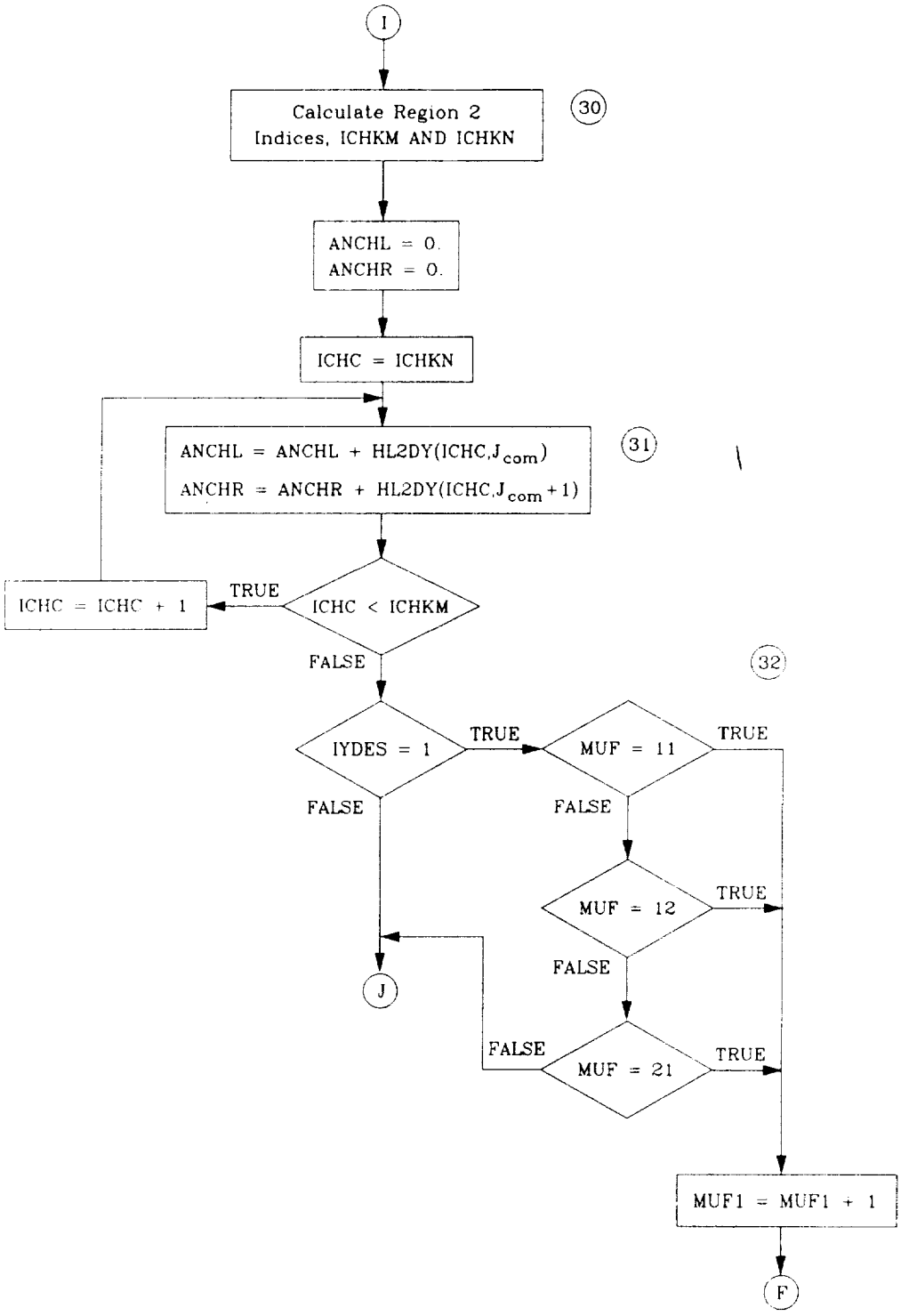

j. Check Destination Path (Section 2)

Figure 4.3 (Continued)

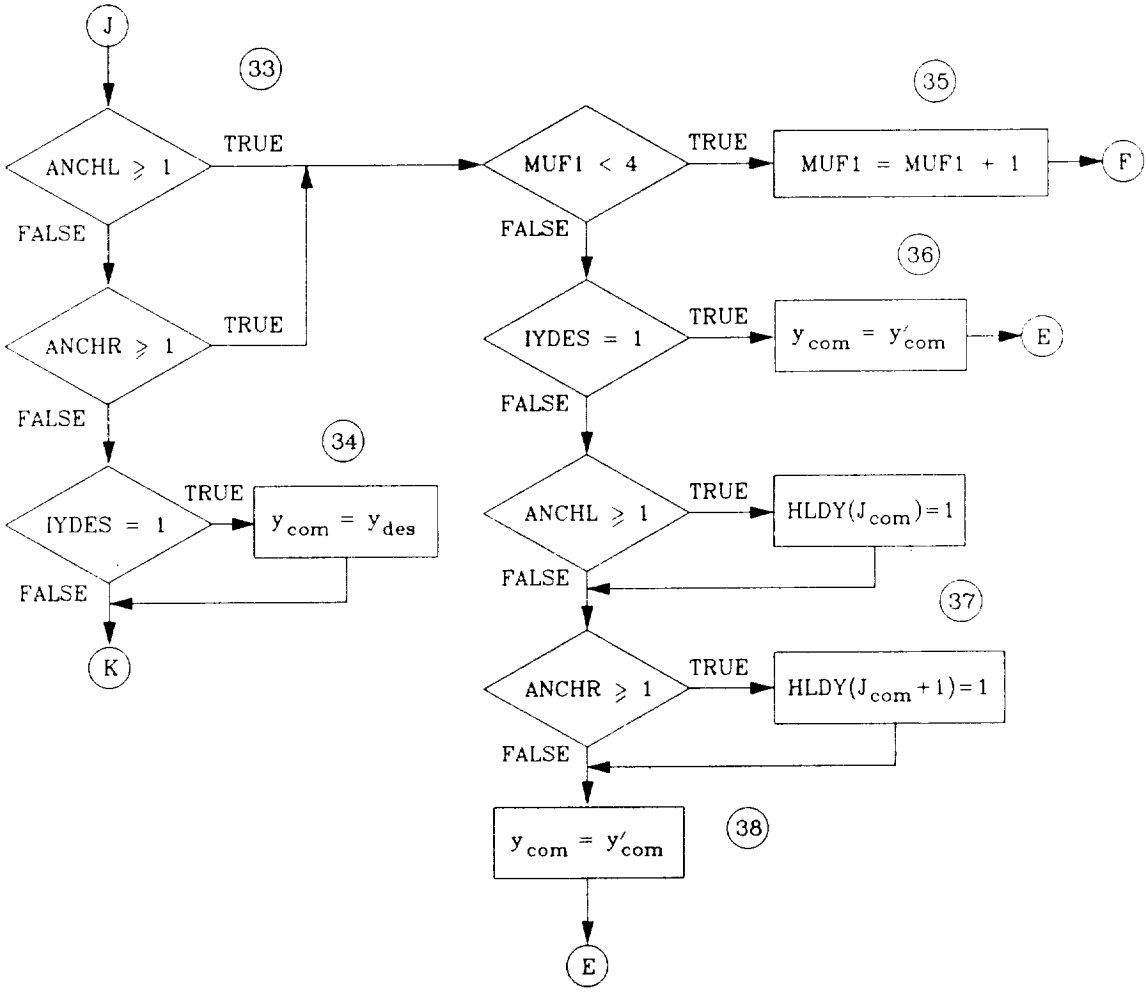

k. Choose Alternate Lateral Evasive Maneuver

Figure 4.3 (Continued)

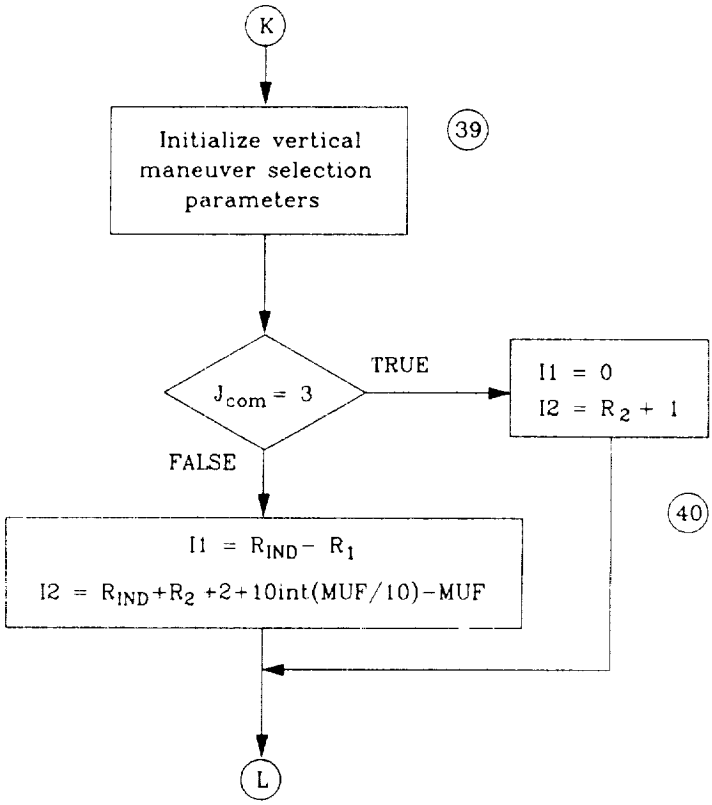

1. Begin Vertical Situation Analysis

Figure 4.3 (Continued)

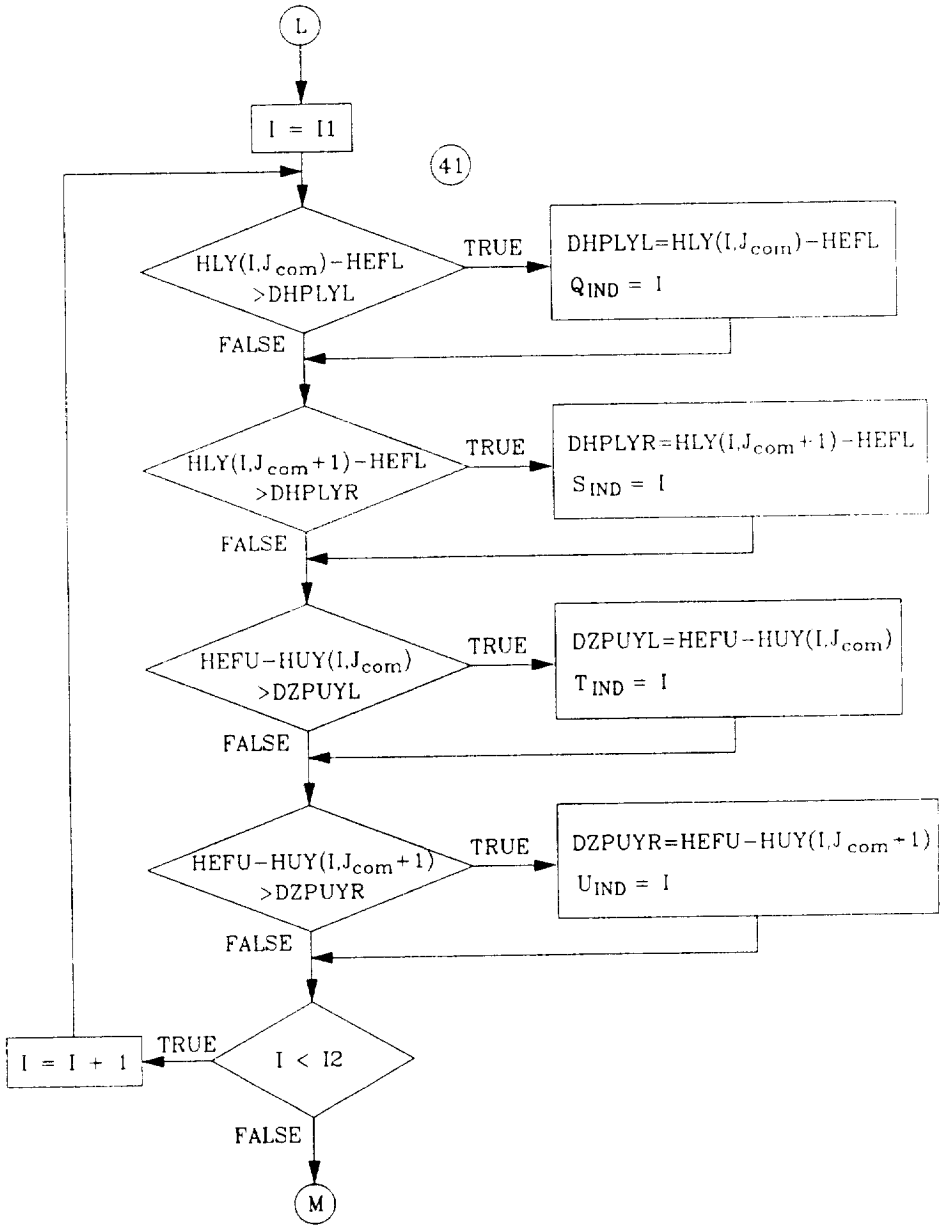

m. Search Vertical Determination Area of Anticipative Array

Figure 4.3 (Continued)

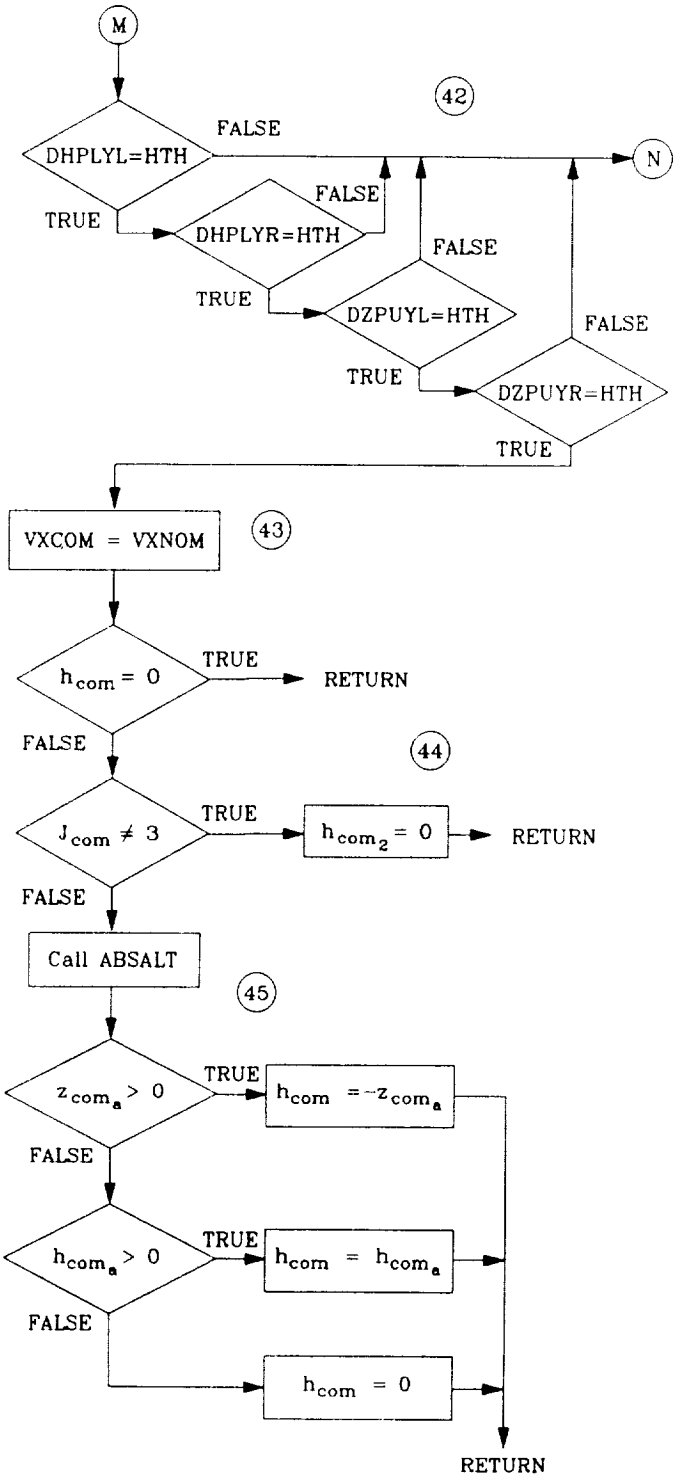

n. Set Vertical Offset Command to Zero

Figure 4.3 (Continued)

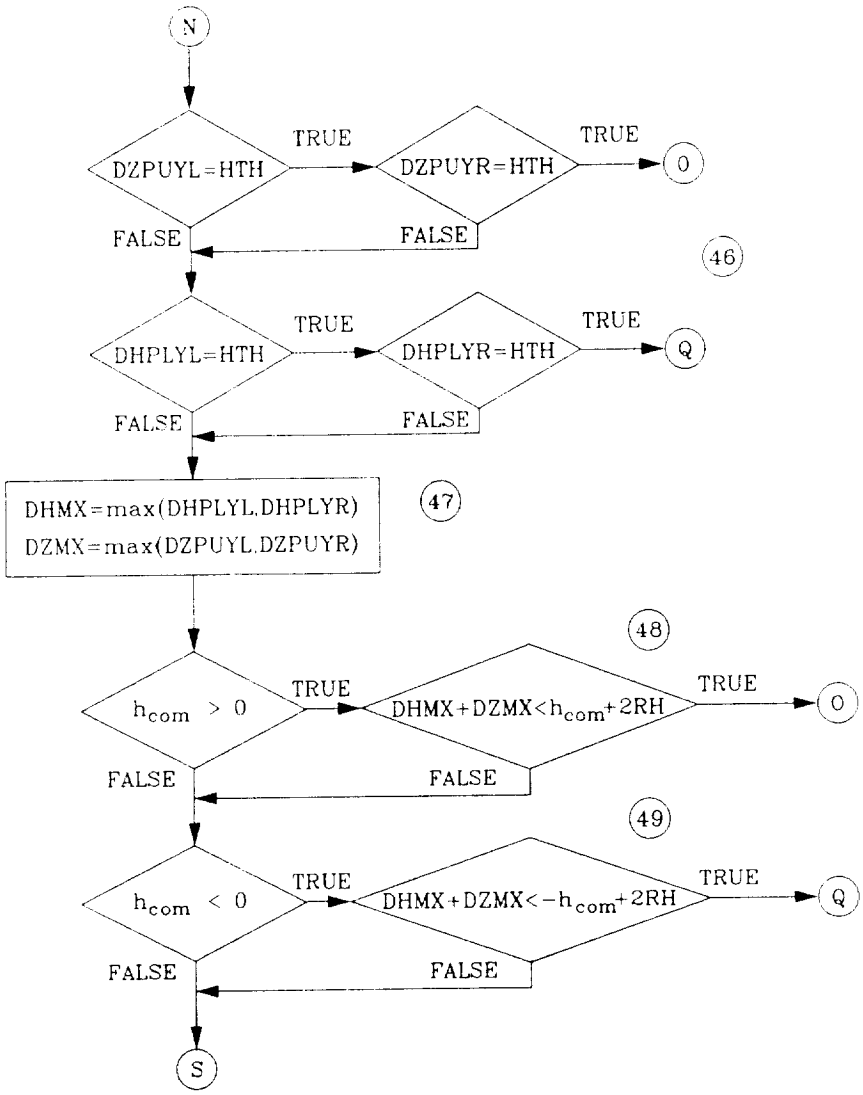

o. Determine if a Climb or Descent will Avoid Detected Obstacle

Figure 4.3 (Continued)

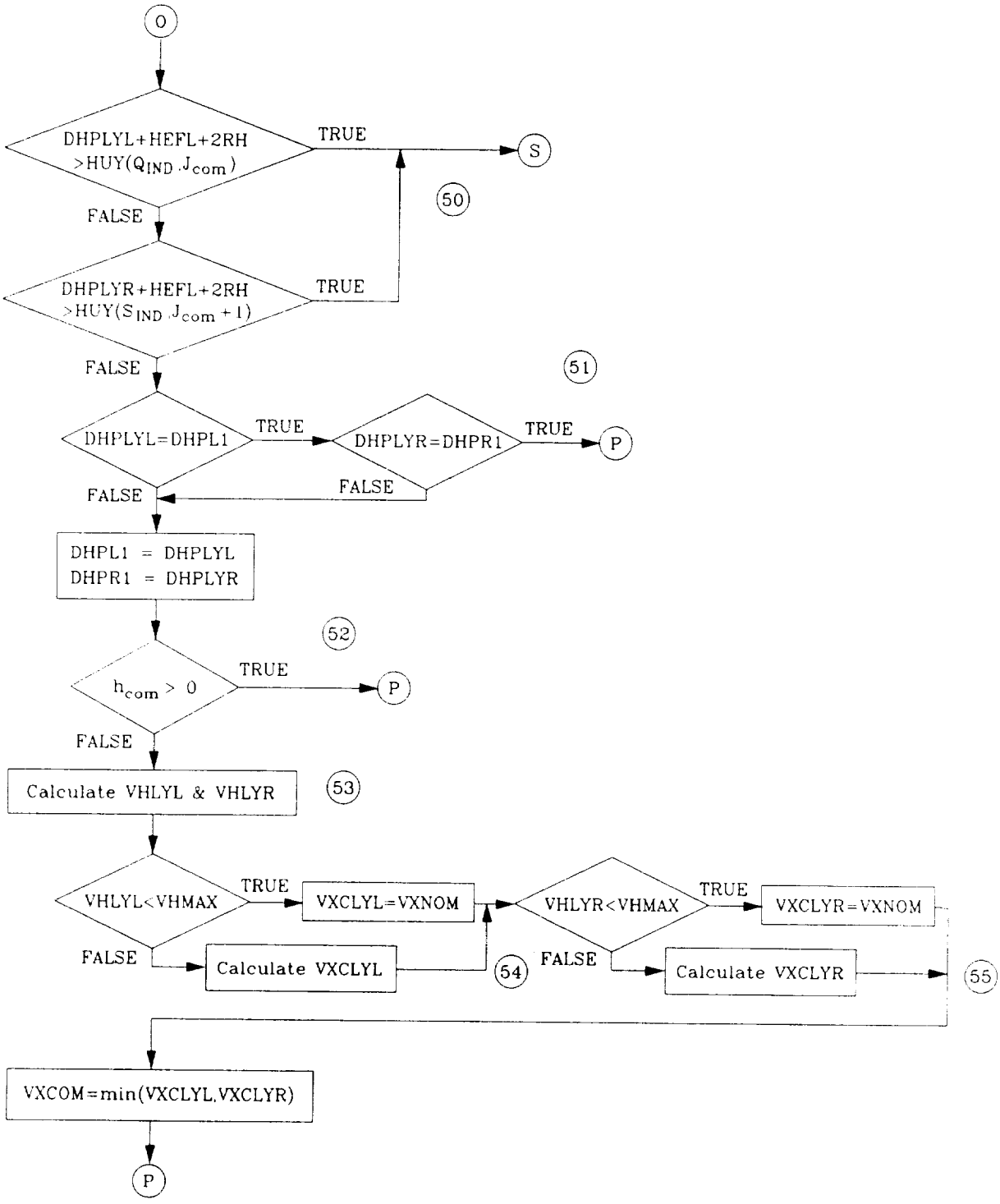

p. Climb Along course

Figure 4.3 (Continued)

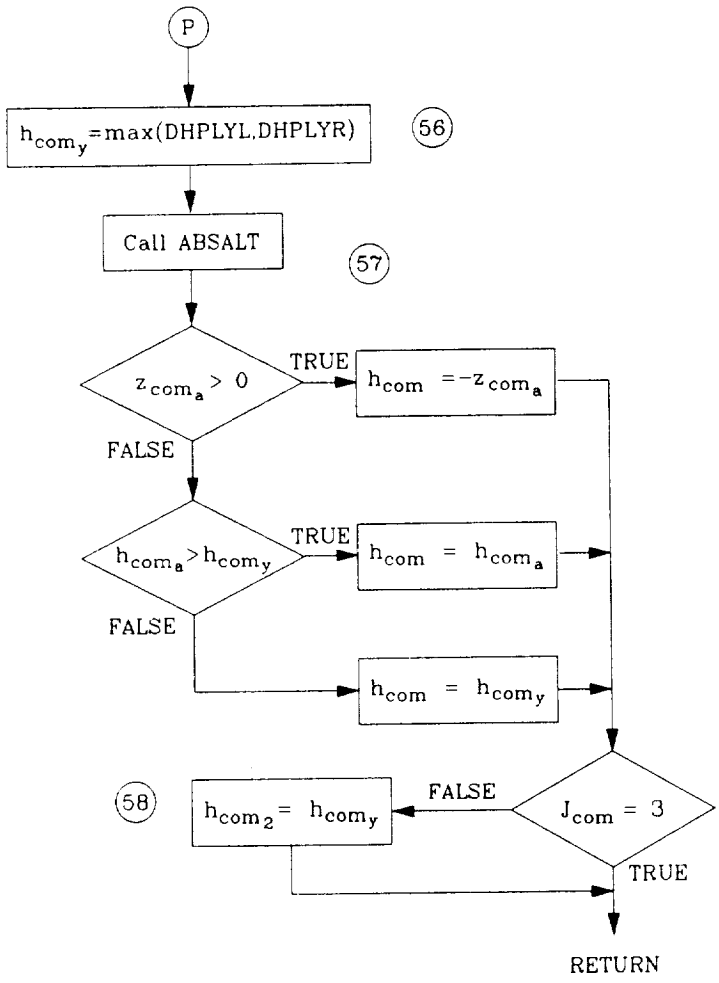

p. Climb Along course (Concluded)

Figure 4.3 (Continued)

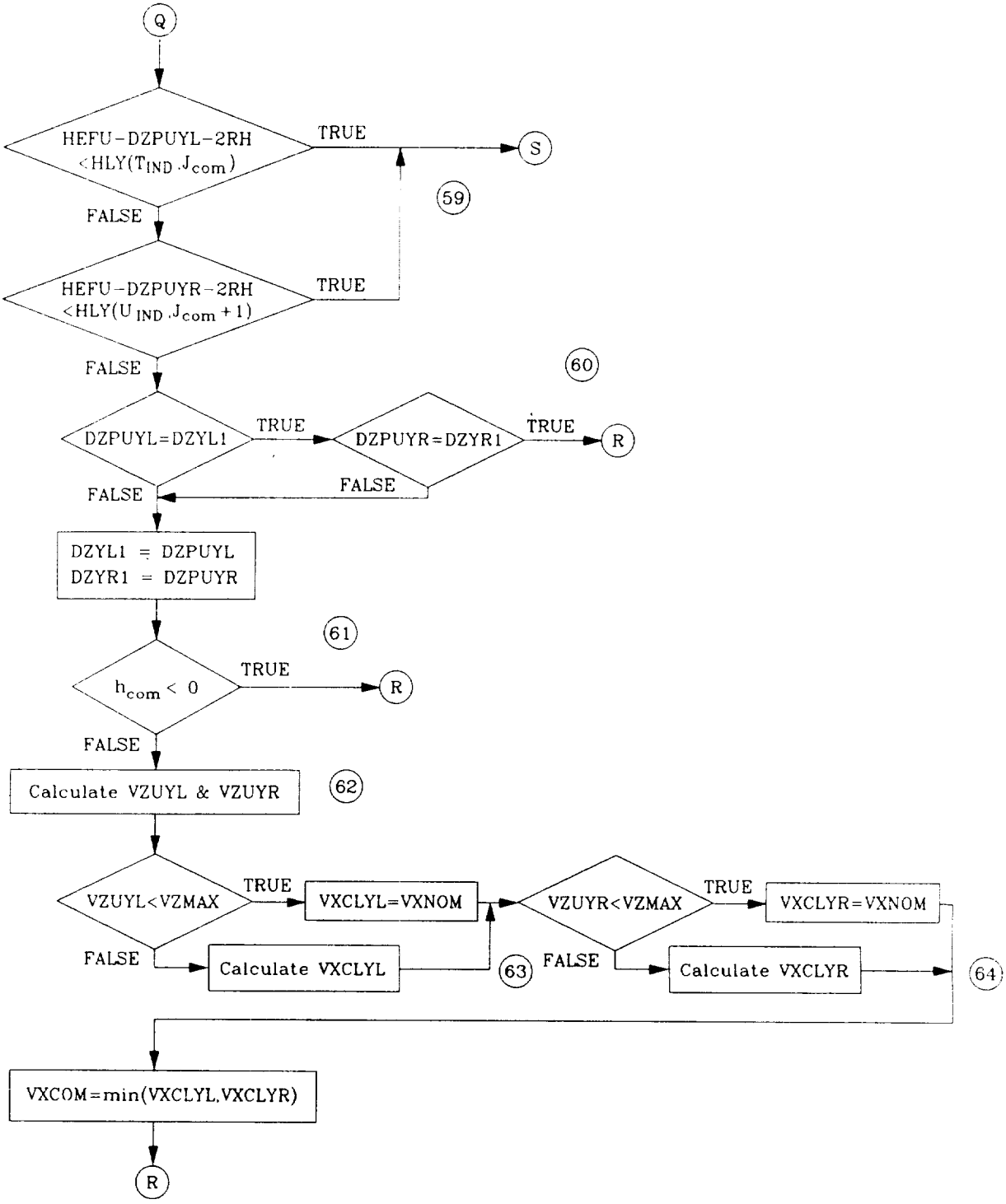

q. Descend Along course

Figure 4.3 (Continued)

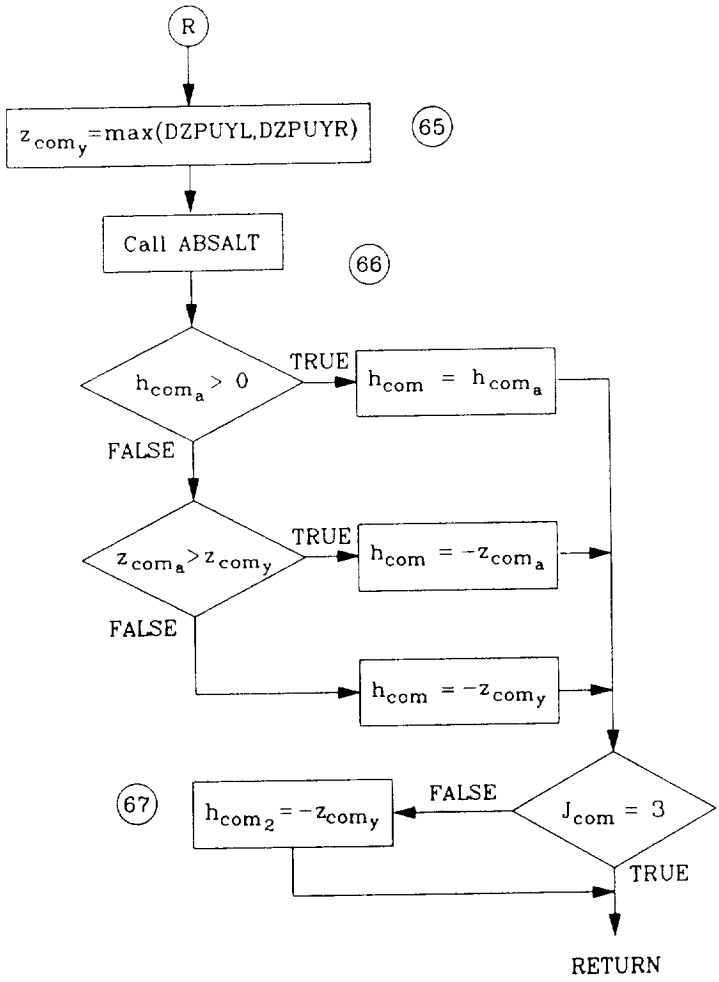

q. Descend Along course (Concluded)

Figure 4.3 (Continued)

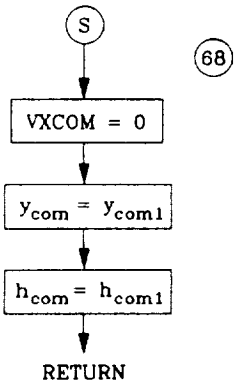

r. Stop Rotorcraft

Figure 4.3 (Continued)

s. Notes (corresponding to circled numbers throughout figure)

1. If the rotorcraft is decelerating to a hover at a waypoint designating aggressive maneuvering while on watch, the obstacle detection logic is bypassed.

2. If the rotorcraft is in the process of performing a lateral evasive maneuver (i.e., constrained time-optimal lateral sidestep), all of the obstacle detection and avoidance maneuver selection logic except the absolute altimetry is bypassed. The length of the safety margin envelope (Fig. 4.4) for this case is doubled.

3. ABSALT is the absolute altimetry subroutine that analyses the immediate vicinity of the rotorcraft to prevent any penetrations of the safety margin envelope (Fig. 4.4) by obstacles. A flow diagram for this subroutine is presented in Fig. 4.5.

4. The initial commands upon entering the obstacle detection and avoidance maneuver selection logic are defined.

5. x_{f_p} and y_{e_f} define the reference point of the along-course anticipative array (see Fig. 4.5).

6. HEFL and HEFU define the vertical locations of the along-course anticipative array (see Fig. 4.7).

7. The value of R2 (defined in Fig. 4.6) is calculated as follows:

$$R_2 = R_1 + \mathrm{INT}\left(\frac{6(V_x - V_{x_{min}})}{RX}\right)$$

8. R_{IND} is the row index of the last row of Section 1 (Fig. 4.6).

9. For the purposes of this simulation, the terrain height under a given cell of the anticipative array is taken to be equal to the approximate terrain height as defined in Section 2.2. Additionally, the threat exposure height will be assumed as a constant height above the terrain corresponding to the average tree along the course.

10. The obstacle search algorithm is defined in the flow diagram presented in Fig. 4.8. Returning from this algorithm are HTOBS(I,J) and DOBS(I,J), the adjusted passable height and threat exposure height due to detected obstacles and threats.

Figure 4.3 (Continued)

s. Notes (Continued)

11. The lower (HLY(I,J)) and upper (HUY(I,J)) navigable heights are determined for the given cell.

12. If the vertical distance between these limits is less than the height of the safety margin envelop (Fig. 4.4), an obstruction is said to exist in that cell.

13. All obstructed cells in a given column of Section 1 of the anticipative array are accounted for.

14. If any obstructions exist in the given column, that column is said to be obstructed.

15. It is desired that the rotorcraft return when possible to the preplanned flight path following a lateral evasive maneuver. Until a clear return is available, however, the obstacle detection and avoidance maneuver selection logic must function for the current course offset. The ICHK counter is used to permit only one check of the return path.

16. Because the half-width of the anticipative array is 4*RY dm, the maximum verifiable lateral offset command magnitude is 3*RY dm. The lateral destination command for the return to the pre-planned flight path is limited to 3*RY dm in the direction of the pre-planned flight path.

17. $y_{com} \neq 0$ indicates an initial lateral offset due to previous lateral evasive maneuvering. ICHK = 1 indicates that the current pass through the lateral evasive maneuver decision logic is the first, and an attempt is therefore made to return the rotorcraft to the pre-planned flight path. IYDES is the return flag (1 = return) and J_{com} is the destination column determined by the lateral destination command. The first check is to see if the destination columns (J_{com} and $J_{com}+1$) are obstructed. If so, the attempt to return is abandoned.

18. The proposed lateral offset command is determined by interrogating Table 4.3. This is a check of the columns of the first section in Fig. 4.6.

19. If no lateral offset is proposed ($J_{com} = 3$), the remainder of the lateral evasive maneuver decision logic is bypassed; otherwise, the proposed lateral offset command is checked before it is accepted.

Figure 4.3 (Continued)

s. Notes (Continued)

20. The first check of the proposed lateral evasive maneuver is of the path through either Section 3 or 4 in Fig. 4.6. Required for this check is the determination of the maneuver urgency factor, which defines the maneuver path. The example depicted in the figure is a specific case in which $J_{com} = 2$. In general, the digits of the maneuver urgency factor, MUF, are defined as follows:

Tens	Ones
$\lvert J_{com} - 3 \rvert$	$R_{IND} - R_{obs} + 1$ or MUF1

where R_{obs} is the row in the anticipative array containing the obstruction necessitating the evasive maneuver, which is determined by interrogating the blocks in the column nearest the center and adjacent to the two destination columns (J_{com} and $J_{com}+1$). In the case depicted in the figure, that column is J = 4. If no obstruction is identified in any of the cells of the column in the area defined as Section 1 in Fig. 4.6, R_{obs} is set to R_{IND}, the last cell of the column.

21. MUF1 is used to artificially increase the urgency of the proposed maneuver (see Note 32 and 35).

22. The flow diagram depicting a sample check of a maneuver path is presented in Fig. 4.9. All possible maneuver paths are shown in Fig. 4.10 through 4.16. A similar procedure to that presented in Fig. 4.9 can be employed to check all of the possible maneuver paths. The output of this routine is IDYST. If IDYST = 0, the maneuver path is clear.

23. If the maneuver path is not clear to return to the preplanned flight path, return to the beginning of the lateral evasive maneuver decision logic.

24. If the maneuver path is not clear and the ones digit of the maneuver urgency factor is equal to 4 due to an obstruction in the nearest cell of the area defined as Section 1 in Fig. 4.6 and not due to an artificial increase of the urgency of the maneuver, an attempt is made to find another navigable path that avoids the obstruction.

25. Before returning to the beginning of the lateral evasive maneuver decision logic for an attempt to find an alternate path, the proposed lateral offset command is discarded by resetting y_{com} to the initial offset command, y'_{com}.

Figure 4.3 (Continued)

s. Notes (Continued)

26. If the formerly proposed lateral offset command was to the left ($J_{com} < 3$), all of the columns of Section 1 of Fig. 4.6 to the left of center are artificially obstructed. This will force the decision logic of Table 4.3 to choose an evasive maneuver to the right, since the leftward maneuver paths are unnavigable.

27. If the formerly proposed lateral offset command was to the right ($J_{com} > 3$), all of the columns of Section 1 of Fig. 4.6 to the right of center are artificially obstructed. This will force the decision logic of Table 4.3 to choose an evasive maneuver to the left, since the rightward maneuver paths are unnavigable.

28. If the maneuver path is not clear but there are no obstructions in the nearest two cells of the center columns of Section 1 as defined in Fig. 4.6, the proposed lateral evasive maneuver is ignored, and the rotorcraft is commanded to continue along the previously commanded course. If, however, obstructions are present in one of these cells, the rotorcraft is commanded to stop.

29. The continuation command is achieved by resetting the lateral offset command to the initial offset command.

30. The last check of the proposed lateral offset command is to check the area beyond the completion of the maneuver, Section 2 in Fig. 4.6. This check is required, because the obstacle detection and avoidance maneuver selection logic is bypassed during a lateral evasive maneuver. If the area beyond the completion of the maneuver is not shown to be free of obstructions, the rotorcraft could run into one obstruction immediately following the avoidance of another. The index ICHKN corresponds to the row number in the current anticipative array coinciding with the location of the first row of the anticipative array following the completion of the evasive maneuver; and ICHKM, to the row number in the current anticipative array coinciding with the location of the row of the anticipative array following the completion of the evasive maneuver immediately preceding the area defined as Section 1 in Fig. 4.6. The calculation of these two indices follows.

$$ICHKM = R_{IND} + R_2 + 2 + 10\,\mathrm{int}\left(\frac{MUF}{10}\right) - MUF$$

$$ICHKN = ICHKM - R_2$$

Figure 4.3 (Continued)

s. Notes (Continued)

31. ANCHL counts the number of obstructions in the left destination column in the prescribed rows, and ANCHR counts the number of obstructions in the right destination column.

32. This section artificially increases the maneuver urgency if the proposed maneuver is a return to the preplanned course.

33. If there are no obstructions detected, the proposed maneuver is allowed.

34. If there are no obstructions, and the proposed maneuver is a return to the preplanned course, the lateral offset command is set to the lateral destination command.

35. If obstructions are detected and the artificial urgency factor is less than 4, the artificial urgency factor is incremented by one. This has the effect of shortening the intrusion of the destination path into the Section 2 area as defined in Fig. 4.6. Ultimately, this may exclude the obstruction from the rows of consideration and thus allow the maneuver.

36. If obstructions are found and altering the urgency of the maneuver has not been able to exclude them, the proposed maneuver is discarded. If the proposed maneuver would have returned the rotorcraft to the preplanned flight path, the lateral offset command is reset, and the lateral evasive maneuver decision logic is restarted.

37. The corresponding column of Section 1 is artificially obstructed as a result of obstructions identified in the columns of Section 2.

38. The lateral offset command is then reset, and the lateral evasive maneuver decision logic, restarted.

39. The vertical maneuver selection parameters are initialized as follows:

DHPLYL = HTH	$Q_{IND} = 0$
DHPLYR = HTH	$S_{IND} = 0$
DZPUYL = HTH	$T_{IND} = 0$
DZPUYR = HTH	$U_{IND} = 0$

40. The search area for the vertical maneuver selection logic varies, depending on the lateral offset command. If the lateral offset command is zero, the search area consists of the cells in the anticipative array that comprise Section 5, as defined in Fig. 4.6. If the lateral offset command is nonzero, the search area is comprised of the destination columns extending from the first row of Section 1 into Section 2, as dictated by ICHKM.

Figure 4.3 (Continued)

s. Notes (Continued)

41. The lower and upper navigable boundaries are compared to the lower and upper surfaces of the anticipative array to determine requisite height changes, if any. The location of the greatest intrusions into the anticipative array is also noted to indicate the distance to the obstacle.

42. The greatest intrusions are compared to an allowable maximum. If any exceeds this maximum, a vertical evasive maneuver is required.

43. If no vertical evasive maneuvers are required, the velocity command is set to the nominal values.

44. If the initial vertical offset command is zero, exit the obstacle detection and avoidance maneuver selection logic. If a lateral offset command has been proposed and approved, the destination vertical offset command (h_{com_2}) is set to zero. This will bring the rotorcraft to the nominal radar altitude at the conclusion of the lateral evasive maneuver.

45. ABSALT is the absolute altimetry subroutine that analyses the immediate vicinity of the rotorcraft to prevent any penetrations of the safety margin envelope (Fig. 4.4) by obstacles. A flow diagram for this subroutine is presented in Fig. 4.5. This logic is exercised if the initial lateral offset command is nonzero

46. A determination is made as to whether a bob-up or -down maneuver is required to avoid the obstacle.

47. If penetrations into the anticipative array exist both from above and below, the maximum of these penetrations is determined to be used in deciding an appropriate course of action.

48. The sum of the maximum penetrations are compared to the width of the anticipative array to determine if there is navigable distance between the penetrating obstacles. If so, the appropriate command is issued.

49. If there is not navigable distance between the penetrating obstacles, the rotorcraft is commanded to stop.

50. For the proposed climb along the course, a check is made to ensure that there is navigable vertical distance above the penetrating obstacle. If not, the rotorcraft is commanded to stop.

51. If the penetrating obstruction has already been identified in a previous pass through the obstacle detection and avoidance maneuver selection logic, the rate of climb calculations are bypassed.

Figure 4.3 (Continued)

s. Notes (Continued)

52. The rate of climb calculations are also bypassed if the rotorcraft is currently responding via a bob-up command to another, albeit shorter, obstacle.

53. The required rates of climb for the penetrations in the left and right columns are calculated as follows:

If the nominal forward velocity, VXNOM, is nonzero (normally true),

$$VHLYL = \frac{DHPLYL}{TPX + (Q_{IND} - R_2 - 1)\frac{RX}{VXNOM}}$$

$$VHLYR = \frac{DHPLYR}{TPX + (S_{IND} - R_2 - 1)\frac{RX}{VXNOM}}$$

If VXNOM = 0,

$$VHLYL = \frac{DHPLYL}{TPH}$$

$$VHLYR = \frac{DHPLYR}{TPH}$$

54. If the required rate of climb due to the penetrating obstacle in the left column exceeds the maximum allowable rate of climb, the forward velocity necessary to enable the rotorcraft to avoid the obstacle, given the rate of climb limit, is calculated as follows:

$$VXCLYL = VHMAX\frac{x_{fp} - x_{pp}}{DHPLYL}$$

55. Similarly, if the required rate of climb due to the penetrating obstacle in the right column exceeds the maximum allowable rate of climb, the forward velocity necessary to enable the rotorcraft to avoid the obstacle, given the rate of climb limit, is calculated as follows:

$$VXCLYR = VHMAX\frac{x_{fp} - x_{pp}}{DHPLYR}$$

The commanded forward velocity is then set to the minimum of the left and right requisite velocities.

Figure 4.3 (Continued)

s. Notes (Continued)

56. The proposed vertical offset command is set as the maximum height of the penetrating obstacles.

57. ABSALT is the absolute altimetry subroutine that analyses the immediate vicinity of the rotorcraft to prevent any penetrations of the safety margin envelope (Fig. 4.4) by obstacles. A flow diagram for this subroutine is presented in Fig. 4.5. This logic is exercised prior to the acceptance of the proposed vertical offset command.

58. If a lateral evasive maneuver has been accepted, the destination vertical offset command is set to the proposed vertical offset command.

59. For the proposed decent along the course, a check is made to ensure that there is navigable vertical distance below the penetrating obstacle. If not, the rotorcraft is commanded to stop.

60. If the penetrating obstruction has already been identified in a previous pass through the obstacle detection and avoidance maneuver selection logic, the rate of descent calculations are bypassed.

61. The rate of descent calculations are also bypassed if the rotorcraft is currently responding via a bob-down command to another, albeit lesser, penetration.

62. The required rates of descent for the penetrations in the left and right columns are calculated as follows:

If the nominal forward velocity, VXNOM, is nonzero (normally true),

$$VZUYL = \frac{DZPUYL}{TPX + (T_{IND} - R_2 - 1)\frac{RX}{VXNOM}}$$

$$VZUYR = \frac{DZPUYR}{TPX + (U_{IND} - R_2 - 1)\frac{RX}{VXNOM}}$$

If VXNOM = 0,

$$VZUYL = \frac{DZPUYL}{TPH}$$

$$VZUYR = \frac{DZPUYR}{TPH}$$

Figure 4.3 (Continued)

s. Notes (Concluded)

63. If the required rate of descent due to the penetrating obstacle in the left column exceeds the maximum allowable rate of descent, the forward velocity necessary to enable the rotorcraft to avoid the obstacle, given the rate of descent limit, is calculated as follows:

$$VXCLYL = VZMAX\frac{x_{fp} - x_{pp}}{DZPUYL}$$

64. Similarly, if the required rate of descent due to the penetrating obstacle in the right column exceeds the maximum allowable rate of descent, the forward velocity necessary to enable the rotorcraft to avoid the obstacle, given the rate of descent limit, is calculated as follows:

$$VXCLYR = VZMAX\frac{x_{fp} - x_{pp}}{DZPUYR}$$

The commanded forward velocity is then set to the minimum of the left and right requisite velocities.

65. The proposed vertical offset command is set as the maximum penetration of the obstacles.

66. ABSALT is the absolute altimetry subroutine that analyses the immediate vicinity of the rotorcraft to prevent any penetrations of the safety margin envelope (Fig. 4.4) by obstacles. A flow diagram for this subroutine is presented in Fig. 4.5. This logic is exercised prior to the acceptance of the proposed vertical offset command.

67. If a lateral evasive maneuver has been accepted, the destination vertical offset command is set to the proposed vertical offset command.

68. The stop command is issued by resetting the lateral and vertical offset commands to their initial values and setting the forward velocity command to zero.

Figure 4.3 (Concluded)

TABLE 4.2

PARAMETER VALUES FOR THE OBSTACLE DETECTION AND AVOIDANCE MANEUVER SELECTION LOGIC

T_{p_x}	Preview time in the longitudinal axis of the anticipative array reference point	6 sec
T_{p_h}	Preview time in the vertical axis for vertical evasive maneuvering	6 sec
RX	Cell length in the anticipative array	32.808 ft (1 dm)
RY	Cell width in the anticipative array	32.808 ft (1 dm)
RX	Cell width in the anticipative array	24.606 ft (3/4 dm)
h_{ALT_c}	Commanded radar altitude	40 ft
$V_{x_{min}}$	Minimum forward velocity to vary dimensions of the anticipative array	21.872 ft/sec
R_1	One less than the number of rows in the lateral evasive maneuver search section (Section 1 in Fig. 4.6)	3
M_{IND}	One less than the number of columns in the anticipative array	7
HTH	Maximum allowable penetration into the anticipative array	0 ft
VXNOM	Nominal along-course velocity command	33.778 ft/sec (20 kt)
VHMAX	Maximum rate of climb	20 ft/sec
VZMAX	Maximum rate of descent	20 ft/sec

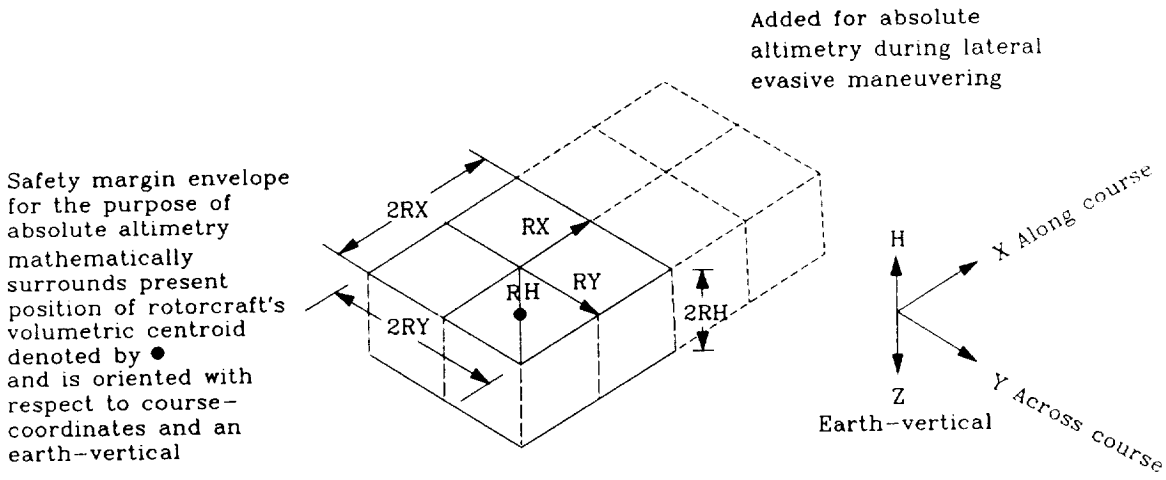

Figure 4.4 Safety Margin Envelope for Applying Absolute Altimetry to the Sensed Data Base to Avoid Obstacles

Inputs:	Waypoint course coordinates	x_{pp} and y_{pp}
	Defined obstacle arrays	$x_{obs}(I_{obs})$, $y_{obs}(I_{obs})$, $w_{obs}(I_{obs})$, and $h_{obs}(I_{obs})$
Outputs:	Absolute Altimetry Vertical Offset Commands	h_{com_a} and z_{com_a}

a. Inputs and Outputs

Figure 4.5 Flow Diagram for Absolute Altimetry Routine

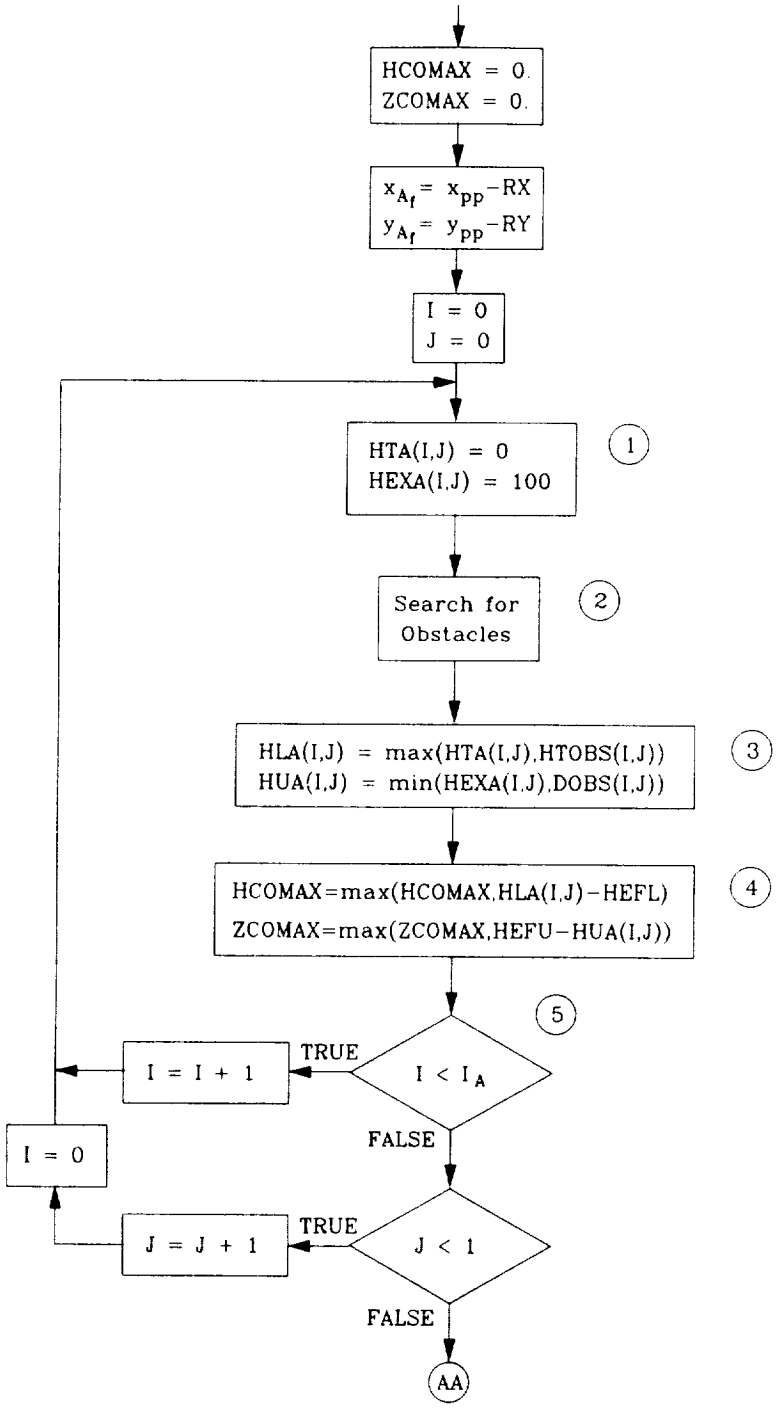

b. Absolute Altimetry Routine

Figure 4.5 (Continued)

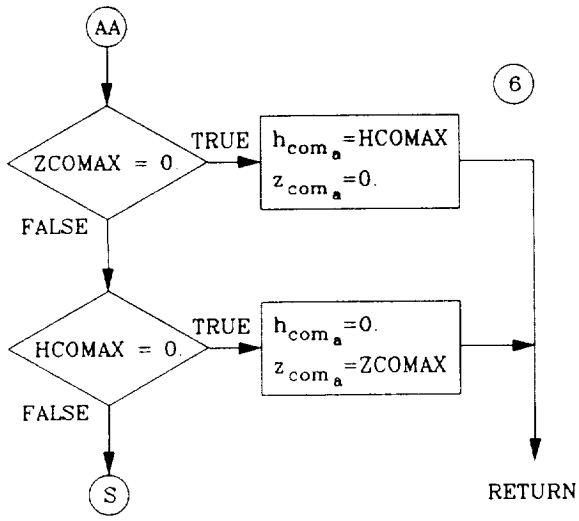

b. Absolute Altimetry Routine (Continued)

Figure 4.5 (Continued)

c. Notes (corresponding to circled numbers throughout figure)

1. For the purposes of this simulation, the terrain height under a given cell of the safety margin envelope is taken to be equal to the approximate terrain height, as defined in Section 2.2. Additionally, the threat exposure height will be assumed as a constant height above the terrain corresponding to the average tree along the course.

2. The obstacle search algorithm is defined in the flow diagram presented in Fig. 4.8. Returning from this algorithm are HTOBS(I,J) and DOBS(I,J), the adjusted passable height and threat exposure height due to detected obstacles and threats.

3. The lower (HLA(I,J)) and upper (HUA(I,J)) navigable heights are determined for the given cell.

4. The maximum penetrations into the safety margin is determined, with HCOMAX corresponding to penetrations from below and ZCOMAX, to penetrations from above.

5. The number of rows in the safety margin envelope varies. During a lateral evasive maneuver, $I_A = 3$, while normally, $I_A = 1$ (see Fig. 4.4).

6. The absolute altimetry vertical offset command is set to the maximum penetration of the anticipative array. If penetrations exist both from above and below, the rotorcraft is commanded to stop.

Figure 4.5 (Concluded)

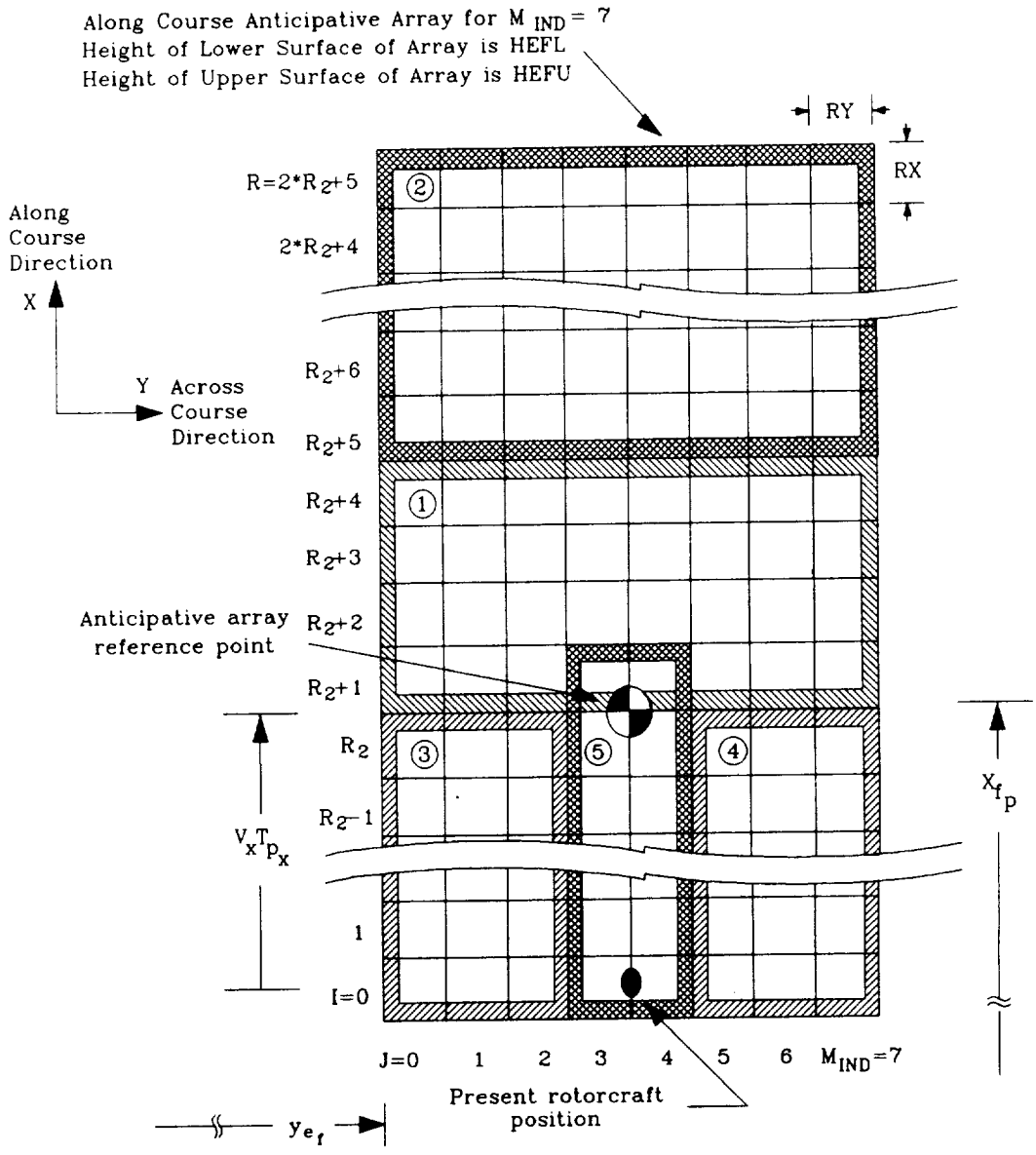

Figure 4.6 Plan View of the Along-Course Anticipative Array of Sensed Terrain, Obstacle, and Threat Elevation Data

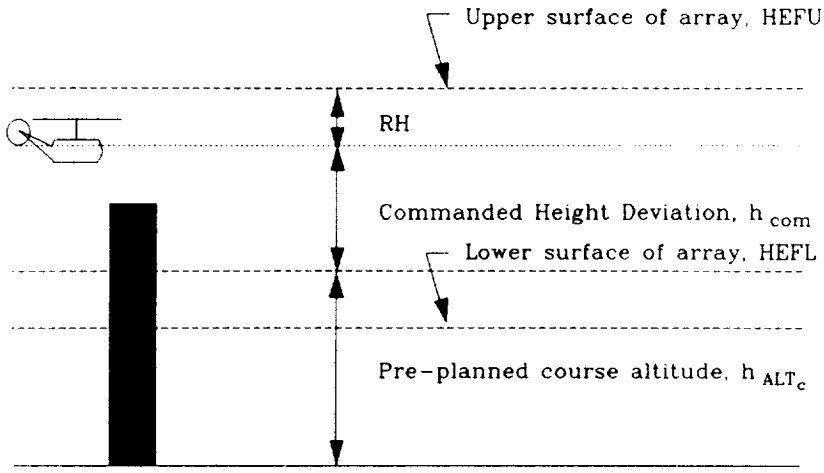

Figure 4.7 Positioning of Upper and Lower Surfaces of the Along-Course Anticipative Array with Current Commanded Height Deviation

TABLE 4.3. PROCEDURAL DECISION LOGIC USING BLOCKS OF SECTION 1 OF THE ALONG-COURSE ANTICIPATIVE ARRAY DEPICTED IN FIG. 4.6

J = Left	0 1 2 3	4 5 6 7	Right	Decision regardless of unspecified elements	Destination Column	Command
	0	0		Continue to follow flight profile	$J_{com} = 3$	$y_{com} = y_{com}$
	0 0	1		Left-step RY	$J_{com} = 2$	$y_{com} = y_{com} - RY$
	1	0 0		Right-step RY	$J_{com} = 4$	$y_{com} = y_{com} + RY$
	0 0 1	1		Left-step 2*RY	$J_{com} = 1$	$y_{com} = y_{com} - 2RY$
	0 0 1	1 0 1		Left-step 2*RY	$J_{com} = 1$	$y_{com} = y_{com} - 2RY$
	1	1 0 0		Right-step 2*RY	$J_{com} = 5$	$y_{com} = y_{com} + 2RY$
	1 0 1	1 0 0		Right-step 2*RY	$J_{com} = 5$	$y_{com} = y_{com} + 2RY$
	0 0 1	1 0 0		Right-step 2*RY if VY $\geq$ 0, Left-step 2*RY if VY < 0	$J_{com} = 5$ or 1	$y_{com} = y_{com} \pm 2RY$
	0 0 1	1 1 1		Left-step 3*RY	$J_{com} = 0$	$y_{com} = y_{com} - 3RY$
	0 0 1	1 0 1		Left-step 3*RY	$J_{com} = 0$	$y_{com} = y_{com} - 3RY$
	0 0 1 1	0 1 1		Left-step 3*RY	$J_{com} = 0$	$y_{com} = y_{com} - 3RY$
	1 1 1	1 0 0		Right-step 3*RY	$J_{com} = 6$	$y_{com} = y_{com} + 3RY$
	1 0 1	1 0 0		Right-step 3*RY	$J_{com} = 6$	$y_{com} = y_{com} + 3RY$
	1 1 0	1 1 0 0		Right-step 3*RY	$J_{com} = 6$	$y_{com} = y_{com} + 3RY$
	0 0 1	1 1 0 0		Right-step 3*RY if VY $\geq$ 0, Left-step 3*RY if VY < 0	$J_{com} = 6$ or 0	$y_{com} = y_{com} \pm 3RY$
	0 0 1 1	0 1 0 0		Right-step 3*RY if VY $\geq$ 0, Left-step 3*RY if VY < 0	$J_{com} = 6$ or 0	$y_{com} = y_{com} \pm 3RY$
	0 0 1	1 1 0 1		Left-step 3*RY	$J_{com} = 6$	$y_{com} = y_{com} - 3RY$
	1 0 1 1	1 0 0		Right-step 3*RY	$J_{com} = 0$	$y_{com} = y_{com} + 3RY$

Legend: 0 = No obstruction present in Jth column of Section 1
1 = At least one element of the Jth column of Section 1 contains an obstruction

Inputs:	Reference point location	
	Anticipative array	x_{fp} and y_{ef}
	Safety margin envelope	x_{Af} and y_{Af}
	Cell indices	I and J
	Defined obstacle arrays	$x_{obs}(I_{obs})$, $y_{obs}(I_{obs})$, $w_{obs}(I_{obs})$, and $h_{obs}(I_{obs})$
Outputs:	Upper and lower navigable boundaries above terrain and below threat exposure height due to detected obstacles in the given cell	HTOBS(I,J) and DOBS(I,J)

a. Inputs and Outputs

Figure 4.8 Flow Diagram for Obstacle Detection Routine

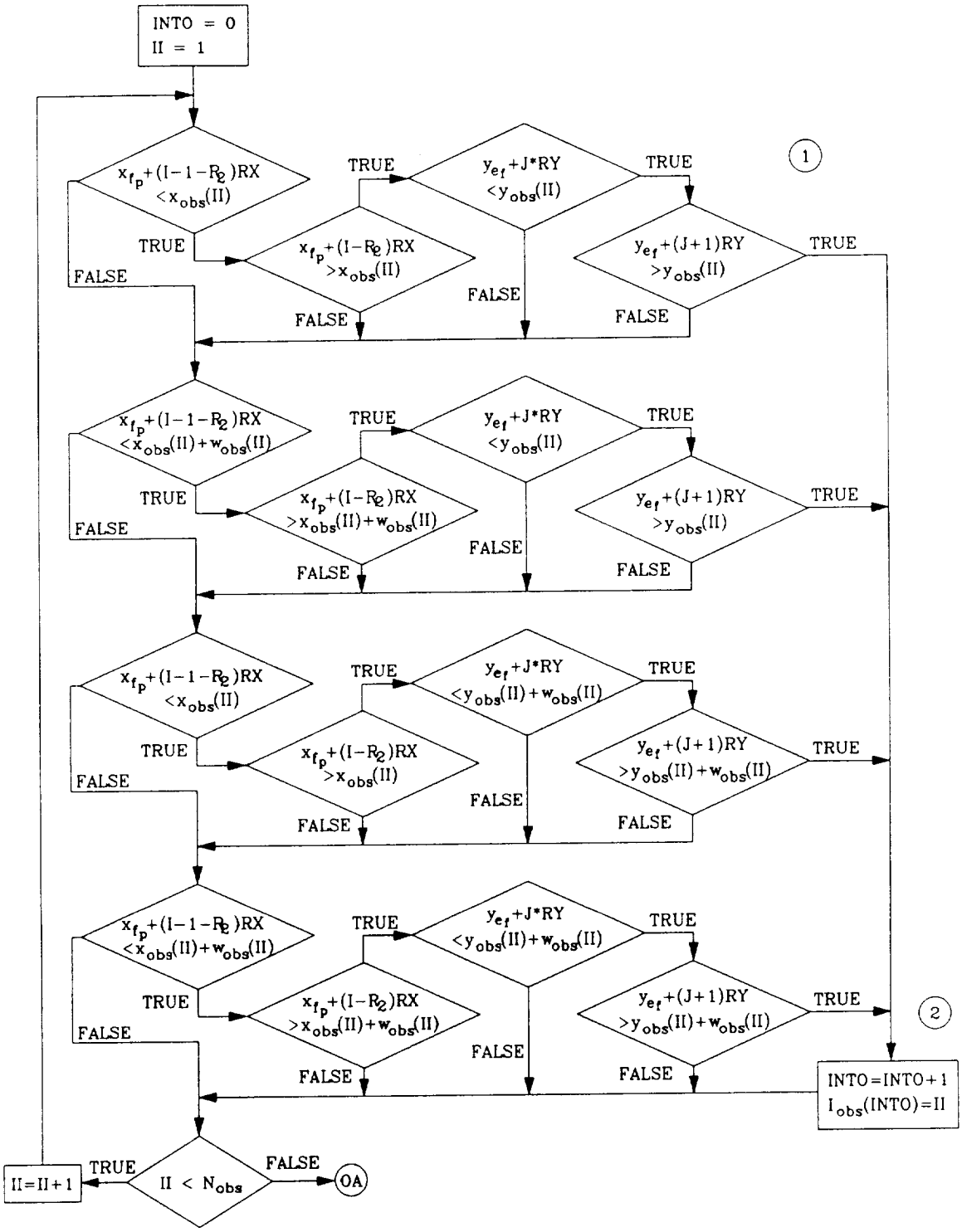

b. Obstacle Detection Routine

Figure 4.8 (Continued)

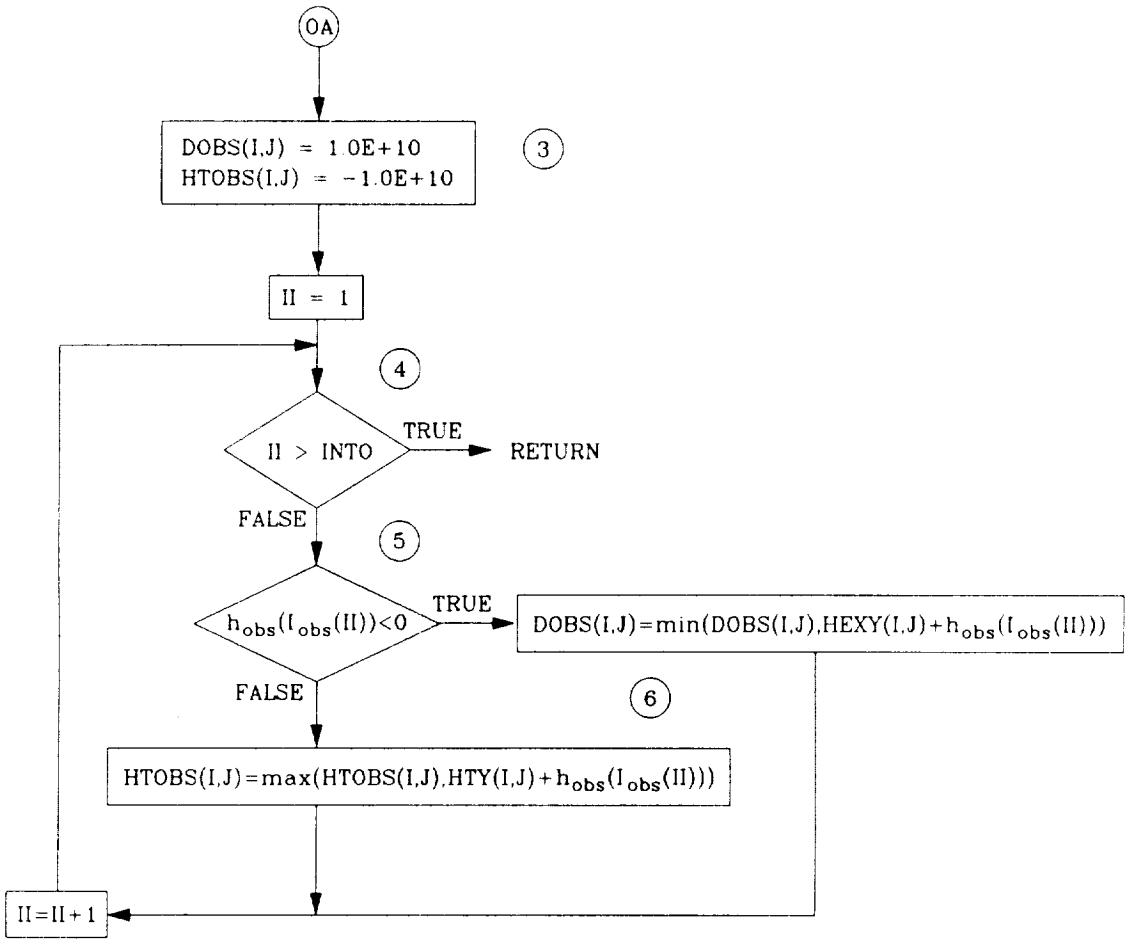

b. Obstacle Detection Routine (Continued)

Figure 4.8 (Continued)

c. Notes (corresponding to circled numbers throughout figure)

1. Each corner of the obstacle is compared to the boundaries of the cell in question to determine if the obstacle encroaches upon that cell. The figure demonstrates this process of identifying obstacles in the anticipative array. In order to identify obstacles in the safety margin envelope, the following substitutions must be made:

Substitute:	For:
$x_{A_f} + I*RX$	$x_{f_p} + (I - 1 - R_2)RX$
$x_{A_f} + (I+1)RX$	$x_{f_p} + (I - R_2)RX$
y_{A_f}	y_{e_f}
HTA(I,J)	HTY(I,J)
HEXA(I,J)	HEXY(I,J)

2. For each obstacle identified in the cell, the INTO obstacle counter is incremented, and the index of the identified obstacle in the obstacle arrays is stored.

3. The navigable boundaries due to obstacles are initialized for the cell at extremes, such that if no obstacles are present in the cell, the terrain and threat exposure heights will govern the navigable boundaries (see Fig. 4.3, Note 11).

4. For each obstacle identified in the cell, the navigable boundaries due to obstacles are modified. If no obstacles are identified, this loop is bypassed.

5. Negative obstacle heights indicate obstacles descending below the threat exposure height.

6. The greatest adjustment to the navigable boundaries caused by obstacles identified in the cell is returned from this routine.

Figure 4.8 (Concluded)

Inputs:	Maneuver urgency factor	MUF
	Destination column	J_{com}
	Heights of the upper and lower surfaces of the anticipative array	HEFL and HEFU
	Upper and lower navigable boundaries	HLY(I,J) and HUY(I,J)
Outputs:	Maneuver check flag	IDYST

a. Inputs and Outputs

Figure 4.9 Flow Diagram Depicting the Procedure Used to Determine if a Proposed Maneuver Path is Clear

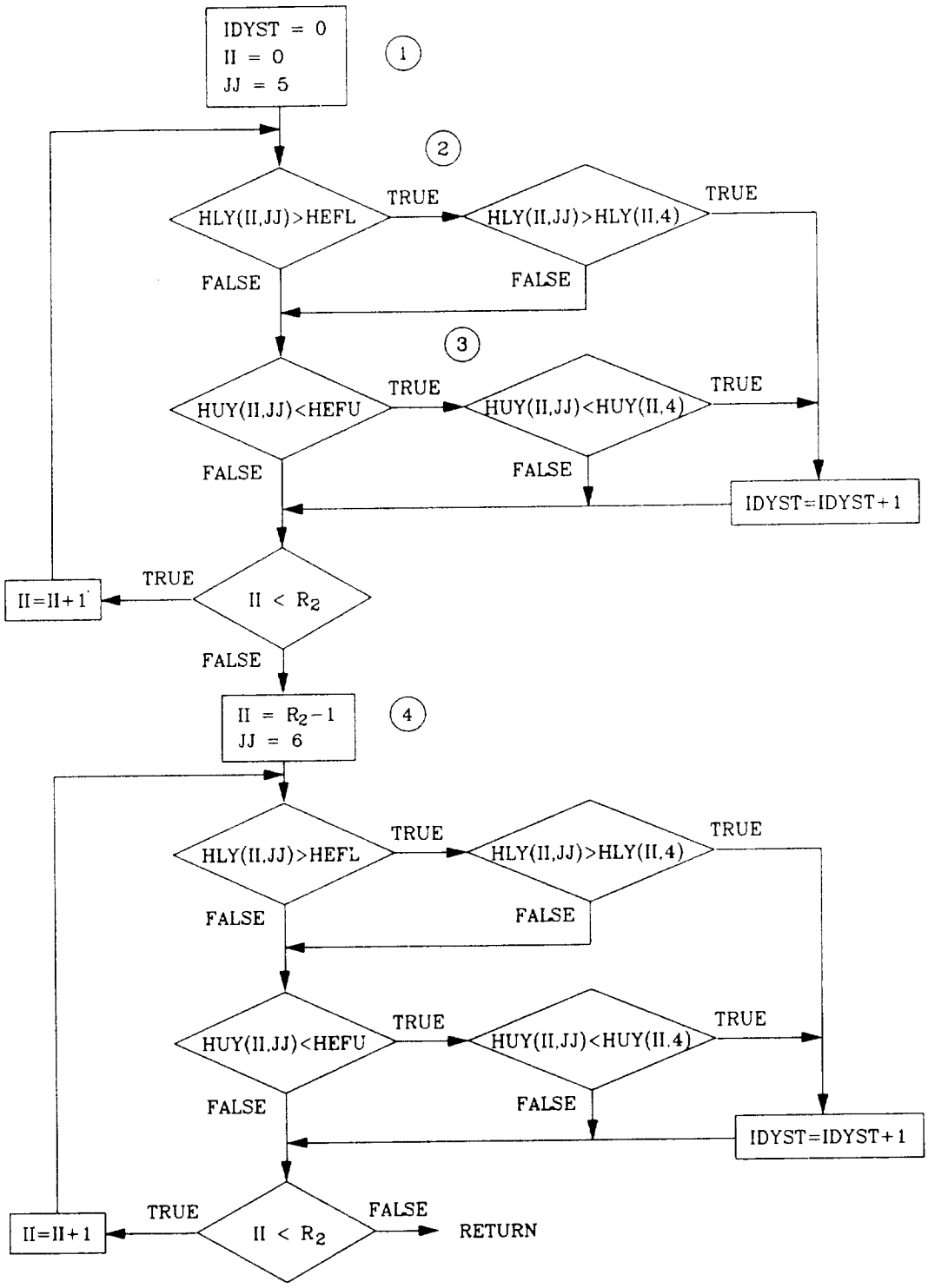

Figure 4.9 (Continued)

b. Sample Maneuver Path Check

c. Notes (corresponding to circled numbers throughout figure)

1. Initially, the maneuver path is assumed to be clear. The maneuver path is determined, based on the maneuver urgency factor, MUF, and the destination column index, J_{com}. The possible maneuver paths are shown in Fig. 4.10. The sample shown in the figure checks the maneuver path of a proposed lateral evasive maneuver rightward with a maneuver urgency factor of 22 ($J_{com} = 5$ and MUF = 22). The ranges for the search indices II and JJ are determined from the specified maneuver path. In the sample shown, the two columns of the maneuver path are JJ = 5 and 6, while II varies from 0 to R_2 in column 5, and from R_2-1 to R_2 in column 6.

2. The lower surface of the anticipative array is searched in the specified cells to determine if any penetrations exist from the lower navigable boundary. If these penetrations do not exceed penetrations in the nearest cell of Section 5 in Fig. 4.6, it can be assumed that the vertical evasive maneuver decision logic has already accounted for this penetration, and it will successfully be avoided. If, however, any penetration exists from below without a corresponding penetration in the vertical decision section, Section 5, the path is considered blocked.

3. The same logic is used when comparing the upper surface of the anticipative array with the upper navigable boundary.

4. The above detailed process is repeated in the search of the cells in the second search column.

Figure 4.9 (Concluded)

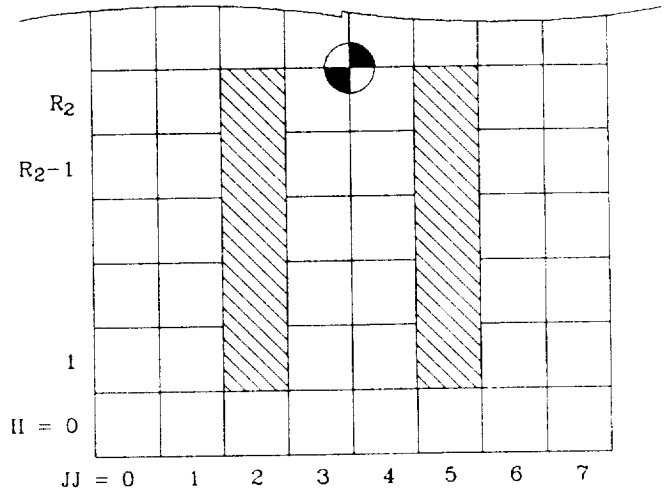

a. MUF = 11, J_{com} = 2 (Left) or 4 (Right)

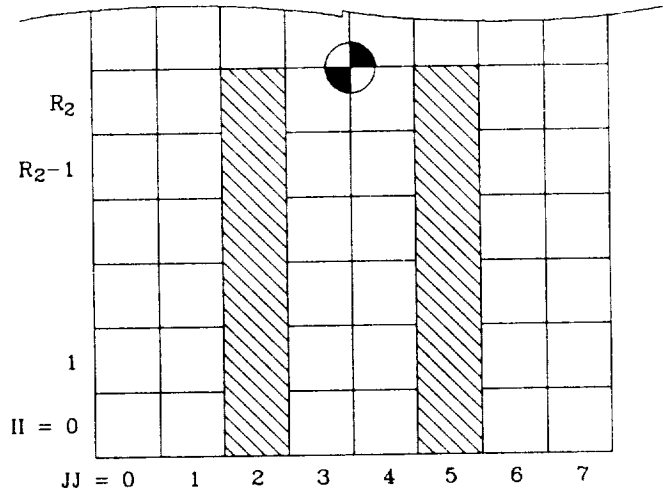

b. MUF = 12, 13, or 14, J_{com} = 2 (Left) or 4 (Right)

Figure 4.10 Possible Maneuver Paths for Lateral Evasive Maneuvers

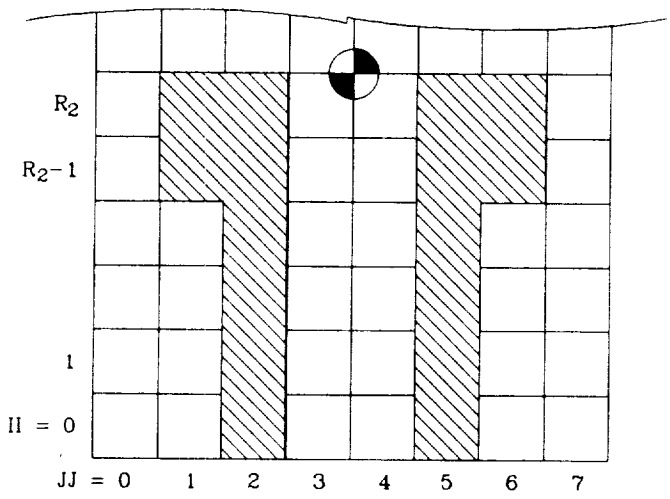

c. MUF = 21 or 22, J_{com} = 1 (Left) or 5 (Right)

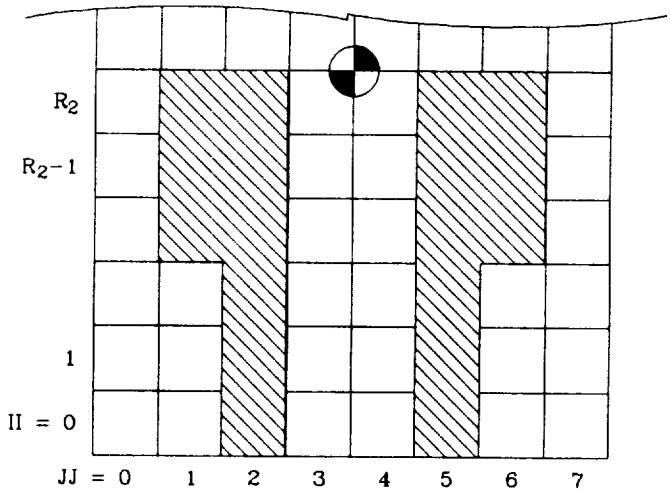

d. MUF = 23, 24, or 31, J_{com} = 0 or 1 (Left) or 5 or 6 (Right)

Figure 4.10 (Continued)

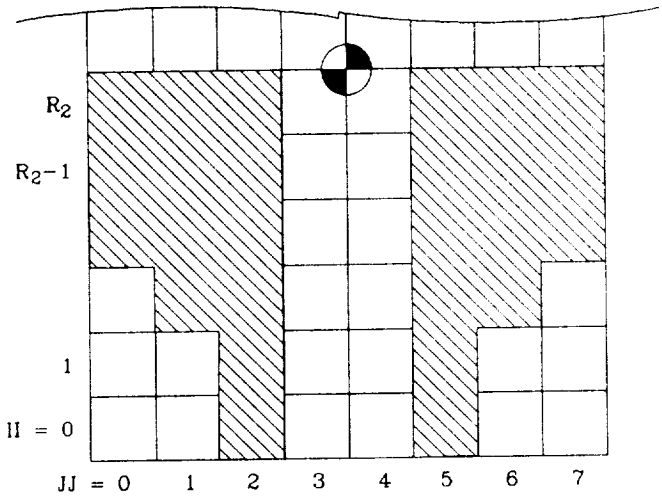

e. MUF = 32, J_{com} = 0 (Left) or 6 (Right)

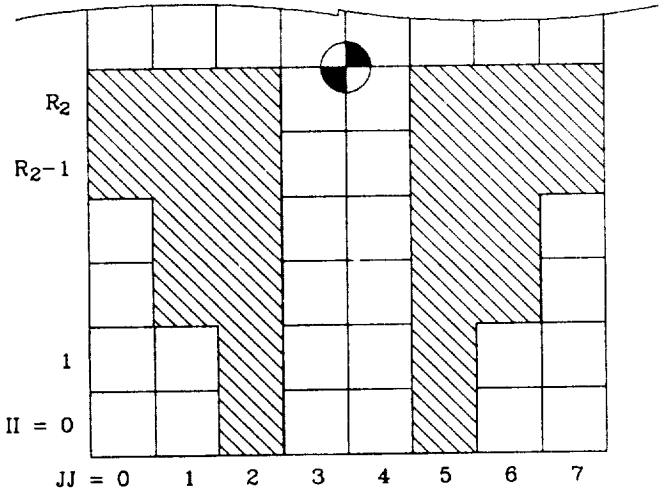

f. MUF = 33, J_{com} = 0 (Left) or 6 (Right)

Figure 4.10 (Continued)

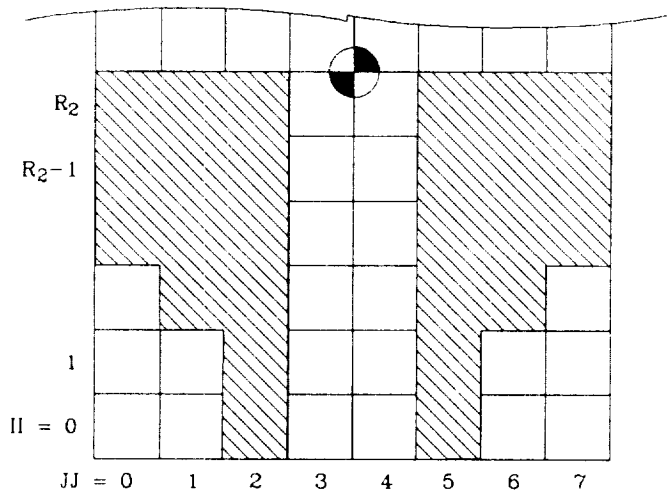

g. MUF = 34, J_{com} = 0 (Left) or 6 (Right)

Figure 4.10 (Concluded)

5. AERODYNAMIC FORCES AND MOMENTS, STEADY WINDS AND TURBULENCE

5.1 Aerodynamic Forces and Moments

The following is a list of equations used in the calculation of the aerodynamic forces and moments. The wind gust terms include the changes in the relative components of the inertially steady wind brought about by changes in heading and orientation of the rotorcraft. The unaugmented stability derivatives in these calculations are presented in Table 5.1.

1. Longitudinal-Vertical

$$\frac{FAX}{m} = X_u(u_b - u'_g)$$

$$\frac{FAZ}{m} = Z_{w_g} w'_g$$

$$XMC7 \cdot TAM = -M_{u_g} u'_g - M_{q_g} q_g$$

2. Lateral-Directional

$$\frac{FAY}{m} = Y_v(v_b - v'_g)$$

$$XMC3 \cdot TAL = -L_{v_g} v'_g - L_{p_g} p_g$$

$$XMC10 \cdot TAN = -N_{r_g} r_g$$

3. Wind gust calculations.

$$\begin{bmatrix} u'_g \\ v'_g \\ w'_g \end{bmatrix} = \begin{bmatrix} u_g \\ v_g \\ w_g \end{bmatrix} + \begin{bmatrix} T_{11} & T_{12} & T_{13} \\ T_{21} & T_{22} & T_{23} \\ T_{31} & T_{32} & T_{33} \end{bmatrix} \begin{bmatrix} u_w \\ v_w \\ w_w \end{bmatrix} - \begin{bmatrix} u_{sw_i} \\ v_{sw_i} \\ w_{sw_i} \end{bmatrix}$$

where u_{sw_i}, v_{sw_i}, and w_{sw_i} are the initial body axis components of the steady wind.

TABLE 5.1

PARAMETER VALUES FOR THE CALCULATION OF THE AERODYNAMIC FORCES AND MOMENTS

X_u	Surge damping stability derivative	-0.04 1/sec
M_{u_g}	Longitudinal velocity stability derivative	-0.001 1/ft-sec
M_{q_g}	Pitch rate stability derivative	-0.871 1/sec
Y_v	Sway damping stability derivative	-0.12 1/sec
L_{v_g}	Lateral velocity stability derivative	-0.039 1/ft-sec
L_{p_g}	Roll rate stability derivative	-3.50 1/sec
Z_{w_g}	Heave damping stability derivative	-0.379
N_{r_g}	Yaw rate stability derivative	-0.366

5.2 Wind Model

Two aspects of the wind conditions are modeled: mean velocity and random turbulence. The turbulence is modeled using the Dryden form for the gust filters. The empirical scale lengths are given in Table 5.2. The gust filters follow.

$$\frac{u_g}{\eta_u} = \frac{(2V_{RW}/L_u)^{\frac{1}{2}}}{s + V_{RW}/L_u}$$

$$\frac{v_g}{\eta_v} = \sigma_{v_g}\sqrt{\frac{3V_{RW}}{L_v}}\left[\frac{s + V_{RW}/\sqrt{3}L_v}{(s + V_{RW}/L_T)^2}\right]$$

$$\frac{w_g}{\eta_w} = \sigma_{w_g}\sqrt{\frac{3V_{RW}}{L_w}}\left[\frac{s + V_{RW}/\sqrt{3}L_w}{(s + V_{RW}/L_T)^2}\right]$$

Also modeled is the variation of the mean-wind velocity and the intensity of the turbulence with changes in absolute altitude. A general expression in terms of absolute altitude, h, is provided for scaling a wind component with absolute altitude. The constants in the expression are given in Table 5.2.

$$V_W = \begin{cases} V_{W_0}\left(\dfrac{h}{h_{tr}}\right)^a & \text{if } h \le h_{tr} \\ V_{W_\infty}\left(\dfrac{h - h'_{tr}}{\delta_0}\right)^{1/b} & \text{if } h_{tr} < h \le \delta_0 + h'_{tr} \\ V_{W_\infty} & \text{if } h > \delta_0 + h'_{tr} \end{cases}$$

$$V_{W_0} = V_{W_\infty}\left(\frac{h_{tr} - h'_{tr}}{\delta_0}\right)^{1/b}$$

$$h'_{tr} = h_{tr}\left(1 - \frac{1}{a \cdot b}\right)$$

Six wind velocities are scaled by this general expression: north, east, and downward steady wind velocity components (VNW, VEW, and VDW) and the gust components defined previously (u_g, v_g, and w_g). These variables substitute for V_{W_∞} in the general expression. For the gust variables, the results of the scaling, V_W, replaces the unscaled value for each. For the steady wind components, the results of the scaling, V_W, are u_w, v_w, and w_w, respectively.

An example of the wind profile resulting from this scaling procedure is presented in Fig. 5.1.

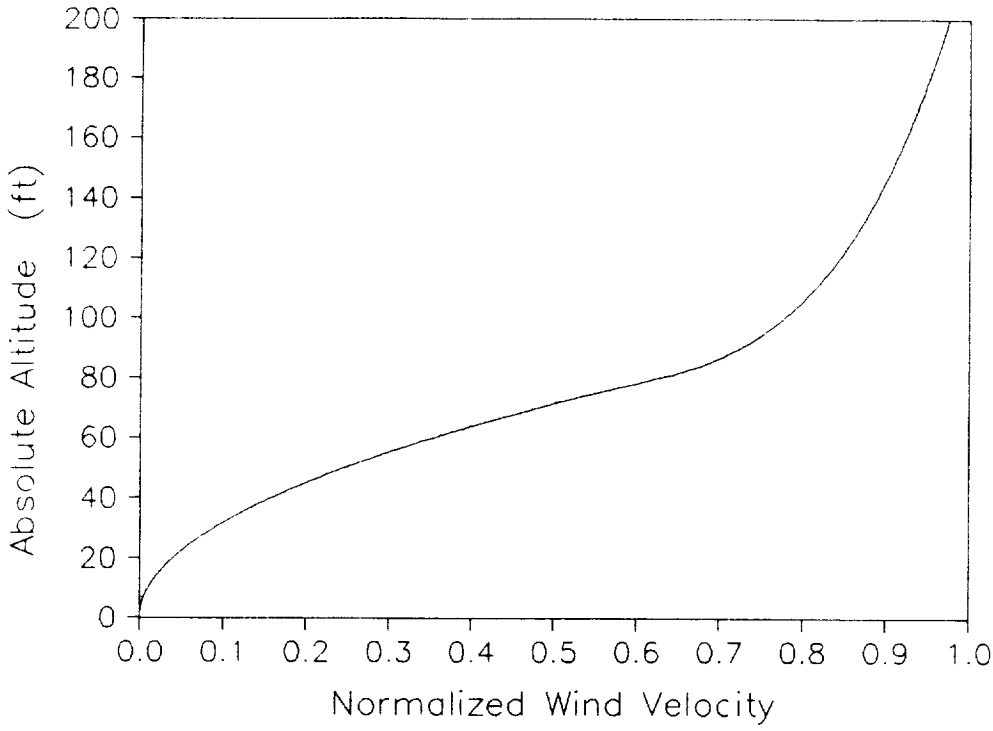

Figure 5.1 Wind Velocity Profile

TABLE 5.2

PARAMETER VALUES FOR THE CALCULATION OF THE WIND MODEL

V_{RW}	Velocity for Dryden form gust filters	≤ 15 ft/sec
L_u	Longitudinal scale length	80 ft
L_v	Lateral scale length	60 ft
L_w	Vertical scale length	10 ft
δ_0	Free stream wind height	150 ft
h_{tr}	Tree canopy height (average)	80 ft
a	First exponential for wind profile	2
b	Second exponential for wind profile	7

6. HEAD-UP DISPLAY (HUD) SPECIFICATIONS

6.1 Format and Symbology

The head-up display (HUD) will be presented in a monochromatic, calligraphic format provided to the pilot by the Evans and Sutherland Picture System through the "HUD Cathode Ray Tube" and optical beam splitter. Detailed requirements for the symbology will be provided in a subsequent section of this specification.

6.2 Display Configurations

There will be two display configurations and two display modes selectable by the research engineer. The symbols to be presented by each of these configuration-mode combinations are illustrated in Figs. 6.1 through 6.4. The first configuration is an elevation-azimuth display format designed for forward flight at the very low speeds typical in NOE operations. The first mode of this configuration is the monitoring display, for use in the pilots' monitoring of the automated flights. The side-task displays (Section 11) are included in this display format. The second elevation-azimuth display mode omits the side-task displays, substituting additional aircraft state information to aid in the manual guidance of the rotorcraft in NOE flight conditions.

The second display configuration is a plan-view format designed for hover tasks in low visibility NOE conditions. The first mode of this configuration is the monitoring display, again for use in the pilots' monitoring of the automated flights. The side-task displays (Section 11) are included in this display format. The second plan-view display mode omits the side-task displays for use in the manual guidance of the rotorcraft.

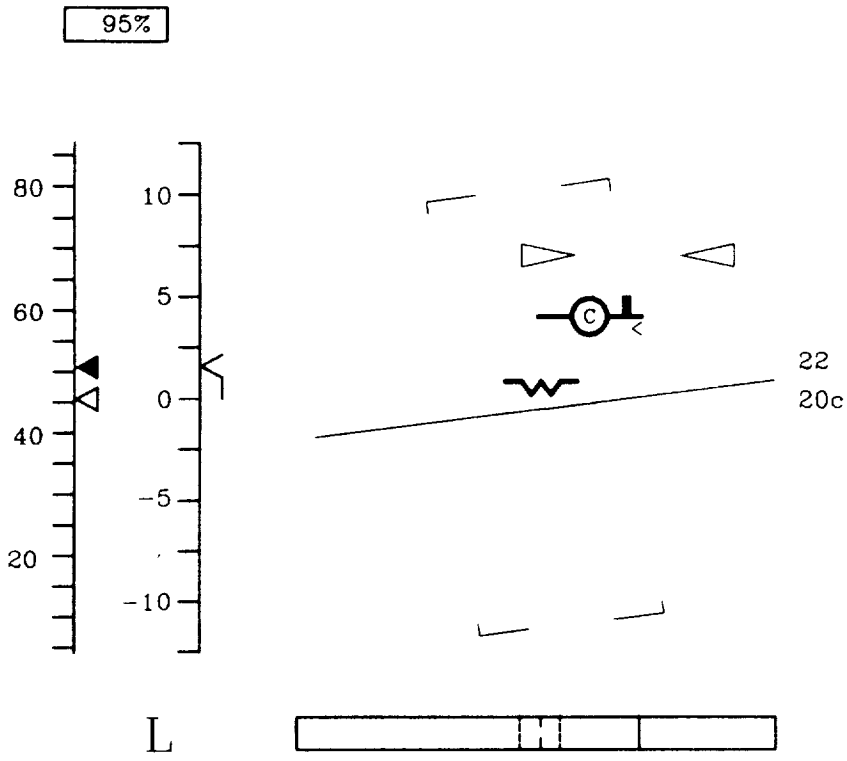

Figure 6.1 Field of View for Elevation-Azimuth Display Monitoring HUD Configuration

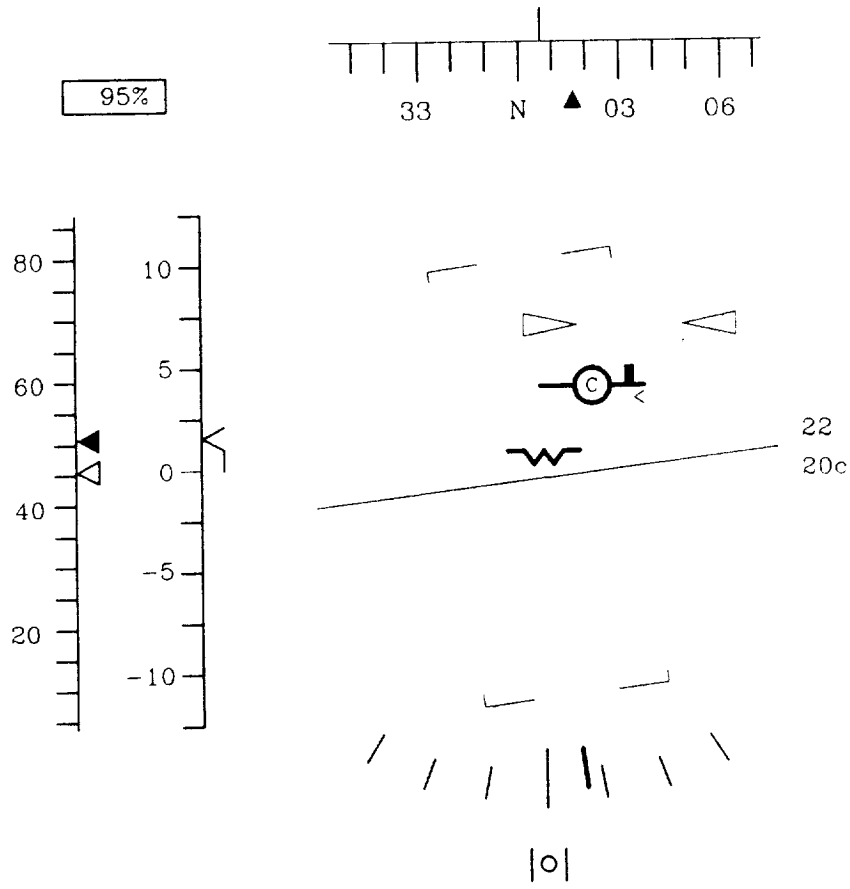

Figure 6.2. Field of View for Elevation-Azimuth Display Manual Guidance HUD Configuration

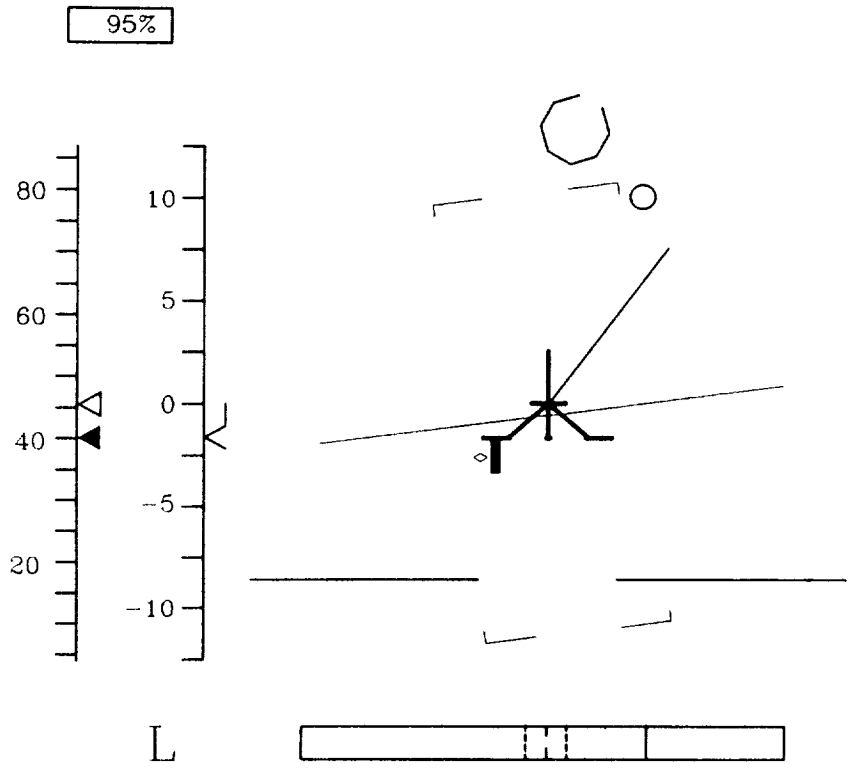

Figure 6.3 Field of View for Plan-View Hover Task Display Monitoring HUD Configuration

6.3 Symbol Size and Shape, General Requirements

a. Symbol Dimensions are expressed in the angle subtended by the symbol or portion thereof at the design eye position defined in MIL-STD-1333.

b. The locations of the case-oriented symbols in the pilot's field of view for the different dispay configurations are shown in Figs. 6.5 amd 6.6.

c. The symbol line width shall subtend 2.0 ± 0.2 milliradians (2σ) with a symbol brightness-to-background ratio of 15 and best focus. (Symbols may, however, be subject to chromatic aberration at the periphery of the field of view required in Fig. 6.3 without violating the intent of this requirement.)

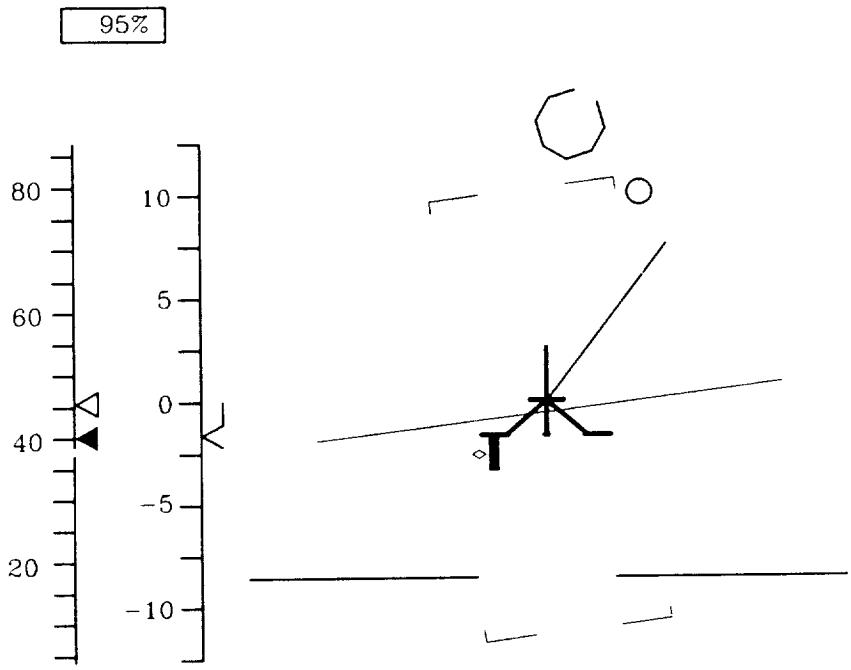

Figure 6.4 Field of View for Plan-View Hover Task Display
Manual Guidance HUD Configuration

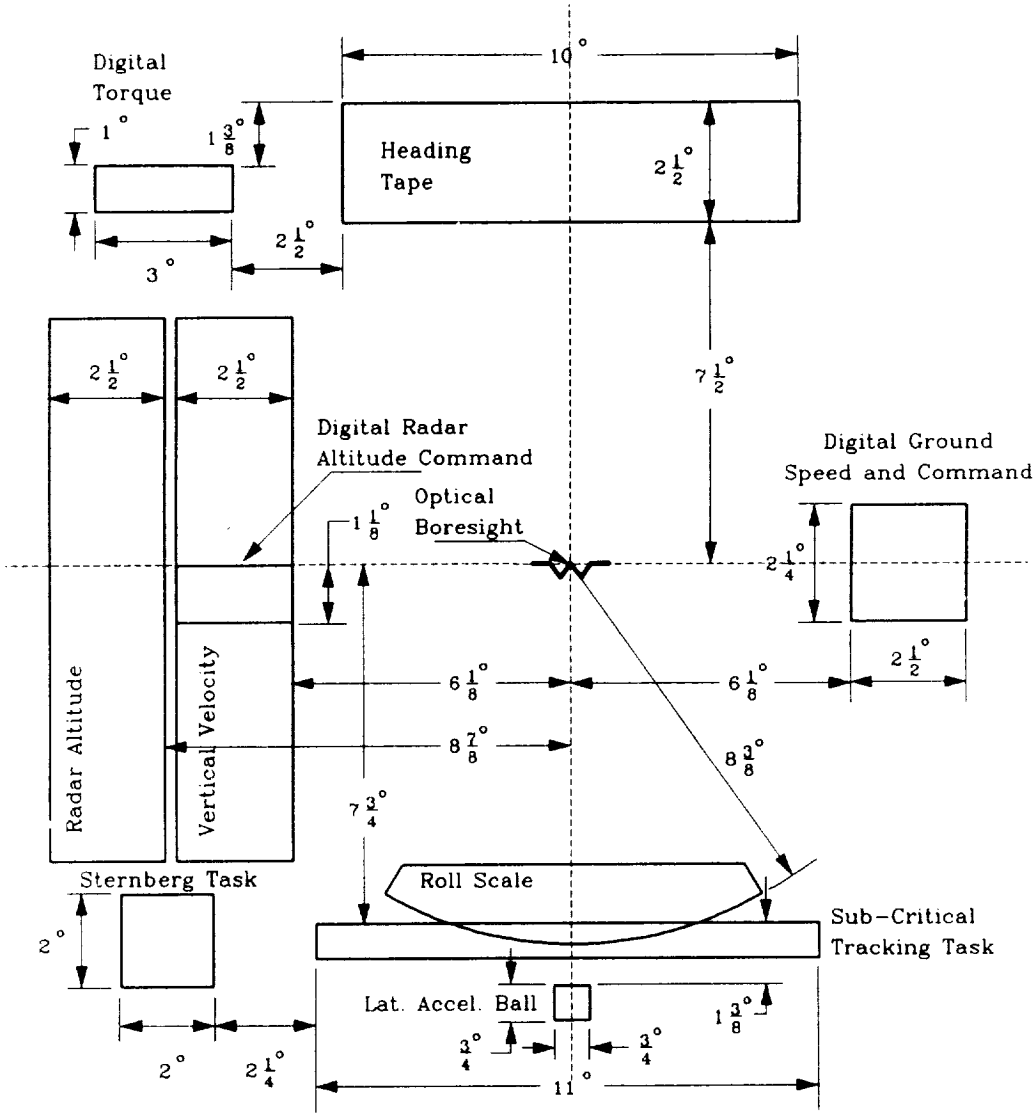

Figure 6.5 Field-of-View Locations for Case-Oriented Symbols Elevation-Azimuth Display Configuration

d. The shape of alphanumeric characters that are incorporated as part of the required symbology shall be as shown in Fig. 6.7. Unless otherwise specified, each character shall be 1/2 deg high by 1/3 deg wide with a corresponding character spacing of 1/6 deg.

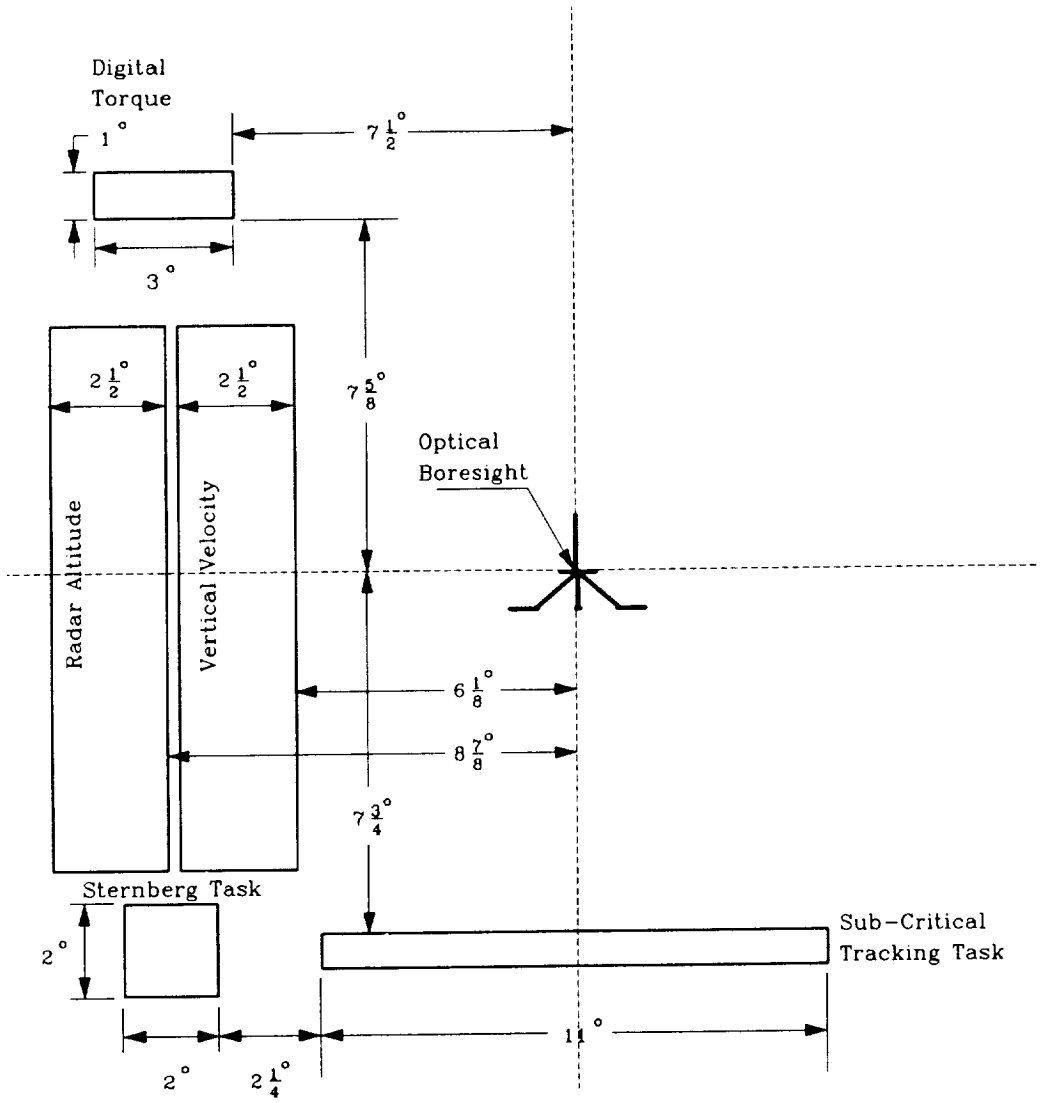

Figure 6.6 Field-of-View Locations for Case-Oriented Symbols Plan-View Display Configuration

Figure 6.7 Alphanumeric Shapes

e. Brightness, gain, and centering controls for the calligraphic HUD CRT are located above the cockpit and can be adjusted only when the cockpit is docked. The color, brightness, and reference/position of each set of symbols described in the next section shall, however, be independently adjustable form the operator's console by means of software and/or hardware controls.

6.4 Individual Requirements for Symbols

a. The shape and dimensions of the center aircraft reference are shown in Fig. 6.8. The boresight reference point shall at all times correspond to the optical boresight of the HUD.

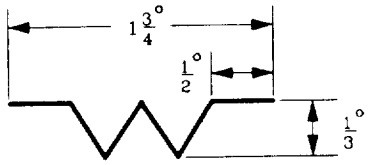

Figure 6.8 Center Aircraft Reference

b. The shape and dimensions of the pseudo-flight path symbol are shown in Fig. 6.9. The location of the symbol is defined in Fig. 6.10 and the following equations.

$$FP_x = K_{v_{HUD}} V_{gd}$$

$$FP_y = -K_{h_{HUD}} v_D$$

where v_D and V_{gd} are defined in Figs. 1.2 and 1.1, respectively. The display scaling gains are defined in Table 6.1.

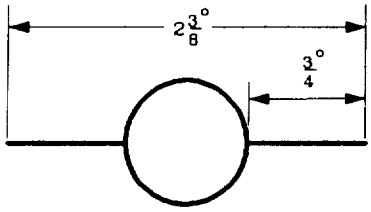

Figure 6.9 Pseudo-Flight Path Symbol

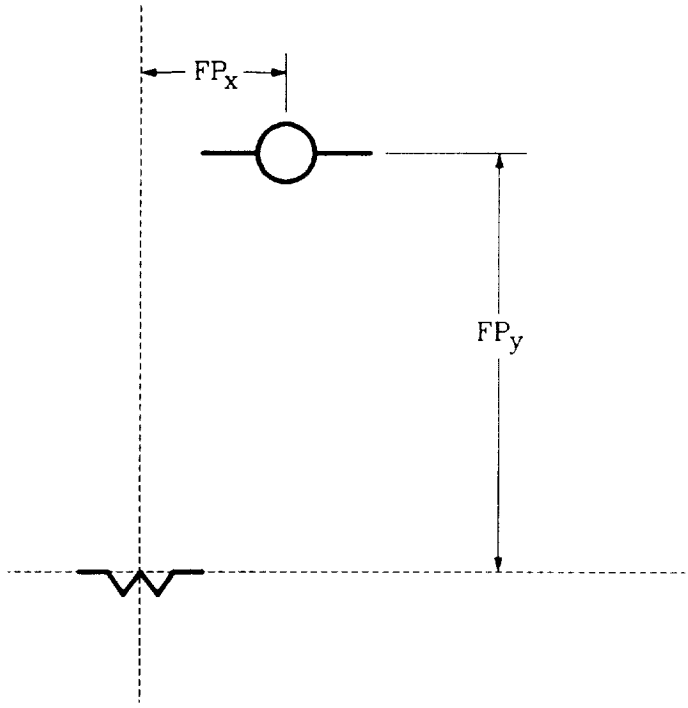

Figure 6.10 Field-of-View Location of the Pseudo-Flight Path Symbol

c. The shape and dimensions of the ghost aircraft are shown in Fig. 6.11. The location of the symbol is defined in Fig. 6.12 and the following equations.

$$G_x = K_{v_{HUD}}\left(-(y_{com} - y_{cs})K_y + \frac{1}{K_{pgy}}\left(\frac{1}{T_{pgy}}\dot{y}_{pg} + \ddot{y}_{pg}\right)\right)\frac{1}{K_{v_c}}$$

$$G_y = K_{h_{HUD}}\left(-(h_{com} + h_{c_{auto}} - h_{cg})K_h + \frac{1}{K_{pgh}}\left(\frac{1}{T_{pgh}}\dot{h}_{pg} + \ddot{h}_{pg}\right)\right)\frac{1}{K_{h_c}}$$

where the parameters of these equations are defined in Section 1.1. This symbol leads the rotorcraft along the preplanned flight profile, modified as necessary to indicate course changes to avoid obstacles.

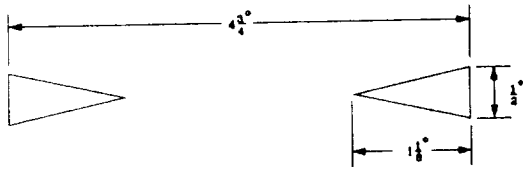

Figure 6.11 Ghost Aircraft Symbol

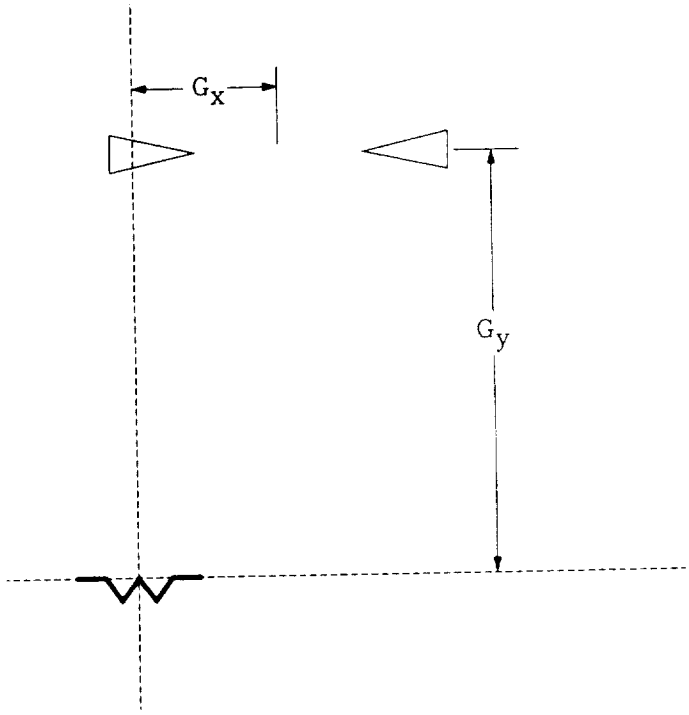

Figure 6.12 Field-of-View Location of the Ghost Aircraft Symbol

d. The longitudinal ground speed error will be displayed as the magnitude of a ribbon referenced to the left wing of the pseudo-flight path symbol. The dimensions and location of the velocity error ribbon are depicted in Fig. 6.13. The equation for the magnitude of the ribbon follows.

$$U_{gd_e} = K_{UERR}\left(U_{gd} - U_{ref} - K_{F_\theta}\left(\frac{\theta s}{s + \frac{1}{\tau_\theta}}\right)\right)$$

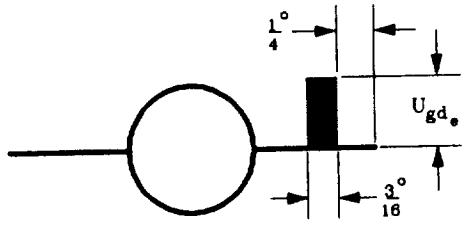

Figure 6.13 Longitudinal Ground Speed Error Ribbon

e. The acceleration caret will display a shaped longitudinal acceleration referenced to the left wing of the pseudo-flight path symbol. The dimensions and location of this symbol are depicted in Fig. 6.14. The equation for the vertical location of this symbol follows.

$$a_{lon} = K_{a_{lon}}\left(\ddot{V}_N \cos\psi + \ddot{V}_E \sin\psi + \frac{1}{\tau_{A_x}} V_{eq}\right)\left(\frac{s}{s + \frac{1}{\tau_{A_x}}}\right)$$

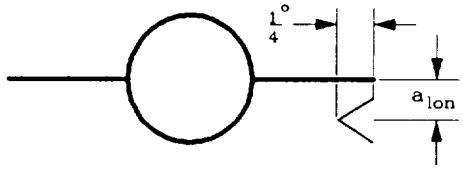

Figure 6.14 Longitudinal Acceleration Caret

f. The alphanumeric symbol "C" (for caution indicator) shall be presented, centered within the pseudo-flight path symbol when any of the three caution lights on the cockpit instrument panel designated for the choice reaction time side task is illuminated (Fig. 6.15).

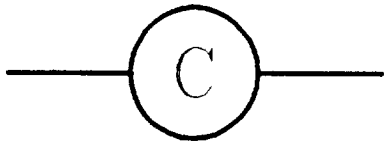

Figure 6.15 Caution Indicator

g. The shape and dimensions of the artificial horizon and pitch ladder are depicted in Fig. 6.16. Downward displacement of the artificial horizon with respect to the boresight shall be in one-to-one proportion to the nose-up elevation or pitch Euler angle of the aircraft with respect to the local horizontal plane. Counterclockwise rotation of the artificial horizon about the boresight shall be in one-to-one proportion to the clockwise roll Euler angle of the aircraft with respect to the local horizontal plane.

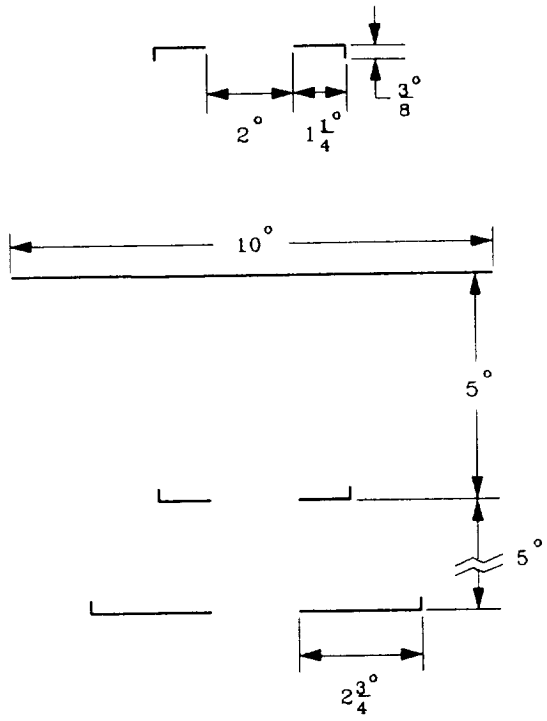

Figure 6.16 Artificial Horizon and Pitch Ladder Specifications

h. The shape and dimensions of the roll scale are shown in Fig. 6.17. The field-of-view location of the symbol is presented in Fig. 6.5. The present roll attitude shall be indicated by the location of the pointer relative to the fixed roll scale. Plus or minus thirty (±30) degrees of the roll attitude scale shall be displayed. The pointer shall move as if it were a segment of a line rotating about the boresight of the display. One degree of rotation shall correspond to minus one degree of roll Euler angle. The scale shall be graduated in ten roll attitude degree increments.

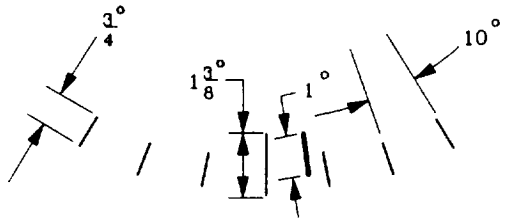

Figure 6.17 Roll Scale Specifications

i. The shape and dimensions of the sliding scale with fixed pointer indicating radar altitude are shown in Fig. 6.18. The sliding tape is to be driven such that the present radar altitude in feet shall be designated by the measure opposite the fixed empty pointer, and the commanded radar altitude shall be designated by the measure opposite the solid moveable pointer. A total of 83 ft will be presented at all times. The empty pointer is case-fixed such that a horizontal line through the HUD boresight bisects the pointer. The command symbol shall remain in view at one degree beyond the nearest degree of presentation when the altitude error exceeds the range of presentation. The scale is graduated into equally spaced, 5 ft increments from 0 to 200 ft. Every 20 ft graduation shall be numbered.

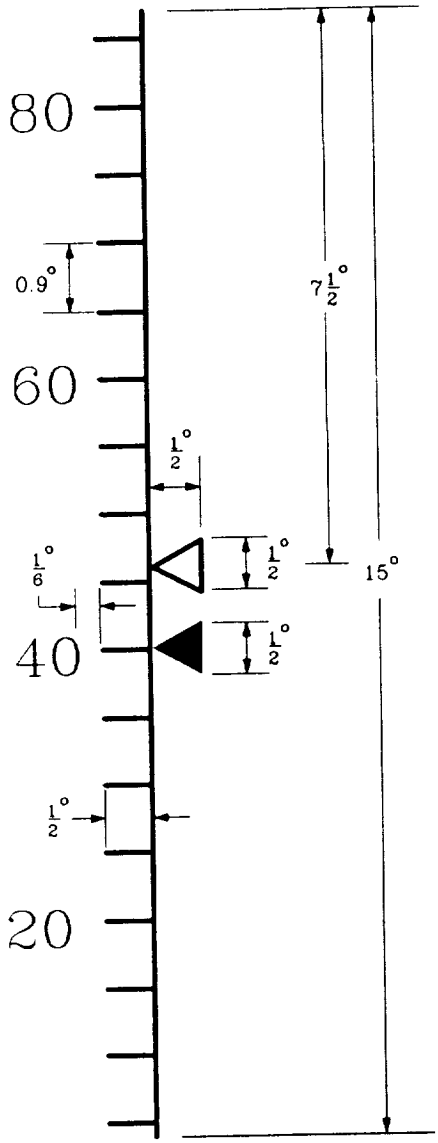

Figure 6.18 Sliding Radar Altitude Tape (ft)

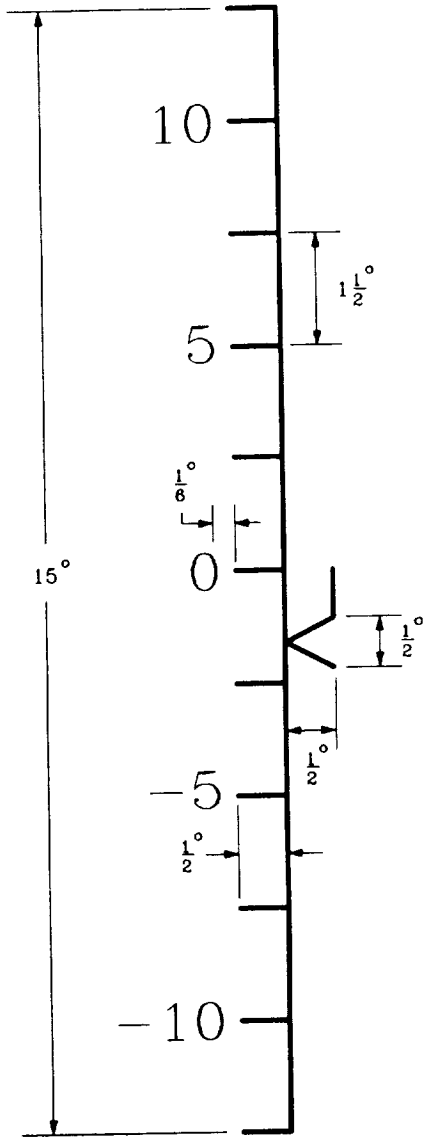

Figure 6.19 Fixed Vertical Velocity Tape (100 fpm)

j. The shape and dimensions of the fixed scale with moving pointer indicating vertical speed are shown in Fig. 6.19. The vertical speed in hundreds of feet per minute (fpm) is designated by the moveable pointer. The moveable pointer shall always be joined with a point beside the zero graduation by a line of adjustable length as shown in Fig. 6.19. The moveable pointer shall remain in the field of view at one degree beyond

the extreme graduation on the scale, and the present indicated vertical speed shall be displayed digitally, to the nearest 100 fpm with the tens and units digits omitted, to the left of the pointer located and in correspondence with the scale of digits shown in Fig. 6.19. The fixed scale shall be graduated into equally spaces 250 fpm increments from -1250 to +1250 fpm. Every 500 fpm graduation shall be numbered with the zero, tens, and units digits omitted.

An option for the research engineer is to omit both the sliding radar altitude tape and the fixed vertical velocity tape and, instead, present the radar altitude digitally together with the letter "R" to designate the number as a radar altitude, tied to the location of the pseudo-flight path symbol (Fig. 6.20). In this case, the commanded radar altitude would be presented digitally, in a location opposite the commanded longitudinal ground speed (Fig. 6.5), with the letter "C" included to designate the number as a command.

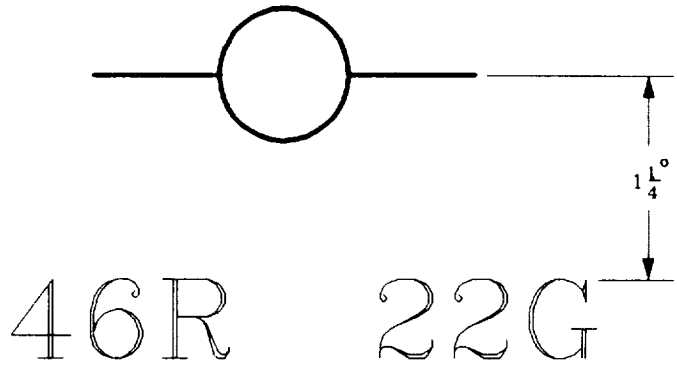

Figure 6.20 Digital Presentation of Radar Altitude and Ground Speed

k. Two methods for displaying heading will be selectable by the research engineer. The first is a sliding heading tape with fixed pointer along the top of the display. The shape and dimensions of this moving scale, to be driven by magnetic heading, are shown in Fig. 6.21. The present magnetic heading in degrees shall be designated by the fixed centrally located line segment, and the commanded magnetic heading, by the moveable solid pointer. The command symbol shall remain in view within one degree of the nearest limit of presentation when the command heading is beyond the range of presentation. Ninety (90) heading degrees of the moveable scale shall be presented within the ten (10) field-of-view degrees allocated in Fig. 6.5. The moving scale shall be graduated in equally spaced, 10-heading-degree increments with every 30th heading-degree numbered with the zero units digit omitted and the numeral

labels replaced with the letters N, E, S, and W for the headings 0, 90, 180, and 270 deg, respectively. The moving scale shall provide a continuous presentation, i.e., 0 deg shall follow 350 deg on the scale as shown in Fig. 6.21.

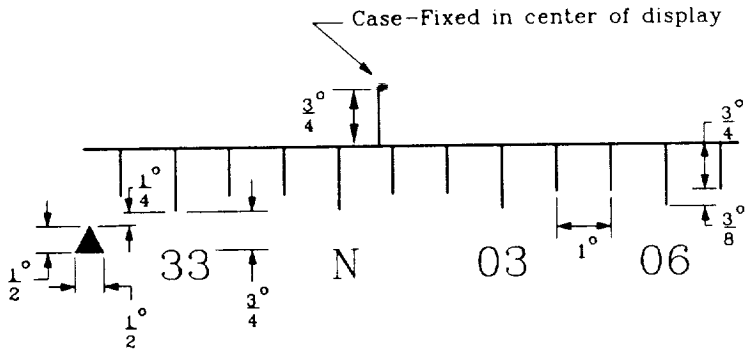

Figure 6.21 Sliding Heading Tape

The second method of presentation of heading is a sliding scale along the artificial horizon, as shown in Fig. 6.22. The sliding scale will not be presented in the center 5 field-of-view degrees of the artificial horizon.

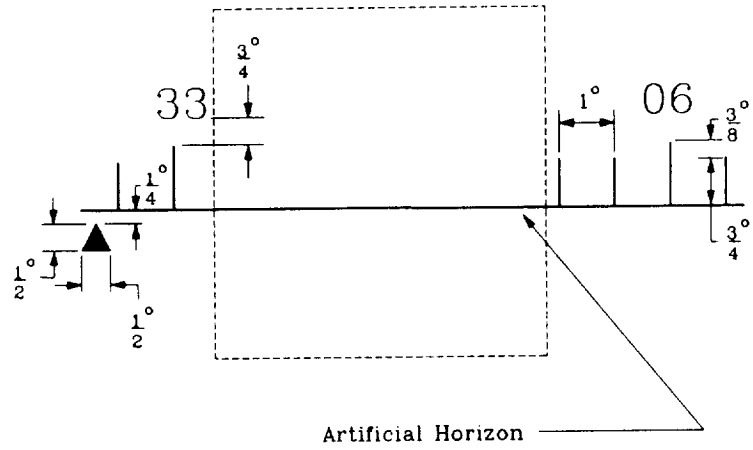

Figure 6.22 Heading Tape on Artificial Horizon

l. The shape and dimensions of the sub-critical tracking task are shown in Fig. 6.23. The moveable line segment shall subtend 4.0 ± 0.2 milliradians (2σ). The lateral positioning of this line segment is governed by the following transfer function:

$$S_x = \frac{K_{sx}\lambda_{sc}}{s - \lambda_{sc}}\delta_{sx}$$

where λ_{sc} is a subcritical value for the unstable pole, $K_{sx} = 7$ deg is the display gain, and δ_{sx} is the normalized, unitless pilot control input through a small side-arm controller. The moveable line segment will flash at the boundary of the assigned range of presentation of the subcritical tracking task when $|S_x| > 7$ deg at a frequency of 3 Hz.

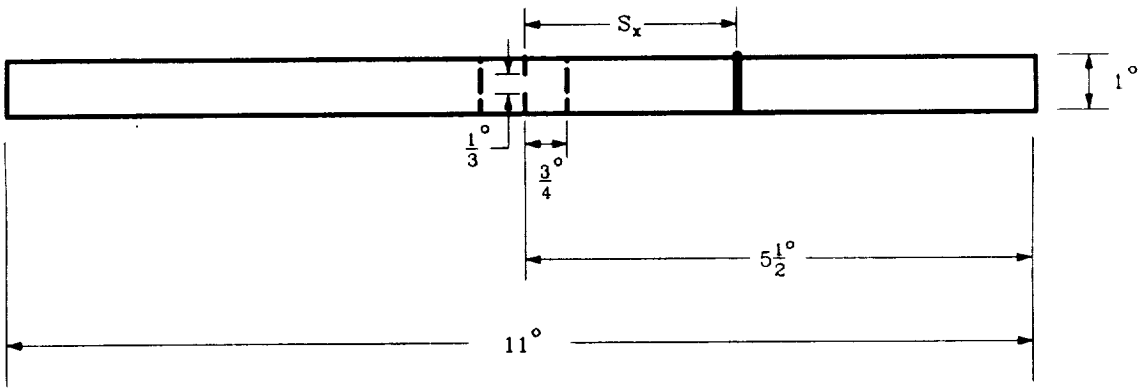

Figure 6.23 Sub-Critical Tracking Task

m. One, two, or three numerals representing the longitudinal ground speed of the aircraft to the nearest units digit, together with the letter "G" to distinguish it from airspeed, shall appear in one of two places in the display, selectable by the research engineer. The first option is to present the digital ground speed in the region of the field of view so designated in Fig. 6.5, along with one, two, or three numerals and the letter "C" representing the commanded ground speed.

The second option is to tie the digital ground speed presentation to the pseudo-flight path symbol, as shown in Fig. 6.20. The commanded ground speed would be presented as before on the right side of the display.

n. Two or three numerals representing the percent rotor torque to the nearest units digit shall appear in the region of the field of view so designated in Fig. 6.4. A calligraphic percent symbol ("%") shall be presented 1/6 field-of-view degrees to the right of the units digit. A box surrounding the range of presentation shall be presented.

o. One calligraphic alphabetic character from those depicted in Fig. 6.5 shall be presented in the region of the field of view so designated in Fig. 6.4 for the Sternberg recognitive task. The height of the character shall be 1 deg, and the width shall be 2/3 deg. No box shall encompass this presentation. Incorrect responses to the presented character will result in the continued presentation of that character for 2 sec with a cross-hatched, 2 deg-by-2 deg box superimposed over the presentation area (see Fig. 6.4) flashing at 3 Hz.

p. The shape and dimensions of the lateral acceleration ball are defined in Fig. 6.24. The field-of-view location of the symbol is defined in Fig. 6.5. The lateral offset of the ball is defined by the following equation.

$$a_{lat} = K_{LA} a_y$$

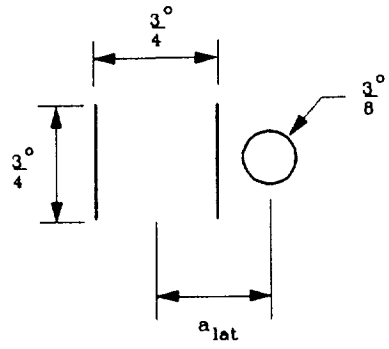

Figure 6.24 Lateral Acceleration Symbol

q. The shape and dimensions of the aircraft trident are shown in Fig. 6.25. The boresight reference point shall at all times correspond to the optical boresight of the HUD and shall correspond to the plan view c.g. of the rotorcraft.

r. The location of the tip of the velocity vector is defined in Fig. 6.26 and by the following equations.

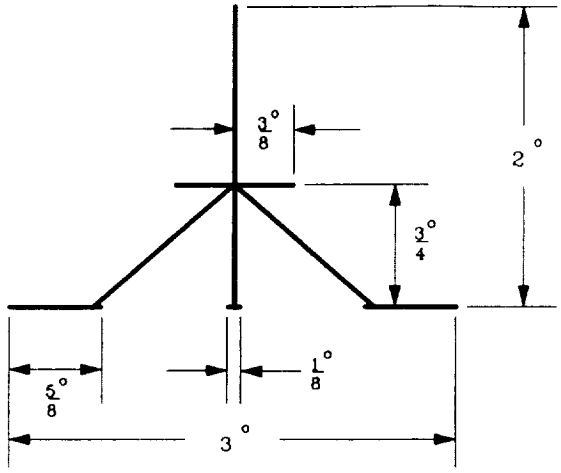

Figure 6.25 Aircraft Trident Symbol

$$V_x = K_{sc} V_{gd}$$

$$V_y = K_{sc} U_{gd}$$

where U_{gd} and V_{gd} are the rotorcraft ground track velocity components rotated into the aircraft heading coordinates.

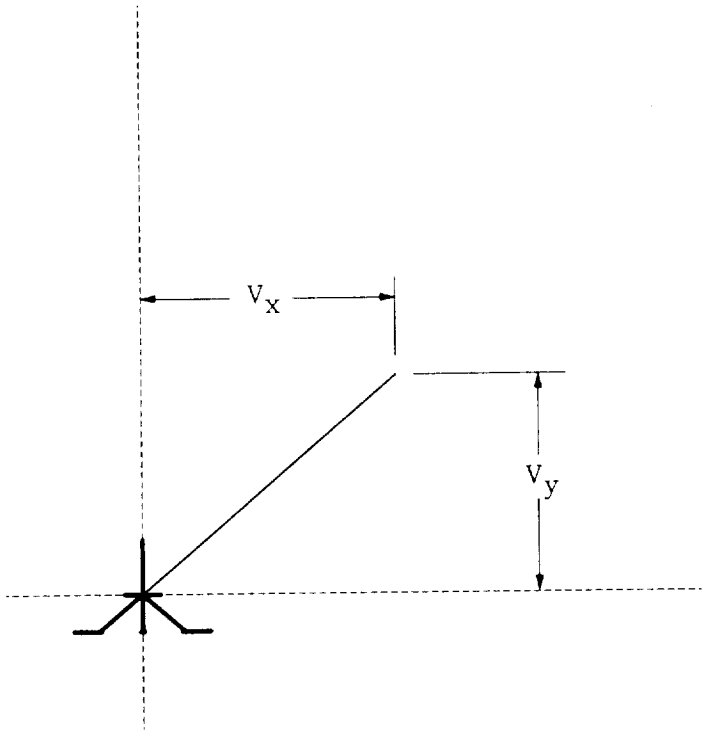

Figure 6.26 Field-of-View Location of the Tip of the Velocity Vector

s. The shape and dimensions of the acceleration symbol (flight command symbol) are shown in Fig. 6.27. The field-of-view location and orientation of the symbol are defined in Fig. 6.28 and by the following equations.

$$A_x = K_{sc} V_{c_{HUD}}$$

$$A_y = K_{sc} U_{c_{HUD}}$$

where $U_{c_{HUD}}$ and $V_{c_{HUD}}$ are defined in Fig. 1.1. In steady-state flight, the symbol rests on the tip of the velocity vector.

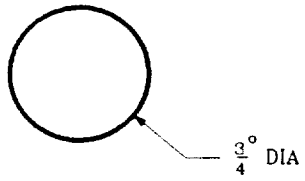

Figure 6.27
Acceleration Symbol

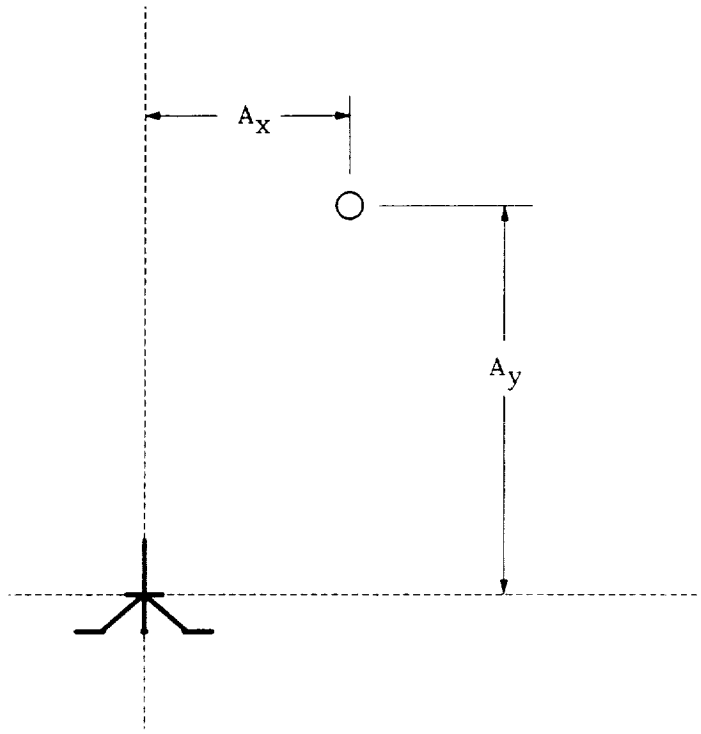

Figure 6.28 Field-of-View Location of the Acceleration Symbol

t. The shape and dimensions of the hover pad symbol are shown in Fig. 6.29. The field-of-view location and orientation of the symbol are defined in Fig. 6.30 and by the following equations.

$$\begin{pmatrix} H_x \\ H_y \end{pmatrix} = K_{hv} \begin{bmatrix} \cos(\psi) & \sin(\psi) \\ -\sin(\psi) & \cos(\psi) \end{bmatrix} \begin{pmatrix} y_e(I_{WP}) - y_{cg} \\ x_e(I_{WP}) - x_{cg} \end{pmatrix}$$

$$H_\psi = \psi_{obs}(I_{AMC}) - \psi$$

where x_{cg} and y_{cg} are the present aircraft location in inertial coordinates, ψ is the present aircraft heading, $x_e(I_{WP})$ and $y_e(I_{WP})$ are the inertial coordinates of the observation waypoint, I_{WP}, and $\psi_{obs}(I_{WP})$ is the observation heading at that waypoint. The symbol will not be presented when the hover location is outside the central field of view of the HUD.

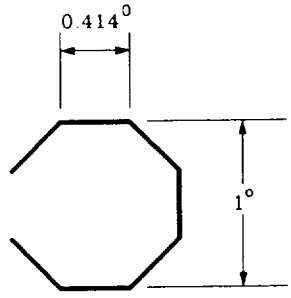

Figure 6.29
Hover Location Symbol

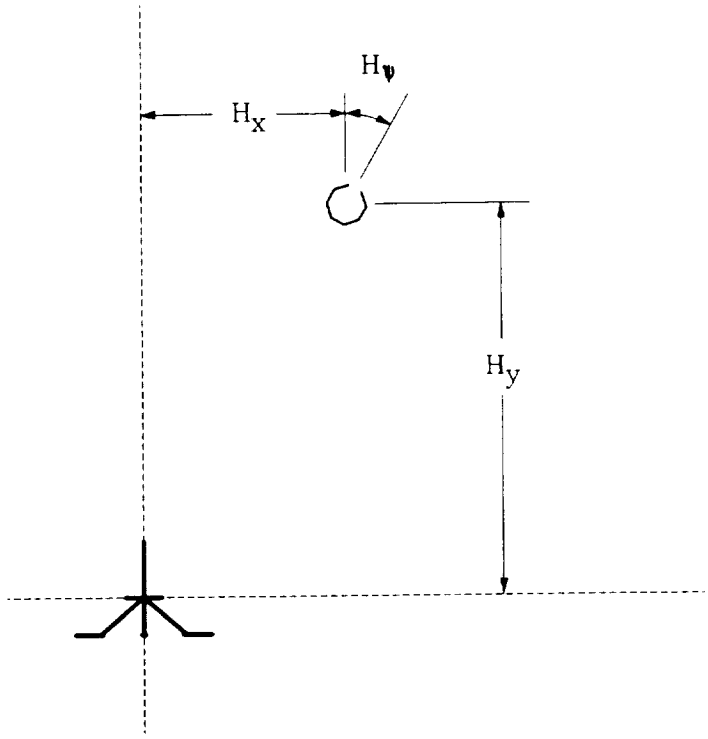

Figure 6.30 Field-of-View Location of the Hover Location Symbol

u. The radar altitude command bar is referenced to the bottom of the aircraft trident symbol and displays the difference between the commanded and actual radar altitude. The dimensions and location of this symbol are defined in Fig. 6.31 and by the following equation.

$$RA_c = K_{h_{HUD}}(h_{com} + h_{c_{auto}} - h_{cg})$$

v. The vertical velocity ribbon is referenced to the lower left "gear" on the aircraft trident symbol. The dimensions and location of this symbol are defined in Fig. 6.32 and by the following equation.

$$VV_r = -K_{h_r} v_D$$

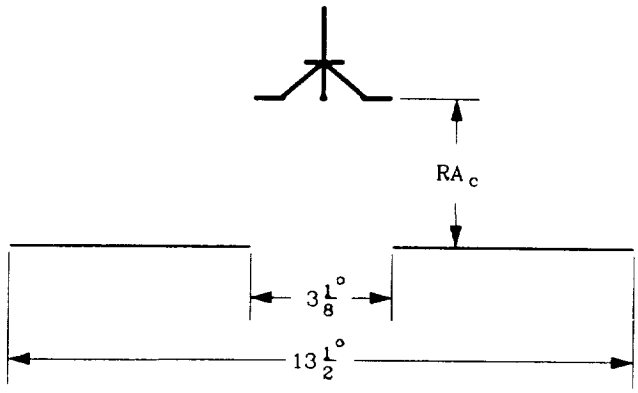

Figure 6.31 Radar Altitude Command Bar

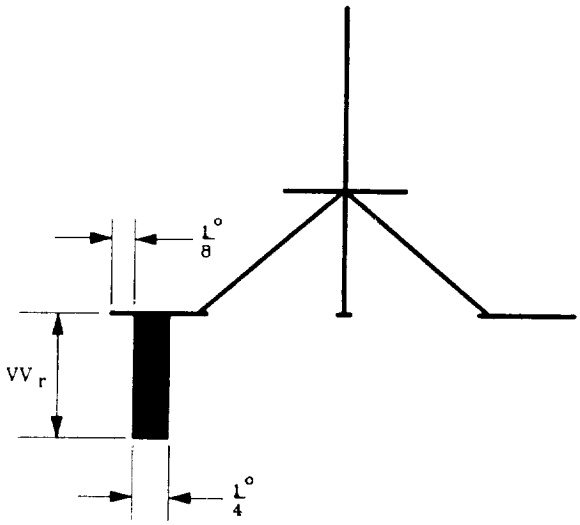

Figure 6.32 Vertical Velocity Ribbon

w. The shape and dimensions of the vertical velocity predictor symbol are presented in Fig. 6.33. This symbol is also referenced to the lower left "gear" of the aircraft trident symbol. The location of this symbol is defined in Fig. 6.34 and by the following equation.

$$VP_r = K_{h_r} \dot{h}_{HUD}$$

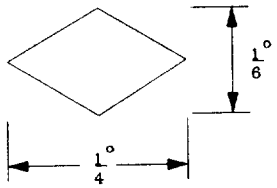

Figure 6.33 Vertical Velocity Predictor

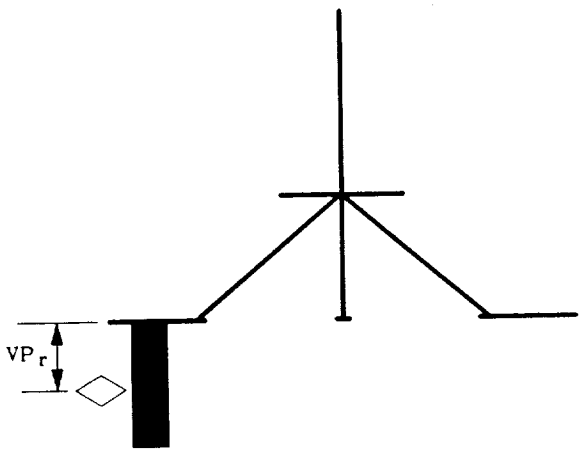

Figure 6.34 Location of the Vertical Velocity Predictor

TABLE 6.1

HEAD-UP DISPLAY GAINS

$K_{v_{HUD}}$	Lateral velocity display scaling gain	0.2 deg/ft/sec
$K_{h_{HUD}}$	Vertical velocity display scaling gain	0.02 deg/fpm
K_{UERR}	Longitudinal velocity error display scaling gain	0.25 deg/kt
τ_{θ}	Pitch attitude washout time constant	25 sec
$K_{F_{\theta}}$	Pitch attitude washout gain	5.62 ft/sec/rad
$K_{a_{lon}}$	Longitudinal acceleration display scaling gain	0.5 deg/ft/sec^2
τ_{A_x}	Acceleration washout time constant	5 sec
K_{LA}	Lateral acceleration display scaling gain	5 deg/g
K_{sc}	Plan view velocity display scaling gain	0.2 deg/ft/sec
K_{hv}	Plan view displacement display scaling gain	0.05 deg/ft
$K_{h_{HUD}}$	Height error display scaling gain	0.1 deg/ft
$K_{h_{HUD}}$	Vertical velocity display scaling gain (Hover)	0.2 deg/ft/sec

7. COCKPIT INSTRUMENT SPECIFICATIONS

The specified cockpit instrument panel layout (Fig. 7.1) resembles that of the pilot station in the Apache attack helicopter. In addition to the toggle switches shown on the left side of the instrument panel and used to control the side tasks, parallel switches shall exist in the console panel to the pilot's left. Numbers on the figure are defined below.

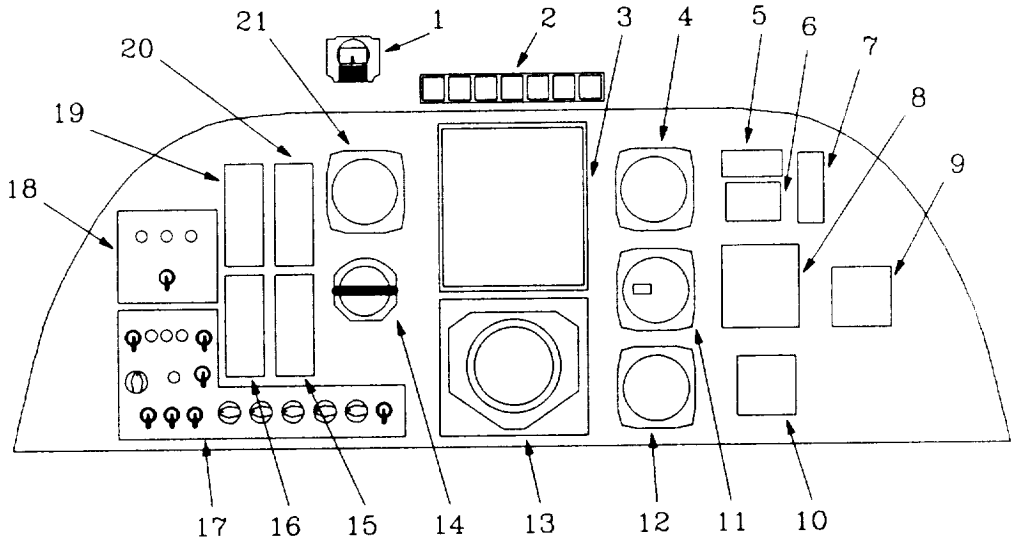

Figure 7.1 AH-64 Pilot Station Instrument Layout

1. Standby magnetic compass
2. Master caution/warning panel (contains lighted auto guidance toggle)
3. CRT for moving map display
4. Radar altimeter
5. Radio call placard
6. Stabilator position indicator
7. Stabilator/airspeed placard

8. Radar warning display

9. Clock

10. Accelerometer

11. Barometric altimeter

12. Instantaneous vertical speed indicator (IVSI)

13. Horizontal situation indicator (HSI)

14. Standby attitude indicator

15. Engine (N_P), rotor (N_R) indicator

16. Engine gas generator (N_G) indicator

17. Fire control panel

18. Choice reaction time side-task control panel

19. Engine turbine gas temperature (TGT) indicator

20. Engine torque indicator

21. Airspeed indicator

8. MOVING MAP DISPLAY (MMD) SPECIFICATIONS

8.1 Format and Symbology

The moving map display (MMD) will be presented on a color cathode-ray tube (CRT) monitor with a 7 inch diagonal screen. This device shall be mounted in the upper center of the cockpit instrument panel (Fig. 7.1). Detailed requirements for the symbology will be provided by a subsequent section of this specification.

8.2 Display Configurations

There will be three display scales selectable by the pilot: 5 dm to 1 in, 20 dm to 1 in, and 100 dm to 1 in. The scaled symbology to be presented by each of these modes is presented in Fig. 8.1, while the unscaled symbology is presented in Fig. 8.2.

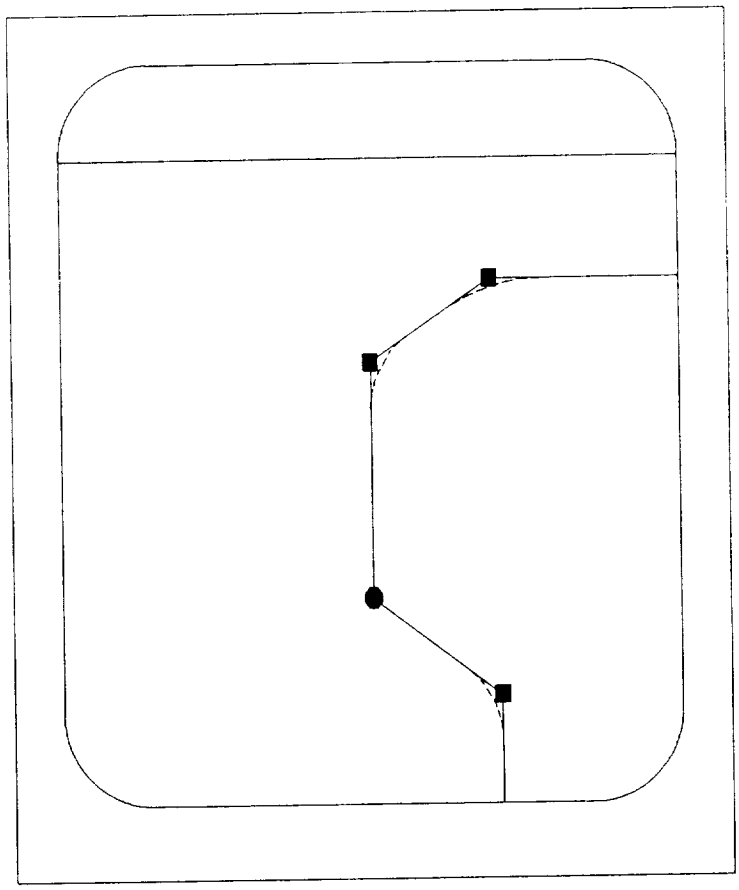

Figure 8.1 Scaled Symbology in the Moving Map Display

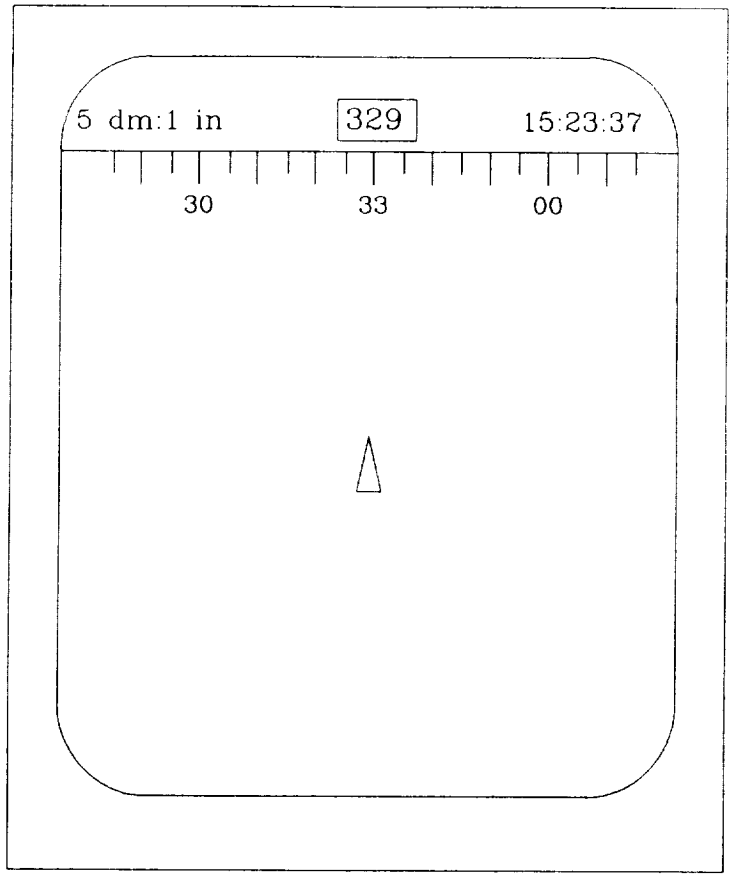

Figure 8.2 Fixed-Scale Symbology in the Moving Map Display

8.3 Symbol Size and Shape, General Requirements

a. Scaled symbol dimensions are expressed in decameters, while fixed-scale symbol dimensions are expressed in inches.

b. The locations of the case-oriented symbols are shown in Fig. 8.3. The dashed line 2.3 inches above the reference point delineates the map display area from the top portion of the display that is dedicated to the heading tape, etc. Above this line, the background is a solid shade equal to that of the level terrain in the map.

c. The symbol line width shall be 20.±2.0 mils (2σ) with a symbol brightness-to-background ratio of 10 at best focus.

d. The shape of alphanumeric characters that are incorporated as part of the required symbology shall be as shown in Fig. 6.4. Unless otherwise specified, each character shall be 0.3 inch high by 0.2 inch wide with a corresponding character spacing of 0.1 inch.

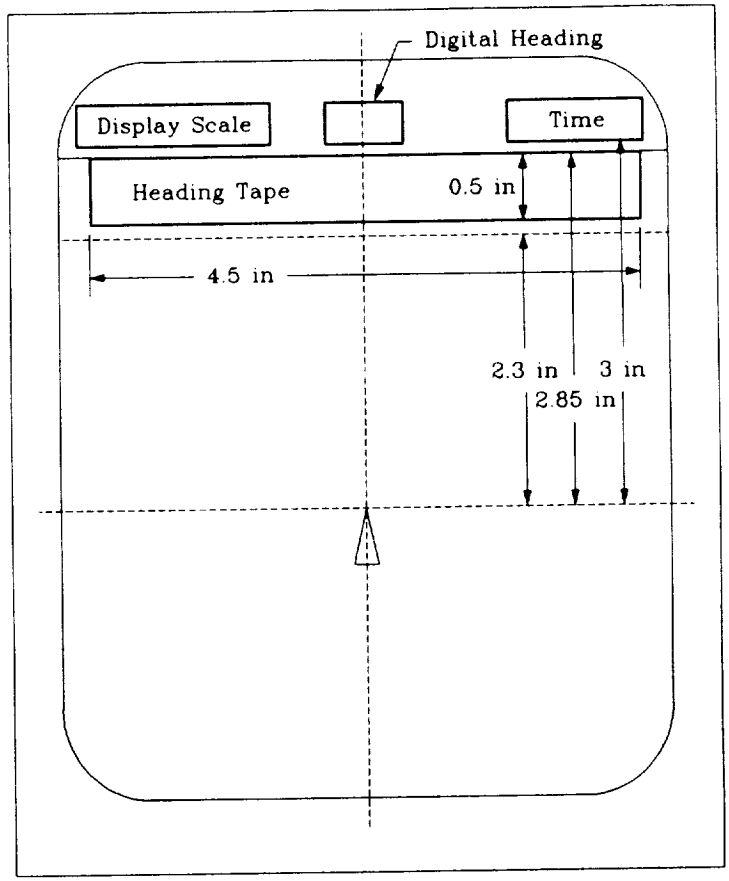

Figure 8.3 Locations for Case-Oriented Symbols

e. Brightness and scaling for the MMD CRT are located on the monitor; however, the color and brightness of each set of symbols described in the next section shall be adjustable independently from the operator's console by means of software and/or hardware controls.

8.4 Individual Requirements for Symbols

a. The shape and dimensions of the aircraft position indicator are shown in Fig. 8.4. The tip of the pointer shall at all times correspond to the center of the map display area. This symbol is fixed in scale, and the tip of the symbol represents the rotorcraft c.g. in plan view.

b. The waypoint course shall be presented to scale via a line connecting the waypoints defined in Section 2.1. The orientation of the presentation shall always be such that the rotorcraft heading is "up" on the display.

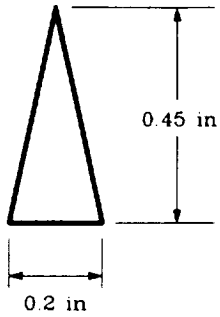

Figure 8.4 Aircraft Position Indicator

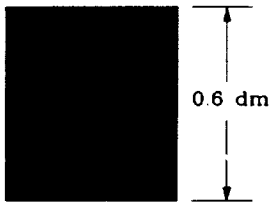

Figure 8.5 Nominal Waypoint Symbol

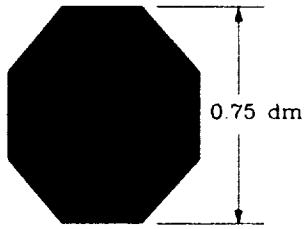

Figure 8.6 Waypoint Symbol Denoting Aggressive Maneuvering while on Watch

c. The waypoints are scaled symbols and are presented in the locations defined in Section 2.1. The shape and dimensions of the two types of waypoint symbols are presented in Figs. 8.5 and 8.6. The two types differentiate waypoints designating aggressive maneuvering while on watch (AMOW) from other waypoints.

d. The hyperbolic transition legs are shown on the waypoint course with dashed lines. Figure 8.7 presents a flow diagram of the generation of these hyperbolic transition legs.

Inputs:	Waypoint specifications:	
	Number of waypoints	N_{wps}
	Longitudinal coordinates of the waypoints	$x_e(I_{wp})$
	Latitudinal coordinates of the waypoints	$y_e(I_{wp})$
	Transitional velocities at the waypoints	$u_{tw}(I_{wp})$
Outputs:	Hyperbolic transition leg coordinates	y_{Eh} and x_{Eh}

a. Inputs and Outputs

Figure 8.7 Flow Diagram for Hyperbolic Transition Leg Calculation

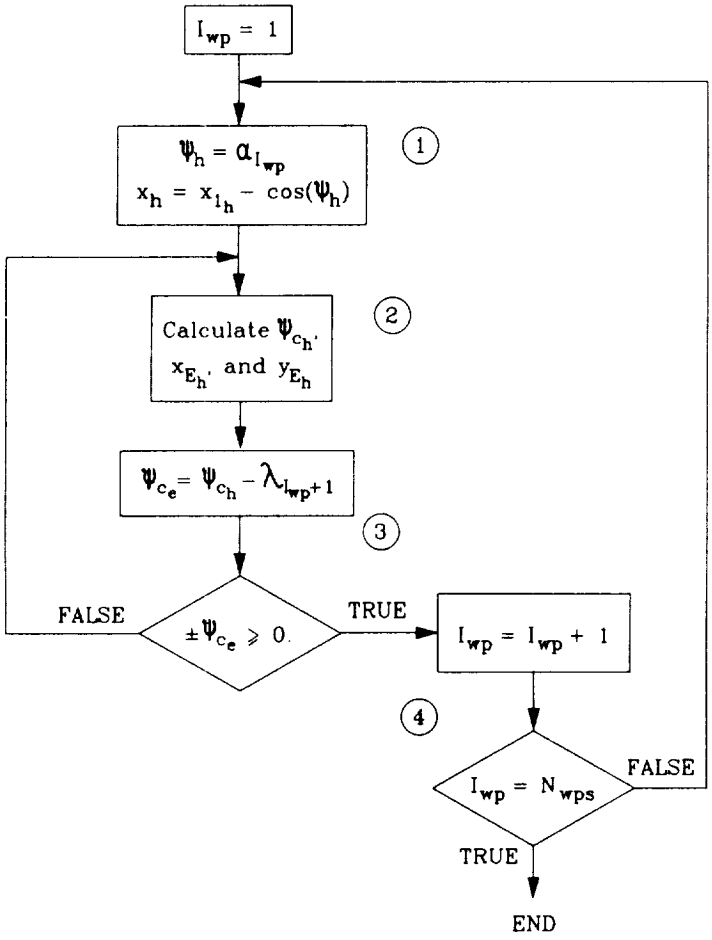

b. Hyperbolic Transition Leg Calculation

Figure 8.7 (Continued)

c. Notes (corresponding to circled numbers throughout figure)

1. For simplicity, the hyperbola calculations are performed in a reference frame in which the equation for the hyperbola is simply

$$\frac{y_h^2}{b^2} - \frac{x_h^2}{a^2} = 1$$

The hyperbolic trajectory is then determined by incrementing x_h, calculating y_h, and then tranforming the coordinate pair into earth-fixed coordinates. The x_h coordinate of the initial point of the hyperbolic trajectory, as well as the heading in the hyperbola reference frame, are calculated as shown to provide a start for the incremental process.

2. The calculation of a set of coordinates that are based on the previous x_h coordinate is accomplished using the following set of equations.

1. $x_h = x_h + \cos(\psi_h)$

2. $y_h = b(I_{wp})\sqrt{1 + \frac{x_h^2}{a^2(I_{wp})}}$

3. $\psi_h = \tan^{-1}\left(\frac{b^2(I_{wp})x_h}{a^2(I_{wp})y_h}\right)$

4. $\psi_{c_h} = \lambda_{I_{wp}} - \alpha_{I_{wp}} \pm \psi_h$

Finally, the transformation to earth-fixed coordinates is performed as follows:

5. $\psi' = \lambda_{I_{wp}} - \alpha_{I_{wp}}$

6. $y'_h = \pm\left(y_h - \sqrt{b^2(I_{wp}) - a^2(I_{wp})\tan^2(\alpha_{I_{wp}})}\right)$

7. $$\begin{bmatrix} x_{E_h} \\ y_{E_h} \end{bmatrix} = \begin{bmatrix} \cos(\psi') & -\sin(\psi') \\ \sin(\psi') & \cos(\psi') \end{bmatrix} \begin{bmatrix} x_h \\ y'_h \end{bmatrix} + \begin{bmatrix} x_{wp}(I_{wp}+1) \\ y_{wp}(I_{wp}+1) \end{bmatrix}$$

Figure 8.7 (Continued)

c. Notes (Concluded)

These equations are to be solved in order, with the initial values of x_h and ψ_h discussed in Note 1. Note that the sign of the $\mp$ in Eqn. 6 is determined by the direction of the turn: (-) for rightward turns and (+) for leftward turns. Refer to Section 2.1 for the calculation of the hyperbolic transition leg parameters.

3. The end of the hyperbolic transition leg occurs when the heading at a point on the leg coincides with the heading of the next waypoint leg. Note that the sign before the ψ_{c_e} term is determined by the direction of the turn: (+) for rightward turns and (-) for leftward turns.

4. The process is repeated until the waypoint counter reaches the total number of waypoints.

Figure 8.7 (Concluded)

e. The gaming area course is the area within which the pilot is required to navigate during the mission. In this case, the gaming area is defined by a series of course points and a course width (see Appendix D). The boundary of this course is presented on the moving map display as a solid line whose width is 40.±2.0 mils (2σ) with a symbol brightness-to-background ratio of 10 at best focus.

f. The shape and dimensions of the fixed pointer with moving scale to be driven by magnetic heading are shown in Fig. 8.8. The present magnetic heading in degrees shall be designated by the fixed centrally located line segment and presented digitally above the center as specified in Fig. 8.3. Ninety (90) heading degrees of the moveable scale shall be presented within the 4-1/2 inches allocated in Fig. 8.3. The moving scale shall be graduated in equally spaced 5 heading degree increments with every 30-heading-degree graduation numbered with the zero units digit omitted. The moving scale shall provide a continuous presentation, i.e., 0 deg shall follow 350 deg on the scale, as shown in Fig. 8.8.

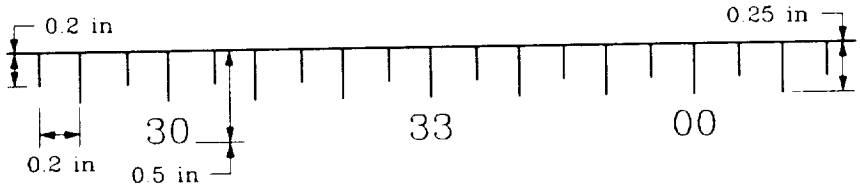

Figure 8.8 Sliding Heading Tape

g. The scale of the display will be presented in the upper left corner of the display, as shown Fig. 8.9. This figure represents sample scalings of the moving map display.

h. The clock time (local CPU is sufficient) will be presented in the upper left corner of the display, as shown in Fig. 8.9.

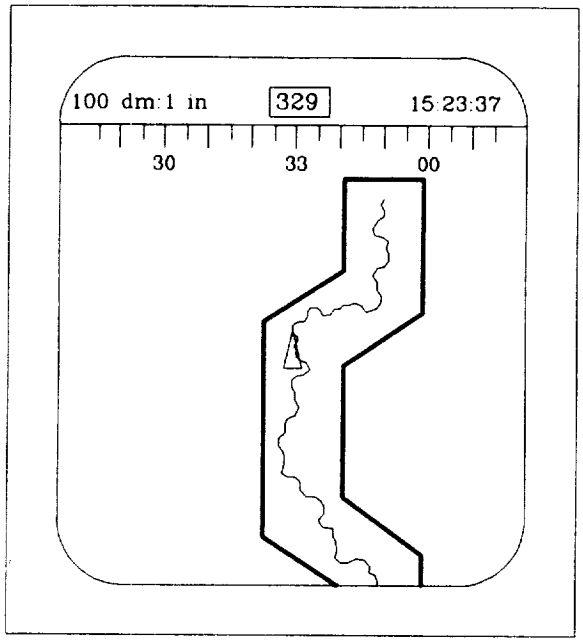

a. 100 dm to 1 in Display Scaling

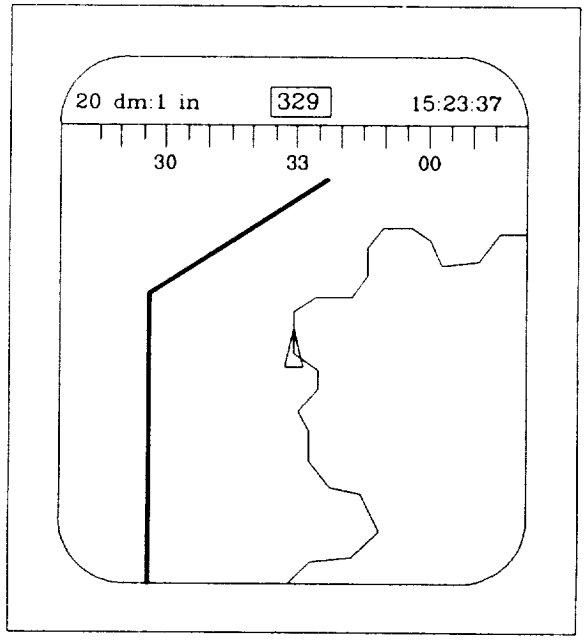

b. 20 dm to 1 in Display Scaling

Figure 8.9 Sample Scalings of the Moving Map Display

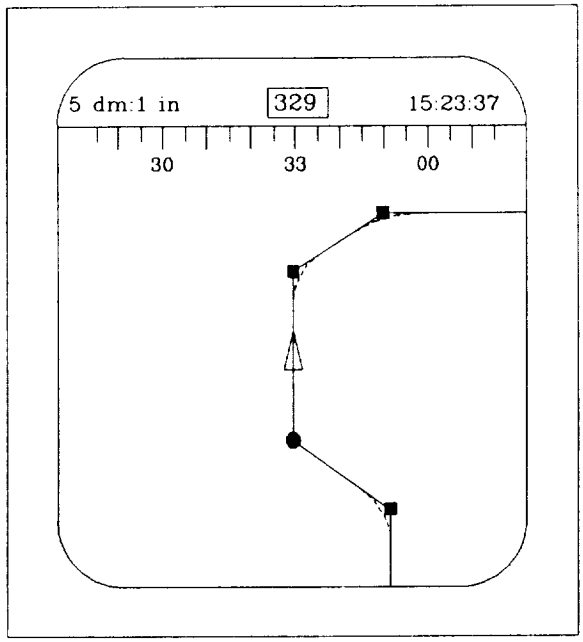

c. 5 dm to 1 in Display Scaling

Figure 8.9 (Concluded)

9. AUDIO ANNUNCIATOR

9.1 Audio Annunciator Specifications

In order to alert the pilot to impending departures from the flight path due to unexpected obstacles, an audio announcement will be presented to the pilot via his head set prior to the execution of the maneuver. The messages for these evasive maneuvers are in two parts: 1) direction and 2) magnitude (and urgency in the case of the lateral maneuvers). The definitions of the possible announcements follow.

TABLE 9.1 LATERAL MANEUVERS ANNOUNCEMENTS

Direction	Magnitude and Urgency (MUF_{AUD})
"Left"	"One-one"
"Right"	"Two-one", etc.

Note: The maneuver urgency factor is used as the second part of the message, because it contains both information about the magnitude (the first digit represents the number of decameters to be traversed during the maneuver) and the urgency (the second digit represents the urgency on a 1-4 scale). There are twelve possible maneuver urgency factors (see Section 4.2).

TABLE 9.2 VERTICAL MANEUVER ANNOUNCEMENTS

Direction	Magnitude
"Up" "Down"	Magnitude of the maneuver to the nearest whole foot

Note: The magnitude of the bob-up and -down maneuvers will vary between 1 and 100 ft. To cover all possible combinations, a voice recording can be made of the numbers 1 through 19, and the tens 20 through 100. An alternate approach would be to use a voice synthesizer to generate the messages.

Another maneuver announced prior to its execution is a speed change at a waypoint transition. Although these maneuvers are not unexpected, as the transition velocities at all of the waypoints are defined prior to the flight (see Section 2.1), they are abrupt and could reduce the pilot's confidence in the automatic system if initiated without warning. There are three messages associated with the speed change maneuvers:

TABLE 9.3 VELOCITY CHANGE ANNOUNCEMENTS

"Transition Velocity Change" - Indicates a reduction in velocity to precede a waypoint transition.

"Transition to hover; prepare for aggressive maneuvering" - Indicates the proximity of a waypoint specifying aggressive maneuvering while on watch.

"Resume nominal velocity" - Indicates an increase in velocity to the nominal velocity following a waypoint transition.

"Obstacle avoidance speed change" - Accompanies a vertical evasive maneuver announcement indicating a change in speed required to avoid a detected obstacle.

9.2 Determination of Audio Annunciator Messages

For imminent lateral and vertical maneuvers, the audio messages are determined by using the obstacle detection and avoidance maneuver selection logic, based on an altered waypoint course position. In the longitudinal axis, the waypoint course position is considered to be a distance ahead of the actual position equal to the current velocity multiplied by the audio preview time, T_{AUD}. In the lateral axis, the waypoint course position is an expected lateral waypoint course position at a time T_{AUD} sec in the future. Imminent speed change messages are based on a distance criteria or the progress through the transition sequence. Figure 9.1 is a flow diagram depicting these procedures.

Inputs:	Waypoint course coordinates	x_{pp} and y_{pp}
	Longitudinal distance to upcoming waypoint	x_{cs}
	Hyperbolic transition parameters	$x_{le}(l_{wp})$, $x_{ant}(l_{wp})$, and $x_{sl}(l_{wp})$
	Current waypoint leg	l_{wp}
	Upcoming waypoint transition velocity	U_{tw}
	Waypoint leg headings	$\lambda_{l_{wp}}$
	Nominal velocity command	u_{nom}
	Current reference velocity	u_{ref}
	Current heading command	$\psi_{c_{auto}}$
	Nominal velocity resumption flag	IRESUM
	Aggressive maneuver counter	IAMFG
Outputs:	Audio annunciator messages	

a. Inputs and Outputs

Figure 9.1 Flow Diagram for Audio Message Determination

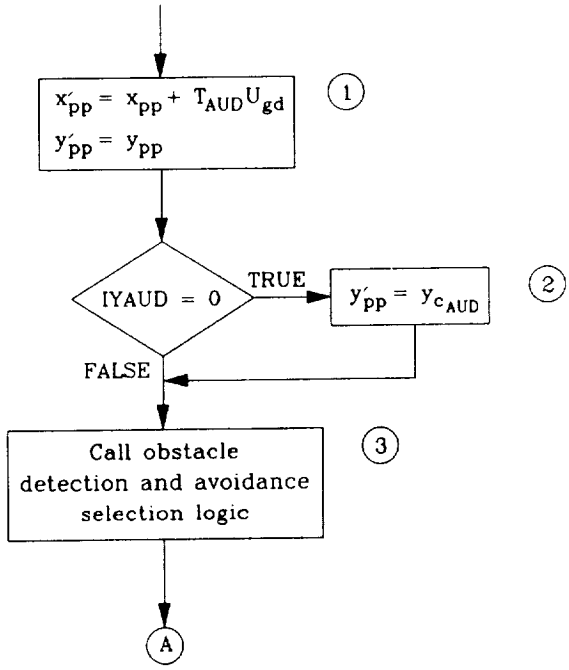

b. Determination of Future Lateral and Vertical Evasive Maneuvers

Figure 9.1 (Continued)

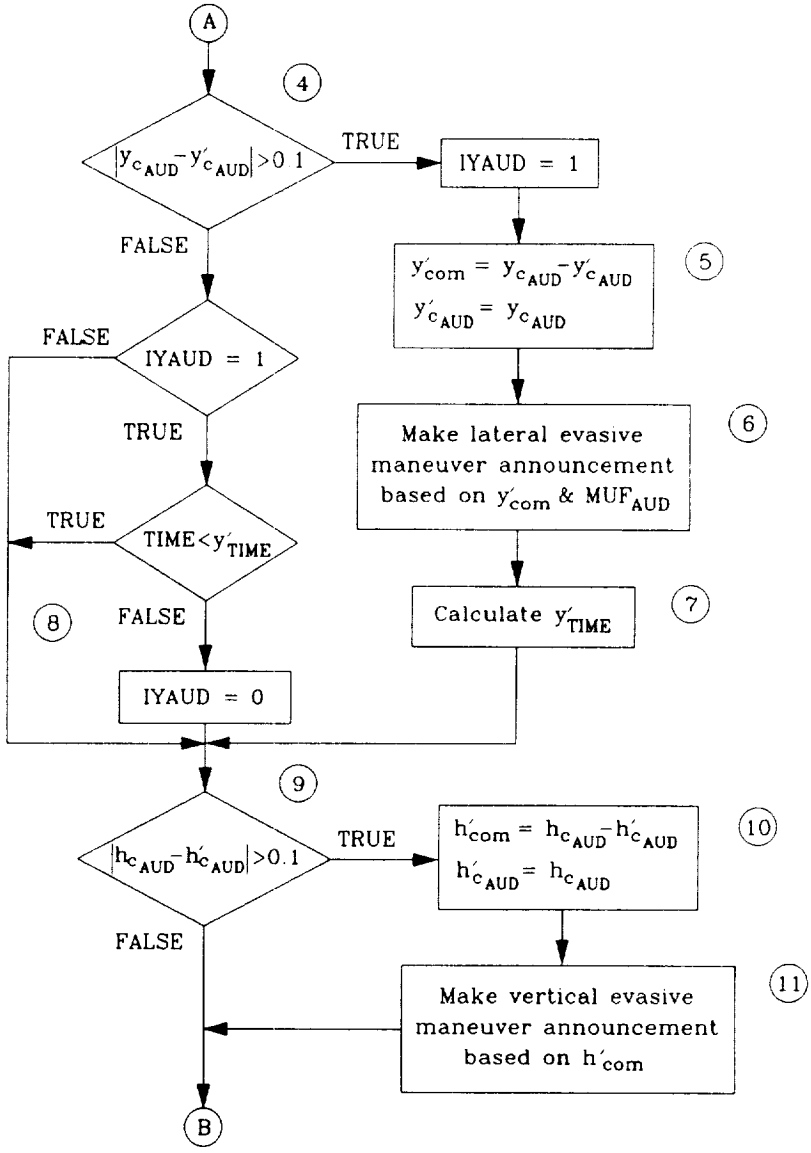

c. Lateral and Vertical Audio Messages

Figure 9.1 (Continued)

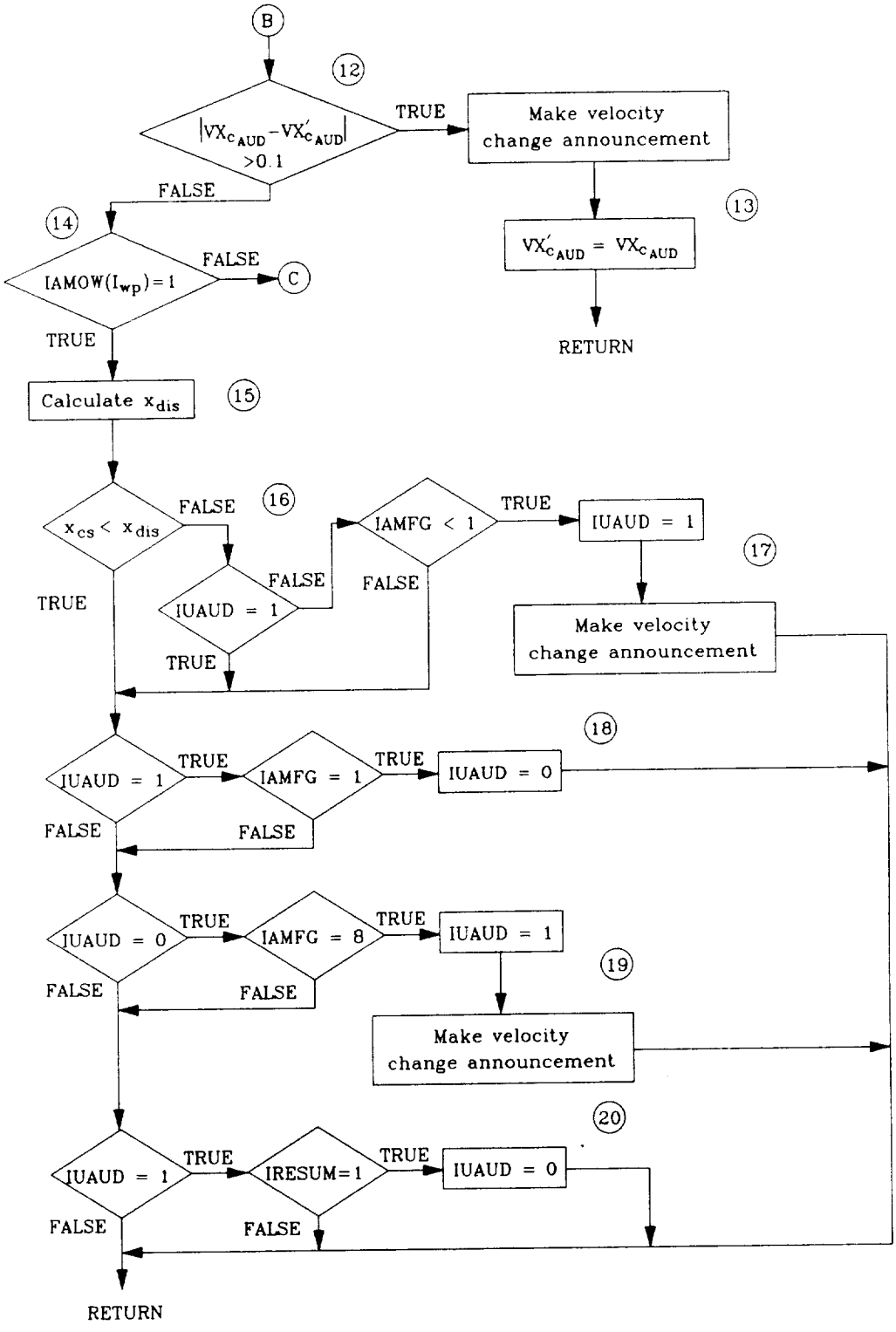

d. Audio Messages Indicating Imminent Velocity Change

Figure 9.1 (Continued)

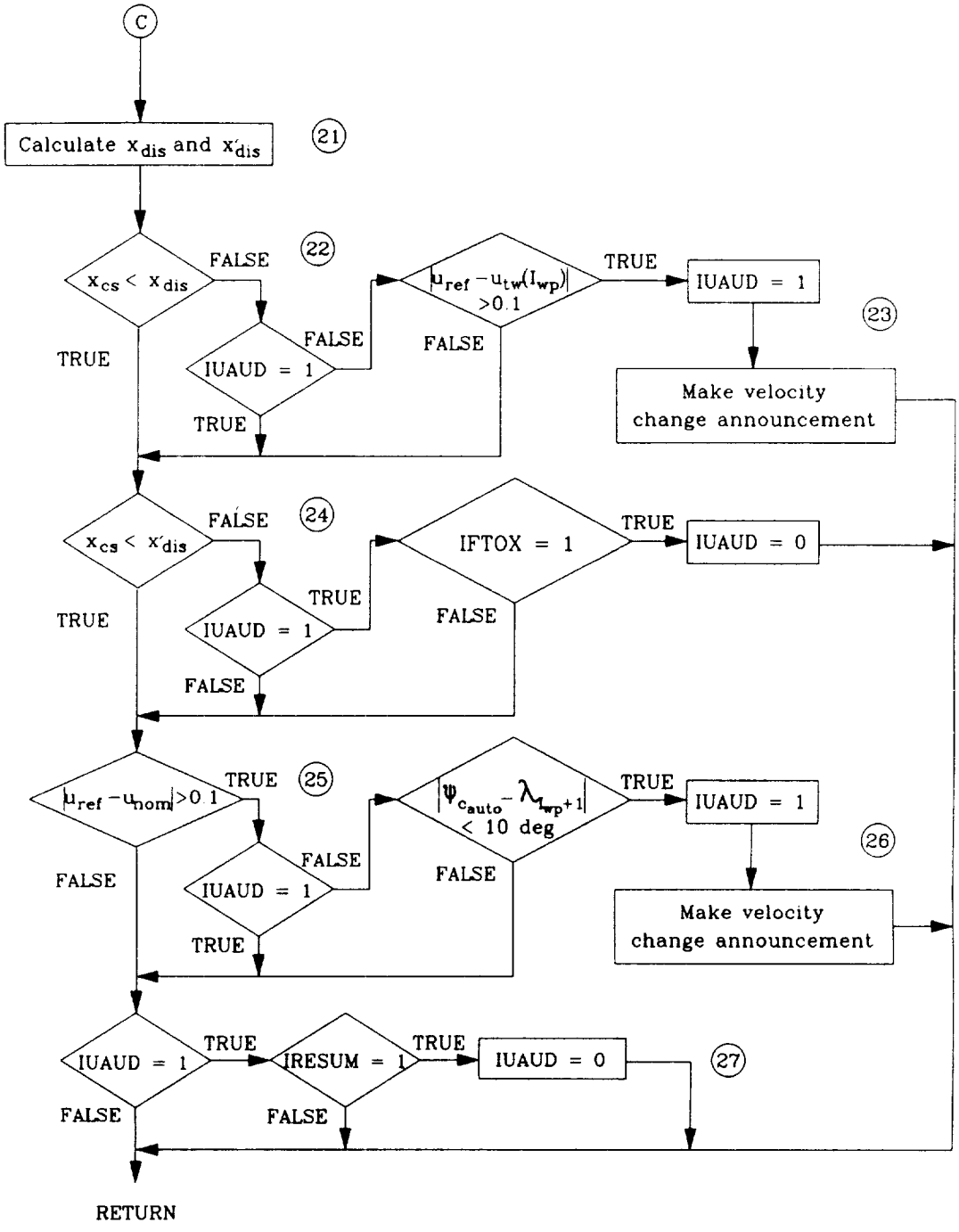

d. (Concluded)

Figure 9.1 (Continued)

e. Notes (corresponding to circled numbers throughout figure)

1. The modified waypoint course location is determined.

2. If the lateral audio flag is zero, the announced lateral maneuver will be complete in T_{AUD} sec; therefore, the modified lateral position is considered equal to the destination of that maneuver.

3. Similar obstacle detection and avoidance maneuver selection logic is used here as in Fig. 4.3 with the exception that the modified waypoint course coordinates are used in place of the current actual waypoint course coordinates. An additional change is in the bypass logic (Fig. 4.3b). The aggressive maneuver flag, IAMFG, is not used as a criterion for bypassing the audio obstacle detection and avoidance maneuver selection logic; and, in place of the lateral evasive maneuver flag, IFTOY, the lateral audio flag, IYAUD, is substituted. To prevent corruption of internal variables, it is necessary to create a duplicate of the original obstacle detection and avoidance maneuver selection logic. The above mentioned changes can then be incorporated into the duplicate. The outputs of this modified obstacle detection logic are: 1) a future lateral offset command, y_{cAUD}, including the maneuver urgency factor, MUF_{AUD}, associated with the maneuver, 2) a future vertical offset command, h_{cAUD}, and 3) a future velocity command, VX_{cAUD}.

4. The future lateral offset command returned by the modified obstacle detection routine is compared with the past value to determine if a new command has been identified.

5. If a new command has been identified, the magnitude of the future lateral offset command is calculated as the difference between the past offset value and the newly identified offset command. Also at this time, the past offset command is set equal to the newly identified lateral offset command.

6. The lateral evasive maneuver announcement is made, based on the maneuver urgency factor, MUF_{AUD}, associated with the predicted maneuver and the direction of the maneuver. The appropriate messages are listed in Table 9.1.

7. y'_{TIME} is the predicted maneuver completion time less the audio preview time, T_{AUD}. It is calculated as follows:

$$y'_{TIME} = TIME + T_{p_x} + (R_1 + 1 - MUF^i_{AUD})\frac{RX}{U_{gd}}$$

where MUF^i_{AUD} is the units digit of MUF_{AUD}.

Figure 9.1 (Continued)

e. Notes (Continued)

8. Until the running time reaches the predicted time, y'_{TIME}, the lateral audio flag remains set to one.

9. The future vertical offset command returned by the modified obstacle detection routine is compared with the past value to determine if a new command has been identified.

10. If a new command has been identified, the magnitude of the future vertical offset command is calculated as the difference between the past offset value and the newly identified offset command. Also at this time, the past offset command is set equal to the newly identified vertical offset command.

11. The vertical evasive maneuver announcement is made, based on the magnitude and direction of the maneuver. The appropriate messages are described in Table 9.2.

12. A comparison is made between the past and current values of the velocity command from the obstacle detection logic, $VX_{c\,AUD}$.

13. If this comparison indicates that a velocity change will be required due to a detected obstacle, the announcement is made, and the past value is set to the current value of $VX_{c\,AUD}$.

14. If the upcoming waypoint is not one that designates aggressive maneuvering while on watch, check for transition speed change requirements.

15. The anticipative distance, x_{dis}, is calculated as follows:

$$x_{dis} = -u_{nom}\left(\frac{1}{K_{hvx}} + T_{AUD}\right)$$

16. If the distance to the upcoming waypoint is less than the anticipative distance, x_{dis}, then ...

17. ... make the transition-to-hover announcement, and set the velocity audio flag, IUAUD, to one.

18. The velocity audio flag is reset to zero when the actual transition to hover has begun, in preparation for the velocity resumption announcement.

19. When the aggressive maneuvering is nearing completion, make the velocity resumption announcement.

Figure 9.1 (Continued)

e. Notes (Concluded)

20. The velocity audio flag is reset to zero in preparation for the next waypoint transition, once the speed change back to the nominal velocity has begun.

21. The anticipative distances, x_{dis} and x'_{dis}, are calculated as follows:

$$x_{dis} = -(x_{lg}(I_{wp}) + x_{ant}(I_{wp}) + x_{sl}(I_{wp}) + U_{gd}T_{AUD})$$

$$x'_{dis} = x_{dis} + U_{gd}T_{AUD}$$

22. If the distance to the upcoming waypoint is less than the anticipative distance, x_{dis}, and a transition speed change is required at the waypoint, then ...

23. ... make the transition speed change announcement, and set the velocity audio flag to one.

24. Once the maneuver has begun, the velocity audio flag is reset to zero in preparation for the velocity resumption announcement.

25. If a transition speed change was required at the waypoint, and the hyperbolic transition is almost complete (the heading change remaining is less than 10 deg), then ...

26. ... make the nominal velocity resumption announcement, and set the velocity audio flag to one.

27. The velocity audio flag is reset to zero in preparation for the next waypoint transition, once the speed change back to the nominal velocity has begun.

Figure 9.1 (Concluded)

TABLE 9.4

PARAMETER VALUES FOR THE AUDIO ANNUNCIATION SYSTEM

T_{AUD}	Audio preview time	2 sec

10. SIDE TASK SPECIFICATIONS

10.1 Divided Attention (Workload) Level

The main application of automatic NOE flight is in a single-pilot rotorcraft in which the mission requirements require an attention level sufficient to compromise the manual guidance and control of the rotorcraft. To simulate this condition, workload intensive side tasks will be included to serve as surrogates for mission tasks other than flight guidance and control. It is the primary responsibility of the evaluation pilot to monitor the rotorcraft's operational performance and his secondary responsibility to perform these side tasks. These side tasks are a choice reaction time task, a "Sternberg" recognitive task, and a sub-critical tracking task.

10.2 Choice Reaction Time Side Task

For the choice reaction time side task, three lights on the cockpit instrument panel will illuminate randomly in pairs ("Indicator Lights" in Fig. 7.1). The pilot is to respond only to the illumination pattern consisting of "ON-OFF-ON." If either of the other two possible illumination patterns appear, the pilot should ignore this side task. The algorithm for turning on the lights is as follows:

a. All lights are initially off.

b. Given the input constant θ_c = mean time between illuminations of the center light in seconds, compute:

$$h_c = \frac{3T_F}{\theta_c} \qquad \text{where } T_F = \text{frame time (seconds)}$$

c. Each frame time, generate (from a uniform distribution) two random numbers (x_1 and x_2) between 0 and 1.

d. If $0 \le x_1 \le h_c$, then illuminate two lights based on the following:

If $0 \le x_2 \le \frac{1}{3}$ then illuminate lights #1 and #2

If $\frac{1}{3} < x_2 \le \frac{2}{3}$ then illuminate lights #2 and # 3

If $\frac{2}{3} < x_2 \le 1$ then illuminate lights #1 and #3

If lights #1 and #2 or lights #2 and #3 are illuminated, disable the test algorithm for τ_p sec (the maximum allowable response time of the pilot) or, in the case of the illumination of lights #1 and #2 until the pilot has correctly responded. Then, restart the test with all lights off.

e. Otherwise, $h_c < x_i \leq 1$ and no lights illuminate.

f. The scoring of this task is based on the average response time over the duration of the run relative to the maximum allowable response time, τ_p. Incorrect pilot responses (i.e., depressing the trigger in response to the illumination of lights #1 and #2 or lights #2 and #3 result in the assessment of the maximum allowable response time while correct pilot responses are assessed the time of illumination of lights #1 and #3.

The values for θ_c and τ_p will be varied for the two levels of divided attention. For the first level, the mean time between illuminations of any two lights will be 48 sec, and the maximum allowable reaction time for the pilot will be set at 3 sec. The second, more workload-intensive level of divided attention will be achieved by reducing θ_c to 8 sec and τ_p to 1.5 sec.

10.3 Sternberg Recognitive Task

The Sternberg recognitive task simulates a target recognition task. The pilot is asked to memorize a limited number of items from a much larger set. Members of the large, complete set of items are then randomly presented to the pilot. The pilot is to respond one way when members of the set of relatively few memorized items are presented, and another when non-member items are presented. For this simulation, the large, complete set of items is the English alphabet. As the number of memorized items increases, the workload on the pilot increases. Thus, the two levels of divided attention will be realized by selecting random sets of three and six for the pilot's memorized sets from these twenty-six items.

The letters from the alphabet will be presented in the lower left-hand corner of the head-up display (Figs. 6.1 and 6.2). Two side-by-side toggles on the cockpit instrument panel (Fig. 7.1) will be required for this task. Upon presentation of members of the memorized set, the pilot shall switch the left toggle, and upon presentation of any other letter, the right. The mean reaction time will be used to score this side task, normalized by the mean reaction times exhibited in trial tests during which all of the pilot's attention is focused on the task. The algorithm for randomly presenting the letters is as follows:

a. The display area for the task is initially blank.

b. Given the input constant θ_S = mean time between the presentation of the letters in seconds, compute:

$$h_S = \frac{T_F}{\theta_S} \qquad \text{where } T_F = \text{frame time (seconds)}$$

c. Each frame time, generate (from a uniform distribution) two random numbers (x_3 and x_4) between 0 and 1.

d. If $0 \le x_3 \le h_S$, then present one letter based on Table 10.1, where each letter of the English alphabet has been assigned a member or nonmember identification (M1, NM20, etc.). Disable the test algorithm until the pilot has responded and then restart the test.

e. Otherwise, $h_S < x_3 \le 1$ and the display area remains blank.

TABLE 10.1 LETTER PRESENTATION CRITERIA FOR STERNBERG RECOGNITIVE TASK

Divided Attention Level 1		Divided Attention Level 2	
Memorized Set		Memorized Set	
$0 \le x_4 \le \frac{1}{6}$	M1	$0 \le x_4 \le \frac{1}{12}$	M1
$\frac{1}{6} < x_4 \le \frac{2}{6}$	M2	$\frac{1}{12} < x_4 \le \frac{2}{12}$	M2
$\frac{2}{6} < x_4 \le \frac{1}{2}$	M3	.	.
		.	.
		.	.
		$\frac{5}{12} < x_4 \le \frac{1}{2}$	M6
Non-Memorized Letters		Non-Memorized Letters	
$\frac{1}{2} < x_4 \le \frac{24}{46}$	NM1	$\frac{1}{2} < x_4 \le \frac{21}{40}$	NM1
.	.	.	.
.	.	.	.
.	.	.	.
$\frac{44}{46} < x_4 \le \frac{45}{46}$	NM22	$\frac{38}{40} < x_4 \le \frac{39}{40}$	NM19
$\frac{45}{46} < x_4 \le 1$	NM23	$\frac{39}{40} < x_4 \le 1$	NM20

The value of θ_s and the number of characters in the the memorized set will be varied for the two levels of divided attention. For the first level, the mean time between presentations of letters is 48 sec, and memorized set will

include three (3) letters. For the second, more workload intensive level of divided attention, the mean time between presentation of letters is 16 sec, and the memorized set will include six (6) letters.

10.4 Sub-Critical Tracking Task

The sub-critical tracking task will be implemented using a short vertical bar traveling horizontally along the bottom of the head-up display. A null point will be displayed using a horizontally-centered vertical marker, and the acceptable position boundaries for the vertical bar are depicted by dashed vertical marks. The limits of travel of the vertical bar are also shown as the bounding box. This symbology is depicted in Figs. 6.1 and 6.2. The positioning of the vertical bar will be a sub-critically unstable process, with the pilot's controlling inputs delivered through a stiff, single-axis side-arm displacement controller on the right armrest of the cockpit seat. The transfer function for this sub-critical tracking task is as follows:

$$\frac{e}{\delta_{sc}} = \frac{K_{sc}\lambda_{sc}}{s - \lambda_{sc}}$$

In order to determine an appropriate value for λ_{sc}, the critical value, λ_c, for each pilot must be determined. This is accomplished by running several critical task test (Ref. 2) training runs with the pilot's full attention given to controlling the position of the vertical bar. λ is increased during each run until the pilot can no longer maintain control of the symbol. After several sets of five training runs each, a mean value for λ_c can be determined, valid only for a particular pilot using a particular controller with a particular control-display lag or delay. Since full attention is required to achieve λ_c, a relative index of sub-critical task workloading, L, where $0 < L < 1$, requiring less than full attention, can then be defined as a fraction of λ_c to provide a sub-critical value, $\lambda_{sc} = L\lambda_c$, that will serve as a surrogate for other control tasks not associated with flight guidance (Ref. 3). The level of relative workload of the sub-critical task will be varied for two levels of divided attention. For the first level of divided attention, the value of λ_{sc} will be set such that the relative workload will be equal to 0.25, or

$$\lambda_{sc} = 0.25\lambda_c$$

The second level of divided attention will be realized by establishing a relative workload of 0.5. This second workload level, in conjunction with the more taxing discrete side-tasks described above, should challenge the evaluation pilot sufficiently to deter him from taking control of the rotorcraft in situations other than dire emergency. As a contingency in case the preliminary trials prove otherwise, the sub-critical task loading, L, must be adjustable as necessary.

The critical task tester used to determine the critical value for the unstable pole is described in Fig. 10.1. The human operator uses the side-arm controller (δ_{sc}), to null the error, e, which is displayed in the head up display. The task is automatically paced in the sense that the unstable pole, λ, increases slowly with time, thus making the task progressively more difficult. At some point, the human operator can no longer control the error, e, and the value of e exceeds the specified bounds. At this point, the task ends, and the corresponding final value of λ is defined to be the critical task score, λ_c. The sub-critical tracking task is operated in a similar manner with the exception that the value of the unstable pole, λ, is fixed as a defined value, λ_{sc}.

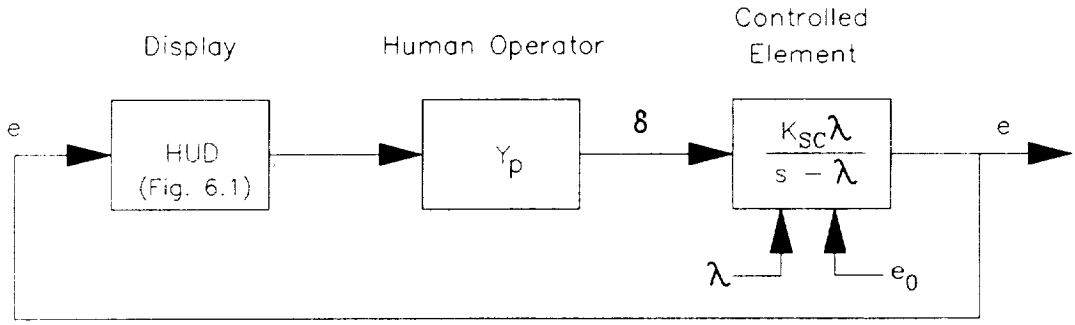

$$\lambda = \lambda_0 + \int \dot{\lambda} dt$$

$$\dot{\lambda} = \begin{cases} 0.20 \text{rad/sec/sec for } |e| < e_c \\ 0.05 \text{rad/sec/sec for } |e| > e_c \end{cases} \quad \text{one-way switch}$$

Note: Task is automatically stopped when $|e| > e_{max}$

Figure 10.1 Functional Block Diagram of Sub-Critical Task Tester (SCTT)

TABLE 10.2

PARAMETER VALUES FOR THE SUB-CRITICAL TASK TESTER

λ_o	Initial magnitude of the unstable pole	0.1 rad/sec
e_o	Initial position error	0.05
e_c	Position error criterion for one-way switch of rate of change of the magnitude of the unstable pole	0.25
e_{max}	Maximum displayed value of e	1.0
K_{sc}	Sub-critical tracking task gain	1.0

REFERENCES

1. Cheng, V. H. L., and B. Sridhar, "Considerations for Automated Nap-of-the-Earth Rotorcraft Flight," Proceedings of the American Control Conference, Atlanta, GA, June 15-17, 1988.

2. Jewell, Wayne, and Warren F. Clement, A Simple Method for Measuring the Effective Delay in Simulator Digital Computing Systems Involving Manual Control, Systems Technology, Inc., Working Paper No. 1156-4, December 1980.

3. Jex, Henry R., "A Proposed Set of Standardized Sub-Critical Tasks for Tracking Workload Calibration," in Neville Moray (Ed.), Mental Workload--Its Theory and Measurement, Plenum Press, 1977.

4. Sinacori, John B., Robert L. Stapleford, Wayne F. Jewell, and John M. Lehman, Researcher's Guide to the NASA Ames Flight Simulator for Advanced Aircraft (FSAA), NASA CR 2875, February 1977.

APPENDIX A

EXCERPTS FROM APPENDIX B OF WORKING PAPER NO. 1254-8

FULLY AUTOMATIC GUIDANCE FOR ROTORCRAFT NAP-OF-THE-EARTH FLIGHT FOLLOWING PLANNED PROFILES

NASA AMES RESEARCH CENTER SIMULATION TEST PLAN

APPENDIX B

COMBINED ROTORCRAFT AND FLIGHT CONTROL SYSTEM EQUATIONS OF MOTION

The equations of motion for the helicopter model are linearized stability derivative equations. These stability derivatives are augmented to achieve the desired dynamics on the combined rotorcraft and stability and control augmentation system (SCAS).

A. LATERAL/DIRECTIONAL

The equations of motion for the latera/directional axes, including the effective stability augmentation in state space form, are as follows:

$$\begin{bmatrix} \dot{v} \\ \dot{r} \\ \dot{p} \\ \dot{\phi} \\ \dot{y} \\ \dot{\psi} \\ \dot{y}_c \\ \dot{\psi}'_c \end{bmatrix} = \begin{bmatrix} Y_v & 0 & 0 & g' & 0 & 0 & 0 & 0 \\ 0 & N_r & 0 & 0 & 0 & K_\psi & 0 & -K_{\psi_c} \\ L_v & 0 & L_p & K_\phi & 0 & -K_{y_c} & 0 & \\ 0 & 0 & 1 & 0 & 0 & 0 & 0 & 0 \\ 1 & 0 & 0 & 0 & 0 & 0 & 0 & 0 \\ 0 & 1 & 0 & 0 & 0 & 0 & 0 & 0 \\ 0 & 0 & 0 & 0 & 0 & 0 & 0 & 0 \\ 0 & 0 & 0 & 0 & 0 & 0 & 0 & 0 \end{bmatrix} \begin{bmatrix} v \\ r \\ p \\ \phi \\ y \\ \psi \\ y_c \\ \psi_c \end{bmatrix} + \begin{bmatrix} 0 & 0 \\ K_{\psi_c} & 0 \\ 0 & K_{y_c} \\ 0 & 0 \\ 0 & 0 \\ 0 & 0 \\ 0 & K'_{y_c} \\ K'_{\psi_c} & 0 \end{bmatrix} \begin{bmatrix} \psi_c \\ v_c \end{bmatrix}$$

$$+ \begin{bmatrix} -Y_v & 0 & 0 \\ 0 & -N_{r_g} & 0 \\ -L_{v_g} & 0 & -L_{p_g} \\ 0 & 0 & 0 \\ 0 & 0 & 0 \\ 0 & 0 & \\ 0 & 0 & \\ 0 & 0 & 0 \end{bmatrix} \begin{bmatrix} v'_g \\ r_g \\ p_g \end{bmatrix}$$

where

$$g' = g\cos(\phi_o) \qquad K'_{y_c} = -\frac{K_{y_c}}{K_y} \qquad K'_{\psi_c} = -\frac{K_{\psi_c}}{K_\psi}$$

and $\dot{\psi}'_c$ is the derivative of ψ_c. So, from:

$$X(s) = (SI - A)^{-1}BU(s)$$

the characteristic equation of the system is:

$$|sI-A| = \begin{vmatrix} s-Y_v & 0 & 0 & -g' & 0 & 0 & 0 & 0 \\ 0 & s-N_r & 0 & 0 & 0 & -K_\psi & 0 & K_\psi \\ -L_v & 0 & s-L_p & -K_\phi & -K_y & 0 & K_y & 0 \\ 0 & 0 & -1 & s & 0 & 0 & 0 & 0 \\ -1 & 0 & 0 & 0 & s & 0 & 0 & 0 \\ 0 & -1 & 0 & 0 & 0 & s & 0 & 0 \\ 0 & 0 & 0 & 0 & 0 & 0 & s & 0 \\ 0 & 0 & 0 & 0 & 0 & 0 & 0 & s \end{vmatrix} = 0$$

$$s^2[s(s-N_r)-K_\psi][(s-Y_v)(s^2(s-L_p)-K_\phi s)-g'(L_v s+K_y)]=0$$

or

$$s^2(s^2-N_r s-K_\psi)(s^4-(Y_v+L_p)s^3+(L_p Y_v-K_\phi)s^2+(K_\phi Y_v-g'L_v)s-g'K_y)=0$$

The transfer functions for the lateral and directional axes are uncoupled and reduce to the following:

$$\frac{v}{v_c} = \frac{g'K_{y_c}\left(\frac{K_{v_c}}{K_{y_c}}s+1\right)}{s^4-(Y_v+L_p)s^3+(L_p Y_v-K_\phi)s^2+(K_\phi Y_v-g'L_v)s-g'K_y}$$

$$\frac{\psi}{\psi_c} = \frac{K_\psi\left(\frac{K_{\psi_c}}{K_{\psi_c}}s+1\right)}{s^2-N_r s-K_\psi}$$

or, with the velocity and yaw rate commands equal to zero, the position and heading hold transfer functions are:

$$\frac{y}{y_c} = \frac{g'K_{y_c}}{s^4-(Y_v+L_p)s^3+(L_p Y_v-K_\phi)s^2+(K_\phi Y_v-g'L_v)s-g'K_y}$$

$$\frac{\psi}{\psi_c} = \frac{K_{\psi_c}}{s^2-N_r s-K_\psi}$$

B. LONGITUDINAL/VERTICAL

The equations of motion for the longitudinal/vertical axes, in state space form, are as follows:

$$\begin{bmatrix} \dot{u} \\ \dot{w} \\ \dot{q} \\ \dot{\theta} \\ \dot{x} \\ \dot{h} \\ \dot{x}_c \\ \dot{h}'_c \end{bmatrix} = \begin{bmatrix} X_u & 0 & 0 & -g' & 0 & 0 & 0 & 0 \\ 0 & Z_w & 0 & 0 & 0 & K_h & 0 & -K_h \\ M_u & 0 & M_q & K_\theta & K_x & 0 & -K_x & 0 \\ 0 & 0 & 1 & 0 & 0 & 0 & 0 & 0 \\ 1 & 0 & 0 & 0 & 0 & 0 & 0 & 0 \\ 0 & -1 & 0 & 0 & 0 & 0 & 0 & 0 \\ 0 & 0 & 0 & 0 & 0 & 0 & 0 & 0 \\ 0 & 0 & 0 & 0 & 0 & 0 & 0 & 0 \end{bmatrix} \begin{bmatrix} u \\ w \\ q \\ \theta \\ x \\ h \\ x_c \\ h_c \end{bmatrix} + \begin{bmatrix} 0 & 0 \\ K_{h_c} & 0 \\ 0 & K_{u_c} \\ 0 & 0 \\ 0 & 0 \\ 0 & 0 \\ 0 & K'_{x_c} \\ K'_{h_c} & 0 \end{bmatrix} \begin{bmatrix} h_c \\ u_c \end{bmatrix}$$

$$+ \begin{bmatrix} -X_u & 0 & 0 \\ 0 & -Z_{w_g} & 0 \\ -M_{u_g} & 0 & -M_{q_g} \\ 0 & 0 & 0 \\ 0 & 0 & 0 \\ 0 & 0 & 0 \\ 0 & 0 & 0 \\ 0 & 0 & 0 \end{bmatrix} \begin{bmatrix} u'_g \\ w'_g \\ q_g \end{bmatrix}$$

where

$$g' = g\cos(\theta_0) \qquad K'_{x_c} = -\frac{K_{x_c}}{K_x} \qquad K'_{h_c} = -\frac{K_{h_c}}{K_h}$$

and h'_c is the derivative of h_c. So, from:

$$X(s) = (sI - A)^{-1}BU(s)$$

the characteristic equation of the system is:

$$|sI - A| = \begin{vmatrix} s - X_u & 0 & 0 & g' & 0 & 0 & 0 & 0 \\ 0 & s - Z_w & 0 & 0 & 0 & -K_h & 0 & K_h \\ -M_u & 0 & s - M_q & -K_\theta & -K_x & 0 & K_x & 0 \\ 0 & 0 & -1 & s & 0 & 0 & 0 & 0 \\ -1 & 0 & 0 & 0 & s & 0 & 0 & 0 \\ 0 & 1 & 0 & 0 & 0 & s & 0 & 0 \\ 0 & 0 & 0 & 0 & 0 & 0 & s & 0 \\ 0 & 0 & 0 & 0 & 0 & 0 & 0 & s \end{vmatrix} = 0$$

$$s^2[s(s - Z_w) + K_h]\{(s - X_u)[s^2(s - M_q) - K_\theta s] + g'(M_u s + K_x)\} = 0$$

or

$$s^2(s^2 - Z_w s + K_h)[s^4 - (X_u + M_q)s^3 + (M_q X_u - K_\theta)s^2 + (K_\theta X_u + g' M_u)s + g' K_x] = 0$$

The transfer functions for the lateral and directional axes are uncoupled and reduce to the following:

$$\frac{u}{u_c} = \frac{-g' K_{x_c}\left(\frac{K_{u_c}}{K_{x_c}}s + 1\right)}{s^4 - (X_u + M_q)s^3 + (M_q X_u - K_\theta)s^2 + (K_\theta X_u + g' M_u)s + g' K_x}$$

$$\frac{h}{h_c} = \frac{-K_{h_c}\left(\frac{K_{h_c}}{K_{h_c}}s + 1\right)}{s^2 - Z_w s + K_h}$$

or, with the velocity and yaw rate commands equal to zero, the position and heading hold transfer functions are:

$$\frac{x}{x_c} = \frac{-g' K_{x_c}}{s^4 - (X_u + M_q)s^3 + (M_q X_u - K_\theta)s^2 + (K_\theta X_u + g' M_u)s + g' K_x}$$

$$\frac{h}{h_c} = \frac{-K_{h_c}}{s^2 - Z_w s + K_h}$$

APPENDIX B

WORKING PAPER NO. 1254-2

CONSTRAINED TIME-OPTIMAL OBSTACLE AVOIDANCE MANEUVERS FOR AUTOMATICALLY GUIDED ROTORCRAFT NAP-OF-THE-EARTH (NOE) FLIGHT

CONSTRAINED TIME OPTIMAL OBSTACLE AVOIDANCE MANEUVERS FOR AUTOMATICALLY GUIDED ROTORCRAFT NAP-OF-THE-EARTH (NOE) FLIGHT

A. INTRODUCTION

In an automatically-piloted vehicle flying in nap-of-the-earth (NOE) conditions along a prescribed course, provisions must be made for unexpected obstacle avoidance. To this end, several rapid response maneuvers have been developed for the automatic guidance system being designed under Ref. 1. The control logic for these maneuvers is represented by the Y_{RR} block of Fig. 1, which is based on Fig. 10 on p. 33 of Ref. 2.

The four maneuvers chosen, each involving primarily one of the rotorcraft's four controllers, were (a) the bob-up and bob-down, (b) the hover turn, (c) the lateral sidestep, and (d) the longitudinal accel-decel. These maneuvers are essential to the completion of most NOE missions, but, in order to be accepted by the pilot when performed automatically, they should emulate the pilot's own tactics and techniques. Recent Black Hawk (UH-60A) flight tests and simulation tests have shown the ability of a pilot to perform nearly time optimal maneuvers when circumstances require an aggressive response (Refs. 3 through 5). The contention is, therefore, that the rapid response obstacle avoidance maneuvers should be constrained time optimal maneuvers in order to ensure pilot acceptance.

The designs of these constrained time optimal maneuver programs are presented in the remainder of this working paper.

B. VERTICAL MANEUVERS

The time optimal control strategy initially considered for performing rapid response maneuvers of rotorcraft in NOE flight was a "bang-bang" manipulation of reference velocities in the McDonnell-Douglas Helicopter Company (MDHC)

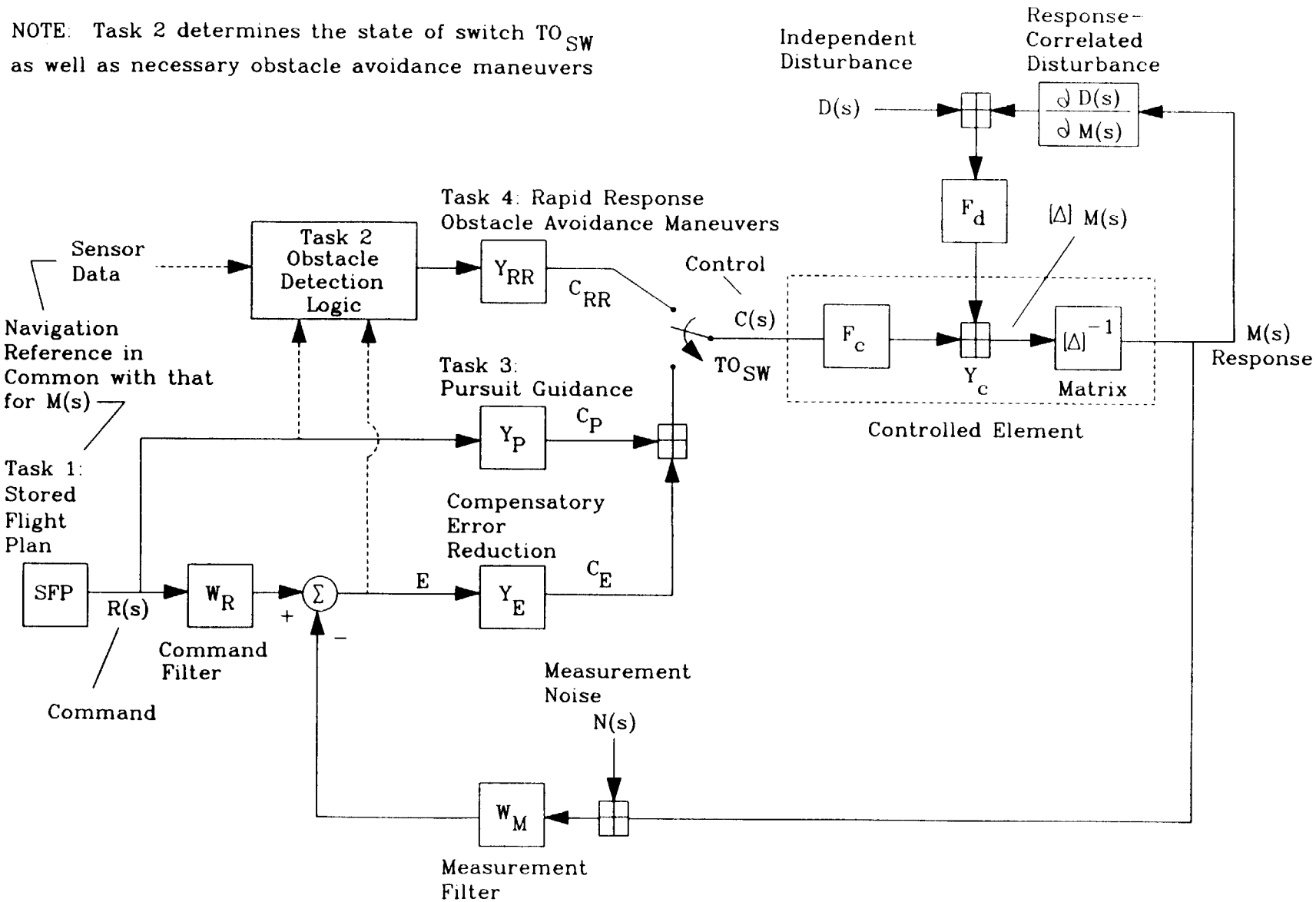

Figure 1. Vector Block Diagram for Multiloop Guidance and Control System

velocity command control system. The commanded velocities would switch instantaneously between maximum and minimum based on a function of the position error and the position error rate.

$$g(e) = \dot{e} + \left(\frac{|e|}{T_L}\right) sgn(e)$$

$$T_L = f\left(\frac{a^2 A}{K_c M}\right)$$

where

$$\frac{h}{h_{ref}} = \frac{K_c}{s(s+a)} = \frac{2}{s(s+2)} \quad *$$

$M = \dot{h}_{ref_{max}}$

A = magnitude of bob-up maneuver

$\dot{h}_{ref} = sgn(g(e)) * M$

There are two problems with this technique. The first is that it does not take into account limits in acceleration, acceleration rate, and/or jerk. These limits exist both as physical limits of the vehicle and as acceptable limits for the pilot. It is the latter that can be considered of utmost importance in an automatically-piloted vehicle flying in NOE conditions. The second problem is that the limit on commanded velocity is not necessarily equivalent to the limit on steady-state velocity. Because there is an inherent lag between commanded velocity and actual vehicle velocity it is acceptable to command a velocity greater than the maximum steady-state velocity until the vehicle velocity actually approaches this limit. Figure 2 shows the constrained time optimal velocity

*This transfer function approximates that for the McDonnell Douglas Helicopter Company (MDHC) vertical velocity command flight control system (Ref. 6).

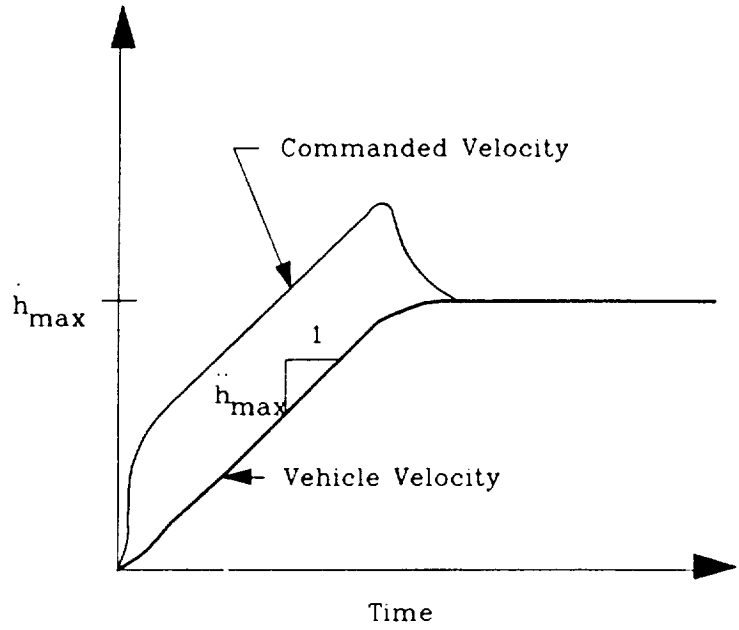

Figure 2. Constrained Time Optimal Vertical Velocity Profile

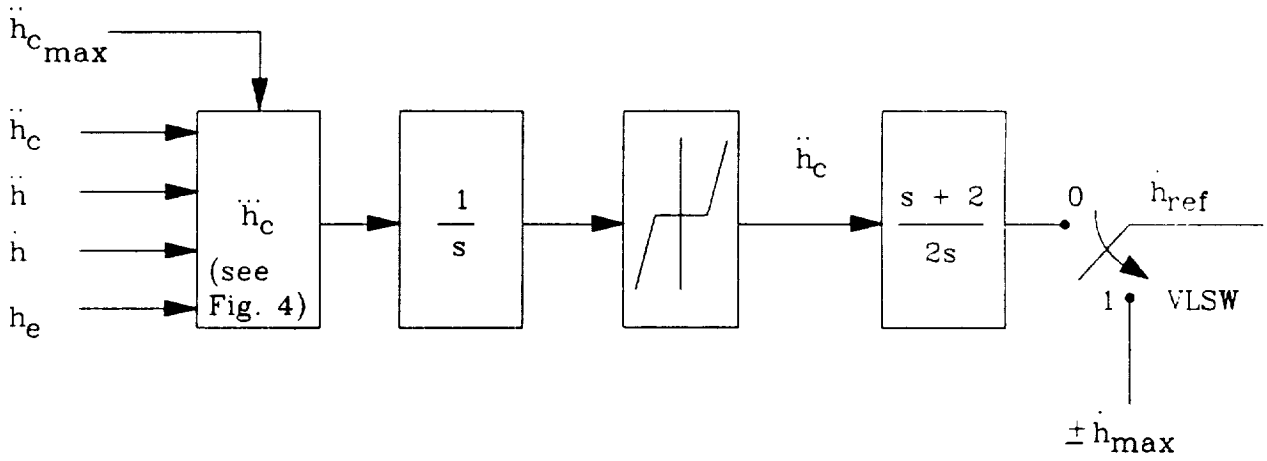

NOTES:

1) $\dddot{h}_c$ is determined by logic presented in Fig. 4
2) The switch, VLSW, is also determined by the logic presented in Fig. 4
3) SGN ($\pm \dot{h}_{max}$) for VLSW=1 is determined by the maneuver (bob-up $+\dot{h}_{max}$, bob-down $-\dot{h}_{max}$)
4) A dead-band ($\pm$ 1/2 dt $\dddot{h}_{max}$) is provided for $\ddot{h}_c$ to insure a region of $\ddot{h}_c = 0$ for logic in Fig. 4

Figure 3. Control Strategy for Starting the Bob-Up Maneuver

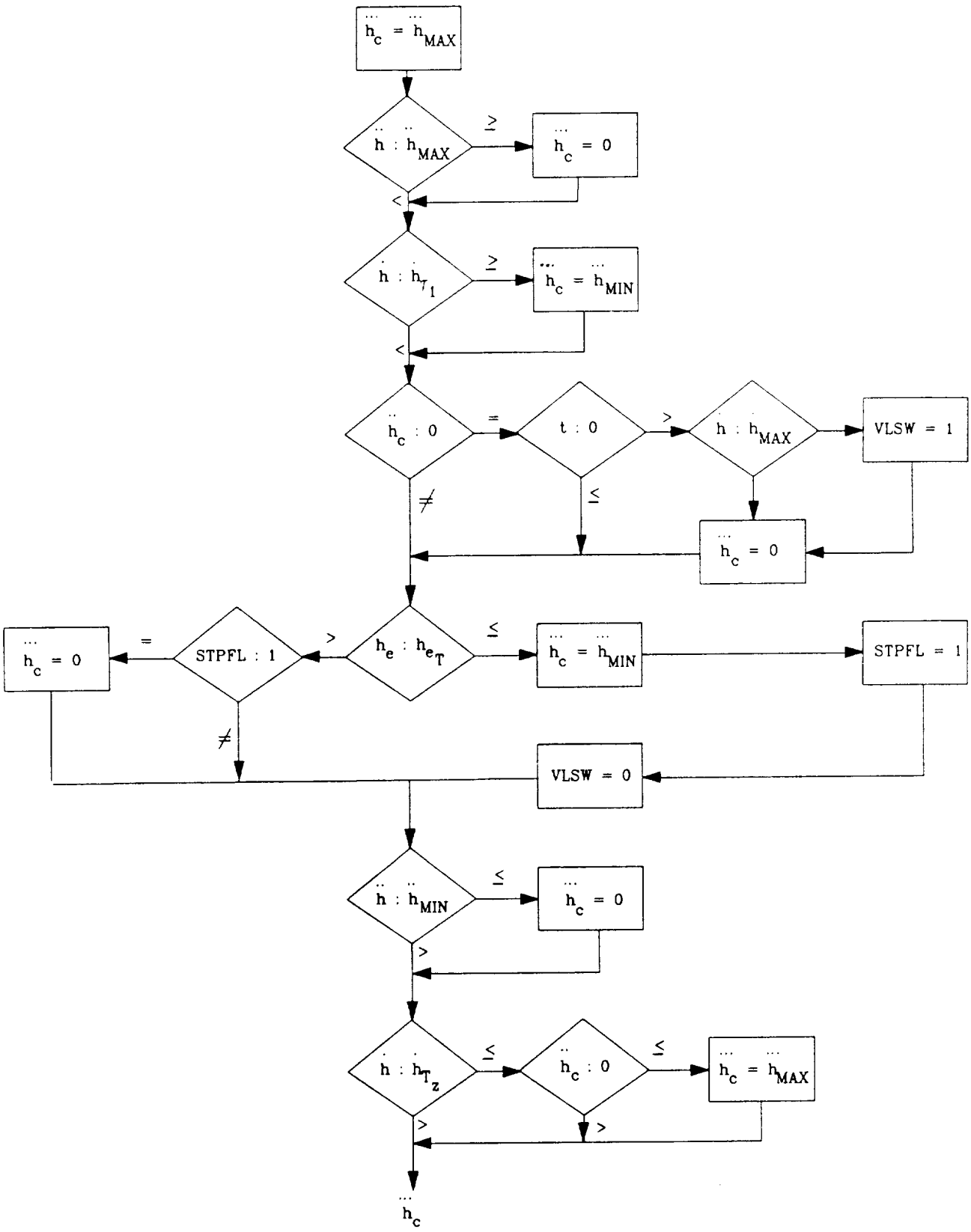

Figure 4. Real-Time Criteria for Determination of $\dddot{h}_c$ Bob-Down

profile. This type of command signal is generated by providing enough lead to the desired velocity command to force the vehicle to accelerate at the acceleration limit until maximum velocity is attained.

To complete the bob-up maneuver in the minimum time given limits on acceleration and jerk, the control strategy shown in Fig. 3 was adopted. This control scheme allows for direct control of the helicopter's vertical acceleration as can be seen in the following derivation:

$$\frac{\dot{h}}{\dot{h}_{ref}} = \frac{2}{s+2} \rightarrow \frac{\ddot{h}}{\dot{h}_{ref}} = \frac{2s}{s+2}$$

$$\frac{\dot{h}_{ref}}{\dot{h}_c} = \frac{s+2}{2s} \quad \text{(Fig. 2)}$$

$$\frac{\ddot{h}}{\dot{h}_c} = \left(\frac{\ddot{h}}{\dot{h}_{ref}}\right)\left(\frac{\dot{h}_{ref}}{\dot{h}_c}\right) = \left(\frac{2s}{s+2}\right)\left(\frac{s+2}{2s}\right) = 1$$

This allows the maximum acceptable performance to be attained. The control logic calls for a multi-step vehicle response in the general case. In the first step, the vehicle starts to build acceleration at the maximum rate until the vehicle has reached maximum acceleration. Next, the vehicle accelerates at this maximum until a point after which the maximum negative jerk will bring the vehicle to a steady climb at the maximum vertical velocity. At this point, the vertical velocity hold is engaged until the altitude error passes through a switching error. This switching error represents the minimum vertical stopping distance given the jerk and deceleration limits. The limits on jerk and acceleration were taken from flight test data (see Appendix A).

It is proposed that the MDHC position hold be used to maintain altitude and make small altitude corrections and that the constrained time optimal control logic be used for gross altitude corrections. The break between constrained

time optimal and compensatory is called the compensatory threshold error. For the following examples of the vehicle response under time optimal control, the threshold error was taken to be 5 ft.

All of the examples were run using a modified version of EVMCEP (Ref. 7). The controller in EVMCEP was changed in order to emulate the MDHC control system, and the time optimal control logic was added. The velocity, acceleration, and jerk limits used in these examples are as follows:

$$\dot{h}_{max} = 20\,ft/sec = 1200\,ft/min$$

$$\ddot{h}_{max} = 16\,ft/sec^2 = 1.5g$$

$$\ddot{h}_{min} = -10\,ft/sec^2 = 0.69g$$

$$\dddot{h}_{max} = 20\,ft/sec^3 = 0.62\,g/sec$$

$$\dddot{h}_{min} = -15\,ft/sec^3 = -0.47\,g/sec$$

These values were taken from time histories of bob-up flight tests and represent a relatively benign control scheme with some sense of urgency that should be acceptable to pilots.

The first three examples in Figs. 5a,b through 7a,b are cases in which the initial forward airspeed was 20 kts. The bob-ups range from 20 ft to 100 ft, encompassing the reasonably expected range of necessary avoidance maneuvers. Any jump over 100 ft would respond identically to the 100 ft jump with the only difference being the time at which the vehicle is climbing at its maximum rate of climb. These examples show comparisons between compensatory and constrained time optimal control schemes. Using either control scheme, the vehicle attains the desired altitude in approximately the same time, but the compensatory controller causes unacceptable acceleration rates. The constrained time optimal controller allowed the vehicle to stay within the constraining limits. The next

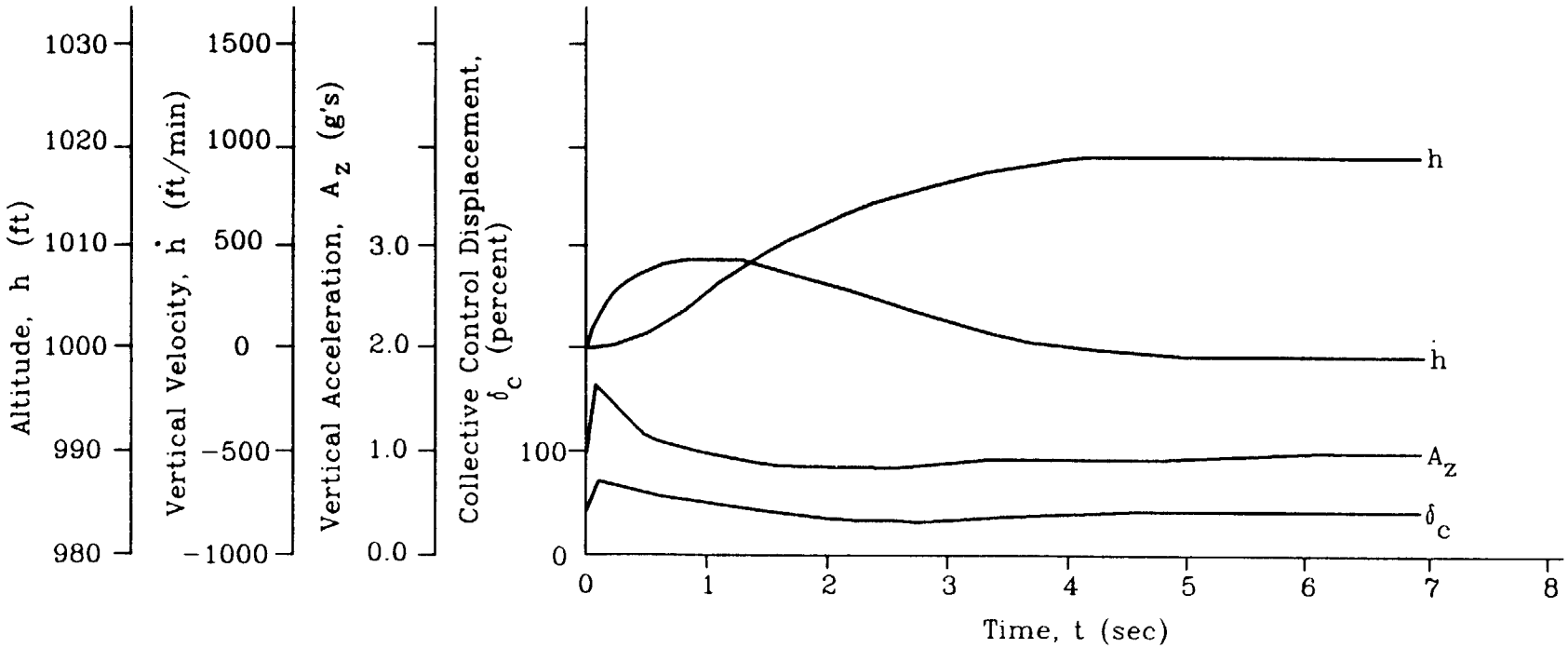

Figure 5a. Time History of 20 ft Bob-Up at 20 kts
Using the Compensatory Control Scheme

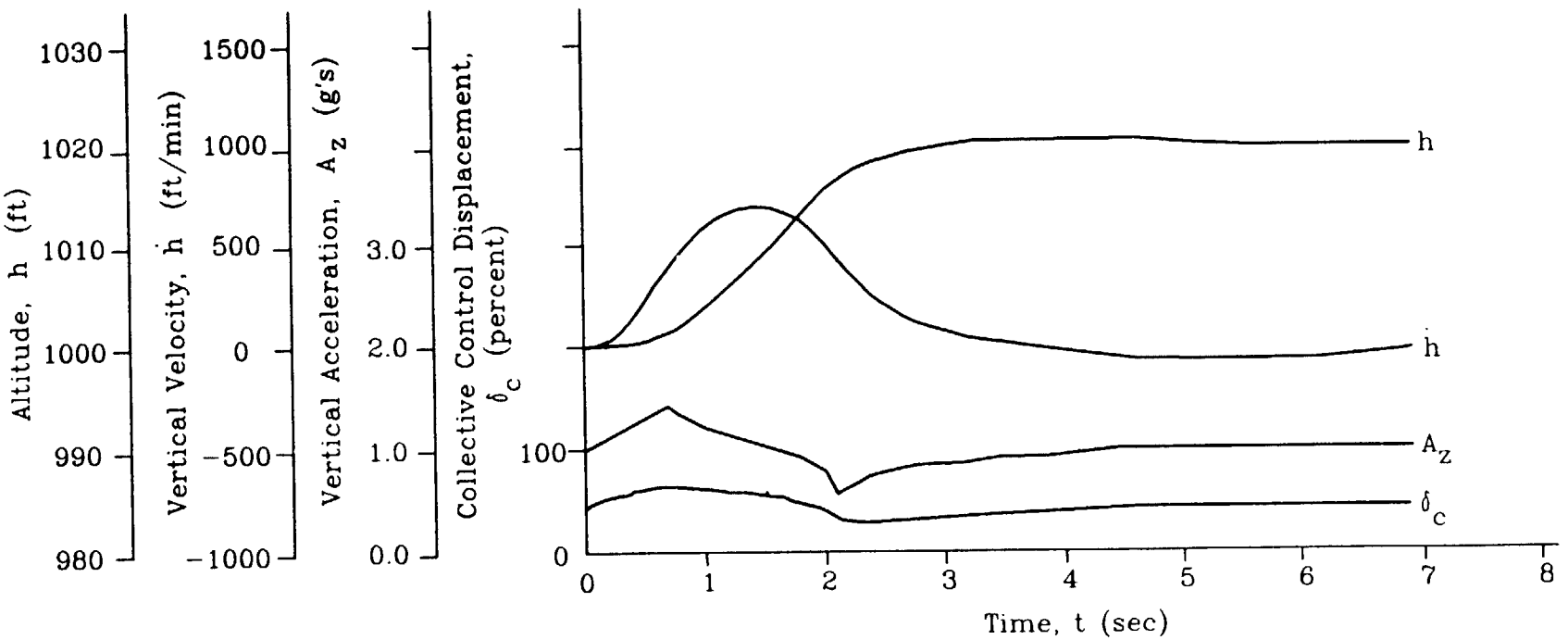

Figure 5b. Time History of 20 ft Bob−Up at 20 kts
Using the Constrained Time Optimal Control Scheme

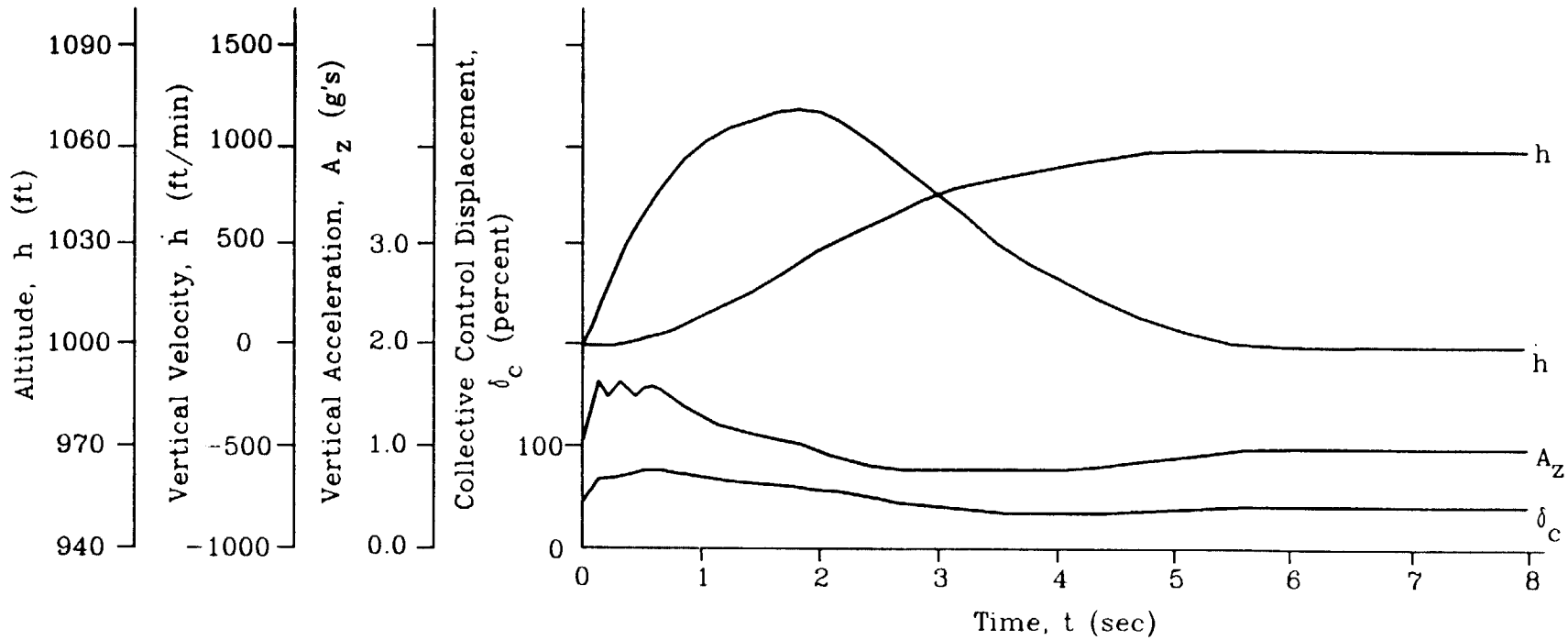

Figure 6a. Time History of 60 ft Bob-Up at 20 kts
Using the Compensatory Control Scheme with Acceleration Limiting

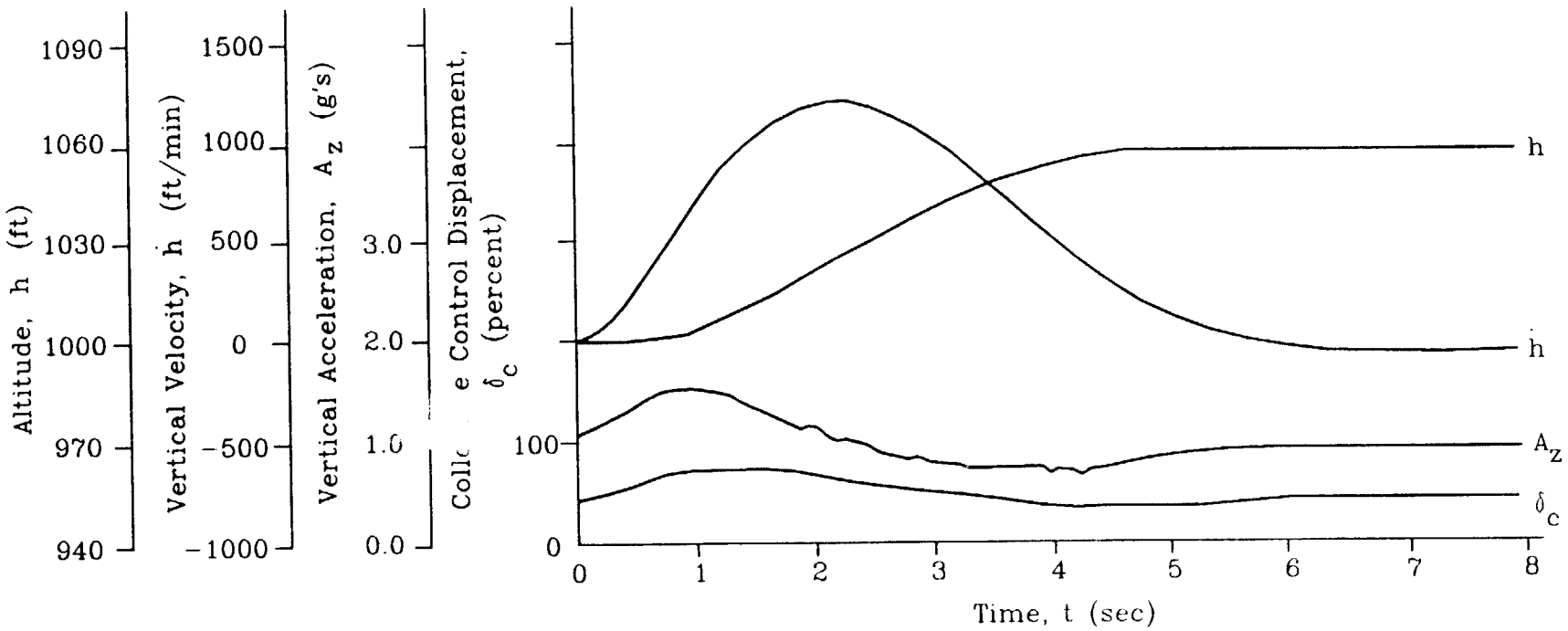

Figure 6b. Time History of 60 ft Bob-Up at 20 kts
Using the Constrained Time Optimal Control Scheme with Acceleration Limiting

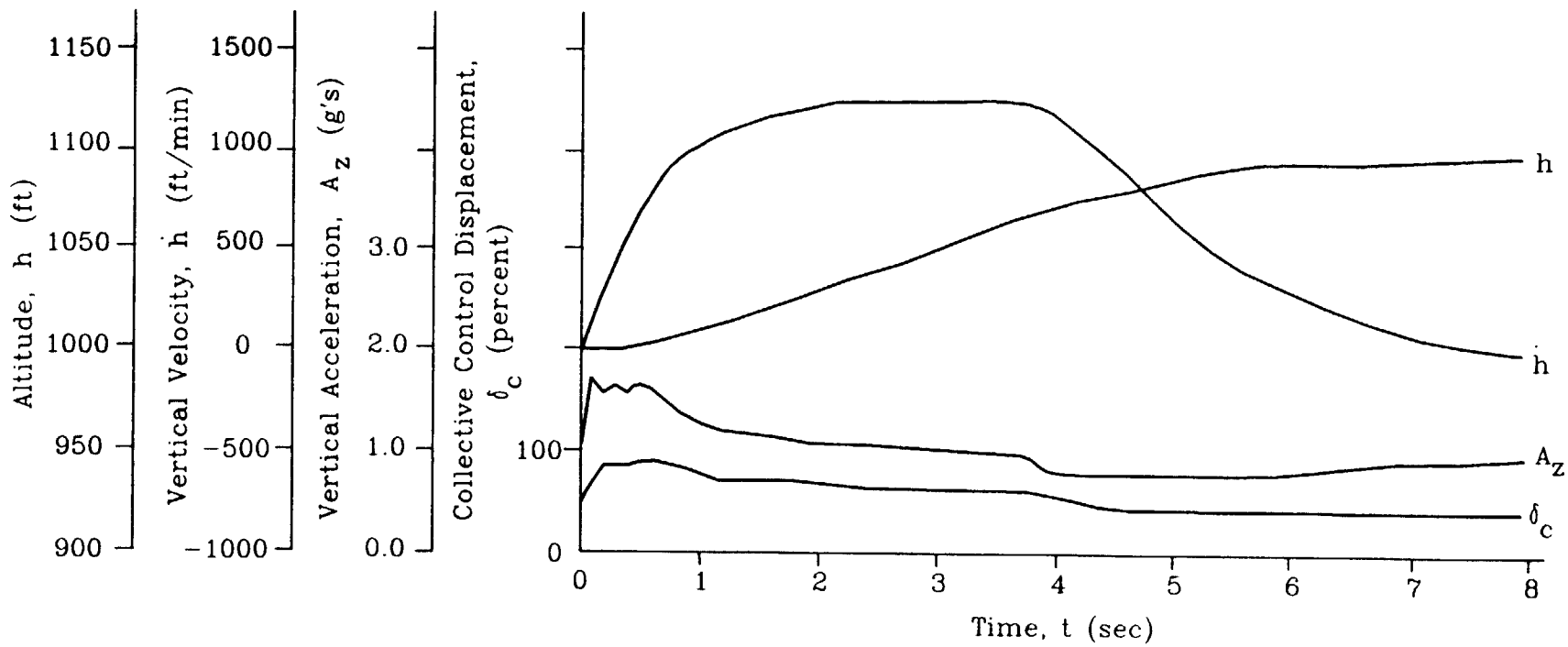

Figure 7a. Time History of 100 ft Bob-Up at 20 kts
Using the Compensatory Control Scheme with Acceleration Limiting

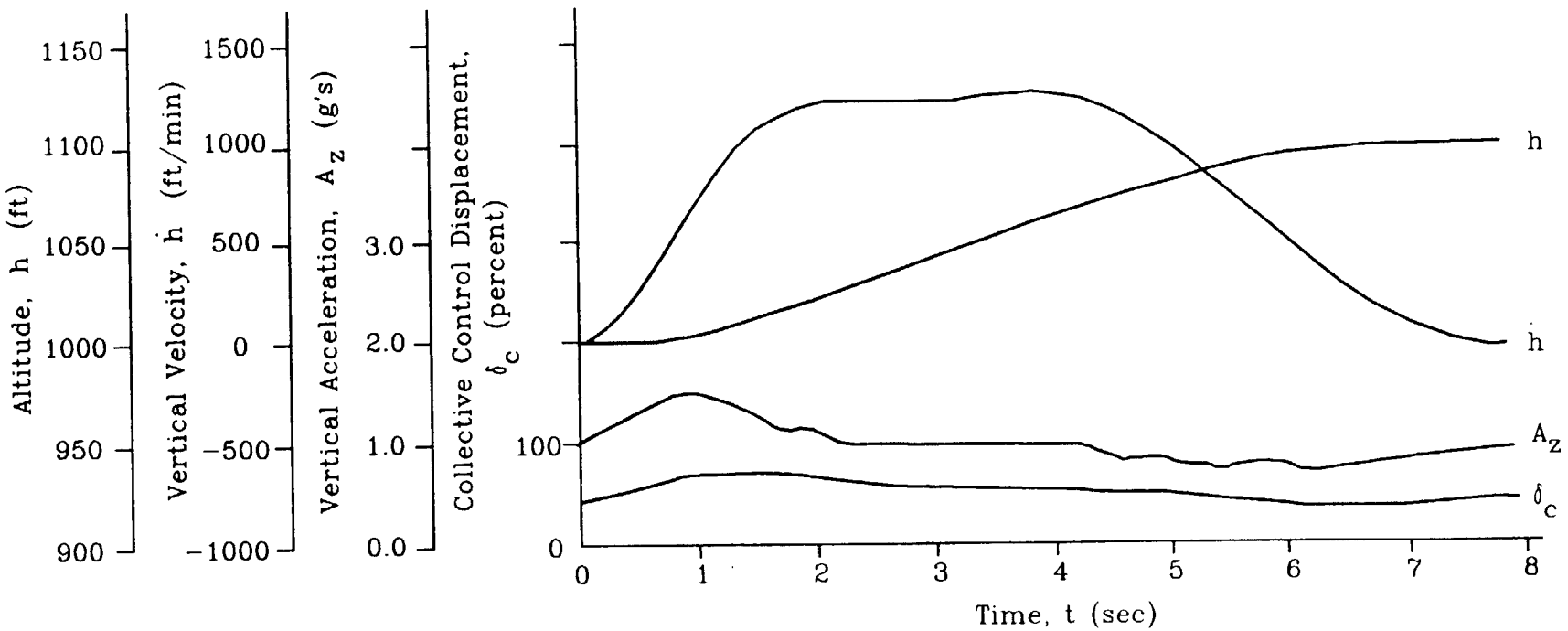

Figure 7b. Time History of 100 ft Bob-Up at 20 kts
Using the Constrained Time Optimal Control Scheme with Acceleration Limiting

two examples in Figs. 8 and 9 are 100 ft bob-ups, with initial forward airspeeds of 0 and 40 kts, respectively. This demonstrates the invariance of the vehicle response throughout the expected range of forward velocities.

Lastly, as is exhibited in Fig. 10 for the 60-ft bob-up, when the controller switches between time optimal and compensatory control, there is the possibility of a discontinuity in the reference velocity signal. This can cause changes in vehicle acceleration exceeding the jerk limits and would thus make the system unacceptable. To solve this problem, a blending switch was implemented so that, instead of an instantaneous switch between time optimal and compensatory control, the switch is made gradually over a specified period of time. The example in Fig. 11 depicts the effect of this blending. The blending time was taken to be 0.5 sec. This blending switch was implemented as shown in Fig. 12.

Besides returning to flight plan height, bob-downs might be used to duck under a suspension or truss bridge to avoid exceeding a threat exposure height. The procedure for performing a constrained time optimal bob-down is identical to that of the bob-up. The modified form of Fig. 4 is presented in Fig. 13 for the bob-down maneuver

Figures 14a, b, and c are included as a comparison among the two control schemes (constrained time optimal and compensatory) and actual flight test time histories. The comparison is particularly applicable for Part a of Fig. 14c. This test was conducted in calm wind conditions, and the instructions to the pilot were that he perform an aggressive bob-up.

The actual vehicle trajectories in all cases are very similar, but the differences can be seen in the collective input. The collective input of the constrained time optimal case resembles much more closely the pilot's collective input than does that of the compensatory case. This supports the premise that

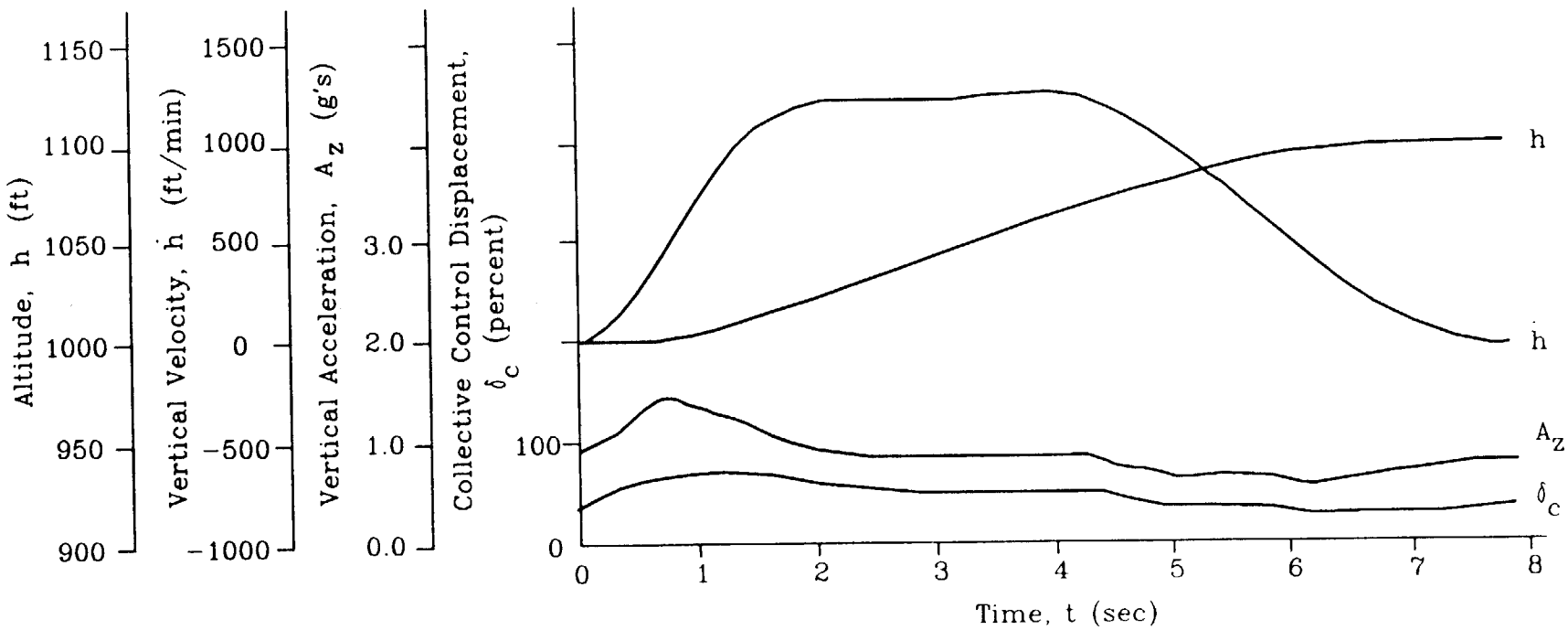

Figure 8. Time History of 100 ft Bob-Up at Hover
Using the Constrained Time Optimal Control Scheme with Acceleration Limiting

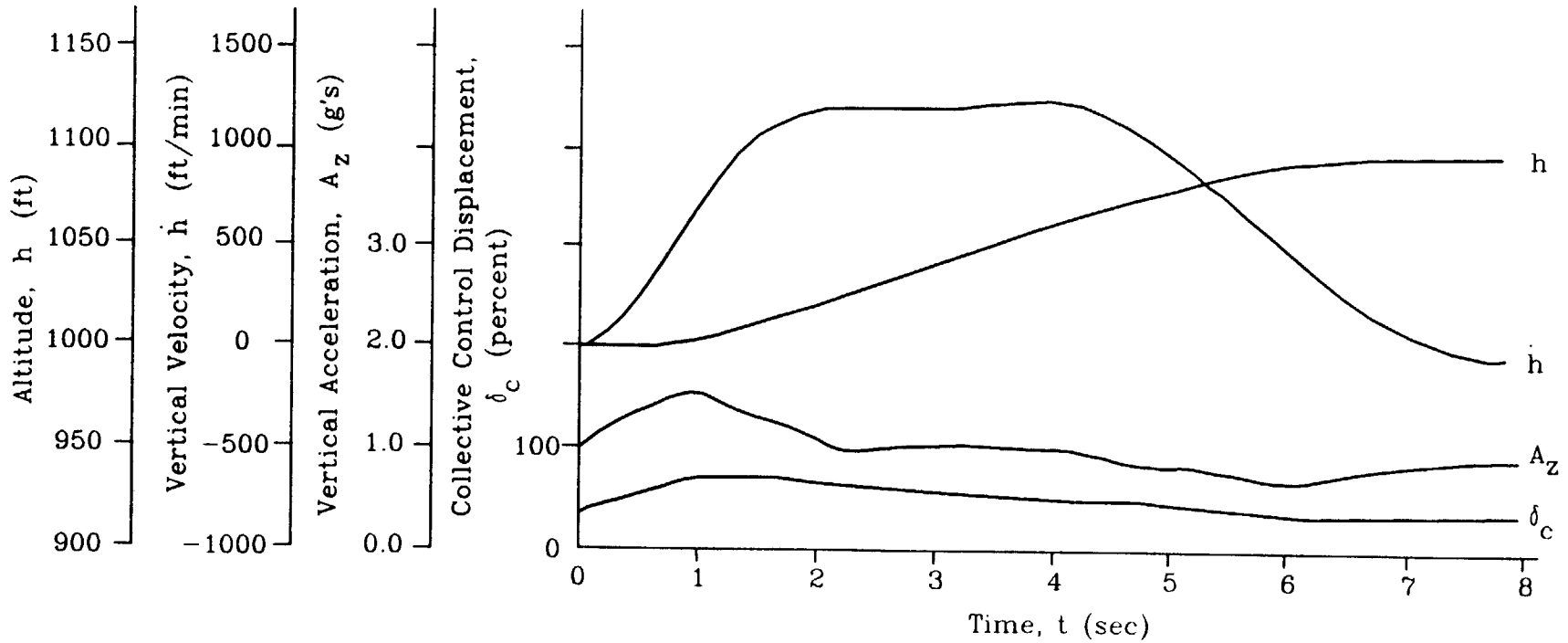

Figure 9. Time History of 100 ft Bob-Up at 40 kts
Using the Constrained Time Optimal Control Scheme with Acceleration Limiting

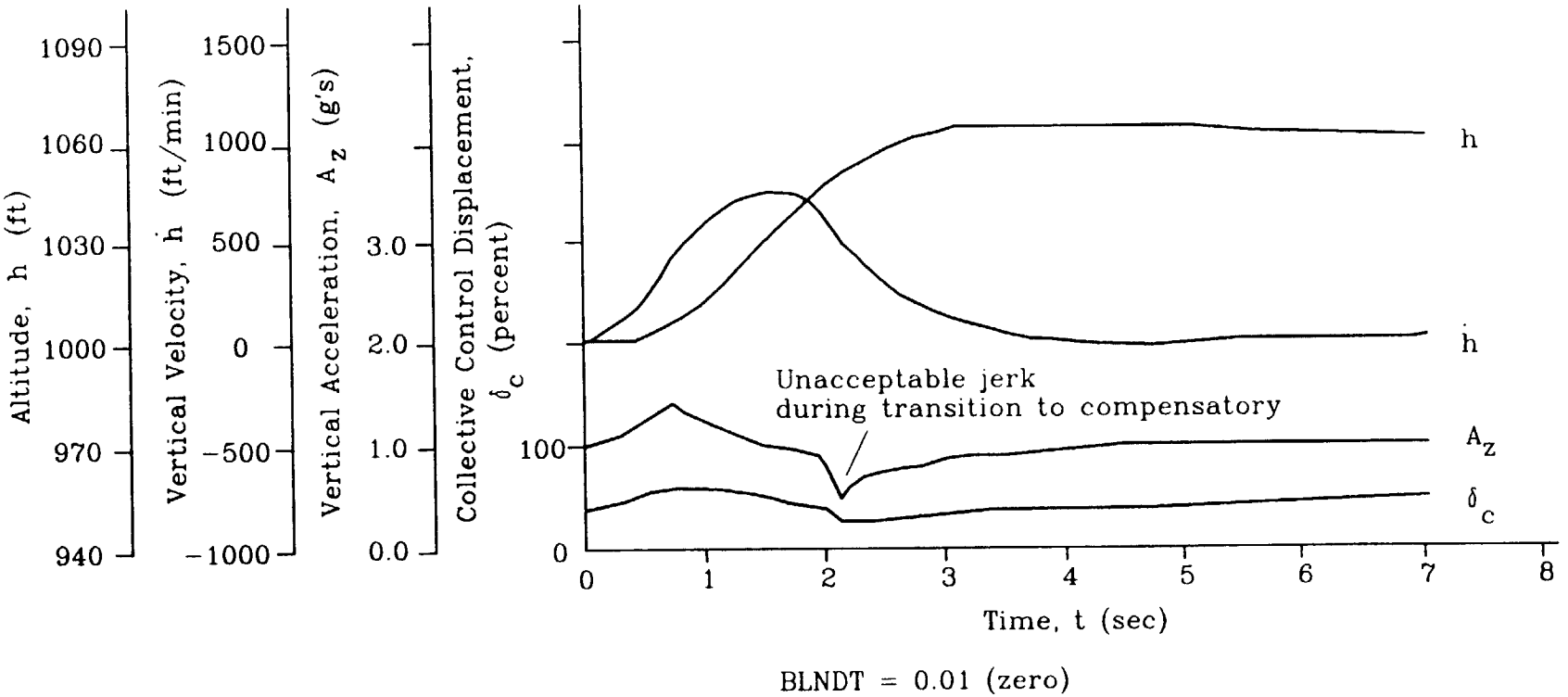

Figure 10. Time History of 60 ft Bob-Up at 20 kts
Using the Constrained Time Optimal Control Scheme
Without Blending Between the Time Optimal and Compensatory Controllers

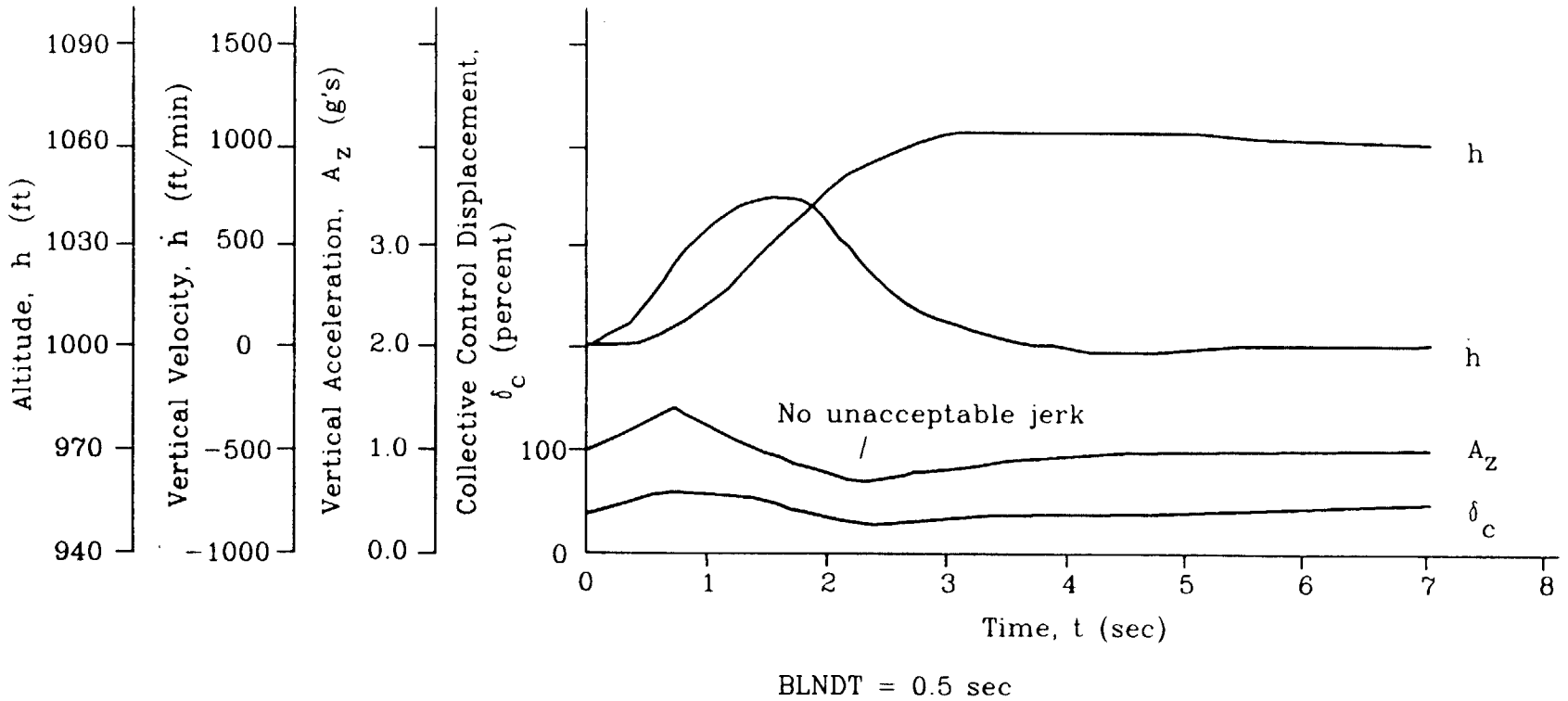

Figure 11. Time History of 60 ft Bob-Up at 20 kts
Using the Constrained Time Optimal Control Scheme With 0.5 sec
Blending time Between the Time Optimal and Compensatory Controllers

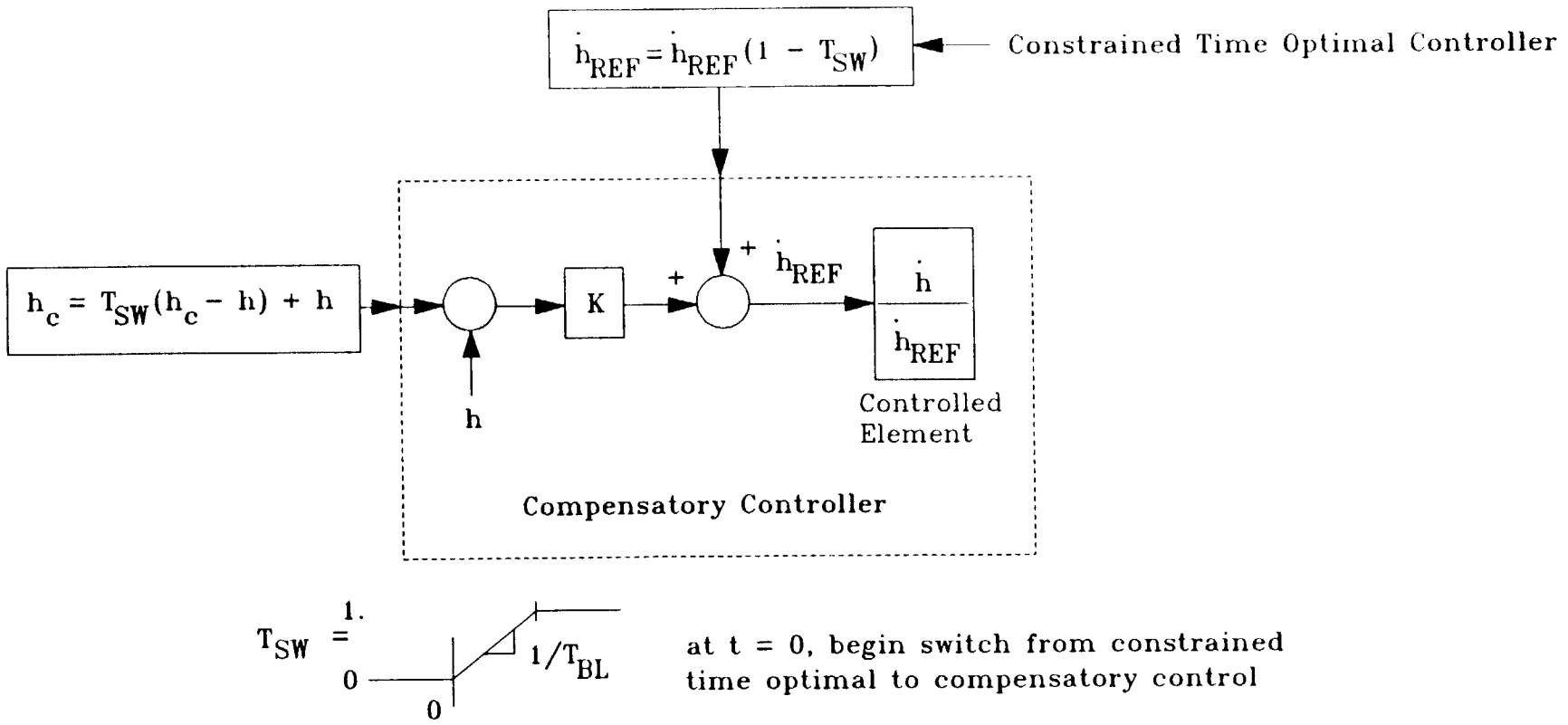

Figure 12. Implementation of the Constrained Time Optimal Controller, Bob-Up Maneuver

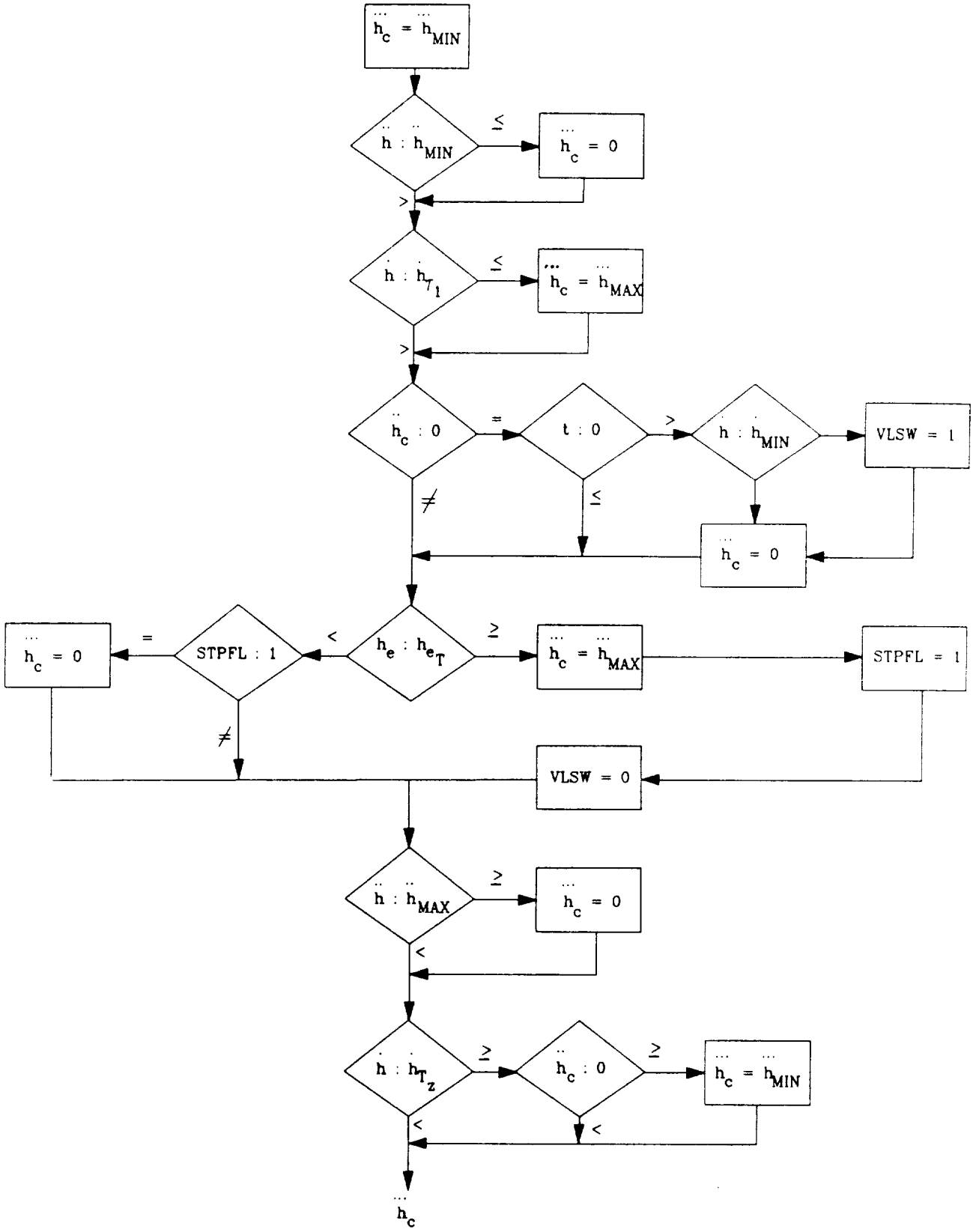

Figure 13. Real-Time Criteria for Determination of $\dddot{h}_c$ Bob-Up

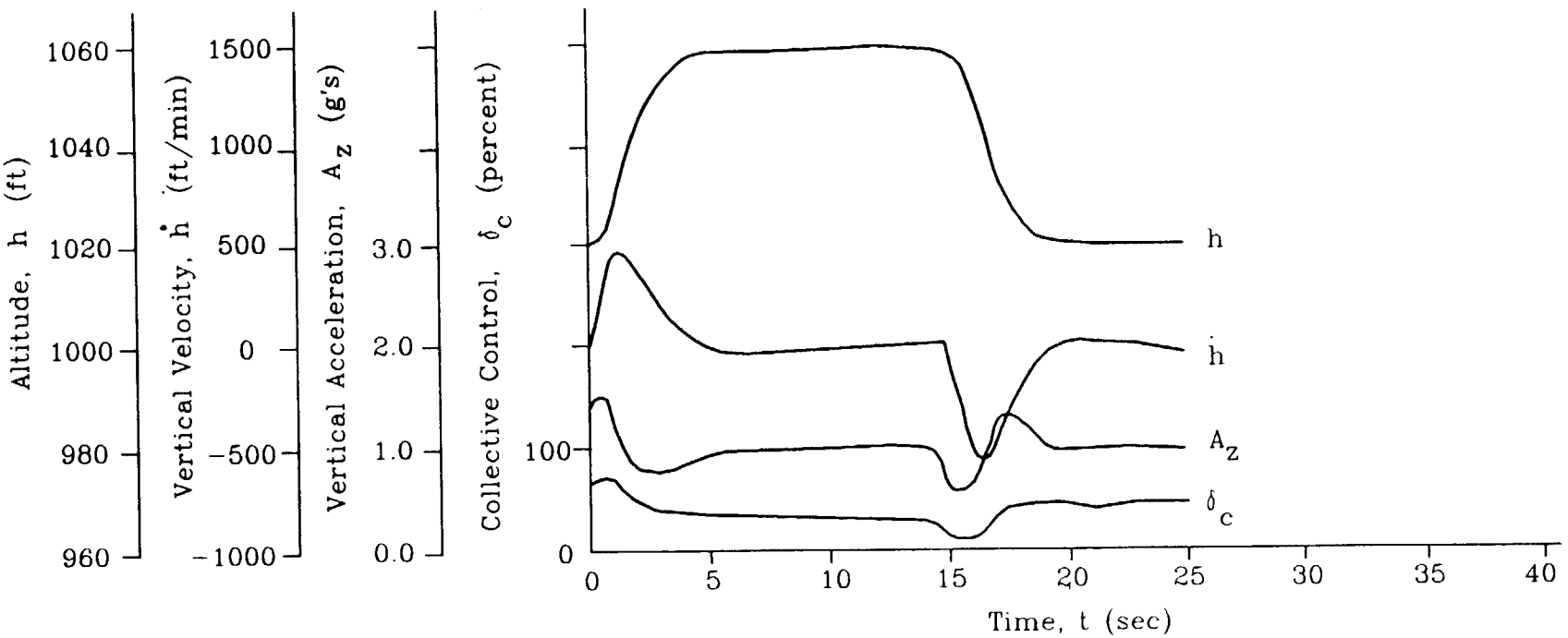

Figure 14a. Time History of 40 ft Bob-Up and Bob-Down at 20 kts Using the Compensatory Control Scheme With Acceleration Limiting

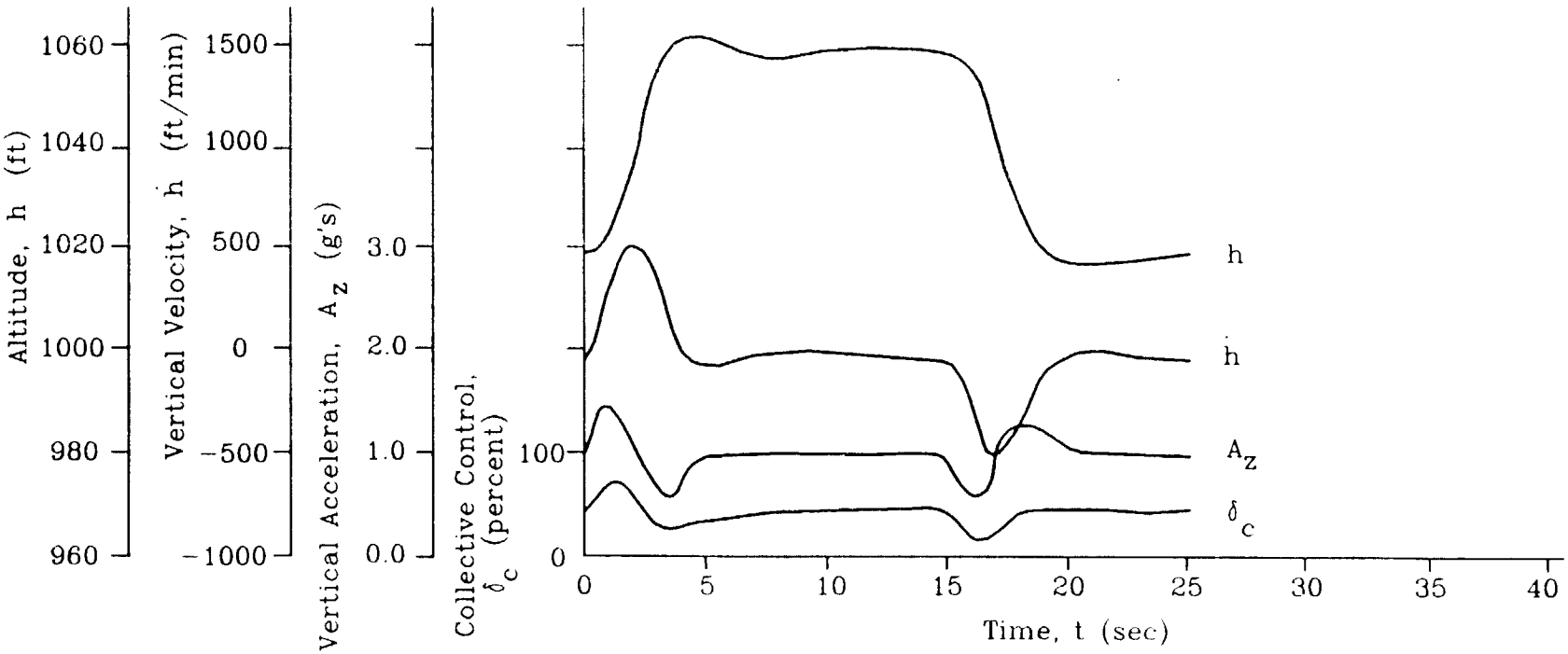

Figure 14b. Time History of 40 ft Bob-Up and Bob-Down at 20 kts
Using the Constrained Time Optimal Control Scheme

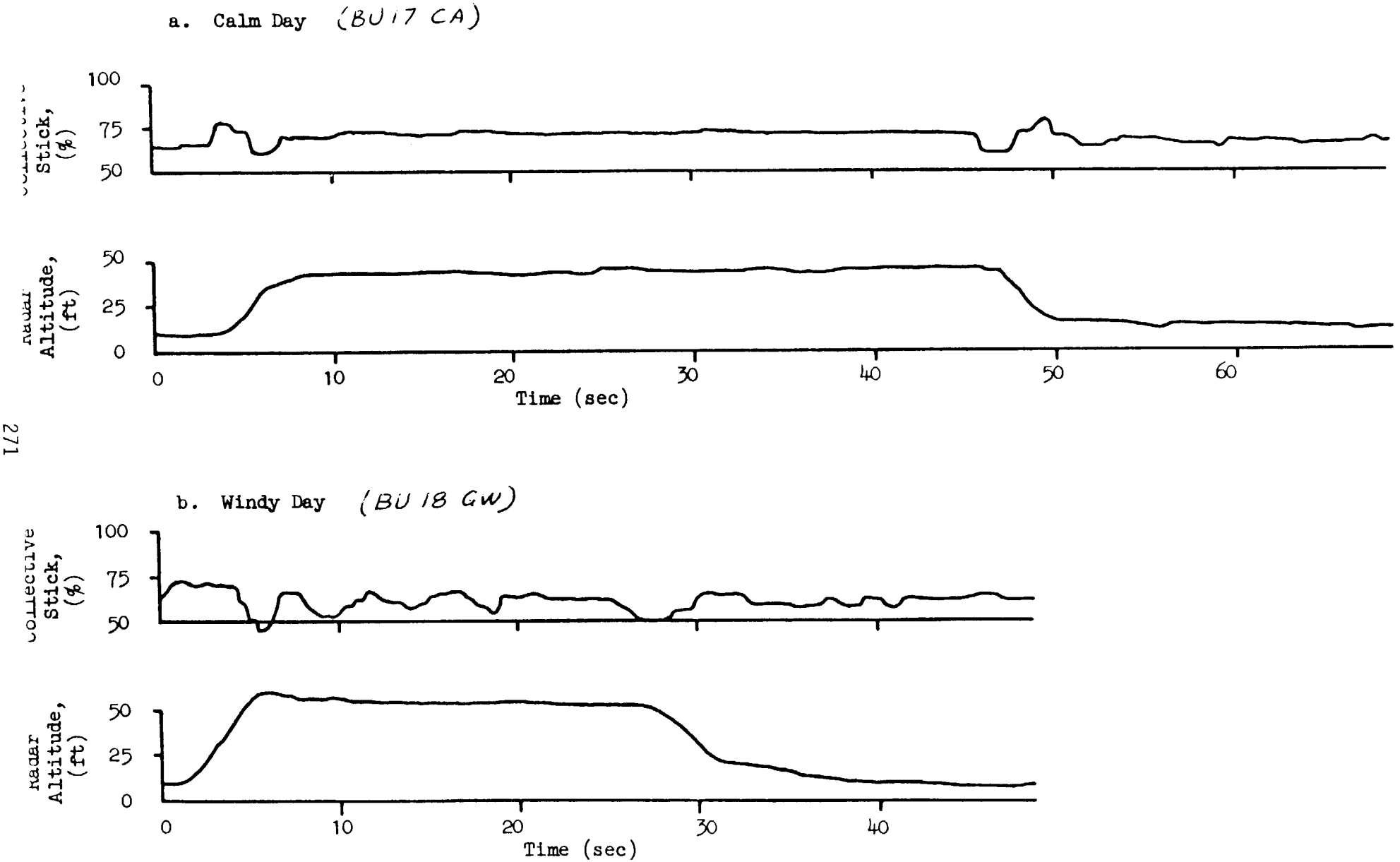

Figure 14c Examples of UH-60A Flight Test Bob-Ups (Ref. 3)

the constrained time optimal control scheme more closely replicates tactics and techniques used by actual pilots and should therefore be more acceptable to the pilots.

C. DIRECTIONAL MANEUVERS

For the constrained "time optimal" pedal turn, an approach similar to that of the bob-up was taken. In this case, however, the implementation of a jerk limit was omitted. This is due to the fact that flight tests (Ref. 3) showed the pilot's willingness to make very abrupt pedal inputs that translate into very large jerk tolerances. Thus, the control strategy in Fig. 15 was used.

A "blended" switch is used for PSDSW; therefore, the equation for $\dot{\psi}_{ref}$ is

$$\dot{\psi}_{ref} = PSDSW\,\dot{\psi}_{a_c} + (1 - PSDSW)\,\dot{\psi}_{b_c}$$

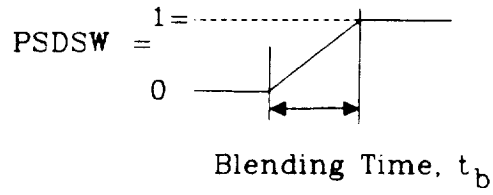

The determination of $\ddot{\psi}_c$ is presented in Fig. 16. Values for $\dot{\psi}_{MAX}$ and $\ddot{\psi}_{MAX}$ were taken from flight test data (see Appendix B).

The control system with which the following test cases were run did not exactly emulate the control system to be used in the future simulation tests. It was obtained by modifying the control system in EVMCEP (Ref. 7). The net result was a control system that had the following dynamic characteristics:

$$\frac{\dot{\psi}}{\dot{\psi}_c} \approx \frac{4}{s+4} \quad \text{but} \quad \frac{\psi}{\psi_c} \sim \frac{15}{[0.6;3.9]}$$

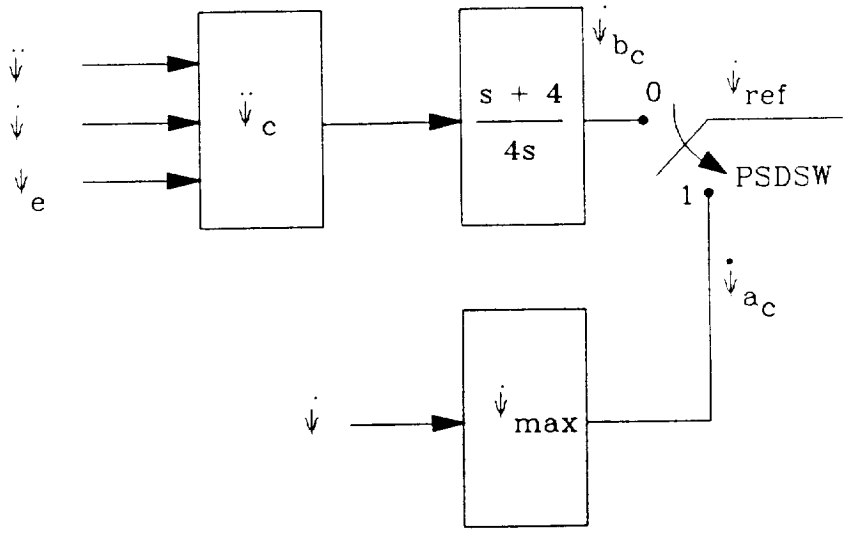

Figure 15. Control Strategy for Completing the Hover Turn Maneuver

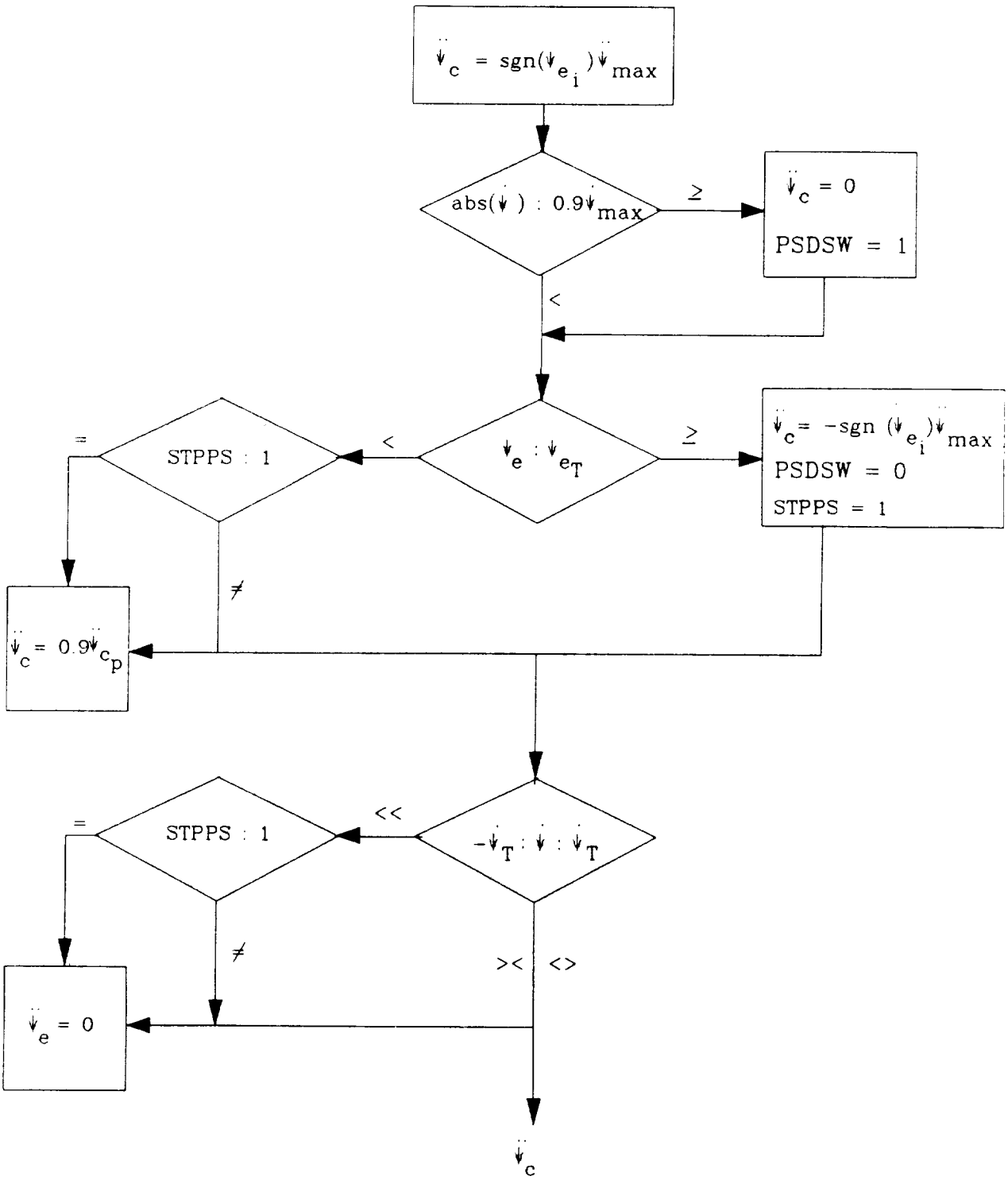

Figure 16. Real-Time Criteria for Determination of $\ddot{\psi}_c$

This is a much faster heading hold response than MDHC's controller,* but, because only a small portion of the ψ_e correction is performed by this compensatory control, it was determined that this model would suffice for this preliminary stage of analysis.

Two test runs are presented. The first is a 90 deg pedal turn at hover (Fig. 17). In this case, the maximum yaw rate was held during the yaw rate hold portion of the maneuver. The time to 90 deg was roughly equal to the aggressive hover turns performed in flight tests (about 3 sec, Ref. 3), but, with the TO controller, the overshoot is almost nonexistent. The total time of the maneuver is therefore substantially less than the piloted tests.

The second example is a 90 deg pedal turn at 20 kts (Fig. 18). The nonzero airspeed changes the dynamics of the vehicle in the yaw axis drastically (Figs. 19a,b). This is evident by the fact that the yaw rate command was unable to hold the maximum yaw rate in the yaw rate hold portion of the task. MDHC yaw rate command of

$$\frac{\dot{\psi}}{\dot{\psi}_c} = \frac{4}{s + 4}$$

is supposed to hold true for up to 20 kts (Ref. 6). If this is the case, the drop in yaw rate will not occur in the future tests with the MDHC control system. This yaw rate drop affects the maneuver only minimally, however; therefore, even if the MDHC control system doesn't take care of this problem, it will not effect the performance significantly.

As with the constrained time optimal bob-up system, the time optimal pedal turn system is to be implemented as in Fig. 20.

*MDHC heading hold transfer function $\Delta\psi/\Delta\psi_c$ is approximately $4/(s + 2)^2$ (Ref. 6).

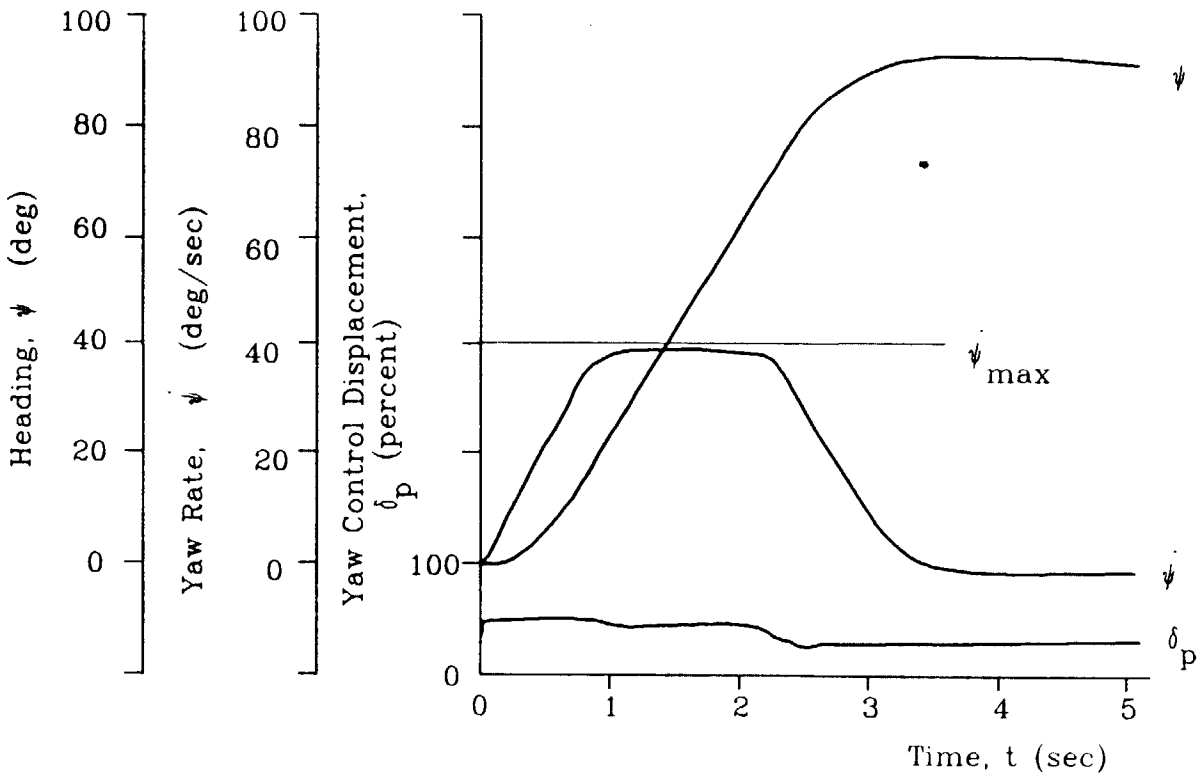

Figure 17. Time History of Pedal Turn at Hover
Using the Constrained Time Optimal Control Scheme

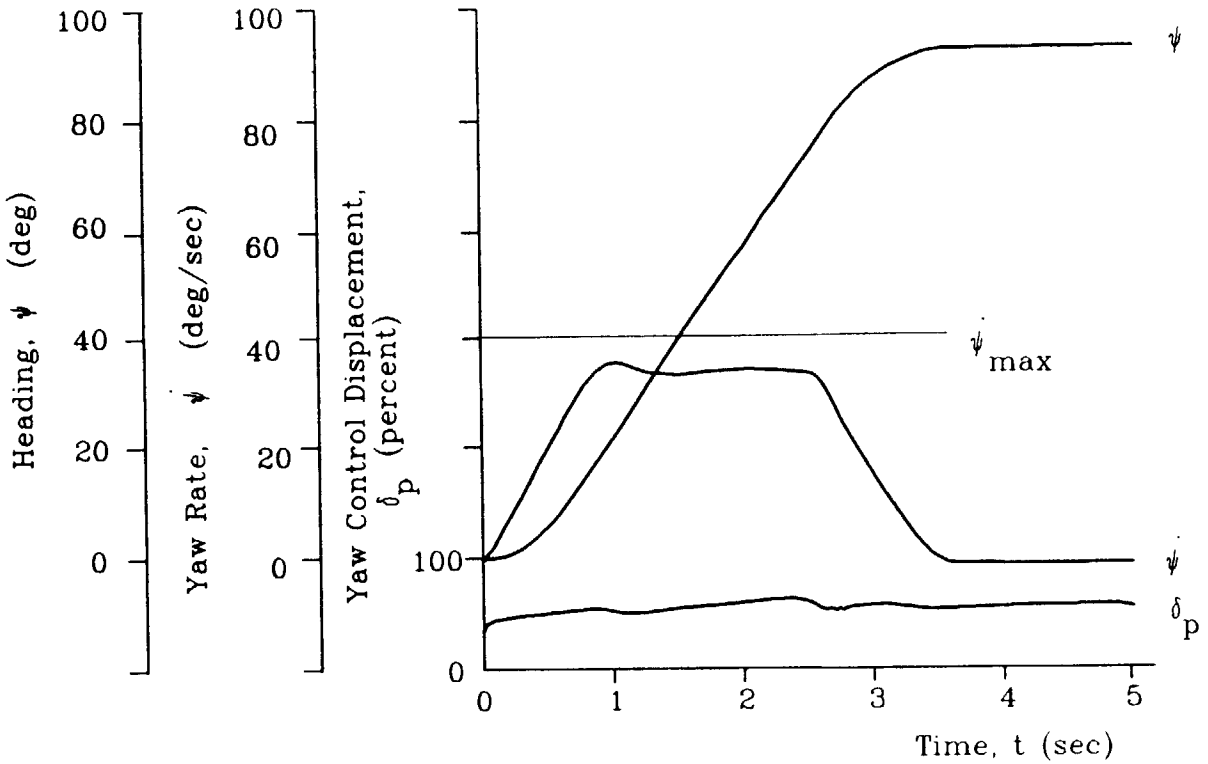

Figure 18. Time History of Pedal Turn at 20 kts
Using the Constrained Time Optimal Control Scheme

a. Hover

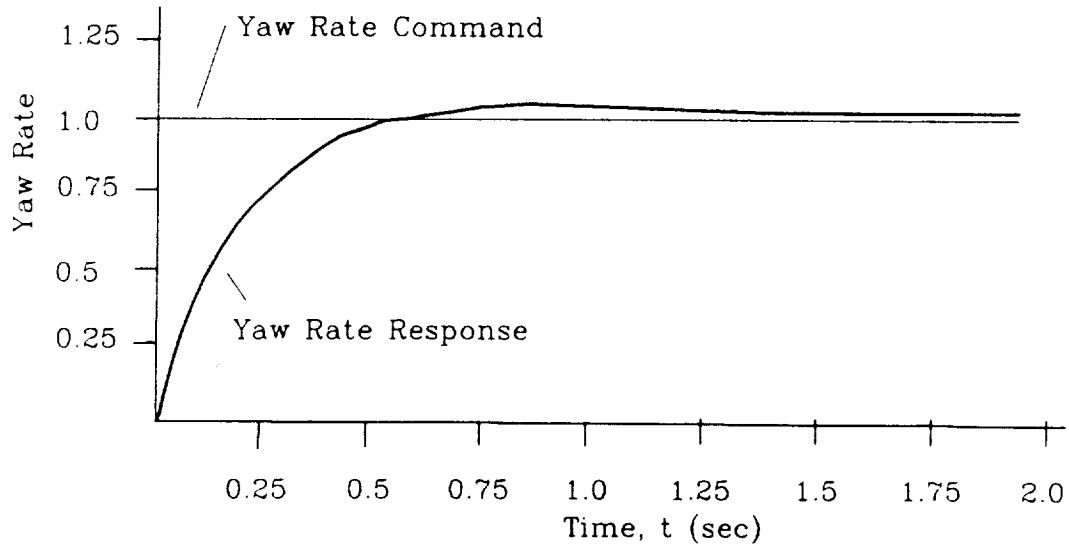

b. 20 kts

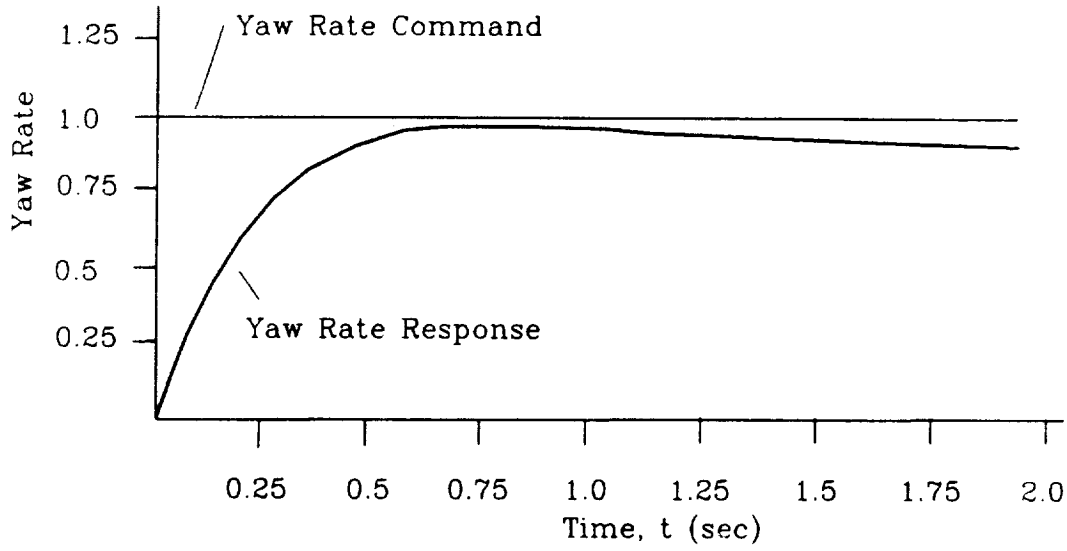

Figure 19. Step Response in Yaw Rate for a Yaw Rate Command

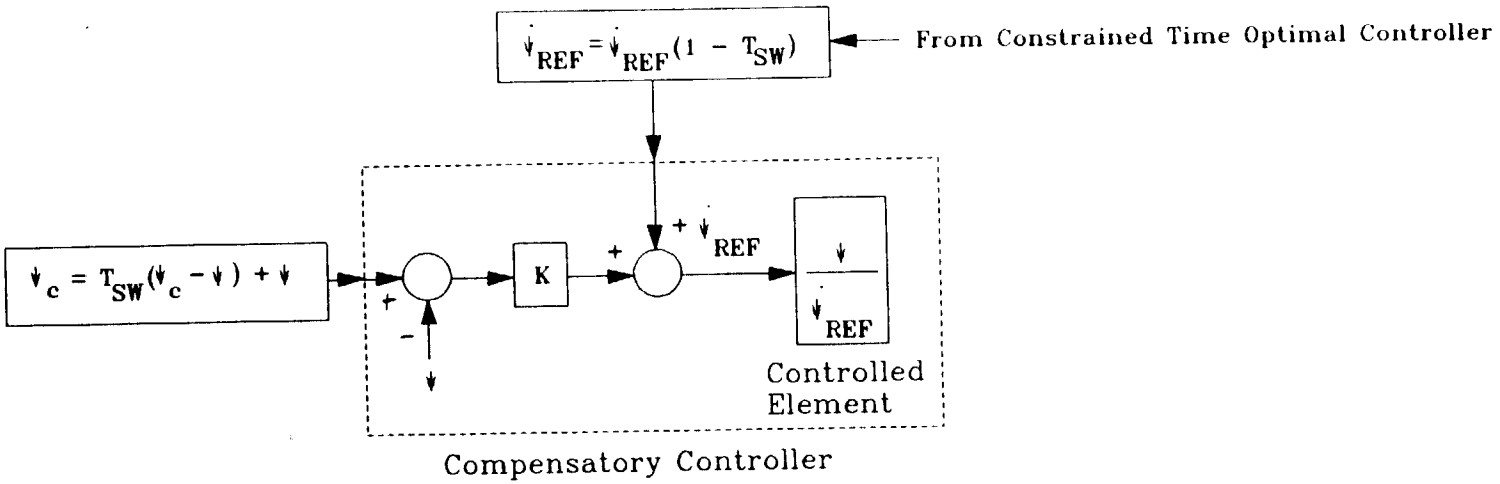

Figure 20. Implementation of the Constrained Time Optimal Controller, Hover–Turn Maneuver

D. LATERAL MANEUVERS

The next obstacle avoidance maneuver is the lateral sidestep. This maneuver presented additional problems to those encountered in the previous maneuvers. Again, the bang-bang manipulation of the reference velocity yields unacceptable results due to higher-order limits. In this case, those limits come in the form of limits on roll rate, roll angle, and roll acceleration. The roll acceleration limit is essentially a limit on cyclic input rate. In order to complete the sidestep in a time optimal fashion while observing these imposed limits, it is necessary to have direct control of the vehicle roll rate. This is analogous to controlling vertical acceleration in the bob-up or yaw acceleration in the hover turn. The problem is that there is no easy way to obtain this control over roll rate by manipulating the lateral reference velocity, especially given only the low frequency response of the vehicle:

$$\frac{\dot{y}}{\dot{y}_{ref}} = \frac{0.8}{s+0.8} \quad *$$

The assumption is made throughout the rest of this discussion that the capability of direct control of roll rate is attainable via a feed-forward command to MDHC's flight control system.

The relationship between y and φ is as follows:

$$\frac{\dot{y}}{\phi} = \frac{g}{s - \hat{Y}_v}$$

Because $\hat{Y}_v$ is generally small, the approximation was made that

$$\dot{y} \approx \frac{g\phi}{s}$$

*This transfer function approximates that for MDHC's lateral velocity command flight control system (Ref. 6).

or

$$\ddot{y} \cong g\phi$$

This indicates that the limits on φ, $\dot{\phi}$, and $\ddot{\phi}$ can be thought of as limits on y, $\dot{y}$, and $\ddot{y}$. The time optimal problem becomes one of controlling a K/s^4 plant with limits on every integrator. As will be seen, this is a much more complicated problem than that of controlling a K/s^3 plant as was the case in both the bob-up and hover turn maneuvers. The commanded $\dot{\phi}_c$ is calculated as shown in Fig. 21. There are three integrators operating serially on $\dot{\phi}_c$, each requiring the switching logic discussed below.

1. **The First Integration of $\dot{\phi}_c$: Attitude ϕ**

The first limited integration of $\dot{\phi}$ is ϕ. The equation for ϕ as a function of $\dot{\phi}_c$ is

$$\phi(t) = \int_0^t \left\{ \int_0^t \ddot{\phi}_c dt \right\} dt = \int_0^t \{\dot{\phi}_c t + \dot{\phi}(0)\} dt$$

$$\phi(t) = \frac{1}{2}\ddot{\phi}_c t^2 + \dot{\phi}(0) + \phi(0)$$

There are four switching points required to control φ throughout the sidestep maneuver, ϕ_{SW1} through ϕ_{SW4} (Fig. 22). The first switch determines the point after which a $\ddot{\phi}_c$ of $-\ddot{\phi}_{max}$ will bring the vehicle to ϕ_{max} as $\dot{\phi}$ reaches zero. The second switch determines the point after which $\ddot{\phi} = \ddot{\phi}_{max}$ will bring the vehicle to the steady state attitude for $\dot{y} = \dot{y}_{max}$. The third switch point is for $\phi = -\phi_{min}$ and the last is for $\phi = \phi_{lc}$. The calculations for these switching points are shown in Fig. 23, wherein the cross-hatched area represents the change in roll attitude following the switch. For the final roll attitude to equal ϕ_{max}, this area must equal $\phi_{max} - \phi_{SW1}$, or

$$\phi_{max} - \phi_{SW1} = \frac{1}{2}\ddot{\phi}_c t^2 + \dot{\phi}(0)t$$

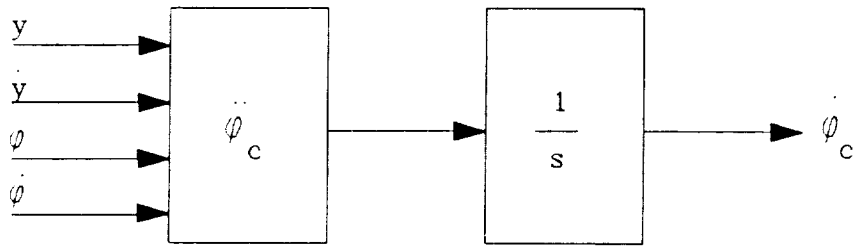

$$\ddot{\varphi}_c = \begin{cases} \ddot{\varphi}_{max} \\ 0 \\ -\ddot{\varphi}_{max} \end{cases}$$ depending on switching criteria

NOTE: $\ddot{\varphi}_c$ is determined by limits on $\ddot{\varphi}_c$ and the switching logic presented later

Figure 21. Constrained Time Optimal Control Scheme for the Lateral Sidestep

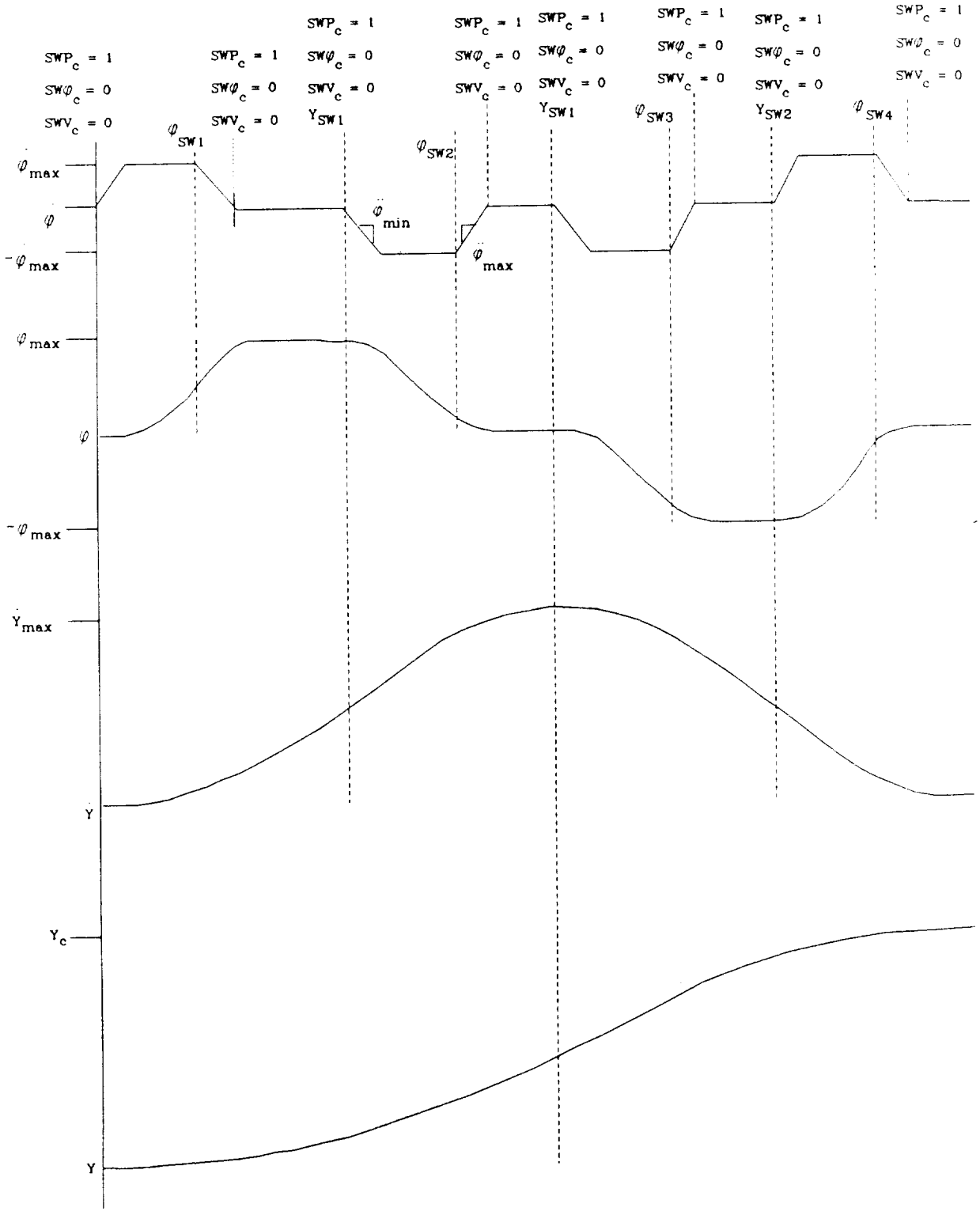

Figure 22. Theoretical Time History of Constrained Time Optimal Sidestep Maneuver

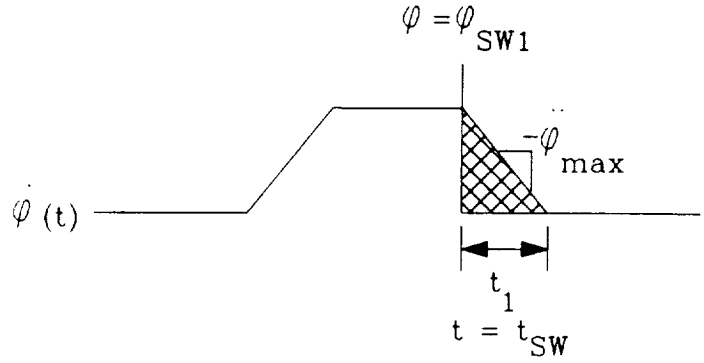

Figure 23. Calculation of Switching Points

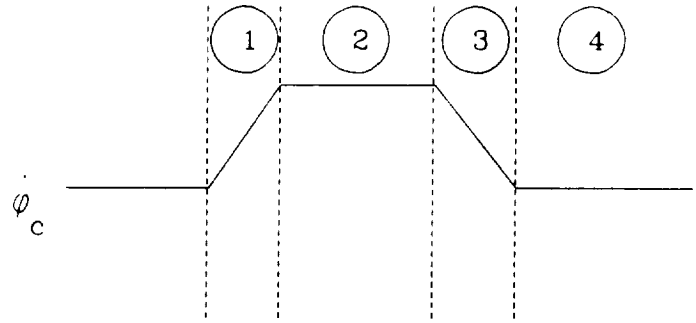

Figure 24. Four Regions of Possible Switching During Maneuver

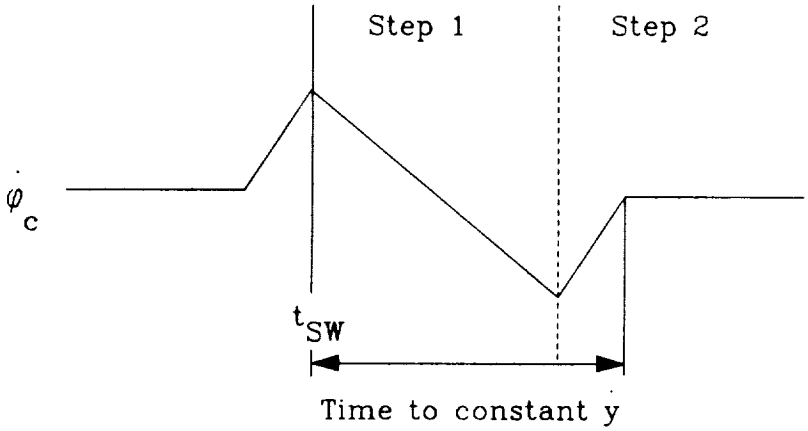

Figure 25. Two Step Response for V_{SW1}, Region 1

Depending on the chosen limits of ϕ and $\dot{\phi}$, this switch could take place before $\dot{\phi}$ reaches $\dot{\phi}_{max}$. The general expression for ϕ_{SW1}, therefore, is calculated as follows:

$$t = \frac{\dot{\phi}(t_{sw})}{\ddot{\phi}_{max}} \text{(the time for } \dot{\phi} \text{ to go to zero)}$$

$$\dot{\phi}(0) = \dot{\phi}(t_{sw})$$

$$\ddot{\phi}_c = -\ddot{\phi}_{max}$$

So

$$\phi_{max} - \phi_{sw1} = -\frac{1}{2}\frac{\dot{\phi}^2(t_{sw})}{\ddot{\phi}_{max}} + \frac{\dot{\phi}^2(t_{sw})}{\ddot{\phi}_{max}} = \frac{1}{2}\frac{\dot{\phi}^2(t_{sw})}{\ddot{\phi}_{max}}$$

$$\boxed{\phi_{sw1} = \phi_{max} - \frac{\dot{\phi}^2(t_{sw})}{2\ddot{\phi}_{max}}}$$

The value of $\dot{\phi}$ at the time of the switch cannot be known ahead of time; therefore, this switch point is calculated on a real-time basis with the current value of $\dot{\phi}$. Because all of the switches require this real-time calculation, notation will be adopted to simplify the expressions. Unsubscripted variables are to be thought of as current values in the on-going real-time calculations. For example:

$$\phi(t) : \phi_{sw1} = \phi_{max} - \frac{\dot{\phi}^2(t)}{2\ddot{\phi}_{max}} \quad = \quad \phi : \phi_{sw1} = \phi_{max} - \frac{\dot{\phi}^2}{2\ddot{\phi}_{max}}$$

where : is the comparison operator

Both equations mean that ϕ is compared to ϕ_{SW1} at all times with ϕ_{SW1} being calculated using the current value of $\dot{\phi}$.

The other three switch points are calculated in a similar fashion with ϕ_{max} replaced with the appropriate desired final value of ϕ.

$$\phi_{ss} - \phi_{sw2} = \frac{1}{2}\frac{\dot{\phi}^2}{\ddot{\phi}_{max}} - \frac{\dot{\phi}^2}{\ddot{\phi}_{max}} = -\frac{\dot{\phi}^2}{2\ddot{\phi}_{max}}$$

$$\boxed{\phi_{sw2} = \phi_{ss} + \frac{\dot{\phi}^2}{2\ddot{\phi}_{max}}}$$

$$\phi_{min} - \phi_{sw3} = -\frac{1}{2}\frac{\dot{\phi}^2}{\ddot{\phi}_{max}} - \frac{\dot{\phi}^2}{\ddot{\phi}_{max}} = -\frac{\dot{\phi}^2}{2\ddot{\phi}_{max}}$$

$$\boxed{\phi_{sw3} = -\phi_{max} + \frac{\dot{\phi}^2}{2\ddot{\phi}_{max}}}$$

$$\phi_{ic} - \phi_{sw4} = -\frac{1}{2}\frac{\dot{\phi}^2}{\ddot{\phi}_{max}} + \frac{\dot{\phi}^2}{\ddot{\phi}_{max}} = \frac{\dot{\phi}^2}{2\ddot{\phi}_{max}}$$

$$\boxed{\phi_{sw4} = \phi_{ic} - \frac{\dot{\phi}^2}{2\ddot{\phi}_{max}}}$$

2. The Second Integration of $\ddot{\phi}_c$: Velocity $\dot{y}$

The second integration of $\dot{\phi}$ is $\dot{y}$. The equation for $\dot{y}$ as a function of $\ddot{\phi}_c$ is:

$$\dot{y}(t) = \int_0^t g\,\phi(t)dt = \int_0^t g\left\{\frac{1}{2}\ddot{\phi}_c t^2 + \dot{\phi}(0)t + \phi(0)\right\}dt$$

$$\dot{y}(t) = g\left(\frac{1}{6}\ddot{\phi}_c t^3 + \frac{1}{2}\dot{\phi}(0)t^2 + \phi(0)t\right) + \dot{y}(0)$$

There are two switching points required to control $\dot{y}$ throughout the sidestep maneuver, $\dot{y}_{sw1}$ and $\dot{y}_{sw2}$ (Fig. 22). The first switch is determined by the minimum change in velocity while bringing φ to φ_{ss}. In these calculations, ϕ_{ss} and ϕ_{ic} are assumed equal. Because $\dot{\Upsilon}_v$ is very small, this is a reasonable assumption. The switching point has the possibility of occurring in four regions of the maneuver depending on chosen limits of $\dot{y}, \phi, \dot{\phi}$, and $\ddot{\phi}$. These regions are defined as follows:

1) $\ddot{\phi}_c = \ddot{\phi}_{max}, \dot{\phi}_c < \dot{\phi}_{max}, \phi < \phi_{SW1}$

2) $\ddot{\phi}_c = 0, \dot{\phi}_c = \dot{\phi}_{max}, \phi < \phi_{SW1}$

3) $\ddot{\phi}_c = -\ddot{\phi}_{max}, \phi_{SW1} < \phi < \phi_{max}$

4) $\ddot{\phi}_c = 0, \dot{\phi}_c = 0, \phi_c = \phi_{max}$

(see Fig. 24)

V_{SW1}, Region 1

In Fig. 25, there is a two step response after the velocity switch is encountered. The total change in velocity is the sum of the change in each part.

For Step 1,

$$\ddot{\phi}_c = -\ddot{\phi}_{max}, \dot{\phi}(0) = \dot{\phi}, \phi(0) = \frac{\dot{\phi}^2}{2\ddot{\phi}_{max}}$$

$$t_1 = \frac{2\dot{\phi}}{\ddot{\phi}_{max}}$$

$$\Delta \dot{y}_1 = g\left\{-\frac{1}{6}\frac{8\dot{\phi}^3}{\ddot{\phi}^2_{max}} + \frac{1}{2}\frac{4\dot{\phi}^3}{\ddot{\phi}^2_{max}} + \frac{\dot{\phi}^3}{\ddot{\phi}^2_{max}}\right\} = g\left(\frac{5\dot{\phi}^3}{3\ddot{\phi}^2_{max}}\right)$$

$\Delta \dot{y}_2 = V_{SW1}$ --This means that the change in velocity for Step 2 is the same as the amount of velocity built up before the switch

Thus,

$$\Delta \dot{y} = V_{SW1} + g\left(\frac{5\dot{\phi}^3}{3\ddot{\phi}^2_{max}}\right)$$

Because the desired final velocity is $\dot{y}_{max}$,

$$\dot{y}_{max} = V_{SW1} + \Delta\dot{y} = 2V_{SW1} + g\frac{5\dot{\phi}^3}{3\ddot{\phi}^2_{max}}$$

$$V_{SW1} = \frac{1}{2}\left(\dot{y}_{max} - g\frac{5\dot{\phi}^3}{3\ddot{\phi}^2_{max}}\right)$$

V_{SW1}, Region 2

In Fig. 26, once again, there is a two-step response following velocity switch point, and the total $\Delta\dot{y}$ is the sum of the two parts.

For Step 1

$$\ddot{\phi}_c = -\ddot{\phi}_{max}, \dot{\phi}(0) = \dot{\phi}_{max}, \phi(0) = \phi$$

$$t = \frac{2\dot{\phi}_{max}}{\ddot{\phi}_{max}}$$

$$\Delta\dot{y}_1 = g\left(-\frac{4\dot{\phi}^3_{max}}{5\ddot{\phi}^2_{max}} + \frac{2\dot{\phi}^3_{max}}{\ddot{\phi}^2_{max}} + \frac{2\phi\dot{\phi}_{max}}{\ddot{\phi}_{max}}\right)$$

$$= g\left(\frac{2\dot{\phi}^3_{max}}{3\ddot{\phi}^2_{max}} + \frac{2\phi\dot{\phi}_{max}}{\ddot{\phi}_{max}}\right)$$

Once again, $\Delta\dot{y}_2 = V_{SW1}$, therefore:

$$V_{SW1} = \frac{1}{2}\left[\dot{y}_{max} - g\left(\frac{2\dot{\phi}^3}{3\ddot{\phi}^2_{max}} + \frac{2\phi\dot{\phi}_{max}}{\ddot{\phi}_{max}}\right)\right]$$

V_{SW1}, Region 3

In Fig. 27, using the same procedure as before, with

$$\ddot{\phi}_c = -\ddot{\phi}_{max}, \dot{\phi}(0) = \dot{\phi}, \phi(0) = \phi, t = \frac{2\dot{\phi}}{\ddot{\phi}_{max}} \text{ for Step 1}$$

we get

$$V_{SW1} = \frac{1}{2}\left[\dot{y}_{max} - g\left(\frac{2\dot{\phi}^3}{3\ddot{\phi}^2_{max}} + \frac{2\phi\dot{\phi}}{\ddot{\phi}_{max}}\right)\right]$$

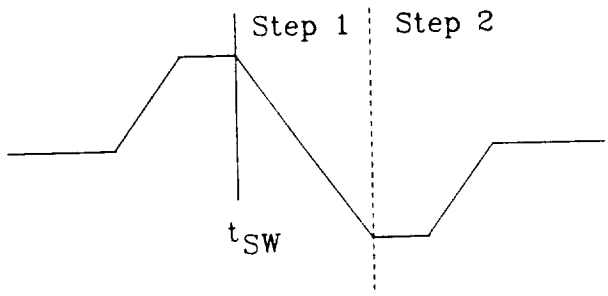

Figure 26. Two-Step Response Following Velocity Switch Point in V_{SW1}, Region 2

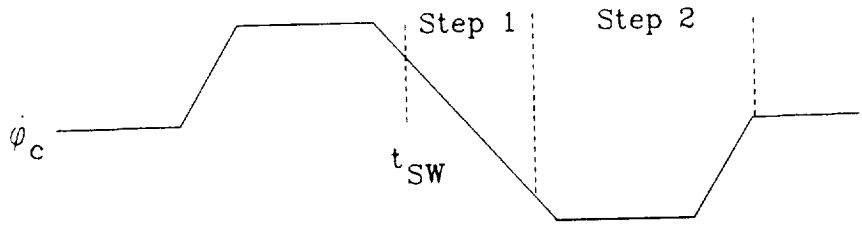

Figure 27. Two-Step Response for V_{SW1}, Region 3

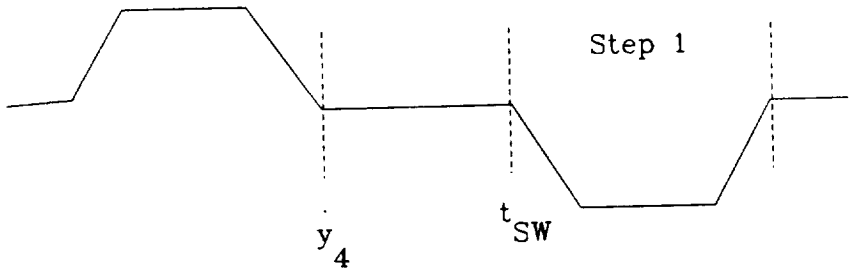

Figure 28. One Step Response for V_{SW1}, Region 4

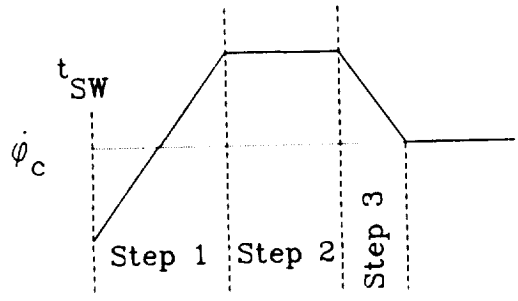

Figure 29. Response After the Second Velocity Switch in V_{SW2}, Region 4

This is the same as was the case in Region 2, where $\dot{\phi} = \dot{\phi}_{max}$. Also, if ϕ is substituted for $\dot{\phi}^2/2\ddot{\phi}_{max}$ in the case of Region 1, the same expression results. Thus, the general expression for V_{SW1} in Regions 1 through 3 is

$$V_{SW1} = \frac{1}{2}\left[\dot{y}_{max} - g\left(\frac{2\dot{\phi}^3}{3\ddot{\phi}_{max}^2} + \frac{2\phi\dot{\phi}}{\ddot{\phi}_{max}}\right)\right]$$

V_{SW1}, Region 4

In the case shown in Fig. 28, the change in velocity during Step 1 is equal to $\dot{y}_4$, where $\dot{y}_4$ is the velocity of the vehicle as it entered Region 4. Therefore,

$$V_{SW1} = \dot{y}_{max} - \dot{y}_4$$

V_{SW2}, Region 4

The second switch point for the velocity, V_{SW2}, is to bring the vehicle to a stop in the lateral direction. This switching velocity represents the minimum change in velocity to bring this about.

In general, the time history of $\dot{\phi}_c$ after the second velocity switch is encountered is shown in Fig. 29. The total change in velocity is calculated as follows:

$$\Delta\dot{y}_1 \Rightarrow \ddot{\phi}_c = \ddot{\phi}_{max}, \dot{\phi}(0) = \dot{\phi}, \phi(0) = \phi, t_1 = \frac{\dot{\phi}_{max} - \dot{\phi}}{\ddot{\phi}_{max}}$$

$$\Delta\dot{y}_1 = g\left[\frac{\dot{\phi}_{max}^3}{6\ddot{\phi}_{max}^2} - \frac{\dot{\phi}^2\dot{\phi}_{max}}{\ddot{\phi}_{max}^2} + \frac{\dot{\phi}^3}{3\ddot{\phi}_{max}^2} + \frac{\phi\dot{\phi}_{max}}{\ddot{\phi}_{max}} - \frac{\dot{\phi}\phi}{\ddot{\phi}_{max}}\right]$$

$$\Delta\dot{y}_2 \Rightarrow \ddot{\phi}_c = 0, \dot{\phi}(0) = \dot{\phi}_{max}, \phi(0) = \phi + \frac{\dot{\phi}_{max}^2 - \dot{\phi}^2}{2\ddot{\phi}_{max}}, t_2 = -\frac{\dot{\phi}}{\ddot{\phi}_{max}} + \frac{\dot{\phi}^2}{2\ddot{\phi}_{max}\dot{\phi}_{max}} - \frac{\ddot{\phi}_{max}}{\ddot{\phi}_{max}}$$

$$\Delta\dot{y}_2 = g\left[-\frac{\dot{\phi}^2}{2\ddot{\phi}_{max}} + \frac{3\phi\dot{\phi}^2}{4\dot{\phi}_{max}\ddot{\phi}_{max}} - \frac{\phi\dot{\phi}_{max}}{2\ddot{\phi}_{max}} + \frac{\dot{\phi}^2\dot{\phi}_{max}}{2\ddot{\phi}_{max}^2} - \frac{\dot{\phi}^4}{8\dot{\phi}_{max}\ddot{\phi}_{max}^2}\right]$$

$$\Delta\dot{y}_3 \Rightarrow \dot{\phi}_c = -\dot{\phi}_{max},\ \dot{\phi}(0) = \dot{\phi}_{max},\ \phi(0) = -\frac{\dot{\phi}_{max}^2}{2\dot{\phi}_{max}},\ t = \frac{\dot{\phi}_{max}}{\dot{\phi}_{max}}$$

$$\Delta\dot{y}_3 = -\frac{g\dot{\phi}_{max}^3}{6\dot{\phi}_{max}^2}$$

So the total $\Delta\dot{y} = V_{SW2}$ is

$$V_{SW2} = -g\left[\frac{\dot{\phi}^3}{3\dot{\phi}_{max}^2} - \frac{\dot{\phi}^2\dot{\phi}_{max}}{2\dot{\phi}_{max}^2} + \frac{\dot{\phi}\dot{\phi}_{max}}{2\dot{\phi}_{max}} - \frac{\dot{\phi}\dot{\phi}}{\dot{\phi}_{max}} + \frac{3\dot{\phi}\dot{\phi}^2}{4\dot{\phi}_{max}\dot{\phi}_{max}} - \frac{\dot{\phi}^2}{2\dot{\phi}_{max}} - \frac{\dot{\phi}^4}{8\dot{\phi}_{max}\dot{\phi}_{max}^2}\right]$$

This is only true if the vehicle passed through Region 2 at the beginning of the maneuver (i.e., if $\dot{\phi}$ reached $\dot{\phi}_{max}$ during the acceleration portion of the maneuver). If one of the switches prevented $\dot{\phi}$ from reaching $\dot{\phi}_{max}$, then the following expression would represent V_{SW2}.

$$V_{SW2} = -g\left[-\frac{\dot{\phi}^2\dot{\phi}_f}{\dot{\phi}_{max}^2} + \frac{\dot{\phi}^3}{3\dot{\phi}_{max}^2} + \frac{\dot{\phi}\dot{\phi}_f}{\dot{\phi}_{max}} - \frac{\dot{\phi}\dot{\phi}}{\dot{\phi}_{max}}\right]$$

where

$$\dot{\phi}_f^2 = -\dot{\phi}\ddot{\phi}_{max} + \frac{1}{2}\dot{\phi}abs(\dot{\phi})$$

3. The Third Integration of $\dot{\phi}_c$: Position y

For the position switch, Y_{SW}, there are many possible regions in which the switch might occur as shown in Fig. 30. Regions 3, 5, and 6 in Fig. 30 depict regions in which the vehicle is already slowing down at its maximum acceptable rate. Therefore, if the position switch were to be encountered during any of these segments, no immediate change would occur. Because of this, the criteria for Region 4 can be used during Region 3, Region 7 can be used for Regions 5 and 6. In this way, if the position switch would have been encountered in Region 3, it will be encountered immediately upon entering Region 4, and likewise with Regions 5, 6, and 7.

The definitions for the various regions are as follows:

1a) $\ddot{\phi}_c = \ddot{\phi}_{max}, \dot{\phi} < \sqrt{\frac{1}{2}}\dot{\phi}_{max}, \phi < \phi_{SW1}, \dot{y} < V_{SW1}$

1b) $\ddot{\phi}_c = \ddot{\phi}_{max}, \sqrt{\frac{1}{2}}\dot{\phi}_{max} < \dot{\phi} < \dot{\phi}_{max}, \phi < \phi_{SW1}, \dot{y} < V_{SW1}$

2) $\ddot{\phi}_c = 0, \dot{\phi}_c = \dot{\phi}_{max}, \phi < \phi_{SW1}, \dot{y} < V_{SW1}$

4) $\ddot{\phi}_c = 0, \dot{\phi}_c = 0, \phi_c = \phi_{max}, \dot{y} < V_{SW1}$

7) $\ddot{\phi}_c = \ddot{\phi}_{max}, 0 > \dot{\phi} > -\dot{\phi}_{max}, 0 < \phi < \phi_{SW2}, \dot{y} > V_{SW1}$

8) $\ddot{\phi}_c = 0, \dot{\phi}_c = 0, \phi_c = 0, \ddot{y}_c = \ddot{y}_{max}$

The expression for y in terms of $\ddot{\phi}_c$ is as follows:

$$y = \int_0^t \dot{y}\,dt = g\left(\frac{1}{24}\ddot{\phi}_c t^4 + \frac{1}{6}\dot{\phi}(0)t^3 + \frac{1}{2}\phi(0)t^2\right) + \dot{y}(0)t + y(0)$$

Y_{SW}, Region 1a

In Fig. 31, there is a two-step response following the position switch and Y_{SW} equals the commanded lateral position less the distance traveled in those deceleration steps.

$$\Delta y_{1a} \rightarrow \ddot{\phi}_c = -\ddot{\phi}_{max}, \dot{\phi}(0) = \dot{\phi}, \phi(0) = \frac{\dot{\phi}^2}{2\ddot{\phi}_{max}}, \dot{y}(0) = g\frac{\dot{\phi}^3}{6\ddot{\phi}_{max}^2}$$

$$t = \frac{\dot{\phi} - \dot{\phi}_f}{\ddot{\phi}_{max}}$$

where $\dot{\phi}_f$ is determined by considering the fact that area A^* must equal area A_2 or $\varphi = 0$ when $\dot{\phi} = \dot{\phi}_f$

$$A_1 = \dot{\phi}\,t_{SW} = \frac{\dot{\phi}^2}{\ddot{\phi}_{max}}$$

$$A_2 = \frac{1}{2}\dot{\phi}_f\,t_{A_2} = \frac{\dot{\phi}_f^2}{2\ddot{\phi}_{max}}$$

*In Fig. 31.

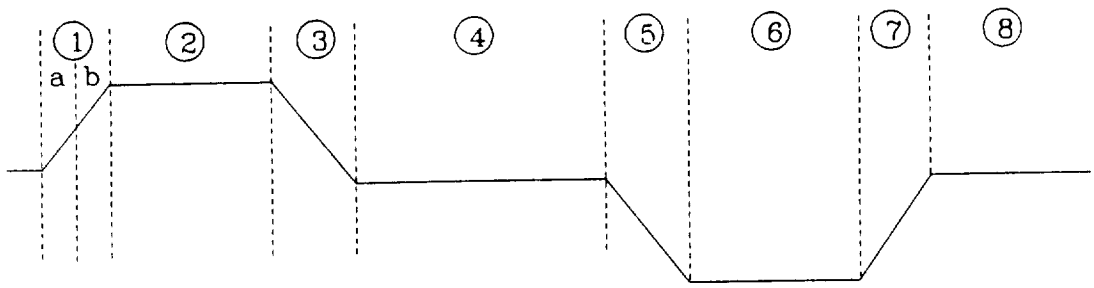

Figure 30. Possible Switching Regions for the Position Switch Y_{SW}

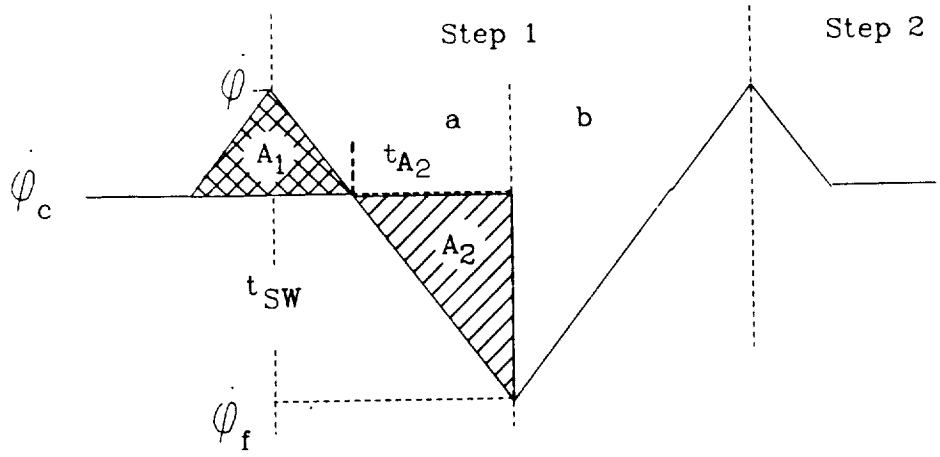

Figure 31. Two-Step Response for Y_{SW}, Region 1a

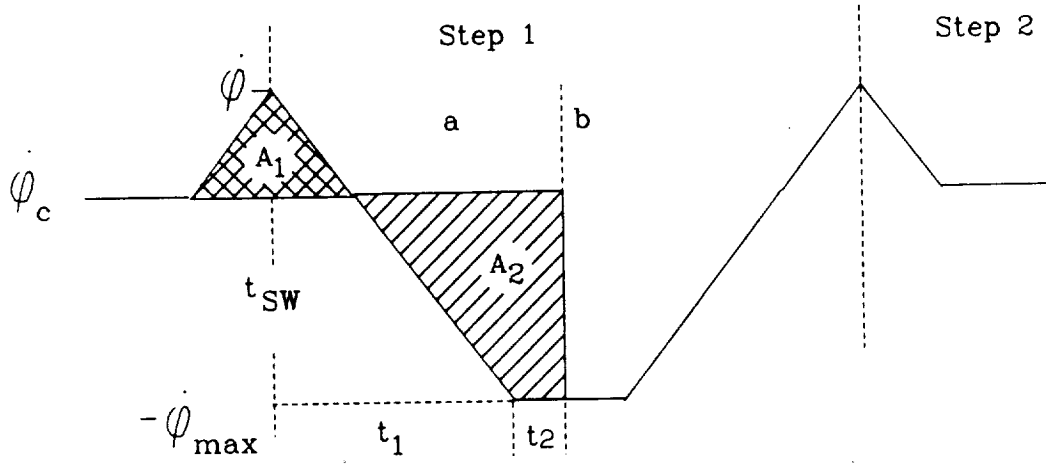

Figure 32. Two-Step Response for Y_{SW}, Region 1b

$$2\dot{\phi}^2 = \dot{\phi}_f^2$$

$$\dot{\phi}_f = -\sqrt{2}\dot{\phi}$$

$$t = \frac{(1+\sqrt{2})\dot{\phi}}{\ddot{\phi}_{max}}$$

$$\Delta y_{1a} = g\left(\frac{-1.415\dot{\phi}^4}{\ddot{\phi}_{max}^3} + \frac{2.345\dot{\phi}^4}{\ddot{\phi}_{max}^3} + \frac{1.457\dot{\phi}^4}{\ddot{\phi}_{max}^3} + \frac{0.402\dot{\phi}^4}{\ddot{\phi}_{max}^3}\right)$$

$$\Delta y_{1a} = g\left(\frac{2.789\dot{\phi}^4}{\ddot{\phi}^3}\right)$$

$$\Delta y_{1b} = \Delta y_{1a}$$

$$\Delta y_2 = Y_{SW}$$

Therefore,

$$Y_{SW} = \frac{1}{2}\left[y_c - g\left(\frac{5.577\dot{\phi}^4}{\ddot{\phi}_{max}^3}\right)\right]$$

Y_{SW}, Region 1b

The distance traveled in Step 1, Fig. 32, of the post position switch response is equal to twice the distance traveled in Part a of that step. Part a can in turn be broken down into two segments of duration t and t_2, respectively. The distance traveled in Step 2 is equal to the distance traveled prior to the position switch being tripped.

$$\Delta y_{1a_1} \rightarrow \ddot{\phi}_c = -\ddot{\phi}_{max}, \dot{\phi}(0) = \dot{\phi}, \phi(0) = \frac{\dot{\phi}^2}{2\ddot{\phi}_{max}}, \dot{y}(0) = \frac{g\dot{\phi}^3}{6\ddot{\phi}_{max}^2}$$

$$t_1 = \frac{\dot{\phi} + \dot{\phi}_{max}}{\ddot{\phi}_{max}}$$

$$\Delta y_{1a_1} = g\left(\frac{0.5417\dot{\phi}^4}{\ddot{\phi}_{max}^3} + \frac{\dot{\phi}^3\dot{\phi}_{max}}{\ddot{\phi}_{max}^3} + \frac{0.5\dot{\phi}^2\dot{\phi}_{max}^2}{\ddot{\phi}_{max}^3} - \frac{0.0417\dot{\phi}_{max}^4}{\ddot{\phi}_{max}^3}\right.$$

$$\Delta y_{1a_2} \Rightarrow \ddot{\phi}_c = 0, \dot{\phi}(0) = -\dot{\phi}_{max}, \phi(0) = \frac{2\dot{\phi}^2 - \dot{\phi}_{max}^2}{2\ddot{\phi}_{max}}$$

$$\ddot{y}(0) = g\left(\frac{\dot{\phi}^3 + \dot{\phi}^2\dot{\phi}_{max} - \frac{1}{6}\dot{\phi}_{max}^3}{\ddot{\phi}_{max}^2}\right)$$

t_2 is defined by the fact that Area A_2 equals Area A, or $\dot{\phi} = 0$ after Step 1a.

$$A_1 = \frac{\dot{\phi}^2}{\ddot{\phi}_{max}}$$

$$A_2 = \frac{1}{2}\left(s t_2 + \frac{\dot{\phi}_{max}}{\ddot{\phi}_{max}}\right)\dot{\phi}_{max}$$

$$t_2 = \frac{\dot{\phi}^2}{\dot{\phi}_{max}\ddot{\phi}_{max}} - \frac{\dot{\phi}_{max}}{2\ddot{\phi}_{max}}$$

$$\Delta y_{1a_2} = g\left(\frac{\dot{\phi}^6}{3\dot{\phi}_{max}^2\ddot{\phi}_{max}^3} + \frac{\dot{\phi}^5}{\dot{\phi}_{max}\ddot{\phi}_{max}^3} + \frac{0.5\dot{\phi}^4}{\ddot{\phi}_{max}^3} - \frac{5\dot{\phi}^2\dot{\phi}_{max}^2}{12\ddot{\phi}_{max}^3} - \frac{0.5\dot{\phi}^3\dot{\phi}_{max}}{\ddot{\phi}_{max}^3} + \frac{0.0417\dot{\phi}_{max}^4}{\ddot{\phi}_{max}^3}\right)$$

$$\Delta y_1 = 2\Delta y_{1a} = g\left(\frac{2\dot{\phi}^6}{3\dot{\phi}_{max}^2\ddot{\phi}_{max}^3} + \frac{2\dot{\phi}^5}{\dot{\phi}_{max}\ddot{\phi}_{max}^3} + \frac{2.0833\dot{\phi}^4}{\ddot{\phi}_{max}^3} + \frac{\dot{\phi}^3\dot{\phi}_{max}}{\ddot{\phi}_{max}^3} + \frac{\dot{\phi}^2\dot{\phi}_{max}^2}{6\ddot{\phi}_{max}^3}\right)$$

and

$$Y_{SW} = \frac{1}{2}(y_c - g\Delta y_1)$$

Y_{SW}, Region 2

The distance traveled during the first part of Step 1a, Fig. 33, is Δy_{1a_1}, and the distance through the second part is Δy_{1a_2}.

$$\Delta y_{1a_1} \Rightarrow \ddot{\phi}_c = -\ddot{\phi}_{max}, \dot{\phi}(0) = \dot{\phi}_{max}, \phi(0) = \phi$$

$$y(0) = g\left(\frac{\dot{\phi}^2}{2\ddot{\phi}_{max}} + \frac{\dot{\phi}_{max}^3}{24\ddot{\phi}_{max}^2}\right)$$

$$t_1 = \frac{2\dot{\phi}_{max}}{\ddot{\phi}_{max}}$$

$$\Delta y_{1a_1} = g\left(\frac{3}{4}\frac{\dot{\phi}_{max}^4}{\ddot{\phi}_{max}^3} + \frac{2\dot{\phi}_{max}^2\dot{\phi}}{\ddot{\phi}_{max}^2} + \frac{\dot{\phi}^2}{\ddot{\phi}_{max}}\right)$$

$$\Delta y_{1a_2} \Rightarrow \ddot{\phi}_c = 0, \dot{\phi}(0) = -\dot{\phi}_{max}, \phi(0) = \phi$$

(because the integral of $\dot{\phi}$ over 1a is 0)

$$\dot{y}(0) = g\left(\frac{17}{24}\frac{\dot{\phi}_{max}^3}{\ddot{\phi}_{max}^2} + \frac{2\phi\dot{\phi}_{max}}{\ddot{\phi}_{max}} + \frac{\phi^2}{2\dot{\phi}_{max}}\right)$$

t_2 is the time to $\varphi = 0$; therefore,

$$t_2 = \frac{\phi}{\dot{\phi}_{max}}$$

$$\Delta y_{1a_2} = g\left(\frac{5}{6}\frac{\phi^3}{\dot{\phi}_{max}^2} + \frac{17}{24}\frac{\dot{\phi}_{max}^2\phi}{\ddot{\phi}_{max}^2} + \frac{2\phi^2}{\dot{\phi}_{max}}\right)$$

The total distance traveled during Step 1 is $2(\Delta y_{1a_1} + \Delta y_{1a_2})$, and the distance traveled during Step 2 is Y_{SW}.

$$\Delta y_1 = g\left(\frac{5}{3}\frac{\phi^3}{\dot{\phi}_{max}^2} + \frac{65}{12}\frac{\dot{\phi}_{max}^2\phi}{\ddot{\phi}_{max}^2} + \frac{6\phi^2}{\dot{\phi}_{max}} + \frac{3}{2}\frac{\dot{\phi}_{max}^4}{\ddot{\phi}_{max}^3}\right)$$

$$Y_{SW} = \frac{1}{2}(y_c - \Delta y_1)$$

Y_{SW}, Region 4

In the case shown in Fig. 34, the vehicle has reached and is holding the maximum allowable roll angle ($\varphi = \varphi_{max}$).

$$\Delta y_{1a_1} \Rightarrow \ddot{\phi}_c = -\ddot{\phi}_{max}, \dot{\phi}(0) = 0, \phi(0) = \phi_{max}, \dot{y}(0) = \dot{y}$$

$$\Delta y_{1a_1} = g\left(-\frac{\dot{\phi}_{max}^4}{24\ddot{\phi}_{max}^3} + \frac{\phi_{max}\dot{\phi}_{max}^2}{2\ddot{\phi}_{max}^2} + \frac{\dot{y}\dot{\phi}_{max}}{g\ddot{\phi}_{max}}\right)$$

$$\Delta y_{1a_2} \Rightarrow \ddot{\phi}_c = 0, \dot{\phi}(0) = -\dot{\phi}_{max}, \phi(0) = \phi_{max} - \frac{\dot{\phi}_{max}^2}{2\ddot{\phi}_{max}}$$

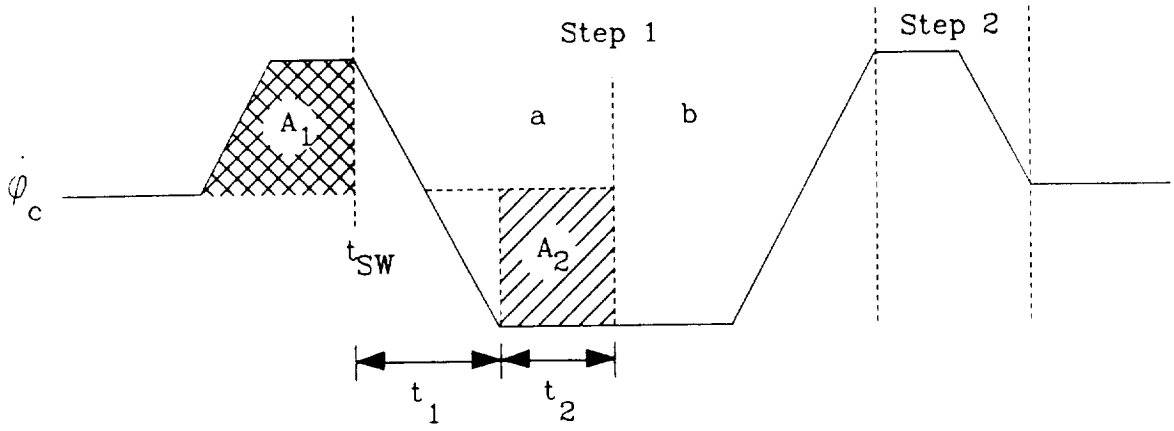

Figure 33. Two-Step Response for Y_{SW}, Region 2

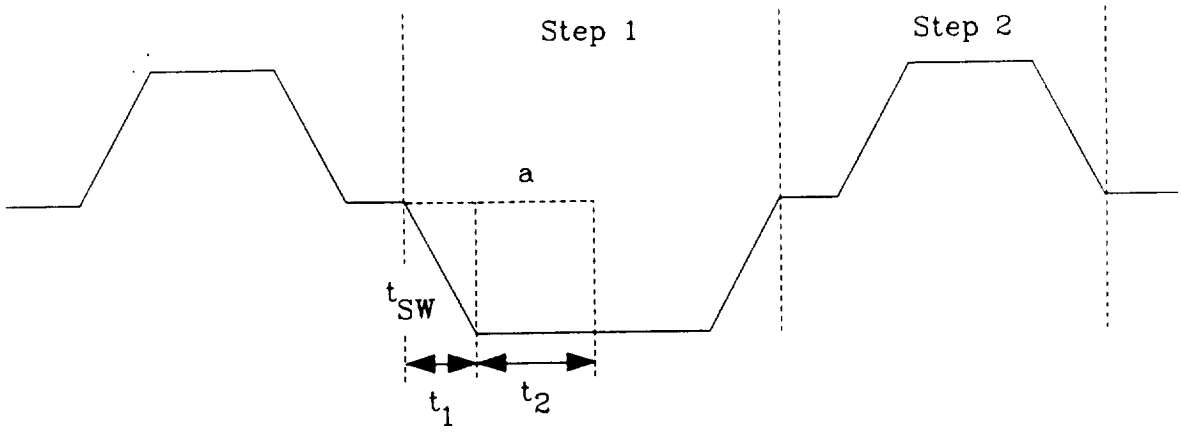

Figure 34. Two-Step Response for Y_{SW}, Region 4

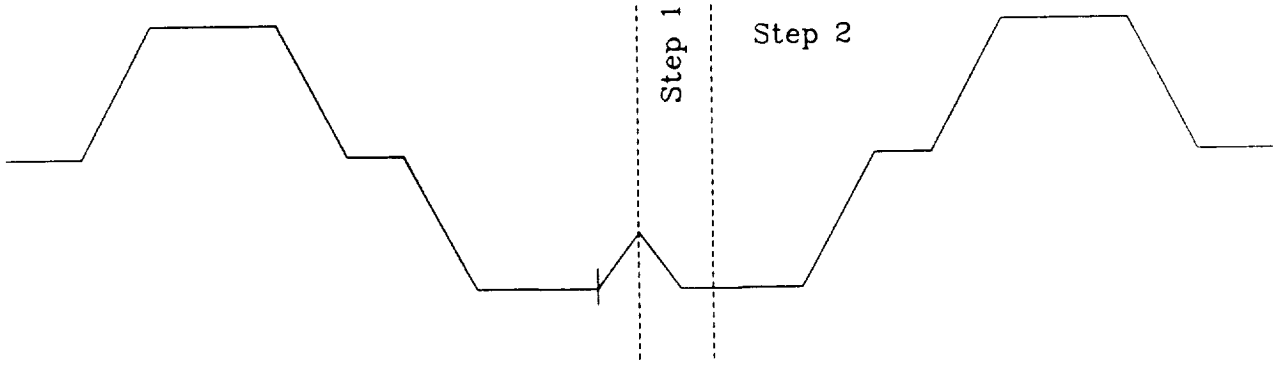

Figure 35. Two-Step Response for Y_{SW}, Region 7

$$y(0) = y + g\left(-\frac{\phi_{max}^3}{6\phi_{max}^2} + \frac{\phi_{max}\dot{\phi}_{max}}{2\phi_{max}}\right)$$

$$t_2 = \frac{\phi_{max} - \frac{\phi_{max}^2}{2\phi_{max}}}{\dot{\phi}_{max}} \text{ (the time to } \phi = 0)$$

$$\Delta y_{1a_2} = g\left(\frac{\phi_{max}^3}{3\phi_{max}^2} - \frac{\phi_{max}\dot{\phi}_{max}^2}{6\phi_{max}^2} + \frac{\dot{\phi}_{max}^4}{24\dot{\phi}_{max}^3} + \frac{\ddot{y}\phi_{max}}{g\dot{\phi}_{max}} - \frac{\dot{y}\dot{\phi}_{max}}{2g\dot{\phi}_{max}}\right)$$

$$\Delta y_1 = 2(\Delta y_{1a_1} + \Delta y_{1a_2}) = g\left(\frac{2}{3}\frac{\phi_{max}^3}{\dot{\phi}_{max}^2} + \frac{2}{3}\frac{\phi_{max}\dot{\phi}_{max}^2}{\dot{\phi}_{max}^2} + \frac{2\ddot{y}\phi_{max}}{g\dot{\phi}_{max}} + \frac{\dot{y}\dot{\phi}_{max}}{g\dot{\phi}_{max}}\right)$$

$$Y_{SW} = \frac{1}{2}(y_c - \Delta y_1)$$

Y_{SW}, Region 7

Once again, the distance traveled in Step 2, Fig. 35, is equal to Y_{SW}, but the origin of that step is not readily apparent. If the position switch took place at or before the instant $\varphi = \varphi_{SW3}$, then Step 2 will start at a time $2\varphi/\varphi_{max}$ after the position switch, and the distance traveled during Step 1 would be

$$\Delta y_1 \Rightarrow \ddot{\phi}_c = 0, \dot{\phi}(0) = -\dot{\phi}_{max}, \phi(0) = \phi, \dot{y}(0) = \dot{y}$$

$$\Delta y_1 = g\left(\frac{-2\phi^3}{3\dot{\phi}_{max}^2} - \frac{2\dot{y}\phi}{g\dot{\phi}_{max}}\right)$$

If the switch occurs at the very end of Region 7, $\varphi \approx 0$, and the second step starts immediately, thus the distance traveled during Step 1 is zero. Thus, the equation above is also satisfied in this case. The actual expression for Δy varies depending on the value of $\dot{\phi}$, but the equation above is an adequate approximation for the far more complicated correct expression.

Y_{SW}, Region 8

After the vehicle has come to steady state at the maximum acceptable lateral velocity, $\dot{\phi} = 0$ and $\varphi = \varphi_{SS}$. This being the case, a commanded $-\ddot{\phi}_{max}$ will immediately start the deceleration of the vehicle, and the distance traveled during that deceleration will equal the distance traveled during the acceleration to $\dot{y} = \dot{y}_{max}$. Thus

$$Y_{SW} = y_c - y_8$$

where y_8 is the lateral position as it entered Region 8.

In order to test this method of control, a control scheme was designed to enable direct control of roll rate, attitude, lateral velocity, or lateral position. This control scheme is diagrammed in Fig. 36. It is STI's understanding that MDHC has access to or can get access to the attitude and rate stabilization loops in their control system, and it is with this access that we propose a similar method to that of Fig. 36 be employed. If MDHC can develop a different method of accurately controlling roll rate, this would also be acceptable.

This control scheme was designed to provide tighter control of attitude, velocity, and position when $\dot{\phi}_c = 0$ and thus better adherence to the theoretical time history of the maneuver. For example, when $\dot{\phi}_c = 0$ is attempting to hold $\varphi = \varphi_{max}$ or $\varphi = -\varphi_{max}$, control is given to the φ loop. Likewise, with velocity command being used to hold $\dot{y} = \dot{y}_{max}$, and position command at the end of the maneuver to hold $y = y_c$. This switching logic is depicted in Fig. 36.

The following test runs are examples of the position switch point being encountered in different regions of the rapid response maneuver. The first is a 25-ft command position change (Fig. 37). In this case, the position switch occurs in Region 2 ($\ddot{\phi} = \ddot{\phi}_{max}, \dot{\phi} < \dot{\phi}_{SW1}$). The limits on $\ddot{\phi}, \dot{\phi}, \phi$, and $\dot{y}$ for all cases were as follows:

$$\ddot{\phi}_{max} = 40 \text{ deg/sec}^2$$

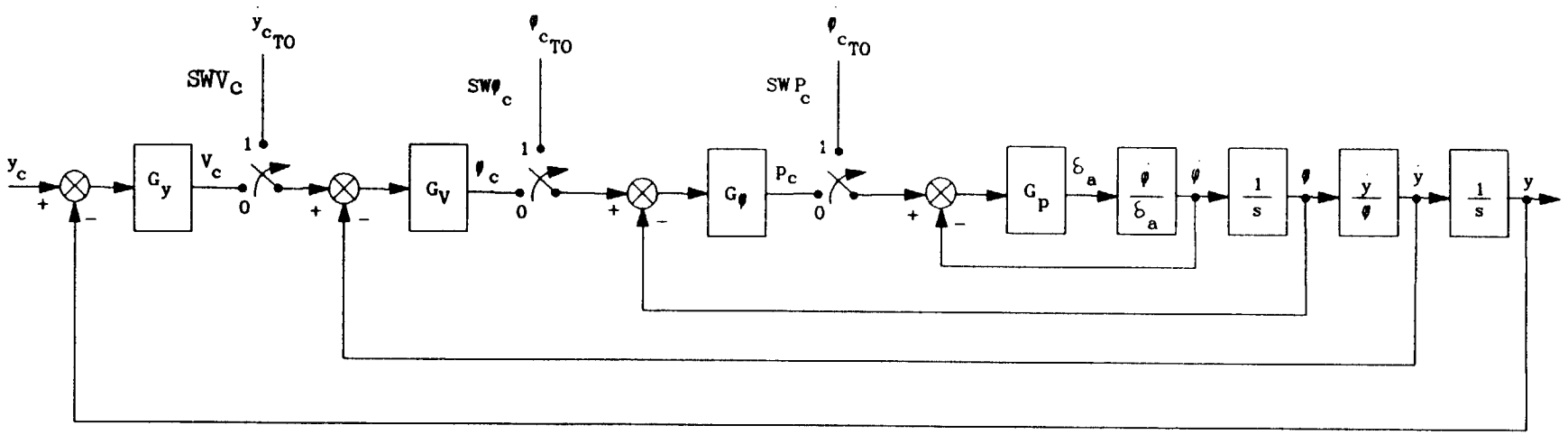

Figure 36. Control Scheme for Testing Constrained Time Optimal Sidestep Maneuver

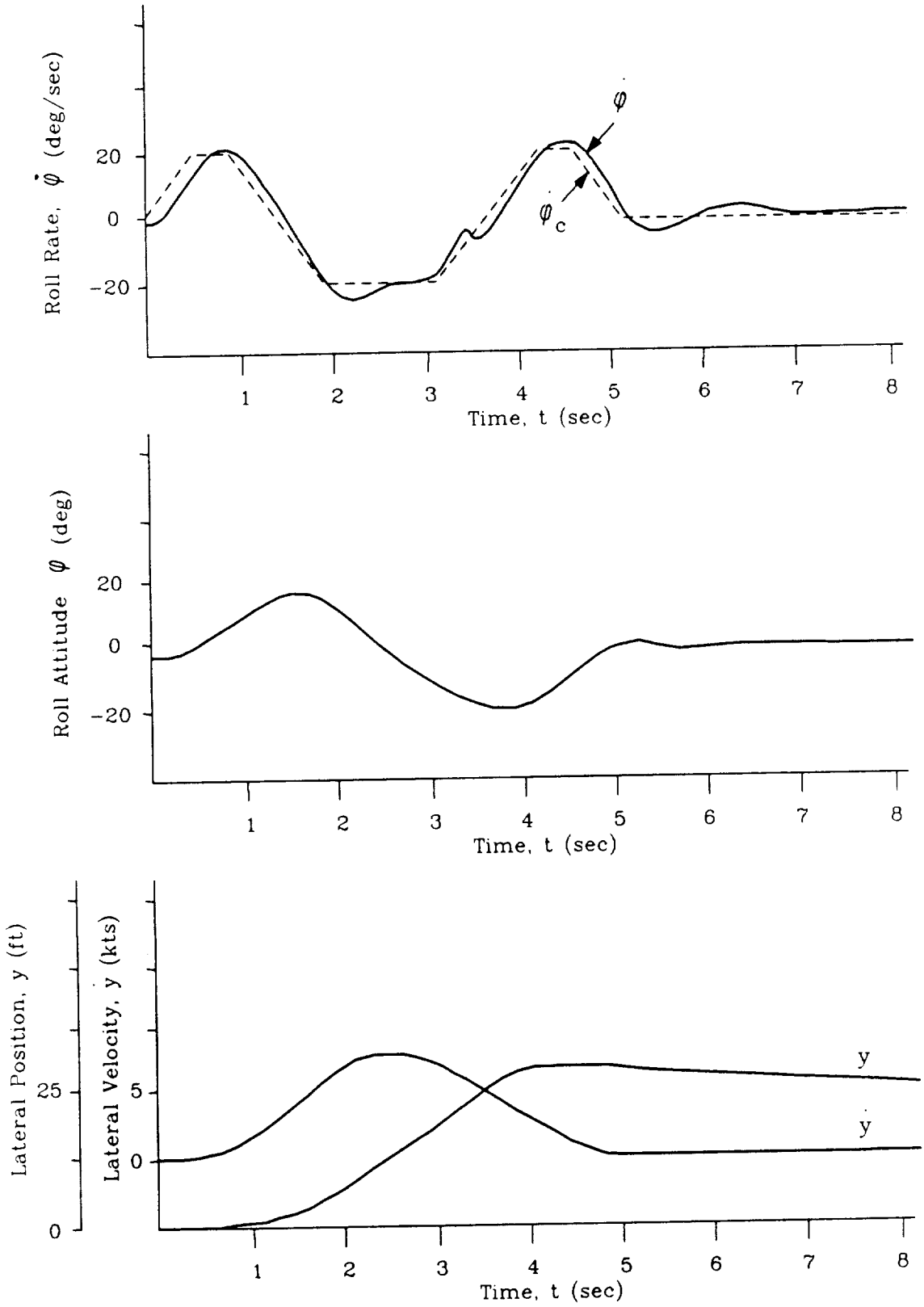

Figure 37. Lateral Sidestep of 25 ft
Using the Constrained Time Optimal Control Scheme

$$\dot{\phi}_{max} = 20 \text{ deg/sec}$$

$$\phi_{max} = 20 \text{ deg}$$

$$\dot{y}_{max} = 20 \text{ kts}$$

With these limits, the commanded position change that would result in the position switching point being encountered in Regions 1a or 1b of the response ($\phi = \phi_{max}, \dot{\phi} < \dot{\phi}_{max}$) is too small to use as a reasonable example.

The second test run was for a commanded displacement of 100 ft (Fig. 38). In this case, the vehicle was able to reach $\varphi = \varphi_{max}$ before encountering the position switch. The switch was encountered in Region 4. Lastly, a test case with a commanded displacement of 300 ft was run (Fig. 39). In this case, the vehicle was able to reach $\dot{y} = \dot{y}_{max}$ before encountering the position switch. Notice the resemblance of this last set of time histories to the ones presented in Fig. 36.

E. LONGITUDINAL MANEUVERS

The last obstacle avoidance maneuver is the longitudinal accel-decel. This maneuver is virtually identical to the lateral sidestep but with one added nuance. It is desirable to have the ability to change <u>relative</u> position rapidly along the flight path as well as absolute position from a hover. To provide this capability, a slight modification is required of the control scheme depicted in Fig. 36. A reference trim velocity (U_T) is added to the velocity command signal so that the velocity command becomes an incremental command as opposed to an absolute command. The position command is also changed. It is incremented with the trim velocity so that it represents a relative commanded position (Fig. 40).

$$x_c(t) = x_{c_{ic}} + \int_0^t U_T dt$$

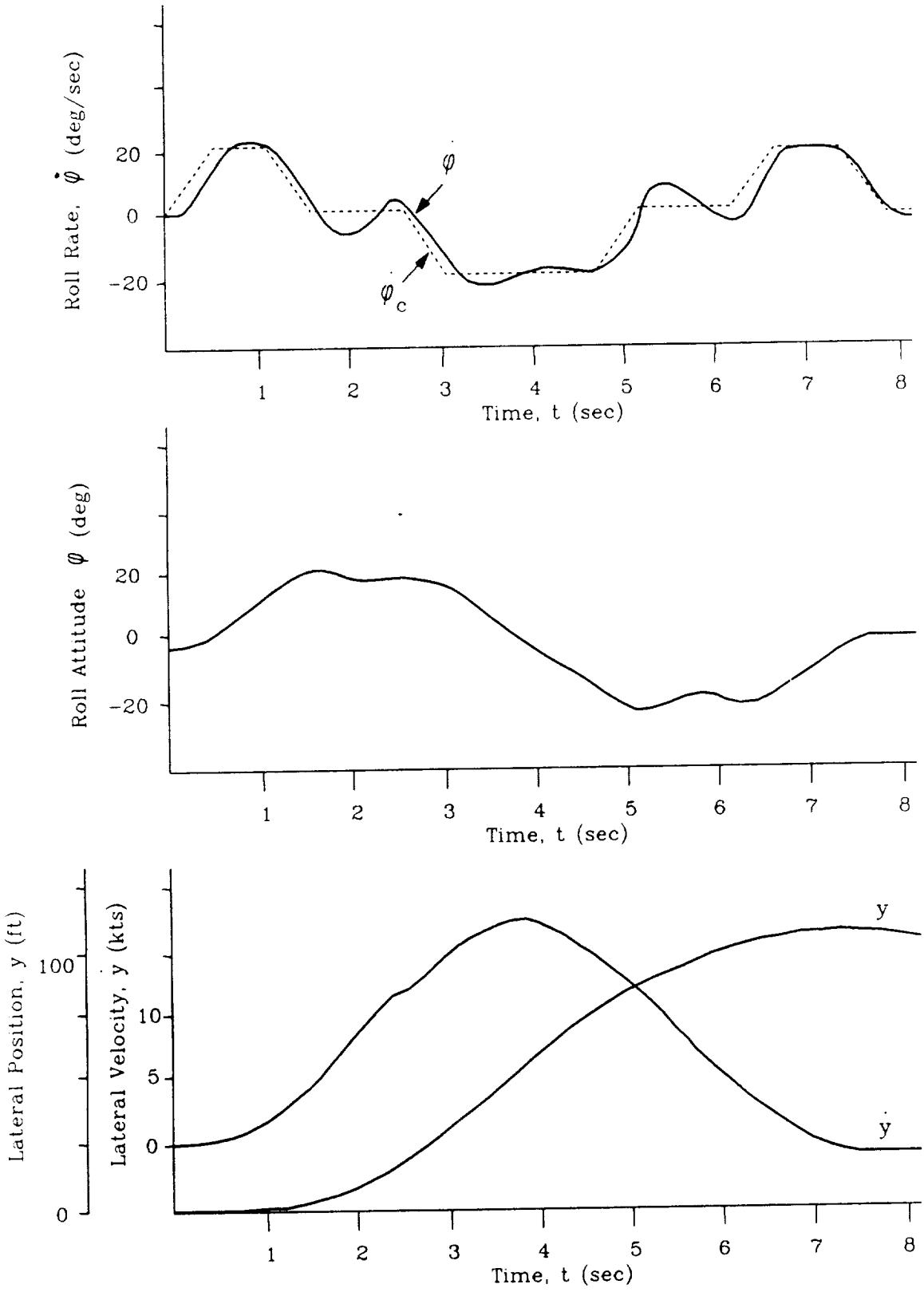

Figure 38. Lateral Sidestep of 100 ft
Using the Constrained Time Optimal Control Scheme

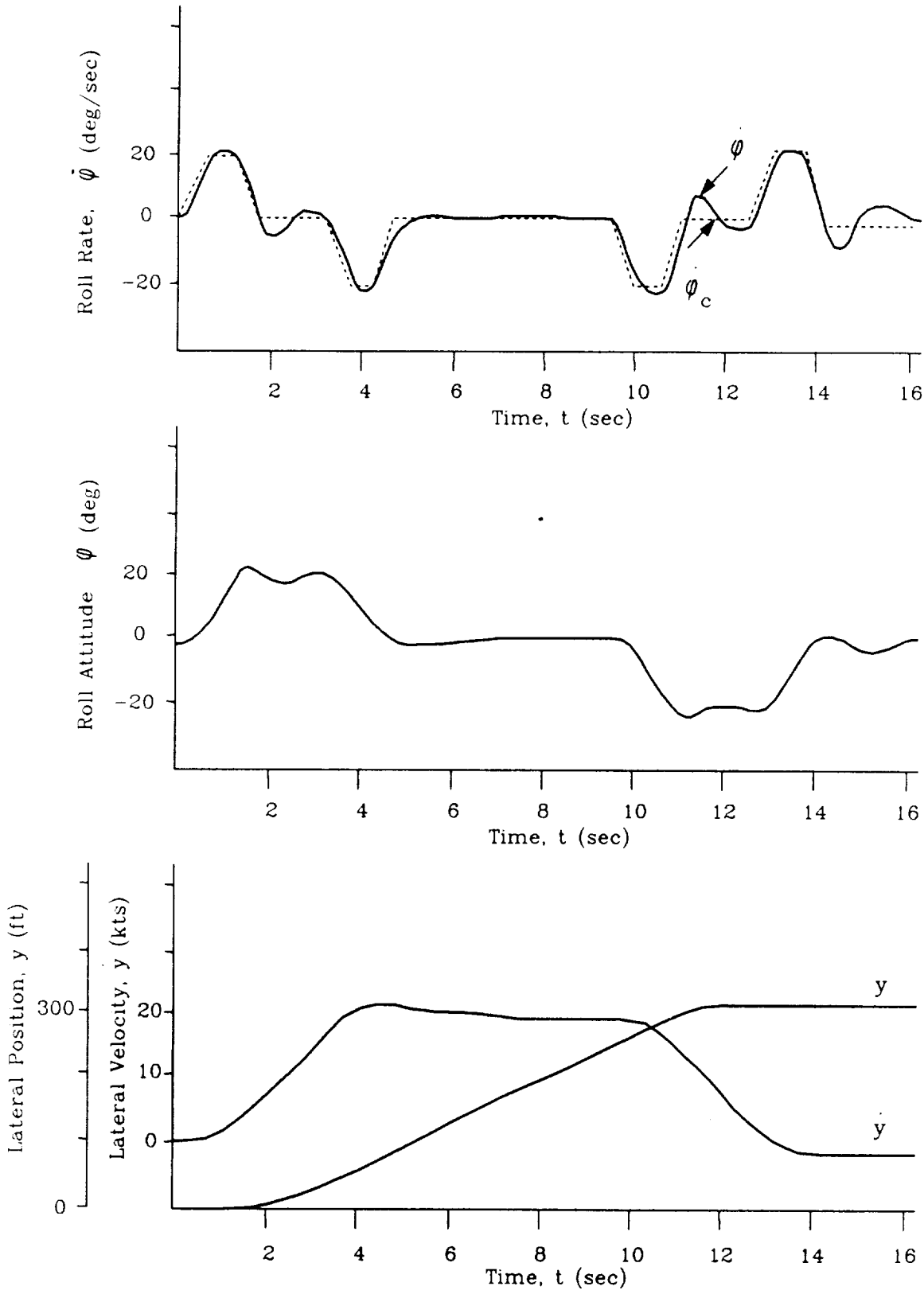

Figure 39. Lateral Sidestep of 300 ft
Using the Constrained Time Optimal Control Scheme

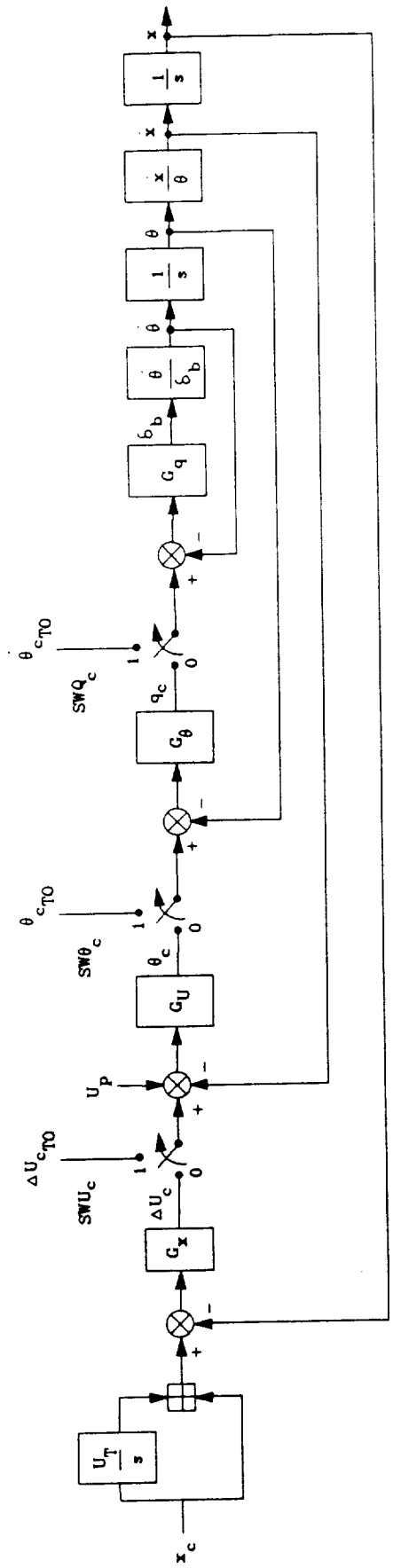

Figure 40. Control Scheme for Testing Constrained Time Optimal Longitudinal Accel-Decel Maneuver

In addition, relative vehicle position is kept track of by subtracting a similarly incremented initial position from the current absolute position

$$x_I(t) = x_{Ic} + \int_0^t U_T\,dt$$

$$x_{rel} = x - x_I$$

The relative values of position, commanded position, and velocity are used in the determination of the velocity and position switching criteria. The switching criteria themselves are similar to the criteria developed for the lateral sidestep with the only difference being the sign of the attitude variables, since

$$\ddot{x} \cong -g\theta \quad \text{whereas} \quad \ddot{y} \cong g\phi$$

The resulting switching criteria are:

U_{SW1}, Region 1-3

$$U_{SW1} = \frac{1}{2}\left[\dot{x}_{max} + g\left(\frac{2}{3}\frac{\dot{\theta}^3}{\ddot{\theta}_{max}^2} - \frac{2\theta\dot{\theta}}{\ddot{\theta}_{max}}\right)\right]$$

U_{SW1}, Region 4

$$U_{SW1} = \dot{x}_{max} - \dot{x}_4$$

where $\dot{x}_4$ is the velocity of the vehicle as it entered Region 4.

U_{SW2}

($\dot{\theta}$ did reach $\dot{\theta}_{max}$ during the acceleration phase of the maneuver)

$$U_{SW2} = g\left(\frac{\dot{\theta}^3}{3\ddot{\theta}_{max}^2} + \frac{\dot{\theta}^2\dot{\theta}_{max}}{2\ddot{\theta}_{max}^2} + \frac{\theta\dot{\theta}_{max}}{2\ddot{\theta}_{max}} + \frac{\theta\dot{\theta}}{\ddot{\theta}_{max}} + \frac{3\theta\dot{\theta}^2}{4\theta_{max}\ddot{\theta}_{max}} + \frac{\theta^2}{2\dot{\theta}_{max}} + \frac{\dot{\theta}^4}{8\theta_{max}\ddot{\theta}_{max}}\right)$$

U_{SW2}

($\dot{\theta}$ did not reach $\dot{\theta}_{max}$ during acceleration phase)

$$U_{SW2} = g\left(\frac{\dot{\theta}^2\dot{\theta}_f}{\ddot{\theta}^2_{max}} + \frac{\dot{\theta}^3}{3\ddot{\theta}^2_{max}} + \frac{\theta\dot{\theta}_f}{\ddot{\theta}_{max}} + \frac{\theta\dot{\theta}}{\ddot{\theta}_{max}}\right)$$

where

$$\dot{\theta}_f^2 = \theta\ddot{\theta}_{max} + \frac{1}{2}\dot{\theta}abs(\dot{\theta})$$

The position switch criteria are defined as follows:

x_{SW}, Region 1a

$$x_{SW} = \frac{1}{2}\left[x_{clc} - g\left(\frac{5.577\dot{\theta}^4}{\ddot{\theta}^3_{max}}\right)\right]$$

x_{SW}, Region 1b

$$x_{SW} = \frac{1}{2}\left[x_{clc} - g\left(\frac{2}{3}\frac{\dot{\theta}^6}{\ddot{\theta}^2_{max}\dot{\theta}^3_{max}} - 2\frac{\dot{\theta}^5}{\dot{\theta}_{max}\ddot{\theta}^3_{max}} + 2.0833\frac{\dot{\theta}^4}{\ddot{\theta}^3_{max}} - \frac{\dot{\theta}^3\dot{\theta}_{max}}{\ddot{\theta}^3_{max}} + \frac{\dot{\theta}^2\dot{\theta}^2_{max}}{6\ddot{\theta}^3_{max}}\right)\right]$$

x_{SW}, Region 2

$$x_{SW} = \frac{1}{2}\left[x_{clc} - g\left(-\frac{5}{3}\frac{\dot{\theta}^3}{\ddot{\theta}^2_{max}} - \frac{65}{12}\frac{\dot{\theta}^2_{max}\theta}{\ddot{\theta}^2_{max}} + 6\frac{\theta^2}{\dot{\theta}_{max}} - \frac{3}{2}\frac{\dot{\theta}^4_{max}}{\ddot{\theta}^3_{max}}\right)\right]$$

x_{SW}, Region 4

$$x_{SW} = \frac{1}{2}\left[x_{clc} - g\left(\frac{2}{3}\frac{\theta^3_{max}}{\ddot{\theta}^2_{max}} + \frac{2}{3}\frac{\theta_{max}\dot{\theta}^2_{max}}{\ddot{\theta}^2_{max}} + 2\frac{\dot{x}\theta_{max}}{g\dot{\theta}_{max}} + \frac{\dot{x}\dot{\theta}_{max}}{g\ddot{\theta}_{max}}\right)\right]$$

x_{SW}, Region 7

$$x_{SW} = \frac{1}{2}\left[x_{clc} + g\left(\frac{2}{3}\frac{\theta^3}{\ddot{\theta}^2_{max}} + \frac{2\dot{x}\theta}{g\dot{\theta}_{max}}\right)\right]$$

x_{SW}, Region 8

$$x_{SW} = x_{c_{lc}} - x_8$$

where x_8 is the relative vehicle position as it entered Region 8.

The first two test cases are examples of the position switch occurring in two different regions, Regions 2 and 4. As was the case with the lateral sidestep, only very small commanded position changes would cause the position switch to be encountered in Regions 1a and 1b. Also, in the longitudinal axis, the maximum velocity is very large and will likely not be attained during a rapid accel-decel maneuver; therefore, the position switch will most likely occur in either Region 2 or Region 4.

The limits on $\ddot{\theta}, \dot{\theta}, \theta$ and $\dot{x}$ used in these test cases were

$$\ddot{\theta}_{max} = 40 \text{ deg/sec}^2$$

$$\dot{\theta}_{max} = 20 \text{ deg/sec}$$

$$\theta_{max} = 20 \text{ deg}$$

$$\dot{x}_{max} = 200 \text{ kts}$$

The first case called for a displacement of 25 ft from hover (Fig. 41). This distance required that the position switch be encountered before θ reached θ_{SW1} (Region 2). The second case called for a 250-ft displacement from hover (Fig. 42). In this case, the vehicle did attain maximum pitch attitude but did not reach the velocity switch point before encountering the position switch (Region 4).

The last test case is an example of a relative position change. The vehicle is travelling at a speed of 20 kts, and a relative position change of 100 ft is commanded (Fig. 43). The vertical distance between the dashed lines in Fig. 43 indicates the 100-ft relative change.

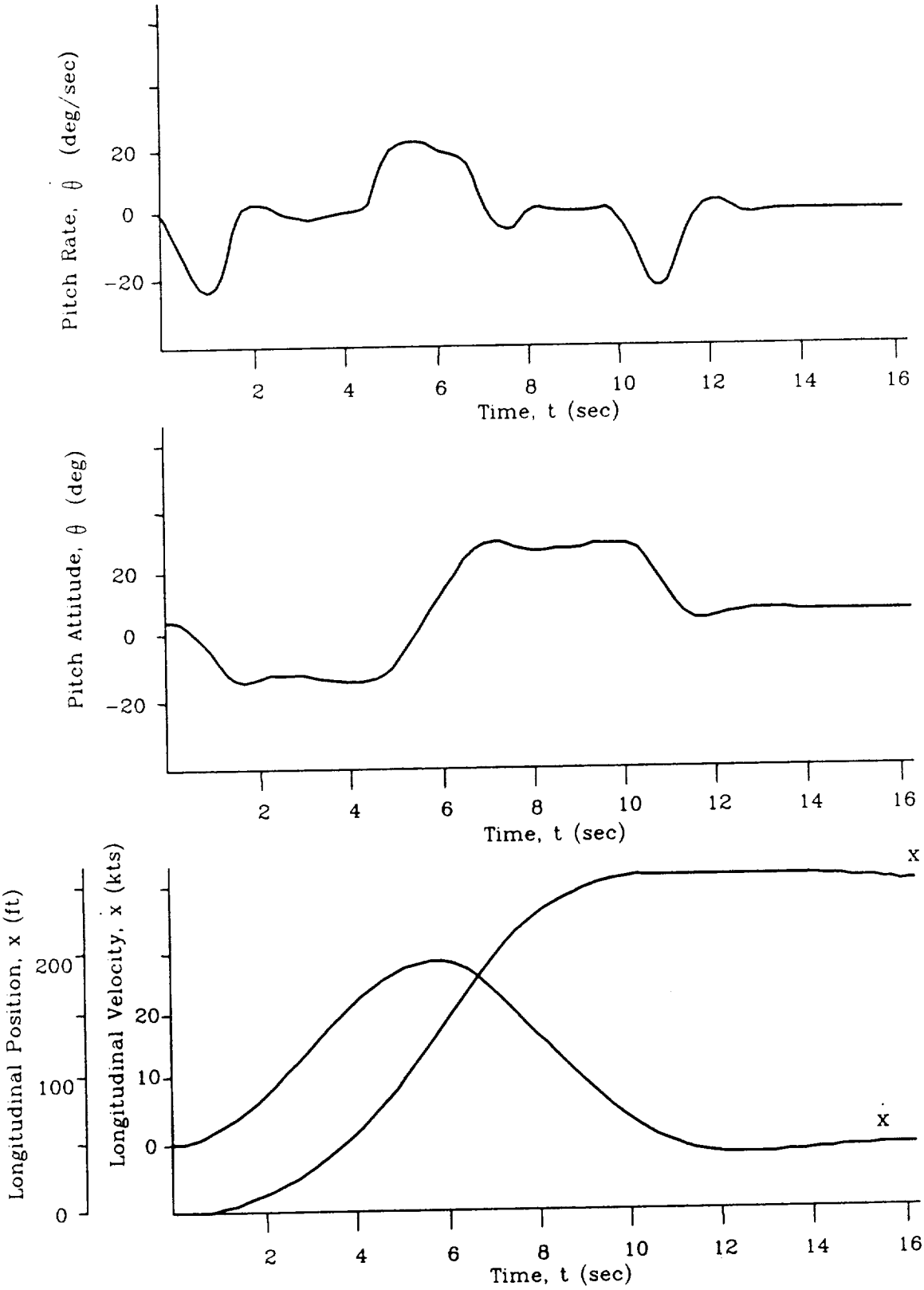

Figure 41. Longitudinal Position Change of 250 ft from Hover Using the Constrained Time Optimal Control Scheme

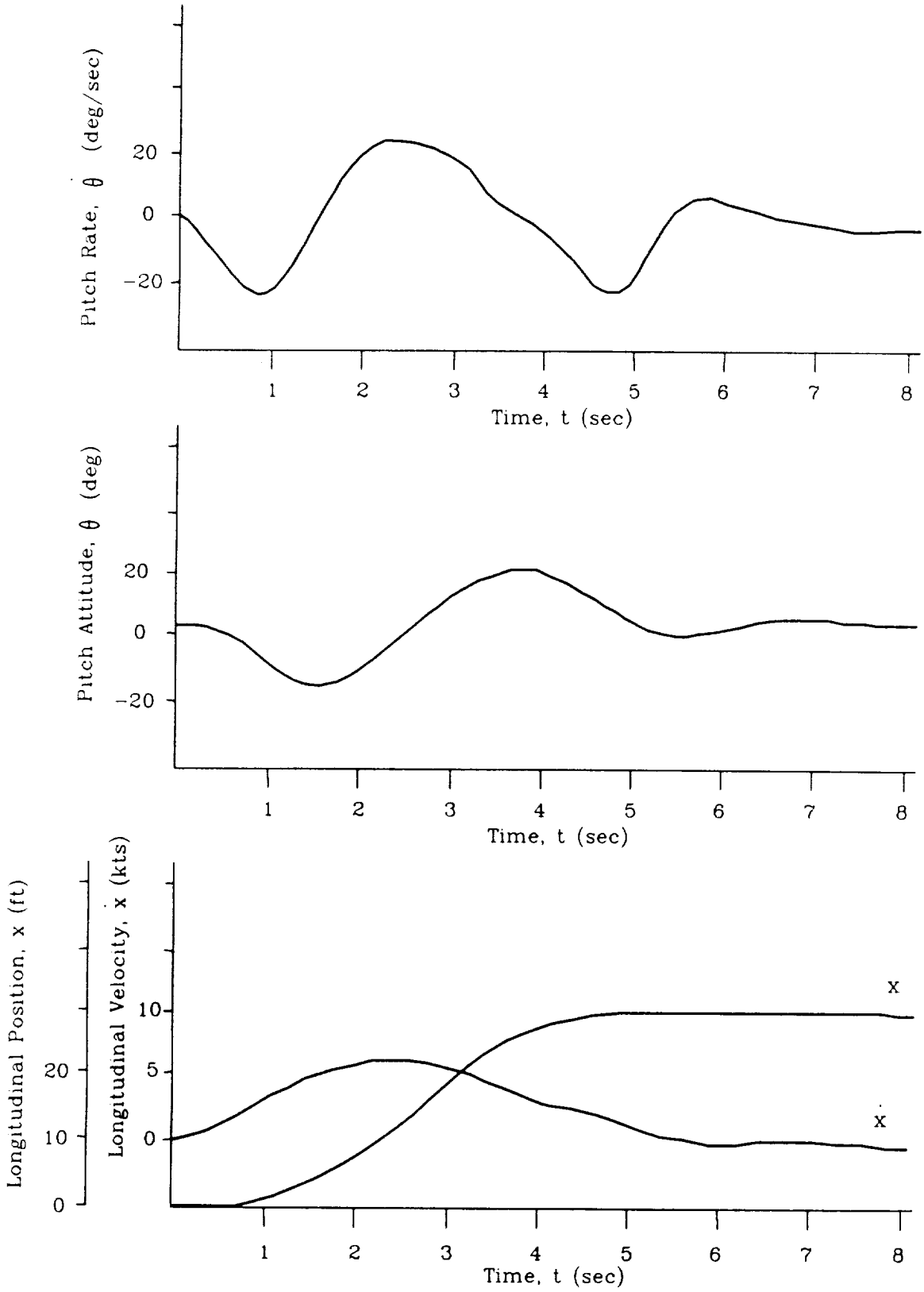

Figure 42. Longitudinal Position Change of 25 ft from Hover Using the Constrained Time Optimal Control Scheme

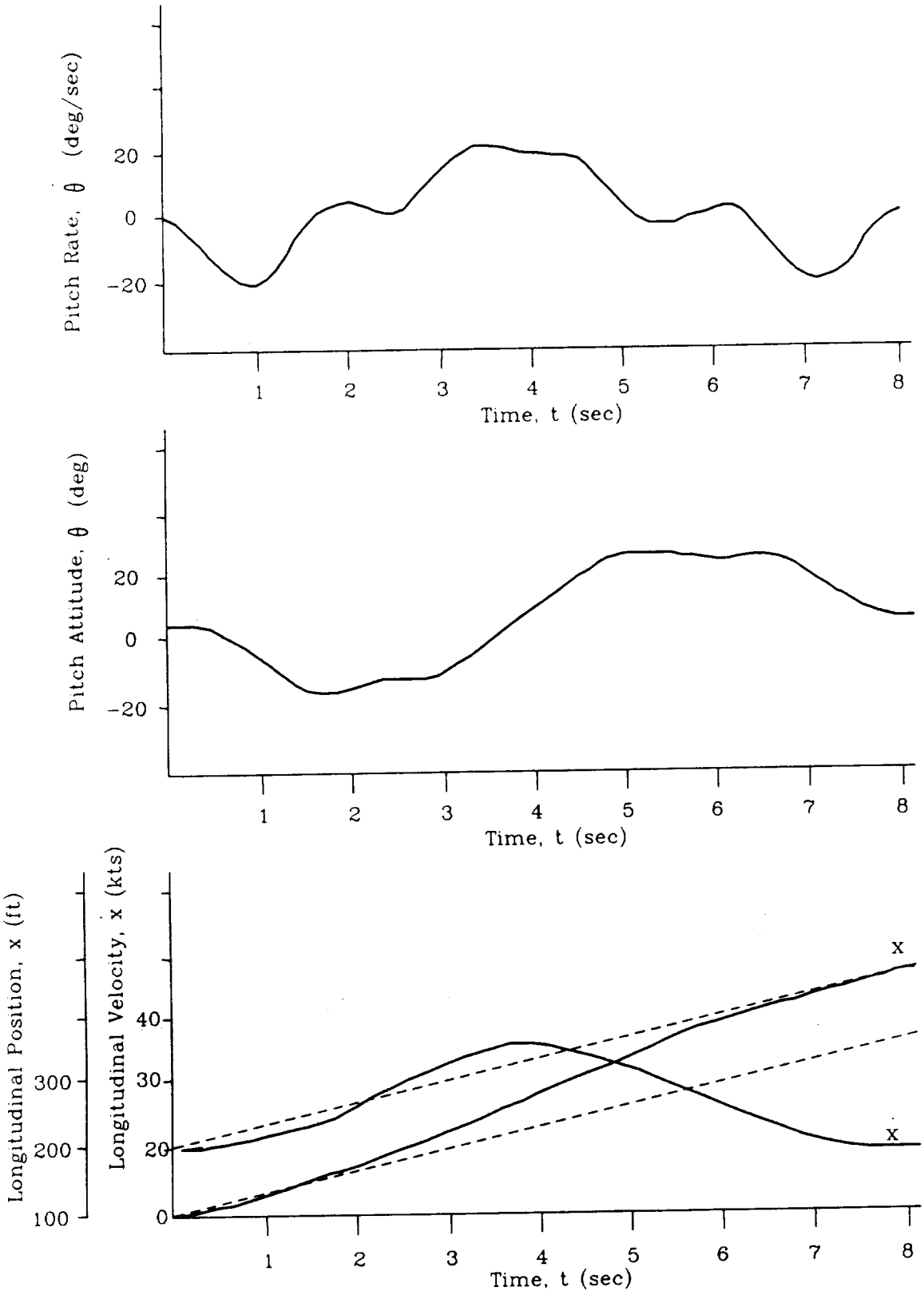

Figure 43. Longitudinal Position Change of 100 ft at 20 kts Using the Constrained Time Optimal Control Scheme

REFERENCES

1. Anon., Development of Fully Automated Guidance for Rotorcraft Nap-of-the-Earth Flight, NASA Contract NAS2-12640, September 3, 1987.

2. Clement, Warren F., Fully Automatic Guidance for Rotorcraft Nap-of-the-Earth Flight, Phase II, Systems Technology, Inc., TP-637, 1987.

3. Ferguson, Samuel W., Warren F. Clement, William B. Cleveland, and David L. Key, "Assessment of Simulation Fidelity Using Measurements of Piloting Technique in Flight," Systems Technology, Inc., Paper No. 347, Presented at the 40th Annual Forum of the American Helicopter Society, Arlington, Virginia, May 1984.

4. Clement, Warren F., William B. Cleveland, and David L. Key, "Assessment of Simulation Fidelity Using Measurements of Piloting Technique in Flight," Systems Technology, Inc., Paper No. 348, Presented at the AGARD Guidance and Control Panel 38th Symposium, Helicopter Guidance and Control Systems for Battlefield Support, Monterey, California, May 1984.

5. Ferguson, Samuel W., Warren F. Clement, Roger H. Hoh, and William B. Cleveland, "Assessment of Simulation Fidelity Using Measurements of Piloting Technique in Flight--Part II," Systems Technology, Inc., Paper No. P-371, Presented at the 41st Annual Forum of the American Helicopter Society, Ft. Worth, Texas, May 1985.

6. Telephone conversation between Donald Caldwell, McDonnell Douglas Helicopter Co., Inc., and Warren Clement, Systems Technology, Inc., November 12, 1987.

7. Jewell, Wayne F., IBM PC Version of the Evasive Maneuver Criteria Evaluation Program, Systems Technology, Inc., Technical Report No. 1230-5, October 1987.

APPENDIX A

Piloted Vertical acceleration rate limits derived from UH-60A Flt tests in Bob-Ups where $Z_{\delta_c} = \frac{-5 \text{ ft/sec}^2}{.8 \text{ in}}$ from step resp.

$Z_{\delta_c} = -0.572 \frac{\text{ft/sec}^2}{\text{percent}}$ from freq. resp.

[10 in δ_c = 100 percent

Use $Z_{\delta_c} = -0.6 \frac{\text{ft/sec}^2}{\text{percent}}$

BU16GW $\dot{\delta}_{c_{max}}$ = −50 percent / 2.8 sec and +50 percent / 3.2 sec; $\Delta(SHPT)_{max}$ = +600 / −650

$Z_{\delta_c}(\dot{\delta}_c)_{max}$ = 10.7 and −9.9 ft/sec³

BU17GW $\dot{\delta}_{c_{max}}$ = −50 percent / 2.0 sec; $\Delta(SHPT)_{max}$ = +550 / −700

$Z_{\delta_c}(\dot{\delta}_c)_{max}$ = 15 ft/sec³

BU18GW $\dot{\delta}_{c_{max}}$ = −50 percent / 2.5 sec and +50 percent / 2.2 sec; $\Delta(SHPT)_{max}$ = +520 / −550

$Z_{\delta_c}(\dot{\delta}_c)_{max}$ = 12 and −13.6 ft/sec³

BU17CA $\dot{\delta}_{c_{max}}$ = −50 percent / 1.5 sec and +50 percent / 1.8 sec; $\Delta(SHPT)_{max}$ = +800 / −500

$Z_{\delta_c}(\dot{\delta}_c)_{max}$ = 20 and −16.7 ft/sec³

" (bob-down) = −50 percent / 1.7 sec and +50 percent / 2.2 sec; $\Delta(SHPT)_{max}$ = −550 / +500

$Z_{\delta_c}(\dot{\delta}_c)_{max}$ = 17.6 and −13.6 ft/sec³

BU18CA $\dot{\delta}_{c_{max}}$ = −50 percent / 1.75 sec; $\Delta(SHPT)_{max}$ = +500 / −850

$Z_{\delta_c}(\dot{\delta}_c)_{max}$ = 17.1 ft/sec³

" (bob-down) $\dot{\delta}_{c_{max}}$ = −50 percent / 2.0 sec and +50 percent / 1.9 sec; $\Delta(SHPT)_{max}$ = −800 / +500

$Z_{\delta_c}(\dot{\delta}_c)_{max}$ = 15 and −15.7 ft/sec³

* BU19CA $\dot{\delta}_{c_{max}}$ = −50 percent / 1.0 sec and +50 percent / 1.2 sec and +50 percent / 1.5 sec; $\Delta(SHPT)_{max}$ = +980 / −640

$Z_{\delta_c}(\dot{\delta}_c)_{max}$ = 30 and −25 ft/sec³ − 20 ft/sec³

BU16DU $\dot{\delta}_{c_{max}}$ = −50 percent / 8.8 sec and +50 percent / 8.1 sec and +50 percent / 10.0 sec; $\Delta(SHPT)_{max}$ = +400 / −100

$Z_{\delta_c}(\dot{\delta}_c)_{max}$ = 3.41 and −3.70 and −3.0 ft/sec³

" (bob-down) = −50 percent / 12.0 sec; $\Delta(SHPT)_{max}$ = −200 / +100

$Z_{\delta_c}(\dot{\delta}_c)_{max}$ = 2.50 ft/sec³

BU17DU $\dot{\delta}_{c_{max}}$ = −50 percent / 7.2 sec and +50 percent / 7.1 sec; $\Delta(SHPT)_{max}$ = +460 / −250

$Z_{\delta_c}(\dot{\delta}_c)_{max}$ = 4.17 and −4.22 ft/sec³

BU18DU $\dot{\delta}_{c_{max}}$ = −50 percent / 3.5 sec and +50 percent / 13.0 sec; $\Delta(SHPT)_{max}$ = +450 / −350

$Z_{\delta_c}(\dot{\delta}_c)_{max}$ = 8.44 and −2.31 ft/sec³

( ) * BU19CA (bob-down) $\dot{\delta}_{c_{max}}$ = −50 percent / 2.0 sec and +50 percent / 2.5 sec; $\Delta(SHPT)_{max}$ = −650 / +550

$Z_{\delta_c}(\dot{\delta}_c)_{max}$ = 15 and −12 ft/sec³

14 Jan 88

Flight Test Measures of $\dddot{h}_{max}$, $\ddot{h}_{max}$, $\dot{h}_{max}$, and $SHPT_{max}$ in Bob-Ups with UH-60A

$Z_{\delta_c} = -0.6 \frac{ft/sec^2}{percent}$

Run No	Pilot	$\dddot{h}_{max}$ (ft/sec^3)	$\lvert\ddot{h}_{max}\rvert$ (ft/sec^2)	$\dot{h}_{max}$ (ft/sec)	$\Delta(SHPT)_{max}$ (HP)
BU 16	GW	+9.4 -10.7	7.2	16.7	+600 -650
BU 17	GW	+? -15.	7.2	17.	+550 -700
BU 18	GW	+13.6 -12.	7.2	15.	+520 -530
BU17	CA	+16.7 -20	6.0	15.	+800 -500
" (bob-down)	"	-17.6 +13.6	6.0	-11.	-550 +500
BU 18	CA	+? -17.1	6.0	18.	+500 -850
" (bob-down)	"	-15 +15.7	7.5	-12.5	-800 +500
BU 19	CA	+25. -30.	7.2	15.	+980 -640
" (bob-down)	"	-15. +12.	6.0	-12.5	-650 +550
BU 16	DU	+3.70 -3.41	1.95	8.	+400 -100
" (bob-down)	"	-2.50 +?	1.5	-6.5	-200 +100
BU17	DU	+4.22 -4.17	2.4	8.	+440 -250
BU18	DU	+2.31 -3.44	3.0	10.	+450 -250

APPENDIX B

PILOTED VEHICLE YAW RATE AND ACCELERATION LIMITS DERIVED FROM UH-60A FLIGHT TESTS IN HOVER TURNS

From Fig. 26 of Ref 3:

$\psi_{max} \sim 40$ deg/sec

From Flight HT2GW

$\psi_{max} \sim 50$ deg/sec

$\dot{\psi}_{max} \sim 40$ deg/sec^2

APPENDIX C

WORKING PAPER NO. 1254-5

AUTOMATIC GUIDANCE ALGORITHMS FOR PURSUIT TRACKING FOR AUTOMATICALLY GUIDED ROTORCRAFT NAP-OF-THE-EARTH FLIGHT FOLLOWING PLANNED FLIGHT PROFILES

AUTOMATIC GUIDANCE ALGORITHMS FOR PURSUIT TRACKING FOR AUTOMATICALLY GUIDED ROTORCRAFT NAP-OF-THE-EARTH FLIGHT FOLLOWING PLANNED FLIGHT PROFILES

A. INTRODUCTION

Extraordinary precision in following guidance commands is required in nap-of-the-earth (NOE) flight. This is dictated chiefly by two considerations:

- The risk of becoming lost because the pattern of the sensed microtexture may not be represented in the stored data base
- The risk of damaging rotors, fuselage, empennage, and undercarriage in NOE operations

In order to attain this level of precision, it is necessary to include pursuit feedforward guidance commands in the anticipative trajectory coupler. The pursuit feedforward guidance algorithms are contained in the box labelled "Y_p" in Fig. 1.

This pursuit guidance requires the (anticipated) acceleration, velocity, and displacement of the commanded courses and profiles, Relatively noise-free acceleration and velocity commands are derived from the data base containing continuous, or piece-wise continuous, equations for the courses and profiles. Thus, the chief sources of noisy acceleration and velocity are contributed by the inherent properties of the navigation errors and the unexpected sensed obstacles that require modification of the stored courses and profiles (Refs. 1 and 2).

Pursuit feedforward guidance will enhance pilot acceptance of automatic NOE, because the pursuit technique is the same as that employed by the pilot in manual curved course-and-profile guidance under visual meteorological conditions (VMC) if sufficient preview is available. Simulation experiments involving human operators have examined varying preview distances in the external visual field in the context of vehicular guidance along curved courses (Ref. 3) to determine conditions that promote pursuit

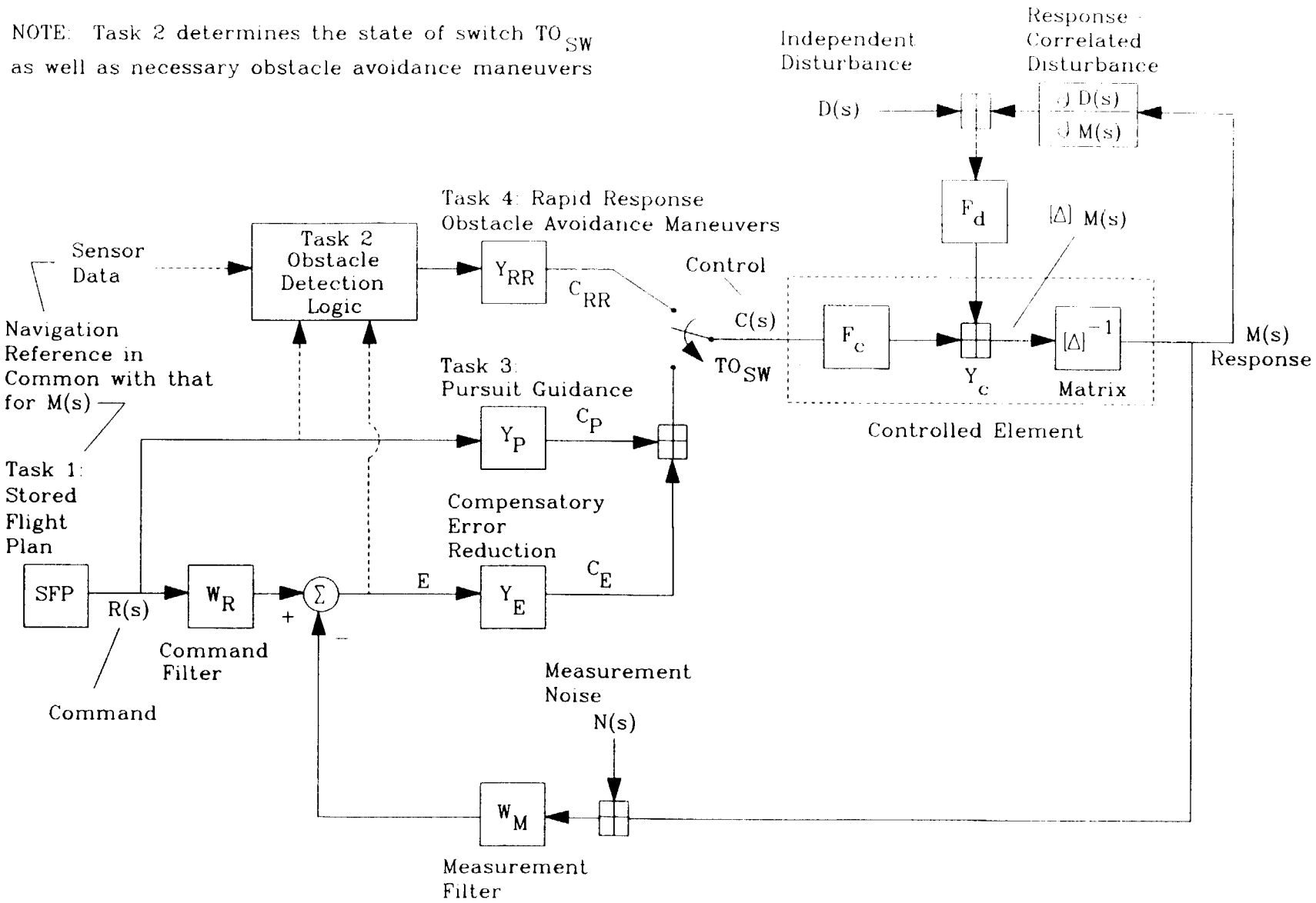

Figure 1. Vector Block Diagram for Multiloop Guidance and Control System

guidance. The results have shown that an experienced human operator will adopt a pursuit feedforward guidance command input when sufficient preview of course curvature is available with consequent reduction in curved course-following error. Pursuit feedforward guidance therefore provides a well-defined and validated form of guidance for corresponding manually and automatically controlled NOE flight.

B. DESIGN OF PURSUIT GUIDANCE CONTROL

A simplified block diagram of the automatic NOE controller is depicted in Fig. 2.

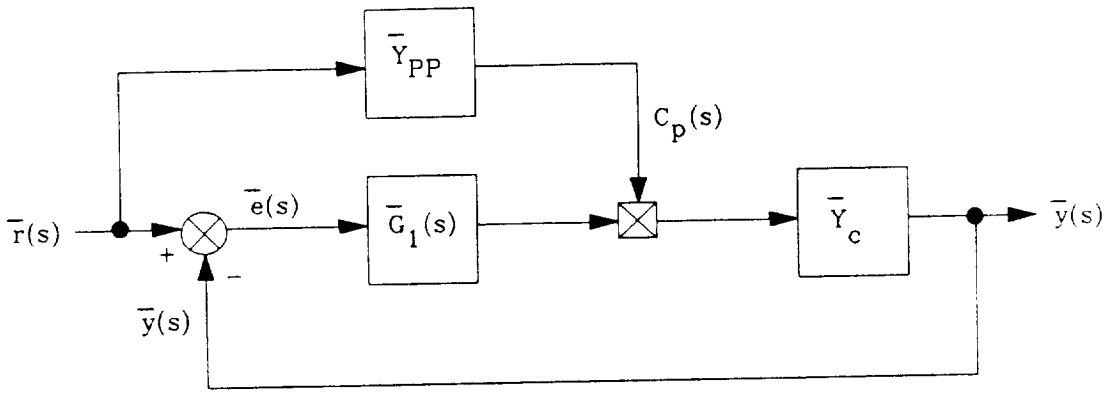

Figure 2. Simplified Block Diagram of the Automatic NOE Controller

where $\bar{G}_1(s)$ represents the compensatory control matrix
$\bar{Y}_{PP}$ represents the feedforward pursuit guidance control matrix
$\bar{Y}_c(s)$ represents the controlled element matrix.

In a decoupled system, these matrices are all diagonal, and the system equations simplify to four independent equations, one each for the heave, sway, surge, and yaw axes. The following derivation will be using scalar quantities and could represent any of the four axes.

The system error, e(s), can be written as follows:

$$e(s) = r(s) - y(s) = r(s) - [e(s)G(s) + r(s)Y_{PP}(s)]Y_c(s)$$

$$\frac{e(s)}{r(s)} = \frac{1 - Y_{PP}Y_c(s)}{1 + G(s)} \tag{1}$$

In order to minimize this error regardless of r(s),

$$1 - Y_{PP}Y_c(s) \to 0$$

or, ideally,

$$Y_{PP}Y_c(s) = 1 \tag{2}$$

Using the McDonnell Douglas Helicopter Co., Inc., (MDHC) velocity command system (Ref. 4), the equation for $Y_c(s)$ in all axes is

$$Y_c(s) = \frac{K_c}{s(s + 1/\tau_c)}$$

where $K_c = 1/\tau_c$, and τ_c represents the augmented heave damping (z axis), swaying damping (y axis), surge damping (x axis), and yaw damping. This requires a Y_{PP} of the form

$$Y_{PP}(s) = \frac{1}{K_c}s(s + 1/\tau_c) \tag{3}$$

in order to satisfy Eqn. 2, or

$$C_p(s) = r(s)Y_{PP}(s) = \frac{1}{K_c}s(s + 1/\tau_c)r(s) \tag{4}$$

In the time domain,

$$C_p(t) = \frac{1}{K_c}[\dot{r}(s) + 1/\tau_c r(s)]$$

With the inclusion, therefore, of the higher order derivatives of the input, r(s), it is ideally possible to negate the error entirely and cause y(s) to follow r(s) exactly.

C. VERTICAL AXIS--TERRAIN FOLLOWING

In NOE operations, it is desirable to maintain a minimum height above the ground throughout changing ground elevations. The course elevation profile, therefore, is

$$h_c = h_{min} + h_E(x,y)$$

where h_c is the commanded altitude

h_{min} is a constant depicting the desired altitude above the ground

$h_E(x,y)$ is the elevation of the terrain at point (x,y)

The required weighted linear combination of predicted commanded acceleration and velocity (Eqn. 4) can be readily derived with a low noise level from the stored flight profile format discussed in Ref. 2, since continuous functions with continuous first and second derivatives are used to represent the required flight profile. The resulting equation for $h_{ref}(s)$, the input to Y_c, is

$$h_{ref}(s) = \underbrace{\left[(h_c - h)\left(1 + \frac{a_1}{s}\right) \right]}_{\substack{\text{Compensatory} \\ \text{Control, } G(s)}} + \underbrace{\left[\frac{1}{K_c}\left(s^2 h_c + \frac{1}{\tau_c} s h_c\right) \right]}_{\substack{\text{Pursuit Feedforward} \\ \text{Guidance, } Y_{pp}(s)}}$$

To gest this control scheme, a truncated sum of sinusoids was developed to simulate a typical, if not extreme, terrain profile. Based on power density spectra of sample terrain profiles presented in Ref. 5, the break frequency is approximately 0.0061 rad/(ft traversed). The sum of sines used contained three frequencies at or below the break and two frequencies above.

$$h_E = 120.57 \sum_{i=1}^{5} A_i \sin(\omega_i t) + 990 \text{ ft}$$

$$h_c = h_E + 10 \text{ ft}$$

$$\dot{h}_c = \dot{h}_E = 120.57 \sum_{i=1}^{5} A_i \omega_i \cos(\omega_i t)$$

$$\ddot{h}_c = \ddot{h}_E = -120.57 \sum_{i=1}^{5} A_i \omega_i^2 \sin(\omega_i t)$$

where $\omega_i = \Omega_i v_T$

v_T = ground track velocity

The magnitude of A_i is determined by the expression

$$|A_i| = \frac{0.0061}{\sqrt{\Omega_i^2 + 0.0061^2}}$$

The sign of A_i, as well as the values for Ω_i, were determined such that $\dot{h}_c(0) = 0$. This was done to prevent the intrusion of transients in the test runs.

i	A_i (ft)	Ω_i (rad/ft)	ω_i (v_T = 20 kts) (rad/sec)
1	-1.0	0.00131	0.0442
2	-1.0	0.00296	0.100
3	0.70	0.0061	0.206
4	0.464	0.0131	0.442
5	-.215	0.0283	0.956

The resulting test run is presented in Fig. 3.

D. LATERAL DIRECTIONAL COURSE FOLLOWING

In the plan view, the course is laid out using a series of waypoints, each having several properties associated with it: north (N) and east (E) geodetic position and longitudinal velocity. The course is defined as the straight lines connecting these sequenced waypoints. This system yields a

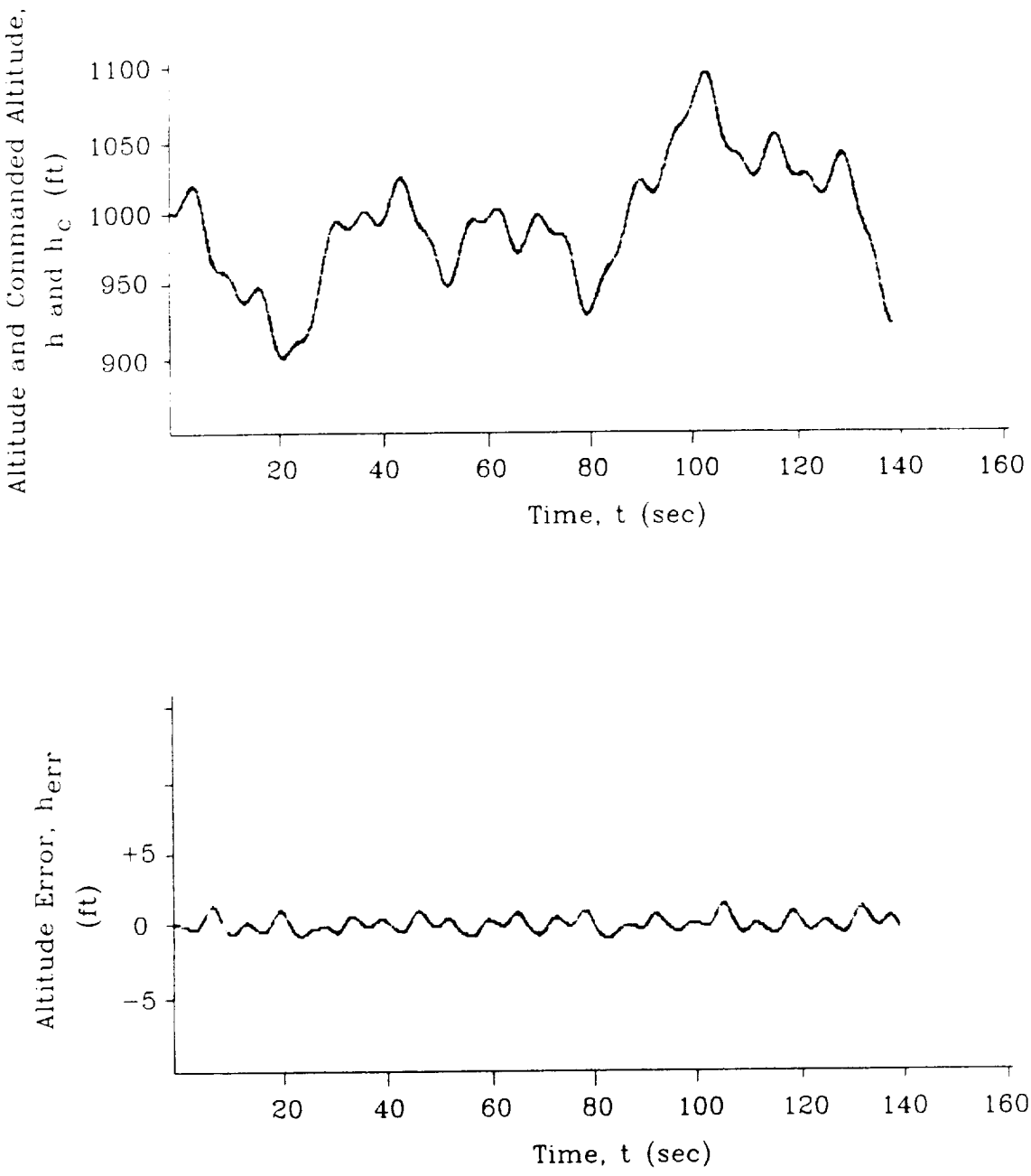

Figure 3. Terrain Following Test Run--Ground Track Velocity Equal to 20 kt

course discontinuous in both $\dot{r}$ and $\ddot{r}$ at the waypoint, and so a transition leg is required.

To be used as this transition leg, a hyperbolic section was chosen. This is because of the relatively gradual entrance and exit from the turn that a hyperbolic section provides. The validity for this choice was confirmed via a curve-fitting program. Test heading changes were conducted using maximum roll rate and attitude to constrain the response. A curve fitting program was then used to find the best conic section fit. The result was a hyperbolic section, confirming the original assumption.

The attributes of the hyperbola are determined by two quantities: (a) the maximum longitudinal velocity in the turn and (b) the desired heading change.

Assuming that the vehicle remains pointed in the direction of travel throughout the (coordinated) turn, a relationship can be made between ϕ and $\dot{\psi}$. $\dot{\psi}$ relates directly to the curvature and velocity at any point as follows:

$$\dot{\psi} = \frac{u}{r}$$

where u is the longitudinal velocity, and r is the instantaneous radius of curvature. In addition,

$$\tan(\phi) = \frac{u^2}{rg}$$

Therefore,

$$\dot{\psi} = \frac{g \tan(\phi)}{u}$$

Thus,

$$\dot{\psi}_{c_{max}} < \frac{g \tan(\phi_{max})}{u}$$

must be satisfied in order that the vehicle be able to hold to the hyperbolic course. $\dot{\psi}_{c_{max}}$ is a property of the hyperbola and is independent of the hyperbola's orientation. Thus, the generic form of the hyperbola, pictured in Fig. 4, is used to ensure satisfaction of this stipulation, and a dummy ψ is used such that

$$\psi_h = \psi_c - \frac{1}{2} \Delta \psi_c$$

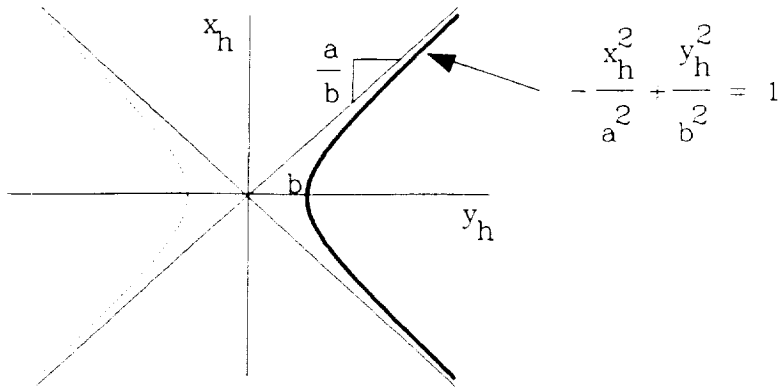

Figure 4. Hyperbolic Section Used for Transition Leg

where $\Delta\psi_c$ is the commanded change of heading through the turn. Because $\Delta\psi_c$ is a constant, $\dot{\psi}_h = \dot{\psi}_c$ and $\ddot{\psi}_h = \ddot{\psi}_c$. ψ_h represents the "heading" at any point along the generic hyperbola, therefore

$$\tan(\psi_h) = \frac{\partial y_h}{\partial x_h}$$

$$-\frac{x_h^2}{a^2} + \frac{y_h^2}{b^2} = 1 \qquad (5)$$

$$\frac{\partial y_h}{\partial x_h} = \left(\frac{b^2}{a^2}\right)\left(\frac{x_h}{y_h}\right)$$

$$\boxed{\tan \psi_h = \left(\frac{b^2}{a^2}\right)\left(\frac{x_h}{y_h}\right)} \qquad (6)$$

$$\dot{\psi}_h = \dot{\psi}_c = \frac{1}{1 + \tan^2 \psi_h}\left(\frac{d}{dt}\right)\left[\left(\frac{b^2}{a^2}\right)\left(\frac{x_h}{y_h}\right)\right] = \frac{\dot{x}_h}{1 + \tan^2 \psi_h}\left(\frac{\partial}{\partial x_h}\right)\left[\left(\frac{b^2}{a^2}\right)\left(\frac{x_h}{y_h}\right)\right]$$

$$\dot{\psi}_h = \frac{\left(\frac{b^2}{a^2} - \tan^2 \psi_h\right)\left(\frac{\dot{x}_h}{y_h}\right)}{1 + \tan^2 \psi_h} = \left(\frac{b^2}{a^2} - \tan^2 \psi_h\right) \frac{\dot{x}_h}{y_h} \cos^2 \psi_h \qquad (7)$$

Assuming the longitudinal velocity of the vehicle remains constant throughout the turn,

$$\dot{x}_h^2 + \dot{y}_h^2 = u^2$$

and

$$\frac{\dot{y}_h}{\dot{x}_h} = \tan \psi$$

therefore,

$$\dot{x}_h = u \cos \psi_h$$

$$\dot{y}_h = u \sin \psi_h$$

ψ_{max} occurs when $\psi_h = 0$, $y_h = b$, $\dot{x}_h = u$

$$\boxed{\dot{\psi}_{h_{max}} = \frac{b}{a^2} u}$$

Therefore, one equation for determining the attributes a and b for the hyperbola is

$$\frac{b}{a^2} < \frac{g \tan\left(\phi_{max}\right)}{u^2} \qquad (8)$$

The other equation has to do with the amount of heading change desired. The maximum heading change is less than 2(b/a) for a given hyperbola.

Thus,

$$\tan^{-1}\left(\frac{b}{a}\right) > \frac{1}{2}\,\Delta\psi_c$$

The general relationship was taken to be

$$\tan^{-1}\left(\frac{b}{a}\right) = \frac{1}{2}\,\Delta\psi_c + K_\psi \tag{9}$$

Because

$$\psi_h < \tan^{-1}\left(\frac{b}{a}\right) < \frac{\pi}{2}$$

$\dot{\psi}$ only reaches zero in the limit; therefore, there is always some degree of curvature and thus some required roll attitude to hold to the hyperbolic course. The compromise with K_ψ is between the arc-length of the transition leg and the entrance and exit course curvature. Smaller K_ψ yields a longer arc-length, since the point at which the hyperbola attains the desired heading is farther out along the asymptotes. Smaller K_ψ also have the desirable effect of decreasing the curvature at entrance and exit from the transition leg. In the limit, with $K_\psi = 0$, the arc-length would be infinite, and the entrance and exit curvature would be zero. The effect of K_ψ can be seen in the following equations. (Subscripts "i" and "o" indicate entrance to and exit from the hyperbolic transition leg, respectively.)

$$\psi_{h_i} = -\frac{1}{2}\,\Delta\psi_c = -\tan^{-1}\left(\frac{b}{a}\right) + K_\psi$$

$$y_{h_i} = \frac{b^2/a^2}{\sqrt{\frac{b^2}{a^2} - \tan^2\left[\tan^{-1}\left(\frac{b}{a}\right) - K_\psi\right]}} \qquad \text{(from Eqns. 5 and 6)}$$

$$\dot{\psi}_{h_i} = \left\{\frac{b^2}{a^2} - \tan^2\left[\tan^{-1}\left(\frac{b}{a}\right) - K_\psi\right]\right\}^{3/2} \frac{a^2}{b^2}\, u \cos^3\left[\tan^{-1}\left(\frac{b}{a}\right) - K_\psi\right]$$

(from Eqn. 7)

The arc-length of the hyperbolic transition leg is related to y_{h_i} in that

$$ds = \sqrt{dx_h^2 + dy_h^2}$$

and

$$y_{h_o} = y_{h_i}$$

$$x_{h_o} = -x_{h_i}$$

$$s = 2 \int_b^{y_o} \sqrt{\frac{(a^2 + b^2)\, y_h^2 - b^4}{b^2\,(y_h^2 - b^2)}}\; dy_h$$

K_ψ = 5 deg seemed to be a reasonable choice for a wide range of $\Delta\psi_c$'s. Using Eqns. 8 and 9 and given u and ϕ_{max}, it is possible to determine the attributes of the hyperbola to be used as the transition leg.

The next step is the determination of the derivatives of the course throughout the transition. To facilitate this step, the derivatives are calculated in the hyperbola's coordinate system and then are transformed into the heading referenced axis system.

These course derivatives are calculated in real time for use in the pursuit feedforward guidance algorithm. To calculate the commanded course (x_h)--the hyperbola coordinate system x-coordinate that varies from $-x_{h_o}$ to x_{h_o} through the transition leg--is incremented using u and ψ_h.

$$x_{h_{k+1}} = x_{h_k} + u \cos\left(\psi_{h_k}\right) \Delta t \tag{10}$$

From this, $y_{h_{k+1}}$ and $\psi_{h_{k+1}}$ are calculated

$$y_{h_{k+1}} = b \sqrt{1 + \frac{x_{h_{k+1}}^2}{a^2}} \tag{11}$$

$$\psi_{h_{k+1}} = \tan^{-1}\left[\left(\frac{b^2}{a^2}\right)\left(\frac{x_{h_{k+1}}}{y_{h_{k+1}}}\right)\right] \tag{12}$$

All of the necessary derivatives can also be calculated given $x_{h_{k+1}}$, a, and b. In the following expressions, each variable can be assumed to have a k+1 subscript. The subscript has been omitted to simplify the expressions. Partial derivatives with respect to x:

$$\frac{\partial y_h}{\partial x_h} = \left(\frac{b^2}{a^2}\right)\left(\frac{x_h}{y_h}\right) \tag{13}$$

$$\frac{\partial^2 y_h}{\partial x_h^2} = \frac{\left(\frac{b^2}{a^2}\right) - \left(\frac{\partial y_h}{\partial x_h}\right)^2}{y_h} \tag{14}$$

$$\frac{\partial^3 y_h}{\partial x_h^3} = \frac{-3\left(\frac{\partial^2 y_h}{\partial x_h^2}\right)\left(\frac{\partial y_h}{\partial x_h}\right)}{y_h} \tag{15}$$

$$\dot{x}_h = u \cos \psi_h \tag{16}$$

$$\dot{y}_h = u \sin \psi_h \tag{17}$$

$$\ddot{y}_h = \left(\frac{d}{dt}\right)(\dot{y}_h) = \left(\frac{d}{dt}\right)\left[\left(\frac{\partial y_h}{\partial x_h}\right)\dot{x}_h\right] = \dot{x}_h\left[\left(\frac{d}{dt}\right)\left(\frac{\partial y_h}{\partial x_h}\right)\right] + (\ddot{x}_h)\left(\frac{\partial y_h}{\partial x_h}\right)$$

$$\ddot{y}_h = \dot{x}_h\left[\left(\frac{\partial^2 y_h}{\partial x_h^2}\right)(\dot{x}_h)\right] + (\ddot{x}_h)\left(\frac{\partial y_h}{\partial x_h}\right)$$

also $u^2 = \dot{x}_h^2 + \dot{y}_h^2$; therefore, $\dot{y}_h \ddot{y}_h + \dot{x}_h \ddot{x}_h = 0$

$$\ddot{y}_h = -\frac{\dot{x}_h}{\dot{y}_h}\ddot{x}_h \rightarrow \ddot{x}_h = -\frac{\partial y_h}{\partial x_h}\ddot{y}_h$$

$$\ddot{y}_h \left[1 + \left(\frac{\partial y_h}{\partial x_h}\right)^2\right] = \left(\frac{\partial^2 y_h}{\partial x_h^2}\right)(\dot{x}_h^2)$$

$$y = \frac{\left(\frac{\partial^2 y_h}{\partial x_h^2}\right)(\dot{x}_h^2)}{1 + \left(\frac{\partial y_h}{\partial x_h}\right)^2} \tag{18}$$

$$\ddot{x}_h = -\left(\frac{\partial y_h}{\partial x_h}\right)\ddot{y}_h = \frac{-\left(\frac{\partial^2 y_h}{\partial x_h^2}\right)(\dot{x}_h^2)\left(\frac{\partial y_h}{\partial x_h}\right)}{1 + \left(\frac{\partial y_h}{\partial x_h}\right)^2} = \frac{-\left(\frac{\partial^2 y_h}{\partial x_h^2}\right)(\dot{x}_h)(\dot{y}_h)}{1 + \left(\frac{\partial y_h}{\partial x_h}\right)^2} \tag{19}$$

$$\frac{d}{dt}\left(\frac{\partial y_h}{\partial x_h}\right) = \frac{d}{dt}\left(\tan \psi_h\right)$$

$$\frac{\partial^2 y_h}{\partial x_h^2}\dot{x}_h = \dot{\psi}_h\left(1 + \tan^2 \psi_h\right) = \dot{\psi}_h\left[1 + \left(\frac{\partial y_h}{\partial x_h}\right)^2\right]$$

$$\dot{\psi}_h = \frac{\left(\frac{\partial^2 y_h}{\partial x_h^2}\right)(\dot{x}_h)}{1 + \left(\frac{\partial y_h}{\partial x_h}\right)^2} \tag{20}$$

$$\ddot{\psi}_h = \left(\frac{d}{dt}\right)\left[\frac{\left(\frac{\partial^2 y_h}{\partial x_h^2}\right)\left(\dot{x}_h\right)}{1 + \left(\frac{\partial y_h}{\partial x_h}\right)^2}\right] = \frac{\left(\frac{\partial^3 y_h}{\partial x_h^3}\right)\left(\dot{x}_h^2\right) + 3\left(\frac{\partial^2 y_h}{\partial x_h^3}\right)\left(\ddot{x}_h\right)}{1 + \left(\frac{\partial y_h}{\partial x_h}\right)^2} \qquad (21)$$

Solving these twelve equations (Eqns. 10 through 21) defines the course and its derivatives in the hyperbola's coordinate system. A simple transformation is required to express these quantities in the heading reference coordinate system.

$$x_E = \left(x_h - x_{h_i}\right) \cos\left(\tfrac{1}{2}\Delta\psi_c\right) - \left(y_h - y_{h_i}\right) \sin\left(\tfrac{1}{2}\Delta\psi_c\right) + x_{WP2} - x_{E_i}$$

$$y_E = \left(x_h - x_{h_i}\right) \sin\left(\tfrac{1}{2}\Delta\psi_c\right) + \left(y_h - y_{h_i}\right) \cos\left(\tfrac{1}{2}\Delta\psi_c\right) + y_{WP2} - y_{E_i}$$

$$\dot{x}_E = \dot{x}_h \cos\left(\tfrac{1}{2}\Delta\psi_c\right) - \dot{y}_h \sin\left(\tfrac{1}{2}\Delta\psi_c\right)$$

$$\dot{y}_E = \dot{x}_h \sin\left(\tfrac{1}{2}\Delta\psi_c\right) + \dot{y}_h \cos\left(\tfrac{1}{2}\Delta\psi_c\right)$$

$$\ddot{x}_E = \ddot{x}_h \cos\left(\tfrac{1}{2}\Delta\psi_c\right) - \ddot{y}_h \sin\left(\tfrac{1}{2}\Delta\psi_c\right)$$

$$\ddot{y}_E = \ddot{x}_h \sin\left(\tfrac{1}{2}\Delta\psi_c\right) + \ddot{y}_h \cos\left(\tfrac{1}{2}\Delta\psi_c\right)$$

$$y_c = - x_E \cos\psi + y_E \sin\psi$$

$$\dot{y}_c = - \dot{x}_E \cos\psi + \dot{y}_E \sin\psi$$

$$\ddot{y}_c = - \ddot{x}_E \cos\psi + \ddot{y}_E \sin\psi$$

$$\psi_c = \psi_h + \frac{1}{2}\Delta\psi_c + \psi_i$$

$$\dot{\psi}_c = \dot{\psi}_h$$

$$\ddot{\psi}_c = \ddot{\psi}_h$$

These command signals are used in the sway and yaw axes pursuit feedforward guidance algorithms. The yaw command signals are designed to provide for a pseudo-coordinated turn at low airspeeds by keeping the nose of the vehicle pointed along the course.

As was previously stated, the initial $\dot{\psi}_c$, although small, is not identically zero; therefore, a small initial roll attitude is required to hold the course. This translates into a small initial $\ddot{y}_c$. Because the vehicle cannot attain a roll attitude instantaneously due to constraints on roll rate, an anticipatory distance is calculated through which $\ddot{y}_c$ is ramped in at a rate corresponding to the maximum roll rate. The anticipatory distance, x_{ant}, is calculated as follows:

$$x_{ant} = \frac{\ddot{y}_{c_i}}{\dddot{y}_{max}} u \quad ; \quad \dddot{y}_{max} \equiv g\,\ddot{\phi}_{max}$$

where $\ddot{y}_{c_i}$ is the initial $\ddot{y}_c$ upon entering the hyperbolic transition leg.

Figures 5 through 7 depict examples of turns using the hyperbolic transition leg. The waypoint legs are indicated by the straight dotted lines. The error, Y_{err}, is a heading-referenced distance to the course at all times (first, waypoint leg No. 1, then the hyperbolic transition leg, and finally the second waypoint leg). The 45 deg and 90 deg turns were conducted at 20 kts, while the 120 deg turn was conducted at 10 kts. One of the benefits of this form of transition compensation is that the closest distance to the waypoint can be calculated ahead of time. This distance is a function of hyperbola attributes and is thus dependent on the speed through the turn as well as total change in heading.

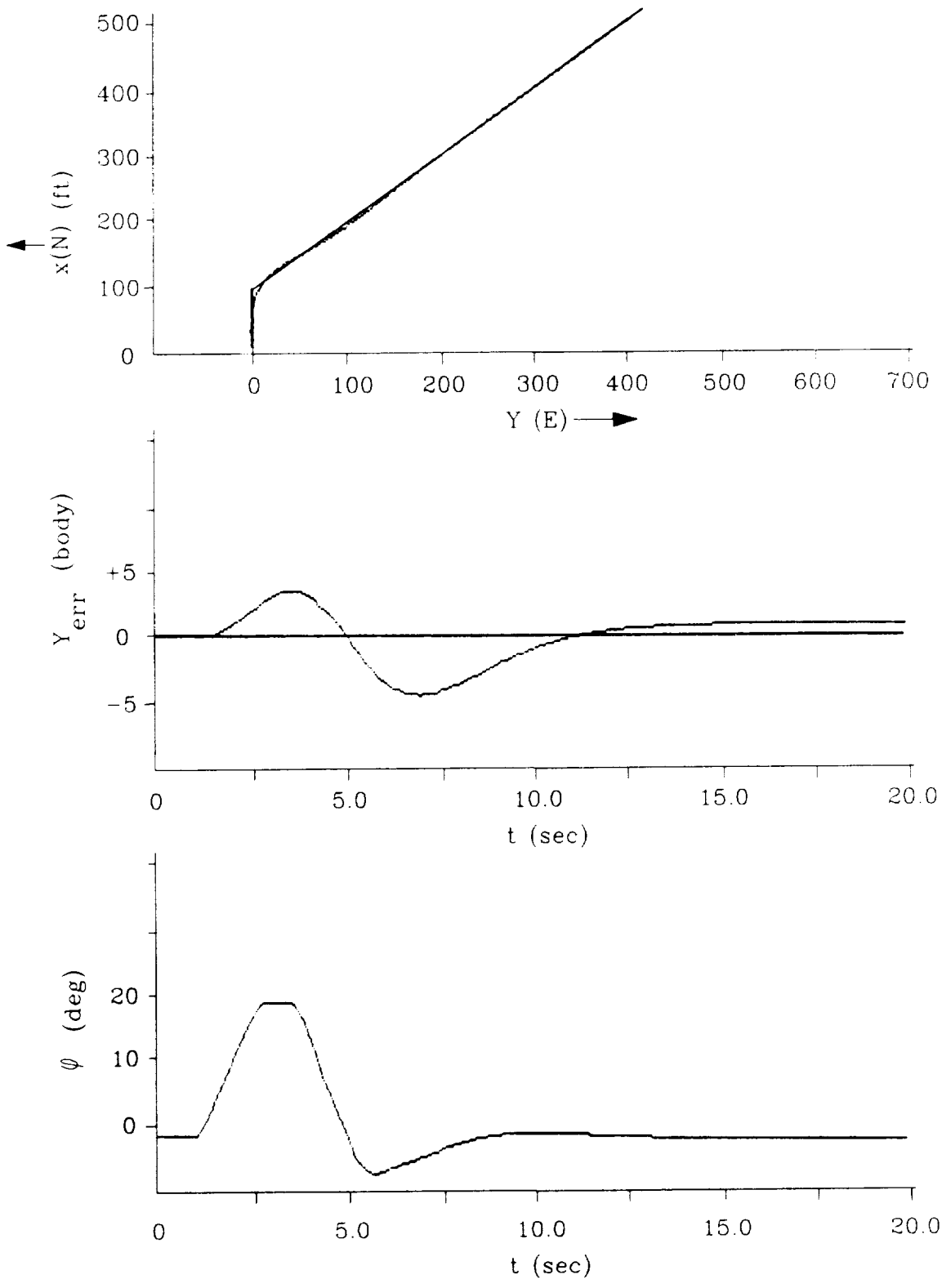

Figure 5. 45 deg Heading Change at 20 kt with No Wind

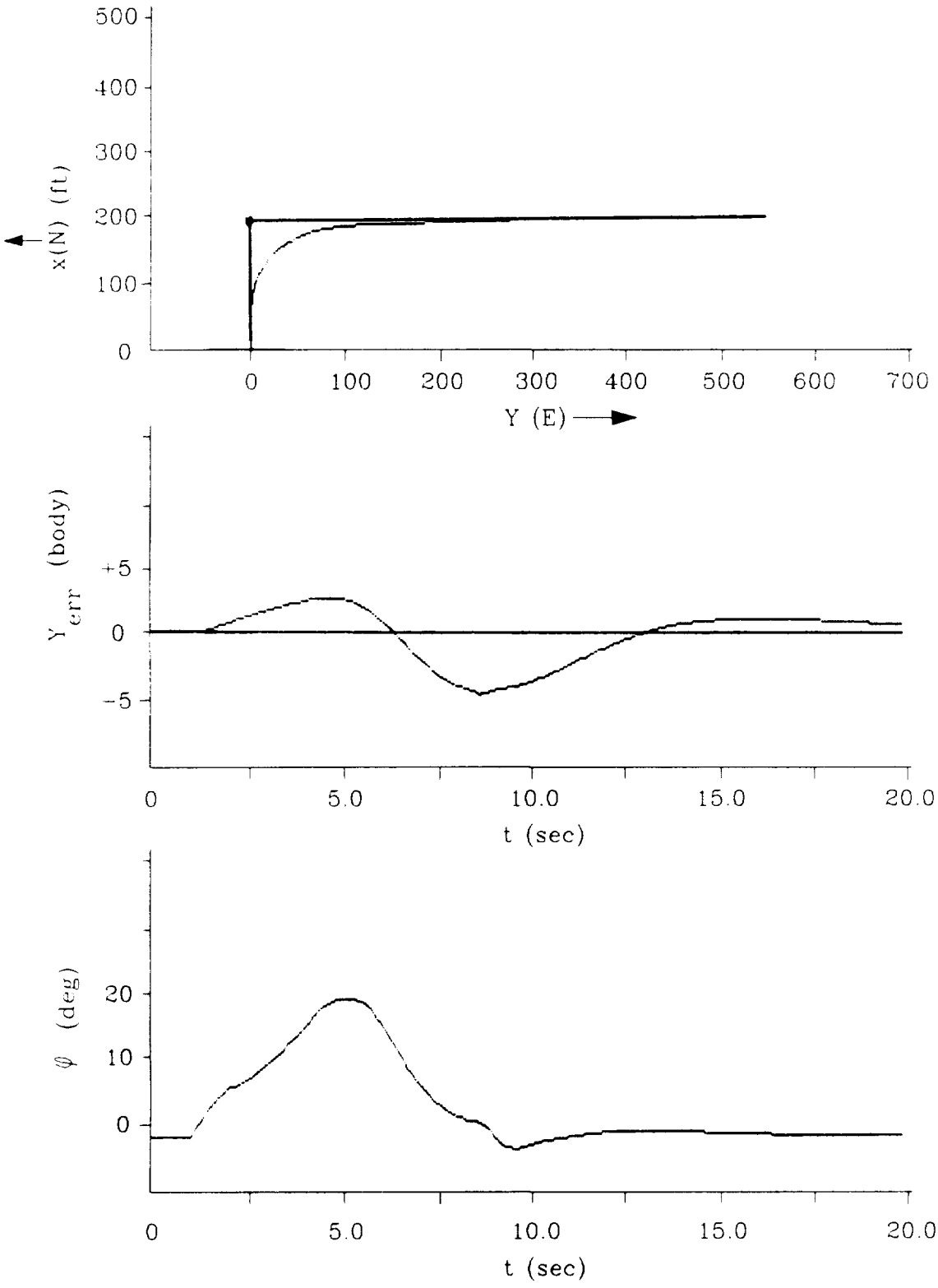

Figure 6. 90 deg Heading Change at 20 kt with No Wind

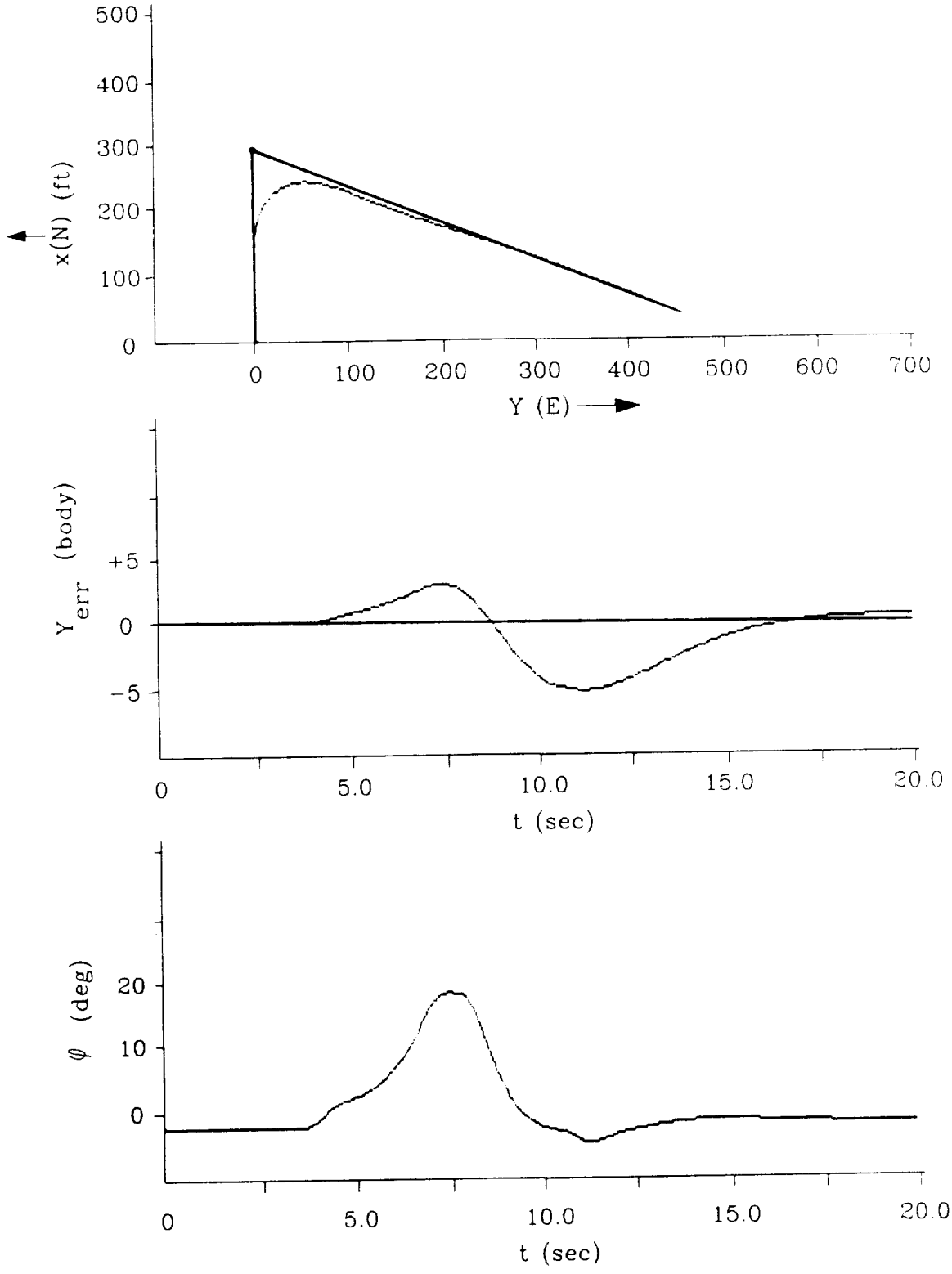

Figure 7. 120 deg Heading Change at 10 kt with No Wind

$$W_d = b - \sqrt{b^2 - a^2 \tan^2 \left(\frac{1}{2} \Delta\psi_c\right)}$$

where W_d is the distance inside the turn.

Because of this relationship, u_c can be adjusted in order that W_d not exceed some maximum value dependent upon the terrain.

E. ACCOUNTING FOR WIND SHEAR

Figures 8 and 9 show 90 deg turns in a steady wind. In the turn, the vehicle experiences a wind shear and is blown off course. The slow integrators then attempt to compensate for the change in wind conditions and bring the vehicle back on course.

To compensate for this problem, a novel technique has been employed. The compensatory control equation for roll rate command, p_c, is

$$p_c = K_p \left(1 + \frac{a_p}{s}\right)\left[\phi_c - \left(\phi - \phi_{ic}\right)\right]$$

where ϕ_{ic} is the trim condition at the start of the run. The integrator a_p/s is initialized to zero in this case. When a wind shear occurs, ϕ_{ic} is no longer the trim condition of the vehicle; therefore, an incorrect signal is being sent as p_c until the integrator spools up to compensate for this error.

The modification made to this controller consists of replacing the ϕ_{ic} with ϕ_{ss}, where ϕ_{ss} is the trim attitude at the current wind condition. This changes with the wind shear and obviates the need for the integrator to compensate for the shear. ϕ_{ss} is obtained using a trim table for the given aircraft and the current wind conditions. Even if the inserted ϕ_{ss} is not exactly equal to the trim attitude, the amount of correction required of the integrator is reduced and thus the time to trim the amount of drift is also reduced.

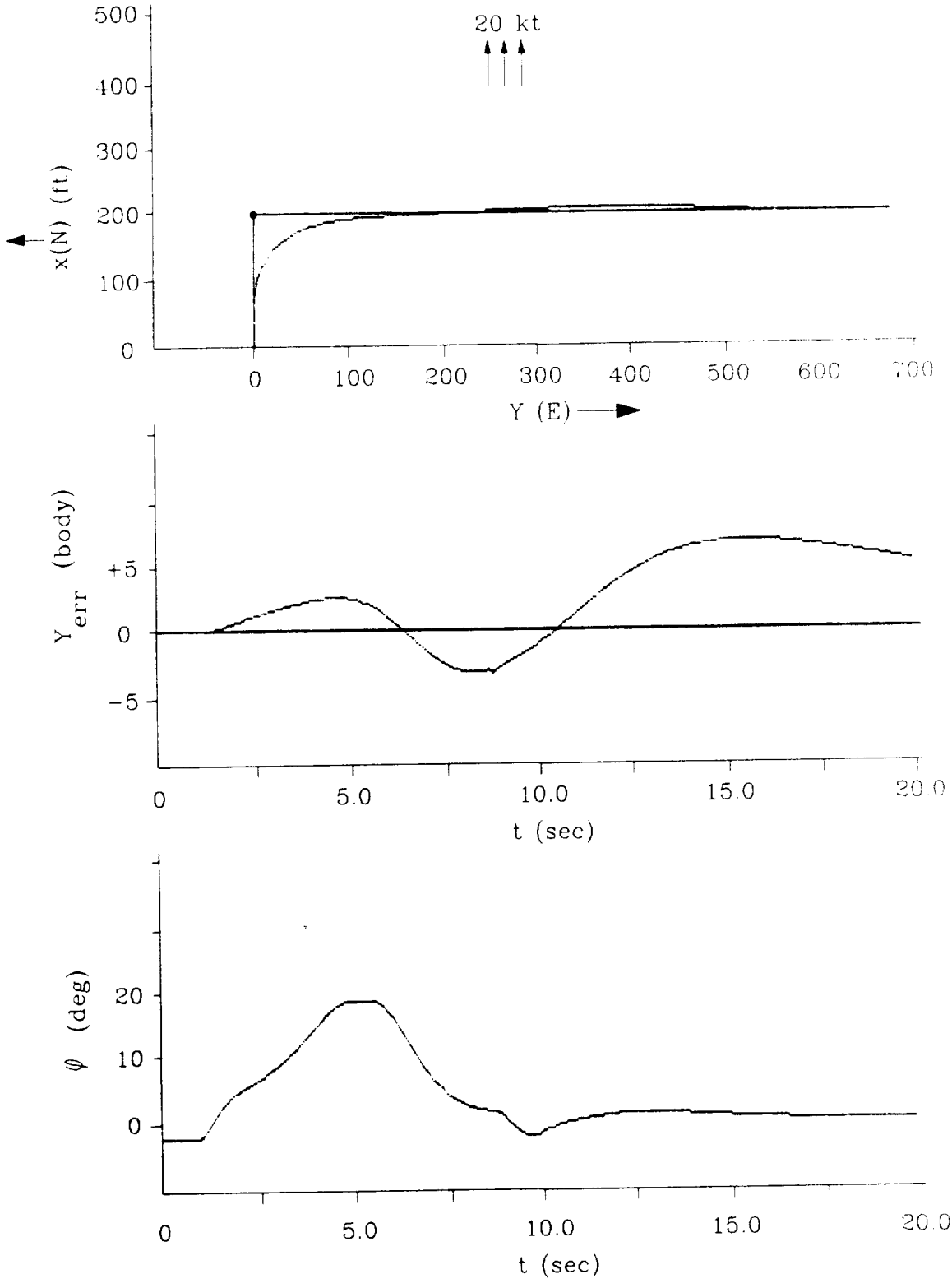

Figure 8. 90 deg Heading Change at 20 kt with 20 kt Northerly Wind

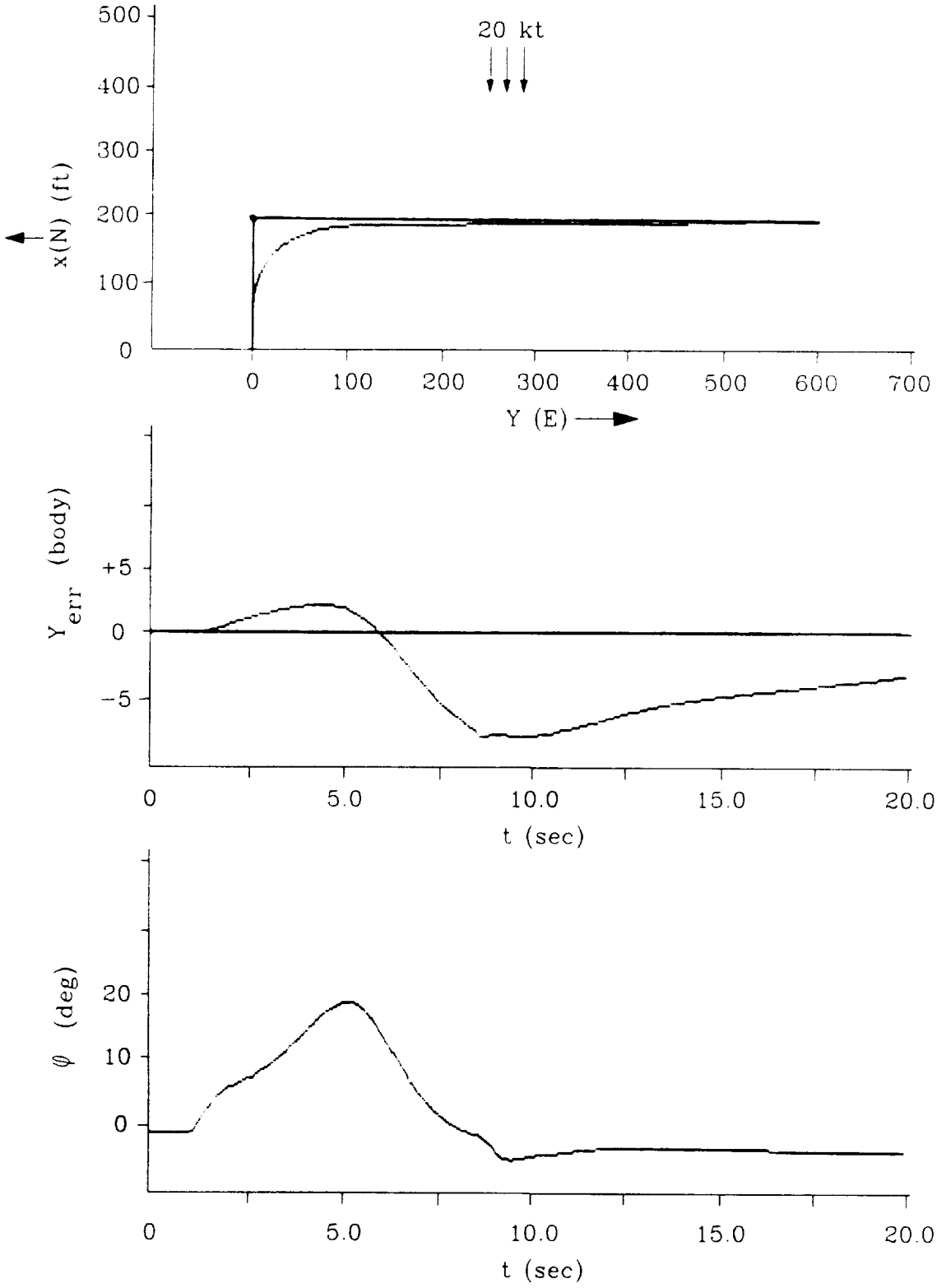

Figure 9. 90 deg Heading Change at 20 kt with 20 kt Southerly Wind

With Wind Shear Compensation

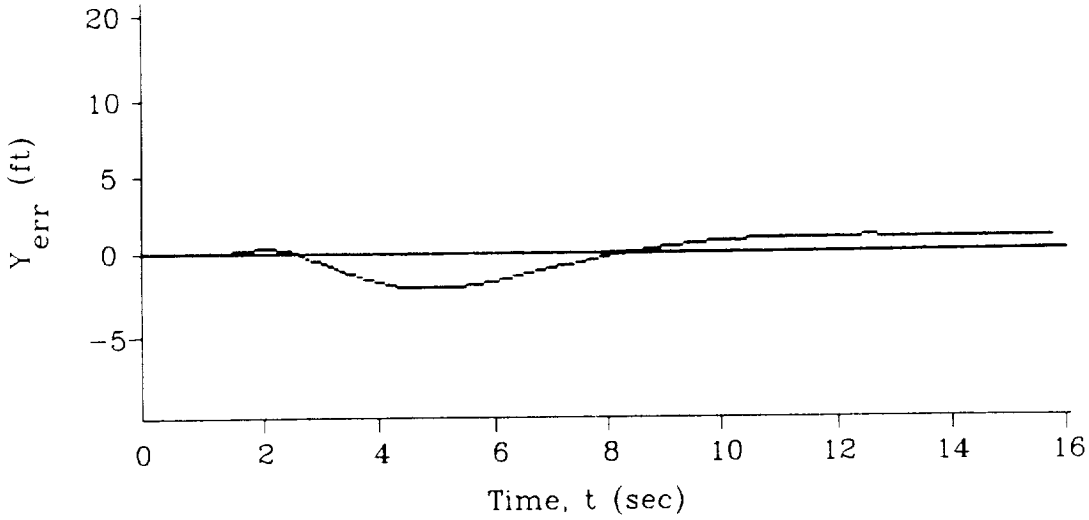

Without Wind Shear Compensation

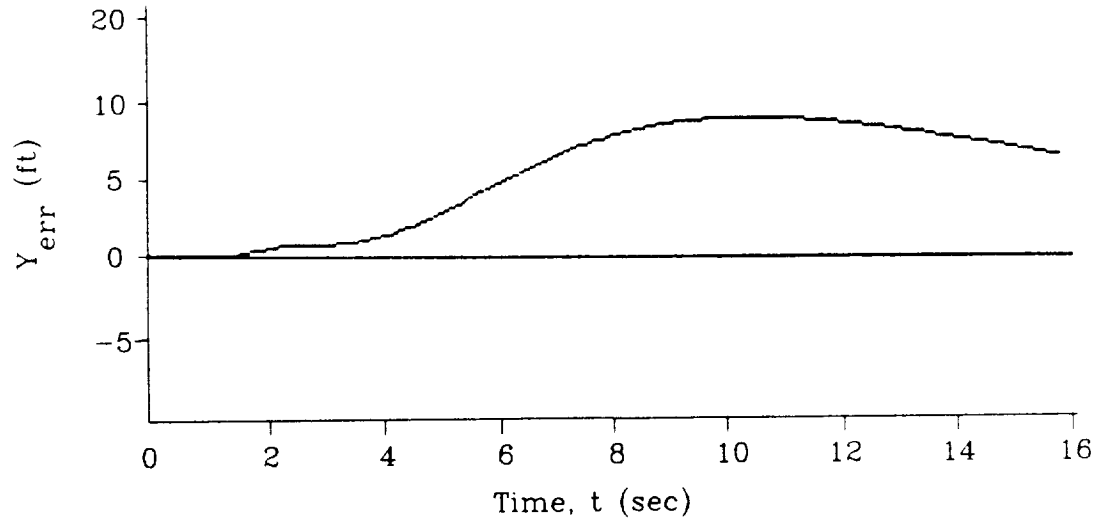

Figure 10. 20 kt Westerly to 20 kt Easterly Wind Shear Over 1 sec Beginning at Time (t) = 1 sec, With and Without Wind Shear Compensation

With Wind Shear Compensation

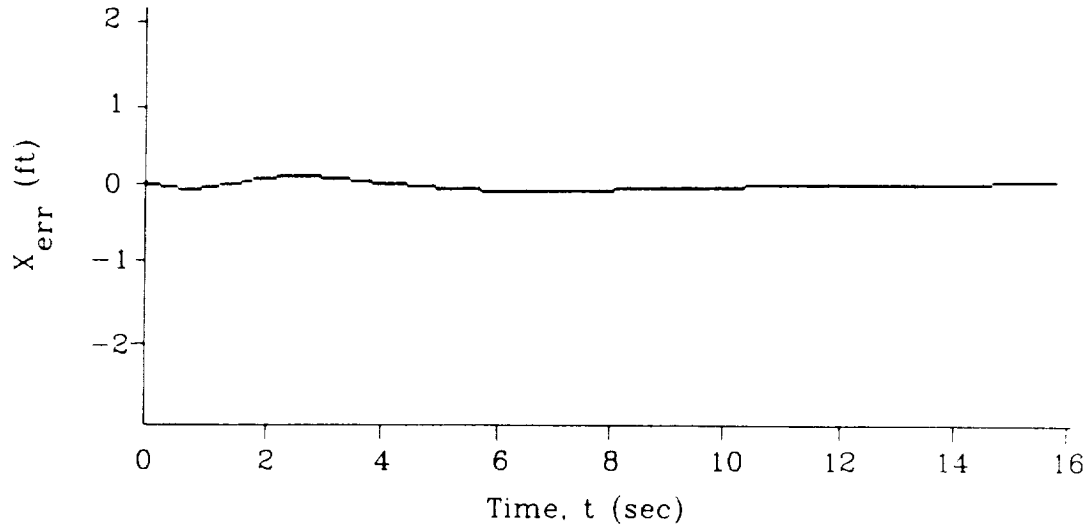

Without Wind Shear Compensation

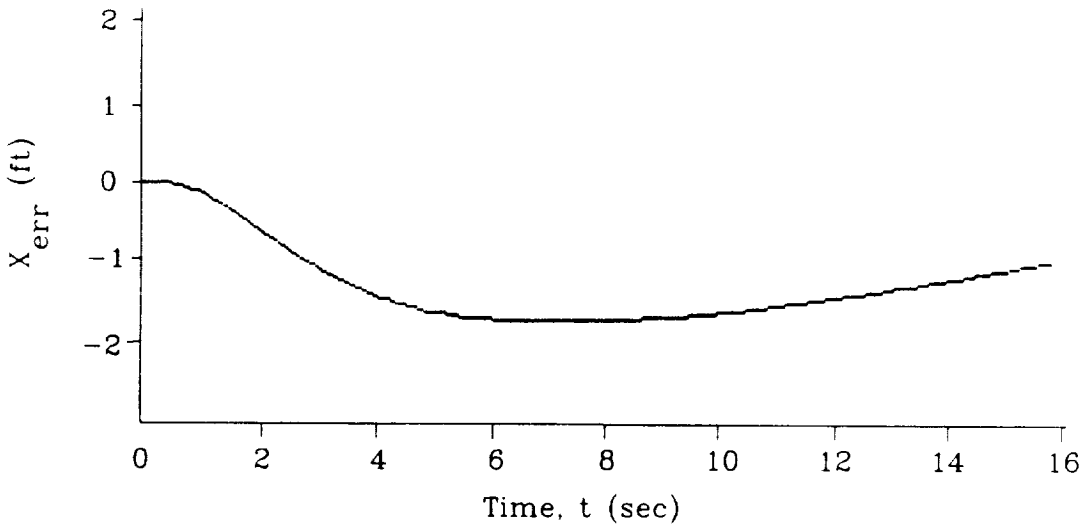

Figure 11. Longitudinal Position Error Generated by a 40 kt Easterly to 40 kt Westerly Wind Shear With and Without Wind Shear Compensation

With Wind Shear Compensation

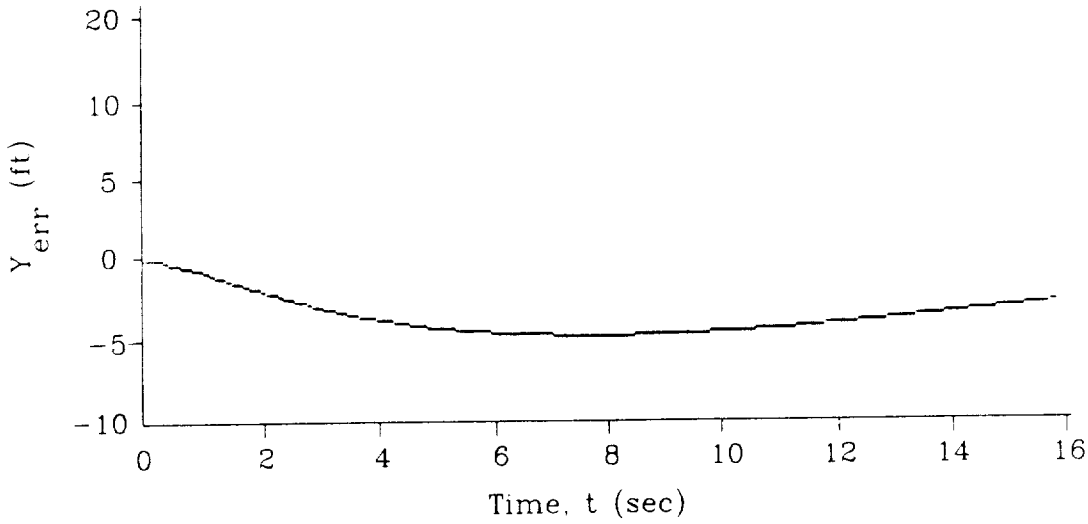

Without Wind Shear Compensation

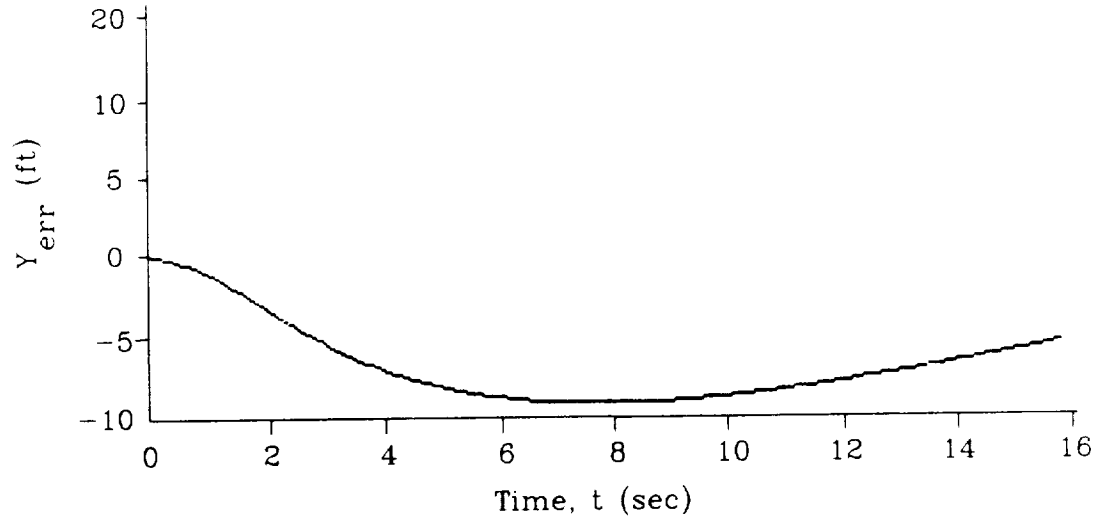

Figure 12. Lateral Position Error Generated by a 20 kt Westerly to 20 kt Easte Wind Shear, With and Without Wind Shear Compensation (ϕ_{ss} outside the trim table)

Examples of this method of wind shear compensation are presented in Figs. 10 through 12. Figures 10 and 11 are examples of this method applied to the lateral and longitudinal axes, respectively, with the trim attitudes interpolated within the trim table. Figure 12 is a case in which the roll trim attitude was determined by extrapolating beyond the trim table and is not an accurate representation of the actual trim attitude in the given wind conditions. Even so, the response of the vehicle is much improved over the unmodified vehicle.

REFERENCES

1. Clement, Warren F., Obstacle Detection and Avoidance Maneuver Selection for Automatically Guided Rotorcraft Nap-of-the-Earth Flight Following Planned Flight Profiles, STI WP-1254-4, April 1988.

2. Jewell, Wayne F., Stored Flight Profiles for the Compuscene IV Display of Automatically Guided Rotorcraft Nap-of-the-Earth Flight, STI WP-1254-6, May 1988.

3. Allen, R. Wade, and Duane McRuer, "The Man/Machine Control Interface--Pursuit Control," Automatica, Vol. 15, No. 6, November 1979, pp. 683-686.

4. Telephone conversation between Donald Caldwell, McDonnell Douglas Helicopter Co., Inc., and Warren Clement, Systems Technology, Inc., November 12, 1987.

5. Clement, Warren F., Duane T. McRuer, and Raymond E. Magdaleno, Some Data Processing Requirements for Precision Nap-of-the-Earth (NOE) Guidance and Control of Rotorcraft, STI TR-1239-1, December 1986, Revised February 1987.

APPENDIX D

WORKING PAPER NO. 1254-7

STORED FLIGHT PROFILES FOR THE COMPUSCENE IV DISPLAY OF AUTOMATICALLY GUIDED ROTORCRAFT NAP-OF-THE-EARTH FLIGHT

Stored Flight Profiles for the Compuscene IV Display of Automatically Guided Rotorcraft Nap-of-the-Earth Flight

A. Introduction

The U.S. Army and helicopter manufacturers are vitally interested in automatic nap-of-the-earth (NOE) flight. It is believed that most of the guidance and control problems associated with Light Helicopter Experimental (LHX) and AH-64X rotorcraft operations have at least interim solutions using a mixture of manual and automatic resources. There is some promise that the range of automatic operations can be extended further to include automatic NOE flight. To accomplish this, at least these three issues must be resolved:

1. Interpolation within the resolution of the stored NOE data base using a stored approximating continuous surface and forward- and side-looking sensors and combining the stored and sensed data for real-time display, guidance, and control purposes.

2. Development of path and attitude command signals from this data array that are appropriate to command safe NOE flight of a three-dimensional helicopter (in contrast to a point mass helicopter).

3. Pilot acceptance of automatic NOE flight.

All of the issues described above are designed to focus on the development of innovative forms of automatic guidance and control which are compatible with piloted guidance strategies and control techniques. Intrinsic to this goal is the interpolation within the resolution of the stored data base to provide guidance for following flight plans.

Described herein is a method for interpolating within the resolution of a stored data base to provide guidance for following flight plans which employs compressed data storage of terrain and threat exposure heights using pre-flight parameter identification of the planned gaming area course. The storage and real-time updating of terrain profiles and obstacles have been organized in gaming area course coordinates that are indexed to the defined gaming area course. Also discussed are the specifications for the waypoint and gaming area course layouts and the cultural feature distribution throughout the data base.

B. Gaming Area Course Coordinate Transformation

The gaming area course is a 100 decameter (dm) wide corridor specified prior to the NOE mission which defines the geographic bounds of the mission. The example terrain used throughout this report is that of the Fulda Gap section of the Compuscene IV data base used at the McDonnell Douglas Helicopter Company (MDHC) at Mesa, Arizona.

The flight plan is defined by waypoints within the gaming area and will, in general, meander with respect to the gaming area course. The gaming area course is transformed from an earth coordinate system to its own coordinate system for convenience in defining the approximate surface of the terrain, as will be described in the next section. In its own coordinate system, the entire gaming area course is straightened into a rectangular corridor 100 dm wide (Fig. 1). This corridor is divided into a number of rectangular sections, based on the number of course points used to define changes in gaming area course direction, each of which defines a course leg in gaming area course coordinates.

The gaming area course coordinate system has a nonlinear relationship with the earth-fixed axis system because, although the lengths of the two sides of the course leg sections are of equal length in the course-oriented coordinate system, the actual distances these two sides represent in the earth-fixed axis system are, in general, different due to turns in the gaming area course. This is demonstrated in Fig. 2 where the third course leg of the defined gaming area course (Fig. 1) is isolated. The following procedure is used to transform earth coordinates into gaming area course coordinates for a given course leg.

Step 1. Calculate the distance from the outbound course point (course point at beginning of course leg n, defined by the earth coordinates $x_e(n)$ and $y_e(n)$) and the point to be transformed (defined by the earth coordinates x_e and y_e).

$$\Delta x_e = x_e - x_e(n)$$

$$\Delta y_e = y_e - y_e(n)$$

Step 2. Project the distances from Step 1 into the course leg direction.

$$\begin{bmatrix} \Delta x_c \\ \Delta y_c \end{bmatrix} = \begin{bmatrix} \cos(\lambda_n) & \sin(\lambda_n) \\ -\sin(\lambda_n) & \cos(\lambda_n) \end{bmatrix} \begin{bmatrix} \Delta x_e \\ \Delta y_e \end{bmatrix}$$

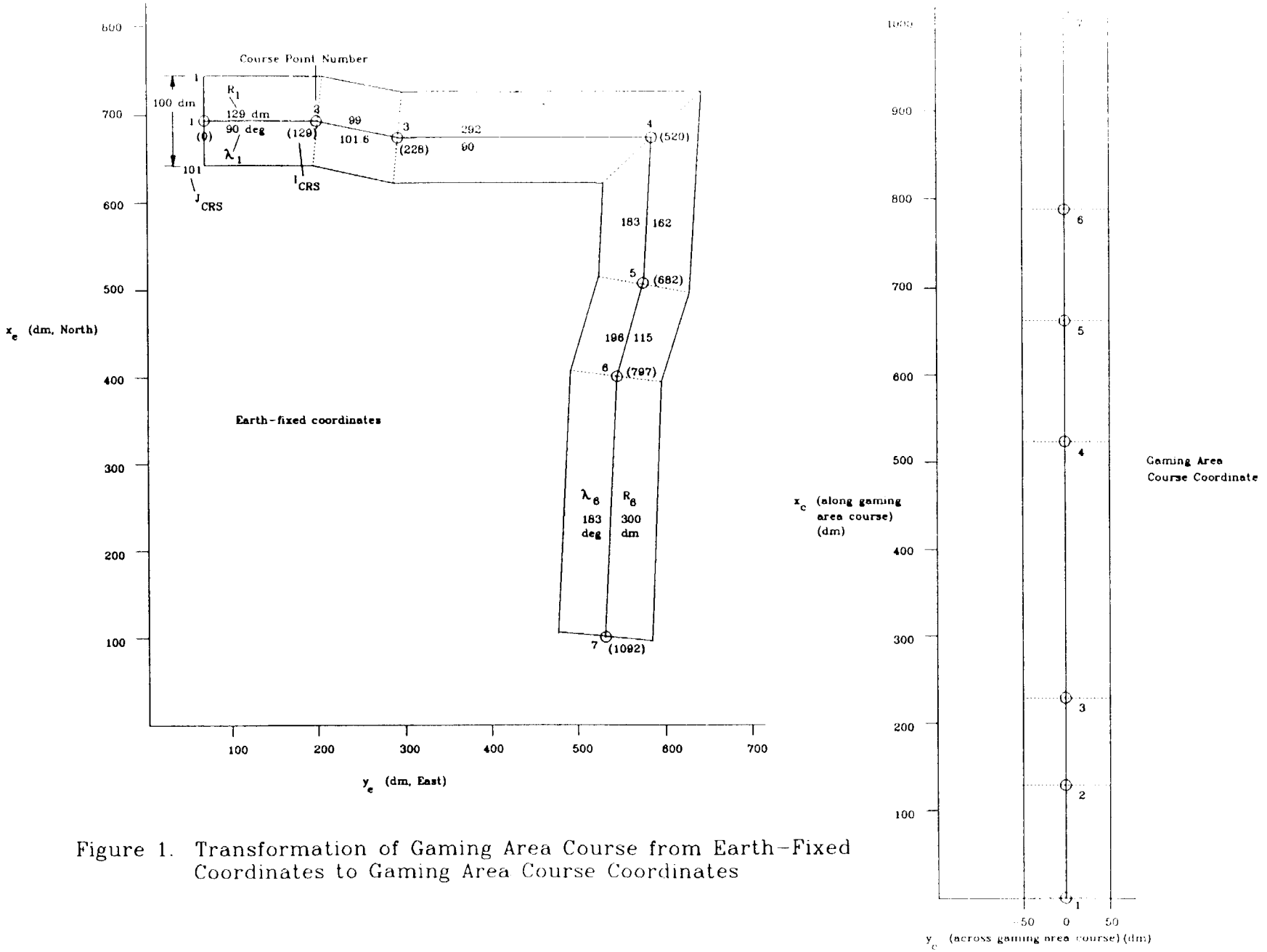

Figure 1. Transformation of Gaming Area Course from Earth-Fixed Coordinates to Gaming Area Course Coordinates

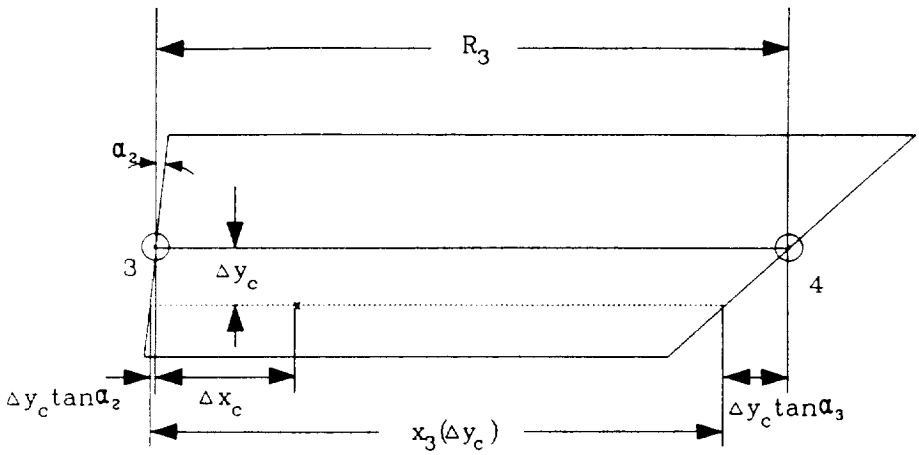

where $\alpha_2 = \frac{1}{2}(\lambda_2 - \lambda_3) = 5.8\,\text{deg}$ and $\alpha_3 = \frac{1}{2}(\lambda_3 - \lambda_4) = -46.5\,\text{deg}$

$$x_3(\Delta y_c) = R_3 + \Delta y_c \tan\alpha_2 + \Delta y_c \tan\alpha_3$$

Figure 2. Third Course Leg of the Gaming Area Course

where λ_n is the direction of the course leg with respect to North,

$$\lambda_n = \tan^{-1}\left(\frac{y_e(n+1) - y_e(n)}{x_e(n+1) - x_e(n)}\right)$$

Step 3. Account for distortion in the along course coordinate caused by unequal lengths of course leg sides. Because the lengths of the sides of the course leg rectangle in the gaming area course coordinates are equal to the distances between the two course points which define the course leg, any distance along a line parallel to the center line of the course leg can be considered as a fraction of the total length in earth coordinates of that parallel line multiplied by the total length of the centerline. From Fig. 2, this translates into

$$\Delta x_{CRS} = R_n\left(\frac{\Delta y_c \tan\alpha_{n-1} + \Delta x_c}{\Delta y_c(\tan\alpha_{n-1} + \tan\alpha_n) + R_n}\right)$$

$$\alpha_n = \frac{1}{2}(\lambda_n - \lambda_{n-1})$$

$$\Delta y_{CRS} = \Delta y_c$$

Step 4. Add previous course leg lengths

$$x_{CRS} = \sum_{i=1}^{n-1} R_i + \Delta x_{CRS}$$

$$y_{CRS} = \Delta y_{CRS}$$

In order to determine into which course leg a particular set of earth coordinates maps, an iterative process is required. First, it is assumed that the earth coordinates in question map into the first course leg and Steps 1 thru 3 are performed based on this assumption. Two conditions are then checked to ensure that the chosen course leg is indeed the correct one. If $\Delta x_{CRS} > R_n$ or $\Delta y_{CRS} > \Delta y_{CRS_{max}}$ (1/2 the gaming area course width), the choice of course leg is incorrect. The next leg is then considered, and Steps 1 thru 3 are repeated. If neither of these inequalities is true, the choice of the course leg was correct, and the transformation proceeds by executing Step 4.

The distortion in the along-course coordinate also adds complication to the calculation of the gaming area course rotorcraft velocities and accelerations. Having already determined the appropriate course leg into which the rotorcraft's position maps, the gaming area course velocities and accelerations are calculated as follows.

Step 1. Project the velocities and accelerations into the course leg direction.

$$\begin{bmatrix} \Delta \dot{x}_c \\ \Delta \dot{y}_c \end{bmatrix} = \begin{bmatrix} \cos(\lambda_n) & \sin(\lambda_n) \\ -\sin(\lambda_n) & \cos(\lambda_n) \end{bmatrix} \begin{bmatrix} \Delta \dot{x}_e \\ \Delta \dot{y}_e \end{bmatrix}$$

$$\begin{bmatrix} \Delta \ddot{x}_c \\ \Delta \ddot{y}_c \end{bmatrix} = \begin{bmatrix} \cos(\lambda_n) & \sin(\lambda_n) \\ -\sin(\lambda_n) & \cos(\lambda_n) \end{bmatrix} \begin{bmatrix} \Delta \ddot{x}_e \\ \Delta \ddot{y}_e \end{bmatrix}$$

Step 2. Calculate gaming area course velocities and accelerations as

$$\dot{x}_{CRS} = \frac{\partial}{\partial \Delta y_c} x_{CRS} \cdot \Delta \dot{y}_c + \frac{\partial}{\partial \Delta x_c} x_{CRS} \cdot \Delta \dot{x}_c$$

$$\dot{y}_{CRS} = \Delta \dot{y}_c$$

and

$$\ddot{x}_{CRS} = \frac{\partial}{\partial \Delta y_c} x_{CRS} \cdot \Delta \ddot{y}_c + \frac{\partial}{\partial \Delta x_c} x_{CRS} \cdot \Delta \ddot{x}_c + \frac{\partial^2}{\partial \Delta y_c^2} x_{CRS} \cdot \Delta \dot{y}_c^2$$
$$+ \frac{\partial^2}{\partial \Delta x_c^2} x_{CRS} \cdot \Delta \dot{x}_c^2 + \frac{\partial^2}{\partial \Delta x_c \partial \Delta y_c} x_{CRS} \cdot \Delta \dot{x}_c \Delta \dot{y}_c$$

$$\ddot{y}_{CRS} = \Delta \ddot{y}_c$$

where

$$\frac{\partial}{\partial \Delta y_c} x_{CRS} = \frac{R_n^2 \tan\alpha_{n-1} - R_n \Delta x_c (\tan\alpha_{n-1} + \tan\alpha_n)}{[\Delta y_c (\tan\alpha_{n-1} + \tan\alpha_n) + R_n]^2}$$

$$\frac{\partial}{\partial \Delta x_c} x_{CRS} = \frac{R_n}{\Delta y_c (\tan\alpha_{n-1} + \tan\alpha_n) + R_n}$$

$$\frac{\partial^2}{\partial \Delta y_c^2} x_{CRS} = -2 \frac{[R_n^2 \tan\alpha_{n-1} - R_n \Delta x_c (\tan\alpha_{n-1} + \tan\alpha_n)](\tan\alpha_{n-1} + \tan\alpha_n)}{[\Delta y_c (\tan\alpha_{n-1} + \tan\alpha_n) + R_n]^3}$$

$$\frac{\partial^2}{\partial \Delta x_c^2} x_{CRS} = 0$$

$$\frac{\partial^2}{\partial \Delta x_c \partial \Delta y_c} x_{CRS} = \frac{-R_n (\tan\alpha_{n-1} + \tan\alpha_n)}{[\Delta y_c (\tan\alpha_{n-1} + \tan\alpha_n) + R_n]^2}$$

These velocities and accelerations are required in order to determine the time rate of change of terrain elevation and slope discussed in a later section.

C. Using Approximating Surface to Represent Terrain Profile

In order to create a continuous representation of the terrain profile and threat exposure height, the rectangular gaming area course corridor is mapped with an approximate terrain surface and threat exposure height function to reduce the storage requirements and facilitate the interpolation within the resolution of the stored data base. To accomplish this, the following steps are taken:

1. **Index Course Coordinates** : The corridor is indexed in an along- and across-course manner, with the i_x index incrementing from 1 to NX along the course, and the j_y index incrementing from 1 to NY from left to right across the course. Each (i_x, j_y) point is then assigned the elevation of the closest data point in the terrain data base. The spacing of these indexed points is determined by the resolution of the terrain data base (Note that a unit of length along the center line of the gaming area course is the same in the gaming area course and the earth-fixed coordinate systems). Each set of NX points along the course for a given j_y will be referred to as a strip from the gaming area course.

2. **Compute the Finite Fourier Transform (FFT) of All Strips** : The FFT for each of the NY strips of NX terrain altitude data points is computed. The mean and trend of the strips are removed prior to computing the FFTs. The altitude profiles are then approximated by including the means and trends to truncated sums of sinusoids using the first MX complex coefficients from the NX/2 complex coefficients resulting from the computation of the FFTs of the strips. These coefficients are stored in four (4) matrices:

$\underline{A}$ - an MX x NY matrix containing the coefficients of the MX sine terms in the NY sums of sinusoids.

$\underline{B}$ - an MX x NY matrix containing the coefficients of the MX cosine terms in the NY sums of sinusoids.

$\underline{c}_0^t$ - an NY row vector containing the NY mean values for each sum.

$\underline{c}_1^t$ - an NY row vector containing the NY trend values for each sum.

If $h_{j_y}(x_{CRS})$ is the approximation of the terrain profile for the j_y^{th} strip of the gaming area course as a function of along-course position, x_{CRS},

$$h_{j_y}(x_{CRS}) = C_{0_{j_y}} + C_{1_{j_y}}(x_{CRS} + 1) + \sum_{i=1}^{MX} [A_{i j_y} \sin \omega_i x_{CRS} + B_{i j_y} \cos \omega_i x_{CRS}]$$

$$\text{where } \omega_i = \frac{2\pi i}{NX}$$

3. **Compute the FFT of the Approximating Coefficient Matrices** : The FFT for each of the MX sets of NY coefficients in the $\underline{A}$ and $\underline{B}$ matrices and the NY coefficients of the $\underline{c}_0^t$ and $\underline{c}_1^t$ row vectors is computed. The means and trends are removed prior to the computation of the FFTs. The coefficients are then approximated by adding the means and trends to truncated sums of sinusoids using the first MY complex coefficients of the NY/2 complex coefficients resulting

from the FFTs of the coefficient matrices. This exercise results in the creation of sixteen (16) more matrices of coefficients, four each for the four matrices of coefficients $\underline{A}$, $\underline{B}$, $\underline{c}_0^t$, and $\underline{c}_1^t$. For the matrix $\underline{A}$, these matrices are:

$\underline{D}$ - an MX x MY matrix containing the coefficients of the MY sine terms in each sum of sinusoid approximations of the MX rows in $\underline{A}$.

$\underline{E}$ - an MX x MY matrix containing the coefficients of the MY cosine terms in each sum of sinusoid approximations of the MX rows in $\underline{A}$.

$\underline{f}_0^t$ - an MX row vector containing the mean values of each of the MX rows in $\underline{A}$.

$\underline{f}_1^t$ - an MX row vector containing the trends of each of the MX rows in $\underline{A}$.

If $A_i(y_{CRS})$ is the continuous function in across-course position, y_{CRS}, approximating the NY discrete values in the i^{th} row of the matrix $\underline{A}$,

$$A_i(y_{CRS}) = F_{0_i} + F_{1_i}(y_{CRS} - 49) + \sum_{j=1}^{MY} [D_{ij}\sin\omega_j(y_{CRS} - 50) + E_{ij}\cos\omega_j(y_{CRS} - 50)]$$

$$\text{where} \quad \omega_j = \frac{2\pi j}{NY}$$

Similarly,

$$B_i(y_{CRS}) = I_{0_i} + I_{1_i}(y_{CRS} - 49) + \sum_{j=1}^{MY} [G_{ij}\sin\omega_j(y_{CRS} - 50) + H_{ij}\cos\omega_j(y_{CRS} - 50)]$$

$$C_0(y_{CRS}) = L_0 + L_1(y_{CRS} - 49) + \sum_{j=1}^{MY} [J_j\sin\omega_j(y_{CRS} - 50) + K_j\cos\omega_j(y_{CRS} - 50)]$$

$$C_1(y_{CRS}) = P_0 + P_1(y_{CRS} - 49) + \sum_{j=1}^{MY} [M_j\sin\omega_j(y_{CRS} - 50) + N_j\cos\omega_j(y_{CRS} - 50)]$$

The final expression for the terrain elevation as a function of both along- and across-course position, $h(x_{CRS}, y_{CRS})$, is,

$$h(x_{CRS}, y_{CRS}) = C_0(y_{CRS}) + C_1(y_{CRS})\cdot(x_{CRS} + 1) + \sum_{i=1}^{MX} [A_i(y_{CRS})\sin\omega_i x_{CRS} + B_i(y_{CRS})\cos\omega_i x_{CRS}]$$

An example showing the ability of this approximating surface to accurately represent the terrain profile is presented in Fig. 3. The longitude and latitude coordinates are congruous with the earth coordinates in Fig. 1.

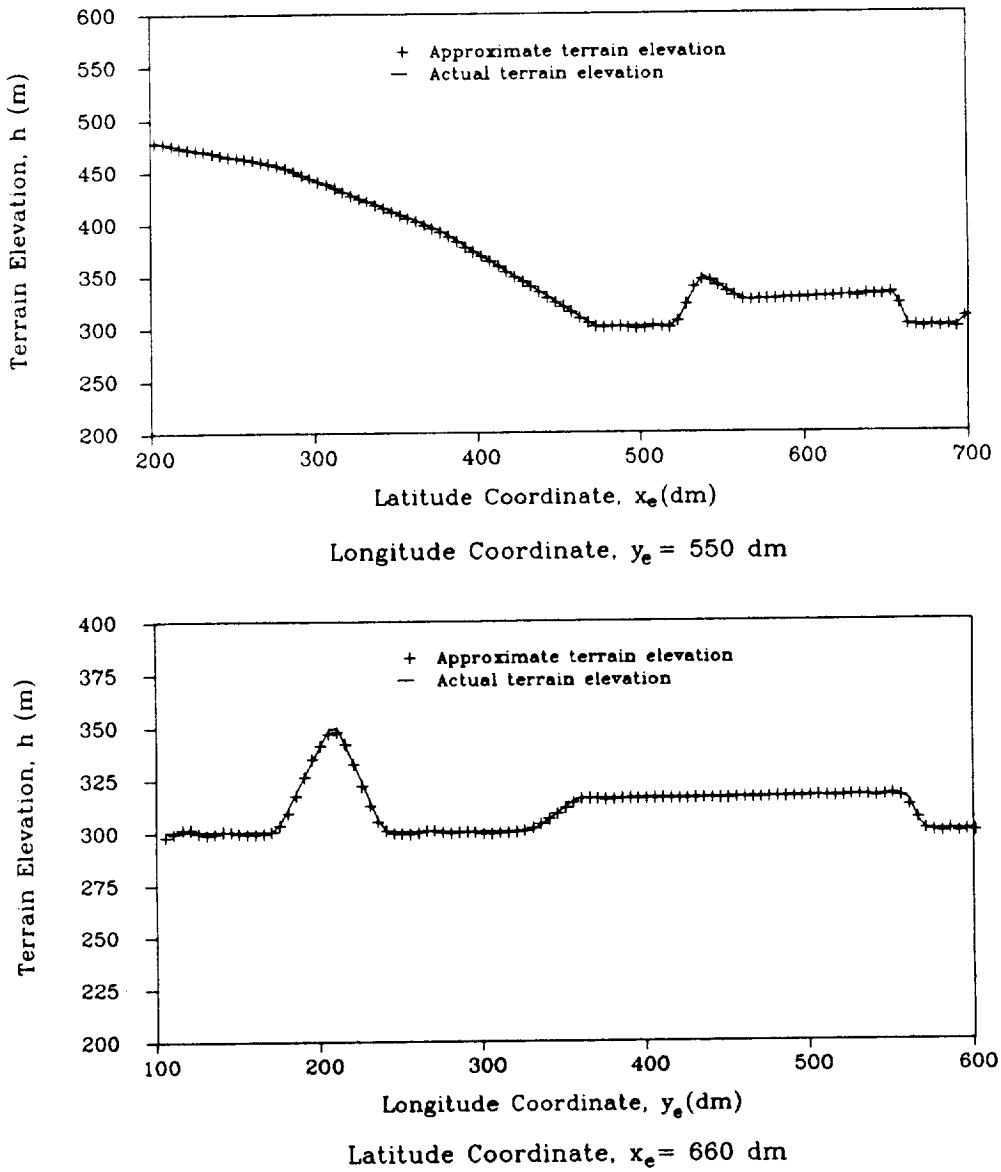

Figure 3. Sample Fulda Gap Terrain Profiles - Approximate and Actual Elevation

4. **Calculation of 1st and 2nd Derivatives for Pursuit Guidance Algorithm** : Because in addition to the terrain elevation the slope and curvature of the terrain are required for the pursuit guidance logic, the following expressions are used in the calculation of these quantities based on the above approximation for the terrain elevation.

$$\dot{h}(x_{CRS}, y_{CRS}) = \frac{\partial}{\partial x_{CRS}}(h(x_{CRS}, y_{CRS}))\cdot \dot{x}_{CRS} + \frac{\partial}{\partial y_{CRS}}(h(x_{CRS}, y_{CRS}))\cdot \dot{y}_{CRS}$$

$$\begin{aligned}\ddot{h}(x_{CRS}, y_{CRS}) = {} & \frac{\partial}{\partial x_{CRS}}(h(x_{CRS}, y_{CRS}))\cdot \ddot{x}_{CRS} + \frac{\partial^2}{\partial x_{CRS}^2}(h(x_{CRS}, y_{CRS}))\cdot \dot{x}_{CRS}^2 \\ & + 2\frac{\partial^2}{\partial x_{CRS}\partial y_{CRS}}(h(x_{CRS}, y_{CRS}))\cdot \dot{x}_{CRS}\dot{y}_{CRS} + \frac{\partial^2}{\partial y_{CRS}^2}(h(x_{CRS}, y_{CRS}))\cdot \dot{y}_{CRS}^2 \\ & + \frac{\partial}{\partial y_{CRS}}(h(x_{CRS}, y_{CRS}))\cdot \ddot{y}_{CRS}\end{aligned}$$

where

$$\frac{\partial}{\partial x_{CRS}}h(x_{CRS}, y_{CRS}) = C_1(y_{CRS}) + \sum_{i=1}^{MX}[A_i(y_{CRS})\omega_i \cos\omega_i x_{CRS} - B_i(y_{CRS})\omega_i \sin\omega_i x_{CRS}]$$

$$\begin{aligned}\frac{\partial}{\partial y_{CRS}}h(x_{CRS}, y_{CRS}) = {} & \frac{d}{dy}C_0(y_{CRS}) + \frac{d}{dy}C_1(y_{CRS})\cdot(x_{CRS}+1) + \sum_{i=1}^{MX}[\frac{d}{dy}A_i(y_{CRS})\sin\omega_i x_{CRS} \\ & + \frac{d}{dy}B_i(y_{CRS})\cos\omega_i x_{CRS}]\end{aligned}$$

$$\frac{\partial^2}{\partial x_{CRS}^2}h(x_{CRS}, y_{CRS}) = -\sum_{i=1}^{MX}[A_i(y_{CRS})\omega_i^2 \sin\omega_i x_{CRS} + B_i(y_{CRS})\omega_i^2 \cos\omega_i x_{CRS}]$$

$$\begin{aligned}\frac{\partial^2}{\partial x_{CRS}\partial y_{CRS}}h(x_{CRS}, y_{CRS}) = {} & \frac{d}{dy}C_1(y_{CRS}) + \sum_{i=1}^{MX}[\frac{d}{dy}A_i(y_{CRS})\omega_i \cos\omega_i x_{CRS} \\ & - \frac{d}{dy}B_i(y_{CRS})\omega_i \sin\omega_i x_{CRS}]\end{aligned}$$

$$\begin{aligned}\frac{\partial^2}{\partial y_{CRS}^2}h(x_{CRS}, y_{CRS}) = {} & \frac{d^2}{dy_{CRS}^2}C_0(y_{CRS}) + \frac{d^2}{dy_{CRS}^2}C_1(y_{CRS})\cdot(x_{CRS}+1) + \sum_{i=1}^{MX}[\frac{d^2}{dy_{CRS}^2}A_i(y_{CRS})\sin\omega_i x_{CRS} \\ & + \frac{d^2}{dy_{CRS}^2}B_i(y_{CRS})\cos\omega_i x_{CRS}]\end{aligned}$$

APPENDIX E

WORKING PAPER NO. 1254-4

OBSTACLE DETECTION AND AVOIDANCE MANEUVER SELECTION FOR AUTOMATICALLY GUIDED ROTORCRAFT NAP-OF-THE-EARTH FLIGHT FOLLOWING PLANNED FLIGHT PROFILES

C. REVISED ANTICIPATORY MULTIRANGE SEARCH PATTERNS ALONG- AND ACROSS-COURSE WITH COMBINED HORIZONTAL AND VERTICAL MANEUVER SELECTION COUPLED WITH CONSTRAINED TIME-OPTIMAL MANEUVERS

OBSTACLE DETECTION AND AVOIDANCE MANEUVER SELECTION FOR AUTOMATICALLY GUIDED ROTORCRAFT NAP-OF-THE-EARTH FLIGHT FOLLOWING PLANNED FLIGHT PROFILES

A. INTRODUCTION

In an automatically-piloted vehicle flying in nap-of-the-earth (NOE) conditions along a prescribed course, provisions must be made for unexpected obstacle avoidance. To this end, obstacle detection and avoidance logic has been developed for the automatic guidance system being designed under Ref. 1. This logic invokes, as necessary, one or more rapid response avoidance maneuvers from among the several described in Ref. 2. The obstacle detection and avoidance maneuver selection logic is represented by the "Task 2" block preceding the "Y_{RR}" block of Fig. 1, which is based on Fig. 10 on p. 33 of Ref. 3.

Automatic processing of stored and sensed terrain and obstacle data will involve sampling, interpolation, extrapolation, smoothing, and comparison of spatial and temporal series of data coupled with priority logic for selection of appropriate evasive maneuvers. An overview of the priority logic for unexpected obstacle avoidance using discrete maneuvers is illustrated in the flow diagram presented in Fig. 2. This working paper presents a detailed description of this priority logic.

B. OUTLINE OF THE PROCEDURE

Obstacle detection and avoidance while following the flight plan depends on the correlation of acquired knowledge from the sensed environment with the forehand knowledge of the recorded environment, i.e., terrain, obstacles, threats, and targets, and the accessing of that correlated knowledge for the purpose of guidance. The correlation procedure to be demonstrated herein is performed in the along-course[1] coordinates. Similar logic could be extended to across-course coordinates. The correlation is provided in a continuous sense using an approximation of the terrain between points from the digital DMA terrain data base. Threats are represented in terms of a threat exposure height function of course coordinates. The "obstacles" are sensed by interrogating a given region for the presence of non-conformity of the observed terrain, cultural features, and threats to the terrain approximation or threat exposure height

1 For the purposes of this discussion, the terms along-course and across-course refer to the rotorcraft total velocity direction relative to the pre-planned flight profile. In the nominal case, therefore, if the rotorcraft is following the pre-planned flight profile, the across-course velocity is zero.

function. These obstacles are characterized by height increments either rising above the terrain height profile or descending below the threat exposure height profile.

A prerequisite for using the forward- and sideward-looking sensed data base to update the flight plan in real time is an independent (navigation) reference system with prescribed uncertainty that is common to the reference system of the preflight stored geodetic and cultural data base. A typical example of such a system would be an inertial system updated by a global positioning system.

Figure 2 illustrates a procedural flow diagram for updating and modifying the stored guidance command flight profiles in real time to provide for unexpected obstacle avoidance. Two data bases having a common navigational reference system (which provides the state vector $\underline{X}$) are identified at the top of the diagram: the stored flight profiles (vector $\underline{R}_n$) at the upper left and the sensed profiles of terrain, obstacles, and threats, together with offset bias requirements for safety, at the upper right (vector $\underline{\hat{R}}_n$).

In principle, it is necessary to compare $\underline{\hat{R}}_n$ with $\underline{R}_n$ in real time, resolve any conflicts with the planned flight profile by automatically selecting a combination of lateral and vertical evasive maneuvers, and return to the planned flight profile where possible. If no combination of lateral and vertical evasive maneuvers will remove a conflict between $\underline{\hat{R}}_n$ and $\underline{R}_n$, the rotorcraft is commanded to stop and let the pilot select another flight plan.

C. DEFINITION OF SAFETY MARGIN ENVELOPES FOR DETECTING OBSTACLES

A three-dimensional safety margin envelope is defined mathematically in the form of a rectangular parallelepiped which encompasses the extremities of the rotorcraft with room to spare, governed by safety margins. This safety margin envelope, shown in Fig. 3, is centered on the position of the rotorcraft at all times for the purpose of absolute altimetry while travelling. Typical dimensions for encompassing the H-60 series rotorcraft or the XV-15 tilt rotorcraft would be : RX = RY = 10 meters (m) and RH = 7.5 m. The upper and lower surfaces of the safety margin envelope are partitioned into four squares each. If sensed obstacles penetrate one or more of these squares, either from above or below, appropriate action will be commanded to counteract the penetration(s). This testing for obstacle penetrations constitutes the absolute altimetry portion of the obstacle avoidance logic, and all vertical maneuvers commanded based on this logic pre-empt vertical maneuvers commanded based on the anticipative enveloping arrays described in Section G.

D. DEFINITION OF ALONG-COURSE ANTICIPATIVE ARRAY FOR SELECTION OF LATERAL EVASIVE MANEUVERS

When the rotorcraft is translating along the course, an augmented anticipative enveloping array extends along and across the course (Fig. 4). This array consists of blocks measuring RX long by RY wide by at least 2*RH high, and is referenced to a point ahead of the vehicle equal to the along-course anticipative time, T_{p_x}, multiplied by the along-course velocity, V_x and at a point above the terrain equal to the rotorcraft's current radar altitude. The height of the blocks varies with commanded vertical deviations from the nominal radar altitude. This is further discussed in Section G. Along the course, the blocks extend back from the reference point to encompass the position of the rotorcraft, and ahead of the reference point $4 \times RX$ plus the magnitude of the rearward extension. Across the course, the blocks extend $\pm 4 \times RY$. This anticipative array is divided into 5 sections, with four contributing to the selection of the lateral evasive maneuvers and the fifth to the vertical vertical evasive maneuvers.

1. The first section (outlined in orange color) consists of the four rows[2] of blocks beginning at the reference point and extending away from the rotorcraft position. The columns of this section are searched to detect obstructions in and around the planned flight path. An obstruction is defined as a point within the block which can not be avoided using a vertical maneuver and staying below the threat exposure threshold. This information is then used to select an appropriate lateral evasive maneuver if necessary. A more thorough description of the maneuver selection procedure is presented in a subsequent section.

2. The second section (outlined in green color) consists of the blocks beyond the first section. These blocks are used to check against unexpected obstructions just beyond the decision section, Section 1. Because the obstacle detection and avoidance logic is disabled during a lateral evasive maneuver, it is essential that there not be an obstruction between the rotorcraft and the along-course anticipative array reference point when the obstacle detection and avoidance logic is enabled at the conclusion of such a maneuver.

2 A row in the along-course anticipative array consists of blocks longitudinally equidistant from the reference point. A column consists of blocks laterally equidistant from the reference point.

3. This section (outlined in dark blue color) consists of the blocks before those of the first section, and to the left of the middle two columns. These blocks will represent obstacle data from the side-looking sensors, and determine whether a proposed leftward lateral evasive maneuver is safe. When a leftward lateral evasive maneuver is proposed, a group of these blocks is chosen representing the path of this maneuver. Only if the path is clear of obstacles is the maneuver executed.

4. This is the mirror to Section 3 and governs rightward lateral evasive maneuvers.

5. The last section (outlined in light blue color) consists of the blocks of the middle two columns before the along-course anticipative array reference point. These blocks govern vertical evasive maneuver commands.

E. SELECTION OF APPROPRIATE LATERAL EVASIVE MANEUVER

The columns of Section 1 are searched for obstructions, and a value 1 or zero is associated with each column depending on whether or not any obstructions are found in that column (1 = yes, 0 = no). These ones and zeros are interpreted as described in Table 1, and a lateral command is proposed.

If a non-zero lateral position command is proposed, the first step is to determine the urgency of the maneuver. This is accomplished by determining which block in Section 1 necessitates the maneuver. The least urgent maneuver (MUF1 = 1) would be necessitated by an obstruction in a block in the furthest row of Section 1 because the rotorcraft would then have the maximum distance in which to maneuver. Conversely, a maneuver necessitated by an obstruction in a block in the nearest row of Section 1 would be the most urgent of maneuvers (MUF1 = 4).

Following the determination of the urgency of the maneuver, all blocks to be passed through by the vehicle's safety margin envelope during the planned maneuver are selected from those of Section 3 or 4. Required of these blocks is that no penetrations exist, either from above or below, in conflict with current height commands. If any of the blocks does not conform to this requirement, the maneuver is disallowed. In this case, if the nearest blocks of both the third and forth columns of the first section are clear of obstructions, the rotorcraft continues without lateral deviation. This phenomenon is exhibited in Fig. 5, where the instigation of the first lateral evasive maneuver was delayed until the maneuver path cleared the obstacle on the right side of the rotorcraft. If either of the nearest blocks of the third or fourth columns

of Section 1 is obstructed, all columns of Section 1 to the side of the originally proposed lateral maneuver are artificially assigned the value 1, and the decision tree of Table 1 is re-inquired, as is demonstrated in Fig. 6. Because the maneuver path did not clear before the obstructions necessitating the maneuver entered the first row of the first section, an alternate, more circuitous route was chosen.

If all of the blocks of the path comply with the above stated requirement, the decision to go ahead with the maneuver is governed by the blocks of Section 2. Blocks in Section 2 constituting the destined path of the rotorcraft following the proposed maneuver are searched to expose obstructions. If no obstruction is detected, the proposed lateral evasive maneuver is so ordered, and the obstacle detection and avoidance logic is disabled until its completion. If, however, an obstruction is detected within a distance from the obstacle necessitating the maneuver equal to the distance from the along-course anticipatory reference point to the vehicle, the maneuver is disallowed. In this case, if MUF1 is less than 4, a maneuver of urgency MUF1 = MUF1 + 1 is proposed, and the decision goes back to the path determination in Section 3 or 4. If MUF1 = 4, than an obstruction is artificially placed in the last row of Section 1 in the column corresponding to the obstruction detected in Section 2, and the decision tree of Table 1 is re-inquired. This is demonstrated in Fig. 7. Though the fifth and sixth obstacles on the course (counted from X=0) were not in Section 1 of the along-course anticipative array when the decision was made to take evasive action, the interogation of Section 2 caused a modification of the original commanded lateral displacement, and these obstacles were safely avoided.

F. RETURNING TO THE PRE-PLANNED FLIGHT PATH FOLLOWING A LATERAL EVASIVE MANEUVER

Upon completion of a lateral evasive maneuver, the automatic guidance routine immediately attempts to return the rotorcraft to the pre-planned flight path via another constrained time optimal lateral maneuver. To this end, the first step of the obstacle detection and avoidance logic is to determine, using criteria described in the previous section, whether such a maneuver is possible given current conditions. If so, the return lateral maneuver is commanded. Otherwise, the obstacle detection and avoidance logic is exercised as described in the previous section. Figure 5 depicts a case in which two lateral evasive maneuvers were required to avoid unexpected obstructions in the pre-planned flight profile. Following the second maneuver, the return path was blocked for some distance, and the return command was thus delayed until the obstacles were cleared.

It is readily apparent that following this procedure, it is quite possible that through a series of lateral translations, the rotorcraft could find itself more than 3*RY laterally displaced from the pre-planned flight path. In this case, with the current width of the along-course anticipative array, a clear return to the flight path could not be confirmed. Because the largest allowable lateral displacement command is 3*RY, it is this command in the direction of the flight path which is sought by the return to path logic. Through a series of such commands, the vehicle can then be brought back to the pre-planned flight path.

G. SELECTION OF APPROPRIATE VERTICAL EVASIVE MANEUVERS

Because in general the rotorcraft will be travelling over uneven terrain, the altitude of the along-course anticipative array is based on the course altitude at the anticipative array reference point. The positions of the upper and lower surfaces of the anticipative array are depicted in Fig. 8, where V_h, is the rate of change of course altitude at the reference point. The positions of the upper and lower surfaces are further modified by the current commanded height deviation from the pre-planned flight path altitude (Fig. 9).

When no lateral evasive maneuver is required, the blocks of Section 5 determine the appropriate height deviation command. Each block is searched to identify penetrations from either above or below. For cases in which there is no current height deviation command, any penetration requires evasive action. If obstacles are discovered penetrating one or more of the blocks from below, the highest among them is determined and the height required to clear it commanded. Similarly, if obstacles are discovered penetrating one or more blocks from above, the lowest among them is determined and the height reqired to clear it commanded. If obstacles are discovered penetrating from both above and below, a stop command is issued and the pilot must determine an appropriate course of action.

For cases in which there is a current height deviation command, the height of the anticipative array blocks is greater than required by the rotorcraft for safe navigation. It is, therefore, unnecessary to respond to all penetrations. The objective of the vertical obstacle avoidance logic in this case is to bring the rotorcraft as close to the pre-planned course altitude as soon as possible, as demonstrated in Fig. 10. If there are penetrations from both above and below, as long as there is navigable vertical distance between them, only the obstacle closest to the desired flight path altitude governs the deviation height command.

If a lateral evasive maneuver is commanded, the search blocks for the commanded height deviation logic consists of those blocks in Sections 1 and 2 which define the proposed post-maneuver flight path. This height command is the destination height command. The absolute altimetry routine continues throughout the lateral evasive maneuver to modify this command appropriately. At the end of the lateral maneuver, however, the rotorcraft should be at the commanded destination height.

Table 1. Modified Procedural Flow Diagram for Obstacle Avoidance using Blocks of Section 1 of the Along-Course Anticipative Array Depicted in Fig. 4 (Each line of the table indicates values in HLDY(J) – the columns of Section 1)

J =	0 1 2 3	4 5 6 7		Decision regardless of unspecified elements in HLDY(J)
Left			Right	
	0	0		Continue to follow flight profile
	0 0	1		Left-step RY
	1	0 0		Right-step RY
	0 0 1	1		Left-step 2*RY
	0 0 1	1 0 1		Left-step 2*RY
	1	1 0 0		Right-step 2*RY
	1 0 1	1 0 0		Right-step 2*RY
	0 0 1	1 0 0		Right-step 2*RY if VY ⩾ 0, Left-step 2*RY if VY < 0
	0 0 1	1 1 1		Left-step 3*RY
	0 0 1	1 0 1		Left-step 3*RY
	0 0 1 1	0 1 1		Left-step 3*RY
	1 1 1	1 0 0		Right-step 3*RY
	1 0 1	1 0 0		Right-step 3*RY
	1 1 0	1 1 0 0		Right-step 3*RY
	0 0 1	1 1 0 0		Right-step 3*RY if VY ⩾ 0, Left-step 3*RY if VY < 0
	0 0 1 1	0 1 0 0		Right-step 3*RY if VY ⩾ 0, Left-step 3*RY if VY < 0

Legend: 0 = No obstruction present in Jth column of Section 1
1 = At least one element of the Jth column of Section 1 contains an obstruction

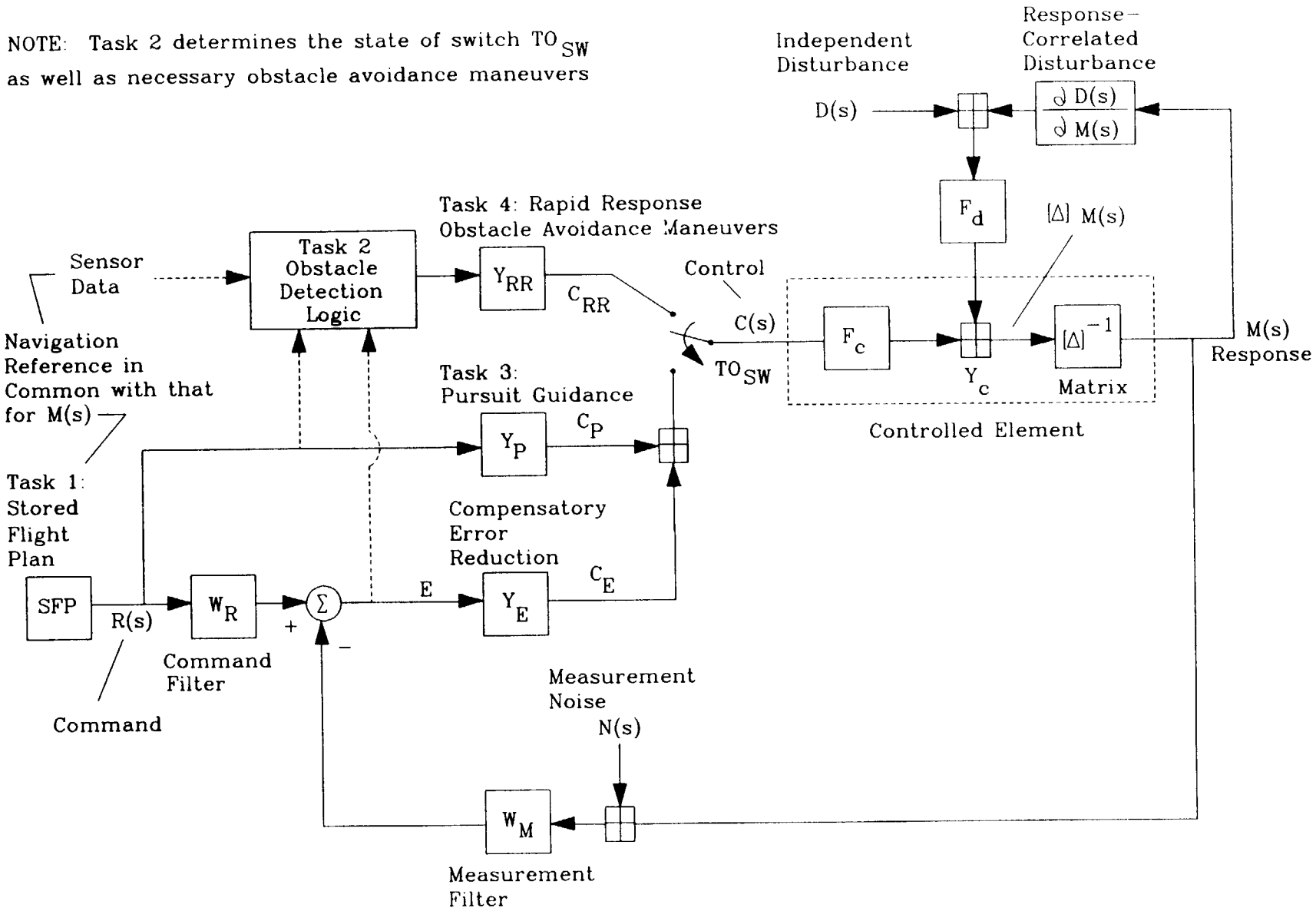

Figure 1. Vector Block Diagram for Multiloop Guidance and Control System

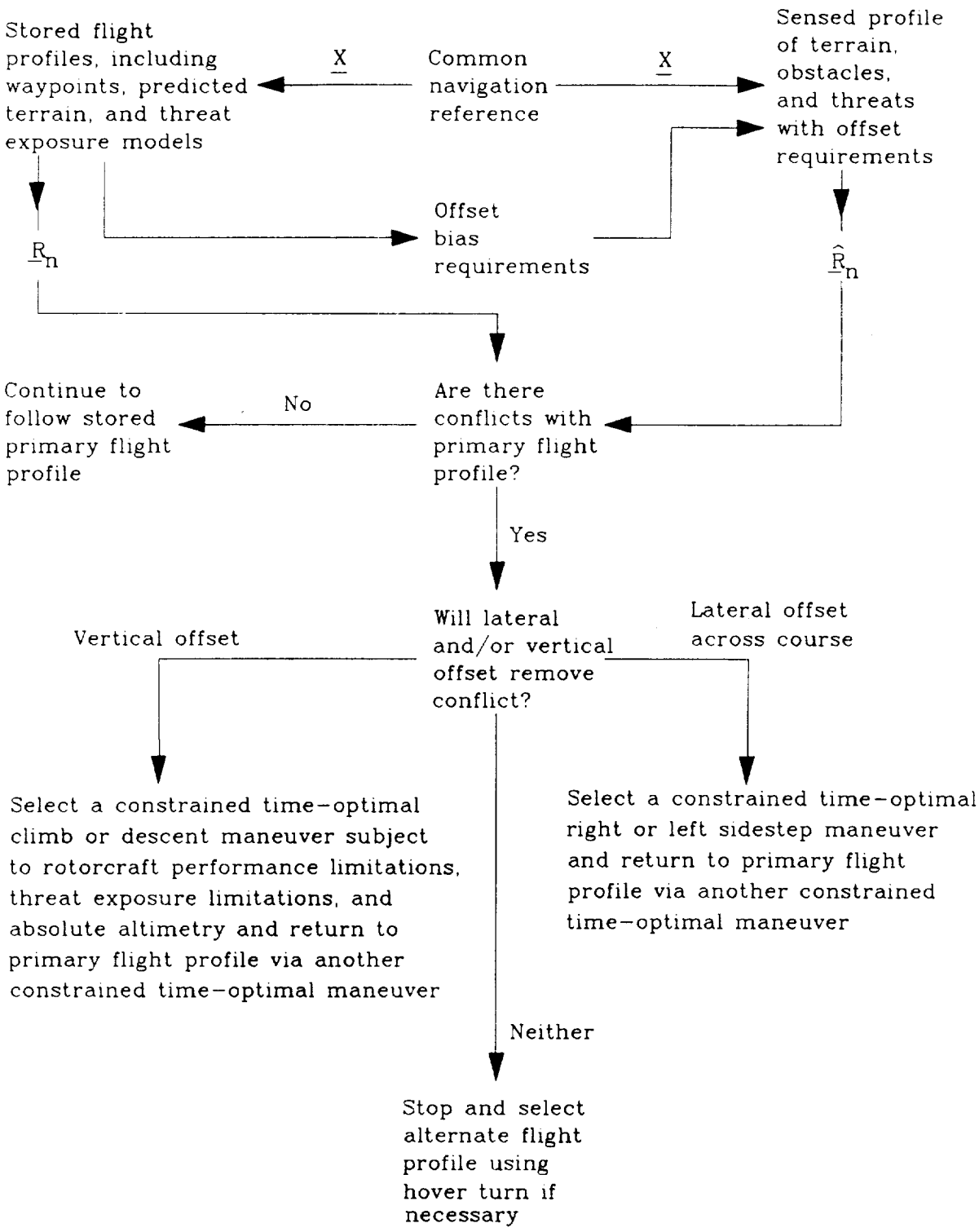

Figure 2. Modified Procedural Flow Diagram for Avoidance of Unexpected Obstacles Encountered in the Along-Course Anticipative Array (Combined vertical and lateral maneuvers are possible)

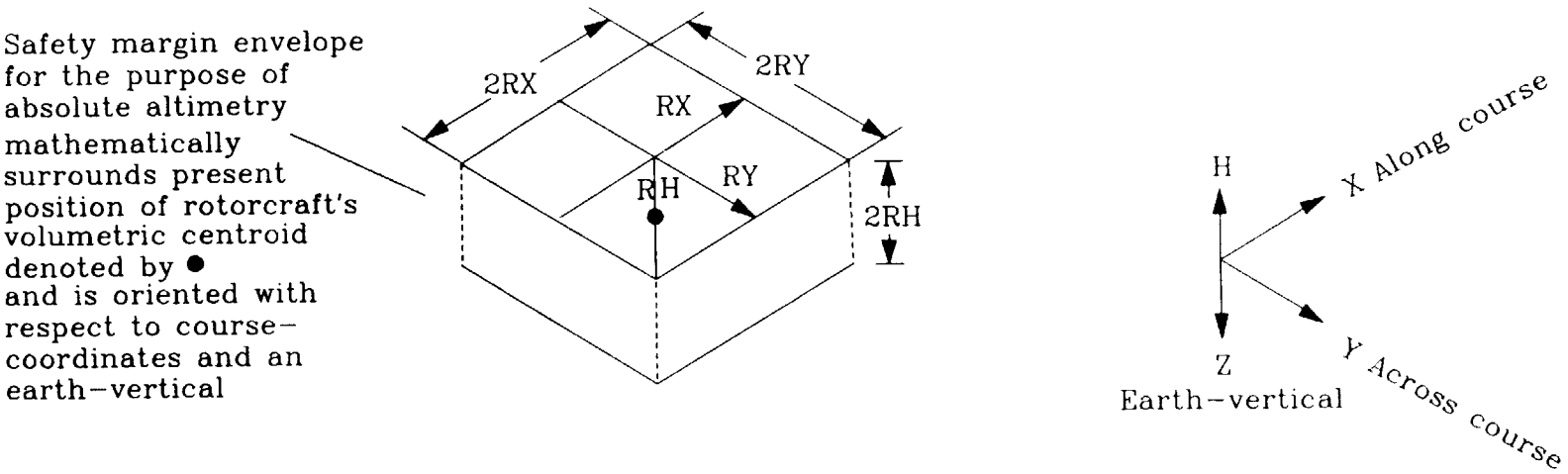

Figure 3. Safety Margin Envelope for Applying Absolute Altimetry to the Sensed Data Base to Avoid Obstacles

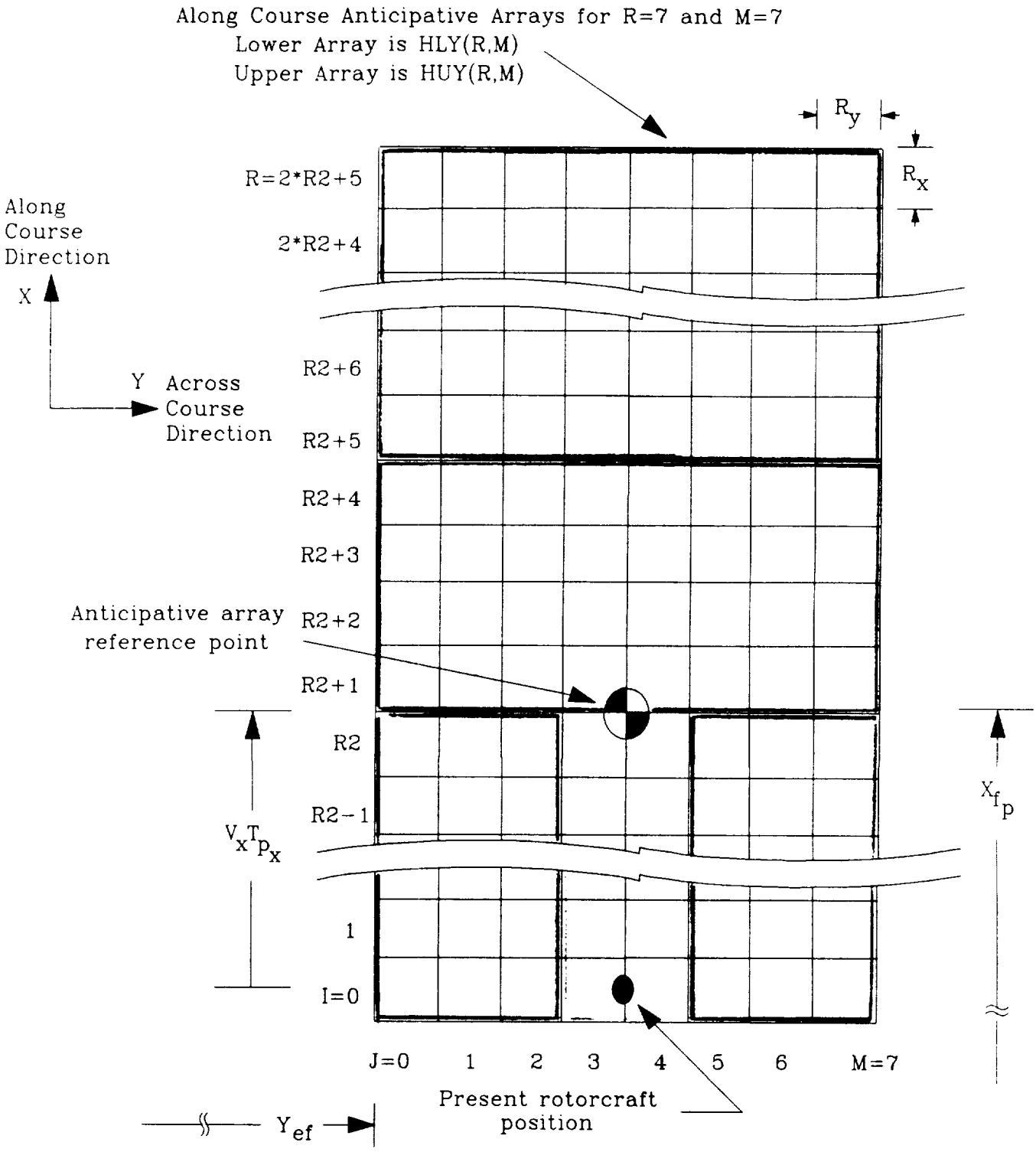

Figure 4. Plan View of Along Course Anticipative Array of Sensed Terrain, Obstacle, and Threat Elevation Data for Safety Margin Envelopes

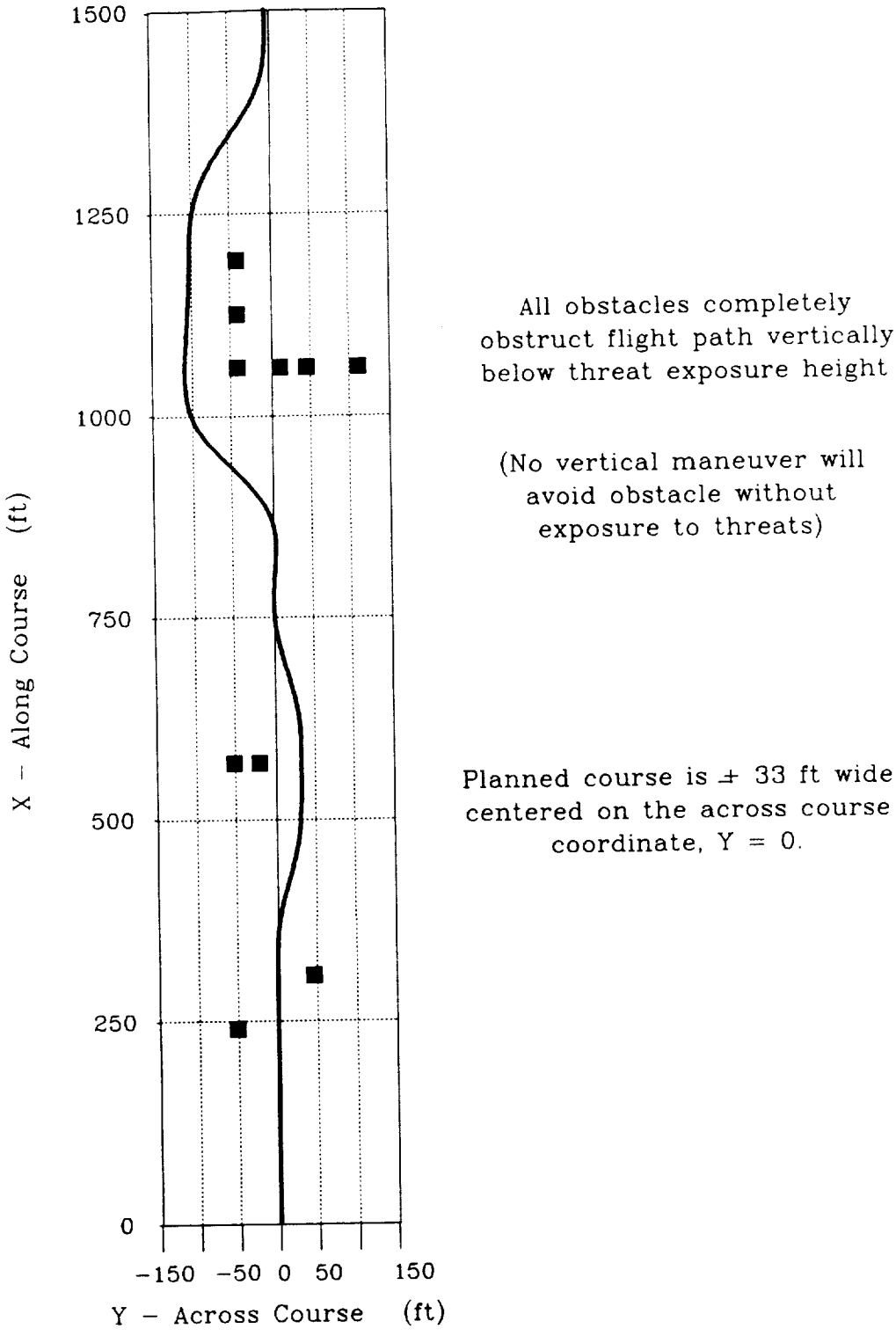

Figure 5. – Unexpected Obstacle Avoidance using Lateral Evasive Maneuvers

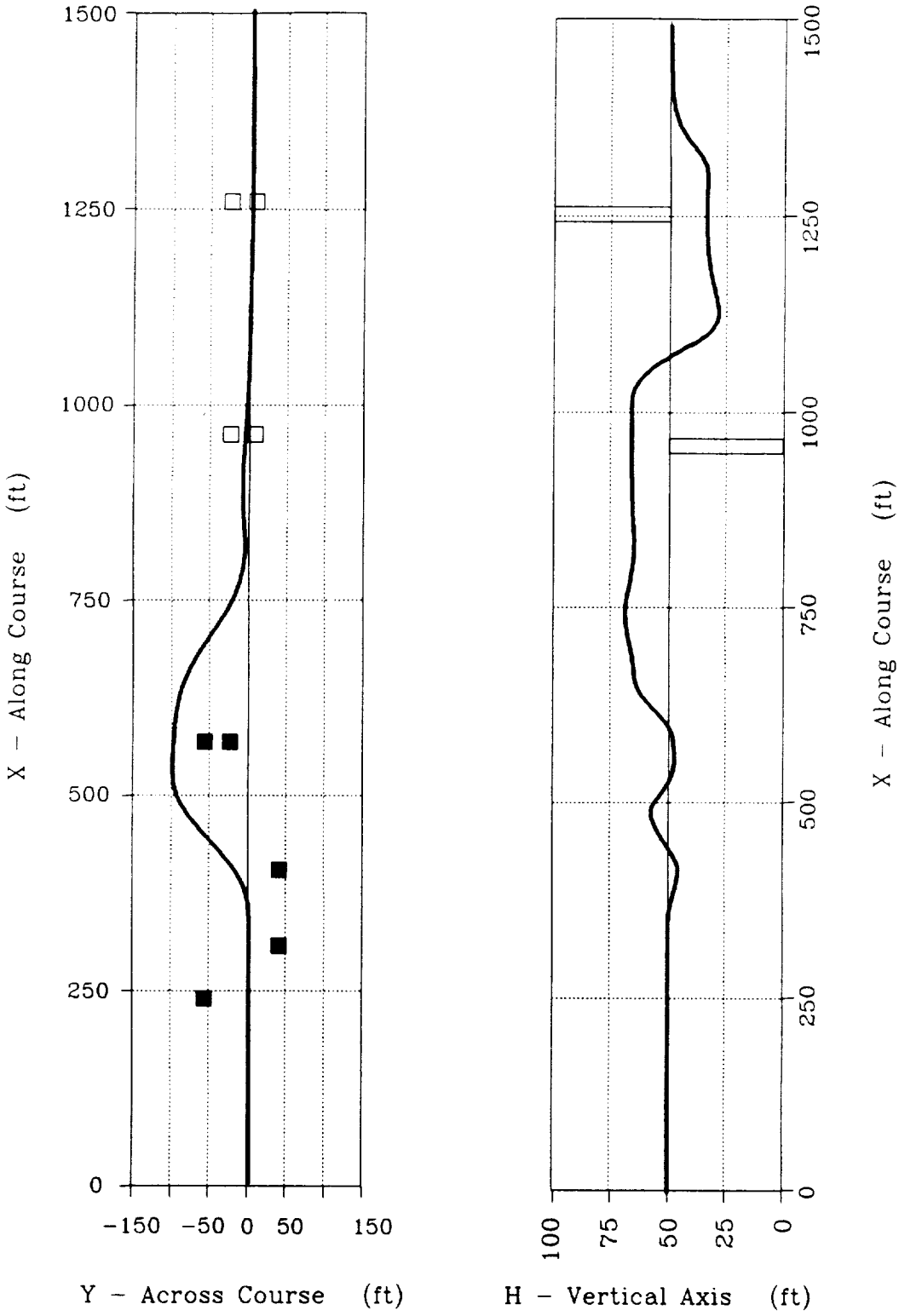

Figure 6. Independent lateral & vertical maneuvering

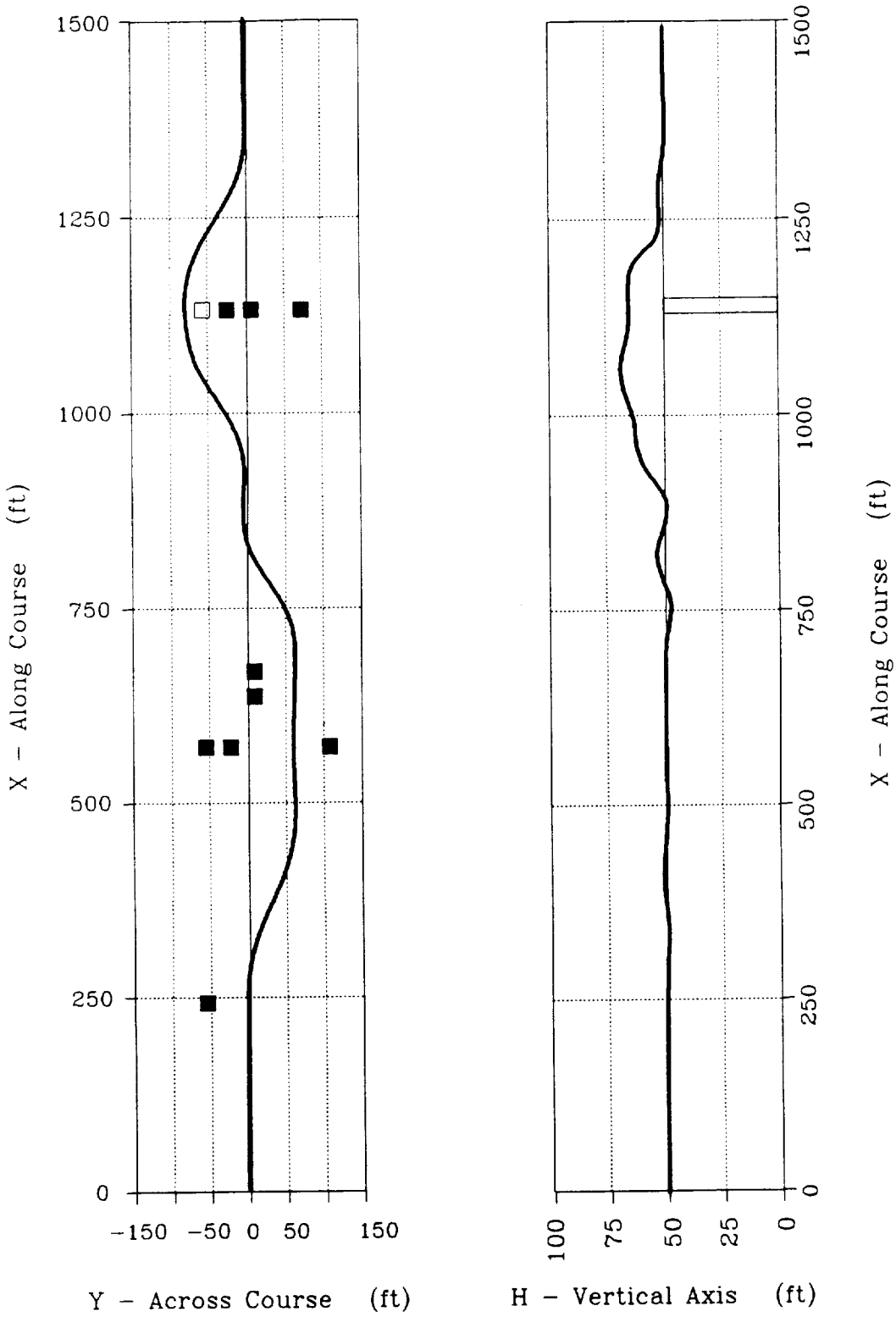

Figure 7. Coupled lateral & vertical maneuvering

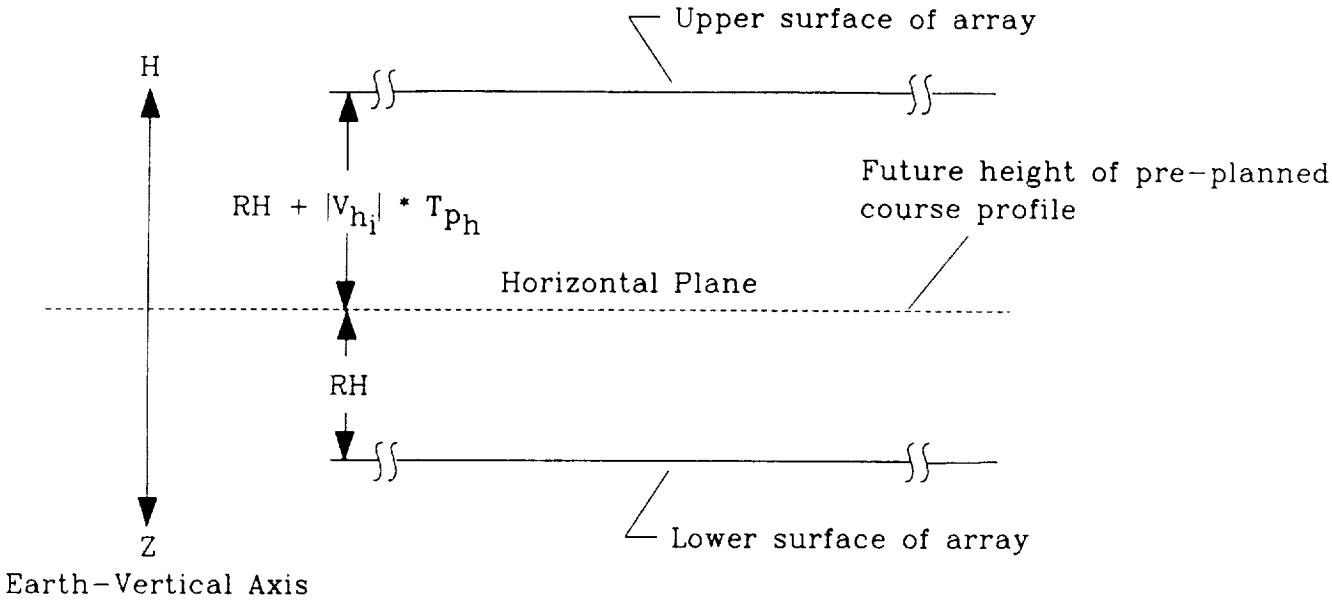

(1) Elevation of Anticipative Array, if Climbing ($V_{h_i} > 0$)

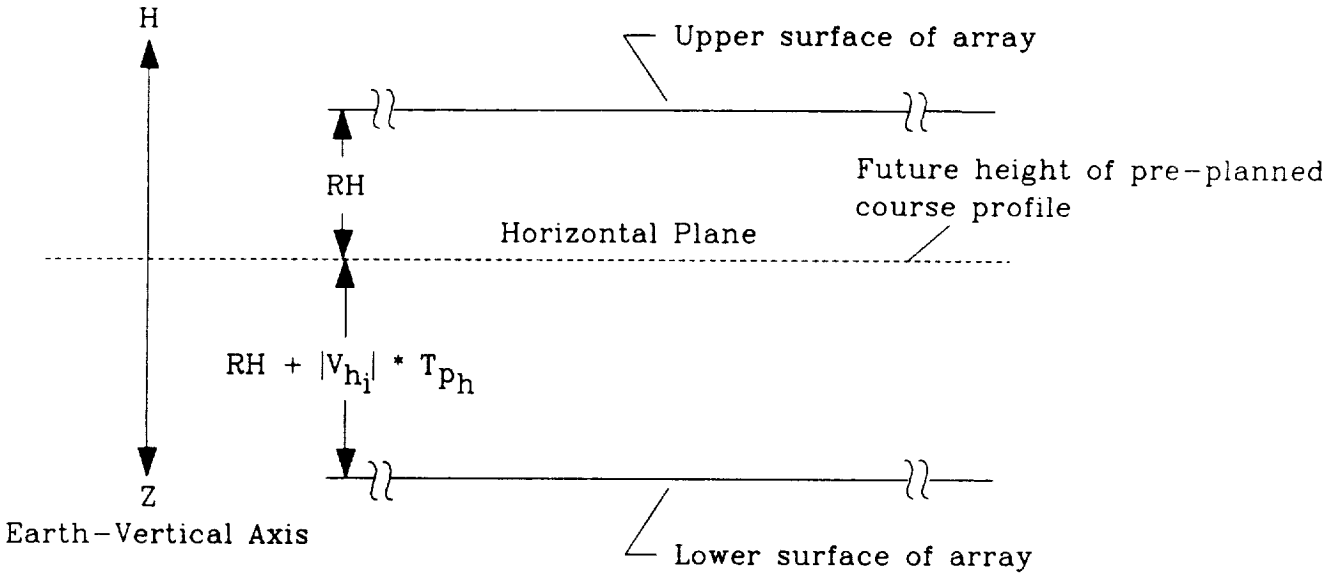

(2) Elevation of Anticipative Array, if Descending ($V_{h_i} < 0$)

Figure 8. Flight Plan with Safety Margin Envelope for Applying Sensed Data Base to Avoid Obstacles
Anticipative Geometry for Vertical Velocity Component

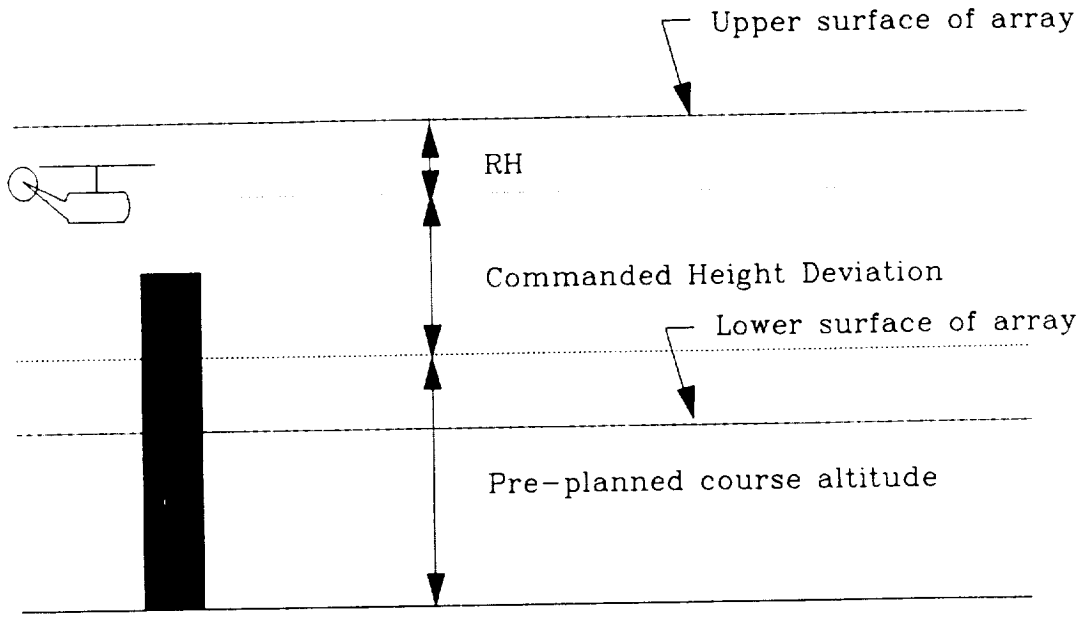

Figure 9. Positioning of Upper and Lower Surfaces of the Along-Course Anticipative Array with Currently Commanded Height Deviation

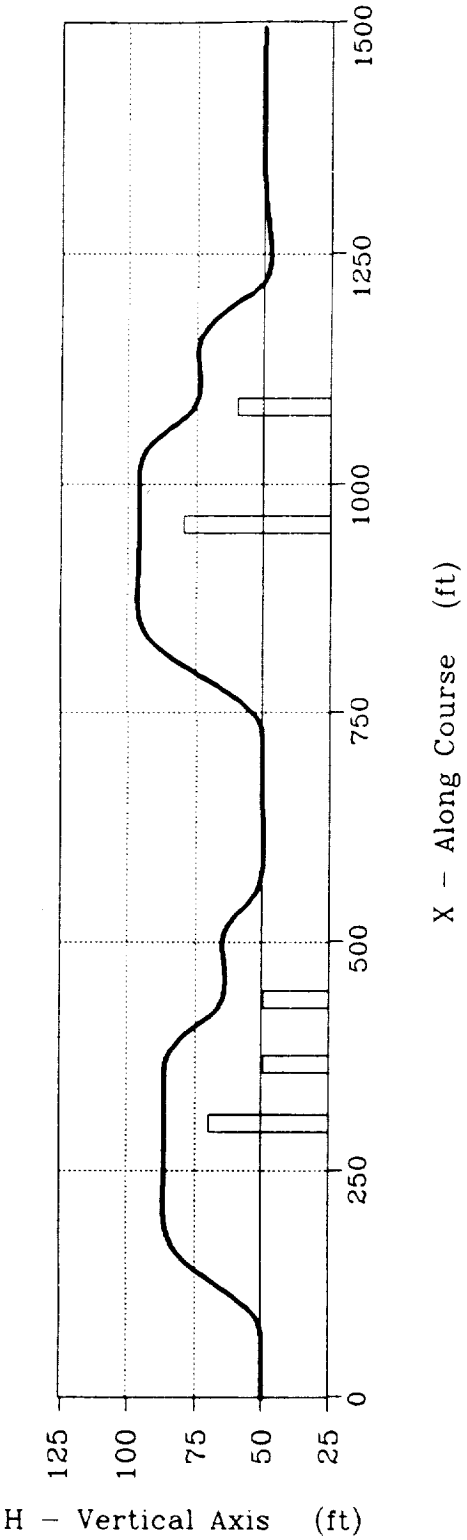

No obstacles completely obstruct flight path

(Vertical maneuvers will avoid obstacle without exposure to threats)

Planned course is ± 16.5 ft high centered on the vertical course coordinate, H = 50. ft

Figure 10. Obstacle avoidance using vertical maneuvering only

APPENDIX F

XFLOAT ARRAY DESIGNATION

XFLOAT array variable designations

Index	Name	Symbol	Units	Description
4	PHIR	ϕ	rad	
5	THETR	Θ	rad	Aircraft Euler angles.
6	PSIR	ψ	rad	
7	PHID	$\dot{\phi}$	rad/sec	
8	THED	$\dot{\Theta}$	rad/sec	Aircraft Euler angle rates.
9	PSID	$\dot{\psi}$	rad/sec	
16	T11		-	
17	T21		-	
18	T31		-	
19	T12		-	
20	T22	T_{ij}	-	Componants of the Local-to-Body axes transformation matrix.
21	T32		-	
22	T13		-	
23	T23		-	
24	T33		-	
37	PB	p	rad/sec	
38	QB	q	rad/sec	Body axis components of the aircraft angular velocity wrt inertial space.
39	RB	r	rad/sec	
52	PTURB	p_g	rad/sec	
53	QTURB	q_g	rad/sec	Body axis components of the equivalent angular velocity due to atmospheric turbulence.
54	RTURB	r_g	rad/sec	

XFLOAT array variable designations (Continued)

Index	Name	Symbol	Units	Description
55	PBD	p	rad/sec^2	
56	QBD	q	rad/sec^2	Body axis components of the angular acceleration wrt inertial space.
57	RBD	r	rad/sec^2	
58	UB	u_b	ft/sec	
59	VB	v_b	ft/sec	Body axis components of the aircraft wrt the air mass.
60	WB	w_b	ft/sec	
61	UTURB	u_g	ft/sec	
62	VTURB	v_g	ft/sec	Body axis components of linear velocity due to atmospheric turbulence.
63	WTURB	w_g	ft/sec	
64	VN	V_N	ft/sec	
65	VE	V_E	ft/sec	Local axis components of the aircraft velocity wrt inertial space.
66	VD	V_D	ft/sec	
80	ALTD	h	ft/sec	Altitude rate.
83	ALT	h	ft	Altitude.
97	G	g	ft/sec^2	Acceleration due to gravity.
122	XMC(3)		$\frac{1}{slug \cdot ft^2}$	
126	XMC(7)	(SAME)	$\frac{1}{slug \cdot ft^2}$	Moment of inertia coefficients used to calculate angular accelerations.
129	XMC(10)		$\frac{1}{slug \cdot ft^2}$	
130	XMASS	m	slug	Aircraft mass

XFLOAT array variable designations (Concluded)

Index	Name	Symbol	Units	Description
136	FAX		lb	
137	FAY	(SAME)	lb	Body axis components of aerodynamic forces.
138	FAZ		lb	
139	FEX		lb	
140	FEY	(SAME)	lb	Body axis components of the applied forces due to the engines.
141	FEZ		lb	
151	FG	FG	lb	Force due to gravity
155	TAL		ft-lb	
156	TAM	(SAME)	ft-lb	Body axis components of applied torque due to aerodynamic loads.
157	TAN		ft-lb	
158	TEL		ft-lb	
159	TEM	(SAME)	ft-lb	Body axis components of applies torque due to engines.
160	TEN		ft-lb	
168	DT2	dt	sec	Loop frame time
174	XCG	x_{EA}	ft	
175	YCG	y_{EA}	ft	Coordinates of the aircraft c.g. wrt the runway axis system.
176	HCG	h_{EA}	ft	
303	TIME	t	sec	Time from start of Operate.

APPENDIX G

TERRAIN APPROXIMATION SUBROUTINE, TERRN

```
      SUBROUTINE TERRAIN(XC,YC,XDCRS,YDCRS,XDDCRS,YDDCRS,
     1                   HXY,HDXY,HDDXY,N1)

C
c**********************************************************************
c
C     Compute approximate terrain elevation given
C        course coordinates adjusted such that the
C        lower left corner of the course is denoted
C        (XX,YY)=(0,0)
C     s.o. 1254-5  Nov. 1988    pjg
C
C**********************************************************************

C
      INCLUDE 'TERRN.CMN'
C
      DIMENSION A(100), B(100), DADY(100), DBDY(100)
      DIMENSION D2ADY2(100), D2BDY2(100)
C
      PI = 3.1415927
C
      XX = XC
      YY = YC + TYRUN/YRES/2.

C
C     Calculate approximate elevation

C
C     C-not term:
C
      C0T=XL0
      DO 562 J=1,MY
         WJ=2.*PI*J/TYRUN
         C0T=C0T+XJJ(J)*SIN(WJ*YY)+XKJ(J)*COS(WJ*YY)
562   CONTINUE

      C0T = C0T + (YY+1.)*XL1

C
C     C-1 term:
C
      C1T=P0
      DO 563 J=1,MY
         WJ=2.*PI*J/TYRUN
         C1T=C1T+XMM(J)*SIN(WJ*YY)+XNM(J)*COS(WJ*YY)
563   CONTINUE
```


PAGE 386 INTENTIONALLY BLANK

```
      C1T = C1T + (YY+1.)*P1

C
C     Ai and Bi terms:
C
      DO 565 I=1,MX
         WI=2.*PI*I/TXRUN
         ANGX=WI*XX
         A(I)=F0(I)
         B(I)=XI0(I)
         DO 570 J=1,MY
            WJ=2.*PI*J/TYRUN
            ANGY=WJ*YY
            SANGY=SIN(ANGY)
            CANGY=COS(ANGY)
            A(I)=A(I)+DIJ(I,J)*SANGY+EIJ(I,J)*CANGY
            B(I)=B(I)+GIJ(I,J)*SANGY+HIJ(I,J)*CANGY
570      CONTINUE

         A(I) = A(I) + (YY+1.)*F1(I)
         B(I) = B(I) + (YY+1.)*XI1(I)

565   CONTINUE
C

C
C     Approximate terrain elevation
C
      HXY = C0T
      DO 567 I=1,MX
         WI=2*PI*I/TXRUN
         HXY=HXY+A(I)*SIN(WI*XX)+B(I)*COS(WI*XX)
567   CONTINUE

      HXY = HXY + (XX+1.)*C1T

C
      IF (N1 .GT. 1) THEN
         HDXY  = 0.
         HDDXY = 0.
         RETURN
      ENDIF
C
C     Total derivatives of approximating surface coefficients
C     wrt across-course position
```

```
C
C     dC-not/dy term:
C
      DC0DY = XL1
      DO 620 J=1,MY
         WJ=2.*PI*J/TYRUN
         DC0DY=DC0DY+XJJ(J)*WJ*COS(WJ*YY)-XKJ(J)*WJ*SIN(WJ*YY)
620   CONTINUE

C
C     dC-1/dy term:
C
      DC1DY=P1
      DO 630 J=1,MY
         WJ=2.*PI*J/TYRUN
         DC1DY=DC1DY+XMM(J)*WJ*COS(WJ*YY)-XNM(J)*WJ*SIN(WJ*YY)
630   CONTINUE

C
C     dAi/dy and dBi/dy terms:
C
      DO 650 I=1,MX
         WI=2.*PI*I/TXRUN
         ANGX=WI*XX
         DADY(I)=F1(I)
         DBDY(I)=XI1(I)
         DO 640 J=1,MY
            WJ=2.*PI*J/TYRUN
            ANGY=WJ*YY
            SANGY=SIN(ANGY)
            CANGY=COS(ANGY)
            DADY(I)=DADY(I)+DIJ(I,J)*WJ*CANGY-EIJ(I,J)*WJ*SANGY
            DBDY(I)=DBDY(I)+GIJ(I,J)*WJ*CANGY-HIJ(I,J)*WJ*SANGY

640      CONTINUE
650   CONTINUE
C

C
C     d2C-not/dy2 term:
C
      DC0DY2=0.0
      DO 660 J=1,MY
         WJ=2.*PI*J/TYRUN
         DC0DY2=DC0DY2-WJ*WJ*(XJJ(J)*SIN(WJ*YY)+XKJ(J)*COS(WJ*YY))
660   CONTINUE
```

```
C
C     d2C-1/dy2 term:
C
      DC1DY2=0.0
      DO 670 J=1,MY
         WJ=2.*PI*J/TYRUN
         DC1DY2=DC1DY2-WJ*WJ*(XMM(J)*SIN(WJ*YY)+XNM(J)*COS(WJ*YY))
670   CONTINUE

C
C     d2Ai/dy2 and d2Bi/dy2 terms:
C
      DO 690 I=1,MX
         WI=2.*PI*I/TXRUN
         ANGX=WI*XX
         D2ADY2(I)=0.0
         D2BDY2(I)=0.0
         DO 680 J=1,MY
            WJ=2.*PI*J/TYRUN
            ANGY=WJ*YY
            SANGY=SIN(ANGY)
            CANGY=COS(ANGY)
            D2ADY2(I)=D2ADY2(I)-WJ*WJ*(DIJ(I,J)*SANGY+EIJ(I,J)*CANGY)
            D2BDY2(I)=D2BDY2(I)-WJ*WJ*(GIJ(I,J)*SANGY+HIJ(I,J)*CANGY)

680      CONTINUE
690   CONTINUE
C

C
C     Partial derivatives of terrain elevation
C
      DHDX = C1T
      DO 600 I=1,MX
         WI = 2*PI*I/TXRUN
         DHDX = DHDX+A(I)*WI*COS(WI*XX)-B(I)*WI*SIN(WI*XX)
600   CONTINUE

C
      D2HDX2 = 0.0
      DO 610 I=1,MX
         WI = 2*PI*I/TXRUN
         D2HDX2 = D2HDX2-A(I)*WI*WI*SIN(WI*XX)-B(I)*WI*WI*COS(WI*XX)
610   CONTINUE
```

```
C
      DHDY = DC0DY
      DO 700 I=1,MX
         WI=2*PI*I/TXRUN
         DHDY=DHDY+DADY(I)*SIN(WI*XX)+DBDY(I)*COS(WI*XX)
700   CONTINUE

      DHDY = DHDY + (XX+1.)*DC1DY

C
      D2HDXY = DC1DY
      DO 710 I=1,MX
         WI = 2*PI*I/TXRUN
         D2HDXY = D2HDXY+DADY(I)*WI*COS(WI*XX)-DBDY(I)*WI*SIN(WI*XX)
710   CONTINUE

C
      D2HDY2 = DC0DY2
      DO 720 I=1,MX
         WI=2*PI*I/TXRUN
         D2HDY2=D2HDY2+D2ADY2(I)*SIN(WI*XX)+D2BDY2(I)*COS(WI*XX)
720   CONTINUE

      D2HDY2 = D2HDY2 + (XX+1.)*DC1DY2

C
C     Total derivative of terrain elevation wrt time

C
      HDXY = DHDX*XDCRS + DHDY*YDCRS

C
      HDDXY = DHDX*XDDCRS + D2HDX2*XDCRS*XDCRS + 2*D2HDXY*XDCRS*YDCRS +
     1        D2HDY2*YDCRS*YDCRS + DHDY*YDDCRS

C
      RETURN
      END
```

APPENDIX H

COMPREHENSIVE INDEXED LIST OF SYMBOLS

The page number on which each symbol in this report appears is given in square brackets [] at the end of the symbol description. Numbers that are bold and underlined (i.e., [**123**]) indicate where the symbols are defined algebraically; numbers that are bold and double underlined (i.e., [**123**]) indicate where the symbols are defined numerically.

SYMBOL	DESCRIPTION
a	First exponential for the wind profile [93, 183, **184**, 219, 251, 293, 297, 327, 328, 329, 330, 331, 338]
$a(I_{wp})$	Hyperbolic transition parameter [88, 89, 90, **98**, 99, 126, 219]
a_{lat}	Lateral acceleration symbol position in the head-up display [**203**]
a_{lon}	Longitudinal acceleration caret position in the head-up display [196]
a_p	Integral-to-proportional gain ratio for the roll rate command [338]
a_y	Lateral acceleration [203]
a_1	Integral-to-proportional gain ratio for the vertical reference velocity [323]
A	Magnitude of the bob-up maneuver [243, 244, 245, 246, 251]
A_i	i^{th} element of the MX sine terms in a sum of sinusoids approximating a given terrain elevation profile [110, 111, 112, 323, **324**, **324**]
$A_i(y_{CRS})$	Continuous function in across-course position, y_{CRS}, approximating the NY discrete values in the i^{th} row of the matrix $\underline{A}$ [**356**, 358]
$A_{i_{Jy}}$	Coefficient of Fourier series representing the terrain profile [355]

A_x	Coordinate of the location of the acceleration symbol in the head-up display [**205**, 206]
A_y	Coordinate of the location of the acceleration symbol in the head-up display [**205**, 206]
A_z	Vertical acceleration (g) [256, 257, 258, 259, 260, 261, 263, 264, 265, 266, 269, 270]
A_1	Shaded area in Figs. 31 and 32 representing the specific time integrals of the roll rate [**292**, 293, **295**, 297]
A_2	Shaded area in Figs. 31 and 32 representing the specific time integrals of the roll rate [**292**, 293, **295**, 297]
$\underline{A}$	MX×NY matrix containing the coefficients of the MX sine terms in the NY sums of sinusoids estimating the terrain elevation profiles of the gaming area course [355, 356]
ABSALT	Absolute altimetry subroutine that analyzes the immediate vicinity of the rotorcraft to prevent any penetrations of the safety margin envelope by obstacles [134, 146, 149, 151, 158, 160, 161]
ANCHL	Counter for the number of obstructions in the left destination column in the prescribed rows of the anticipative array [**142**, **142**, 143, 157]
ANCHR	Counter for the number of obstructions in the right destination column in the prescribed rows of the anticipative array [**142**, **142**, 143, 157]
b	Second exponential for the wind profile [93, 183, **184**, 219, 293, 297, 327, 328, 329, 330, 331, 338]
$b(I_{wp})$	Hyperbolic transition parameter [88, 89, 90, **98**, 99, 126, 219]
B_i	i^{th} element of the MX cosine terms in a sum of sinusoids approximating a given terrain profile [110, 111, 112]
$B_i(y_{CRS})$	Continuous function in across-course position, y_{CRS}, approximating the NY discrete values in the ith row of the matrix $\underline{B}$ [**356**, 358]

$B_{i_{1y}}$	Coefficient of the Fourier series representing the terrain profile [355]
$\underline{B}$	MX×NY matrix containing the coefficients of the MX cosine terms in the NY sums of sinusoids estimating the terrain elevation profiles of the gaming area course [355, 356]
$BLND_{pg}$	Blended value of the pursuit feedforward guidance command [84, 90]
BO_A	Breakout in the roll force feel system [5]
BO_B	Breakout in the pitch force feel system [4]
BO_C	Breakout in the collective force feel system [13]
BO_P	Breakout in the yaw force feel system [18]
BU(s)	Laplace transform of the vector U of the independent variables premultiplied by its coefficient matrix B [243, 245]
$\underline{C}_0^t$	NY row vector containing the NY mean values for each sum of sinusoids estimating the terrain elevation profiles of the gaming area course [355, 356]
$\underline{C}_1^t$	NY row vector containing the NY trend values for each sum of sinusoids estimating the terrain elevation profiles of the gaming area course [355, 356]
c(s)	Control [250, 320, 362]
C_E	Compensatory error reduction control vector [250, 320, 362]
C_p	Pursuit feedforward guidance control vector [250, 320, 362]
$C_p(s)$	Laplace transform of the pursuit feedforward guidance control vector [321, 322]
C_{RR}	Evasive maneuver control vector [250, 320, 362]
C_0	Constant added to the sum of sinusoids approximating a given terrain elevation profile [110, 111, 112]
$C_0(y_{CRS})$	Continuous function of the across-course position, y_{CRS}, approximating the mean terrain elevation [356, 358]

$C_{0_{j_y}}$	Coefficient representing the mean terrain elevation in the j_yth strip of the gaming area course as a function of the along-course position, x_{CRS} [355]
C_1	Trend added to the sum of sinusoids approximating a given terrain elevation profile [110, 111, 112]
$C_1(y_{CRS})$	Continuous function of the across-course position, y_{CRS}, approximating the trend in terrain elevation [356, 358]
$C_{1_{j_y}}$	Coefficient representing the trend in terrain elevation in the j_yth strip of the gaming area course as a function of the along-course position, x_{CRS} [355]
C(s)	Resultant automatic guidance control vector [250, 320, 362]
d	Differential operator [111, 112, 327, 331, 332, 333, 358]
ds	Differential arc distance [330]
dt	Frame time of the digital computer (sec) [61, 70, 73, 79, 87, 88, 91, 238, 252, 281, 286, 292, 302, 306, 327, 331, 332, 333]
D_A	Damping in the roll force feel system [5]
D_B	Damping in the pitch force feel system [4]
D_C	Damping in the collective force feel system [13]
D_{ij}	The (i,j) element of the coefficient matrix $\underline{D}$ [109, 110, 111, 112, 356]
D_N	Range to the nearest waypoint [115, 115]
D_P	Damping in the yaw force feel system [18]
$\underline{D}$	MX x MY matrix containing the coefficients of the MY sine terms in each sum of sinusoid approximations of the MX rows in $\underline{A}$ [356]
D(s)	Independent disturbance vector [250, 320, 362]
DHMX	Maximum penetration from below of the vertical evasive maneuver decision section [147]

DHPL1	Previously identified maximum penetration from below into the left column of the vertical evasive maneuver decision section [148]
DHPLYL	Maximum penetration from below into the left column of the vertical evasive maneuver decision section [145, 146, 147, 148, 149, 157, 159]
DHPLYR	Maximum penetration from below into the right column of the vertical evasive maneuver decision section [145, 146, 147, 148, 149, 157, 159]
DHPR1	Previously identified maximum penetration from below into the right column of the vertical evasive maneuver decision section [148]
DISABL	Logical switch disabling the recapture of automatic guidance [103, 106, 119, 128]
DOBS(I,J)	Threat exposure height due to the detected obstacles and threats [136, 153, 164, 166, 170, 172, 172]
DZMX	Maximum penetration from above of the vertical evasive maneuver decision section [147]
DZPUYL	Maximum penetration from above into the left column of the vertical evasive maneuver decision section [145, 146, 147, 150, 151, 157, 160, 161]
DZPUYR	Maximum penetration from above into the right column of the vertical evasive maneuver decision section [145, 146, 147, 150, 151, 157, 160, 161]
DZYL1	Penetrating obstruction identified from DZPUYL [150]
DZYR2	Penetrating obstruction identified from DZPUYR [150]
e	Error in the subcritical tracking task [237, 238, 251]
e_c	Position error criterion for the one-way switch of the rate of change of the magnitude of the unstable pole for the critical task tester [238, 239]
e_{max}	Maximum displayed value of e for the critical task tester [238, 239]

e_0	Initial position error for the critical task tester and subcritical tracking task [238, **239**]
$e(s)$	System error [**322**]
$\bar{e}(s)$	System error vector [321]
E	Error vector [250, 320, 362]
E_{ij}	The (i,j) element of the coefficient matrix $\underline{E}$ [109, 110, 111, 112, 356]
$\underline{E}$	MX×MY matrix containing the coefficients of the MY cosine terms in each sum of sinusoid approximations of the MX rows in $\underline{A}$ [356]
$\underline{f}_0^t$	MX row vector containing the NY mean values for each of the MX rows in $\underline{A}$ [356]
$\underline{f}_1^t$	MX row vector containing the NY trends values for each of the MX rows in $\underline{A}$ [356]
F_A	Friction in the roll force feel system [**5**]
F_{A_p}	Pilot's lateral force on the cyclic controller [2, **5**]
F_E	Friction in the pitch force feel system [**4**]
F_{E_p}	Pilot's longitudinal force on the cyclic controller [2, **4**]
F_C	Friction in the collective force feel system; the controlled element transfer function [**13**, 250, 320, 362]
F_{C_p}	Pilot's force on the collective controller [2, **13**]
F_d	Disturbance transfer function [250, 320, 362]
F_F	Friction in the yaw force feel system [**18**]
F_{F_p}	Pilot's force on the pedal controllers [2, **18**]
F_{0_i}	The i^{th} element in the coefficient matrix $\underline{f}_0^t$ [109, 110, 356]
F_{1_i}	The i^{th} element in the coefficient matrix $\underline{f}_1^t$ [109, 110, 111, 356]

FP_x	x coordinates of the flight path symbol in the head-up display [193, 194]
FP_y	y coordinates of the flight path symbol in the head-up display [193, 194]
FAX	Aerodynamic force in the body x-direction [2, 181]
FAY	Aerodynamic force in the body y-direction [2, 181]
FAZ	Aerodynamic force in the body z-direction [2, 181]
FEX	Engine force in the body x-direction [2]
FEY	Engine force in the body y-direction [2]
FEZ	Engine force in the body z-direction [2, 14]
FG	Weight of the rotorcraft (lb) [14]
FT2DM	Feet to decameters transformation (dm/ft) [104, 108]
g	Gravitational acceleration [35, 36, 37, 49, 50, 70, 73, 76, 243, 245, 255, 280, 286, 287, 288, 290, 291, 292, 294, 295, 296, 298, 306, 307, 326, 328, 334]
g(e)	Time-optimal "bang-bang" switching criterion for vertical maneuvers [251]
g'	Gravitational acceleration in body axis z-direction [243, 244, 245, 246]
G_A	Gradient in the roll force feel system [5]
G_B	Gradient in the pitch force feel system [4]
G_C	Gradient in the collective force feel system [13]
G_{ij}	The (i,j) element in the coefficient matrix $\underline{G}$ [109, 110, 111, 112, 356]
G_p	Roll rate feedback transfer function [18, 300]
G_P	Gradient in the yaw force feel system [18]
G_q	Pitch rate feedback transfer function [305]

G_U	Longitudinal velocity feedback transfer function [305]
G_v	Lateral velocity feedback transfer function [300]
G_x	x coordinates of the ghost aircraft symbol in the head-up display [**194**, 195, 305]
G_y	y coordinates of the ghost aircraft symbol in the head-up display [**194**, 195, 300]
G_θ	Pitch attitude feedback transfer function [305]
G_ϕ	Roll attitude feedback transfer function [300]
$G(s)$	Control compensation [322, 323]
$\overline{G}_1(s)$	Compensatory control matrix [321]
h	Altitude (ft) [3, 87, 110, 111, 112, 183, 245, 246, 251, 256, 257, 258, 259, 260, 261, 263, 264, 265, 266, 267, 269, 270, 323, 325, 357]
h_{ALT_c}	Commanded radar altitude (ft) [87, **99**, 112, 120, 135, **162**]; Pre-planned course altitude [168]
h_c	Odds that the choice reaction time test lights will illuminate in a given time interval [3, **57**, **234**, 235, 245, 246, **267**]; Commanded altitude [**323**, 325]
$h_{c_{AUD}}$	Future vertical offset audio command [228, 231]
$h_{c_{auto}}$	Automatic guidance altitude command (based on approximate terrain surface) [2, 15, 110, **112**, 194, 207]
h_{cg}	Height of the rotorcraft center of gravity [14, 15, 16, 194, 207]
h_{com}	Vertical offset command [2, 54, 55, 57, **87**, 133, **134**, 135, **146**, **146**, 147, 148, **149**, 150, **151**, **152**]; Commanded height deviation in the head-up display [168, 194, 207]
h^p_{com}	Previous altitude offset command [54, **55**]
h_{com_2}	Vertical offset destination command [**87**, **87**, 134, **146**, **149**, **151**, 158]

h_{com_a}	Upward vertical offset command from absolute altimetry [134, 146, 149, 151, 163, **165**, **165**]
$h_{com_{tmp}}$	Vertical offset command upon arrival at and departure from an aggressive maneuver waypoint [**87**]
h_{com_y}	Proposed upward vertical offset command [149]
h_{com_l}	Vertical offset command upon entering the obstacle detection and avoidance maneuver selection logic
h_e	Altitude error (ft) [252, 253, 268]
h_{e_T}	Altitude error switching criteria for constrained time-optimal vertical maneuvers [253, 268]
h_{ea}	Vertical offset switching criterion [55]
h_{err}	Altitude error (ft) [325]
h_{err_l}	Initial altitude error [55, 58, 59]
h_E	Elevation of the terrain [**323**]
$h_E(x,y)$	The elevation of the terrain at point (x,y) [323]
$h_{j_y}(x_{CRS})$	Approximation of the terrain profile for the j_y^{th} strip of the gaming area course as a function of the along-course position, x_{CRS} [**355**]
h_m	Model altitude for model following aggressive maneuvering [15, 54, 55, **57**, 75, **76**]
h_m^p	Previous vertical maneuver model altitude [**55**, 75, 76]
h_{min}	A constant depicting the desired altitude above the ground [323]
$h_{mum}(I_{AMC})$	Absolute height of the unmask bob-up maneuver [82, 87, 94, 97, **120**]
$h_{obs}(I_{obs})$	Height of obstacles in defined obstacle array [133, 163, 170]
$h_{obs}(I_{obs(ll)})$	Height of the obstacle identified by the index in ( ) [172]
h_{R_P}	Nonlinear collective gain [3]

h_s Odds that a letter for the Sternburg recognitive side task will illuminate in a given time interval [236]

h_{tr} Tree canopy height (average, ft) [183, **184**]

$h(x_{CRS}, y_{CRS})$ Final expression for the terrain elevation as a function of both along- and across-course position [**356**, 358]

$\dot{h}$ Vertical velocity (ft/sec) [3, 111, 112, 245, 246, 252, 253, 254, 256, 257, 258, 259, 260, 261, 263, 264, 265, 266, 267, 268, 269, 270]

$\dot{h}_c$ Vertical velocity command (ft/sec) [14, 16, **56**, **57**, 58, 245, 246, 323, **324**, **324**]

$\dot{h}_c^{TO}$ Vertical velocity command for the model, following aggressive maneuvering [54, **58**, 75, 76]

$\dot{h}_E$ Effective time rate of change of terrain elevation (ft/sec) [**324**]

$\dot{h}_{HUD}$ Vertical velocity command displayed in the head-up display [209]

$\dot{h}_m$ Model vertical velocity for the model following aggressive maneuvering [54, 55, **57**, 75, **76**]

$\dot{h}_m^P$ Previous vertical maneuver model velocity [**55**, 75, 76]

$\dot{h}_{max}$ Upward vertical velocity limit (ft/sec) [53, **55**, 56, 61, 252, 253, **255**, *314*]]

$\dot{h}_{MAX}$ Maximum vertical velocity (ft/sec) [268]

$\dot{h}_{min}$ Downward vertical velocity limit (ft/sec) [**55**]

$\dot{h}_{MIN}$ Minimum vertical velocity (ft/sec) [268]

$\dot{h}_{\theta r1}$ Intermediate vertical velocity function used in calculating the altitude offset switching criterion for the constrained time optimal bob-up and -down maneuver [**59**]

$\dot{h}_{\theta r2}$ Intermediate vertical velocity function used in calculating the altitude offset switching criterion for the constrained time optimal bob-up and -down maneuver [**59**, 60]

$\dot{h}_{or3}$ Intermediate vertical velocity function used in calculating the altitude offset switching criterion for the constrained time optimal bob-up and -down maneuver [60]

$\dot{h}_{or4}$ Intermediate vertical velocity function used in calculating the altitude offset switching criterion for the constrained time optimal bob-up and -down maneuver [60, 61]

$\dot{h}_{pg}$ Vertical velocity pursuit feedforward guidance command [2, 15, 110, 112, 194]

$\dot{h}_{ref}$ Vertical reference velocity [15, 251, 252, 254, 267, 323]

$\dot{h}_{ref\,max}$ Maximum value of the vertical reference velocity [251]

$\dot{h}_{R_{auto}}$ Effective vertical reference velocity from the automatic guidance [13, 16]

$\dot{h}_{R_p}$ Vertical velocity reference supplied by the pilot's supervisory override option [14]

$\dot{h}_{T_z}$ Vertical velocity switching criterion for the bob-up and -down maneuver [253, 268]

$\dot{h}_{\tau_1}$ Vertical velocity switching criterion for the bob-up and -down maneuver [253, 268]

$\dot{h}(x_{CRS}, y_{CRS})$ First derivative of terrain elevation for the pursuit guidance algorithm [358]

$\dot{h}_1$ Intermediate vertical velocity function used in calculating the vertical velocity switching criterion for the contrained time-optimal bob-up and -down maneuver [55, 56, 57, 59]

$\ddot{h}$ Vertical acceleration (ft/sec^2) [111, 112, 252, 253, 254, 268]

$\ddot{h}_c$ Vertical acceleration command (ft/sec^2) [56, 56, 57, 57, 58, 58, 252, 253, 254, 268, 323, 324]

$\ddot{h}_c^{TO}$ Vertical acceleration command for the model following aggressive maneuvering [54, 58, 75, 76]

$\ddot{h}_{c\,max}$ Maximum vertical acceleration command (ft/sec^2) [252]

$\ddot{h}_E$ Effective time rate of change of $\dot{h}_E$ (ft/sec^2) [324]

$\ddot{h}_m$ Vertical model acceleration [15, 54, 55, 57, 75, 76]

$\ddot{h}_m^p$ Previous vertical maneuver model acceleration [55, 76]

$\ddot{h}_{max}$ Maximum upward vertical acceleration (ft/sec^2) [53, 55, 56, 58, 252, 253, 255, 314]

$\ddot{h}_{min}$ Maximum downward vertical acceleration (ft/sec^2) [55, 57, 58, 59, 60, 253, 255, 268]

$\ddot{h}_{or1}$ Intermediate vertical acceleration function used in calculating the altitude offset switching criterion for the constrained time-optimal bob-up and -down maneuver [59]

$\ddot{h}_{or2}$ Intermediate vertical acceleration function used in calculating the altitude offset switching criterion for the constrained time-optimal bob-up and -down maneuver [60]

$\ddot{h}_{or3}$ Intermediate vertical acceleration function used in calculating the altitude offset switching criterion for the constrained time-optimal bob-up and -down maneuver [60]

$\ddot{h}_{or4}$ Intermediate vertical acceleration function used in calculating altitude offset switching criterion for the constrained time-optimal bob-up and -down maneuver [61]

$\ddot{h}_{pg}$ Vertical acceleration pursuit feedforward guidance command [2, 15, 110, 112, 194]

$\ddot{h}_{tr}$ Vertical acceleration threshold [56, 57, 58, 61]

$\ddot{h}_1$ Intermediate vertical acceleration function used in calculating the vertical velocity and altitude offset switching criterion for the constrained time-optimal bob-up and -down maneuver [55, 59, 61, 62]

$\ddot{h}(x_{CRS}, y_{CRS})$ Second derivative for the pursuit guidance algorithm [358]

$\dddot{h}_c$ Commanded vertical jerk (acceleration rate) [56, 56, 57, 57, 58, 252, 253, 253, 268, 268]

$\dddot{h}_{cr1}$ Intermediate jerk function used in calculating the altitude offset switching criterion for the constrained time-optimal bob-up and -down maneuver [59]

$\dddot{h}_{cr2}$ Intermediate jerk function used in calculating the altitude offset switching criterion for the constrained time-optimal bob-up and -down maneuver [60]

$\dddot{h}_{cr3}$ Intermediate jerk function used in calculating the altitude offset switching criterion for the constrained time-optimal bob-up and -down maneuver [60]

$\dddot{h}_{cr4}$ Intermediate jerk function used in calculating the altitude offset switching criterion for the constrained time-optimal bob-up and -down maneuver [60, 61]

$\dddot{h}_{max}$ Maximum vertical jerk [55, 56, 57, 59, 60, 62, 252, 253, 255, 268, 314]

$\dddot{h}_{min}$ Minimum vertical jerk [55, 56, 57, 59, 60, 61, 253, 255, 268]

h'_{cAUD} Past value of the audio annunciator vertical offset command [228]

h'_{com} Vertical offset command upon entering the obstacle detection and avoidance maneuver selection logic; past value of the vertical offset command [135, 152, 228]

h'_{tr} Modified tree canopy height for estimating the wind velocity profile in the surface boundary layer [183]

$\dot{h}'_c$ Effective vertical velocity command [15, 16, 245]

$\ddot{h}'_{mn}$ Intermediate vertical acceleration function used in calculating the altitude offset switching criterion for the constrained time-optimal bob-up and -down maneuver [59, 60, 61]

H Height expressed in an earth vertical axis coordinate (ft) [163, 365, 372, 373, 375, 377]

H_{ij} The (i,j) element in the coefficient matrix $\underline{H}$ [109, 110, 111, 112, 356]

H_x Coordinate of the location of the hover location symbol in the head-up display [206, 207]

H_y Coordinate of the location of the hover location symbol in the head-up display [206, 207]

H_v	Angular orientation of the hover location symbol in the head-up display [206, 207]
H3DMN	Positive vertical acceleration rate limit (ft/sec^3) [55, 61, **63**]
H3DMX	Negative vertical acceleration rate limit (ft/sec^3) [55, **63**]
HCOMAX	Maximum penetration of the safety margin envelope from above [**164**, **164**, **165**]
HDDMN	Positive vertical acceleration limit (ft/sec^2) [55, **63**]
HDDMX	Negative vertical acceleration limit (ft/sec^2) [55, **63**]
HDMN	Positive vertical velocity limit (ft/sec) [55, **63**]
HDMX	Negative vertical velocity limit (ft/sec) [55, **63**]
HDSWT	Vertical velocity switching criterion [56, 57, **61**, **62**]
HEFL	Defines the vertical location of the lower surface of the along-course anticipative array [**135**, 145, 153, 164, 167, 168, 174, 175]
HEFU	Defines the vertical location of the upper surface of the along-course anticipative array [**135**, 145, 150, 153, 164, 167, 168, 174, 175]
HEXA(I,J)	Threat exposure height in the (i,j) cell of the absolute altimetry array [**164**, 173]
HEXY(I,J)	Threat exposure height in the (i,j) cell of the along-course anticipative array [**136**, 172, 173]
HLA(I,J)	Lower navigable boundary of the (i,j) cell of the absolute altimetry array [**164**, 166]
HL2DY	Identification of obstructions of the along-course anticipative array [139, 141, 142]
HL2DY(I,J)	Identification of obstructions in the (i,j) cell of the along-course anticipative array [**136**, 137]
HLDY(J)	Identification of obstructions in the j^{th} column of the along-course anticipative array [**137**, 371]

HLDY(J_{com})	Identification of obstructions in the destination column J_{com} of the along-course anticipative array [138, 143]
HLDY($J_{com}+1$)	Identification of obstructions in the destination column $J_{com}+1$ of the along-course anticipative array [138, 143, 143]
HLDY(LL)	Identification of obstructions in the destination column LL of the along-course anticipative array [140]
HLY(I,J)	Lower navigable boundary of the (i,j) cell of the along-course anticipative array [136, 154, 174]
HLY(II,JJ)	Lower navigable height boundary identified by the indices in ( ) [175]
HLY(II,4)	Lower navigable height boundary identified by the indices in ( ) [175]
HLY(I,J_{com})	Lower navigable height boundary identified by the indices in ( ) [145]
HLY(R,M)	Lower navigable height boundary identified by the indices in ( ) [367]
HLY(T_{IND},J_{com})	Lower navigable height boundary identified by the indices in ( ) [150]
HLY(U_{IND},J_{com})	Lower navigable height boundary identified by the indices in ( ) [150]
HOVR	Logical flag enabling the automatic position hold [2, 8, 9, 82, 86, 87, 91]
HTA(I,J)	Terrain height in the (i,j) cell of the absolute altimetry array [164, 173]
HTH	Maximum allowable penetration into the anticipative array (ft) [146, 147, 157, 162]
HTOBS(I,J)	Adjusted passable height [136, 153, 164, 166, 170, 172, 172]
HTSW	Altitude offset switching criterion that initiates the deceleration phase of the maneuver [55, 59, 61]
$HTSW_1$	Altitude offset switching criterion for initiating the deceleration phase of the bob-up or -down maneuver [59]

$HTSW_2$	Altitude offset switching criterion for initiating the deceleration phase of the bob-up or -down maneuver [60]
$HTSW_3$	Altitude offset switching criterion for initiating the deceleration phase of the bob-up or -down maneuver [60, 60]
$HTSW_4$	Altitude offset switching criterion for initiating the deceleration phase of the bob-up or -down maneuver [61]
HTY(I,J)	Terrain height in the (i,j) cell of the along-course anticipative array [136, 172, 173]
HUA(I,J)	Upper navigable boundary of the (i,j) cell of the absolute altimetry array [164, 166]
HUY(I,J)	Upper navigable boundary of the (i,j) cell of the along-course anticipative array [136, 154, 174]
HUY(II,JJ)	Upper navigable height boundaries identified by the indices in ( ) [175]
HUY(II,4)	Altitude offset switching criterion for initiating the deceleration phase of the bob-up or -down maneuver [175]
$HUY(I,J_{com})$	Altitude offset switching criterion for initiating the deceleration phase of the bob-up or -down maneuver [145]
$HUY(Q_{IND},J_{com})$	Altitude offset switching criterion for initiating the deceleration phase of the bob-up or -down maneuver [148]
HUY(R,M)	Altitude offset switching criterion for initiating the deceleration phase of the bob-up or -down maneuver [367]
$HUY(S_{IND},J_{com})$	Altitude offset switching criterion for initiating the deceleration phase of the bob-up or -down maneuver [148]
i	Index [109, 110, 111, 323, 324, 353, 355, 356, 358]
i_x	Index of points within a gaming area course terrain elevation profile [355]
I	Row index integer in the along-course anticipative array of the sensed obstacles [115, 136, 137, 145, 164, 164, 167, 170, 171, 173, 367]; identity matrix [243, 244, 245, 246]
I_A	Two-axis trim button on the cyclic stick in the roll force feel system [5, 164, 166]

I_{AMC}	Aggressive maneuver counter [87, 120, 120]
I_B	Two-axis trim button on the cyclic stick in the pitch force feel system [4]
I_{cp}	Course point index [101, 104, 107, 107]
I_{CRS}	Gaming area course index [351]
I_{obs}(INTO)	Index of the identified obstacle in the obstacle array [171]
I_{wp}	Waypoint counter for automatic guidance [2, 82, 84, 87, 90, 95, 95, 96, 96, 114, 115, 115, 116, 119, 119, 120, 120, 121, 126, 129, 206, 218, 218, 226]
I_{O_i}	The i^{th} element in the coefficient vector $\underline{i}_O^t$ [109, 110, 356]
I_{I_i}	The i^{th} element in the coefficient vector $\underline{i}_I^t$ [109, 110, 111, 356]
I1	Obstacle array counter for vertical situation analysis [144, 144, 145]
I2	Obstacle array counter for vertical situation analysis [144, 145]
IAMOW(I_{AMC})	Aggressive maneuver station tags in the automatic guidance recapture logic [83, 88, 114]
IAMOW(I_{wp})	Station tag for aggressive maneuvering at waypoint index in ( ) [83, 88, 94, 96, 119, 120, 121, 229]
IAMOW(N)	Aggressive maneuver station tag in the automatic guidance recapture logic [120]
IAMFG	Aggressive maneuver flag [86, 86, 87, 91, 134, 226, 229, 231]
IAZCFG	Vertical acceleration command flag [54, 55, 56, 57, 75, 76]
ICHC	Index counter for checking the destination path in Section 2 Fig. 4.3 of the obstacle detection and avoidance maneuver selection logic [142]
ICHK	Flag controlling check for return to the nominal flight path following the lateral evasive maneuver [138, 138, 154]

ICHKM	Index corresponding to the row number in the current anticipative array coinciding with the location of the first row of the anticipative array following the completion of the evasive maneuver immediately preceding the area defined as Section 1 in Fig. 4.6 [142, **156**, 157]
ICHKN	Index corresponding to the row number in the current anticipative array coinciding with the location of the first row of the anticipative array following the completion of the evasive maneuver [142, **156**]
IDYST	Maneuver check flag [**139**, **155**, 174, **175**, *175*]
IFTOH	Vertical evasive maneuver flag [54, **55**, **57**, **58**, **59**]
IFTOPS	Directional evasive maneuver flag [64, **65**, **66**]
IFTOX	Longitudinal evasive maneuver flag [**9**, 42, 43, **44**, **46**, **47**, 48, **230**]
IFTOY	Lateral evasive maneuver flag [2, 26, **27**, **33**, **34**, **35**, **134**, 231]
IHDCFG	Vertical velocity command flag [54, **55**, **56**, **57**, 61, 75, **76**]
IHSWFG	Control flag for calculating $HTSW_n$ [55, **57**]
II	Along-course index [**171**, **171**, **172**, **172**, **175**, **175**, 176, **177**, **178**, **179**, **180**]
INCAP	Initial capture flag [**115**, 122]
INTO	Number of obstacles resident in a given cell of the along-course anticipative array [**171**, 172, 173]
IPCFG	Roll rate command flag [26, **27**, **30**, **31**, **32**, **33**, 69, **70**]
IPHCFG	Roll attitude command flag [26, **27**, **28**, **29**, **30**, **31**, **32**, **33**, 35, 36, 37, 69, **70**]
IPHTFG	Intermediate flag used in calculating the switching criteria for the lateral constrained time-optimal maneuvers [**27**, **28**, **30**, **33**, 35, 37]
IPSWFG	Intermediate flag used in calculating the switching criteria for the constrained time-optimal pedal turn [**65**]

IQCFG	Pitch rate command flag [42, **44**, **45**, **46**, 72, **73**]
IRESUM	Nominal velocity resumption flag [2, 42, **43**, 48, 82, **84**, **87**, 90, 226, **229**, **230**]
IRGNY	Counter in the lateral constrained time-optimal maneuver [**30**, **31**, **32**, **33**, **36**, **37**]
IRMP	Number of time intervals through which $\dot{\gamma}_{c_{pg}}$ is ramped up in preparation of a hyperbolic trajectory [83, **88**]
ITHCFG	Pitch attitude command flag [42, **44**, **45**, **46**, 50, 72, **73**]
ITRN	Intermediate flag used in the waypoint sequencing logic [83, **84**]
IUAUD	Longitudinal audio flag [**229**, **230**, 232]
IUMFSW	Longitudinal model following switch [8, **9**]
IUSWFG	An intermediate control flag in the longitudinal constrained time-optimal maneuver [**44**, **46**, 50]
IUTWP	Intermediate flag used in initiating the constrained time-optimal speed change [**43**, 48]
IVLFGY	Velocity switch in the lateral constrained time-optimal maneuver [**27**, **31**, **33**, 35, 38]
IVTSWF	Velocity switch in the lateral constrained time-optimal maneuver [**27**, **28**, **29**, **31**, **33**, 35, 36]
IVTSWO	Intermediate control flag in the lateral constrained time-optimal maneuver [**27**, **33**, 35]
IYAUD	Lateral audio flag [**227**, **228**, 231]
IYDCFG	Lateral velocity command flag [26, **27**, **31**, **32**, **33**, 37, 69, **70**]
IYDES	Return to nominal course flag [**138**, **139**, **142**, **143**, 154]
IYTSWF	Intermediate control flag in the lateral constrained time-optimal maneuver [**27**, 28, **32**, **33**]
j	Across-course index used in approximating the terrain profile [**109**, **110**, **111**, **112**, 356]

j_y	Index of gaming area course terrain elevation profiles [355]
J	Column index integer in the along-course anticipative array of sensed obstacles [136, 136, 137, 137, 155, 164, 167, 169, 170, 171, 367, 371]
J_{com}	Column index integer in the along-course anticipative array of sensed obstacles determined by the lateral destination command [138, 138, 140, 142, 144, 146, 149, 151, 154, 155, 156, 169, 174, 176, 177, 178, 179, 180]
J_{CRS}	Width index of the gaming area course [351]
J_j	The j^{th} column in the coefficient matrix J [109, 110, 112, 356]
JJ	Across-course index used in the obstacle detection and avoidance maneuver selection logic [175, 176, 177, 178, 179, 180]
K	Controlled element gain [267, 279, 281]
$K_{a_{lon}}$	Longitudinal acceleration display scaling gain (deg/ft/sec^2) [196, 210]
K_A	Lateral cyclic trim integrator gain (in/sec) [5]
K_B	Longitudinal cyclic trim integrator gain (in/sec) [4]
K_c	Controlled element gain [23, 251, 322, 323]
K_{F_θ}	Pitch attitude washout gain (HUD) (ft/sec/rad) [195, 210)
K_h	Vertical position error gain (1/sec^2) [14, 15, 16, 17, 194, 245, 246]
K_{h_c}	Height command gain for rotorcraft control (1/sec) [245, 246]
$K_{h_{HUD}}$	Height error display scaling gain (deg/ft) [207, 210]
$K_{\dot{h}_c}$	Vertical velocity gain (1/sec) [14, 15, 16, 17, 194, 245, 246]
$K_{\dot{h}_{HUD}}$	Vertical velocity display scaling gain (deg/fpm or deg/fps) [193, 194, 210]

K_{h_r} Vertical velocity display scale factor for the head-up display [207, 208]

K_{hv} Plan view displacement display scaling gain (deg/ft) [206, **210**]

K_{hvx} Position error feedback gain (1/sec) [86, 96, **99**, 119, 232]

K_j The j^{th} column of the coefficient matrix $\underline{K}$ [109, 110, 112, 356]

K_{LA} Lateral acceleration display scaling gain (deg/g) [203, **210**]

K_p Compensatory proportional gain (1/sec) for the roll rate command [338]

K_{pgh} Vertical pursuit guidance model gain (dimensionless) [15, **17**, 23, 194]

K_{pgp} Directional pursuit guidance model gain (dimensionless) [20, **22**, 23]

K_{pgy} Lateral pursuit guidance model gain (ft/rad) [8, 10, **12**, 23, 194]

K_{p_m} Lateral model roll rate feedforward gain (1/sec) [8, 10, **12**]

K_{q_m} Longitudinal model pitch rate feedforward gain (1/sec) [8, **12**]

K_{sc} Plan view velocity display scaling gain (deg/ft/sec) [204, 205, **210**]; Sub-critical tracking task gain [237, 238, **239**]

K_{sx} Velocity display scaling gain (deg/ft/sec); Sub-critical tracking task gain [**202**]

K_{u_c} Longitudinal velocity command gain (rad/ft·sec) [6, 8, 10, **11**, 245, 246]

K_{UERR} Longitudinal velocity error display scaling gain (deg/kt) [195, **210**]

K_{u_m} Longitudinal model velocity feedforward gain (rad/ft·sec) [8, 10, **12**]

K_{v_c} Lateral velocity command gain (rad/ft·sec) [6, 8, 10, **11**, 194, 243, 244]

$K_{v_{HUD}}$ Lateral velocity display scaling gain (FPS or deg/ft/sec) [193, 194, **210**]

K_{v_m} Lateral model velocity feedforward gain (rad/ft·sec) [8, 10, **12**]

K_x Longitudinal position error gain (rad/ft·sec^2) [6, 8, 10, **11**, 245, 246]

K_{x_c} Longitudinal displacement command gain for rotorcraft control (1/sec) [245, 246]

K'_{x_c} Normalized longitudinal position command gain (dimensionless) [6, 8, **11**]

K_y Lateral position error gain (rad/ft·sec^2) [6, 8, 10, **11**, 194, 243, 244]

K_{y_c} Lateral displacement command gain for rotorcraft control (1/sec) [243, 244]

K_{δ_A} Lateral cyclic gain (ft/sec) [**5**]

K_{δ_B} Longitudinal cyclic gain (ft/sec) [**4**]

K_{δ_C} Collective gain (ft/sec) [**13**]

K_{δ_P} Pedal gain (deg/sec) [**18**]

K_θ Pitch attitude feedback gain (1/sec^2) [6, 8, 10, **11**, 245, 246]

K_{θ_m} Longitudinal model pitch attitude feedforward gain (1/sec^2) [8, 10, **12**]

K_ϕ Roll attitude feedback gain (1/sec^2) [6, 8, 10, **11**, 243, 244]

K_{ϕ_m} Lateral model roll attitude feedforward gain (1/sec^2) [8, **12**]

K_ψ Heading error feedback gain (1/sec^2) [19, 20, 21, **22**, 243, 244, **329**, **330**]

K_{ψ_c} Heading command gain for rotorcraft control (1/sec) [243, 244]

K_{ψ_c} Yaw rate command gain (1/sec) [19, 20, 21, **22**, 243, 244]

K'_{h_c} Vertical position command gain ($1/sec^2$) [14, 17, 245]

K'_{x_c} Normalized longitudinal displacement command gain for rotorcraft control (dmls) [245]

K'_{y_c} Normalized lateral position command gain (dimensionless) [6, 8, 11, 243]

K'_{ψ_c} Normalized heading command gain ($1/sec^2$) [19, 20, 22, 243]

L Relative index of the sub-critical task workloading [237]

L_p Augmented roll rate stability derivative (1/sec) [6, 9, 11, 243, 244]

L_{p_g} Roll rate gust stability derivative (1/sec) [181, 182, 243]

L_u Longitudinal scale length (ft) [183, 184]

L_v Augmented lateral velocity stability derivative (rad/ft·sec) [6, 8, 10, 11, 183]; Lateral scale length (ft) [184, 243, 244]

L_w Vertical scale length [183, 184]

L_{v_g} Lateral velocity gust stability derivative (1/ft-sec) [181, 182, 243]

L_0 Mean value of the MX rows in the coefficient matrix $\underline{c}_0^t$ [109, 110, 356]

L_1 Trend value of the MX rows in the coefficient matrix $\underline{c}_0^t$ [109, 110, 112, 356]

LL Across-course index for the lateral evasive maneuver command (see note 26, p. 156) [140, 140]

m Effective mass [181]

M Generalized position: the maximum value of the across-course column index integer J in the anticipative array of the obstacle detection and maneuver selection logic [135, 367]; Maximum value of h_{ref} for the constrained time-optimal vertical maneuver [251]

M_{IND}	One less than the number of columns in the anticipative array [136, 137, 140, 162, **167**]
M_j	The j^{th} column of the coefficient matrix M [109, 110, 112, 356]
M_q	Augmented pitch rate stability derivative (1/sec) [6, 9, **11**, 245, 246]
M_{q_g}	Pitch rate gust stability derivative (1/sec) [181, **182**, 245]
M_u	Augmented longitudinal velocity stability derivative (rad/ft·sec) [6, 8, 10, **11**, 245, 246]
M_{u_g}	Longitudinal velocity stability derivative (rad/ft·sec) [181, **182**, 245]
M(s)	Vehicle response vector [250, 320, 362]
MUF	Maneuver urgency factor [26, **139**, **142**, 144, 155, 156, 174, **176**, **177**, **178**, **179**, **180**]
MUFI	First of two digits of the maneuver urgency factor[**27**]
MUFJ	Second of two digits of the maneuver urgency factor [**27**]
MUF1	Artificially increased maneuver urgency factor [**139**, **139**, **142**, **143**, 155, 368, 370]
MUF_{AUD}	Predicted maneuver urgency factor for the audio annunciator [224, 228, 231]
MUF^J_{AUD}	Units digit of MUF_{AUD} [231]
MX	Number of approximating complex coefficients used for the along-course approximation of terrain [109, 110, 111, 355, 356, 358]
MY	Number of approximating complex coefficients used for the across-course approximation of terrain [109, 110, 111, 112, 355, 356]
n	Course leg counter [**353**]
n_{cp}	Course point counter [**103**, **103**]

n_{cps}	Number of course points in the gaming area course [102, 103, 107, 108]
n_{wp}	Candidate waypoint leg in the waypoint course coordinate transformation [**128**, **128**, 129]
n_{wps}	Number of waypoints [127, 128]
N	Temporary waypoint [**116**, 119, 120]
N_{AMC}	Number of waypoints commanding zero-transition velocity [**97**]
$N_{C\,trm}$	Trim release button on the collective [**13**]
N_C	Engine gas generator indicator in the cockpit instrument panel layout [212]
N_j	The j^{th} column of the coefficient matrix $\underline{N}$ [109, 110, 112, 356]
N_{obs}	Number of obstacles in a cell of the anticipative array [171]
N_P	Engine indicator in the cockpit instrument panel layout [212]
$N_{P\,trm}$	Trim release for the pedals [**18**]
$N_{PR\,trm}$	Trim release button on the cyclic stick (button on the top of the stick) [**4**, **5**]
N_r	Augmented yaw rate stability derivative [19, **22**, 243, 244]
N_{r_g}	Yaw rate gust stability derivative [181, **182**, 243]
N_R	Rotor indicator in the cockpit instrument panel layout [212]
N_{wp}	Waypoint number [121]
N_{wps}	Number of waypoints in the automatic guidance recapture logic [82, 95, 96, 97, 114, 115, 119, 217, 218]
N(s)	Measurement noise vector [250, 320, 362]
NX	Number of points in each terrain elevation profile of the gaming area course used in the approximation of that profile [110, 355]

NY	Number of terrain elevation profiles used to approximate the terrain surface [110, 355, 356]
p	Roll rate (rad/sec) [6, 243]
p_c	Roll rate command (rad/sec) [8, 10, 300, 338]
p_c^{TO}	Roll rate command for the constrained time-optimal lateral evasive maneuver (rad/sec) [26, 34, 69, 70]
p_g	Gust induced roll rate (rad/sec) [181, 243]
p_m	Lateral model roll rate [8, 26, 27, 33, 69, 70, 70]
p_m^p	Previous lateral maneuver roll rate [27, 69, 70]
P_0	The mean value of the MX rows in the coefficient matrix $\underline{c}_0^t$ [109, 110, 356]
P_1	The mean value of the MX rows in the coefficient matrix $\underline{c}_1^t$ [109, 110, 112, 356]
$\dot{p}$	Roll acceleration [243]
PHDDMX	Roll acceleration limits associated with the two digits of the maneuver urgency factor (deg/sec^2) [40]
PHDMX	Roll rate limits (deg/sec) [40]
PHIMX	Roll attitude limits (deg/sec) [40]
PHIT	Altitude switching criterion [25, 30, 31, 32, 33, 37, 38]
PILIM	pi (π) limiter function defined on p. 91, note no. 19 [87, 91]
PSDSW	Time-optimal switching function for the yaw rate reference in a pedal turn [272, 273, 274]
PSSWT	Heading error switching criterion [65, 67]
q	Pitch rate (rad/sec) [6, 245]
q_c	Pitch rate command (rad/sec) [8, 10, 305]

q_c^{TO} Pitch rate command for the constrained time-optimal speed change [42, 47, 72, 73]

q_g Gust induced pitch rate (rad/sec) [181, 245]

q_m Longitudinal model pitch rate [8, 42, 44, 46, 72, 73, 73]

q_m^p Previous longitudinal maneuver model pitch rate [44, 72, 73]

$q_{o_{r1}}$ Intermediate pitch rate function used in calculating the longitudinal velocity switching criterion for the constrained time-optimal longitudinal acceleration-deceleration maneuver [49]

$q_{o_{r2}}$ Intermediate pitch rate function used in calculating the longitudinal velocity switching criterion for the constrained time-optimal longitudinal acceleration-deceleration maneuver [49]

$q_{o_{r3}}$ Intermediate pitch rate function used in calculating the longitudinal velocity switching criterion for the constrained time-optimal longitudinal acceleration-deceleration maneuver [50]

$q_{o_{r4}}$ Intermediate pitch rate function used in calculating the longitudinal velocity switching criterion for the constrained time-optimal longitudinal acceleration-deceleration maneuver [50]

q_1 Intermediate pitch rate function used in calculating the longitudinal velocity switching criterion for the constrained time-optimal longitudinal acceleration-deceleration maneuver [49, 51]

$\dot{q}$ Pitch acceleration (rad/sec^2) [245]

$\dot{q}_{c_{r1}}$ Intermediate pitch acceleration function used in calculating the longitudinal velocity switching criterion for the constrained time-optimal longitudinal acceleration-deceleration maneuver [49]

$\dot{q}_{c_{r2}}$ Intermediate pitch acceleration function used in calculating the longitudinal velocity switching criterion for the constrained time-optimal longitudinal acceleration-deceleration maneuver [49]

$\dot{q}_{cr3}$	Intermediate pitch acceleration function used in calculating the longitudinal velocity switching criterion for the constrained time-optimal longitudinal acceleration-deceleration maneuver [50]
$\dot{q}_{cr4}$	Intermediate pitch acceleration function used in calculating the longitudinal velocity switching criterion for the constrained time-optimal longitudinal acceleration-deceleration maneuver [50]
q'_{mx}	Minimax pitch rate function used in calculating the velocity switching criterion for the final acceleration phase of the constrained time-optimal acceleration-deceleration maneuver [49, 50]
Q_{IND}	Row location of the maximum penetration from below in the left column of the vertical evasive maneuver decision section [145, 157, 159]
r	Instantaneous radius of curvature [243, 326]
r_g	Gust induced yaw rate [181, 243]
r(s)	General expression for the Laplace transform of the course position command array and its derivatives [23, 322]
$\dot{r}$	Yaw acceleration (rad/sec^2) [243, 326]
$\dot{r}(s)$	General expression for the Laplace transform of the course velocity command array and its derivatives [23, 322]
$\ddot{r}$	Yaw jerk (rad/sec^3) [326]
$\ddot{r}(s)$	General expression for the Laplace transform of the course acceleration command array and its derivatives [23, 322]
$\bar{r}(s)$	Vector representing r(s) [321]
R	Maximum value of the integer I [167, 367, 367]
R(s)	General expression for the Laplace transform of the course position command array and its derivatives [250, 320, 362]
R_B	Body axis yaw rate [19]
R_i	Length of the ith course leg of the gaming area course [105, 353]

R_{lcp} Gaming area course leg length [101, 104, 106, 107, **108**]

R_{lwp} Waypoint leg length [82, 95, **97**, 114, **119**, 120, 121, 127, 129]

R_{IND} Row index of the last row of Section 1 (Fig. 4.6) [**135**, 136, 137, 139, 141, 144, 153, 155, 156]

R_n Length of the nth course leg of the gaming area course [352, 353, 354]

R_{ncp} Gaming area course leg length [103]

R_{nwp} Waypoint leg length [128, 129]

R_{obs} Row in the anticipative array containing the obstruction necessitating the evasive maneuver [155]

R_T Waypoint course distance preceding the recapture waypoint [**119**, **119**, 120]

R_x Cell length along course in the anticipative array (ft or dm) of the sensed obstacles [367]

R_y Cell length across course in the anticipative array (ft or dm) of the sensed obstacles [367]

R_1 One less than the number of rows in the lateral evasive maneuver search section (Section 1 in Fig. 4.6) [135, 137, 141, 144, 153, **162**, 231]; Length of the first course leg of the gaming area course [351]

R_2 One less than the number of rows preceding the lateral evasive maneuver search section in the along-course anticipative array [**135**, 136, 144, **153**, 156, 159, 160, 167, 171, 173, 175, 176, 177, 178, 179, 180, 367]

R_3 Length of the third course leg of the gaming area course [352]

R_6 Length of the sixth course leg of the gaming area course [351]

R_{lwp} Temporary waypoint by length [116, **122**]

$\underline{R}_n$	Sensed profile of the terrain, obstacles, and threats with offset requirements [131, 132, 133, 363, 364]
$\underline{\hat{R}}_n$	Stored flight profiles, including waypoints, predicted terrain, and threat exposure models [131, 132, 133, 363, 364]
RA_c	Radar altitude command bar location in the head-up display [207, 208]
RECAP	Logical flag controlling the initiation of the automatic guidance recapture [113, 120, 121]
RECAPT	Logical flag controlling the initiation of the automatic guidance recapture [115]
RH	Half the minimum vertical separation of the upper and lower surfaces of the anticipative array [135, 136, 147, 163, 364, 365, 366, 375, 376]
RX	Cell length in the anticipative array (ft or dm) [153, 159, 160, 162, 163, 164, 167, 171, 173, 231, 364, 364, 365, 366]
RY	Cell width in the anticipative array (ft or dm) [135, 138, 154, 162, 163, 164, 167, 169, 171, 364, 365, 366, 371, 374]
RZ	Cell width in the anticipative array (ft or dm) [162]
s	Laplace transform operator [4, 5, 183, 195, 196, 202, 237, 238, 243, 244, 246, 251, 252, 254, 273, 275, 280, 281, 282, 295, 300, 305, 322, 323, 330, 338]
sI	Laplace transform operator multiplied by the identity matrix [243, 244, 245, 246]
S_{IND}	Row location of the maximum penetration from below in the right column of the vertical evasive maneuver decision section [145, 157, 159]
S_x	Position of the sub-critical-tracking-task controlled vertical bar in the head-up display [202]
SFP	Stored flight plan [250, 320, 362]
SHLDY(J)	Identification of the obstructions in the j^{th} column of section 1 of the anticipative array [137, 137]
$SHPT_{max}$	Shaft horsepower of the turbine [2, 314]

SMART	Ames Research Center numerical integration program for the vehicle dynamic equations of motion [2]
STPFL	Flag indicating the vertical deceleration at the conclusion of the constrained time-optimal vertical maneuver [253, 268]
STPPS	Flag indicating the yaw rate deceleration at the conclusion of the constrained time-optimal directional maneuver [274]
SUPOV	Supervisory override flag [4, 5, 9, 13, 113, 120, 121]
$SW\phi_c$	(PHCFG) roll attitude command flag [283, 300]
$SW\theta_c$	(THCFG) pitch attitude command flag [305]
SWP_c	(PCFG) roll rate command flag [283, 300]
SWQ_c	(QCFG) pitch rate command flag [305]
SWU_c	Longitudinal velocity command flag [305]
SWV_c	(YDCFG) lateral velocity command flag [283, 300]
t	Time (sec) [256, 257, 258, 259, 260, 261, 263, 264, 265, 266, 267, 268, 276, 277, 278, 284, 285, 287, 288, 291, 292, 294, 301, 303, 304, 309, 310, 311, 323, 324, 325, 335, 336, 337, 339, 340, 341, 342, 343]
t_{A_2}	Time interval associated with the shaded area A_2 in Fig. 31 representing a specific time integral of roll rate [292, 293]
t_b	Blending time [272]
t_{sw}	Switching time in the constrained time-optimal maneuver logic [284, 285, 289, 292, 293, 297]
t_1	Duration of the first step of the constrained time-optimal response following switch [284, 287, 290, 293, 294, 295, 297]
t_2	Duration of the second step of the constrained time-optimal response following switch [290, 293, 294, 295, 296, 297, 298]
T_{AM}	Accumulated time on watch during aggressive unmask/mask maneuvers [87, 87, 92]
T_{AUD}	Audio preview time (sec) [225, 227, 231, 232, 233]

T_{BL}	Blending switch time
T_F	Frame time (sec) [234, 235]
T_{IND}	Row location of the maximum penetration from above in the left column of the vertical evasive maneuver decision section [145, 157, 160]
T_L	Switching time for the bang-bang type time-optimal controller [251]
T_m	Range to the given waypoint [115, 122]
T_{min}	Minimum distance to the recapture waypoint (ft) [115, 126]
$T_{mum}(I_{AMC})$	Desired time on watch during the aggressive unmask/mask maneuvers [82, 87, 92, 94, 97, 120]
T_{ph}	Preview time in the vertical axis for the vertical evasive maneuvering (sec) [162, 375]
T_{pgh}	Vertical pursuit guidance model time constant (sec) [15, 17, 23, 194]
T_{pgp}	Directional pursuit guidance model time constant [20, 22, 23]
T_{px}	Preview time in the longitudinal axis of the anticipative array reference point (sec) [135, 162, 167, 231, 367]
T_{pgy}	Lateral pursuit guidance model time constant (sec) [8, 10, 12, 23, 194]
T_{r1}	Time to establish a pitch rate at the maximum pitch acceleration used in calculating the velocity switching criterion for the final acceleration phase of the constrained time-optimal acceleration-deceleration maneuver [49, 59]
T_{r2}	Time to establish a pitch rate at the maximum pitch acceleration used in calculating the velocity switching criterion for the final acceleration phase of the constrained time-optimal acceleration-deceleration maneuver [49, 60]
T_{r3}	Time to establish a pitch rate at the maximum pitch acceleration used in calculating the velocity switching criterion for the final acceleration phase of the constrained time-optimal acceleration-deceleration maneuver [50, 60]

T_{r4}	Time to establish a pitch rate at the maximum pitch acceleration used in calculating the velocity switching criterion for the final acceleration phase of the constrained time-optimal acceleration-deceleration maneuver [50, 60, 61]
T_{sw}	Switching time in the constrained time-optimal maneuver logic [267, 279]
T'_{min}	Initial length of the first temporary waypoint leg (ft) [122, 126]
TO_{SW}	Constrained time-optimal maneuver switch [250, 320, 362]
TR_{δ_A}	Lateral limits of travel of the cyclic controller (in) [5]
TR_{δ_B}	Longitudinal limits of travel of the cyclic controller (in) [4]
TR_{δ_C}	Limits of travel of the collective controller (in) [13]
TR_{δ_P}	Directional limits of travel of the cyclic controller (in) [18]
TAL	Aerodynamic rolling moment [2, 181]
TAM	Aerodynamic pitching moment [2, 181]
TAN	Aerodynamic yawing moment [2, 181]
TEL	Engine induced rolling moment [2, 6]
TEM	Engine induced pitching moment [2, 6]
TEN	Engine induced yawing moment [2, 19]
THET	Pitch attitude at which the pitch acceleration switching based on THSWT occurs during the acceleration phases of the constrained time-optimal acceleration-deceleration maneuver [41, 45, 46]
THSWT	Pitch attitude switching criterion for the acceleration phases of the constrained time-optimal acceleration-deceleration maneuver [51]
TIME	Real clock time in the simulation [228, 231]

TPH	Preview time in the vertical axis of the anticipative array reference point [159, 160]
TPX	Preview time in the longitudinal axis of the anticipative array reference point (sec) [159, 160]
u	Longitudinal velocity [245, 246, 326, 328, 329, 330, 331, **332**, 334]
u_b	Longitudinal body axis component of velocity of the rotorcraft [181]
u_c	Longitudinal velocity command [245, 246, 338]
u_{ea}	Intermediate longitudinal velocity used in calculating the velocity switching criterion for the constrained time-optimal acceleration-deceleration maneuver [**44**]
u_{et}	Longitudinal velocity error threshold (ft/sec or kt) [44, **52**]
u_g	Longitudinal wind gust velocity [181, 183]
u_m	Longitudinal model velocity [8, 42, **44**, **46**, 72, **73**]
u_m^p	Previous longitudinal maneuver model velocity [**44**, 72, 73]
u_{nom}	Nominal along-course velocity (ft/sec or kt) [2, 43, 96, 98, **99**, 114, 116, 117, 119, 226, 230, 232]
$u_{R_{auto}}$	Effective longitudinal velocity command based on the automatic guidance [4, 8, 10]
u_{ref}	Longitudinal reference velocity [2, 8, 42, **43**, 44, 46, **86**, **86**, **120**, **121**, 226, 230]
u_{ref}^p	Previous along-course velocity command [42, **44**]
u_{R_p}	Nonlinear longitudinal cyclic gain [3, 6]
u_{sw_i}	Initial longitudinal body axis component of the steady wind [181]
u_{tw}	Longitudinal along-course velocity command from the waypoint sequencing [2, 42, 43, 99]
$u_{tw}(I_{wp})$	Transition velocities at the waypoints [81, 82, 91, 94, 97, 98, 114, **116**, 217, 230]

$u_{tw}(N)$	Transition velocity of the first temporary waypoint leg in the automatic guidance recapture logic [117, 117, *120*]
u_w	Northward component of the steady wind [181, 183]
u	Longitudinal body axis acceleration component [245]
u'_g	Longitudinal body axis effective wind gust component, including shear due to turns in steady wind [181, 245]
U_c	Velocity command from the automatic guidance system
$U_{c_{HUD}}$	Velocity command for the head-up display [205]
U_{gd}	Rotorcraft ground track velocity component rotated into the aircraft heading coordinate [6, 7, 8, 9, 10, 86, 88, 89, 117, 120, 121, 195, 204, 227, 231, 233]
U_{gd_e}	Longitudinal velocity error ribbon length in the head-up display [195]
U_{IND}	Row location of maximum penetration from above in the right column of the vertical evasive maneuver decision section (145, 157, 160]
U_P	Pursuit feedforward guidance component of the longitudinal velocity [305]
U_{ref}	Longitudinal reference velocity [195]
U_{SW1}	First longitudinal velocity switching criterion for the constrained time-optimal maneuvers [306]
U_{SW2}	Second longitudinal velocity switching criterion for the constrained time-optimal maneuvers [306, 307]
U_{tw}	Upcoming waypoint transition velocity [226]
U_T	Reference trim velocity (kt) [302, 305, 306]
UTSW	Velocity switching criterion that initiates the final acceleration phase of the longitudinal constrained time-optimal maneuver [41, 44, 49]
$UTSW_1$	Intermediate steps in calculating the velocity switching criterion for the final acceleration phase of the constrained time-optimal acceleration-deceleration maneuver [49]

$UTSW_2$ Intermediate steps in calculating the velocity switching criterion for the final acceleration phase of the constrained time-optimal acceleration-deceleration maneuver [49]

$UTSW_3$ Intermediate steps in calculating the velocity switching criterion for the final acceleration phase of the constrained time-optimal acceleration-deceleration maneuver [50, 50]

$UTSW_4$ Intermediate steps in calculating the velocity switching criterion for the final acceleration phase of the constrained time-optimal acceleration-deceleration maneuver [51]

v Lateral component of velocity of the rotorcraft [25, 243, 244]

v_b Lateral velocity, body axis (ft/sec) [181]

v_c Lateral velocity command (ft/sec) [243, 244]

v_D Vertical velocity [14, 193, 207]

v_g Lateral wind gust velocity (ft/sec) [181, 183]

v_m Lateral model velocity [8, 26, 27, 33, 69, 70]

v_m^p Previous lateral maneuver model velocity [27, 69, 70]

v_{ref} Lateral velocity reference [8]

$v_{R_{auto}}$ Equivalent lateral velocity command based on the automatic guidance [5, 8, 10]

v_{R_p} Nonlinear lateral cyclic gain [3, 6]

v_{sw_1} Initial lateral body axis component of the steady wind [181]

v_T Ground track velocity [324]

v_w Eastward component of the steady wind [181, 183]

$v_{x_{com}}$ Longitudinal along-course velocity command from the obstacle detection logic [42]

v_1 Intermediate lateral velocity used in calculating the switching criteria for the constrained time-optimal sidestep [27, 28, 29, 30, 31, 36, 37]

$\dot{v}$	Lateral acceleration [243]
v'_g	Lateral body-axis effective wind gust component, including shears due to turns in steady wind [181, 243]
V	Generalized velocity
V_c	Generalized velocity command from the automatic guidance system [300]
$V_{c_{HUD}}$	Lateral velocity command for the head-up display [205]
V_{eq}	Equivalent airspeed [196]
V_E	Eastward component of inertial velocity [6, 9, 102, 127]
V_{gd}	Rotorcraft ground track velocity component rotated into the aircraft heading coordinate [6, 7, 8, 9, 10, 193, 204]
V_{h_i}	Rate of change of the course altitude at the reference point [374, 375]
V_N	Northward component of the inertial velocity [6, 9, 102, 127]
V_{ref}	Rotorcraft body axis velocity command signal
V_{RW}	Velocity for the Dryden form gust filters (ft/sec) [183, 184]
V_{SW1}	First lateral velocity switching criterion for the constrained time-optimal maneuvers [284, 287, 288, 289, 290, 292]
V_{SW2}	Second lateral velocity switching criterion for the constrained time-optimal maneuvers [290, 291]
V_W	Mean wind velocity [183]
V_{W_0}	Reference value of the wind velocity in the logarithmic portion of the surface boundary layer transition [183]
V_{W_∞}	Free stream value of the wind velocity above the surface boundary layer [183]
V_x	Waypoint course resolved velocity component [127, 133, 135, 153, 167, 367]; Component of the velocity vector in the head-up display [204, 205]

V_y	Waypoint course resolved velocity component [127, 133]; Component of the velocity vector in the head-up display [204, 205]
$V_{x_{min}}$	Minimum forward velocity to vary the dimensions of the anticipative array (ft/sec) [135, 153, 162]
V_E	Eastward component of linear acceleration [102, 196]
V_N	Northward component of linear acceleration [102, 196]
VP_r	Vertical velocity predictor in the head-up display
$VX_{c_{AUD}}$	Future velocity audio command [229, 231, 232]
$VX'_{c_{AUD}}$	Past value of velocity audio command [229]
VDW	Downward steady wind velocity component [183]
VEW	Eastward steady wind velocity component [183]
VHLYL	Required upward vertical velocity to clear the obstacles detected in the left column of the vertical evasive maneuver decision section [148, 159]
VHLYR	Required upward vertical velocity to clear the obstacles detected in the right column of the vertical evasive maneuver decision section [148, 159]
VHMAX	Maximum rate of climb (ft/sec) [148, 159, 162]
VLSW	Vertical velocity switch flag [252, 253, 268]
VNW	Northward steady wind velocity component [183]
VTSW	Velocity switching criterion that initiates the final acceleration phase of the lateral constrained time-optimal maneuver [25, 28, 29, 30, 31, 35, 36]
VTSWO	Velocity switching criterion that initiates the final deceleration phase of the lateral constrained time-optimal maneuver [25, 29, 35]
VP_r	Vertical velocity predictor [209]
VV_r	Vertical velocity ribbon [208]

VXCLYL	Required forward velocity to allow vertical clearing of the obstacles detected in the left column of the vertical evasive maneuver decision section given the rate of climb and descent limits [148, 150, 159, 161]
VXCLYR	Required forward velocity to allow vertical clearing of the obstacles detected in the right column of the vertical evasive maneuver decision section given the rate of climb and descent limits [148, 150, 159, 161]
VXCOM	Forward velocity command [2, 43, 48, 133, 146, 148, 150, 152]
VXNOM	Nominal along-course forward velocity command (ft/sec or kt) [146, 148, 150, 159, 160, 162]
VY	Across-course component of the ground velocity (ft/sec or m/s) [169, 371]
VZMAX	Maximum rate of descent (ft/sec) [150, 161, 162]
VZUYL	Required downward vertical velocity to clear the obstacles detected in the left column of the vertical evasive maneuver decision section [150, 160]
VZUYR	Required downward vertical velocity to clear the obstacles detected in the right column of the vertical evasive maneuver decision section [150, 160]
w	Downward vertical velocity [245]
w_g	Downward vertical wind gust velocity [181, 183]
$w_{obs}(I_{obs})$	Width of obstacles in the defined obstacle array [133, 163, 170]
$w_{obs}(II)$	Threat exposure height of an obstacle in the cell identified by counter II [171]
w_{sw_i}	Initial downward body axis component of the steady wind [181]
w_w	Downward component of the steady wind [181, 183]
w'_g	Downward body-axis wind gust component, including shears due to turns in steady wind [181, 245]
W_d	Distance inside the turn [338]

W_M	Measurement filter [250, 320, 362]
W_R	Command filter [250, 320, 362]
x	Longitudinal position (ft) [3, 245, 246, 305, 306, 309, 310, 311, 331]
x_{ant}	Anticipatory distance [2, 42, 43, 93, **334**]
$x_{ant}(I_{wp})$	Hyperbolic transition parameter--anticipative distance [82, 83, 88, 96, **99**, 114, 226, 233]
$x_{ant}(N)$	Anticipatory distance for the Nth temporary waypoint [**117**, 124]
$x_{ant}(N+1)$	Anticipatory distance for the (N+1)th temporary waypoint [**119**]
x_{Af}	Along-course location of the safety margin envelope reference point [**164**, 170, 173]
x_c	Longitudinal position command [3, 245, 246, 302, 305, 351]
x_{cic}	Initial longitudinal position command [302, 307, 308]
x_{cg}	Present aircraft location inertial coordinate [206]
$x_{cp}(I_{cp})$	North coordinate of the I_{cp} course point [102, 104, 107, 108]
x_{CRS}	Along-course position relative to the upcoming waypoint [**353**, 354, 355, 356, 358]
x_{cs}	Along-course position relative to the upcoming waypoint [2, 42, 43, 48, 82, 83, **84**, 86, 87, **88**, **90**, **92**, 121, **126**, 226, 229, 230]
x_{dis}	Anticipative distance for the audio annunciator logic [229, 230, **232**, **233**]
x_{dm}	Northerly coordinate of the rotorcraft location (dm) [104]
x_e	Longitudinal position error [6, **7**, 8, **9**, 350, 351, 357]
$x_e(I_{wp})$	Northerly earth coordinates of the waypoints (earth coordinate system) [82, 114, 206, 217]
$x_e(n)$	Earth coordinate, north, of the nth waypoint (dm) [350, 352]

$x_e(n+1)$	Earth coordinate, north, of the (n+1)th waypoint (dm) [352]
$x_{e_{stk}}$	Longitudinal position error for calculation of the equivalent longitudinal velocity command [8, 10]
x_{err1}	Initial velocity error in the longitudinal constrained time-optimal maneuver [**44**, 47, 48]
x_E	Northerly earth coordinate of the hyperbolic course transition leg [**333**]
x_{Eh}	Earth axis longitudinal position of a point specified in the hyperbola's coordinate system [217, 218, 219]
x_{E_1}	X_E at the entrance to the hyperbolic course transition leg [333]
x_{EA}	Earth axis longitudinal position coordinate [6, 8, 9, 88, 90, 91, 92, 102, 117, 122, 123, 126, 127, 129]
x_{EA_c}	Earth axis longitudinal position command [6, 8, 9, **86**]
x_{fp}	Along-course coordinate of the reference point of the along-course anticipative array of sensed obstacles [**135**, 153, 159, 161, 167, 170, 171, 173, 367]
x_{gc}	Gaming area along course coordinate [102, 105, 106, 110, 115]
x_h	Longitudinal position in the hyperbola's coordinate system [85, **88**, 89, 90, **91**, 121, **126**, **218**, **219**, 220, 327, 330, 331, 332, 333]
x_{h_1}	x_h at the entrance to the hyperbolic course transition leg [330, 333]
x_{h_k}	kth sequential value of x_h [330]
$x_{h_{k+1}}$	(k+1)th sequential value of X_h [**330**, 331]
x_{h_o}	x_h at the exit from the hyperbolic course transition leg [**330**]
x_{ic}	Initial longitudinal position [306]
$x_{l_{cp}}(\Delta y_c)$	Along-course distance between waypoints as a function of off-course displacement [101]

$x_{obs}(I_{obs})$ North position coordinate of obstacles in the defined obstacle array [133, 163, 170]

$x_{obs}(II)$ Same as $x_{obs}(I_{obs})$, except that the obstacle counter $II \leq I_{obs}$ [171]

x_{pp} Waypoint course coordinate [127, 128, **129**, 133, 135, 159, 161, 163, 164, 226, 227]

x_{rel} Relative longitudinal position given the constant reference velocity [306]

x_{sl} Waypoint course parameter in the longitudinal constrained time-optimal maneuvers [2, 42, 43, 93, 123]

$x_{sl}(I_{wp})$ Hyperbolic transition parameter--distance required to slow to the transition velocity [82, 86, **96**, **98**, 114, 121, 226, 233]

$x_{sl}(N)$ (See note 11, p. 123 for definition) [**117**, **119**, 124]

x_{SW} Relative longitudinal position switching criteria for the constrained time-optimal maneuvers [**307**, **308**]

x_{ter} Gaming area course coordinate modified to accommodate the terrain approximation routine [**110**, 111, 112]

$x_{TN\,min}$ Minimum length of the second temporary waypoint leg in the automatic guidance recapture logic [119]

x_{wc} Waypoint course coordinates of the point at which recapture is initiated [121]

x_{wcs} Gaming area course coordinate of a waypoint [115]

$x_{wp}(I)$ Northerly earth-axis location of the waypoint designated by the integer in ( ) [115]

$x_{wp}(I_{wp})$ Northerly earth-axis location of the waypoint designated by the integer in ( ) [81, 86, 88, 90, 91, 92, 94, 97, 122, 123, 126, 127, 219]

$x_{wp}(n_{wp})$ Northerly earth-axis location of the waypoint designated by the integer in ( ) [129]

$x_{wp}(N)$ Northerly earth-axis location of the waypoint designated by the integer in ( ) [**117**, **118**, **122**, **123**]

x_{WP2}	Northerly earth coordinate of waypoint number 2 before which a hyperbolic course transition leg is required [333]
x_0	(see Eq. 19, p. 90 for the definition used in calculating the hyperbolic course transitions) [**90**]
x_1	Random number governing discrete side-tasks [234, 235, 306]
x_2	Random number governing discrete side-tasks [234]
x_3	Random number governing discrete side-tasks [236]
$x_3(\Delta y_c)$	Along-course length of the third leg of the gaming area course coordinate at a constant lateral off-course displacement Δy_c [352]
x_4	Random number governing discrete side-tasks [236]
x_8	Relative vehicle position (longitudinal) as it entered Region 8 [308]
x_{1_E}	Waypoint course parameter in the longitudinal constrained time-optimal maneuver [2, 42, 43, 93]
$x_{1_E}(I_{wp})$	Hyperbolic transition parameter--entrance to the hyperbolic transition leg [82, 83, 91, **96**, **98**, **99**, 114, 121, 226, 233]
$x_{1_E}(N)$	First hyperbolic transition leg parameters[**117**, 124]
$x_{1_E}(N+1)$	Second hyperbolic transition leg parameter [**119**]
x_{1_h}	Entrance to hyperbolic transition leg--hyperbola coordinate system [93, 218]
$x_{1_h}(I_{wp})$	(See Eq. 4, p. 98 for the definition used in calculating the hyperbolic course transitions) [**98**, 99]
$\dot{x}$	Longitudinal velocity (kt) [3, 245, 305, 307, 308, 309, 310, 311]
$\dot{x}_c$	Longitudinal velocity command [6, 8, 9, 245]
$\dot{x}_{cp}$	Along-course component of velocity with respect to a course point [103]

$\dot{x}_{CRS}$ Longitudinal velocity--gaming area course coordinate system [353, 358]

$\dot{x}_E$ Northerly component of velocity in earth coordinates in a hyperbolic course transition [333]

$\dot{x}_{EA_c}$ Earth axis longitudinal velocity command [7, 9]

$\dot{x}_{gc}$ Gaming area along course inertial velocity component [102, 105, 110, 111]

$\dot{x}_h$ Longitudinal velocity--hyperbola coordinate system [89, 327, 328, 331, 332, 333]

$\dot{x}_{max}$ Maximum value of longitudinal velocity for the constrained time optimal acceleration-deceleration maneuver [306, 308]

$\dot{x}_4$ Longitudinal velocity of the vehicle as it entered Region 4 [306]

$\ddot{x}$ Longitudinal acceleration [306]

$\ddot{x}_{cp}$ Along-course component of acceleration with respect to a course point [103]

$\ddot{x}_{CRS}$ Longitudinal acceleration--gaming area course coordinate system [354, 358]

$\ddot{x}_E$ Northerly component of acceleration in earth coordinates in a hyperbolic course transition [333]

$\ddot{x}_h$ Longitudinal acceleration--hyperbola coordinate system [89, 331, 332, 333]

$\ddot{x}_{gc}$ Gaming area course linear acceleration component [102, 105, 110, 111]

x'_{cs} Along-course distance to the next waypoint in the waypoint sequencing logic [86, 91]

x'_{pp} Waypoint course coordinate for the audio annunciator [227]

x'_{wp} Longitudinal earth-axis location of a temporary waypoint [118, 124]

x'_{dis} Anticipative distance [230, 233]

x(N)	Northerly coordinate of position [335, 336, 337, 339, 340]
X	Along-course direction [163, 167, 367, 369, 372, 373, 377]
X(s)	Laplace transform of the vector X of the dependent variables [**243**, **245**]
X_{TR1}	Entrance hyperbolic transition distances for the purposes of automatic guidance recapture [**121**, **121**]
X_{TR2}	Exit hyperbolic transition distances for the purposes of automatic guidance recapture [**121**]
$X_{TN\,min}$	Minimum length of the second temporary waypoint leg
X_u	Surge damping stability derivative (1/sec) [181, **182**, 245, 246]
$\underline{X}$	Common navigational reference [131, 132, 363, 364]
XH	X-coordinate of the hyperbolic transition between the course legs at a waypoint [93]
XMASS	Effective mass (slug) [14, **17**]
XMC(3)	Effecting rolling moment of inertia (ft-lb-sec^2) [6, **12**, 181]
XMC(7)	Effecting pitching moment of inertia (ft-lb-sec^2) [6, **11**, 181]
XMC(10)	Effecting yawing moment of inertia (ft-lb-sec^2) [19, **22**, 181]
y	Lateral position (ft) [3, 25, 111, 112, 243, 244, 280, 281, 282, 291, **292**, **295**, **299**, 300, 301, 303, 304, **332**]
y_{A_f}	Across-course location of the safety margin envelope reference point [**164**, 170]
y_c	Across-course position [3, 243, 244, 294, 295, 296, 297, 299, 300, **333**, 351]
$y_{c_{AUD}}$	Future lateral offset command (audio annunciator) [227, 228, 231]
y_{cg}	Present aircraft location inertial coordinate [266]
y_{cp}	Easterly coordinate of any (unspecified) course point [103]

$y_{cp}(I_{cp})$ Easterly coordinate of the I_{cp} course point [102, 104, 107, 108]

y_{com} Lateral offset command [2, 26, 27, 33, 133, 135, 138, **140**, **141**, **143**, **152**, 154, 155, **169**, 194]

y^{p}_{com} Previous value of lateral offset command [26, **27**]

y_{coml} Lateral offset command upon entering the obstacle detection and avoidance maneuver selection logic

y_{cs} Lateral offset from the waypoint course [2, 8, 82, **83**, 84, **85**, **87**, **90**, 194]

y_{CRS} Lateral offset from the waypoint course [353, 356, 358]

y_{des} Lateral destination of the evasive maneuver [**138**, **138**, 143]

y_{dm} Easterly coordinate of the rotorcraft location (dm) [104]

y_{e} Lateral position error [6, **7**, 8, **9**, 350, 351, 357]

$y_{e}(I_{wp})$ Easterly earth coordinates of the waypoints [82, 114, 206, 217]

$y_{e}(n)$ Earth coordinate, east, of the nth waypoint (dm) [350, 352]

$y_{e}(n+1)$ Earth coordinate, east, of the (n+1)th waypoint (dm) [352]

y_{ea} Lateral offset used in calculating the switching criteria for the constrained time-optimal sidestep [**27**, 29, 31]

y_{errt} Lateral position error threshold (ft) [40]

y_{errl} Lateral offset error threshold [25, **27**, 29, 34, 35, 36, 37]

y_{ef} Across-course coordinate of the reference point of the along-course anticipative array of sensed obstacles [**135**, 153, 167, 170, 171]

y_{estk} Lateral position error for calculation of the equivalent lateral velocity command [8, 10]

y_{Eh} Earth-axis lateral position of the point specified in the hyperbola's coordinate system [217, 218, 219]

y_E Easterly earth coordinate of the hyperbolic course transition leg [333]

y_{E_i} y_E at the entrance to the hyperbolic course transition leg [333]

y_{EA} Earth-axis lateral position coordinate [6, 8, 9, 88, 90, 91, 92, 102, 117, 122, 123, 126, 127, 129]

y_{EA_c} Earth-axis lateral position command [6, 8, 9, 86]

y_{gc} Gaming area across-course coordinate [102, 105, 110]

y_h Lateral position--hyperbola coordinate system [88, 89, 90, 219, 327, 328]

y_{h_i} y_h at the entrance to the hyperbolic course transition leg [329, 330, 333]

$y_{h_{k+1}}$ (k+1)th sequential value of y_h [350]

y_{h_o} y_h at the exit from the hyperbolic course transition leg [330]

y_m Lateral model position [8, 26, 27, 33, 69, 70]

y_m^p Previous lateral maneuver model position [27, 69, 70]

y_{mx} Maximum lateral deviation from the waypoint course [103, 108, 110]

y_o Exit coordinate of the hyperbolic course transition in the hyperbolic y-coordinate [330]

$y_{obs}(I_{obs})$ East position coordinate of obstacles in the defined obstacle array [133, 163, 170]

$y_{obs}(II)$ Same as $y_{obs}(I_{obs})$, except that the obstacle counter $II \leq I_{obs}$ [171]

y_{pg} Pursuit feedforward guidance command [84]

y_{pp} Waypoint course coordinate [127, 128, 129, 135, 163, 164, 226, 227]

y_{ter} Gaming area course coordinate modified to accommodate terrain-approximation routine [110, 111, 112]

y_{wc}	Waypoint course coordinates of the point at which the recapture is initiated [121]
y_{wcs}	Gaming area course coordinate of a waypoint [115]
$y_{wp}(1)$	Easterly earth-axis coordinate of the waypoint designated by the integer in ( ) [115]
$y_{wp}(I_{wp})$	Easterly earth-axis coordinate of the waypoint designated by the integer in ( ) [81, 94, 97, 122, 127]
$y_{wp}(I_{wp}+1)$	Easterly earth-axis coordinate of the waypoint designated by the integer in ( ) [86, 88, 90, 91, 92, 97, 122, 126, 219]
$y_{wp}(I_{wp}-1)$	Easterly earth-axis coordinate of the waypoint designated by the integer in ( ) [123]
$y_{wp}(n_{wp})$	Easterly earth-axis coordinate of the waypoint designated by the integer in ( ) [129]
$y_{wp}(N)$	Easterly earth-axis coordinate of the waypoint designated by the integer in ( ) [124]
$y_{wp}(N+1)$	Easterly earth-axis coordinate of the waypoint designated by the integer in ( ) [**117**, **118**, **122**, **123**]
y_{WP2}	Easterly earth coordinate of waypoint number 2 before which a hyperbolic course transition is required [333]
y_o	Intermediate variable used in calculating the hyperbolic course transitions [**90**]
y_{l_h}	Lateral coordinate of the hyperbolic trajectory entrance (Hyperbola coordinate system) [88, 93]
$y_{l_h}(I_{wp})$	Lateral coordinate of the hyperbolic trajectory entrance (Hyperbola coordinate system) for the waypoint designated by the integer in ( ) [**98**, 99]
y_s	Lateral position of the vehicle as it entered Region 8 [299]
$\dot{y}$	Lateral velocity (ft/sec) [3, 243, **280**, **281**, 282, 284, 286, 292, **295**, **297**, **299**, 300, 301, **302**, 303, 304]
$\dot{y}_4$	Lateral velocity of the vehicle as it entered Region 4 [289, 290, **296**]

$\dot{y}_c$	Lateral velocity command [6, 8, 9, 243, **292**, **333**]
$\dot{y}_c^{TO}$	Lateral velocity command from the constrained time-optimal maneuver logic [26, **34**, 69, 70]
$\dot{y}_{cTO}$	Constrained time-optimal lateral velocity command for the sidestep maneuver [300]
$\dot{y}_{cp}$	Easterly coordinate of velocity with respect to an (unspecified) course point [103]
$\dot{y}_{CRS}$	Gaming area course inertial velocity component [**353**, 358]
$\dot{y}_E$	Easterly component of velocity in the earth coordinates in a hyperbolic course transition [**333**]
$\dot{y}_{EA_c}$	Earth-axis lateral velocity command [**7**, **9**]
$\dot{y}_{gc}$	Gaming area across-course inertial velocity component [102, **105**, 110, 111]
$\dot{y}_h$	Lateral velocity in the hyperbolic coordinate system [**89**, **328**, **331**, 332, 333]
$\dot{y}_{max}$	Lateral velocity command limit (ft/sec or kt) [25, 27, 28, 30, 34, 35, **40**, 281, **288**, 290, 292, 299, *302*]
$\dot{y}_{pg}$	Lateral velocity pursuit feedforward guidance command [2, 82, **83**, **84**, **85**, **89**, 194]
$\dot{y}_{ref}$	Reference lateral velocity (same as V_{ref}) [280]
$\dot{y}_{SW1}$	Lateral velocity at the first switching point required to control the sidestep maneuver [286]
$\dot{y}_{SW2}$	Lateral velocity at the second switching point required to control the sidestep maneuver [286]
$\ddot{y}$	Lateral acceleration [281, 306]
$\ddot{y}_c$	Lateral acceleration command in the heading reference coordinate system during a hyperbolic course transition [**333**, 334]
$\ddot{y}_{c_1}$	Initial $\ddot{y}_c$ upon entering the hyperbolic transition leg (334]

$\ddot{y}_{CRS}$ Gaming area course linear acceleration component [354, 358]

$\ddot{y}_E$ Easterly component of acceleration in earth coordinates in a hyperbolic course transition [333]

$\ddot{y}_{gc}$ Gaming area course linear acceleration component [105, 110, 111]

$\ddot{y}_h$ Lateral acceleration in the hyperbola coordinate system [89, 331, 332, 333]

$\ddot{y}_i$ Initial lateral acceleration command upon entering the hyperbolic trajectory [83, 88]

$\ddot{y}_{pg}$ Lateral acceleration pursuit feedforward guidance command [2, 82, 83, 83, 84, 85, 102, 194]

$\dddot{y}_{max}$ Maximum lateral jerk [334]

$y'_{c_{AUD}}$ Past value of the audio annunciator lateral offset command [228]

y'_{com} Lateral offset command upon entering the obstacle detection and avoidance maneuver selection logic [135, 140, 141, 143, 152, 155, 228]

y'_{cs} Lateral offset from the waypoint course leg [83, 84, 85, 87, 88, 90, 92, 121, 126]

y'_h Modified value of y_h for use in transforming the hyperbolic transition coordinates to earth-fixed coordinates [90, 219]

y'_{mx} Maximum deviation allowed from the waypoint course (ft or dm) [128, 130]

y'_{pp} Waypoint course coordinate for the audio annunciator [227]

y'_{TIME} Predicted maneuver completion time less the audio preview time [228, 231, 232]

y'_{wp} Earth-axis coordinate of the temporary waypoint [118, 124]

$y(s)$ Laplace transformed system position output response of the controlled element in general [322]

$\bar{y}(s)$	Laplace transformed system position output response vector of the controlled element in general [321]
Y	Across-course direction [163, 167, 283, 365, 367, **369**, 372, 373]
Y_c	Controlled element matrix [250, 283, 323]
$Y_c(s)$	Controlled element matrix [**23**, **322**]
Y_{ef}	Across-course coordinate of the reference point of the along-course anticipative array of sensed obstacles [367]
Y_{err}	Lateral course displacement error in body axis [335, 336, 337, 339, 340, 341, 342, 343]
Y_E	Compensatory error reduction control matrix [250, 320, 362]
Y_P	Pursuit feedforward guidance control matrix [250, 320, 362]; Human operator [238]
Y_{PP}	Pursuit feedforward guidance control matrix [319, 322]
$Y_{PP}(s)$	Pursuit feedforward guidance transfer function [**322**, 323]
Y_{RR}	Constrained time-optimal evasive maneuver control matrix [249, 250, 320, 361, 362]
Y_{SW}	Lateral position switch for the constrained time-optimal sidestep maneuver [291, 292, 293, **294**, **295**, 296, 297, **298**, **299**]
Y_{SWn}	Lateral position switching criteria for the constrained time-optimal maneuvers [283]
Y_v	Sway damping stability derivative (1/sec) [**40**, 181, **182**, 243, 244]
$\dot{Y}$	Lateral velocity [283]
$\dot{Y}_{max}$	Maximum lateral velocity [283]
$\hat{Y}_v$	Sway damping stability derivative (1/sec) [280, 286]
$\bar{Y}_c(s)$	Controlled element matrix [321]
$\bar{Y}_{PP}$	Pursuit feedforward guidance control matrix [321]

Y(E)	Easterly coordinate of position [335, 336, 337, 339, 340]
YH	Y-coordinate of hyperbolic transition between the course legs at a waypoint [93]
YTSW	Position switching criterion in the lateral constrained time-optimal maneuver [25, **27**, 28, 29, **31**, 35, **36**, **37**, 38]
z_{com_a}	Downward vertical offset command from the absolute altimetry [134, 146, 149, 151, 163, **165**, **165**]
z_{com_y}	Proposed downward vertical offset command [151]
Z	Earth-vertical direction [163, 365, 375]
Z_w	Augmented heave damping stability derivative (1/sec) [14, *17*, 245, 246]
Z_{w_g}	Heaving damping gust stability derivative [181, **182**, 245]
Z_{δ_c}	Partial derivative of heaving acceleration with respect to the collective control displacement [**313**, **314**]
$Z_{\delta_c}(\Delta\delta_c)_{max}$	Heaving jerk due to the maximum collective control velocity [**313**]
ZCOMAX	Maximum penetration of the safety margin envelope from below [**164**, **164**, **165**, 166]
$\alpha_{l_{cp}}$	Minus one-half the heading change of the given course point [101, 104, 106, **107**, 108]
$\alpha_{l_{wp}}$	Minus one-half the heading change at the given waypoint [88, 89, 90, 91, 98, 99, **116**, 126, 218, 219]
$\alpha_{l_{wp-1}}$	Minus one-half the heading change at the given waypoint [**95**, **95**, **116**]
α_n	Minus one-half the heading change of the nth waypoint [**352**, 354]
α_{n-1}	Minus one-half the heading change of the n-1th waypoint [352, 354]
$\alpha_{n_{wp}}$	Minus one-half the heading change of the given waypoint [**129**]

$\alpha_{N_{cps}}$ Minus one-half the heading change of the given course point [107, 107]

$\alpha_{N_{cps-1}}$ Minus one-half the heading change of the given course point [107, 107]

$\alpha_{N_{wps}}$ Minus one-half the heading change of the given waypoint [95, 95]

$\alpha_{N_{wps-1}}$ Minus one-half the heading change of the given waypoint [95, 95]

α_{N-1} Minus one-half the heading change of the given waypoint [117]

α_2 Minus one-half the heading change of the given waypoint, with α_n for n=2 [352, 352]

α_3 Minus one-half the heading change of the given waypoint, with α_n for n=3 [352, 352]

δ Human operator's control displacement for the subcritical tracking task [238]

δ_a Lateral deflection of the cyclic controller (in) [300]

$\delta_{A_{auto}}$ Lateral deflection of the cyclic controller as determined by the automatic system [5]

δ_{A_p} Lateral deflection of the cyclic controller due to pilot inputs [5, 6]

$\delta_{A_{trm}}$ Trim lateral deflection of the cyclic controller [5]

δ_b Longitudinal deflection of the cyclic controller (in) [305]

$\delta_{B_{auto}}$ Longitudinal deflection of the cyclic controller as determined by the automatic system [4]

δ_{B_p} Longitudinal deflection of the cyclic controller due to pilot inputs [4, 6]

$\delta_{B_{trm}}$ Trim longitudinal deflection of the cyclic controller [4]

δ_c Collective control displacement (in) [256, 257, 258, 259, 260, 261, 263, 264, 265, 266, 269, 270]

$\delta_{C_{auto}}$	Collective control displacement as determined by the automatic system [13]
δ_{C_p}	Collective control displacement due to pilot inputs [13, 14]
$\delta_{C_{trm}}$	Trim collective control displacement [13]
δ_P	Yaw control displacement (in or percent) [276, 277]
$\delta_{P_{auto}}$	Yaw control displacement as determined by the automatic system [18]
δ_{P_p}	Yaw control displacement due to pilot inputs [18, 19]
$\delta_{P_{trm}}$	Trim yaw control displacement [16]
δ_{SC}	Side arm controller [237, 238]
δ_{sx}	Normalized, unitless pilot control input through the joystick controller for the subcritical tracking task [202]
δ_0	Free stream wind height (ft) [183, 184]
δ_{A_p}	Lateral velocity of the cyclic controller due to pilot input [5]
δ_{B_p}	Longitudinal velocity of the cyclic controller due to pilot inputs [4]
$\delta_{\dot{C}_p}$	Collective control velocity due to pilot inputs [13]
$\delta_{\dot{P}_p}$	Yaw control velocity due to pilot inputs [18]
ΔD_{max}	Maximum change in length of the first waypoint leg from the previous iteration (ft) [118, 126]
ΔD_{wp}	Distance between the nearest and the actual second temporary waypoint [118, 124]
$\Delta(SHPT)_{max}$	Maximum change in the turbine shaft horsepower [313, 314]
Δt	Time interval [330]
Δu	Incremental longitudinal velocity [41]
Δu_{com}	Incremental commanded longitudinal velocity [41]

ΔU_c Change in the commanded longitudinal velocity [305]

$\Delta U_{c_{TO}}$ Time-optimal change in the commanded longitudinal velocity [305]

Δx_c Along course leg distance from the previous waypoint [101, 104, 105, 106, 129, 350, 352, 353, 354]

Δx_{cp} Change in the northerly coordinate of any (unspecified) course point [103]

Δx_{CRS} Along-course coordinate distance between two waypoints along a line parallel to but laterally offset with respect to the centerline of the course leg of the gaming area course [352, 353]

Δx_e Northerly incremental distance (in earth coordinates) of the rotorcraft from the previous waypoint [104, 129, 350]

Δx_{gc} Change in the gaming area along-course coordinate [104, 105, 106]

Δx_{wp} Change in the distance along course from the previous waypoint [128, 129]

$\Delta \dot{x}_c$ Along-course leg velocity of the rotorcraft [353, 354]

$\Delta \dot{x}_{dm}$ Change in northerly velocity (in earth coordinates) of the rotorcraft (dm/sec) [105]

$\Delta \dot{x}_e$ Northerly component of velocity (in earth coordinates) of the rotorcraft with respect to the previous waypoint [353]

$\Delta \dot{x}_{gc}$ Change in the gaming area along-course velocity of the rotorcraft [105]

$\Delta \ddot{x}_c$ Along-course leg acceleration of the rotorcraft [353, 354]

$\Delta \ddot{x}_{dm}$ Northerly component of acceleration (in earth coordinates) of the rotorcraft (dm/sec) [105]

$\Delta \ddot{x}_e$ Northerly component of acceleration (in earth coordinates) of the rotorcraft with respect to the previous waypoint [353]

$\Delta \ddot{x}_{gc}$ Along-course acceleration (in gaming area coordinates) of the rotorcraft [105]

Δy_c Across-course leg distance from the centerline [101, 104, 105, 106, 129, 350, 352, 354]

Δy_{cp} Change in the easterly coordinate of any (unspecified) course point [103]

Δy_{CRS} Across-course leg displacement from the centerline of the course leg [353]

$\Delta y_{CRS_{max}}$ Maximum semi-width with respect to the centerline of a leg of the gaming area course [353]

Δy_e Change in the lateral position error [104, 129, 350]

Δy_{gc} Change in the gaming area across-course coordinate [104, 105, 106]

Δy_{wp} Change in the distance across course from the previous waypoint [128, 129]

Δy_1 Incremental lateral displacement during Step 1 of the constrained time-optimal sidestep [295, 296, 298]

Δy_{1a} Incremental lateral displacement during Step 1a of the constrained time-optimal sidestep [292, 294]

Δy_{1a_1} Incremental lateral displacement during Step 1a1 of the constrained time-optimal sidestep [294, 295, 296, 298]

Δy_{1a_2} Incremental lateral displacement during Step 1a2 of the constrained time-optimal sidestep [295, 296, 298]

Δy_{1b} Incremental lateral displacement during Step 1b of the constrained time-optimal sidestep [294]

Δy_2 Incremental lateral displacement during Step 2 of the constrained time-optimal sidestep [294]

$\Delta \dot{y}$ $\Delta \dot{y}_1 + \Delta \dot{y}_2 + \Delta \dot{y}_3$ in Region 4 at the second switching point for the lateral velocity to bring the rotorcraft to a stop in the lateral direction of the constrained time-optimal sidestep [287, 288, 291]

$\Delta \dot{y}_c$ Across-course leg velocity of the rotorcraft [353, 354]

$\Delta \dot{y}_{dm}$ Change in the easterly velocity (in earth coordinates) of the rotorcraft (dm/sec) [105]

$\Delta \dot{y}_e$ Easterly component of velocity (in earth coordinates) of the rotorcraft with respect to the previous waypoint [353]

$\Delta \dot{y}_{gc}$ Change in the gaming area across-course velocity of the rotorcraft [105]

$\Delta \dot{y}_1$ Incremental lateral velocity change during Step 1 in Region 4 at the second switching point for the lateral velocity to bring the rotorcraft to a step in the lateral direction of the constrained time-optimal sidestep [287, 288, 290, 295]

$\Delta \dot{y}_2$ Incremental lateral velocity change during Step 2 in Region 4 at the second switching point for the lateral velocity to bring the rotorcraft to a step in the lateral direction of the constrained time-optimal sidestep [287, 288, 290]

$\Delta \dot{y}_3$ Incremental lateral velocity change during Step 3 in Region 4 at the second switching point for the lateral velocity to bring the rotorcraft to a step in the lateral direction of the constrained time-optimal sidestep [291]

$\Delta \ddot{y}_c$ Across-course leg acceleration of the rotorcraft [353, 354]

$\Delta \ddot{y}_{dm}$ Easterly component of acceleration (in earth coordinates) of the rotorcraft (dm/sec) [105]

$\Delta \ddot{y}_e$ Easterly component of acceleration (in earth coordinates) of the rotorcraft with respect to the previous waypoint [353]

$\Delta \ddot{y}_{gc}$ Across-course acceleration (in gaming area coordinates) of the rotorcraft [105]

$\Delta \dot{\delta}_{c_{max}}$ Maximum incremental collective control velocity with respect to trim [313]

$\Delta \psi$ Change of heading [275]

$\Delta \psi_c$ Commanded change of heading through the turn [275, 327, 329, 330, 333, 334, 338]

$\Delta \psi_{cp}$ Change in heading at a course point [107]

$\Delta \psi_c(I_{wp})$ Change in commanded heading during the hyperbolic transition at a waypoint identified in ( ) [95, 98, 99, 116]

$\Delta\psi_c(N)$	Change in commanded heading at the first temporary waypoint identified in ( ) for the automatic guidance recapture of the course [117, 119]
$\Delta\psi_c(N-1)$	Change in commanded heading at the previous temporary waypoint identified in ( ) for the automatic guidance recapture of the course [117]
$\Delta\psi_m$	Change in the heading command for the constrained time-optimal pedal turn [87]
$[\Delta]$	Characteristic determinant of the dependent variables in the response of the controlled element [250, 320, 362]
η_u	Independent white noise source for the longitudinal component of stochastic atmospheric turbulence [183]
η_v	Independent white noise source for the lateral component of stochastic atmospheric turbulence [183]
η_w	Independent white noise source for the normal component of stochastic atmospheric turbulence [183]
Θ	Pitch attitude (rad) [6, 8, 10, 12, 41, 195, 245, 305, 306, 307, 308, 309, 310, 311]
θ_c	Mean time between illumination of the correct pattern for the choice reaction time side task (sec) [45, 46, 47, 234, 235, 305]
θ_c^{TO}	Pitch attitude command from the constrained time-optimal speed change [42, 47, 72, 73]
$\theta_{c_{TO}}$	Pitch attitude command for the constrained time-optimal longitudinal acceleration-deceleration maneuver [305]
θ_m	Longitudinal model pitch attitude [42, 44, 46, 72, 73]
θ_m^p	Previous value of θ_m [44, 72, 73]
θ_{max}	Maximum pitch attitude limit (deg) [41, 51, 52, 307, 308]
θ_{min}	Minimum pitch attitude limit (deg) [41, 51, 52]
θ_o	Trim pitch attitude at hover (rad) [6, 8, 10, 12, 245]

θ_s Mean time between the presentation of the letters for the Sternberg recognitive side task (sec) [236]

θ_{SW1} Switching point required to control pitch attitude throughout the constrained time-optimal sidestep maneuver [308]

$\theta_{o_{r1}}$ Intermediate pitch attitude function used in calculating the longitudinal velocity switching criterion for the constrained time-optimal longitudinal acceleration-deceleration maneuver [**49**, 50]

$\theta_{o_{r2}}$ Intermediate pitch attitude function used in calculating the longitudinal velocity switching criterion for the constrained time-optimal longitudinal acceleration-deceleration maneuver [**49**]

$\theta_{o_{r3}}$ Intermediate pitch attitude function used in calculating the longitudinal velocity switching criterion for the constrained time-optimal longitudinal acceleration-deceleration maneuver [**49**]

$\theta_{o_{r4}}$ Intermediate pitch attitude function used in calculating the longitudinal velocity switching criterion for the constrained time-optimal longitudinal acceleration-deceleration maneuver [**49**, 50]

θ_1 Intermediate pitch attitude function used in calculating the longitudinal velocity switching criterion for the constrained time-optimal longitudinal acceleration-deceleration maneuver [**44**, 45, 46, 49]

$\dot{\theta}$ Pitch rate (deg/sec) [41, 245, 305, 306, 307, 308, 309, 310, 311]

$\dot{\theta}_c$ Pitch rate command [**45**, **45**, **46**, **46**, **47**, **47**]

$\dot{\theta}_{c_{TO}}$ Constrained time-optimal pitch rate command [305]

$\dot{\theta}_f$ Intermediate pitch rate function used in calculating the longitudinal velocity switching criteria for the constrained time-optimal longitudinal acceleration-deceleration maneuver [307]

$\dot{\theta}_{max}$ Pitch rate limit (deg/sec) [41, 46, 47, 49, 50, *52*, 306, 307, **308**]

$\dot{\theta}_{min}$ Pitch rate limit (deg/sec) [41, 45, **52**]

$\dot{\theta}_I$ Intermediate pitch rate function used in calculating the longitudinal velocity switching criteria for the constrained time-optimal longitudinal acceleration-deceleration maneuver [44]

$\ddot{\theta}$ Pitch angular acceleration [308]

$\ddot{\theta}_c$ Pitch angular acceleration command [45, 45, 46, 46, 47]

$\ddot{\theta}_{max}$ Maximum pitch angular acceleration limit (deg/sec^2) [45, 46, 47, 49, 50, 51, *52*, 306, 307, 308]

$\ddot{\theta}_{min}$ Minimum pitch angular acceleration limit (deg/sec^2) [45, 46, 52]

λ Magnitude of the unstable pole for the tracking side task (rad/sec) [237, 238]

λ_c Critical value for the unstable pole for the tracking side task (rad/sec) [237, 238]

$\lambda_{i_{wp}}$ Course angle at the ith waypoint [84]

$\lambda_{i_{cp}}$ Course angle at the ith course point [104, 105, 107, 108]

$\lambda_{i_{wp}}$ Waypoint leg headings in the automatic guidance recapture logic [82, 85, 87, 88, 89, 90, 92, 95, 97, 114, 116, 121, 123, 126, 127, 218, 219, 226, 230]

λ_n Direction of the course leg with respect to north at the nth waypoint [350, 352, 353]

λ_{n+1} Direction of the course leg with respect to north at the (n+1)th waypoint [352]

$\lambda_{n_{wp}}$ Waypoint leg headings in the automatic guidance recapture logic [129]

$\lambda_{N_{cps}}$ Course angle at the last course point [107]

$\lambda_{N_{wps}}$ Course angle at the last waypoint [95]

λ_{sc} Subcritical value for the unstable pole for tracking the side task (rad/sec) [202, 237, 238]

λ_0 Initial magnitude of the unstable pole (rad/sec) [238, 239]

λ_1 Direction of the course leg with respect to north at the 1st waypoint [351]

λ_2 Direction of the course leg with respect to north at the 2nd waypoint [352]

λ_3 Direction of the course leg with respect to north at the 3rd waypoint [352]

λ_4 Direction of the course leg with respect to north at the 4th waypoint [352]

λ_5 Direction of the course leg with respect to north at the 5th waypoint [351]

λ_6 Direction of the course leg with respect to north at the 6th waypoint [351]

$\dot{\lambda}$ Time derivative of the unstable pole in the subcritical tracking task [238]

σ Standard deviation [188, 214, 221]

τ_{A_x} Longitudinal acceleration washout time constant in the head-up display (sec) [196, **210**]

τ_c Represents the augmented heave damping (z axis), sway damping (y axis), surge damping (x axis), and yaw damping time constants (sec) [23, 322, 323]

τ_p Maximum allowable response time of the pilot for the choice reaction time side task (sec) [235]

τ_θ Pitch attitude washout time constant in the head-up display (sec) [**210**]

ϕ Roll attitude (rad) [6, 8, 10, 25, 243, 280, **281**, 282, 283, **284**, 285, 286, 287, 288, **290**, **291**, **292**, **292**, **294**, **295**, **295**, **296**, **296**, **298**, **298**, **299**, 300, 301, **302**, 303, 304, 326, 338, 339, 340]

ϕ_c Roll attitude command [287, **292**, **292**, 300, 338]

ϕ_{ct} Intermediate variable in calculating the time-optimal roll attitude command for the constrained time-optimal lateral maneuver logic [**30**, **32**, 34]

ϕ_c^{TO} Roll attitude command from the constrained time-optimal lateral maneuver logic [26, **34**, 69, 70]

$\phi_{c_{TO}}$ Constrained time-optimal roll attitude command [300]

ϕ_{ic} Initial trim condition in roll attitude [281, 286, 338]

ϕ_m Lateral model roll attitude [26, **27**, **33**, 69, **70**, **70**]

ϕ_m^p Previous value of ϕ_m[**27**, 69, 70]

ϕ_{max} Turn bank angle limit (deg) [25, **27**, 28, 30, 37, 98, **99**, 281, 283, 285, 286, 287, 292, 296, 298, 299, **302**, 326, 328, 330]

ϕ_{min} Minimum roll attitude used in calculating the constrained time-optimal sidestep maneuver [25, **27**, 32, 38, 281, 286]

ϕ_{ss} Trim roll attitude at the current wind condition and desired lateral velocity

ϕ_{SS} Trim roll attitude at the current wind condition and desired lateral velocity [286, 299, 338]

ϕ_{SW1} Switching points required to control roll attitude throughout the constrained time-optimal sidestep maneuver [284, **285**, 287, 292, 299]

ϕ_{SW2} Switching points required to control roll attitude throughout the constrained time-optimal sidestep maneuver [281, 283, **286**, 292]

ϕ_{SW3} Switching points required to control roll attitude throughout the constrained time-optimal sidestep maneuver [281, 283, **286**, 298]

ϕ_{SW4} Switching points required to control roll attitude throughout the constrained time-optimal sidestep maneuver [281, 283, **286**]

ϕ_0 Trim roll attitude at hover (rad) [6, 8, 10, **12**, 243]

ϕ_1 Intermediate roll attitude variable [$\phi_1 = \phi_m sgn(y_{err1})$] used in calculating the constrained time-optimal sidestep maneuver [**27**, 28, **30**, 31, 32, 33, 35, 36, 37]

$\dot{\phi}$ Roll rate (deg/sec) [25, 243, 281, 282, 283, 284, 285, 286, 287, 288, **290**, **291**, **292**, 293, **294**, **295**, **296**, **298**, **299**, **299**, 300, 301, 302, 303, 304]

$\dot{\phi}_c$ Roll rate command [30, 31, 32, **33**, *33*, **34**, *34*, 36, 281, 282, 284, 286, 287, 289, 290, 291, **292**, **292**, 293, 297, *299*, 301]

$\dot{\phi}_{cTO}$ Constrained time-optimal roll rate command [300]

$\dot{\phi}_f$ Intermediate roll rate function used in calculating the lateral velocity and displacement switching criteria for the constrained time-optimal sidestep maneuver [**291**, 292, 293, **294**]

$\dot{\phi}_{ic}$ Initial roll rate command

$\dot{\phi}_m$ Model roll rate [27]

$\dot{\phi}_{max}$ Turn roll rate limit (deg/sec) [25, **27**, 30, 33, 34, 35, 36, 37, **99**, 283, 285, 287, 288, 290, 291, 292, 293, 294, 295, 296, 298, 299, **302**]

$\dot{\phi}_{min}$ Minimum roll rate used in calculating the constrained time-optimal sidestep maneuver [25, **27**, 31, 32]

$\dot{\phi}_1$ Intermediate roll rate variable [$\dot{\phi}_1 = \dot{\phi}_m sgn(y_{err1})$] used in calculating the constrained time-optimal sidestep maneuver [**27**, 33, 35, 36, 38]

$\ddot{\phi}$ Roll angular acceleration [**281**, 286, 294, 299, **302**]

$\ddot{\phi}_c$ Commanded roll acceleration [**30**, **30**, **31**, **31**, **32**, **32**, **33**, **33**, **34**, 37, 281, 282, **285**, 286, **287**, **288**, **289**, **291**, **292**, **292**, 294, **295**, **295**, **296**, **296**]

$\ddot{\phi}_{max}$ Roll angular acceleration limit [25, **27**, 31, 32, 33, 34, 35, 36, 37, 38, 281, 282, 283, 284, 285, 286, 287, 288, 290, 291, 294, 295, 296, 298, 299, 302, 334]

$\ddot{\phi}_{min}$ Minimum roll acceleration for calculation of the constrained time-optimal sidestep maneuver [25, **27**, 31, 32, 33, 283]

ψ Heading (deg) [3, 9, 19, 20, 21, 87, 88, 91, 120, 121, 122, 123, 124, 126, 196, 206, 243, 244, 272, 276, 277, 279, 326, 328, 333, 335, 336, 337]

ψ_c Commanded heading [3, 95, 243, 244, 272, **279**, 327, 334]

$\psi_{c_{auto}}$ Effective heading command based on automatic guidance [2, 20, 64, 65, 82, 84, **85**, **87**, **89**, **90**, **92**, 226, 230]

ψ_{c_e} Difference between the commanded heading and the heading of the next waypoint leg [**84**, 218, 220]

ψ_{c_h} Heading at the specified point along the hyperbolic transition leg [218, **219**]

ψ^p_{com} Previous value of ψ_{com}[64, **65**]

ψ_{cs} Commanded heading with respect to the heading of the current waypoint leg [83, **88**]

ψ_e Heading error [273, 274, 275]

ψ_{e_i} Initial heading error of the constrained time-optimal heading change [274]

ψ_{e_T} Heading error threshold [274]

ψ_{ea} Intermediate heading error variable [$\psi_{ea} = (\psi_{c_{auto}} - \psi_m)sgn(\psi_{err1})$] used in calculation of the constrained time-optimal pedal turn maneuver [65]

ψ_{errt} Threshold heading error for the constrained time optimal maneuver (deg) [65, **68**]

ψ_{err1} Intermediate heading error variable [$\psi_{err1} = \psi_{c_{auto}} - \psi^p_{com}$] used in calculation of the constrained time-optimal pedal turn [**65**, 66, 67]

ψ_h Heading in hyperbola coordinate system [85, **88**, 89, 90, **91**, 121, **126**, **218**, **219**, 220, **327**, **328**, 329, 330, 331, 332, 334]

ψ_{h_i} Heading at the entrance to the hyperbolic transition leg between courses in the gaming area [329]

ψ_{h_k} kth extrapolated valued of ψ_h in real time [330]

$\psi_{h_{k+1}}$ (k+1)th extrapolated valued of ψ_h in real time [**330**]

ψ_i Initial heading for use in the pursuit feedforward algorithm during an hyperbolic transition between courses in the gaming area [334]

ψ_m	Directional model heading [20, **65**, 78, **79**]
ψ_m^p	Previous value of ψ_m [**65**, 78, 79]
$\psi_{mum}(I_{AMC})$	Observation heading at the observation waypoint [82, 87, 94, 97, **120**]
$\psi_{obs}(I_{AMC})$	Observation heading at the observation waypoint [206]
ψ_{tr}	Threshold heading error to be considered in the hyperbolic transition leg (deg) [121, **126**]
$\dot{\psi}$	Yaw rate (deg/sec) [3, 243, 244, 272, 273, 274, 275, 276, 277, **326**, 329]
$\dot{\psi}_{ac}$	Yaw rate command from automatic guidance [272, 273]
$\dot{\psi}_{bc}$	Yaw rate command from automatic guidance [272, 273]
$\dot{\psi}_c$	Yaw rate command [19, 20, **65**, **66**, **66**, 243, 244, 275, **327**, **334**]
$\dot{\psi}_{cmax}$	Yaw rate command limit [**326**]
$\dot{\psi}_c^{TO}$	Yaw rate command from the constrained time optimal maneuver logic [64, **66**, 78, 79]
$\dot{\psi}_e$	Yaw rate error [272]
$\dot{\psi}_{ei}$	ith value of $\dot{\psi}_e$ in real time sequence [274]
$\dot{\psi}_h$	Yaw rate in hyperbola coordinate system [**89**, **327**, **328**, **332**, 334]
$\dot{\psi}_{hmax}$	Maximum yaw rate during an hyperbolic transition between course legs in the gaming area [**328**]
$\dot{\psi}_{hi}$	Yaw rate at the entrance to an hyperbolic transition between course legs in the gaming area [**329**]
$\dot{\psi}_m$	Directional model yaw rate [20, 64, **65**, 78, **79**]
$\dot{\psi}_m^p$	Previous value of $\dot{\psi}_m$[**65**, 78, 79]

$\dot{\psi}_{max}$ Yaw rate limit (rad/sec) [65, 66, 67, **68**, 272, 273, 274, 276, 277, **315**, 328]

$\dot{\psi}_{min}$ Minimum yaw rate for calculation of the constrained time-optimal yaw rate command [66]

$\dot{\psi}_{pg}$ Yaw rate pursuit feedforward guidance command [2, 20, 82, **83**, **84**, **85**, **89**]

$\dot{\psi}_{ref}$ Reference value of yaw rate from the constrained time-optimal controller for compensatory control [20, **272**, 273, **279**]

$\dot{\psi}_{R_{auto}}$ Equivalent yaw rate command based on automatic guidance [21]

$\dot{\psi}_{R_p}$ Nonlinear pedal gain [3, 19]

$\dot{\psi}_{tr}$ Yaw rate threshold for calculation of the constrained time-optimal yaw rate command [65, 66]

$\dot{\psi}_T$ Yaw rate switching criteria for the constrained time-optimal directional maneuver logic [274]

$\dot{\psi}_1$ Intermediate yaw rate variable [$\dot{\psi}_1 = \dot{\psi}_m sgn(\psi_{err1})$] used in calculation of the constrained time-optimal pedal turn [65, 67]

$\ddot{\psi}$ Yaw angular acceleration [273]

$\ddot{\psi}_c$ Yaw angular acceleration command [**65**, **65**, 66, 272, 273, **274**, **274**, 327, **334**]

$\ddot{\psi}_c^{TO}$ Yaw angular acceleration command from the constrained time-optimal maneuver logic [64, **66**, 78, 79]

$\ddot{\psi}_{cp}$ Past value of the yaw angular acceleration command [274]

$\ddot{\psi}_e$ Acceleration of yaw error [**274**]

$\ddot{\psi}_h$ Yaw angular acceleration in the hyperbola coordinate system [**89**, **327**, **333**, 334]

$\ddot{\psi}_m$ Directional model yaw acceleration [20, 64, **65**, **79**]

$\ddot{\psi}_{max}$ Yaw angular acceleration limit (rad/sec^2) [65, 67, **68**, 272, 274, **315**]

$\ddot{\psi}_{min}$ Minimum yaw acceleration used in the calculation of the constrained time-optimal pedal turn [65]

$\ddot{\psi}_{pg}$ Yaw angular acceleration pursuit feedforward guidance command [2, 20, 82, **83**, **84**, **85**, **89**]

ψ' Heading of the hyperbolic coordinate x-axis [**219**]

$\dot{\psi}'_c$ Effective yaw rate command [20, 21], 243

ω_a Circular frequency bandwidth for position hold (rad/sec) [**3**]

ω_b Circular frequency bandwidth for velocity command (rad/sec) [**3**]

ω_i Circular temporal frequency component of the encountered terrain profile (rad/sec) [**110**, 111, 323, **324**, **324**, **355**, 356, 358]

ω_j jth circular frequency (rad/sec) in a Fourier series [110, 111, 112, **356**]

Ω_i Spatial frequency component of the terrain profile (1/length) [**324**]

NASA
National Aeronautics and Space Administration

Report Documentation Page

1. Report No.	2. Government Accession No.	3. Recipient's Catalog No.
NASA CR-177571		

4. Title and Subtitle

Fully Automatic Guidance and Control for Rotorcraft Nap-of-the-Earth Flight Following Planned Profiles. Volume II – Mathematical Model

5. Report Date

January 1991

6. Performing Organization Code

7. Author(s)

Warren F. Clement, Peter J. Gorder, and Wayne F. Jewell

8. Performing Organization Report No.

STI TR-1254-2

10. Work Unit No.

9. Performing Organization Name and Address

Systems Technology, Inc.
2672 Bayshore Parkway, Suite 505
Mountain View, CA 94043

11. Contract or Grant No.

NAS2-12640

13. Type of Report and Period Covered

Contractor Report

12. Sponsoring Agency Name and Address

National Aeronautics and Space Administration
Washington, DC 20546-0001

14. Sponsoring Agency Code

15. Supplementary Notes

Point of Contact: Harry Swenson, Ames Research Center, MS 210-9, Moffett Field, CA 94035-1000
(415) 604-5469 or FTS 464-5469

16. Abstract

Developing a single-pilot, all-weather nap-of-the-Earth (NOE) capability requires fully automatic NOE (ANOE) navigation and flight control. Innovative guidance and control concepts are investigated in a four-fold research effort that: (1) organizes the on-board computer-based storage and real-time updating of NOE terrain profiles and obstacles in course-oriented coordinates indexed to the mission flight plan; (2) defines a class of automatic anticipative pursuit guidance algorithms and necessary data preview requirements to follow the vertical, lateral, and longitudinal guidance commands dictated by the updated flight profiles; (3) automates a decision-making process for unexpected obstacle avoidance; and (4) provides several rapid response maneuvers. Acquired knowledge from the sensed environment is correlated with the forehand knowledge of the recorded environment (terrain, cultural features, threats, and targets), which is then used to determine an appropriate evasive maneuver if a non-conformity of the sensed and recorded environments is observed. This four-fold research effort has been evaluated in both fixed-base and moving-base real-time piloted simulations, thereby providing a practical demonstration for evaluating pilot acceptance of the automated concepts, supervisory override, manual operation, and re-engagement of the automatic system. Volume I describes the major components of the guidance and control laws as well as the results of the piloted simulations. Volume II describes the complete mathematical model of the fully automatic guidance system for rotorcraft NOE flight following planned flight profiles.

17. Key Words (Suggested by Author(s))	18. Distribution Statement
Automatic flight guidance and control Rotorcraft Nap of the Earth	Unclassified-Unlimited Subject Category - 08

19. Security Classif. (of this report)	20. Security Classif. (of this page)	21. No. of Pages	22. Price
Unclassified	Unclassified	480	A21

For sale by the National Technical Information Service, Springfield, Virginia 22161 GPO 586-319/59100